TURBULENT NATURAL CONVECTION IN RECTANGULAR ~~AIR~~-CAVITIES

A THESIS SUBMITTED FOR THE DEGREE OF
DOCTOR OF PHILOSOPHY

AUTHOR:
KEVIN JOHN KING

INSTITUTE:
QUEEN MARY COLLEGE
UNIVERSITY OF LONDON

DATE:
APRIL 1989

BIBL. LONDIN. UNIV

ABSTRACT

The velocity and temperature fields of several air cavities have been surveyed.

The cavities operated in the transitional boundary layer regime with vertical, opposing, isothermal heated and cooled walls.

The cavity height, width, temperature difference and wall insulation were all changed during the study, with the aspect ratio varying from 4 to 10, and Ra_H varying from 2.263×10^{10} to 4.486×10^{10}.

The local velocity and temperature were measured simultaneously using a laser Doppler anemometer and a 25μm chromel-alumel thermocouple. This allowed the turbulence quantity $\overline{u'T'}$ to be measured directly, as well as the mean and root mean square of the fluctuations of velocity and temperature.

Several other quantities, which have not previously been available, were derived from the measured data, these were the wall shear stress, the mean lateral velocity, $\overline{u'v'}$, and $\overline{v'T'}$.

The effect of a decrease of the level of insulation on the vertical walls was to decrease the non-dimensional temperature of the fluid at the vertical centre-line.

Different thermal boundary conditions on the horizontal walls resulted in significant differences between the heated and cooled wall, thermal and velocity, boundary layers.

A decrease in the cavity width was seen to alter the characteristics of the mean velocity and temperature profiles when the width was less than twice the lateral extent of either boundary layer in a cavity with a larger width.

Near wall distributions of $\overline{u'v'}$ have shown that the viscous sub-layer was approximately 4mm thick.

Calculations of power spectral density, together with inspection of time histories, have confirmed that a laminar flow was present at the bottom of the heated wall.

P.S.D. calculations showed that the dominant frequencies of transition were multiples of a base frequency and dependent on the local temperature drop between the wall and the "environment".

The power relationship between frequency and power spectral density has been shown to depend on the local vertical temperature gradient.

Three sub-ranges were identified in the velocity spectra, whereas four were identified in the temperature spectra. The equivalent ranges in the

velocity and temperature spectra exhibited different powers on the frequency, with those of the temperature field being larger.

ACKNOWLEDGEMENTS

The author would primarily like to thank Dr. R. Cheesewright for his support and encouragement during the course of the present study, and for arranging the opportunity to undertake experimental work at E.N.S.M.A. in Poitiers, France. In this respect thanks are given to Doan-Kim-Son for his hospitality at E.N.S.M.A. and for the friendliness of the students and technical staff there. More specifically, the author would like to extend his gratitude to Rene Albert, Jean-Claude Pret, Juan-Carlos Elicer, Fakhreddine Chabchoub and Laziz Jemai.

At Q.M.C., thanks are given to the technical staff who promptly dealt with problems which arose during the experimental periods, and who helped with some of the work in the latter stages of the study. Specfically, the author would like to thank Tony Burn, Tony Turner and Vince Ford.

Grateful acknowledgement is given to the S.E.R.C. who provided the funding which allowed the study to go ahead, and for the opportunity to attend a summer school which has proved very valuable in the personal development of the author.

Finally, the author would like to thank his parents for providing financial and moral support whenever necessary, and without hesitation.

TO

MY MOTHER & MY FATHER

CONTENTS

LIST OF FIGURES 11
LIST OF TABLES 21
LIST OF PLATES 25
LIST OF SYMBOLS 26

CHAPTER 1 - INTRODUCTION

1.1 INITIATION OF THE PRESENT STUDY 30
1.2 THE CAVITY CONFIGURATION 31
1.3 THE DEFINITION AND EQUATIONS OF NATURAL CONVECTION ... 32
1.4 PREVIOUS WORK 33
1.5 THE PRESENT STUDY 35

CHAPTER 2 - LITERATURE SURVEY

2.1 INTRODUCTION 38
2.2 FLOW REGIMES 39
2.3 TRANSITION 41
2.3.1 ONSET OF TRANSITION 42
2.3.2 INSTABILITY MODE 45
2.3.3 TRANSITION FREQUENCIES 47
2.4 TRANSITIONAL BOUNDARY LAYER REGIME 49
2.5 TURBULENT BOUNDARY LAYER REGIME 54
2.6 VELOCITY BOUNDARY LAYER 56
2.7 THERMAL BOUNDARY LAYER 60
2.8 CORE STRATIFICATION 64
2.9 TURBULENCE QUANTITIES 67
2.9.1 THE REYNOLDS STRESS $\rho\overline{u'v'}$ 68
2.9.2 THE LATERAL AND VERTICAL TURBULENCE HEAT FLUXES . 69
2.9.3 THE TRANSITION REGION 69
2.9.4 TURBULENCE KINETIC ENERGY 70
2.10 TURBULENCE SPECTRA 71
2.11 VELOCITY LENGTH AND TEMPERATURE SCALES 74
2.11.1 SCALES IN THE NEAR WALL REGION 75
2.11.1.1 TEMPERATURE SCALES 75
2.11.1.2 VELOCITY SCALES 77
2.11.2 THE OUTER REGION 79

2.12 FLOOR AND CEILING BOUNDARY CONDITIONS 81
2.13 VERTICAL SIDE WALL BOUNDARY CONDITIONS 86
2.14 HEAT TRANSFER CORRELATIONS 87
2.14.1 OVERALL HEAT TRANSFER CORRELATIONS 87
2.14.2 LOCAL HEAT TRANSFER CORRELATIONS 90
2.15 RESUME 90
2.16 OBJECTIVES OF THE PRESENT STUDY IN RELATION TO POINTS BROUGHT FORTH BY THE LITERATURE SURVEY 92

CHAPTER 3 - APPARATUS

3.1 THE APPARATUS AT QUEEN MARY COLLEGE 110
3.1.1 THE CAVITY 110
3.1.1.1 THE BASE FRAME 110
3.1.1.2 THE A-FRAME 111
3.1.1.3 THE COOLED WALL 114
3.1.1.4 THE HEATED WALL 115
3.1.1.5 THE VERTICAL SIDE WALLS 116
3.1.1.6 THE FLOOR AND CEILING 116
3.1.2 THE THERMOCOUPLE SIGNAL PROCESSING INSTRUMENTATION 117
3.1.3 THE LASER DOPPLER ANEMOMETRY SYSTEM 118
3.1.4 THE DATA LOGGING SYSTEM 119
3.2 THE APPARATUS AT POITIERS 121
3.2.1 THE CAVITY 121
3.2.1.1 THE COOLED WALL 121
3.2.1.2 THE HEATED WALL 122
3.2.1.3 THE VERTICAL SIDE WALLS 122
3.2.1.4 THE FLOOR AND CEILING 123
3.2.2 THE TEMPERATURE MEASURING EQUIPMENT 123
3.2.3 THE LASER DOPPLER ANEMOMETRY SYSTEM 124

CHAPTER 4 - EXPERIMENTAL PROCEDURE

4.1 INTRODUCTION 137
4.2 PROCEDURE FOR SERIES 1 137
4.2.1 PROBE PREPARATION 137
4.2.2 LASER DOPPLER ANEMOMETER PREPARATION AND PARAMETERS 138

4.2.3 INITIAL CAVITY PREPARATION 140
4.2.4 RUN PROCEDURE 140
4.3 PROCEDURE FOR SERIES 2 144
4.4 PROCEDURE FOR SERIES 3 145
4.4.1 PROBE PREPARATION 145
4.4.2 LASER DOPPLER ANEMOMETER PARAMETERS 146
4.4.3 INITIAL CAVITY PREPARATION 146
4.4.4 RUN PROCEDURE 147
4.5 PROCEDURE FOR SERIES 4 147
4.6 PROCEDURE FOR SERIES 5 147
4.7 PROCEDURE FOR SERIES 6 148
4.7.1 PROBE PREPARATION 148
4.7.2 LASER DOPPLER ANEMOMETER PREPARATION AND PARAMETERS 149
4.7.3 INITIAL CAVITY PREPARATION 150
4.7.4 RUN PROCEDURE FOR VELOCITY MEASUREMENTS 150
4.7.5 RUN PROCEDURE FOR TEMPERATURE MEASUREMENTS 151
4.8 PROCEDURE FOR SERIES 7 152

CHAPTER 5 - SUMMARY OF THE EXPERIMENTAL SERIES

5.1 INTRODUCTION 155
5.2 EXPERIMENTAL SERIES DESCRIPTION 155
5.2.1 SERIES 1 155
5.2.2 SERIES 2 156
5.2.3 SERIES 3 156
5.2.4 SERIES 4 156
5.2.5 SERIES 5 156
5.2.6 SERIES 6 157
5.2.7 SERIES 7 157

CHAPTER 6 - UNCERTAINTY ESTIMATIONS

6.1 INTRODUCTION 159
6.2 CONSECUTIVE REPEATABILITY OF DATA 159
6.2.1 VELOCITY DATA 159
6.2.2 TEMPERATURE DATA 160
6.3 DAY TO DAY REPEATABILITY OF DATA 161
6.3.1 VELOCITY PROFILES 161

6.3.2 TEMPERATURE PROFILES 162
6.3.3 WALL HEAT TRANSFER RATES 162
6.4 THE EFFECT OF THE THERMOCOUPLE ON VELOCITY 163
6.5 SUMMARY OF UNCERTAINTIES IN THE Q.M.C. DATA 166
6.5.1 UNCERTAINTIES IN INDIVIDUAL RUNS 167
6.5.2 UNCERTAINTIES IN RELATION TO SPECIFIC CAVITY CONDITIONS 168
6.6 UNCERTAINTIES IN THE POITIERS CAVITY DATA 168

CHAPTER 7 - RESULTS AND DISCUSSIONS

7.1 INTRODUCTION 196
7.2 THE TEMPERATURE FIELD 197
7.2.1 THE MEAN AND FLUCTUATING COMPONENTS OF TEMPERATURE 197
7.2.2 THE MEAN TEMPERATURE IN θ AND Nu_v FORMAT 202
7.2.3 THE VERTICAL CENTRE-LINE TEMPERATURE DISTRIBUTION 206
7.2.4 THE HEAT TRANSFER COEFFICIENTS 210
7.2.5 THE LOCAL HEAT TRANSFER 212
7.2.6 OVERALL HEAT TRANSFER 215
7.2.7 TWO-DIMENSIONAL CHECKS 217
7.2.8 SUMMARY OF THE FINDINGS FROM THE TEMPERATURE RESULTS 217
7.3 THE VELOCITY FIELD 218
7.3.1 THE MEAN AND FLUCTUATING COMPONENTS OF VELOCITY . 219
7.3.2 COMMENTS ARISING OUT OF THE USE OF THE LASER DOPPLER ANEMOMETER 227
7.3.3 THE WALL SHEAR STRESS 229
7.3.3.1 THE WALL SHEAR STRESS AT THE HEATED WALL ... 231
7.3.3.2 THE WALL SHEAR STRESS AT THE COOLED WALL ... 231
7.3.3.3 REPEATABILITY, VELOCITY CORRECTION AND UNCERTAINTY ESTIMATION WITH REGARD TO THE WALL SHEAR STRESS 232
7.3.4 VELOCITY SCALES 233
7.3.5 PROBABILITY DISTRIBUTIONS OF VELOCITY 236
7.3.6 THE RATIO $u'_{r.m.s.}/v'_{r.m.s.}$ 238
7.3.7 MASS FLOW CALCULATIONS 239
7.3.8 COMPARISON OF PROFILES AT SIMILAR Ra_x 240
7.3.9 THE LATERAL MEAN VELOCITY 241

7.3.10 COMPARISON WITH HOT-WIRE DATA ON A QUALITATIVE BASIS 244
7.3.11 HEATED CEILING 244
7.3.12 FLOW VISUALISATION 245
7.3.13 SUMMARY OF THE FINDINGS FROM THE VELOCITY RESULTS 245
7.4 TURBULENCE QUANTITIES 248
7.4.1 THE VERTICAL TURBULENCE HEAT FLUX 248
7.4.2 THE LATERAL TURBULENCE HEAT FLUX 250
7.4.3 THE REYNOLDS STRESS $\rho\overline{u'v'}$ 252
7.4.4 THE TOTAL SHEAR STRESS 258
7.4.5 TURBULENCE KINETIC ENERGY 258
7.4.6 SUMMARY OF THE FINDINGS FROM THE TURBULENCE QUANTITIES 260
7.5 POWER SPECTRAL DENSITY CALCULATIONS 261
7.5.1 THE MATHEMATICAL TECHNIQUE 263
7.5.2 VELOCITY TIME HISTORIES 266
7.5.3 VELOCITY P.S.D. DISTRIBUTIONS 267
7.5.4 COMPARISON OF EXPERIMENTAL AND THEORETICALLY PREDICTED SUB-RANGE EXPONENTS FOR VELOCITY P.S.D. DISTRIBUTIONS 273
7.5.5 TEMPERATURE P.S.D. DISTRIBUTIONS 276
7.5.6 COMPARISON OF EXPERIMENTAL AND THEORETICALLY PREDICTED SUB-RANGE EXPONENTS FOR TEMPERATURE P.S.D. DISTRIBUTIONS 279
7.5.7 FREQUENCY AND WAVENUMBER RANGES IN RELATION TO THE SUB-RANGES 281
7.5.8 JUSTIFICATION OF THE VALIDITY OF THE P.S.D. CALCULATIONS 281
7.5.9 SUMMARY OF THE FINDINGS FROM THE P.S.D. CALCULATIONS 282

CONCLUSIONS 462
REFERENCES 465
PUBLISHED MATERIAL 476
APPENDIX A 477

LIST OF FIGURES

CHAPTER 1 - INTRODUCTION

1.1 CAVITY CONFIGURATION AND CO-ORDINATE SYSTEM 36

1.2 CO-ORDINATE DEFINITION PLUS VELOCITY AND TEMPERATURE PROFILES FOR NATURAL CONVECTION OF AIR ALONG A VERTICAL WALL 37

CHAPTER 2 - LITERATURE SURVEY

2.1 MAXIMUM AND MINIMUM VELOCITY ENVELOPES DUE TO UNSTEADY MOTIONS 94

2.2 THE INFLUENCE OF ASPECT RATIO ON THE ONSET OF UNSTEADY MOTIONS AND TURBULENCE 95

2.3 THE INFLUENCE OF STRATIFICATION ON CRITICAL Gr_L FOR $0.73 < Pr < 12.7$ 97

2.4 THE INFLUENCE OF STRATIFICATION ON CRITICAL Gr_L FOR $Pr > 20$ 98

2.5 THE INFLUENCE OF STRATIFICATION ON CRITICAL Ra_L FOR $Pr > 0.73$ 99

2.6 VARIATION OF $f/C\dot{Q}^{*0.5}$ WITH $Gr_{x\dot{Q}*}$ 100

2.7 VARIATION OF DOMINANT TRANSITION FREQUENCY WITH HEIGHT FOR THE VELOCITY FIELD 100

2.8 VARIATION OF DOMINANT TRANSITION FREQUENCY WITH HEIGHT FOR THE TEMPERATURE FIELD 100

2.9 SKETCH OF THE VELOCITY BOUNDARY LAYER FROM A WATER CAVITY OPERATING IN THE TRANSITIONAL BOUNDARY LAYER REGIME 101

2.10 VELOCITY AND TEMPERATURE PROFILES FROM A WATER CAVITY OPERATING IN THE TRANSITIONAL BOUNDARY LAYER REGIME .. 102

2.11 VELOCITY AND TEMPEARTURE PROFILES FROM A RELATIVELY NARROW AIR CAVITY OPERATING IN THE TRANSITIONAL BOUNDARY LAYER REGIME 103

2.12 OVERALL HEAT TRANSFER IN THE TRANSITIONAL AND TURBULENT BOUNDARY LAYER REGIMES 104

2.13 VELOCITY AND TEMPERATURE PROFILES FROM A WATER CAVITY NOMINALLY OPERATING IN THE TRANSITIONAL BOUNDARY LAYER REGIME 105

2.14 VARIATION OF REYNOLDS NUMBER AT THE MEAN VELOCITY PEAK WITH STRATIFICATION 106
2.15 THE EFFECT ON THE MEAN VELOCITY PROFILE OF REDUCING THE CAVITY WIDTH AT CONSTANT Ra_H 106
2.16A CORE STRATIFICATIONS FROM CAVITIES OPERATING IN THE TRANSITIONAL BOUNDARY LAYER REGIME 107
2.16B CORE STRATIFICATIONS FROM CAVITIES OPERATING IN THE TRANSITIONAL BOUNDARY LAYER REGIME 108
2.17 IDEAL ADIABATIC AND EXPERIMENTAL TEMPERATURE DISTRIBUTIONS ON THE FLOORS AND CEILINGS OF TWO CAVITIES 109

CHAPTER 3 - APPARATUS

3.1 THE Q.M.C. CAVITY 126
3.2 SKETCH SHOWING THE OPTICAL ACCESS BLOCKS REMOVED 127
3.3 ADDITIONAL SEALS AT THE TOP AND BOTTOM OF THE Q.M.C. CAVITY 128
3.4 UNITS OF THE Q.M.C. LASER DOPPLER ANEMOMETRY SYSTEM .. 129
3.5 DISA TRACKER CALIBRATION GRAPH 130A
3.6 THE POITIERS CAVITY HEATED WALL 130B

CHAPTER 4 - EXPERIMENTAL PROCEDURE

4.1 CO-ORDINATE SYSTEM FOR THE LASER DOPPLER ANEMOMETER .. 153

CHAPTER 5 - SUMMARY OF THE EXPERIMENTAL SERIES

5.1 SUMMARY OF THE EXPERIMENTAL SERIES 158

CHAPTER 6 - UNCERTAINTY ESTIMATIONS

6.1 REPEATABILITY OF MEAN VELOCITY - HEATED WALL 170
6.2 REPEATABILITY OF R.M.S. OF VELOCITY FLUCTUATIONS - HEATED WALL 171
6.3 REPEATABILITY OF MEAN VELOCITY - COOLED WALL 172
6.4 REPEATABILITY OF R.M.S. OF VELOCITY FLUCTUATIONS - COOLED WALL 173
6.5 REPEATABILTY OF MEAN TEMPERATURE - HEATED WALL 174

6.6 REPEATABILITY OF R.M.S. OF TEMPERATURE FLUCTUATIONS - HEATED WALL 175
6.7 REPEATABILITY OF MEAN TEMPERATURE - COOLED WALL 176
6.8 REPEATABILITY OF R.M.S. OF TEMPERATURE FLUCTUATIONS - COOLED WALL 177
6.9 CO-ORDINATE SYSTEM FOR CREEPING FLOW AROUND A SPHERE . 178
6.10 THERMOCOUPLE EFFECT ON MEAN VELOCITY - HEATED WALL - FULL BOUNDARY LAYER 179
6.11 THERMOCOUPLE EFFECT ON MEAN VELOCITY - HEATED WALL - FROM WALL TO y = 20mm 180
6.12 THERMOCOUPLE EFFECT ON MEAN VELOCITY - HEATED WALL - FROM WALL TO y = 5mm 181
6.13 THERMOCOUPLE EFFECT ON R.M.S. OF VELOCITY FLUCTUATIONS - HEATED WALL - FULL BOUNDARY LAYER 182
6.14 THERMOCOUPLE EFFECT ON R.M.S. OF VELOCITY FLUCTUATIONS - HEATED WALL - FROM WALL TO y = 20mm ... 183
6.15 THERMOCOUPLE EFFECT ON MEAN VELOCITY - COOLED WALL - FULL BOUNDARY LAYER 184
6.16 THERMOCOUPLE EFFECT ON MEAN VELOCITY - COOLED WALL - FROM WALL TO y = 20mm 185
6.17 THERMOCOUPLE EFFECT ON MEAN VELOCITY - COOLED WALL - FROM WALL TO y = 5mm 186
6.18 THERMOCOUPLE EFFECT ON R.M.S. OF VELOCITY FLUCTUATIONS - COOLED WALL - FULL BOUNDARY LAYER 187
6.19 THERMOCOUPLE EFFECT ON R.M.S. OF VELOCITY FLUCTUATIONS - COOLED WALL - FROM WALL TO y = 20mm 188
6.20 VARIATION OF VELOCITY CORRECTION WITH TURBULENCE INTENSITY 189
6.21 VARIATION OF VELOCITY CORRECTION WITH HORIZONTAL SEPARATION OF THERMOCOUPLE JUNCTION AND PROBE VOLUME . 190

<u>CHAPTER 7 - RESULTS AND DISCUSSIONS</u>

7.1 PROFILES OF NON-DIMENSIONAL MEAN TEMPERATURE FOR SERIES 3 ($\Delta T \simeq 45.8K$) 284
7.2 PROFILES OF NON-DIMENSIONAL MEAN TEMPERATURE FOR SERIES 6 ($\Delta T \simeq 42.5K$) 285
7.3 PROFILES OF NON-DIMENSIONAL $T'_{R.M.S.}$ FOR SERIES 3 ($\Delta T \simeq 45.8K$) 286

7.4 PROFILES OF NON-DIMENSIONAL $T'_{R.M.S.}$ FOR SERIES 6 ($\Delta T \simeq 42.5K$) 287
7.5 THETA AGAINST Nu_Y AT THE HEATED WALL OF SERIES 3, WITH T_{MIN} AS THE REFERENCE TEMPERATURE 288
7.6 THETA AGAINST Nu_Y AT THE HEATED WALL OF SERIES 3, WITH T_∞ AS THE REFERENCE TEMPERATURE 289
7.7 THETA AGAINST Nu_Y AT THE HEATED WALL OF SERIES 4, WITH T_{MIN} AS THE REFERENCE TEMPERATURE 290
7.8 THETA AGAINST Nu_Y AT THE HEATED WALL OF SERIES 4, WITH T_∞ AS THE REFERENCE TEMPERATURE 291
7.9 THETA AGAINST Nu_Y AT THE HEATED WALL OF SERIES 5, WITH T_{MIN} AS THE REFERENCE TEMPERATURE 292
7.10 THETA AGAINST Nu_Y AT THE HEATED WALL OF SERIES 6, WITH T_{MIN} AS THE REFERENCE TEMPERATURE 293
7.11 THETA AGAINST Nu_Y AT THE HEATED WALL OF SERIES 3, 4, 5 AND 6, WITH T_{MIN} AS THE REFERENCE TEMPERATURE 294
7.12 THETA AGAINST Nu_Y AT THE COOLED WALL OF SERIES 3, WITH T_{MIN} AS THE REFERENCE TEMPERATURE 295
7.13 THETA AGAINST Nu_Y AT THE COOLED WALL OF SERIES 4, WITH T_{MIN} AS THE REFERENCE TEMPERATURE 296
7.14 THETA AGAINST Nu_Y AT THE HEATED AND COOLED WALLS OF SERIES 3 AND 4, WITH T_{MIN} AS THE REFERENCE TEMPERATURE 297
7.15 THETA AGAINST $\ln(Nu_Y)$ AT THE HEATED WALL OF SERIES 3, WITH T_{MIN} AS THE REFERENCE TEMPERATURE 298
7.16 THETA AGAINST $\ln(Nu_Y)$ AT THE HEATED WALL OF SERIES 3, WITH T_{MIN} AS THE REFERENCE TEMPERATURE 299
7.17 NON-DIMENSIONAL VERTICAL CENTRE-LINE TEMPERATURE DISTRIBUTIONS FOR SERIES 1, 2, 3 AND 4 300
7.18 NON-DIMENSIONAL VERTICAL CENTRE-LINE TEMPERATURE DISTRIBUTIONS FOR SERIES 5, 6 AND 7 301
7.19 NON-DIMENSIONAL VERTICAL CENTRE-LINE TEMPERATURE DISTRIBUTIONS FOR SERIES 2, 3 AND 5 302
7.20 LOCAL Nu_x AGAINST LOCAL Gr_x AT THE HEATED WALL FOR SERIES 2, 3, 4 AND 5 303
7.21 LOCAL Nu_x AGAINST LOCAL Gr_x AT THE COOLED WALL FOR SERIES 2, 3, 4 AND 5 304
7.22 LOCAL Nu_x AGAINST LOCAL Gr_x AT THE HEATED WALL FOR SERIES 5, 6 AND 7 305

7.23 LOCAL Nu_x AGAINST LOCAL Gr_x AT THE COOLED WALL FOR SERIES 5, 6 AND 7 306
7.24 LOCAL Nu_x AGAINST LOCAL Gr_x AT THE HEATED WALL FROM COWAN ET AL [12] AND THE PRESENT STUDY 307
7.25 LOCAL Nu_x AGAINST LOCAL Ra_x AT THE HEATED WALL FROM COWAN ET AL [12] AND THE PRESENT STUDY 308
7.26 PROFILES OF MEAN VELOCITY FOR SERIES 3 ($\Delta T \simeq 45.8K$) .. 309
7.27 PROFILES OF MEAN VELOCITY FOR SERIES 6 ($\Delta T \simeq 42.5K$) .. 310
7.28 PROFILES OF $u'_{R.M.S.}$ FOR SERIES 3 ($\Delta T \simeq 45.8K$) 311
7.29 PROFILES OF $u'_{R.M.S.}$ FOR SERIES 6 ($\Delta T \simeq 42.5K$) 312
7.30 VARIATION OF % DROPOUT WITH TIME 313
7.31 COMPARISON BETWEEN EXPERIMENTAL AND PREDICTED MEAN VELOCITY FROM SERIES 3 AT $x/H = 0.765$ 314
7.32 WALL SHEAR STRESS DATA FOR SERIES 3, 4 AND 5 315
7.33 WALL SHEAR STRESS DATA FOR SERIES 5, 6 AND 7 316
7.34 SERIES 3 MEAN VELOCITY SCALED WITH SHEAR VELOCITY IN THE NEAR WALL REGION WITH Nu_y AS THE DIMENSIONLESS LENGTH 317
7.35 SERIES 4 MEAN VELOCITY SCALED WITH SHEAR VELOCITY IN THE NEAR WALL REGION WITH Nu_y AS THE DIMENSIONLESS LENGTH 318
7.36 SERIES 5 MEAN VELOCITY SCALED WITH SHEAR VELOCITY IN THE NEAR WALL REGION WITH Nu_y AS THE DIMENSIONLESS LENGTH 319
7.37 SERIES 6 MEAN VELOCITY SCALED WITH SHEAR VELOCITY IN THE NEAR WALL REGION WITH Nu_y AS THE DIMENSIONLESS LENGTH 320
7.38 SERIES 7 MEAN VELOCITY SCALED WITH SHEAR VELOCITY IN THE NEAR WALL REGION WITH Nu_y AS THE DIMENSIONLESS LENGTH 321
7.39 SERIES 3 MEAN VELOCITY SCALED WITH THE BUOYANCY SCALE IN THE NEAR WALL REGION WITH Nu_y AS THE DIMENSIONLESS LENGTH 322
7.40 SERIES 4 MEAN VELOCITY SCALED WITH THE BUOYANCY SCALE IN THE NEAR WALL REGION WITH Nu_y AS THE DIMENSIONLESS LENGTH 323
7.41 SERIES 5 MEAN VELOCITY SCALED WITH THE BUOYANCY SCALE IN THE NEAR WALL REGION WITH Nu_y AS THE DIMENSIONLESS LENGTH 324

7.42 SERIES 6 MEAN VELOCITY SCALED WITH THE BUOYANCY SCALE IN THE NEAR WALL REGION WITH Nu_y AS THE DIMENSIONLESS LENGTH 325
7.43 SERIES 7 MEAN VELOCITY SCALED WITH THE BUOYANCY SCALE IN THE NEAR WALL REGION WITH Nu_y AS THE DIMENSIONLESS LENGTH 326
7.44 SERIES 3 MEAN VELOCITY SCALED WITH THE THERMAL SCALE IN THE NEAR WALL REGION WITH Nu_y AS THE DIMENSIONLESS LENGTH 327
7.45 SERIES 4 MEAN VELOCITY SCALED WITH THE THERMAL SCALE IN THE NEAR WALL REGION WITH Nu_y AS THE DIMENSIONLESS LENGTH 328
7.46 SERIES 5 MEAN VELOCITY SCALED WITH THE THERMAL SCALE IN THE NEAR WALL REGION WITH Nu_y AS THE DIMENSIONLESS LENGTH 329
7.47 SERIES 6 MEAN VELOCITY SCALED WITH THE THERMAL SCALE IN THE NEAR WALL REGION WITH Nu_y AS THE DIMENSIONLESS LENGTH 330
7.48 SERIES 7 MEAN VELOCITY SCALED WITH THE THERMAL SCALE IN THE NEAR WALL REGION WITH Nu_y AS THE DIMENSIONLESS LENGTH 331
7.49 SERIES 3 MEAN VELOCITY SCALED FOR THE OUTER PART OF THE NEAR WALL REGION WITH Nu_y AS THE DIMENSIONLESS LENGTH 332
7.50 SERIES 4 MEAN VELOCITY SCALED FOR THE OUTER PART OF THE NEAR WALL REGION WITH Nu_y AS THE DIMENSIONLESS LENGTH 333
7.51 SERIES 3 MEAN VELOCITY SCALED WITH THE SHEAR VELOCITY AGAINST y SCALED WITH δ 334
7.52 SERIES 4 MEAN VELOCITY SCALED WITH THE SHEAR VELOCITY AGAINST y SCALED WITH δ 335
7.53 SERIES 6 MEAN VELOCITY SCALED WITH THR SHEAR VELOCITY AGAINST y SCALED WITH δ 336
7.54 SERIES 7 MEAN VELOCITY SCALED WITH THE SHEAR VELOCITY AGAINST y SCALED WITH δ 337
7.55 SERIES 3 MEAN VELOCITY SCALED WITH $[g\beta_T(T_w-T_\infty)\delta]^{1/2}$ AGAINST y SCALED WITH δ 338
7.56 SERIES 4 MEAN VELOCITY SCALED WITH $[g\beta_T(T_w-T_\infty)\delta]^{1/2}$ AGAINST y SCALED WITH δ 339

7.57 SERIES 6 MEAN VELOCITY SCALED WITH $[g\beta_T(T_w-T_\infty)\delta]^{1/2}$ AGAINST y SCALED WITH δ 340
7.58 SERIES 7 MEAN VELOCITY SCALED WITH $[g\beta_T(T_w-T_\infty)\delta]^{1/2}$ AGAINST y SCALED WITH δ 341
7.59 SERIES 3 MEAN VELOCITY SCALED WITH $[kg\beta_T(T_w-T_\infty)^2/\dot{Q}''_w]^{1/2}$ AGAINST y SCALED WITH δ 342
7.60 SERIES 4 MEAN VELOCITY SCALED WITH $[kg\beta_T(T_w-T_\infty)^2/\dot{Q}''_w]^{1/2}$ AGAINST y SCALED WITH δ 343
7.61 SERIES 6 MEAN VELOCITY SCALED WITH $[kg\beta_T(T_w-T_\infty)^2/\dot{Q}''_w]^{1/2}$ AGAINST y SCALED WITH δ 344
7.62 SERIES 7 MEAN VELOCITY SCALED WITH $[kg\beta_T(T_w-T_\infty)^2/\dot{Q}''_w]^{1/2}$ AGAINST y SCALED WITH δ 345
7.63 SERIES 3, 4 AND 6 MEAN VELOCITY SCALED WITH SHEAR VELOCITY IN THE NEAR WALL REGION WITH Nu_v AS THE DIMENSIONLESS LENGTH 346
7.64 SERIES 3, 4 AND 6 MEAN VELOCITY SCALED WITH THE SHEAR VELOCITY AGAINST y SCALED WITH δ 347
7.65 PROBABILITY DISTRIBUTION OF VELOCITY FOR SERIES 3 AT x/H = 0.229 348
7.66 PROBABILITY DISTRIBUTION OF VELOCITY FOR SERIES 3 AT x/H = 0.497 349
7.67 PROBABILITY DISTRIBUTION OF VELOCITY FOR SERIES 3 AT x/H = 0.497 350
7.68 MINIMUM, AVERAGE AND MAXIMUM VELOCITY PROFILES FOR SERIES 3 AT x/H = 0.497 351
7.69 SERIES 3 PROFILES OF $u'_{R.M.S.}/v'_{R.M.S.}$ 352
7.70 COMPARISION OF CALCULATED AND MEASURED MEAN LATERAL VELOCITY FOR SERIES 3 353
7.71 COMPARISON OF L.D.A. AND HOT-WIRE PROFILES AT MID-HEIGHT 354
7.72 MEAN VELOCITY PROFILES FOR SERIES 3 AT x/H = 0.949 FOR INCREASES OF CEILING TEMPERATURE OF 0, 0.95 AND 2.28K 355
7.73 $u'_{R.M.S.}$ PROFILES FOR SERIES 3 AT x/H = 0.949 FOR INCREASES OF CEILING TEMPERATURE OF 0, 0.95 AND 2.28K 356
7.74 PROFILES OF $\overline{u'T'}$ FOR SERIES 3 357
7.75 PROFILE OF $\overline{u'T'}$ CORRELATION COEFFICIENT FOR SERIES 3 AT x/H = 0.497 358
7.76 COMPARISON OF CALCULATED AND MEASURED VALUES OF $\overline{v'T'}$ FOR SERIES 3 359

7.77 PROFILES OF $\overline{u'v'}$ FOR SERIES 3 360
7.78 SAMPLE PROFILES OF $\overline{u'v'}$ CORRELATION COEFFICIENT FOR SERIES 3 361
7.79 SAMPLE PROFILES OF τ FOR SERIES 3 362
7.80 PROFILES OF P FOR SERIES 3 363
7.81 PROFILES OF G FOR SERIES 3 364
7.82 COMPARISON OF FULL PROFILES OF P AND G FOR SERIES 3 .. 365
7.83 COMPARISON OF NEAR WALL PROFILES OF P AND G FOR SERIES 3 366
7.84 PROGRAM RESULTS FROM TEST DATA WITH A SINGLE FREQUENCY COMPONENT OF 10Hz 367
7.85 SAMPLE VELOCITY TIME HISTORY FROM SERIES 4 AT x/H = 0.046 AND 3.20mm FROM THE HEATED WALL 368
7.86 SAMPLE VELOCITY TIME HISTORY FROM SERIES 4 AT x/H = 0.096 AND 3.11mm FROM THE HEATED WALL 369
7.87 SAMPLE VELOCITY TIME HISTORY FROM SERIES 4 AT x/H = 0.143 AND 3.07mm FROM THE HEATED WALL 370
7.88 SAMPLE VELOCITY TIME HISTORY FROM SERIES 4 AT x/H = 0.229 AND 2.94mm FROM THE HEATED WALL 371
7.89 SAMPLE VELOCITY TIME HISTORY FROM SERIES 3 AT x/H = 0.497 AND 6.63mm FROM THE HEATED WALL 372
7.90 SAMPLE VELOCITY TIME HISTORY FROM SERIES 5 AT x/H = 0.118 AND 3.59mm FROM THE HEATED WALL WITH THE TRACKER FREQUENCY RANGE SET TO 33-333kHz 373
7.91 SAMPLE VELOCITY TIME HISTORY FROM SERIES 5 AT x/H = 0.118 AND 3.59mm FROM THE HEATED WALL WITH THE TRACKER FREQUENCY RANGE SET TO 10-100Hz 374
7.92 VELOCITY P.S.D.'s FROM SERIES 3 AT x/H = 0.046, 0.096 AND 0.143, AND APPROXIMATELY 3.7mm FROM THE HEATED WALL 375
7.93 VELOCITY P.S.D.'s FROM SERIES 3 AT x/H = 0.046, 0.096 AND 0.143, AND APPROXIMATELY 7.7mm FROM THE HEATED WALL 376
7.94 VELOCITY P.S.D. FROM SERIES 3 AT x/H = 0.229 AND 3.95mm FROM THE HEATED WALL 377
7.95 VELOCITY P.S.D. FROM SERIES 4 AT x/H = 0.229 AND 3.96mm FROM THE HEATED WALL 378

7.96 VELOCITY P.S.D.'s FROM SERIES 3 AT x/H = 0.849, 0.898 AND 0.949, AND APPROXIMATELY 4.9mm FROM THE COOLED WALL 379
7.97 VELOCITY P.S.D.'s FROM SERIES 3 AT x/H = 0.849, 0.898 AND 0.949, AND APPROXIMATELY 7.9mm FROM THE COOLED WALL 380
7.98 VELOCITY P.S.D.'s FROM SERIES 3 AT x/H = 0.046, 0.096 AND 0.143, AND APPROXIMATELY 6.2mm FROM THE COOLED WALL 381
7.99 VELOCITY P.S.D.'s FROM SERIES 3 AT x/H = 0.046, 0.096 AND 0.143, AND APPROXIMATELY 11.7mm FROM THE COOLED WALL 382
7.100 VELOCITY P.S.D.'s FROM SERIES 3 AT x/H = 0.849, 0.898 AND 0.949, AND THE CAVITY VERTICAL CENTRE-LINE 383
7.101 VELOCITY P.S.D.'s FROM SERIES 3 AT x/H = 0.849, 0.898 AND 0.949, AND APPROXIMATELY 8.8mm FROM THE HEATED WALL 384
7.102 VELOCITY P.S.D.'s FROM SERIES 3 AT x/H = 0.849, 0.898 AND 0.949, AND APPROXIMATELY 16.4mm FROM THE HEATED WALL 385
7.103 VELOCITY P.S.D. FROM SERIES 3 AT x/H = 0.497 AND 2.61mm FROM THE HEATED WALL 386
7.104 VELOCITY P.S.D. FROM SERIES 3 AT x/H = 0.497 AND 6.63mm FROM THE HEATED WALL 387
7.105 VELOCITY BUOYANCY SUB-RANGE INDEX AGAINST dT/dx, R_G AND R_F 388
7.106 VELOCITY INERTIAL SUB-RANGE INDEX AGAINST dT/dx, R_G AND R_F 389
7.107 VELOCITY DISSIPATION SUB-RANGE INDEX AGAINST dT/dx, R_G AND R_F 390
7.108 TEMPERATURE P.S.D's FROM SERIES 3 AT x/H = 0.096 AND 4.24mm AND 8.24mm FROM THE HEATED WALL 391
7.109 TEMPERATURE P.S.D's FROM SERIES 3 AT x/H = 0.143 AND 3.99mm AND 8.03mm FROM THE HEATED WALL 392
7.110 TEMPERATURE P.S.D's FROM SERIES 4 AT x/H = 0.229 AND 4.26mm AND 8.26mm FROM THE HEATED WALL 393
7.111 TEMPERATURE P.S.D's FROM SERIES 4 AT x/H = 0.096 AND 4.02mm, 8.02mm AND 60mm FROM THE HEATED WALL 394

7.112 TEMPERATURE P.S.D's FROM SERIES 3 AT x/H = 0.497 AND 4.16mm AND 8.15mm FROM THE HEATED WALL 395
7.113 TEMPERATURE P.S.D.'s FROM SERIES 3 AT x/H = 0.849, 0.898 AND 0.949, AND APPROXIMATELY 3.5mm FROM THE HEATED WALL 396
7.114 TEMPERATURE P.S.D.'s FROM SERIES 3 AT x/H = 0.849, 0.898 AND 0.949, AND APPROXIMATELY 3.4mm FROM THE HEATED WALL 397
7.115 TEMPERATURE BUOYANCY SUB-RANGE INDEX AGAINST dT/dx, R_G AND R_F 398
7.116 TEMPERATURE INERTIAL SUB-RANGE INDEX AGAINST dT/dx, R_G AND R_F 399
7.117 TEMPERATURE THIRD SUB-RANGE INDEX AGAINST dT/dx, R_G AND R_F 400
7.118 TEMPERATURE DISSIPATION SUB-RANGE INDEX AGAINST dT/dx, R_G AND R_F 401

LIST OF TABLES

CHAPTER 3 - APPARATUS

3.1 COOLED WALL CHANNEL AND THERMOCOUPLE HEIGHTS FOR ORIGINAL 3.0m HIGH Q.M.C. CAVITY 131

3.2 COOLED WALL THERMOCOUPLE POSITIONS RELATIVE TO FALSE FLOOR FOR Q.M.C. CAVITY HEIGHTS OF 2.5 AND 2.0m 131

3.3 HEATER DATA FOR Q.M.C. CAVITY HEIGHTS OF 2.5 AND 2.0m 132

3.4 HEATED WALL THERMOCOUPLE POSITIONS RELATIVE TO FALSE FLOOR FOR Q.M.C. CAVITY HEIGHTS OF 2.5 AND 2.0m 133

CHAPTER 4 - EXPERIMENTAL PROCEDURE

4.1 NOMINAL POSITIONS FOR DATA COLLECTION - Q.M.C. CAVITY 154

CHAPTER 6 - UNCERTAINTY ESTIMATIONS

6.1 VARIATION OF MEAN VELOCITY AND R.M.S. OF VELOCITY FLUCTUATIONS WITH TIME 191

6.2 REPEATABILITY OF MEAN VELOCITY AND R.M.S. OF VELOCITY FLUCTUATIONS FOR THE Q.M.C. CAVITY 191

6.3 VARIATION OF MEAN TEMPERATURE AND R.M.S. OF TEMPERATURE FLUCTUATIONS WITH TIME 192

6.4 REPEATABILITY OF MEAN TEMPERATURE AND R.M.S. OF TEMPERATURE FLUCTUATIONS 192

6.5 VARIATION OF VELOCITY CORRECTION WITH UPSTREAM DISTANCE, x, FOR LAMINAR FLOW 193

6.6 EXPERIMENTALLY DETERMINED EFFECT OF THERMOCOUPLE JUNCTION ON VELOCITY 193

6.7 VELOCITY MEASUREMENTS WITH AND WITHOUT A THERMOCOUPLE IN BOTH WALL BOUNDARY LAYERS 194

6.8 RE-SAMPLING OF Q.M.C. DATA AT 3.125Hz AND 6.25Hz 194

6.9 REPEATABILITY OF MEAN VELOCITY AND R.M.S. OF VELOCITY FLUCTUATIONS FOR THE POITIERS CAVITY 195

CHAPTER 7 - RESULTS AND DISCUSSIONS

7.1 HEAT TRANSFER COEFFICIENTS FOR SERIES 1 AND 2 402

7.2 HEAT TRANSFER COEFFICIENTS FOR SERIES 3 AND 4 402
7.3 HEAT TRANSFER COEFFICIENTS FOR SERIES 5 403
7.4 HEAT TRANSFER COEFFICIENTS FOR SERIES 6 AND 7 403
7.5 LOCAL VALUES OF Nu_x, Gr_x AND Ra_x FROM SERIES 2 404
7.6 LOCAL VALUES OF Nu_x, Gr_x AND Ra_x FROM SERIES 3 404
7.7 LOCAL VALUES OF Nu_x, Gr_x AND Ra_x FROM SERIES 4 405
7.8 LOCAL VALUES OF Nu_x, Gr_x AND Ra_x FROM SERIES 5 405
7.9 LOCAL VALUES OF Nu_x, Gr_x AND Ra_x FROM SERIES 6 406
7.10 LOCAL VALUES OF Nu_x, Gr_x AND Ra_x FROM SERIES 7 406
7.11 OVERALL HEAT TRANSFER SERIES 1-7 407
7.12 EXAMPLES OF THE AGREEMENT BETWEEN PREDICTED AND EXPERIMENTAL VELOCITIES 408
7.13 WALL SHEAR STRESS DATA FOR SERIES 3 408
7.14 WALL SHEAR STRESS DATA FOR SERIES 4 409
7.15 WALL SHEAR STRESS DATA FOR SERIES 5 409
7.16 WALL SHEAR STRESS DATA FOR SERIES 6 410
7.17 WALL SHEAR STRESS DATA FOR SERIES 7 410
7.18 GROUPS FOR PROBABILITY DISTRIBUTION OF VELOCITY 411
7.19 MASS FLOW FOR SERIES 1 412
7.20 MASS FLOW FOR SERIES 3 412
7.21 MASS FLOW FOR SERIES 4 413
7.22 MEASURED v FOR SERIES 7, x/H = 0.50 413
7.23 MEASURED v FOR SERIES 7, x/H = 0.65 414
7.24 MEASURED v FOR SERIES 7, x/H = 0.80 414
7.25 THE TURBULENCE QUANTITY $\overline{u'T'}$ AND G, THE PRODUCTION OF TURBULENCE KINETIC ENERGY BY BUOYANCY FOR x/H = 0.046 415
7.26 THE TURBULENCE QUANTITY $\overline{u'T'}$ AND G, THE PRODUCTION OF TURBULENCE KINETIC ENERGY BY BUOYANCY FOR x/H = 0.096 416
7.27 THE TURBULENCE QUANTITY $\overline{u'T'}$ AND G, THE PRODUCTION OF TURBULENCE KINETIC ENERGY BY BUOYANCY FOR x/H = 0.143 417
7.28 THE TURBULENCE QUANTITY $\overline{u'T'}$ AND G, THE PRODUCTION OF TURBULENCE KINETIC ENERGY BY BUOYANCY FOR x/H = 0.229 418
7.29 THE TURBULENCE QUANTITY $\overline{u'T'}$ AND G, THE PRODUCTION OF TURBULENCE KINETIC ENERGY BY BUOYANCY FOR x/H = 0.360 419
7.30 THE TURBULENCE QUANTITY $\overline{u'T'}$ AND G, THE PRODUCTION OF TURBULENCE KINETIC ENERGY BY BUOYANCY FOR x/H = 0.497 420
7.31 THE TURBULENCE QUANTITY $\overline{u'T'}$ AND G, THE PRODUCTION OF TURBULENCE KINETIC ENERGY BY BUOYANCY FOR x/H = 0.630 421

7.32 THE TURBULENCE QUANTITY $\overline{u'T'}$ AND G, THE PRODUCTION OF TURBULENCE KINETIC ENERGY BY BUOYANCY FOR x/H = 0.765 422
7.33 THE TURBULENCE QUANTITY $\overline{u'T'}$ AND G, THE PRODUCTION OF TURBULENCE KINETIC ENERGY BY BUOYANCY FOR x/H = 0.849 423
7.34 THE TURBULENCE QUANTITY $\overline{u'T'}$ AND G, THE PRODUCTION OF TURBULENCE KINETIC ENERGY BY BUOYANCY FOR x/H = 0.898 424
7.35 THE TURBULENCE QUANTITY $\overline{u'T'}$ AND G, THE PRODUCTION OF TURBULENCE KINETIC ENERGY BY BUOYANCY FOR x/H = 0.949 425
7.36 THE TURBULENCE QUANTITY $\overline{v'T'}$ FOR x/H = 0.046 426
7.37 THE TURBULENCE QUANTITY $\overline{v'T'}$ FOR x/H = 0.096 427
7.38 THE TURBULENCE QUANTITY $\overline{v'T'}$ FOR x/H = 0.143 428
7.39 THE TURBULENCE QUANTITY $\overline{v'T'}$ FOR x/H = 0.229 429
7.40 THE TURBULENCE QUANTITY $\overline{v'T'}$ FOR x/H = 0.360 430
7.41 THE TURBULENCE QUANTITY $\overline{v'T'}$ FOR x/H = 0.497 431
7.42 THE TURBULENCE QUANTITY $\overline{v'T'}$ FOR x/H = 0.630 432
7.43 THE TURBULENCE QUANTITY $\overline{v'T'}$ FOR x/H = 0.765 433
7.44 THE TURBULENCE QUANTITY $\overline{v'T'}$ FOR x/H = 0.849 434
7.45 THE TURBULENCE QUANTITY $\overline{v'T'}$ FOR x/H = 0.898 435
7.46 THE TURBULENCE QUANTITY $\overline{v'T'}$ FOR x/H = 0.949 436
7.47 THE TURBULENCE QUANTITY $\overline{u'v'}$ FOR x/H = 0.046 437
7.48 THE TURBULENCE QUANTITY $\overline{u'v'}$ FOR x/H = 0.096 438
7.49 THE TURBULENCE QUANTITY $\overline{u'v'}$ FOR x/H = 0.143 439
7.50 THE TURBULENCE QUANTITY $\overline{u'v'}$ FOR x/H = 0.229 440
7.51 THE TURBULENCE QUANTITY $\overline{u'v'}$ FOR x/H = 0.360 441
7.52 THE TURBULENCE QUANTITY $\overline{u'v'}$ FOR x/H = 0.497 442
7.53 THE TURBULENCE QUANTITY $\overline{u'v'}$ FOR x/H = 0.630 443
7.54 THE TURBULENCE QUANTITY $\overline{u'v'}$ FOR x/H = 0.765 444
7.55 THE TURBULENCE QUANTITY $\overline{u'v'}$ FOR x/H = 0.849 445
7.56 THE TURBULENCE QUANTITY $\overline{u'v'}$ FOR x/H = 0.898 446
7.57 THE TURBULENCE QUANTITY $\overline{u'v'}$ FOR x/H = 0.949 447
7.58 VALUES OF $\overline{u'v'}$ AT THE CAVITY CENTRE LINE CALCULATED FROM EXPERIMENTAL DATA USING THE TURBULENCE ENERGY EQUATION 448
7.59 VALUES OF $\overline{u'v'}$ AT THE CAVITY CENTRE LINE CALCULATED FROM EXPERIMENTAL DATA USING THE CORRELATION COEFFICIENT 448
7.60 EFFECT OF CORRECTION TO CENTRE-LINE TEMPERATURE ON VALUES OF THE TURBULENCE QUANTITY $\overline{u'v'}$ 449
7.61 EXPERIMENTAL AND CORRECTED CENTRE-LINE TEMPERATURES .. 450

7.62 FLOW REVERSALS AND TEMPERATURE INVERSION 450
7.63 DENSITY, REYNOLDS STRESS $\rho\overline{u'v'}$, TOTAL SHEAR STRESS, PRODUCTION OF TURBULENCE KINETIC ENERGY BY SHEAR AND MEAN LATERAL VELOCITY, v, FOR x/H = 0.046 451
7.64 DENSITY, REYNOLDS STRESS $\rho\overline{u'v'}$, TOTAL SHEAR STRESS, PRODUCTION OF TURBULENCE KINETIC ENERGY BY SHEAR AND MEAN LATERAL VELOCITY, v, FOR x/H = 0.096 452
7.65 DENSITY, REYNOLDS STRESS $\rho\overline{u'v'}$, TOTAL SHEAR STRESS, PRODUCTION OF TURBULENCE KINETIC ENERGY BY SHEAR AND MEAN LATERAL VELOCITY, v, FOR x/H = 0.143 453
7.66 DENSITY, REYNOLDS STRESS $\rho\overline{u'v'}$, TOTAL SHEAR STRESS, PRODUCTION OF TURBULENCE KINETIC ENERGY BY SHEAR AND MEAN LATERAL VELOCITY, v, FOR x/H = 0.229 454
7.67 DENSITY, REYNOLDS STRESS $\rho\overline{u'v'}$, TOTAL SHEAR STRESS, PRODUCTION OF TURBULENCE KINETIC ENERGY BY SHEAR AND MEAN LATERAL VELOCITY, v, FOR x/H = 0.360 455
7.68 DENSITY, REYNOLDS STRESS $\rho\overline{u'v'}$, TOTAL SHEAR STRESS, PRODUCTION OF TURBULENCE KINETIC ENERGY BY SHEAR AND MEAN LATERAL VELOCITY, v, FOR x/H = 0.497 456
7.69 DENSITY, REYNOLDS STRESS $\rho\overline{u'v'}$, TOTAL SHEAR STRESS, PRODUCTION OF TURBULENCE KINETIC ENERGY BY SHEAR AND MEAN LATERAL VELOCITY, v, FOR x/H = 0.630 457
7.70 DENSITY, REYNOLDS STRESS $\rho\overline{u'v'}$, TOTAL SHEAR STRESS, PRODUCTION OF TURBULENCE KINETIC ENERGY BY SHEAR AND MEAN LATERAL VELOCITY, v, FOR x/H = 0.765 458
7.71 DENSITY, REYNOLDS STRESS $\rho\overline{u'v'}$, TOTAL SHEAR STRESS, PRODUCTION OF TURBULENCE KINETIC ENERGY BY SHEAR AND MEAN LATERAL VELOCITY, v, FOR x/H = 0.849 459
7.72 DENSITY, REYNOLDS STRESS $\rho\overline{u'v'}$, TOTAL SHEAR STRESS, PRODUCTION OF TURBULENCE KINETIC ENERGY BY SHEAR AND MEAN LATERAL VELOCITY, v, FOR x/H = 0.898 460
7.73 DENSITY, REYNOLDS STRESS $\rho\overline{u'v'}$, TOTAL SHEAR STRESS, PRODUCTION OF TURBULENCE KINETIC ENERGY BY SHEAR AND MEAN LATERAL VELOCITY, v, FOR x/H = 0.949 461

LIST OF PLATES

CHAPTER 3 - APPARATUS

3.1 Q.M.C. CAVITY SIDE WALL WITH OPTICAL ACCESS 134

3.2 THE POITIERS CAVITY - HEATED WALL VIEW 135

3.3 THE POITIERS CAVITY - COOLED WALL VIEW 136

LIST OF SYMBOLS

A	Counter D/A gain setting
B	Cavity breadth
B	Characteristic non-dimensional frequency quoted in equation (2.2) $\beta Gr_{x*}^{1/3}$ (for air B = 0.35, for water B = 0.25)
C	Defined in equation (2.1) $(g\beta_T/k)^{0.5}/2\pi$
Cp	Specific heat capacity at constant pressure
f	Frequency (cycles per second)
f_D	Doppler frequency
f_s	Frequency shift
g	Specific gravitational force 9.81m/s^2
G	Production of turbulence kinetic energy by buoyancy $-g\overline{u'\rho'}$
Gr	Grashof number
Gr_H	Global Grashof number based on H $g\beta_T(T_H-T_C)H^3/(\mu/\rho)^2$
Gr_L	Global Grashof number based on L $g\beta_T(T_H-T_C)L^3/(\mu/\rho)^2$
Gr_x	Local Grashof number based on x $g\beta_T(T_H-T_C)x^3/(\mu/\rho)^2$
Gr_{xQ}	Local Grashof number based on x for a constant heat flux plate $g\beta_T Q''_\omega x^4/k(\mu/\rho)^2$
Gr_{x*}	Modified Grashof number $4(Gr_x/4)^{1/4}$
Gr_{xQ*}	Modified Grashof number for constant heat flux plate $5(Gr_{xQ}/5)^{1/5}$
$G_x(f)$	Raw estimate of power spectral density at frequency f
h	Heat transfer coefficient
h	Time between samples
H	Cavity height
H/L	Aspect ratio
j	$-1^{0.5}$
k	Turbulence kinetic energy $(\overline{u'u'} + \overline{v'v'} + \overline{w'w'})/2$
k	Thermal conductivity
k	Counter variable
L	Cavity width
$\dot{m}$	Mass flow rate
$\dot{m}'$	Mass flow rate per length
n	Wavenumber $2\pi f/u$
n	Counter variable
N	Total number of samples
Nu	Nusselt number
Nu_H	Global Nusselt number based on H $\dot{Q}''_\omega H/[k(T_H-T_C)]$

Nu_L	Global Nusselt number based on L $\dot{Q}''_\omega L/[k(T_H-T_C)]$
Nu_x	Local Nusselt number based on x $\dot{Q}''_\omega x/[k(T_\omega-T_\infty)]$
Nu_y	Local Nusselt number based on y $\dot{Q}''_\omega y/[k(T_\omega-T_\infty)]$
P	Pressure
P	Production of turbulence kinetic energy by shear $-\rho\overline{u'v'}du/dy$
Pr	Prandtl number $(\mu/\rho)/\alpha$ or $\mu Cp/k$
$\dot{Q}'$	Heat transfer rate per length
$\dot{Q}''$	Heat transfer rate per area
Ra	Rayleigh number GrPr
Ra_H	Global Rayleigh number based on H Gr_HPr
Ra_L	Global Rayleigh number based on L Gr_LPr
Ra_x	Local Rayleigh number based on x Gr_xPr
R_F	Flux Richardson number $\overline{u'T'}g\beta_T/[\overline{u'v'}dv/dx]$
R_G	Gradient Richardson number $[g\beta_T dT/dx]/[dv/dx]^2$
S	Non-dimensional temperature gradient $dT/dx[H/(T_\omega-T_\infty)]$ or $dT/dx[H/(T_H-T_C)]$
T	Local mean temperature
T	Sample time
T'	Local fluctuating component of temperature
u	Mean velocity in x direction
u'	Fluctuating component of velocity in x direction
u_1	Velocity scale defined by Bayley [32]
$\overline{u'v'}$	Two component correlation
$\overline{u'T'}$	Two component correlation
$\overline{u'\rho'}$	Two component correlation
u_{MAX}	Maximum profile velocity or peak velocity
u_1	Characteristic velocity defined by Bayley [36]
u_τ	Shear velocity $(\tau_\omega/\rho_\omega)^{0.5}$
V	Voltage
v	Mean velocity in y direction
v'	Fluctuating component of velocity in y direction
$\overline{v'T'}$	Two component correlation
w	Mean velocity in z direction
w'	Fluctuating component of velocity in z direction
x	Vertical co-ordinate
x(f,T)	Defined in equation (7.41)
x(t)	Time history value at time t
X_k	X(f,T)/h
y	Horizontal co-ordinate (associated with cavity width)

y^+	Non-dimensional distance $yu_\tau/(\mu/\rho)$
z	Horizontal co-ordinate (associated with cavity breadth)

GREEK SYMBOLS

α	Thermal diffusivity $k/\rho Cp$
β	Non-dimensional frequency determined from equation (2.2)
β_T	Coefficient of thermal expansion
γ	Non-dimensional temperature gradient $dT/dx[L/(T_H-T_C)]$
γ_1	Non-dimensional temperature gradient at which stability mode changes
δ	Boundary layer thickness
δ	Measure of boundary layer thickness in equation (2.32)
δT	Change of temperature
Δ	Increment
ΔT	Temperature difference
Δu	Velocity difference
ϵ	Rate of dissipation of turbulence kinetic energy
θ	Non-dimensional temperature $(T-T_C)/(T_H-T_C)$ or $(T-T_\infty)/(T_W-T_\infty)$
θ	Angle between laser beams
λ	Wavelength
μ	Coefficient of viscosity
π	Pi 3.142
ρ	Mean density
ρ'	Local fluctuating component of density
τ	Shear stress

SUBSCRIPTS

C	Conditions at the cooled wall
CL	Conditions at the vertical cavity centre-line
COR	Correction to be applied to relevant quantity
D	Negative x direction
E	Experimental value
H	Conditions at the heated wall
MIN	Conditions at the position of maximum horizontal temperature inversion
P	Predicted value
R	Conditions at a reference temperature
R.M.S.	Root mean square of relevant quantity
REF	Conditions at a reference temperature

U	Positive x direction
W	Conditions at the wall
∞	Environmental conditions away from the wall (considered to be those of the environment for the case of a vertical flat plate and those at the vertical centre-line in a cavity)

CHAPTER 1 - INTRODUCTION

1.1 INITIATION OF THE PRESENT STUDY

Natural convection in rectangular cavities arises in a number of heat transfer scenarios which are of importance to Engineers. Examples include: nuclear reactor cooling systems; insulation systems, such as double glazing and cavity walls; the heating and ventilation in buildings, including the spread of fire; the growth of crystals, particularly in the cooling of castings; and solar heat collectors.

A very important practical scenario involves the use of molten sodium, to transfer heat by turbulent natural convection, within various geometrically shaped cavities which form part of the proposed designs for the cooling system of the Commercial Demonstration Fast Reactor (C.D.F.R.).

To design such a cooling system sucessfully it is necessary to be able to predict the heat transfer, and flow characteristics, of the sodium within the cavities.

As it is both difficult and very expensive to undertake experimental studies using sodium, a programme of data collection using fluids of different Prandtl numbers was initiated by the National Nuclear Corporation (N.N.C.) who are responsible for the design of the C.D.F.R. The data collected by this programme will serve as a check against the computer codes which have been, and are being, developed.

The numerical solution of turbulent natural convection flow within cavities is complex and one faces two tasks. Firstly the qualitative understanding of a given fluid's motion (what are the flow patterns, general features, structures and mechanisms?) and secondly the quantitative prediction of a given fluid's motion, and the turbulent transport quantities, by reliable computer codes (what are the suitable mathematical models, the permissible approximations and the empirical input?).

In the development of a full three-dimensional computer code it was decided, by N.N.C., that initial efforts would be put into the development of two-dimensional codes. Once these had been verified by experimental data progress could then be made to three-dimensional codes. Indeeed, this is the approach which has been taken by most researchers.

The Department of Mechanical Engineering at Queen Mary College was commissioned to carry out extensive measurements of: the velocity and temperature fields; the turbulence quantities; and the local heat transfer, within a large air cavity across which there existed a temperature difference which was large enough to induce a mainly turbulent natural

convection flow. The flow was to be two-dimensional and all closing boundaries were to be adiabatic. During the study the cavity Rayleigh number and the aspect ratio were to be varied to examine their effects on the flow.

There is a need for all the quantities, described in the previous paragraph, to be predicted accurately in any given scenario.

The temperature field is required in order that the heat transfer across the cavity can be determined. In addition, when one considers the effect of cyclic, temperature induced, stresses on the cavity structure, the prediction of the root mean square (R.M.S.) of temperature fluctuations, near the closing boundaries, becomes important.

The mean velocity must be predicted correctly so that one may have confidence in the temperature predictions, as temperature and velocity are linked by the equations of conservation of mass, momentum and energy.

The turbulence quantities are important in that they are required to establish the empirical constants for the computer codes.

All of the quantities are very important when one considers the large range of fluids (whose Prandtl number varies typically from 0.005-1000) that the computer codes must deal with.

1.2 THE CAVITY CONFIGURATION

There are many possible cavity configurations. The most notable variables are: the thermal boundary conditions on the active and closing boundaries (the active boundaries may be isothermal or subjected to a constant heat flux, and the closing boundaries may be adiabatic or subject to a condition such as a linear temperature gradient); the aspect ratio (in respect of it being less than or greater than one); the angle of tilt; the position of the heated and cooled boundaries; the geometry of the cavity; and the surface roughness of the boundaries. Therefore it is necessary to define the exact configuration which has been studied.

The configuration studied was that of a rectangular cavity with a vertical isothermal heated wall and an opposing isothermal cooled wall. The four remaining boundaries which closed the cavity were nominally adiabatic, but in practice allowed heat transfer. The cavity aspect ratio of height to width was varied between 4 and 10, and all boundaries were plane so that there was no artificial enhancement of heat transfer. A basic sketch of the cavity configuration, and co-ordinate system, is shown in Figure 1.1.

The flow within the cavity is of great importance and has been categorized in terms of flow regimes. These flow regimes are known as

conduction, asymptotic, laminar boundary layer, transitional boundary layer and turbulent boundary layer. The cavity was designed to operate primarily with the latter two flow regimes present.

In practice, the basic configuration described here does not occur very frequently (indeed there are no instances of a rectangular cavity in the design proposals of the C.D.F.R.) but in order to develop and verify the computer codes, for any fluid or cavity geometry, one must first successfully predict data for a basic configuration such as the one studied.

The configuration is basic in that the cavity is rectangular, the flow is nominally two-dimensional and the boundary condition on the closing boundaries is nominally one of zero temperature gradient in the perpendicular direction.

1.3 THE DEFINITION AND EQUATIONS OF NATURAL CONVECTION

A free convective flow is one that is driven by body forces so that the momentum equation is coupled to either the energy or diffusion equation. (In the present study one is concerned with a flow driven by temperature differences, therefore it is the momentum and energy equations which are coupled).

Natural convection is a sub-division of free convection where the body force is that due to gravity.

For two-dimensional flow there are initially four equations of interest. These are the equations representing the conservation of mass, momentum (in the vertical and horizontal directions) and energy.

The full equations describing variable properties are too complicated for most needs and so use is made of the Boussinesq approximation. This approximation considers all properties to be constant (i.e. evaluated at a reference temperature) except for density when it contributes to a buoyancy force. The resulting equations are:

$$\frac{du}{dx} + \frac{dv}{dy} = 0 \qquad (1.1)$$

Equation (1.1) represents the conservation of mass.

$$u\frac{du}{dx} + v\frac{du}{dy} = \frac{-1}{\rho_R}\frac{dP}{dx} + \frac{d}{dx}\left[-\overline{u'u'} + \frac{(\mu_R)du}{(\rho_R)dx}\right] - \frac{g(\rho - \rho_\infty)}{\rho_R}$$
$$+ \frac{d}{dy}\left[-\overline{u'v'} + \frac{(\mu_R)du}{(\rho_R)dy}\right] \qquad (1.2)$$

Equation (1.2) represents the conservation of momentum in the vertical direction. The pressure, P, is the absolute pressure minus the hydrostatic

pressure, and the subscript ∞ indicates conditions at the cavity centre-line.

$$u\frac{dv}{dx} + v\frac{dv}{dy} = \frac{-1}{\rho_R}\frac{dP}{dy} + \frac{d}{dx}\left[-\overline{u'v'} + \frac{(\mu_R)dv}{(\rho_R)dx}\right]$$
$$+ \frac{d}{dy}\left[-\overline{v'v'} + \frac{(\mu_R)dv}{(\rho_R)dy}\right] \qquad (1.3)$$

Equation (1.3) represents the conservation of momentum in the horizontal direction. The pressure, P, is the absolute pressure minus the hydrostatic pressure.

$$u\frac{dT}{dx} + v\frac{dT}{dy} = \frac{d}{dx}\left[-\overline{u'T'} + \alpha_R\frac{dT}{dx}\right] + \frac{d}{dy}\left[-\overline{v'T'} + \alpha_R\frac{dT}{dy}\right] \qquad (1.4)$$

Equation (1.4) represents the conservation of energy.

Equations (1.1) to (1.4) are for cavity flow, the equivalent flat plate flow equations utilise the absolute pressure in equations (1.2) and (1.3) and the subscript ∞ indicates environmental conditions.

All properties with the subscript R are evaluated at an appropriate reference temperature.

The present author's choice for the representation of the buoyancy term (the alternative being $g\beta_T\Delta T$) will become clear when the calculation of wall shear stresses is explained in Chapter 7.

For the boundary layer on each wall of a cavity, equations (1.2)-(1.4) can be further reduced when the boundary layer approximations are applied. The resulting equations are given below.

$$u\frac{du}{dx} + v\frac{du}{dy} = \frac{d}{dy}\left[-\overline{u'v'} + \frac{(\mu_R)du}{(\rho_R)dy}\right] - \frac{g(\rho - \rho_\infty)}{\rho_R} \qquad (1.5)$$

$$u\frac{dT}{dx} + v\frac{dT}{dy} = \frac{d}{dy}\left[-\overline{v'T'} + \alpha_R\frac{dT}{dy}\right] \qquad (1.6)$$

The co-ordinate system, used in equations (1.1)-(1.6), is defined in Figure 1.2, which also shows a typical velocity and temperature profile.

1.4 PREVIOUS WORK

Early work on cavity problems only considered the overall heat transfer and considerable effort was given to provide experimental correlations on the basis of a power law relating the relevant non-dimensional groups. This work covered all types of flow regime, from conduction through to turbulent boundary layer, and was sadly lacking in proper co-ordination.

Work then progressed to computer simulation of the laminar boundary layer regime, with only a small amount of associated experimental work.

The main thrust of recent work has been in the field of computer code development, although only a few attempts have been made at predicting the turbulent boundary layer regime.

Most recently a few papers have been available which have presented experimentally measured mean temperature and velocity fields in turbulent cavity flow, but no data on two-component turbulence quantities have been published.

Although a few researchers had presented experimental mean velocity profiles in the past, the most recent measurements are notable because they were made using laser Doppler anemometry (L.D.A.).

L.D.A. has many advantages over the possible alternatives (such as hot-wire anemometry) and has lead to reduced uncertainties in the data.

The present study has utilised L.D.A. which is an improvement on hot-wire anemometry, used by a previous researcher on the same cavity, most notably in being able to measure velocities below 0.1m/s, including negative velocities.

Among the standard list of comments which are made about L.D.A. is that it does not disrupt the flow. This is clearly a plus in it's favour.

Obviously, if one were to use hot-wire anemometry in cavity flow, then it would be necessary to calibrate the hot-wire for many temperatures within any range of practical interest. With L.D.A. all one requires is one initial, relatively fast, calibration of the signal processing system before work can begin.

In assessing data from cavities one cannot forget the parallel classical problem of natural convection from a vertical plane surface. Research for this problem has been proceeding for a longer time than that for cavities.

A number of theoretical studies of cavity heat transfer have assumed that a cavity can be considered to be the equivalent of two vertical plates in a stratified environment. A comparison of the results for the heated and cooled walls and similar plate scenarios is useful. However, data for a vertical plate in a stratified environment (the cores of the cavities studied here were startified) are extremely limited and use has to be made of data from vertical plates in isothermal environments.

Because it is simpler, the plate problem has received more attention in the derivation of an analytical description than the cavity. It is,

therefore, a natural first step to apply the scaling parameters for velocity, length and temperature (so far derived) to the data from cavities.

1.5 THE PRESENT STUDY

Data has been collected from two air cavities, one at Queen Mary College (Q.M.C.) and one at L'Ecole Nationale Superieure de Mecanique et d'Aerotechnique (E.N.S.M.A.) Poitiers, France. The major differences between the two cavities was the level of insulation provided on their four closing boundaries, and their aspect ratios.

A systematic study was carried out where the temperature difference across the cavity, the cavity height and cavity width were all varied.

The Q.M.C. cavity allowed the height to be varied whilst the width was kept constant. The variation of width was achieved with the Poitiers cavity.

Both cavities allowed the variation of temperature difference.

Seven surveys were carried out, using two heights (2.5m and 2.0m) two widths (0.5m and 0.2m) and three temperature differences (32K, 46K and 61K).

The temperature fields were surveyed using 25μm chromel-alumel thermocouples, and the velocity fields with laser Doppler anemometers.

The same type of thermocouples had been used successfully by previous researchers at Q.M.C. and so there was no need to choose an alternative temperature measuring technique.

A different signal processor was used in each of the laser Doppler anemometry systems, namely a tracker at Q.M.C., and a counter at Poitiers.

The Poitiers counter was configured to yield a near continuous output similar to that of a tracker.

Both systems utilised frequency shift to allow the measurement of negative velocities.

The Q.M.C. data were digitised and stored on magnetic tape for subsequent analysis. This allowed the calculation of power spectral densities in order to obtain a better understanding of the flow.

Data from two of the Q.M.C. surveys have been kept which will allow the calculation of additional turbulence quantities in the future.

Unfortunately, the Poitiers data could not be stored and consisted only of the mean quantity and R.M.S. of the fluctuating components.

Many of the quantities presented in this thesis are the first of their kind to be published. This, together with the practical and commercial use to which they will be put, justifies the research undertaken.

FIGURE 1.1

CAVITY CONFIGURATION AND CO-ORDINATE SYSTEM

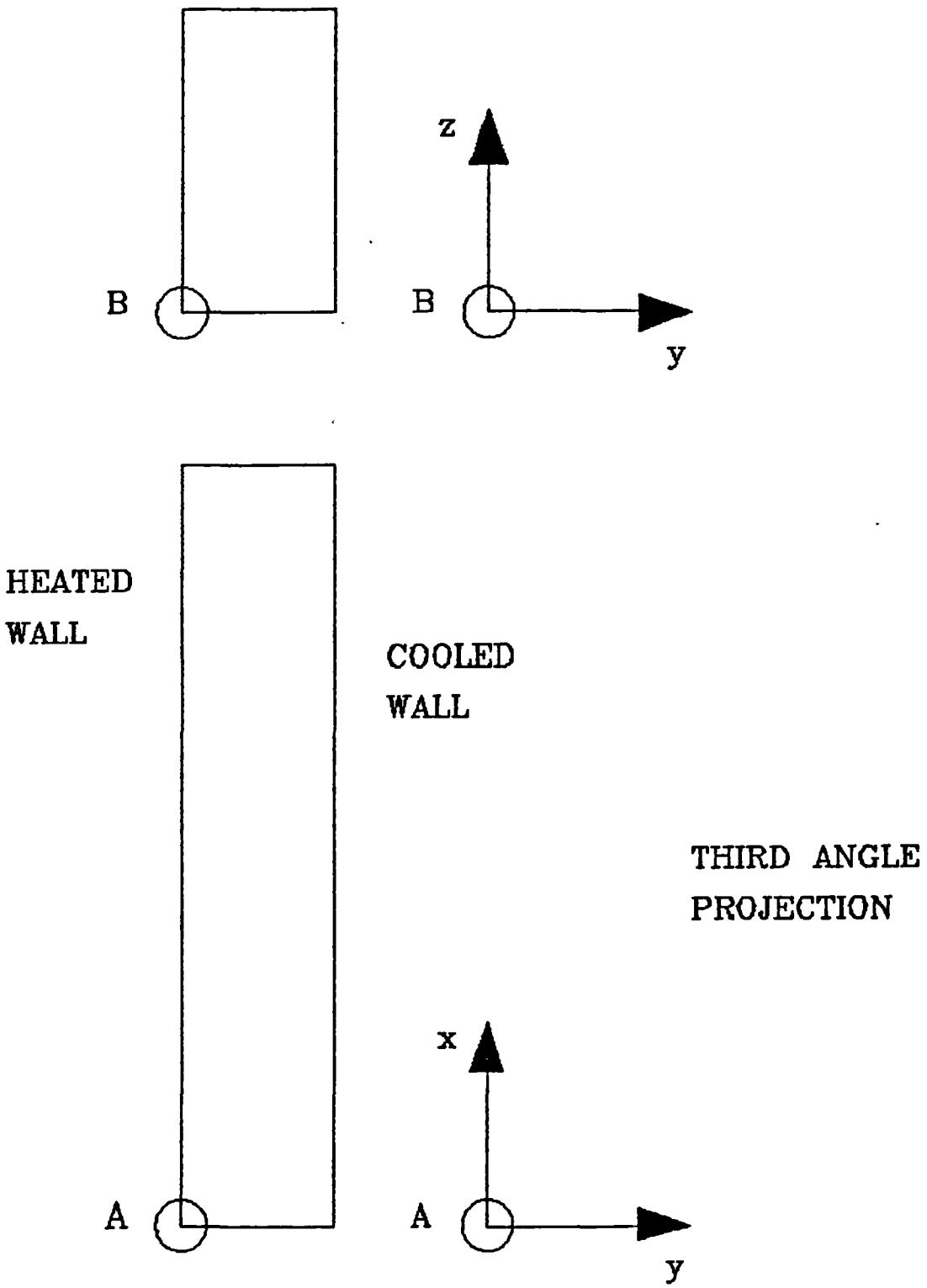

FIGURE 1.2

CO-ORDINATE DEFINITION PLUS VELOCITY AND TEMPERATURE PROFILES FOR NATURAL CONVECTION OF AIR ALONG A VERTICAL WALL

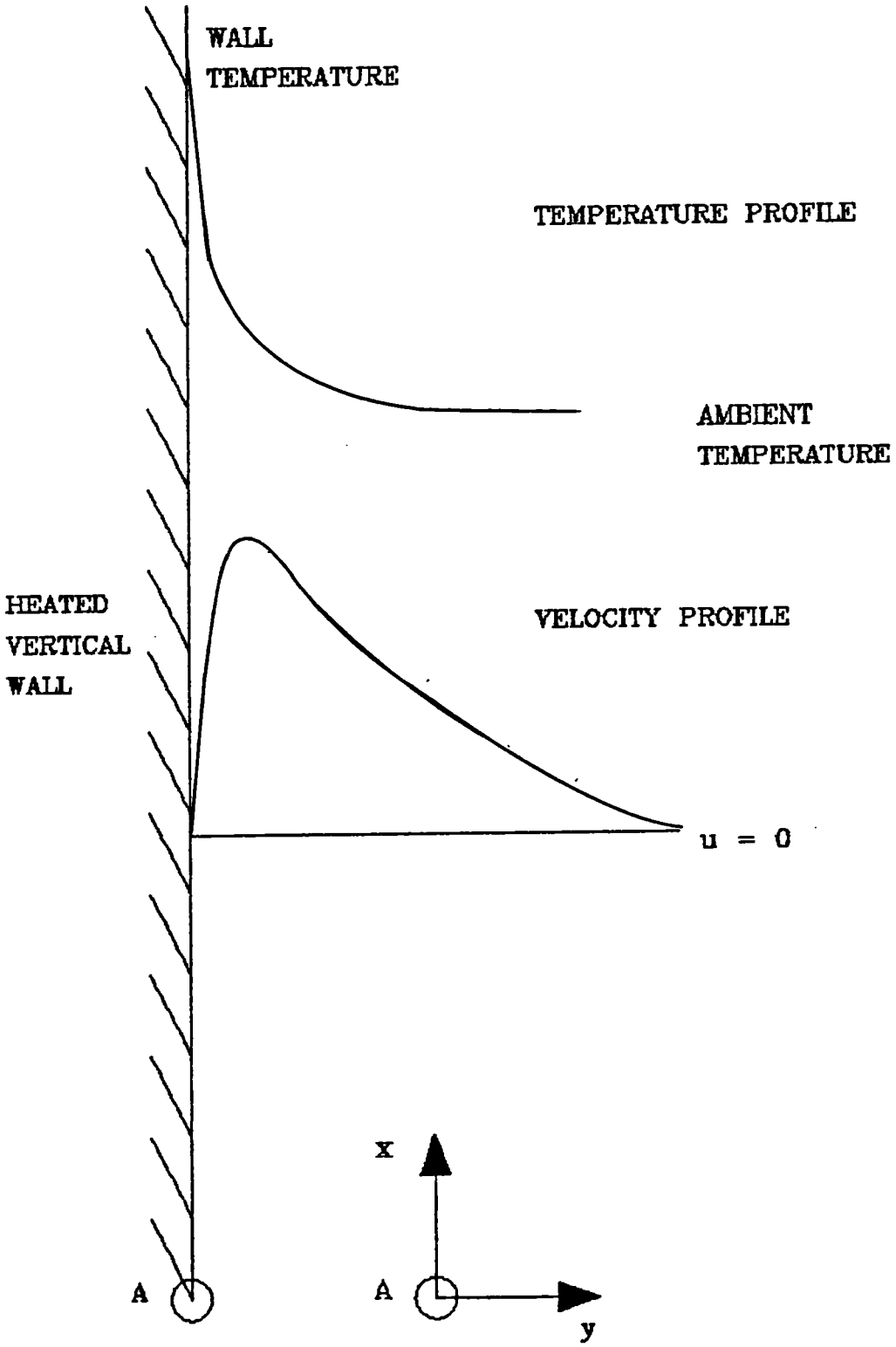

CHAPTER 2 - LITERATURE SURVEY

2.1 INTRODUCTION

This survey follows on from that of Ziai [1] who concentrated on describing the various types of flow regime; the heat transfer relationships for each regime; and pertinent flat plate data. In addition to the presentation of new material some of the points discussed by Ziai [1] will be investigated in greater depth as they are relevant to the research undertaken for this thesis.

Most Sections deal with particular points which are of relevance to the results presented later. However, some Sections discuss additional topics which are clearly not fully appreciated by current researchers in the field of natural convection in vertical cavities.

The survey starts with a consideration of the flow regimes within a cavity and the dimensionless groups whose magnitudes indicate the presence of each regime. It is known, from dimensional analysis, that, for a two-dimensional flow, $Nu = Nu(Gr,Pr,H/L)$, but the choice of the characteristic length for Nu and Gr is not straightforward. The situations in which H or L should be used are discussed and the available experimental data, in subsequent Sections, are recalculated to fit in with the recommendations.

Having established the relevant characteristic lengths, the survey then goes on to discuss the information available for the two flow regimes which are of direct concern to the author. These are the transitional and turbulent boundary layer regimes which both exhibit regions of turbulent flow.

Before discussing the transitional boundary layer regime, the important phenomenon of transition is described with reference to cavity and vertical flat plate work.

Transition, from laminar to turbulent flow, is a very important feature of the transitional boundary layer regime. Indeed, in the analysis of the experimental results, considerable effort was put into the calculation of power spectral densities in order to establish the frequencies of transition, and the nature of the turbulence.

The general characteristics of the transitional and turbulent boundary layer regimes are reviewed in general, with separate Sections describing the mean, and R.M.S. of the fluctuating components, of the velocity and temperature fields.

The "core" region is discussed next, with particular reference to the thermal stratification which exists in both regimes of interest, and the definition which one may use to determine the lateral extent of the "core".

Having dealt with the basic aspects of the two flow regimes (these have formed the bulk of material published) the turbulence quantities, including turbulence spectra, are then discussed. Because of the unavailability of cavity data for most of these quantities, recourse to the limited amount of data from flat plate work has been made. It is expected that the general characteristics of these quantities will be similar for cavity and flat plate scenarios, especially near the wall.

Following the discussion of the turbulence quantities comes a complementary Section on the attempts to provide velocity, length and temperature scales. These attempts have so far been restricted to the case of a vertical flat plate in an isothermal environment and are reassessed with particular emphasis on the effects of a stratified environment.

Thereafter, attention is turned to the effects of the cavity structure on the internal flow. These Sections deal mainly with the effect of heat transfer through the closing boundaries, and the associated difficulties in obtaining truely two-dimensional and anti-symmetric flow. Bearing the former in mind, some global heat transfer correlations (which were the objective of much early research) are reassessed, and the added complication of temperature dependent properties is also considered.

The survey finishes with a resume of the important points brought forth by the survey and an outline of how they have affected some details of the objectives of the present study.

Please note that throughout the text the term "boundary layer" will refer to the velocity boundary layer. Whenever the thermal boundary layer is under discussion it will be referred to in full.

2.2 FLOW REGIMES

Batchelor [2] undertook the earliest analytical work on cavity flow and found that, for a two-dimensional flow with a moderate temperature difference between the walls ($(T_H-T_C)/T_C < 0.2$) non-dimensionalisation of the governing equations gave $Nu = Nu(Ra,Pr,H/L)$. The use of Ra (which incorporates both the kinematic viscosity and the thermal diffusivity) rather than Gr, has resulted in Nu being less dependent on Pr.

The Rayleigh number has also been shown to be a reasonable first choice as an indicator of the presence of flow regimes, however, it must be stressed that this finding is limited in the range of Pr investigated, and

that there is no guarantee that the use of Ra (in the manner to be described) will be valid when dealing with liquid metals, as in such cases molecular heat transfer is a significant factor, even in regions of intense turbulence.

Batchelor [2] chose the characteristic length, for Ra_L, to be L. His choice of L was due to his interest in the application of his work to the insulation of buildings (by cavity walls) where L was easily changed. He predicted that the existence of each flow regime would be governed by the magnitude of Ra_L. He only concerned himself with four flow regimes but it is now known that there are five possible flow regimes within a vertical cavity; conduction; asymptotic; laminar boundary layer; transitional boundary layer; and turbulent boundary layer. Please note that some early researchers have incorrectly termed the asymptotic regime, the "transitional" regime.

The dominant parameters governing the existence of each regime are now clear. The conduction and asymptotic regimes are governed predominantly by Ra_L, as is the onset of the laminar boundary layer regime. The transitional and turbulent regimes are governed by Ra_H.

Dixon and Probert [3] and Eckert and Carlson [4] confirmed that, as Batchelor [2] suggested, Ra_L was the correct choice for the conduction and asymptotic regimes, and for the indication of the onset of the laminar boundary layer regime.

The use of Ra_L was extended to the laminar, transitional and turbulent boundary layer regimes until Seki et al [5] showed that for these regimes the use of Ra_H was significantly superior. They considered that as the occurrence of transition (and so turbulence) in the case of natural convection on a vertical flat plate was dependent on the height, then once a laminar boundary layer regime had developed in a cavity any subsequent change would be governed predominantly by the cavity height rather than the width (when (T_H-T_C) remained constant).

This is an instinctive assumption which is supported by the work of a number of researchers. Batchelor [2] had tentatively suggested that inasmuch as the convective motion is in the vertical direction, the cavity height would have an influence on the heat transfer (and so the flow regime, as the heat transfer coefficient for turbulent flow is higher than that for laminar flow).

Bauman et al [6] also expressed the view that a choice of Ra_H would be more meaningful since heat transfer rates and transition to turbulence are dominated by the height of vertical surfaces.

The experimental work of Mull and Reiher [7] found a dependency of the heat transfer coefficient on height.

In addition, MacGregor and Emery [8] indicated a dependency on Ra_H at the asymptotic/laminar boundary layer interface, and that significant changes in the global heat transfer coefficient occurred as H/L increased.

Elsherbiny et al [9] noted that, at constant Ra_L, the trend toward a 1/3 power on Ra_L in a power law heat transfer relationship (indicative of a turbulent boundary layer regime) was quicker for higher aspect ratio, thereby showing the effect of H.

Griffiths and Davis [10] concluded that heat transfer in the laminar boundary layer regime was unaffected by an increase in cavity width, providing the width was greater than the lateral extent of an equivalent boundary layer on a vertical flat plate (by boundary layer it is presumed that they were referring to the velocity boundary layer). Ziai [1] in his survey determined that once the laminar boundary layer regime was fully established, any increase in the cavity width only had a minor influence on the centre-line temperature distribution. These findings show that for a given temperature difference any increase in the cavity width does not result in the transitional or turbulent regimes, as the heat transfer characteristics and centre-line temperature remain essentially unchanged with increasing width.

The presentation of data in terms of Ra_L in some recent papers, dealing with the transitional and turbulent regimes, appears to indicate that the importance of Ra_H has not been fully appreciated by current researchers.

However, one must bear in mind that the Rayleigh number is only the dominant parameter, and that in the cases of large and small H/L this second parameter will have an important influence. It will be seen in subsequent Sections just how this parameter influences the flow patterns of the transitional and turbulent regimes.

The Prandtl number is also of importance, mainly in governing the thickness of the boundary layers and the effect this has on heat transfer. This will be discussed later.

2.3 TRANSITION

Before discussing the transitional boundary layer regime it is logical to first consider the phenomenon of transition which occurs in this regime. The onset of transition is examined with particular reference to the values

of Ra_H and H/L. The instability mode and transition frequencies are also considered.

2.3.1 ONSET OF TRANSITION

The criteria for the onset of transition to turbulent flow have not been properly established, but it is clear that there is a dependency on Ra_H, H/L and Pr (the dimensionless groups resulting from the dimensional analysis of a two-dimensional flow).

The most important point to note is that when transition occurs the entire flow does not become turbulent, which is the impression that some early researchers gave. The transitional regime exhibits regions of laminar, transitional and turbulent flow.

Most estimates of the onset of transition make use of experimental data and are primarily based on Ra_H, but two studies have been carried out, using numerical techniques, which have attempted to account for both Ra_H and H/L. When assessing these two numerical studies it must be borne in mind that no numerical code exists which is able to predict the onset of transitional flow accurately, so that the results can only be used to indicate possible trends, and are not to be used for hard and fast demarkations of the existence of flow regimes.

The first attempt to provide a criterion for the existence of turbulence in a vertical cavity (taking into account different Ra_L and H/L) was by Elder [11] who suggested that turbulence was present in a cavity for $Ra_H > 10^{10}$. Another suggestion (for different Ra_H and H/L) has come from Seki et al [5], who suggested (from experimental data at H/L = 5-47.5) that turbulent fluctuations exist when $Ra_H > 4\times10^9$.

Cowan et al [12] investigated the first occurence of temperature fluctuations in high aspect ratio water cavities. They positioned a fast response thermocouple in the geometric centre of the cavity and recorded Gr_L at which fluctuations first appeared. Assuming a Prandtl number of 3.26 for their experimental conditions, turbulence first occurred at Ra_H = 1.9×10^{11} for H/L = 45.6 and at $Ra_H = 5.2\times10^{11}$ for H/L = 60.8.

MacGregor and Emery [8] observed turbulence at $Ra_H = 10^{10}$ with H/L = 10 and at $Ra_H = 10^{11}$ with H/L = 20, for a fluid of moderate Prandtl number. They concluded that the difference was due to the narrow vertical cavity damping oscillations and so delaying transition. The results of Cowan et al [12] support this, and indeed, it is a reasonable explanation.

In a subsequent paper, MacGregor and Emery [13] went on to comment on their previous data of [8], stating that there were other examples of

increasing critical Ra_H with decreasing L at constant H. However, the effect was only noticed for L below certain values.

One must ask why some research has not produced an H/L dependency. It is possible that, for those cases which have exhibited an H/L dependency, the boundary layers on each wall have met at the centre of the cavity. In this scenario the volume of fluid available to form the boundary layers is reduced and the flow pattern must suffer some change. Thus one may propose that the walls only influence the critical Rayleigh number when the boundary layers meet. The influence becoming stronger as the distance between the walls decreases.

Based on the boundary layer thicknesses of Schmidt and Wang [14], and Giel and Schmidt [15], one may estimate that the boundary layers have only met for the highest aspect ratio studied by Cowan et al [12]. This would explain why they found no aspect ratio dependence, as the majority of their data was taken from cavities with lower aspect ratios than the highest one they studied.

The comments of MacGregor and Emery [13] concerning a limiting value of L beyond which there is no effect would also tend to support the proposal. If, then, the proposal is correct, one sees that it is not possible to consider only Ra_H and H/L as affecting the onset of transition, as the boundary layer thickness will be dependent on Pr. Normally Pr is only associated with the ratio of the thicknesses of the thermal and velocity boundary layers, but the dependency of the absolute thickness is shown by comparing water and air boundary layer thicknesses at similar values of Ra_H (i.e. comparison of the present results with those of Schmidt and Wang [14] and Giel and Schmidt [15]).

In attempting to assess the experimental results one must bear in mind that the position at which turbulent fluctuations first occur need not necessarily be at the geometric centre.

The view that turbulent fluctuations first occur at mid-height and in the boundary layer was supported by the work of Elder [11] who found temperature fluctuations to be largest in the thermal sub-layer and mixing region of the boundary layer. Batchelor [2] also proposed that the amplification of a natural disturbance would be at the position of maximum velocity gradient, which would be nearer the wall than the centre.

However, the view that turbulent fluctuations first occur at mid-height was challenged by the work of Seki et al [5] who reported turbulent fluctuations as occurring near the top of the heated wall as H was increased for constant Ra_L, and by MacGregor and Emery [13] who reported

initial fluctuations at x/H = 0.1 which then took the form of a sinuous motion at x/H = 0.2, finally tripping again at x/H = 0.9.

There have also been some attempts to determine a local Rayleigh number at which transition starts. For a vertical flat plate in an isothermal environment the value has been quoted as $Ra_x = 2\times10^9$ by Saunders [16] and $Ra_x > 10^9$ by Bauman et al [6]. For a cavity, the value has been quoted as $Ra_x = 4.85\times10^8$ for air by Raithby and Hollands [17], and 9.44×10^8 for water by Bohn et al [18].

Bohn et al [18] carried out experiments using a cubical water cavity, and observed travelling waves between $Ra_x = 10^8$ and 10^9. They compared their experimental result to the estimate of Elder [11], for the initial presence of travelling waves in water ($Ra_x = 3\times10^8$).

Travelling waves are essentially unsteady motions (also referred to as instabilities) which are a precursor to turbulence as described later in this Section. Unfortunately Ra_x itself cannot be considered an absolute indicator of the onset of these waves or transition.

Godeaux and Gebhart [19] conducted a thorough analytical and experimental study for a constant heat flux vertical plate in an isothermal water environment and concluded that transition was dependent on Gr_x, Pr and the energy imparted to the flow. Although the general conclusion was that transition could be reasonably estimated to occur at $Gr_x > 10^9$.

Under similar circumstances Jaluria and Gebhart [20] speculated that the onset of transition was dependent upon a number of parameters such as the total heat transfer to the flow; the local momentum flux; and the kinetic energy flux.

Elder [11] made a brief note that an increase of Pr from 6 to 1000 increased the critical Rayleigh number for a cavity. This observation was not followed up at the time but it does have support from the numerical work of Bergholz [21] which is described in Section 2.3.2.

Briggs and Jones [22] surveyed the velocity field of a square air cavity, with a linear temperature gradient on the horizontal closing boundaries, and found unsteady motions to occur at $Ra_H = 0.3\times10^7$. There was a considerable variation in velocity envelopes (which are shown in Figure 2.1) the maximum peak being nearly twice that of the minimum peak. These unsteady motions are of considerable importance for they mark the beginning of the transition process and do not represent turbulence which only occurs after Ra_H is increased to a value beyond that at which the unsteady motions occur. This was first noted by Elder [11] who found that unsteady motions, in the form of travelling waves, appeared at

approximately $Ra_H = 8\times10^{6}Pr^{0.6}$. These unsteady motions have been the subject of two numerical studies.

Chenoweth and Paolucci [23] undertook numerous numerical calculations in an attempt to show the dependence of the flow regime on H/L and Ra_L. The fact that the Rayleigh number was based on L rather than H for this 1986 paper is an indication of the lack of understanding of the importance of Ra_H. Their data, in the form of Ra_H, are replotted in Figure 2.2 along with the other data presented in this Section and in Section 2.4. (Figure 2.2 represents the best available criterion on which to predict the presence of unsteady motions and turbulence in a cavity). Their predictions of unsteady motions compared extremely well with the experimental data available to them, however, their predictions of the presence of turbulence are only of use in showing the general effect of H/L on the critical value of Ra_H.

Le Quere and Alziary de Roquefort [24] suggested (from numerical work at H/L = 4-6 and with an adiabatic floor and ceiling) that unsteady motions occurred when $Ra_H > 10^{6}$. The influences of the floor and ceiling are discussed in Section 2.12, and are shown to be of considerable importance, so much so that some of the experimental critical Rayleigh numbers quoted in this Section may be subject to significant uncertainty.

From Figure 2.2 one notes that the two sets of numerical data for an adiabatic floor and ceiling agree very well in predicting the presence of instabilities (unsteady motions) in the range H/L = 1-10. The prediction of the presence of turbulence by Chenoweth and Paolucci [23] is in reasonable agreement with all the available experimental data but care must be taken when estimating uncertainty on the log-log graph at H/L > 30.

Clearly this area requires more thorough experimental investigation, especially with reference to the Prandtl number, but one postulate is confirmed by Figure 2.2, and that is that the critical value of Ra_H for the presence of turbulent fluctuations increases as H/L exceeds a certain value. The numerical predictions plotted on Figure 2.2 indicate that this value may be approximately 6 for adiabatic horizontal closing boundaries.

2.3.2 INSTABILITY MODE

Bergholz [21] undertook numerical calculations to investigate the instability of flow in a cavity, with special emphasis on the stratification and the Prandtl number. He concluded that both had a significant effect on the mode of instability and the critical value of Gr_L. He defined a non-dimensional temperature gradient, γ, which was the vertical temperature

gradient non-dimensionalised with L and (T_H-T_C). The choice of L was unfortunate as was the lack of any mention of H in the analysis. However, there are certain trends in the results which are of considerable interest. One must note that he considered $0 < \gamma < 15$ and that the lower values of γ are not applicable to the boundary layer regimes. He predicted horizontal temperature inversions at $\gamma = 4.8$ and velocity reversals at $\gamma = 8$. This latter value may be considered to be the point at which a boundary layer regime exists. But more important is the proposal from the results that the existence of a temperature inversion does not guarantee a velocity reversal.

At both low and high Pr Bergholz [21] noted a change in the mode of instability as γ changed. He defined the value of γ at which this change occurred as γ_1. For $0.73 < Pr < 12.7$ the instability was of stationary mode for $\gamma < \gamma_1$ and travelling wave mode for $\gamma > \gamma_1$. γ_1 decreased with increasing Pr and became zero at Pr = 12.7, thus resulting in travelling wave instability for all γ. However, at higher values of Pr (considered to be above 20) the critical mode was travelling waves for $\gamma < \gamma_1$ but stationary for $\gamma > \gamma_1$. γ_1 decreased as Pr increased, and approached zero as Pr approached infinity.

For the boundary layer regime ($\gamma > 8$) at constant Pr (in the range $0.73 < Pr < 1000$) Bergholz [21] found that an increase in γ resulted in an increase in critical Gr_L. At constant γ an increase in Pr resulted in a decrease in critical Gr_L. Bergholz's graphs, for low and high Pr, of critical Gr_L against γ are reproduced as Figures 2.3 and 2.4. In general, for the boundary layer regime and $Pr < 50$, the mode of instability was predicted to be that of travelling waves. These have been observed experimentally by Elder [11] and Bohn et al [18]. For $Pr > 50$ the instabilty mode was predicted to be stationary.

Although most of Bergholz's [21] work was concerned with the Grashof number he did present a graph of critical Ra_L against γ which is of some significance, in that, for a constant γ, it shows that the variation of critical Ra_L is small within the ranges $0.73 < Pr < 12.7$ and $50 < Pr < \infty$, although different for each. This graph is reproduced as Figure 2.5 and supports the observations of Elder [11] mentioned in Section 2.3.1.

For the boundary layer regime Bergholz [21] found the stationary and travelling wave instability modes to be dominated by the buoyancy force, except at the lower values of Pr, in which case shear instabilities could occur if γ was not too large. Unfortunately no numerical values were quoted for γ in this case.

2.3.3 TRANSITION FREQUENCIES

Godaux and Gebhart [19] carried out experiments for the natural convection flow of water along a vertical flat plate and found the initial disturbance frequency for temperature to be approximately 0.08Hz, increasing to 0.35Hz during transition. It was found that small disturbances entered the laminar flow from the environment, and as they were convected downstream a narrow band of frequencies were amplified, initially resulting in one dominant frequency. The position at which initial amplification of disturbances first occured was at the outer inflexion point of the boundary layer ($d^2u/dy^2 = 0$).

Jaluria and Gebhart [20] investigated experimentally the processes occurring in the transition of the natural convection flow of water next to a vertical constant heat flux surface. They presented a graph of $f/CQ^{*0.5}$ against Gr_{xQ*}. The definition of C was:

$$C \equiv (g\beta_T/k)^{0.5}/2\pi \qquad (2.1)$$

On this graph (reproduced as Figure 2.6) Jaluria and Gebhart [20] plotted a line predicted by linear stability theory. For the range of Gr_{xQ*} = 400 to 1400, the value of $f/C\dot{Q}^{*0.5}$ varied from 0.6 to 0.74. Their results at the onset of transition did agree with this prediction, but it was found that during transition the dominant frequency increased. Thus the values were replotted to show an approximately linear dependency of f on $Gr_{xQ*}/x^{0.5}$. For a range of $Gr_{xQ*}/x^{0.5}$ of 400 to 700, the dominant disturbance frequency was in the range 0.13 to 0.59Hz for velocity, and 0.07 to 0.44Hz for temperature. (The graphs are reproduced in Figures 2.7 and 2.8).

Jaluria and Gebhart [20] observed the transition process to start first in the velocity boundary layer, which then promoted thermal transition. Subsequently the dominant temperature frequency lagged that of the velocity.

Gebhart and Mahajan [25] presented a number of analytical relations for the prediction of the initial dominant frequency, of transition, which were apparently incorrect. They presented equations which involved the quantity β which was defined as the dimensionless frequency for the case of an isothermal flat plate in isothermal surroundings. One equation described a characteristic frequency, B, as a multiple of β and the 1/3 power of a modified Grashof number and is shown below.

$$B = \beta Gr_{x*}^{1/3} \qquad (2.2)$$

In the text the value of B for air (Pr = 0.733) was quoted by Gebhart and Mahajan [25] as 0.35 based on stablity theory, but also as 0.315Pr

(which for air is 0.231) again supposedly based on stability theory. The quantity B was further equated to another grouping:

$$B = 2\pi f\{g\beta_T(T_\omega - T_\infty)/(\mu/\rho)^2\}^{-2/3} \qquad (2.3)$$

Now, considering that β and Gr_{x*} are both dimensionless, then the right-hand side of equation (2.3) should also be dimensionless. This is not the case, and the present author could not find a correction for this equation.

The last equation of interest presented by Gebhart and Mahajan [25] was:

$$f = (\mu/\rho)Gr_{x*}^3/32\pi x^2\beta \qquad (2.4)$$

Assuming that at transition $Gr_x = 10^9$, and $(\mu/\rho) = 1.8\times10^{-5}$ (air) then it is clear that β in equation (2.4) is incorrectly positioned in the denominator and should be in the numerator. Support for this reasoning comes from Jaluria and Gebhart [20] whose similar equations for a constant heat flux wall can be compared to equation (2.4), and the equation quoted by Gebhart and Mahajan [25] for the constant heat flux case which was identical except for an error in the positioning of β^*, the constant heat flux equivalent of β.

The corrected version of equation (2.4) is:

$$f = \beta(\mu/\rho)Gr_{x*}^3/32\pi x^2 \qquad (2.5)$$

Using example data for the natural convection flow of air along a vertical flat plate with $(T_\omega - T_\infty) = 55K$, $x = 0.56m$ and $Gr_x = 10^9$ one calculates $Gr_{x*} = 503$. Therefore if $B = 0.35$ then $\beta = 0.044$, and if $B = 0.231$ then $\beta = 0.029$. These predict f to be 3.2Hz and 2.1Hz respectively. The validity of these two predictions can be assessed by the work of a number of authors with similar conditions.

Dastbaz [26] conducted an experimental investigation of the transition region in air along an isothermal vertical flat plate. He found the dominant frequency at the start of transition to be 3.2Hz which agrees with the use of $B = 0.35$. He also detected what he termed an harmonic at 2.8Hz. This value is too large to consider the use of $B = 0.315Pr$ to be correct.

Smith [27] and Cheesewright and Doan [28], all using the same apparatus as Dastbaz [26], reported the dominant frequency to be 3.6Hz and 3.5Hz respectively. Different experimental conditions probably account for the difference between these values and the previous one reported by Dastbaz [26].

Departing from flat plate work one turns to the only information available on cavity transition frequencies presented by Giel and Schmidt [15]. For the temperature field in a water cavity, on the heated wall, the

first observed frequency was 0.96Hz. On the cooled wall it was 0.82Hz. At a height further downstream on the heated wall, but still during transition, the temperature spectra exhibited peaks at 0.9, 1.8, 2.7 and 3.4Hz, the dominant being at 0.9Hz. They claimed that using the work of Gebhart and Mahajan [25] the frequency predicted by linear stability theory was 0.97Hz. B for Pr = 6.7 was quoted as 0.25, although using B = 0.315Pr gives B as 2.11. It is clear from approximate calculations that the value which will give the most meaningful result is that of B = 0.25, therefore the use of the relationship B = 0.315Pr has been shown to be undesirable for air and water. It is regretable that Giel and Schmidt [15] have not commented on the presentation of Gebhart and Mahajan [25].

Finally, one notes that Pera and Gebhart [29] carried out experimental work for the natural convection flow of air over surfaces slightly inclined from the horizontal. They introduced artificial disturbances into the flow for a frequency range of 1.5-4.6Hz. The frequency which was amplified most was 1.7Hz, which is approximately one-half of that reported for vertical flat plate work.

From the results presented in this Section it appears that frequencies associated with the transition of natural convection flow for air and water are multiples of a base frequency close to 0.9Hz. It will be interesting to see if the present results indicate this also.

2.4 TRANSITIONAL BOUNDARY LAYER REGIME

The transitional boundary layer regime has been observed by Seki et al [5], Cowan et al [12], Renault and Doan-Kim-Son [30] and Giel and Schmidt [15]. Each case had a unique and interesting aspect.

Giel and Schmidt [15] presented the "best" example of a transitional boundary layer regime, where laminar, transitional and turbulent regions were observed on both the heated and the cooled walls (with the flow being close to being anti-symmetric). They surveyed the velocity and temperature fields of a water cavity using L.D.A. and a thermocouple. The cavity was operated at $Ra_H = 8.0\times10^{10}$ and H/L = 10. The vertical walls, floor and ceiling were all insulated with 50mm of expanded polystyrene. A laminar region occupied approximately 43% of the upstream part of the heated wall and another laminar region occupied approximately 37% of the upstream part of the cooled wall. Re-laminarization occurred on both the ceiling and floor. No detail was given as to the point at which the re-laminarization was completed, but a rough sketch showed it as being completed after the flow had travelled approximately 60% of the distance along both the floor

BIBL. LONDIN. UNIV

and the ceiling. This finite distance required for re-laminarization is important as one must ask what might have happened to the flow if the cavity width had been reduced to this distance (and below it) for the same Ra_H. (Figure 2.9 is a reproduction of the sketch of the flow pattern from Giel and Schmidt [15]).

The re-laminarization phenomenon is discussed further in Section 2.12 with particular reference to: the heat transfer through the floor and the ceiling; the local Richardson number; and the cavity width in relation to the boundary layer width.

The velocity and thermal boundary layers are discussed separately in Sections 2.6 and 2.7, but it is pertinent to mention here that at the outer edge of the boundary layers of Giel and Schmidt [15], regions of reversed flow were observed over the downstream 70% of each wall, and that horizontal temperature inversions also occurred. (Typical profiles of velocity and temperature are shown in Figure 2.10). The main feature of the flow reversal regions was that they did not extend to the cavity centre. The maximum peak velocity was said to have occurred at mid-height for both boundary layers. This was accounted for by the decrease in the local (T_w-T_∞) with height, but since this occurs for all x it is not an acceptable explanation. One would only expect the velocity to decrease as a result of two things. Firstly, due to a reduction in mass flow caused by fluid leaving the boundary layer, and secondly, the balance and subsequent domination of viscous and turbulence shear forces compared to those of buoyancy. One must also remember that velocities were only recorded for specific heights and that the regions above and below mid-height, and the next experimental stations, may have incorporated the maximum peak velocity.

Renault and Doan-Kim-Son [30] surveyed the velocity and temperature fields of an air cavity (using L.D.A. and resistance thermometry) at $Ra_H = 6.2\times10^{10}$ and H/L = 10. Although the value of Ra_H was very close to that of Giel and Schmidt [15], and the aspect ratio the same, there were considerable differences between the two flow patterns. (The profiles presented by Renault and Doan-Kim-Son [30] are reproduced in Figure 2.11). On the heated wall the velocity profiles had a "laminar aspect" up to x/H = 0.2 where $Ra_x = 4.26\times10^9$. The root mean square (R.M.S.) of the velocity fluctuations peaked at this position, indicating a transition process, and fully developed turbulent flow appeared to have developed by x/H = 0.5 where $Ra_x = 4.54\times10^9$. From x/H = 0.5 upwards the boundary layers met in the centre of the cavity and no flow reversal regions were present. (This

was in contrast to the boundary layers of Giel and Schmidt [15]). The peak velocity at the heated wall did not start to decrease until close to the ceiling at x/H = 0.95. The velocity profiles were said to exhibit "self-preservation" for x/H = 0.5-0.95, but because the temperature profiles changed with height one would have expected to see a reduction in mass flow with increasing height. Re-laminarization did not occur over the ceiling but began as the flow moved from the bottom of the cooled wall to the floor. There was also an imbalance of mass flow at mid-height which was attributed to the poor level of insulation on all closing boundaries. *This is discussed in Section 2.13.*

For fluids with differing Pr Seki et al [5] found that 20% of the height of the heated wall was laminar for the range $Ra_H = 4\times10^9$ to 4×10^{12} with H and L both varied. Whilst this result agreed with that of Renault and Doan-Kim-Son [30], the idea that this is always the case was contradicted by Giel and Schmidt [15]. One would not expect a fixed percentage of the height to be covered by laminar flow as transition to turbulence is not governed by this. One may attempt to explain why Seki et al [5] found the 20% height a common factor as either coincidence in that all their experiments happened to have similar Ra_x at x/H = 0.2, or that their interpretation of their visual observations left something to be desired. Their heat transfer relation for the transitional boundary layer regime was given as:

$$Nu_H = 0.084Pr^{-0.51}Ra_H^{0.3} \qquad (2.6)$$

The limits of the transitional regime were considered to be:

$$4.0\times10^9 \leq Ra_H \leq 2.0\times10^{12} \qquad (2.7)$$

Cowan et al [12] carried out heat transfer measurements for a water cavity with fixed H, but varying L and Ra_L. Their results have been recalculated as Ra_H and are plotted on Figure 2.12 (which is a reproduction of the transitional boundary layer regime graph presented by Seki et al [5]). Although they did not present velocity data they did comment that their variation of local heat transfer coefficient with height, on the heated wall, could only be explained by the formation of a laminar boundary layer at the bottom, which eventually underwent transition to a turbulent boundary layer. No measurements were presented for the cooled wall, but considering that the boundary layers would not have met at the centre, and the very high level of insulation, one would have expected a laminar region on the cooled wall for aspect ratios 5.7 and 11.4 at least.

Schmidt and Wang [14] claimed that an experiment with a water filled cavity at $Ra_H = 4.64\times10^{10}$ and H/L = 2 was for a turbulent boundary layer

regime. If the limits for the transitional boundary layer regime proposed by Seki et al [5] are correct, then this cannot be true. They did observe that at the top of the heated wall, and at the bottom of the cooled wall, the velocity profiles taken with a Laser Doppler anemometer exhibited scatter. This was attributed to turbulence. However, profiles taken at the bottom of the heated wall, and the top of the cooled wall, did not exhibit any scatter. This certainly indicated that the turbulence level was reduced in these regions, and that laminar flow might possibly have been present. Without velocity fluctuation data one is unable to comment further on this point. (Relevant profiles from Schmidt and Wang [14] are reproduced in Figure 2.13).

Schmidt and Wang [14] reported that the maximum peak velocity occurred at mid-height, and explained this in the same manner as Giel and Schmidt [15] which has been shown to be inadequate.

Ralph et al [31] presented profiles of mean velocity and R.M.S. of velocity fluctuations for x/H = 0.7, 0.9 and 0.95 from an air cavity, with a constant heat flux heated wall and an isothermal cooled wall, operating at $Ra_H = 1.25 \times 10^{10}$ and H/L = 28.68. They claimed that no steady laminar region was observed. If this was true then doubt is cast on the criteria for the existence of the transitional boundary layer regime as given by Figure 2.2. One may only propose that, as the size of the eddies were said to be comparable with the distance between the mean velocity peaks in each boundary layer, the laminar region that would have existed for a larger cavity width was affected by surrounding turbulent regions, or that their investigations of any possible laminar region were not thorough enough. If the former is the correct explanation then they have produced evidence of another Prandtl number effect. Apart from re-stating that this whole area needs careful examination one must attempt to recommend a common approach to the problem. The simplest would appear to be to examine time-histories of the flow and to undertake a spectral analysis. They appear to have undertaken the latter and reported no obvious predominant frequency. If the heated wall has been surveyed properly this would indicate that a transition process was not observed and that all the flow was turbulent.

One looks back at the comment of Renault and Doan-Kim-Son [30] who reported the region at the bottom of the heated wall as having a "laminar aspect". It is known from Renault [32] (the work which formed the basis for Renault and Doan-Kim-Son [30]) that data were recorded on magnetic tape and that spectral analysis was undertaken. Perhaps the choice of the term "aspect" was meant to indicate that the flow was only laminar for some

percentage of time, and indeed, even the comment of Ralph et al [31] that there was no steady laminar region, could be taken to mean this. If this is so then one must classify the work of Ralph et al [31] as being in the transitional boundary layer regime, as all the flow was not turbulent all the time.

The only other experimental work has been that of Bohn et al [18] who observed that turbulent flow existed on the downstream third of each wall in a cubical water cavity at $Ra_H = 10^{10}$. This experimental arrangement was somewhat different in that all four walls were capable of being heated or cooled.

This Section is completed with a look at two numerical studies which used $k-\epsilon$ models in an attempt to predict the transitional and turbulent boundary layer regimes. Such studies are confronted by severe problems when it is required that both laminar and turbulent regions exist in the cavity. The use of a $k-\epsilon$ model requires that all parts of the flow are turbulent, therefore making the modelling of potential laminar regions impossible. These regions can only be approximated as regions of low turbulence intensity. If one is to attempt to predict the laminar regions using a laminar model then one must provide empirical input to switch over to a turbulent model. Indeed, if re-laminarization is to be taken into account empirical input is required for this also. Therefore the first attempts to predict flow patterns must rely on the judgement of the researcher as to what empirical input is relevant. As this survey has already shown, the relevant empirical input cannot be considered to be fully known. One must bear these points in mind when attempting to glean information from numerical work, as only general trends may be considered as having any worthwhile use.

Clearly one can only assess the validity of numerical predictions by comparing them with existing experimental data from cavities subject to the same boundary conditions as the numerical cases.

Ozoe et al [33] undertook numerical calculations for a square water cavity ($Pr = 6.7$) for $Ra_H = 6.3\times10^{10}$ and 1.09×10^{11}, but only the heated wall boundary layer profile results for $Ra_H = 6.3\times10^{10}$ were presented. They accounted for the transition on the heated wall but it's location depended on the set of $k-\epsilon$ model constants used. Two sets of data were presented, one for a standard set of $k-\epsilon$ model constants, and one for a modified set of constants which resulted in the closest agreement between their predictions and experimental results available at the time. In both cases the absolute location of transition could not be determined from the

limited data they presented, but there was a trend for the region where the transition process was still evident to be associated with the maximum peak of turbulence kinetic energy, and the maximum peak velocity. For the second case of comparable experimental and numerical results the maximum peak velocity did not occur at mid-height but around the position of transition above which the peak velocities decreased and reversed flows occured. There was a flow reversal at the very bottom of the heated wall at x/H = 0.008 which has not been observed by any of the experimental works described so far. (The lowest value of x/H investigated experimentally by other researchers was 0.036).

Perhaps the most important trend found by Ozoe et al [33] was that as Ra_H increased so did the boundary layer thickness.

Markatos and Pericleous [34] numerically predicted the flow in a square air cavity at different values of Ra_H. They assumed that turbulent conditions existed for $Ra_H > 10^6$ which was too low a value. However, the results that are of interest were in the range $Ra_H = 10^{10}$ to 10^{15}. They tabulated values which showed that in the transitional boundary layer regime, the non-dimensional height at which the maximum peak velocity occurred, decreased as Ra_H increased. If the suggestion from Ozoe et al [33], that the position of transition is the same as that of maximum peak velocity, is correct, then the above observation is the logical progression which one would expect, and contradicts Seki et al [5] who considered transition to occur at a constant non-dimensional height.

2.5 TURBULENT BOUNDARY LAYER REGIME

MacGregor and Emery [13] and Seki et al [5] are the only authors to have presented experimental data for high Ra_H ($Ra_H > 10^{12}$) whilst Markatos and Pericleous [34] have attempted to predict data for high Ra_H.

Using the data of MacGregor and Emery [13] and their own, Seki et al [5] determined the start of the turbulent boundary layer regime to be at $Ra_H \approx 2.0 \times 10^{12}$. For this regime one would anticipate that, as Ra_H increases above this limit, there would be little change in heat transfer characteristics (i.e. the heat transfer coefficient) so that for a power relationship between Nu_H and Ra_H there would be a 1/3 power on Ra_H, indicating that the characteristic length does not affect heat transfer.

Seki et al [5] assumed this to be so and proposed the following relationship.

$$Nu_H = 0.039 Ra_H^{1/3} \qquad (2.8)$$

Their plot for this region showed that this did not agree fully with the data of MacGregor and Emery [13] whose data lead to:

$$Nu_H = 0.046Ra_H^{1/3} \qquad (2.9)$$

Clearly there must be some dependence on Pr which Seki et al [5] were unable to ascertain given the small amount of data available to them. Their graph for this regime is presented as Figure 2.12.

Markatatos and Pericleous [34] predicted data for a constant sized square cavity at $Ra_H = 10^{12}$, 10^{14} and 10^{16}. There is a reasonable level of confidence (as is possible for numerical predictions) in the results for the first two values, but not for the third. Considering the height of the position of maximum velocity, one sees that it changed from x/H = 0.3179 to 0.594 to 0.2865 as Ra_H increased. One expects the velocity to decrease after the height at which buoyancy forces are matched by shear forces. As the temperature difference is increased, to increase Ra_H, one would expect this height to increase, as reflected by the first two results. Therefore doubt is cast on the third result. In addition one notes that their comments implied that the boundary layer thickness had decreased from $Ra_H = 10^{14}$ to 10^{16}, which would not be expected. Certainly their numerical technique had one major flaw which was the use of existing forced flow wall functions to predict the wall shear stress. These are not applicable to natural convection flow.

Perhaps the most interesting observation from the predictions of Markatatos and Pericleous [34] is that their results were delineated into three ranges of Ra_H as regards heat transfer correlations. The first was for their laminar calculations and the other two were for their turbulent calculations. As stated previously they considered a turbulent regime to exist for too low a value of Ra_H, which formed the demarkation between the first and second ranges. But the demarkation between their two turbulent ranges was $Ra_H = 10^{12}$ which is very close to that proposed for the start of the turbulent boundary layer regime by Seki et al [5]. When a 1/3 power was imposed on Ra_H for the whole of their turbulent range the resulting heat transfer correlation was:

$$Nu_H = 0.060Ra_H^{1/3} \qquad (2.10)$$

The coefficient of 0.060 was significantly different from that found by Seki et al [5] and MacGregor and Emery [13], which would again indicate a Pr effect. For $Ra_H > 10^{12}$ Markatatos and Pericleous [34] had initially calculated the correlation by a least squares analysis to be:

$$Nu_H = 1.325Ra_H^{0.245} \qquad (2.11)$$

2.6 VELOCITY BOUNDARY LAYER

Firstly one must define what the boundary layer is considered to be. It is considered to be that region which extends from the wall to the first zero crossing and does not include the region of reversed flow.

Giel and Schmidt [15] presented profiles of mean velocity and R.M.S. of velocity fluctuations for a water cavity at $Ra_H = 8.0 \times 10^{10}$ and H/L = 10. Velocity reversals were noted for the upstream 70% of the heated and cooled walls. The thickness of the boundary layer was reported as being approximately constant except at the corner regions. From the graphs presented for the heated wall, one notes that the distance from the wall to the first point of zero mean velocity was constant at approximately 4mm for x/H = 0.346 to 0.964. The second point of zero mean velocity, denoting the end of the region of reversed flow, varied from 8 to 11mm for the same range of x/H. The dimensions, and trends, of the boundary layer and reversed flow region on the cooled wall were more or less the same.

Raithby and Hollands [17] claimed that for a vertical flat plate in an isothermal environment the thickness of the turbulent boundary layer is essentially constant, and so independent of height. Although the environment for a cavity is stratified this was also the case for Giel and Schmidt [15].

The Laser Doppler anemometer data of Giel and Schmidt [15] produced apparent velocity fluctuation data in the laminar flow regions which were shown to be fully explainable in terms of the uncertainty introduced by the finite size of the measuring volume. Further confirmation of the laminar characteristics of these regions was provided by spectral analysis. The apparent velocity fluctuation data introduced by the finite size of the measuring volume were shown to be insignificant in the turbulent regions of the flow, where the R.M.S. of the velocity fluctuations was of the same order of magnitude as the mean velocity.

Giel and Schmidt [15] measured the horizontal velocity at the vertical cavity centre-line and showed that crossflow occurred from the cooled wall to the heated wall for x/H = 0.0-0.4. The crossflow from the heated to the cooled wall appeared to be concentrated in the region x/H = 0.9-1.0, with some flow in this direction at x/H = 0.7 which corresponded with the start of transition on the cooled wall. As noted in Section 2.4 the flow was not perfectly anti-symmetric, with transition occurring at different distances downstream of each wall. Therefore it is not surprising to note that there was some difference in the mean horizontal velocity profile either side of mid-height. The difference between the location of transition on each wall can be accounted for by the variation of temperature dependent properties

and the small difference in heat transfer through the floor and ceiling (indicated by the centre-line temperature distribution).

Schmidt and Wang [14] presented velocity profiles from a water cavity at $Ra_H = 4.64 \times 10^{10}$ and H/L = 2. The cavity was essentially the same as that used by Giel and Schmidt [15] except that the cavity width had been increased. The similar values of Ra_H provide a chance to examine the effect of the cavity width. As for Giel and Schmidt [15] flow reversals were observed just outside of the boundary layers on both walls. These reversals were confined to the upstream 60% of each wall. This is compared to approximately 70% for the higher Ra_H case of Giel and Schmidt [15] (×1.7 that of Schmidt and Wang [14]). The regions of reversed flow were of limited extent and the core quiescent as before.

For the heated wall Schmidt and Wang [14] reported the boundary layer thickness to be 4-5mm to the first zero crossing and 8-10mm to the second. The cooled wall B.L. was larger at 5-6mm and 9-13mm. Thus the heated wall boundary layer thickness characteristics were virtually the same as for Giel and Schmidt [15], with the cooled wall boundary layer slightly larger. However, there were considerable differences in the peak velocities. The peak velocity at each height on the heated wall was higher for Schmidt and Wang [14]. This was also true for the furthest upstream and downstream heights on the cooled wall.

One may seek to explain the increase in mass flow for the lower value of Ra_H by postulating that the larger cavity provided a greater reservoir of fluid from which to form the boundary layers. Certainly there must be a limiting value of L beyond which the boundary layers, for constant and ideal conditions, do not grow further and are the equivalent of that resulting on a vertical flat plate under the same environmental conditions. One other explanation is that the different mass flows have resulted from a different centre-line temperature distribution which is examined in Sections 2.8 and 2.13.

The horizontal mean velocity profile measured by Schmidt and Wang [14] at the cavity centre-line was also different from that of Giel and Schmidt [15] with most of the crossflow in the regions x/H = 0.0-0.27 and 0.73-1.0. The profile was much more anti-symmetric for the larger cavity with peak velocities differing mainly because of temperature dependent properties.

Downstream from mid-height Schmidt and Wang [14] stated that the general trend was for the peak velocity to decrease and move away from the wall, however, the velocity profiles they presented lent poor support to the

comment that the peak moved away from the wall. No comment on such a movement was made by Giel and Schmidt [15].

Schmidt and Wang [14] compared mean velocity profiles at similar values of a local Rayleigh number (which they defined) and found them to be similar. On closer examination one sees that, because all the profiles were taken at the same height, Ra_x was similar also.

Kutateladze et al [35] presented profiles of mean velocity and R.M.S. of velocity fluctuations for an ethyl-alcohol cavity operating at several aspect ratios (with constant height) and $Ra_H > 10^{10}$. They only reported measurements in a turbulent region of the flow. The type of regime was not fully specified, but is likely to have been transitional boundary layer. For the turbulent region, a Reynolds number based on the peak velocity, and distance of the peak velocity from the wall, was found to be a constant for a given temperature stratification. Their graph of stratification and Re is reproduced as Figure 2.14. No other researchers have presented data to support the idea of a constant Re, but Schmidt and Wang [14] and Ziai [1] both support the observation of decreasing peak velocity being associated with movement of the peak away from the wall. When checking the work of other researchers it must be borne in mind that the constant Re will only apply to that region where the temperature stratification is constant.

The work of Kutateladze et al [35] contained a most interesting result which was not apparent to them at the time, as they were concerned with Ra_L. At a value of $Ra_H = 1.9\times10^{11}$ they measured the mean velocity, and the R.M.S. of the velocity fluctuations, for cavity widths of 30mm and 15mm (H/L = 13.17 and 26.33 respectively). The larger width showed a boundary layer thickness estimated to be greater than 9mm, which was more than half the second cavity width. The result of the reduction in width was to significantly increase the velocity in the region of the peak (y = 0.5-3mm) with only a small increase elsewhere. Here then is the only documented effect on the boundary layers of reducing the cavity width so that they meet in the cavity centre. Their graph is reproduced as Figure 2.15.

The results of Kutateladze et al [35] also showed that at a constant aspect ratio (H/L = 26.33) an increase of Ra_H from 8.69×10^{10} to 1.9×10^{11} produced a substantial change in the velocity profile (see Figure 2.15). For an increase of Ra_H of $\times2.2$ ($(T_\omega-T_\infty)$ increased by $\times1.9$) the peak velocity at mid-height increased by $\times1.7$. This suggests an almost linear relation between the temperature drop across the cavity and the peak velocity at mid-height. Such an increase in peak velocity with Ra_H is surprisingly high. This was not observed in the comparison of the results of Giel and Schmidt

[15] and Schmidt and Wang [14], but it could be that the change in cavity width for these cases dominated any change brought about by the change in Ra_H.

The peak of the R.M.S. of velocity fluctuations was seen by Kutateladze et al [35] to coincide with the peak of the mean velocity. The peak of the R.M.S. of velocity fluctuations reported by Giel and Schmidt [15] was on the core side of the peak mean velocity.

Renault and Doan-Kim-Son [30] presented mean velocity profiles which met at the cavity centre and showed no regions of flow reversal. No change of peak mean velocity, with height, was found in the turbulent region on the heated wall, although it was seen to move away from the wall with increasing height. There was a reduction in peak mean velocity below mid-height at the cooled wall. This was due to fluid being expelled from the boundary layer and travelling to the heated wall where a transition process was taking place.

None of the researchers mentioned up to now have attempted to fit an equation to the mean velocity profiles they have measured. To find such an attempt one must look to the early work of Bayley [36]. He fitted a curve to the then available experimental data for turbulent natural convection flow along a vertical flat plate in an isothermal environment. The resulting equation was:

$$u = u_1 (y/\delta)^{1/7} (1-y/\delta)^4 \qquad (2.12)$$

u_1 was described as a characteristic velocity (which for forced flow would be the free stream velocity). For the case of natural convection flow u_1 was derived as a function of Gr_x, Pr, the temperature field, μ/ρ and x. A graph indicated that for natural convection u_1 might have been considered as the free stream velocity which would have resulted in the viscous sub-layer mean velocity distribution. It is known that the equation for mean velocity in the viscous sub-layer is a cubic, unlike the linear distribution that Bayley assumed. Therefore his definition of u_1 is most likely to be proved unacceptable, even if his equation describing the mean velocity distribution is shown to be basically correct. (One notes from these points that forced flow predictions of wall shear stress cannot be used for turbulent natural convection flow). The boundary layer thickness was δ, and must be considered to be the distance from the wall to the first position of zero velocity. In some cases the constraints of the cavity width will determine this value. The work of Bayley [36] is worthy of comparison with future data as the term $(y/\delta)^{1/7}$ was considered to be typical of turbulent conditions for both forced and natural convection flow. One point

emphasised by Bayley's work, which is still valid, is that no-one has presented data which attempt to describe the viscous sub-layer thickness. He considered the non-dimensional thickness of the viscous sub-layer to be $12y^+$, but this is very likely to be proved incorrect.

Very little work has been carried out, either experimentally or numerically, for scenarios incorporating environmental stratification. A numerical investigation by Jaluria and Gebhart [37] did show that the level of stratification had a very important effect on all characteristics. For a constant heat flux heated wall in a stratified environment they found that increasing stratification lead to a larger temperature inversion; a higher heat transfer rate; a decrease in the peak mean velocity; a flattening of the velocity profile; and reduced wall shear stress. The reduction in velocity was due to the modification of the temperature profile resulting in reduced buoyancy forces. It is immediately apparent that when seeking to scale temperature and velocity profiles one must account for the level of stratification. This is discussed in Section 2.11.

Chen and Eichorn [38] presented experimental results of natural convection flow along a vertical cylinder in a stratified environment. They proposed that $Nu_x = Nu_x(Ra_x, Pr, S)$ where S was the non-dimensional temperature gradient (a measure of the stratification). It was shown that the ratio of the total heat transfer from the cylinder in a stratified environment, to that of a cylinder in an isothermal environment, was always greater than one. (Their definition of the environmental temperature for a comparable isothermal environment was very important, they used the average environmental temperature from the stratified scenario). This ratio was seen to increase with increasing stratification, with good agreement between their experimental and numerical results.

2.7 THERMAL BOUNDARY LAYER

The thermal boundary layer is straightforward to define when a horizontal temperature inversion is not present. It is defined as extending to that position where the fluid temperature reaches that of the fluid at the cavity centre. However, it is not easy to define when a horizontal temperature inversion is present. There are three possibilities. Firstly, one may define the thermal boundary layer as extending to the position where the modulus of $(T_\omega - T)$ is a maximum and $dT/dy = 0$. Secondly, the thermal boundary layer may be defined as extending to a position beyond the maximum of the modulus of $(T_\omega - T)$ where the fluid temperature reaches that of the fluid at the centre of the cavity. This position could be at the

cavity centre or before the cavity centre where $dT/dy = d^2T/dy^2 = 0$. The third possibility is that the thermal boundary layer may be defined as extending to that position at which the fluid temperature first reaches that of the fluid at the cavity centre. As the temperature at the cavity centre is regarded as the reference temperature for the buoyancy term in the x direction momentum equation, then the second and third proposals may be considered more suitable. Alternatively, it may be argued that, in general, dT/dy beyond the position at which the modulus of $(T_\omega - T)$ is a maximum, is small compared to dT/dy near to the wall, and so this outer region may be ignored, thus favouring the first proposal. The author has chosen the third proposal for three reasons. Firstly, high levels of stratification at the cavity centre-line can invalidate the first proposal, secondly, because the cavity centre-line temperature is used in the x direction momentum equation, and thirdly, because this definition is consistent with that of the velocity boundary layer.

Giel and Schmidt [15] reported the thermal boundary layer to be approximately 1.5mm thick for the fully developed turbulent regions on both walls, with the region of inversion extending to 6mm. Schmidt and Wang [14] reported a slightly higher boundary layer thickness of 1.7mm, but as scaling off the graphs from both papers is difficult one may consider the boundary layer thicknesses to be the same. Therefore, it would appear that at similar Ra_H for water the thickness of the thermal boundary layer was unaffected by the change of cavity width.

In both of the above cases the fluid along the vertical cavity centre-line was stratified and all temperature profiles exhibited horizontal inversions. Jaluria and Gebhart [37] have explained that these temperature inversions are a result of the centre-line stratification. For a heated wall the fluid entering the boundary layer from below is lower in temperature than that at the local centre-line, and, if the vertical temperature gradient exceeds a certain value, then the incoming fluid will not attain this temperature. Obviously, the larger the gradient the greater the inversion. Events are similar for the cooled wall except that the incoming fluid remains above the local centre-line value.

There has only been one reported case where the fluid along the entire vertical centre-line has not been stratified. Ralph et al [31] found the region x/H = 0.2-0.7 to be essentially unstratified. No explanation was put forward for this but one may speculate that there are two possible explanations for this. Firstly, as noted previously, the eddy sizes were reported as being comparable to the distance between velocity peaks. This

may have resulted in substantial mixing which effectively smeared out the stratification. The second possible explanation comes from the work of Gill [39].

Gill [39] stated that one would expect fluid to be entrained into the boundary layer at the bottom of the heated wall, so bringing in cooler fluid, and at the top of the cooled wall bringing in warmer fluid, thus strong horizontal temperature gradients would be maintained at the top and bottom of the cavity resulting in a stable stratification. One notes that in the case of Ralph et al [31] the regions where stratification was present were those which one would associate with entrainment. The lack of stratification in the central region might possibly have been associated with a constant mass flow (i.e. no entrainment) but as no data for this region were available this cannot be checked. However, it would be interesting to examine the magnitude of temperature inversions in relation to the derivative of mass flow with height. If the foregoing explanation has some basis then one would expect comparatively small inversions at positions of lower dm/dx, i.e. near cavity mid-height. It may be that both the turbulent mixing and the cavity size (restricting the mass flow) are both contributors to the non-stratification.

Whilst investigating the laminar boundary layer regime in a square cavity, deVahl Davis [40] noted that regions of reversed velocity were associated with temperature inversions. He proposed that the reverse velocity was due to the temperature inversion. Since the governing equations of natural convection require simultaneous solution for velocity and temperature, this simple explanation cannot fully explain the observation. One notes that the temperature inversion results from fluid entrainment which then promotes velocity reversal. One also has to consider the local forces of shear and buoyancy which may combine so that a zero mean velocity may not result at the position of zero buoyancy force. In addition one notes that the presence of a temperature inversion is no guarantee of velocity reversal as shown by Jaluria and Gebhart [37].

Giel and Schmidt [15], Schmidt and Wang [14] and Cowan et al [12] have all found that the thermal boundary layer has been thinner than the velocity boundary layer. In addition they found that the regions of temperature inversion were of limited extent, with the central portions of the cavity temperature profiles being horizontal. This was not the case for Ziai [1] and Renault and Doan-Kim-Son [30] who found that the regions of temperature inversion met at the centre-line of their air cavities. The inversions observed by Renault and Doan-Kim-Son [30] did not result in a

velocity reversal because of the restrictions of their relatively small cavity width, but those of Ziai [1] are predicted to have done so. The temperature inversions observed by Schmidt and Wang [14] did not superimpose on the region of velocity reversal indicating that local buoyancy forces were less than those of shear (see Figure 2.13).

Zhukauskas [41] in a study of the effect of surface roughness on forced convective heat transfer along horizontal boundaries, stated that the heat transfer was related to the thickness of the thermal sub-layer. The greater the thickness, or the lower the thermal conductivity of the fluid, the lower the heat transfer rate. With an increase in Pr the percentage of the local temperature drop through the thermal sub-layer was said to increase. Typically it was 25% for air and 90% for transformer oil. Ziai [1] has been the only researcher to report on the size of the thermal sub-layer for an air cavity. He found it to be approximately 1.6mm, as compared to aproximately 2.0mm for an isothermal vertical flat plate, in an isothermal environment, reported by Ierokipiotis [42]. Ziai [1] found the thermal sub-layer to account for approximately 25% of the local temperature drop.

Zhukauskas [41] also reported that any surface roughness which enhanced heat transfer was comparable in height to that of the thermal sub-layer, thus indicating the dominance of the thermal sub-layer in heat transfer. This also shows that walls constructed from materials which have undergone standard surface forming processes will not be rough enough to promote enhanced heat transfer.

Sparrow and Azevedo [43] carried out experiments in water using a heated wall, and an inert wall, where the spacing between the two was varied with all ends left open. The range of Ra_H investigated was 10^5-10^9 which meant that the flow was laminar. The spacing, L, was varied from approximately 30% of the thermal boundary layer thickness to infinity (i.e. a vertical flat plate). It was found that for a constant Ra_H a change in the overall heat transfer occurred at L/H = 0.032, where decreasing L resulted in decreasing heat transfer. The spacing at which the change was noted was essentially that of the thickness of the thermal boundary layer on the heated wall, which was calculated to fully occupy the spacing at L/H = 0.028 (making the thickness of the thermal boundary layer approximately 4mm). Therefore it is certainly probable that when the thermal boundary layers on the two walls of a cavity meet in the centre, the heat transfer will be different to the case when they do not. It has been previously suggested that the meeting of the velocity boundary layers affects the onset of transition and so any change of heat transfer. It certainly seems

likely that restriction of both the thermal and velocity boundary layers contribute to changes in heat transfer.

2.8 CORE STRATIFICATION

As previously stated the vertical centre-line temperature for boundary layer regimes is virtually always stratified. This is generally referred to as the core stratification. However, one must be very careful in defining a "core". Early researchers considered the core to be a region of fluid around which there was a flow which was responsible for heat transfer. But now one may attempt to define the core relative to the velocity or thermal boundary layers, or to the magnitude of the turbulence heat flux across the cavity. When choosing between a definition based on the velocity or thermal boundary layers one notes that the work discussed in Section 2.3.3, showed that during transition the temperature fluctuations occurred as a result of fluctuations in velocity. Therefore one may favour the definition of a core in relation to the velocity boundary layer as temperature fluctuations are more dependent on velocity fluctuations, rather than vice versa.

When considering the velocity boundary layer there are two possible definitions. Firstly, the core is that region which exists beyond the velocity boundary layer which ends at the first position of zero velocity. Secondly, the core is that region which exists beyond the region of reversed flow outside the boundary layer. The logical choice is the first definition, so that one need only consider two regions, the boundary layer and the core. Of course, this does mean that the core may be divided into two regions; one of non-zero, and one of zero, mean vertical velocity.

In the case of Schmidt and Wang [14], the reversed flow regions were of limited extent and a quiescent region was found to exist where the mean vertical velocity was zero. The work reported by Ziai [1] indicated that the regions of reversed flow met at the cavity centre-line, and that the core exhibited fluctuations in temperature. Ziai [1] expressed surprise at the existence of these temperature fluctuations because Schmidt and Wang [14] had described their core as quiescent. But one can clearly see that it was the lack of appreciation of the division of the core into two regions which lead to Ziai's comments.

As for the work of Renault and Doan-Kim-Son [30], one sees that with the boundary layers meeting at the centre-line without flow reversal, no core could possibly exist when using the current definition.

A definition of a core in relation to the turbulence heat flux across the cavity is in keeping with the early view that the core was not

responsible for heat transfer. The only known data for $\rho Cp\overline{v'T'}$ from a cavity is that which was measured by another researcher at Q.M.C. (Mr. A. Bowles [89] as the present study was drawing to a close. These data, and their relation to the thermal boundary layer, are reviewed in the Results and Discussion.

One other frequently claimed feature of the vertical centre-line temperature distribution is that it is linear. One notes from Cowan et al [12] and Schmidt and Wang [14] that if all closing boundaries are well insulated, and there is a substantial core, then there is a linear stratification.

Giel and Schmidt [15] showed a linear stratification up to x/H = 0.67 from which point the temperature gradient started to increase, whereas Ziai [1] showed a linear region up to x/H = 0.77 from which point the temperature gradient decreased. It is possible that the different flow regions may have some effect as Renault [32] found that the centre-line stratification was linear except for the section below x/H = 0.2 where a much thinner "laminar aspect" region existed.

Ziai [1], whose velocity profiles suggested similar flow regions to those of Renault [32], showed that the data for the region up to x/H = 0.23 could form their own region of linear stratification. The remaining data would then form a linear region extending much further than x/H = 0.77. The data of Giel and Schmidt [15], with laminar regions on both walls, are harder to account for, but it is possible to construct separate linear regions of stratification above and below mid-height. These can be seen to be mirror images, either one acting as the original and being subject to two reflections.

Perhaps the most surprising difference in the core stratification has been the equation of the line representing it. All data for transitional and turbulent boundary layer regimes are plotted on Figure 2.16. Cowan et al [12] reported the equation of the non-dimensional temperature, as a function of non-dimensional height, to be:

$$\theta = 0.54(x/H) + 0.34 \qquad (2.13)$$

Schmidt and Wang [14] reported:

$$\theta = 0.70(x/H) + 0.11 \qquad (2.14)$$

Giel and Schmidt [15] reported:

$$\theta = 0.65(x/H) + 0.11 \qquad (2.15)$$

Equation (2.13) is an average of measurements from four runs utilizing different cavity aspect ratios. There was some scatter exhibited by the data, so one cannot be too surprised at the difference between equations

(2.14) and (2.15) which are from the same apparatus, but at different aspect ratios. No trend indicating an increase of the centre-line temperature, with increasing aspect ratio, was found by Cowan et al [12]. One might have expected this if the cavity insulation had not been adequate, since the decrease in L would have decreased the surface area through which heat transfer losses could have taken place, so generally increasing the temperature at the vertical centre-line.

For air cavities the following have been reported. Firstly Ziai [1]:

$$\theta \simeq 0.50(x/H) + 0.19 \qquad (2.16)$$

Secondly Renault [32]:

$$\theta \simeq 0.41(x/H) + 0.14 \qquad (2.17)$$

It is thought that the poor levels of insulation on the air cavities resulted in lower temperatures at the centre-line than would have occurred for adiabatic boundaries. Hence, generally speaking, the magnitude of θ at any x/H is greater for a well insulated water cavity than a poorly insulated air cavity. This is discussed further in Section 2.13.

For an ethyl-alcohol cavity Kutateladze [35] presented two centre-line temperature distributions. Firstly for $Ra_H = 5.55\times10^{10}$ and H/L = 8.06:

$$\theta = 0.55(x/H) + 0.23 \qquad (2.18)$$

Secondly for $Ra_H = 9.34\times10^{10}$ and H/L = 21.94:

$$\theta \simeq 0.38(x/H) + 0.35 \qquad (2.19)$$

Equation (2.18) has a gradient which is compatible with the general value of 0.55 found by Ziai [1] to exist for all boundary layer regimes. But the most interesting observation arises from Figure 2.16 which depicts the data giving rise to equation (2.19). Here one can see that the stratification at the end of each cavity is stronger than for the data for equation (2.18), but is less in the central region. It would appear that the increase in aspect ratio (brought about by an increase in H and a decrease in L) has started a trend towards the centre-line temperature distribution reported by Ralph et al [31]. Regretably no boundary layer information was presented for these conditions to compare with that of Ralph et al [31].

For the case of a fluid (whose only temperature dependent property is density) enclosed in a cavity with adiabatic closing boundaries, one would expect θ to be 0.5 at x/H = 0.5 because all features (e.g. flow pattern and temperature distribution) would be expected to be anti-symmetric. With heat loss through the closing boundaries one might expect θ at mid-height to be less than 0.5 as was reported by those using air cavities. The ethyl-alcohol cavity of Kutateladze [35] showed $\theta \simeq 0.51$, whereas the well

insulated water cavity of Schmidt and Wang [14] showed $\theta \simeq 0.46$, both at mid-height.

The water cavity of Cowan et al [12] showed $\theta \simeq 0.61$ at mid-height. One may consider this to be: the true value, as the cavity was well insulated against heat losses; a false value, because of additional heat input by the incorrect setting of guard heaters; or a false value due to a constant uncertainty in the y intercept of the equation. Without recourse to the original data one cannot claim that either of the last two explanations are correct. However, one may try to gain an indication as to whether θ should be greater than 0.5 at mid-height by assuming that the heat transfer from the heated wall and to the cooled wall, are equal at mid-height. Taking into account the temperature dependence of the thermal conductivity of air and water, one finds that the greater temperature difference, between wall and cavity centre, should be on the cooled wall side, thus indicating that at $x/H = 0.5$ one should expect $\theta > 0.5$.

Eckert and Carlson [4] reported the centre-line temperature for a laminar boundary layer regime in an air cavity to be:

$$\theta \simeq 0.54(x/H) + 0.17 \qquad (2.20)$$

This is very similar to equations (2.16) and (2.17) indicating either that the centre-line temperature distribution for different regimes is very similar, or that researchers have tended to use the lower points on a graph (which are associated with a laminar region) to draw a line of best fit.

Ostrach [44] proposed that the non-dimensional temperature gradient may decrease as Pr increases, but this has not been supported by the available evidence for the transitional and turbulent boundary layer regimes.

2.9 TURBULENCE QUANTITIES

Apart from the R.M.S. of velocity and temperature fluctuation data, no experimental data on turbulence quantities have been reported for cavity flow. One must therefore turn to the limited amount of experimental and numerical data available for the vertical flat plate, to gain an insight into the likely distributions of turbulence quantities in cavity flow. Certainly one would expect the near wall region in both cases to be similar.

Before proceeding one should note that some of the data presented in experimental papers has been derived from graphical interpretation because of the limitations of the measuring equipment used. These data are generally subject to unknown levels of uncertainty, due to both the

measuring equipment and the subjective interpretation of graphs. In addition one must note that the available numerical data are generally unsubstantiated by direct comparison with experimental work in identical conditions. These numerical data are only expected to indicate possible trends, but, because of the lack of any type of data, they must be included in this survey.

2.9.1 THE REYNOLDS STRESS $\rho\overline{u'v'}$

Miyamoto et al [45] undertook measurements, using a one-component Laser Doppler anemometer and a thermocouple, of the natural convection flow of air on a constant heat flux, heated, vertical plate. Profiles of $\overline{u'T'}$, $\overline{v'T'}$ and $\overline{u'v'}$ were presented.

Miyamoto et al [45] had to calculate $\overline{u'v'}$ using graphical interpretation because only a one-component anemometer was available. In order to do this the wall shear stresses would have had to be estimated, but no such data were reported. The calculations indicated that $\overline{u'v'}$ was negative in a small region near the wall up to $Nu_y = 0.8\text{-}1.0$, after which $\overline{u'v'}$ was positive for the remainder of the profile which peaked at $Nu_y \approx 10$. The magnitude of the negative peak was approximately 6% of the positive peak.

Ierokipiotis [42] also presented profiles of $\overline{u'v'}$ derived from one-component Laser Doppler anemometer data, which again showed the negative region extending up to $Nu_y \approx 1.1$. The positive peak occurred at $Nu_y \approx 17$, and the magnitude of the negative peak was approximately 9% of the positive one.

Visual observations of the large eddy structure of the natural convection flow of water along a constant heat flux wall were made by Kitamura et al [46]. They observed that high velocity fluid was ejected outwards and that low velocity fluid flowed towards the wall to replace that ejected. At $Nu_y = 0.86$ and 4.9 they deduced that $\overline{u'v'}$ should be positive, thus confirming the quality of the data at $Nu_y = 4.9$ of Miyamoto et al [45] and Ierokipiotis [42].

The only other $\overline{u'v'}$ data available were presented by To and Humphrey [47] who undertook numerical calculations for the natural convection of air along a vertical flat plate. They reported the existence of the negative region but it's peak was much higher than those of the previously decribed experimental data, with the zero position at $Nu_y = 1.7$. The high magnitude of the peak invalidates the results as it is generally accepted that $\overline{u'v'}$ must be very small in the near wall region. In addition they did comment

that their scaling of mean velocity using the shear velocity produced meaningless results which was surprising as Ierokipiotis [42] had found reasonable agreement using this scale. One can see the reason for this in their Figure 8. It showed the calculated velocity gradient as decreasing very close to the wall. This is impossible, and so all their near wall results must be considered to be of little value, if any.

For positions far from the wall the numerical results of To and Humphrey [47] for $\overline{u'v'}$ did exhibit the positive peak in approximately the same position indicated by Miyamoto et al [45].

2.9.2 THE LATERAL AND VERTICAL TURBULENCE HEAT FLUXES

Turning attention to $\overline{v'T'}$, which is representative of the lateral turbulence heat flux $\rho C_p\overline{v'T'}$, one notes that the experimental work of Ierokipiotis [42] and Miyamoto et al [45], and the numerical work of To and Humphrey [47], have all produced results exhibiting the same general graphical trend, but with $\overline{v'T'}$ taking different magnitudes in each case. The quantity $\overline{v'T'}$ was seen to be positive everywhere, peaking at $Nu_Y \approx 2.4$ (the region of values extending to $Nu_Y \approx 30$).

Rather curiously Miyamoto et al [45] and To and Humphrey [47] both presented the profile of $\overline{u'T'}/(\overline{u'u'})^{0.5}(\overline{T'T'})^{0.5}$ (the correlation coefficient) instead of $\overline{u'T'}$ (which is representative of the vertical turbulence heat flux $\rho C_p\overline{u'T'}$). Both sets of data agree well for $Nu_Y > 3.5$ where they are constant at approximately 0.6. Close to the wall Miyamoto et al [45] reported negative values out to $Nu_Y \approx 0.4$.

2.9.3 THE TRANSITION REGION

The transition region was considered by Jaluria and Gebhart [20] who presented plots of the normalised local maximum of u' and T' across the boundary layers. The velocity plot was found to exhibit two peaks and the temperature plot one peak. This confirmed previous observations by other researchers. The flattening of the graph towards the end of transition was attributed to the increase in eddy size which was damped by the external low velocity flow.

Miyamoto et al [45] found differences between the transitional and fully developed turbulent regions, which was to be expected. A profile of $(\overline{u'u'}/\overline{v'v'})^{0.5}$ was approximately constant at 2 for all Nu_Y in the transitional region. Whereas the turbulent region differed near to the wall ($Nu_Y < 3$) by showing a much larger value. For the turbulent region their profiles of $(\overline{u'u'})^{0.5}/u_{max}$ had a maximum peak at $Nu_Y \approx 6$ compared to 1.5

for u/u_{MAX}. This was in contrast to that of Giel and Schmidt [15] whose water cavity data showed that the mean velocity and R.M.S. of velocity fluctuations peaked at approximately the same position.

The $(\overline{v'v'})^{0.5}/u_{MAX}$ data of Miyamoto et al [45] at three different heights, in the fully developed turbulent region, collapsed reasonably well peaking at $Nu_Y \approx 10$.

Bill and Gebhart [48] reported on the development of turbulence quantities during transition along a vertical flat plate, using hot-wire anemometers. Miyamoto et al [45] and Ierokipiotis [42] have shown that data from hot-wire anemometers are not reliable in natural convection flow, and so only general trends from hot-wire data are useful. The data of Bill and Gebhart [48] showed that during transition the non-dimensionalised peak values of $\overline{u'u'}$, $\overline{v'v'}$, $\overline{u'T'}$ and $\overline{v'T'}$ all increased to a maximum at the end of transition. The non-dimensionalising quantity in each case was the maximum peak value in the transition region.

2.9.4 TURBULENCE KINETIC ENERGY

For a water cavity operating at $Ra_H \approx 6.3\times10^{10}$ Ozoe et al [33] reported numerically predicted profiles of turbulence kinetic energy with two peaks, which were most noticeable at mid-height. The magnitude of the inner peak, compared to that of the outer one, varied with height. They claimed the two-peak profile to be characteristic of turbulent natural convection, and stated further that Miyamoto et al [45] also showed the two peak phenomenon in a profile of $\overline{u'u'}$. Examination of this data revealed that there was a very small secondary peak on the wall side of the main peak. But, the $\overline{v'v'}$ data did not show such a peak and neither did the sum of $\overline{u'u'}$ and $\overline{v'v'}$.

To and Humphrey [47] looked at G, the production of turbulence kinetic energy by buoyancy, $-g\overline{u'\rho'}$, and P, the production of turbulence kinetic energy by shear, $-\rho\overline{u'v'}du/dy$. It has already been noted that their near wall results were invalid, just how this may have affected their outer region results is unclear, but these results are worthy of comment for future comparison. Both buoyancy and shear production were positive at all positions away from the near wall region (shear production zero at the mean velocity peak). Buoyancy production was always less than that of shear. Dissipation and convection were the major sink mechanisms of the turbulence kinetic energy.

Fraikin et al [49] numerically predicted G and P for an air cavity at $Ra_H = 10^6$ with a linear temperature gradient on both the floor and ceiling.

For this case, where one expects most of the flow to be laminar with turbulent regions only in the vicinity of the floor and ceiling (see Section 2.12) G was found to be negative everywhere except in the starting corners and in the flow along the floor and ceiling, where it was of a comparable magnitude to *P*. For an adiabatic floor and ceiling one would have expected G to be negative rather than positive. As would be expected, the sum G + P was found to be negative in the central region of the cavity.

The temperature spectra of Ziai [1] were said to support the idea that in the core the dominant source/sink term, in the turbulence kinetic energy equation, was the sink term due to buoyancy effects. Whilst in the boundary layer the shear stress term dominated that of the buoyancy term. This agrees with the work of Fraikin et al [49].

2.10 TURBULENCE SPECTRA

Corrsin [50] considered the one and three-dimensional spectral equations for a field of temperature fluctuations, in stationary isotropic turbulence. He predicted the dependence of the power spectral density on wavenumber, for what he termed intermediate and high wavenumber ranges. He considered the intermediate wavenumber range to be where all of the fluctuation "energy", entering such a range, passed through the range with no appreciable "dissipation" by molecular effects. This "dissipation" was meant to describe the smearing out of temperature fluctuations by thermal conductivity. His postulates rendered his results applicable only to the intermediate wavenumber range for temperature which overlapped with that of the velocity spectrum. The result was that the power spectral density was proportional to wavenumber, and hence frequency, to the power -5/3. He compared this to previous work on velocity spectra which yielded the same result.

For a high wavenumber range, considered to be where molecular effects were not negligible, the power spectral density was predicted by Corrsin [50] to be proportional to wavenumber to the power -7 (the same as previous predictions for velocity). He postulated the existence of a cut-off wavenumber where viscous effects were dominant. The suggestion was that as Pr goes to zero the temperature spectrum would cut-off at a lower value than the velocity spectrum, with the opposite as Pr approached infinity. The ratio of the thermal to velocity cut-off numbers was predicted to be $Pr^{0.75}$. For the case of air this would be 0.77.

Bolgiano [51] went a stage further and considered turbulent spectra in a stably stratified atmosphere. The primary thought was that the buoyancy

forces would modify the turbulence spectra by removing kinetic energy from the turbulent field at the driving scales, and also (because of the anisotropic fluctuations caused by the stratification) to "bleed" the turbulence over a wide range of scales. He postulated that the spectrum may be divided into three ranges. Firstly a buoyancy sub-range, associated with lower wavenumbers, and characterising the larger anisotropic eddies directly influenced by the stratification. Secondly, an inertial sub-range where anisotropy had been erased, and thirdly a dissipation sub-range at high wavenumbers where molecular effects dominated. Corrsin [50] had already described the latter two sub-ranges. The new power dependencies of the wavenumber for the buoyancy sub-range were -11/5 for the velocity spectrum and -7/5 for the temperature spectrum.

Bolgiano [51] went on to say that there were two limits which would determine the existence of the buoyancy and inertial sub-ranges. Firstly, and most obvious, is that under neutral conditions the buoyancy sub-range would not exist. Secondly, above a given level of stratification the flow would be entirely anisotropic and the inertial sub-range would not exist.

Perhaps of some interest is the note in the introduction of Bolgiano [51], that the exponent in the inertial sub-range of the atmosphere had been observed to be in the range -4 to -7, the exact value depending on the Richardson number of the atmospheric layer (which is in turn dependent on the temperature gradient). From this observation one might expect to see the exponent in any inertial sub-range, found in cavity flow, to vary across the thermal boundary layer because of the variation of the vertical temperature gradient.

A number of researchers have presented turbulence spectra for a natural convection flow along a vertical flat plate in a practically isothermal environment. Bill and Gebhart [48] using water presented velocity and temperature spectra for different lateral positions at a height corresponding to just downstream of the completion of transition. The frequency range covered was 0.006-10Hz, the upper limit being determined by their measuring equipment. At the lower frequencies substantial differences were found between the spectra, indicating that the energy within the larger eddies changed across the boundary layer. At higher frequencies ($f > 0.5$Hz) the agreement between spectra was good and an exponent of -3 was found. Although they did not attempt to fit an exponent to the low frequency data one can quite easily fit a -5/3 exponent to this data at the near wall position.

Dastbaz [26] presented spectra for the latter stages of transition of the natural convection of air along a vertical flat plate. He found that three exponents existed. They were -5/3, -3 and -17/3, and were applicable to low, intermediate and high frequencies (up to 25Hz) respectively. These can be compared to those of -1, -5/3 and -5 found by Smith [27] in the fully developed turbulent region using the same apparatus.

Papailou and Lykoudis [52] presented temperature spectra for the natural convection flow of mercury next to a heated wall in a cell. The -5/3 range was not observed at lateral stations close to the wall and was only present for a small frequency range in data from the edge of the boundary layer. This indicated substantial anisotropy of the turbulence. At all lateral stations a substantial -3 range was observed (where both -5/3 and -3 were observed the latter was at higher frequencies).

Ziai [1] was the first to present velocity and temperature spectra for the transitional boundary layer regime in a cavity. His spectra indicated wavenumber exponents of -5/3 and -3 for both velocity and temperature. The -5/3 range existed at lower frequencies than did the -3 range for all the fully developed, turbulent region, data. However, the reverse was true for the data taken close to the bottom of the heated wall where the flow was speculated to have a "laminar aspect".

One notes that whenever a -3 exponent has been observed the general trend is for a -5/3 exponent to have existed at the lower frequencies. All researchers have stated that the -3 exponent was predicted by Shur [53] and Lumley [54]. But Shur [53] proposed the opposite, with -3 at the lower wavenumbers.

Shur [53] presented spectra of velocity measured in clear air turbulence which exhibited a -3 exponent at low wave-numbers and one of -5/3 at higher wave-numbers. Lumley [54] had proposed that this would result if the transfer of energy, due to work done by buoyancy forces against gravity, was small compared to the local spectral density flux and was indicative of the effects of G (the production of turbulence kinetic energy by buoyancy forces) upon the cascade of energy.

The reason why Ziai [1] observed the exponent characteristics proposed by Shur [53] at the bottom of the heated wall and the top of the cooled wall is not known. Clearly one must attempt to investigate the local temperature gradient and value of G (the production of turbulence kinetic energy due to buoyancy) in all cases to see if an increase in the temperature gradient or decrease in G promotes such a result.

As regards the dissipation sub-range proposed by Corrsin [50] no evidence of the -7 exponent has been found. The only dissipation sub-ranges to have been observed were those of Dastbaz [26] and Smith [27] of -17/3 and -5 respectively. The difference between the two may have been due to different environmental conditions resulting in different local Richardson numbers, whose effect has been noted by Bolgiano [51].

The buoyancy sub-range of Bolgiano [51] has had limited support from the work of Smith [27].

Regrettably most researchers have only presented their spectra based *on frequency instead of wavenumber (wavenumber can be considered to be* $2\pi f/u$ as proposed by Taylor, but, such a definition is not satisfactory for all examples of turbulent flow). It is clear from the extensive work of Ziai [1] that the frequency ranges which are applicable to an exponent vary with lateral position (and so local velocity) therefore it is quite possible that the wavenumber ranges may be constant.

Temperature spectra were presented by Giel and Schmidt [15] for cavity flow for the height at which transition commenced, and at a height where turbulent flow conditions had been established. One can estimate from their data that two exponent ranges existed. The exponents were -3.75 and -6.

2.11 VELOCITY, LENGTH AND TEMPERATURE SCALES

Ostrach [55] commented on the lack of any standard in the scaling of velocity, length and temperature, and rightly pointed out that this makes the comparison of different sets of data difficult. He also noted the lack of uncertainty estimations which increases the difficulty of appraising any proposed scale when using existing data.

There have been only two attempts to analytically predict appropriate scales. Those of George and Capp [56] and Cheesewright [57]. Both analyses have been carried out for a vertical flat plate in an isothermal environment. The main problem, which they both comment on, is that natural convection flow is one of multiple scales, with different scales being applicable in inner and outer regions. This viewpoint was confirmed by Zhong et al [58].

Any attempt to derive velocity, length and temperature scales must begin with the conservation equations of mass, momentum and energy. For different regions of the boundary layers one may, by order of magnitude arguments, reduce the equations to slightly different forms. The variables left in the equations, and any relevant boundary conditions, must then form the set from which scales may be constructed.

2.11.1 SCALES IN THE NEAR WALL REGION

Consider the region near the wall which is normally considered to extend to the velocity peak. This region can be sub-divided into an inner one which includes both the thermal and viscous sub-layers, and an outer one. For the whole region, it can be shown that the inertia terms on the left hand side of equations (1.5) and (1.6) are negligible so that one has equations (2.21) and (2.22) representing the momentum and energy equations, respectively. Note that the common representation of the buoyancy term is used in equation (2.21), rather than that used in equation (1.5).

$$0 = g\beta_T(T-T_\infty) + (\mu/\rho)\frac{d^2u}{dy^2} - \frac{d\overline{u'v'}}{dy} \qquad (2.21)$$

$$0 = \alpha\frac{d^2T}{dy^2} - \frac{d\overline{v'T'}}{dy} \qquad (2.22)$$

The boundary conditions at y = 0 are as follows.

(i) $u = 0$, (ii) $\mu du/dy = \tau_\omega$, (iii) $T = T_\omega$, (iv) $-k_\omega dT/dy = \dot{Q}''_\omega$

The work of George and Capp [56] has been superseded by the work of Cheesewright [57] which has shown that a number of false assumptions were made in the former. Cheesewright [57] identified three velocity, three length and one temperature scale in the region under consideration. Cheesewright integrated the momentum and energy equations, once, and used all the variables in the two equations for his dimensional analysis. In doing this he also defined a number of quantities. The integrated equations were:

$$u_\tau^2 = B\,\theta\,dy + (\mu/\rho)\frac{du}{dy} - \overline{u'v'} \qquad (2.23)$$

$$-Q_T = \alpha\frac{d\theta}{dy} - \overline{v'\theta'} \qquad (2.24)$$

Where $\theta = (T-T_\infty)/(T_\omega-T_\infty)$; $B = g\beta_T(T_\omega-T_\infty)$; $Q_T = \dot{Q}''_\omega/[\rho Cp(T_\omega-T_\infty)]$

2.11.1.1 TEMPERATURE SCALES

From equations (2.23) and (2.24) Cheesewright [57] wrote:

$\theta = \theta(Q_T,\alpha,y,(\mu/\rho),u_\tau,B)$ and $u = u(Q_T,\alpha,y,(\mu/\rho),u_\tau,B)$

From dimensional analysis Cheesewright [57] determined that:

$\theta = \theta(Nu_v,Gr_v,y^+,Pr)$

The above function shows the non-dimensional temperature as a function of three non-dimensional lengths and the Prandtl number. Cheesewright [57] showed that if the overall heat transfer relationship was of the form $Nu_x = Gr_x^{1/3}\, f_1(Pr)$ then $Nu_v = Gr_v^{1/3}\, f_1(Pr)$ and that if the wall shear stress relationship was of the form $\tau_\omega/[\rho_\omega Bx] = Gr_x^{-1/3}\, f_2(Pr)$

then one could write $y^+ = Gr_y^{1/3} f_2(Pr)$. Therefore each non-dimensional length could be represented as a function of another with the constant of proportionality being a function of the Prandtl number.

In examining the temperature profile in close detail Cheesewright [57] found that in the thermal sub-layer, where $\overline{v'\theta'}$ is negligible, equation (2.24) could be written as:

$$\theta \approx 1 - Nu_y \qquad (2.25)$$

In the outer part of the near wall region Cheesewright [57] presented arguments to support the proposal that $d\theta/dy$ is independent of (μ/ρ) and α. In addition he argued that as $Gr_\infty \to \infty$ the temperature profile would only be dependent on one non-dimensional length. He chose Nu_y and proposed that for $d\theta/dy$ to be independent of (μ/ρ) and α then:

$$\theta = C_0 \ln(Nu_y) + C_1(Pr) \qquad (2.26)$$

From experimental data, for $1.0 < Nu_y < 3.0$, and $0.7 < Pr < 33$ Cheesewright [57] proposed that:

$$\theta = 0.28 - 0.08 \ln(Nu_y) \qquad (2.27)$$

The non-dimensional temperature θ was used sucessfully in conjunction with Nu_y by Jarokipiotis [42] to collapse his full temperature profiles. Cheesewright and Ziai [59] used the same scales for the temperature profiles from an air cavity. They found excellent collapse of profiles and agreement with flat plate profiles out to $Nu_y \approx 0.7$. Beyond this position the profiles from the fully developed turbulent region showed very good agreement between themselves, but there was no agreement with the flat plate data. This disagreement arose from the stratification present at the cavity centre-line giving rise to negative values of θ. From this observation it was suggested that the stratification introduced an additional length scale in the outer region. However, it remains to be seen if an improvement in agreement between the flat plate and cavity profiles can be achieved by using the maximum value of $(T_w - T)$, to which the heat transfer rate responds, instead of $(T_w - T_\infty)$.

Cheesewright and Ziai [59] had suggested that the thermal sub-layer ended at $Nu_y \approx 0.35$ and that the region where the thermal transport was dominated by turbulence effects began at $Nu_y \approx 2$. The more rapid fall off of the cavity temperature profile beyond this point indicated to Cheesewright and Ziai [59] that the turbulence levels in this region were reduced as compared to those for a vertical flat plate. This must have been due to the damping effect of the stratification. The stratification has also been seen to delay transition which is characterised by amplification of disturbances at the outer inflexion point of the boundary layer.

Most surprising of all was the disagreement of the temperature profiles for the heated and cooled walls of Cheesewright and Ziai [59]. Agreement out to the edge of the thermal sub-layer was reasonable but otherwise poor. One notes from Ziai [1] that there was some doubt as to the validity of his heat transfer rates at both walls. His graph of local Nusselt number against Grashof number showed a lower heat transfer for the cooled region. One would certainly not have expected this as his cooled wall flow was initially more turbulent than his heated wall flow. Thus one would have anticipated the reverse. It is therefore possible that some of the disagreement between heated and cooled wall temperature profiles has resulted from uncertainties in the data.

The $[\overline{T'T'}]^{0.5}$ data of Cheesewright and Ziai [59] collapsed reasonably well and agreed with flat plate data, except at the outer edge of the boundary layer, when using Nu_y and (T_w-T_∞).

The dimensionless group θ was used in conjunction with the length scale $[\alpha^2/g\beta_T(T_w-T_\infty)]^{1/3}$ by George and Capp [56] who found their data to collapse well. Subsequent work by Ierokipiotis [42] did show some support for these scales, as did Siebers et al [60] who included a multiplier in the length scale to account for temperature dependent properties when they were calculated at T_∞. The multiplier was:

$$(k_w/k_\infty)(T_w/T_\infty)^{0.14}$$

One must note that the data presented for these scales has been for air only. Siebers et al [60] did present water data but used a different length scale. The scale they used was the integral with respect to y of θ. They found the data to collapse very well claiming that the integral of $(T-T_\infty)$ with respect to y was dynamically significant as it appears in the x direction momentum equation when it is integrated with respect to y. George and Capp [56] had dismissed this as not being significant.

Further support for the modified George and Capp [56] length scale came from To and Humphrey [47] who found their numerical calculations for air to collapse with the air data of Siebers et al [60].

2.11.1.2 VELOCITY SCALES

In the case of velocity Cheesewright [57] found that any of three non-dimensional velocities could be represented as a function of the three non-dimensional lengths and the Prandtl number. The velocity scales which he identified were:

(i) $(\tau_w/\rho_w)^{1/2} = u_\tau$ (ii) $[g\beta_T(T_w-T_\infty)(\mu/\rho)]^{1/3} = [B(\mu/\rho)]^{1/3}$

(iii) $\dot{Q}''_w/[\rho Cp(T_w-T_\infty)] = Q_T$

Alternatively, any of the non-dimensional velocities could be represented as a function of the Prandtl number, a non-dimensional length and two ratios of the velocity scales. Most notably Cheesewright [57] proposed:

$$\frac{u}{[B(\mu/\rho)]^{1/3}} = f(Gr_v, \frac{u_\tau}{[B(\mu/\rho)]^{1/3}}, \frac{Q_T}{[B(\mu/\rho)]^{1/3}}, Pr)$$

In the region common to both the viscous and thermal sub-layers Cheesewright [57] showed that the equation in this region could be written as:

$$\frac{u}{[B(\mu/\rho)]^{1/3}} = \frac{u_\tau^2}{[B(\mu/\rho)]^{2/3}} Nu_v - \frac{Nu_v^2}{2}\left\{1 - \frac{Nu_v}{3}\frac{Q_T}{[B(\mu/\rho)]^{1/3}} Pr\right\} \quad (2.28)$$

In attempting to derive an equation for the velocity profile in the outer part of the near wall region Cheesewright [57] argued that du/dy was not independent of α, but may be considered to be independent of (μ/ρ). He proposed that:

$$\frac{u}{B\alpha/Q_T^2} = \frac{-C_\theta}{0.92}\left\{\frac{u_\tau^2 Q_T}{B\alpha} ln(Nu_v) - (C_1 - 2C_\theta)Nu_v + C_\theta Nu_v ln Nu_v\right\} + C_3 \quad (2.29)$$

One may comment on the probable applicability of the length scales in relation to a stratified environment, as the scales in the near wall region for an isothermal and stratified environment are expected to be the same. Bergholz [21] and Jaluria and Gebhart [37] have shown that with increasing stratification, for a constant temperature difference $(T_\omega - T_\infty)$, the position of the mean velocity peak moves towards the wall; the wall shear stress decreases; and the wall heat flux increases. One clearly sees that any attempt to use the buoyancy and wall shear stress length scales out to the peak will not be acceptable, as they will not account for the movement of the peak. Only the thermal length scale exhibits the potential to do this by itself. If the thermal length scale were suitable then one notes that the heat transfer coefficient would have to vary slightly to take into account any movement of the peak away from the wall as x increases within a cavity.

The change of the magnitude of the mean velocity peak with changing stratification indicates that the thermal and buoyancy velocity scales cannot be applicable themselves. However, virtually the same velocity scale as the buoyancy one was proposed by George and Capp [56] except they used α instead of (μ/ρ). This, they claimed, collapsed the data available to them in conjunction with $[\alpha^2/g\beta_T(T_\omega - T_\infty)]^{1/3}$ for length. The numerical data of To

and Humphrey [47] and the L.D.A. data of Cheesewright and Ierikipiotis [61] and Miyamoto et al [45] all lent support to the use of these scales for an isothermal environment, but the resulting graphs using the data from these researchers were different to that of George and Capp [56] who only had hot-wire data to work from.

Turning back to the numerical work of Jaluria and Gebhart [37] for a stratified environment, one notes that for a given local temperature drop the heat transfer and mean velocity are dependent on the stratification. This suggests that the shear velocity may be a suitable velocity scale, or that any velocity scale should take into account the heat transfer coefficient and the temperature difference (the latter must be used as the heat transfer coefficient is expected to be approximately constant with height for specific boundary conditions).

The shear velocity was considered as a scale by George and Capp [56]. However, they were not happy with this choice as it could not be predicted, and was not considered to be a fundamental parameter because the viscous sub-layer was not one of constant shear stress. Cheesewright [57] has dismissed their views on the non-importance of the wall shear stress, and indeed, Ierokipiotis [42] did find reasonable agreement between full boundary layer profiles whilst using the shear velocity scale in conjunction with the length non-dimensionalised as Nu_v.

Chen and Eichorn [38] performed observations in water using a dye technique for the interesting case where at some height on a cylinder in a stratified environment $T_w = T_\infty$. For $S < 1.4$ the height at which the flow spread horizontally was below that at which $T_w = T_\infty$, which showed that for those conditions the actions of shear forces were easily able to eliminate the vertical motion before $T_w = T_\infty$. For $S > 1.4$ the flow did not spread horizontally until a height just above $T_w = T_\infty$, which indicated that the actions of shear forces were not able to overcome the flow's momentum at $T_w = T_\infty$. These observations present a minor problem in determining a velocity scale based on the heat transfer coefficient for small values of $(T_w - T_\infty)$.

2.11.2 THE OUTER REGION

In the outer region the inertia terms on the left hand side of equations (1.5) and (1.6) are not negligible, but those involving molecular transport are. Therefore one can write equations (2.30) and (2.31) which are the momentum and energy equations, respectively.

$$u\frac{du}{dx} + v\frac{du}{dy} = g\beta_T(T-T_\infty) - \frac{d\overline{u'v'}}{dy} \qquad (2.30)$$

$$u\frac{dT}{dx} + v\frac{dT}{dy} = \frac{d\overline{v'T'}}{dy} \qquad (2.31)$$

Cheesewright [57] put forward velocity scales for the outer region, they were:

(i) $(\tau_w/\rho_w)^{1/2}$ (ii) $[g\beta_T(T_w-T_\infty)\delta]^{1/2}$

(iii) $[kg\beta_T(T_w-T_\infty)^2/\dot{Q}''_w]^{1/2}$

The second velocity scale contains δ which was defined as the boundary layer thickness. This was the only length scale proposed.

The first and third velocity scales are seen to show some promise. Ierokipiotis [42] has presented full profiles using the first in conjunction with Nu_Y which collapsed his data quite well. But it is the third which may hold most promise as it incorporates the heat transfer coefficient and the temperature difference in the correct manner to account for the effects of stratification near the peak. However, in the region of reversed flow it would not account for the effects of stratification and another scale, as yet unknown, will be applicable in this region.

The current definition of δ does present some problems when one takes into account the boundary conditions of $u = 0$ and $T = T_\infty$ at $y = \delta$. The water data of Schmidt and Wang [14] show that at $y = \delta$ $u = 0$ and $T < T_\infty$. However, sufficient data do not exist for any further comment to be made.

George and Capp [56] did discuss the outer region proposing the velocity scale:

$[g\beta_T\delta\dot{Q}''_w/(\rho Cp)]^{1/3}$

The length scale, δ, was quoted as being an "appropriate" outer length scale and likely to be x dependent. The "boundary layer thickness" was the only offer of a measure of δ put forward by George and Capp [56] who claimed that it had been used as a scale, in conjunction with u_{MAX} for velocity, to collapse mean velocity profiles over the outer 90% of the boundary layer. However, what they defined as a boundary layer thickness was not the true value but a measure of it. They defined "boundary layer thickness" as:

$$\delta^* = \int \frac{u}{u_{MAX}}\,dy \qquad (2.32)$$

From data available to them, George and Capp [56] found that the ratio of u_{MAX} to their outer scale incorporating their version of δ ranged from 8.19 to 8.73 which forms a range of ±3% from the average.

Whilst the velocity scale proposed by George and Capp [56] for the outer region may have been suitable for the case of an isothermal environment, it does not necessarily follow that it would be applicable to the case of a stratified environment.

Catton et al [62] showed, for the laminar boundary layer regime, that as H/L increased for constant Ra_L the mid-height mass flow increased together with the boundary layer thickness, and that the velocity peak moved away from the wall. This indicated that scaling the entire velocity profile using u/u_{MAX} would prove difficult unless a suitable length scale, such as the boundary layer thickness, could be found to account for the movement of the peak.

2.12 FLOOR AND CEILING BOUNDARY CONDITIONS

The thermal boundary conditions on the floor and ceilinghave been shown to be of considerable importance to the levels of turbulence within a cavity.

Bauman et al [6] investigated the flow in a cavity of aspect ratio 0.5 and found that for a range of Ra_H of 2.0×10^6 to 6.75×10^9, the flow could be either laminar or turbulent, depending on the specific temperature distributions on the floor and ceiling.

Le Quere and Alziary de Roquefort [24] investigated numerically the influence of adiabatic and linear temperature gradient boundary conditions. Their study indicated that for aspect ratios in the range 1-10 the different conditions affected the critical Rayleigh number for the onset of unsteady motions. The linear temperature boundary condition lead to a decrease in the critical number for any given aspect ratio. As a consequence they pointed out the need to specify the boundary conditions of experimental work, in order that the validity of numerical calculations may be judged properly.

Le Quere and Alziary de Roquefort [24] also found that the critical Rayleigh number for linear temperature gradient boundary conditions increased as aspect ratio increased, and approached that for adiabatic conditions which was practically constant with changing aspect ratio. One associates this with the level of heat transfer through the boundaries which decreases with increasing aspect ratio. The aspect ratio was also noted to have one other effect. For large cavities the instability mechanism was hydrodynamic whereas for aspect ratio less than ≈ 2 it was thermal.

Briggs and Jones [22] found the linear temperature gradient boundary condition to be destabilizing. Heat transfer from the floor to the fluid

lead to locally upward moving fluid, and heat transfer from the fluid to the ceiling lead to locally downward moving fluid.

Elsherbiny et al [63] set out to study the effects of the floor and ceiling thermal boundary conditions on the flow and heat transfer. They stated that for most of the previous air experiments the boundary conditions will have probably been the linear temperature gradient type, as adiabatic conditions require that the effective thermal conductivity of the floor, or ceiling, and it's insulation be an order of magnitude less than that of the fluid. Having noted the importance of the floor and ceiling they then wrongly dismissed the vertical side walls as having little influence.

For the case of a linear temperature gradient Elsherbiny et al [63] expected heat transfer to the fluid at the floor and heat transfer from the fluid at the ceiling. This was assuming that the temperature of most of the fluid close to the floor was at or very near to T_c and that at the ceiling at or very near to T_H. They also distinguished between boundary conditions on the inner and outer faces of the finite walls which formed the floor and ceiling, saying that one may have an initially linear temperature gradient inner profile which would be influenced by the outer condition which could be a linear temperature gradient or constant temperature type. The extended linear temperature profile (linear temperature gradient at inner and outer faces) gave rise to a lower heat transfer (through floor or ceiling) for air at moderate to high Rayleigh number ($Ra_H \simeq 10^8$ to 10^{10}) than the normal case of inner linear temperature gradient and outer constant temperature.

Fraikin et al [49] undertook numerical calculations for a square cavity at $Ra_H = 10^8$, which they considered would give rise to turbulent flow. From Figure 2.2 one sees that with their floor and ceiling conditions of linear temperature gradient, most of the flow would have been laminar, with only small localised regions of turbulence due to heat transfer through the floor and ceiling. As previously stated, their model would have had to approximate the laminar regions as regions of low turbulence intensity and re-laminarization could not have been predicted, therefore strictly, the results were invalid.

However, it is worth noting some general trends in the results of Fraikin et al [49]. The maximum turbulent viscosity was predicted to be up to four times larger than the molecular viscosity and occurred at the starting corners (i.e. bottom of heated wall and top of cooled wall). The variation of turbulent viscosity confirmed that a laminar region should have occupied most of the cavity. The maximum values of turbulent viscosity were associated with the turbulent flow induced by heat transfer through

the floor and ceiling. Hence the previous observations of the destabilizing nature of the linear temperature gradient boundary condition are supported.

The only two reported distributions of temperature on the floor and ceiling have come from Bilski et al [64], who showed temperature distributions for ideal adiabatic and experimental conditions from a square air cavity, and Ziai [1]. Their data are reproduced as Figure 2.17, from which it can be seen that the experimental conditions are approximately that of a linear temperature gradient.

Catton et al [62] claimed the boundary conditions also affected the boundary layer. Linear temperature gradient conditions were said to yield higher peak velocities than adiabatic conditions, and flow reversals were claimed to be larger for adiabatic conditions. The former observation was substantiated by Kim and Viskanta [65], in a numerical study of laminar natural convection within thick conducting wall air cavities. They showed that heat transfer to the floor and ceiling increased as the ratio of the thermal conductivities of the wall to the fluid increased. Horizontal and vertical velocities also increased with increasing ratio of thermal conductivities, which would make the floor and ceiling thermal boundary conditions tend towards a linear temperature gradient type.

Ozoe et al [66] carried out an experimental investigation of laminar flow at $Ra_H = 1.5\times10^8$ and observed that the flow up the heated wall was two-dimensional, but that three-dimensional spiral streaklines developed across the ceiling. The cause of these vortices was speculated as being either centrifugal forces produced in the change from vertical to horizontal flow (giving rise to Gortler-type vortices) or heat transfer from the fluid to the ceiling (giving rise to Benard-type vortices). The vortices apparently persisted down the cooled wall and were then damped along the floor. The width of the ceiling boundary layer was seen to increase downstream.

Mallinson [67] indicated that for a laminar boundary layer regime, a three-dimensional double spiral was induced due to heat transfer through the ceiling.

The velocity surveys of cavities operating in the transitional boundary layer regime have generally shown the velocity profiles not to be anti-symmetric. More importantly, only one survey has definitely shown re-laminarization along the cavity ceiling, whilst all surveys have shown re-laminarization along the cavity floor. All the different observations can be accounted for by two cavity characteristics. These are the thermal boundary conditions on the floor and ceiling, and the cavity width.

The thermal boundary conditions, in practice, fall within the two extremes of adiabatic and linear temperature gradient. In the case of adiabatic boundary conditions the local temperature gradient never becomes negative, whereas this can occur, at some positions, for all other boundary conditions. Now, it is known that buoyancy forces, resulting from stratification, influence the turbulence quantities. The effects of a stable stratification have been investigated experimentally by Webster [68] and Ayra [69] and considered theoretically by Gibson and Launder [70] and [71]. The conclusion of this work is that collapse of the turbulence will occur at a critical value of the flux Richardson number.

The flux Richardson number is the ratio of the rate of turbulence energy removal by buoyancy forces to the rate of turbulence energy creation by mean shear, and is defined in equation (2.33).

$$R_F \equiv \frac{\overline{u'T'}g\beta_T}{\overline{u'v'}\frac{dv}{dx}} \qquad (2.33)$$

An alternative representation of the Richardson number is the gradient Richardson number. This is the flux Richardson number multiplied by the turbulent Prandtl number and is defined in equation (2.34).

$$R_G \equiv \frac{g\beta_T dT/dx}{(dv/dx)^2} \qquad (2.34)$$

It is easier to see from this representation that the Richardson number will only be positive when dT/dx is positive (i.e. when a stable stratification exists).

The effect of a stable stratification is to extract energy directly from the vertical component, so reducing $\overline{u'u'}$ and, as a consequence, $\overline{u'v'}$. The interaction of $\overline{u'v'}$ with the mean velocity gradient contributes directly only to the v' component from where energy is redistributed to the u' and w' components. Therefore one sees that all three fluctuating components of velocity are reduced, and as temperature fluctuations are a result of velocity fluctuations, T' is also reduced.

Gibson and Launder [70] reported that early simplified models yielded a range of 0.15-0.5 for the critical flux Richardson number, but the models only considered free shear flows thereby neglecting the influence of a wall. It is now known that the presence of a wall substantially alters the character of pressure fluctuations in it's vicinity which in turn affects the turbulence stresses and heat fluxes. In addition, the presence of a horizontal boundary will tend to reduce vertical fluctuations and so the

critical value of R_F. Gibson and Launder [70] stated that measured values of critical R_F, relating to experiments in wall affected turbulence, put the critical value at which turbulence collapsed as 0.07-0.2. In a later paper, Gibson and Launder [71], the critical value of R_F was put at 0.25 for the atmospheric boundary layer.

One now sees that re-laminarization can occur on the floor or ceiling of a cavity if a stable stratification is present which gives rise to a value of R_F above the critical value. One must now consider the effects of $R_F < 0$ which will arise near the cooled wall side of the ceiling, and the heated wall side of the floor, when the boundary conditions depart from the adiabatic case. For the ceiling flow, one sees that as heat is lost from the fluid the buoyancy force will result in immediate downward motion of the fluid, thus promoting turbulence and so bring a halt to re-laminarization. In the case of the flow along the floor, upward fluid motion will only occur if the buoyancy force is able to overcome the weight of the fluid above, just as in Rayleigh-Benard flow in horizontal cavities. Thus a value of R_F less than zero is no guarantee of upward fluid motion from the floor near to the heated wall, and so re-laminarization may not be arrested.

The survey of Giel and Schmidt [15] would appear to be the only one which had near adiabatic conditions at the floor and ceiling. This may be deduced by noting the high level of insulation used, and the fact that the working fluid was water which greatly eases the practical problems of reducing heat transfer.

The consequence of non-adiabatic boundary conditions for the survey of Ziai [1] has been to prevent full re-laminarization along the ceiling, but to allow it to happen along the floor. Re-laminarization along the floor was also aided by the transition process at $x/H \simeq 0.25$ on the heated wall, which reduced the mass flow in the boundary layer at the bottom of the cooled wall. The temperature data of Ziai [1] have indicated that the flux Richardson number, along the ceiling near the heated wall and along the floor near the cooled wall, was positive and greater than 0.25, which was the value of critical R_F proposed by Gibson and Launder [70] for the collapse of turbulence. Certainly, collapse of the turbulence did occur at the beginning of Ziai's floor and ceiling boundary layers, but this collapse was arrested as the local heat transfer reduced the local Richardson number with distance along the ceiling.

One now turns to the effect of the cavity width on re-laminarization. Launder [72] noted that in free stream turbulence the magnitude of $\overline{T'T'}$ has been found to decrease with the -1.5 power of distance, and that the

magnitude of the turbulence kinetic energy has been found to decrease with the -1.2 power of distance. This obviously shows that one expects turbulence to be destroyed over a specific distance, which is dependent on initial conditions, for both neutral and stably stratified flows. One may now consider the survey of Renault and Doan-Kim-Son [30] which showed the boundary layers meeting in the centre of the cavity. Here the restriction of the cavity width may very well have prevented full re-laminarization along the floor, resulting in the flow at the base of the heated wall exhibiting a "laminar aspect" instead of true laminar characteristics.

2.13 VERTICAL SIDE WALL BOUNDARY CONDITIONS

The vertical side wall boundary conditions are important in three respects. Firstly, they can affect the heat transfer rates at each wall, secondly, they can affect the flow pattern causing three-dimensional effects, and thirdly, heat loss through the vertical side walls can reduce the temperature at the vertical centre-line.

A number of researchers have automatically assumed that their cavity flows have been perfectly two-dimensional, and as a consequence they have presumed that the heat transfer from the heated wall is identical to that to the cooled wall. They then based the global Nusselt number on the heat transfer data at the heated wall.

Ziai [1] has shown that, for his air cavity with relatively poor closing wall insulation, the average heat transfer rate at the centre-line of each active wall is not identical. This discrepancy was accounted for as a combination of heat transfer through the closing walls, and additional heat transfer at the heated wall arising from a leakage flow from the bottom probe access slot up to, and through, the top probe access slot. Calculations indicated that the latter effect gave rise to only a very small proportion of the heat transfer imbalance.

If all the closing boundaries (especially the vertical side walls) of Ziai's [1] cavity had been insulated so that adiabatic conditions had been obtained, then the heat transfer at each active wall would have been identical. For this ideal case, the heat transfer at the heated wall would have been lower than that measured by Ziai, and the heat transfer at the cooled wall would have been higher than that measured by Ziai. This shows that the use of the heated wall heat transfer data as a basis for the Nusselt number can result in too high a value. This uncertainty is less likely to arise with other frequently used fluids, such as water, because of their higher thermal conductivities. Air has a very low thermal conductivity

and as a consequence adiabatic conditions on the closing boundaries are very hard to obtain.

MacGregor and Emery [8] found a distinct lack of symmetry in their temperature profiles, this was attributed to the effect of temperature dependent properties, however, the more likely explanation is one of heat loss through the closing boundaries, causing a lowering of the fluid temperature in the region of the cavity centre.

Morrison and Tran [73] investigated the laminar boundary layer regime for an air cavity at $Ra_H = 6.25 \times 10^6$ and H/L = 5. By increasing the insulation on the vertical side walls the region exhibiting identical lateral mean velocity profiles increased from z/B = 0.2-0.8 to 0.1-0.9. There was also a significant effect on the mean velocity profile. The heated wall velocities decreased and the cooled wall velocities increased, resulting in a decrease of volume flux imbalance at mid-height from 10% to 2%. As might be expected the region at the bottom of the heated wall was virtually unaffected with the flow at the top of the cooled wall reduced. L.D.A. measurements also showed horizontal components towards the centre-line as the flow went up the heated wall and horizontal components away from the centre-line as the flow went down the cooled wall. This indicated that a proportion of the flow up the heated wall travelled down each side wall.

Linthorst et al [74] also found that improving the vertical side wall insulation led to an improved mass balance at mid-height.

2.14 HEAT TRANSFER CORRELATIONS

The provision of an overall heat transfer equation was not the purpose of the research undertaken for this thesis. However, whilst reading through the literature it became obvious that no equations exist which can reliably predict the heat transfer for any given situation. Therefore it was decided to include this Section which comments on overall heat transfer and the dimensionless groups which are important in two and three-dimensional cavity flow. Also included are the limited data on local heat transfer equations within cavities, and a comment on the importance of temperature dependent properties used in overall and local heat transfer equations.

2.14.1 OVERALL HEAT TRANSFER CORRELATIONS

The correlations used to-date, for both cavity and flat plate scenarios, have made use of the non-dimensional groups resulting from dimensional analysis. The first analytical approach by Batchelor [2] for the

cavity problem proposed that $Nu_L = Nu_L(Ra_L, Pr, H/L)$. For the boundary layer regimes the characteristic length H now replaces L.

The form of the function has generally been that of a constant times the non-dimensional groups each raised to a different power. There is no full analytical support for this method, but it remains the best avenue of approach available, especially when one considers the potential levels of uncertainty in data already available, and the poorly structured manner in which research has been carried out, which has by no means fully accounted for the three basic variables, Ra_H, Pr and H/L. A typical example is the use of constant height cavities which have not fully accounted for the variation of H/L but only that of L.

Elsherbiny et al [9] have stated that for cavities the simple power law is insuffucient to fully describe the heat transfer function. In addition, the empirical analysis of vertical flat plate data by Churchill and Chu [75] has indicated that a power law function is too simple for this case also.

Other researchers have indicated that the Nusselt number for a cavity is dependent on other non-dimensional groups which introduce three-dimensional effects into the flow. Elsherbiny et al [63] considered the parameters influencing Nu_H (in the general case of a tilted cavity) to be Ra_H, Pr, H/L, B/L, angle of tilt, ratio of wall to fluid thermal conductivities, a radiation-conduction group, the emissivities of the heated and cooled walls ceiling and floor and T_H/T_C. They correctly stated that all researchers should strive to quote these values for all experimental results. However, in the case of vertical cavities in the boundary layer regimes, the emissivities, radiation-conduction group and the angle of tilt have negligible influence.

Support for the inclusion of B/L came from Eckert and Carlson [4] and those investigating the influence of insulation on the vertical side walls. The main argument was that this variable determines the two-dimensional nature of the cavity flow. Viskanta et al [76] in a numerical study reported three-dimensional effects as being very important at low Pr. Both flow pattern and heat transfer were affected.

Support for the inclusion of the ratio of wall to fluid thermal conductivities came from those investigating the effect of heat loss through all closing boundaries

B/L and the thermal conductivity ratio may be combined in a variable describing the heat loss from the cavity, which could be used to estimate

the uncertainty in the heat transfer at either wall, so allowing the uncertainty in Nu_H to be reduced.

Support for the inclusion of T_H/T_C came from Siebers et al [60] who undertook experiments with an isothermal vertical flat plate in air at very large temperature differences. The non-dimensional group T_ω/T_∞ was included in a power law function to compensate for temperature dependent properties when they were all evaluated at the environmental temperature T_∞. The exponent was -0.14. A similar group using $(\mu/\rho)_\omega/(\mu/\rho)_\infty$ was proposed by George and Capp [56] with an exponent of -0.21. For air in the range T_ω/T_∞ = 1-1.3 with T_∞ = 293.15K the two are related as:

$$[(\mu/\rho)_\omega/(\mu/\rho)_\infty]^{-0.21} = 2.533[T_\omega/T_\infty]^{-0.14} - 1.534 \qquad (2.35)$$

If the group of Siebers et al [60] is considered correct then the maximum uncertainy when using the George and Capp [56] group is 6.5% which increases for T_ω/T_∞ above 1.3.

The only new group which could feasibly be introduced is T_H/T_C, which one would use to account for temperature dependent properties once they had been evaluated at T_C, instead of using some other reference temperature.

The inclusion of the Gebhart number ($g\beta_T H/Cp$) was proposed by Fand and Brucker [77], but this is only valid for conduction and aysmptotic flow regimes.

By staying with the power law function one must attempt to comment on the likely size of the power for each group. The powers proposed by Seki et al [5] for Ra_H in the transitional and turbulent boundary layer regimes are probably correct. One would expect 1/3 for the turbulent case where the heat transfer coefficient remains essentially constant, with increasing Ra_H, and heat transfer becomes independent of the characteristic length, and less than this, but greater than 1/4 (the experimentally observed value for the laminar boundary layer regime) for the transitional case.

As regards H/L one notes that as it increases the heat transfer rate is likely to decrease, but would only be noticeable at aspect ratios of, say, greater than 10. Therefore a value for the power of -1/9 proposed by Jakob [78] would be a reasonable expectation.

The effect of Pr is that, as it decreases so the boundary layer thickness increases, hence the heat transfer rate would tend to decrease, although the effect above Pr = 1 would be minimal. Therefore something in the region of 0.03 would be a likely power.

One other matter complicates things, and that is the thermal boundary conditions on the floor and ceiling. It is highly likely that the heat transfer will be different (all other parameters being kept constant) for

the extremes of adiabatic and linear temperature gradient boundary conditions. This should be most notable at low values of H/L, where the characteristics of the flow at the top of the cooled wall could be altered significantly in the case of a linear temperature gradient.

2.14.2 LOCAL HEAT TRANSFER CORRELATIONS

Local heat transfer values were reported by Cowan et al [12] for water and by Ziai [1] for air, but were not found to be consistent with one another, thus indicating a Pr effect. Detailed comparison between these data and those resulting from the present research is left until Chapter 7.

Eckert and Carlson [4] reported the local heat transfer for the laminar boundary layer regime of an air cavity as $Nu_x = 0.231 Gr_x^{0.3}$. They correctly stated that if the centre-line temperature could be predicted then the local heat transfer could be calculated if a reliable function was known.

2.15 RESUME

There now follows a resume of all the important points brought forth by the Literature Survey.

Dimensional analysis shows that, for two-dimensional flow within a cavity, $Nu = Nu(Gr,Pr,H/L)$ but for the range of Pr investigated to-date it is advantagous to replace Gr with Ra so that $Nu = Nu(Ra,Pr,H/L)$.

The characteristic length to be used when considering Nu and Ra for the boundary layer regimes is H.

When attempting to predict the presence of turbulent fluctuations within a cavity, the dominant non-dimensional groups are Ra_H and H/L. H/L becomes irrelevant below a certain (as yet undetermined) value. A third group, Pr, does have an effect by determining the boundary layer thickness, but not enough data exist to attempt to incorporate it into a criterion for the presence of turbulent fluctuations. Even the available data for Ra_H and H/L are insufficient to provide anything other than a reasonable estimation.

There is a considerable need for a properly co-ordinated research study which takes account of the variation of Ra_H, H/L and Pr. Most research has only involved the variation of L, keeping H constant, therefore making it difficult to determine the true influence of H/L.

The discrete frequencies of transition within cavities and for vertical flat plate flow have been in a range of 0.9-3.6Hz. These data originated from experiments using air and water and there appears to be a common factor, in each discrete frequency, of approximately 0.9Hz.

The flow pattern in the transitional boundary layer regime has not always been observed to be anti-symmetric. It's departure from this ideal has been primarily due to heat transfer losses through all closing boundaries. This has introduced three-dimensional effects, which coupled with the influence of temperature dependent properties, has resulted in non-symmetric mean velocity profiles and mass flow imbalance at mid-height.

Heat transfer through the ceiling has been responsible for negative values of the local Richardson number between the cavity centre-line and the cooled wall, preventing complete re-laminarization of the flow along some cavity ceilings.

The core region of a cavity can be considered to be comprised of two sub-regions when it is defined relative to the boundary layer. These are a region of non-zero mean velocity (a reversed flow region) and a zero mean velocity region.

The temperature stratification of the fluid at the cavity centre-line, for the boundary layer regimes, has not been observed to be consistent. Some of the discrepancy between different data (for the same fluid) can be attributed to different levels of heat loss through the closing boundaries which reduces, at all heights, the value of θ.

There appears to be an effect on the non-dimensional gradient of the temperature stratification (for the same fluid) when L is reduced below a critical value (with H kept constant). In such a case the gradient decreases.

The stratification has not always been observed to be linear for all x. There is an indication that the non-dimensional gradient is different in regions where the flow exhibits "laminar aspects" and where it is fully turbulent.

Very little quantitative turbulence data exist. Those that do suggest that there is a region, between the mean velocity peak and the wall, where $\overline{u'v'}$ is negative. Far from the wall $\overline{u'v'}$ is positive.

The only sub-range consistently found with a constant exponent on frequency (or wavenumber) for both temperature and velocity fluctuation spectra from cavities and flat plates, is an inertial sub-range with an exponent of -5/3. The dissipation sub-range has been shown to exhibit exponents of -17/3 and -5.

Mean temperature profiles have been shown to scale reasonably well with the non-dimensional group $(T-T_\infty)/(T_\omega-T_\infty)$ in conjunction with the non-dimensional group Nu_y. Less success has been achieved with mean velocity profiles.

When considering overall heat transfer equations the use of the film temperature ($(T_H-T_C)/2$) is recommended in order to facilitate easy comparison of different data sets.

2.16 OBJECTIVES OF THE PRESENT STUDY IN RELATION TO POINTS BROUGHT FORTH BY THE LITERATURE SURVEY

The major objectives of the present study have been set out in Chapter 1, the Introduction. This Section points out some minor objectives which were set after the Literature Survey was undertaken.

The present study has concentrated on the charcteristics of the velocity and temperature fields. Within the study itself, seven scenarios have been studied which have involved the logical variation of H, L and (T_H-T_C). Mean values and R.M.S. of fluctuations for velocity and temperature have been calculated which will be used to compare with those already available and between different scenarios within the study.

The cavity height was varied as this has only been carried out in a few studies. The variation of cavity width became important in the investigation of the effect of the width on the velocity and thermal boundary layers for constant height and Ra_H.

An attempt has been made to provide direct measurements of $\overrightarrow{u'T'}$ and hence $\overrightarrow{u'\rho'}$ (production of turbulence kinetic energy by buoyancy is $-g\overrightarrow{u'\rho'}$) and graphical interpretaion of data to provide profiles of $\overrightarrow{u'v'}$ and $\overrightarrow{v'T'}$. These represent the first turbulence quantities to be presented for cavity flow.

In addition, turbulence spectra are presented which investigate the dominant frequencies of transition for both velocity and temperature fields, and the effect of the variation of the vertical temperature gradient on the frequency exponent.

Estimates of the wall shear stress have also been made and are presented here for the first time. These were necessary to calculate $\overrightarrow{u'v'}$, and have aided in estimating the thickness of the viscous sub-layer.

Measurements of local heat transfer have been made which have provided a basis on which to attempt a correction for three-dimensional effects brought about by heat loss through the closing boundaries. Included in this process is a prediction of the stratification for a cavity with adiabatic closing boundaries. The local heat transfer data also provide a further estimate of the value of Ra_x at which transition may be considered to occur in a cavity.

Velocity, length and temperature scales are investigated together with an attempt to provide a universal velocity profile near to the peak velocity using the early research of Bayley [36]. The limit at which u_τ may be considered an appropriate scale for the near wall profile is also considered.

FIGURE 2.1

MAXIMUM AND MINIMUM VELOCITY

ENVELOPES DUE TO UNSTEADY MOTIONS

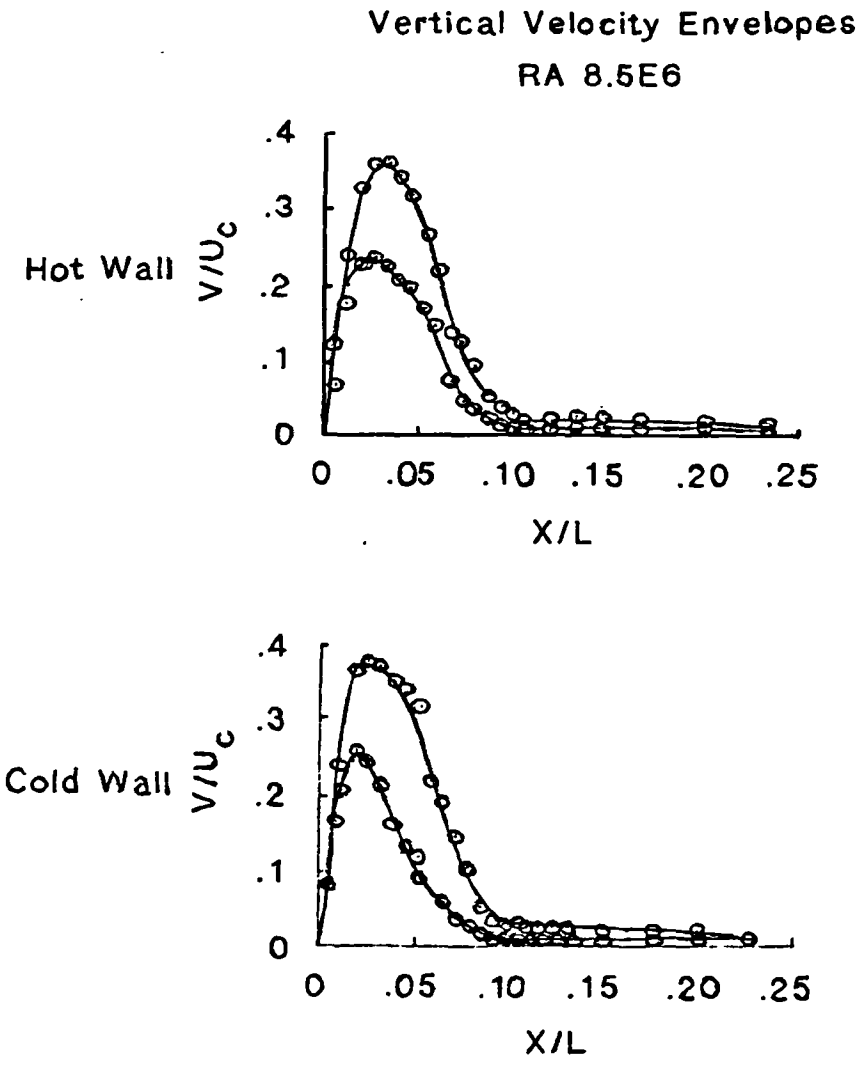

Vertical velocity envelopes at Rayleigh number 8.5 x 10^6

REPRODUCED FROM BRIGG AND JONES [22]

FIGURE 2.2

THE INFLUENCE OF ASPECT RATIO ON THE

ONSET OF UNSTEADY MOTIONS AND TURBULENCE

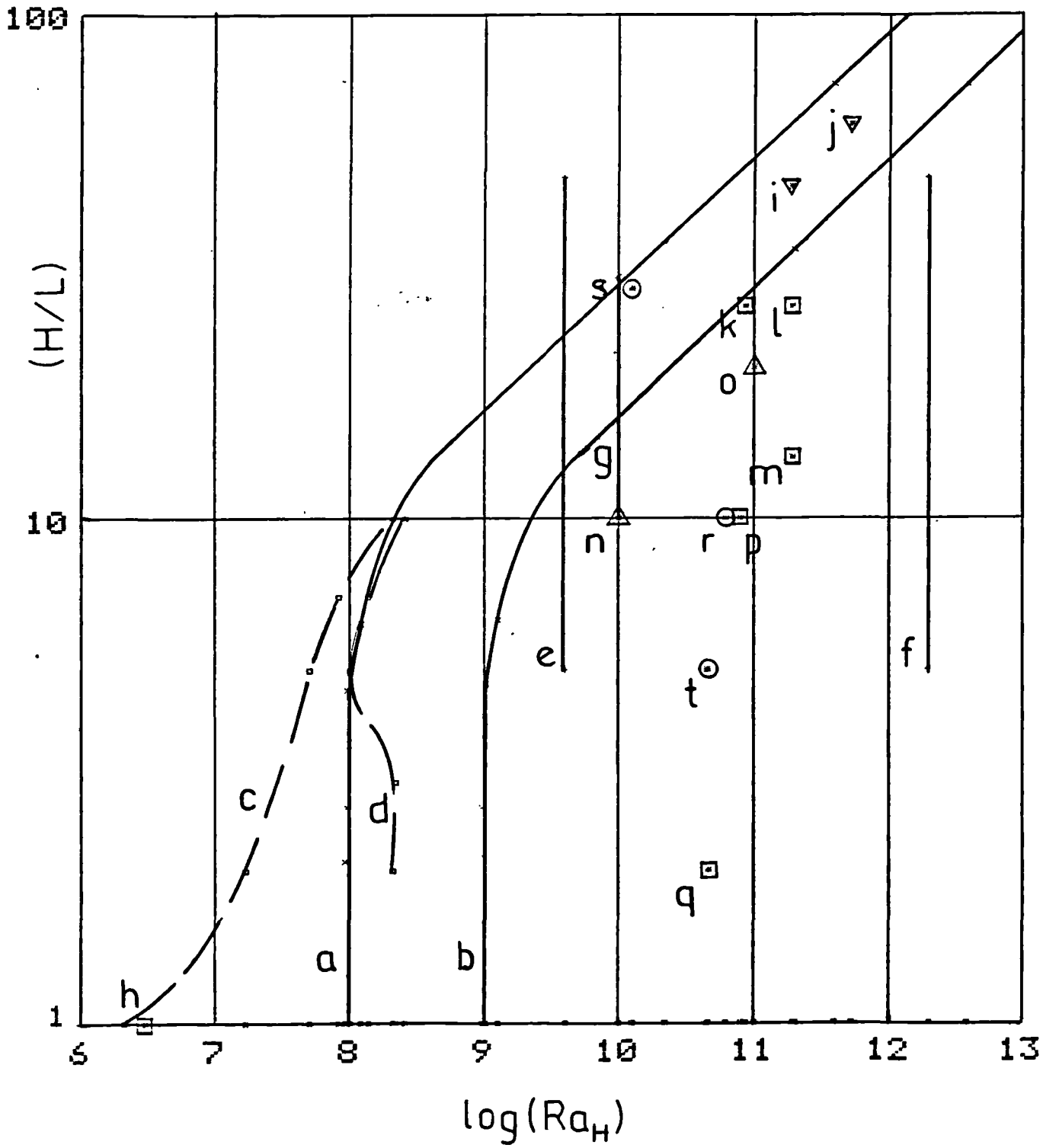

KEY TO FIGURE 2.2

a	Chenoweth and Paolucci [23], onset of instabilities
b	Chenoweth and Paolucci [23], onset of turbulence
c	Le Quere and Alziary de Roquefort [24], linear temperature profile on floor and ceiling
d	Le Quere and Alziary de Roquefort [24], adiabatic conditions on floor and ceiling
e	Seki et al [5], transitional boundary layer regime
f	Seki et al [5], turbulent boundary layer regime
g	Elder [11], transitional boundary layer regime
h	Briggs and Jones [22], onset of instabilities
i,j	Cowan et al [12], first indications of turbulence
k,l,m	Kutateladze et al [35], experimental data shows transitional boundary layer regime
n,o	MacGregor and Emery [8], first indications of turbulence
p	Giel and Schmidt [15], experimental data shows transitional boundary layer regime
q	Schmidt and Wang [14], experimental data presumed by authors to indicate turbulent boundary layer regime
r	Renault and Doan-Kim-Son [31], experimental data shows transitional boundary layer regime
s	Ralph et al [32], experimental data shows turbulent boundary layer regime
t	Cheesewright et al [85], experimental data shows transitional boundary layer regime

FIGURE 2.3

THE INFLUENCE OF STRATIFICATION

ON CRITICAL Gr_L FOR $0.73 < Pr < 12.7$

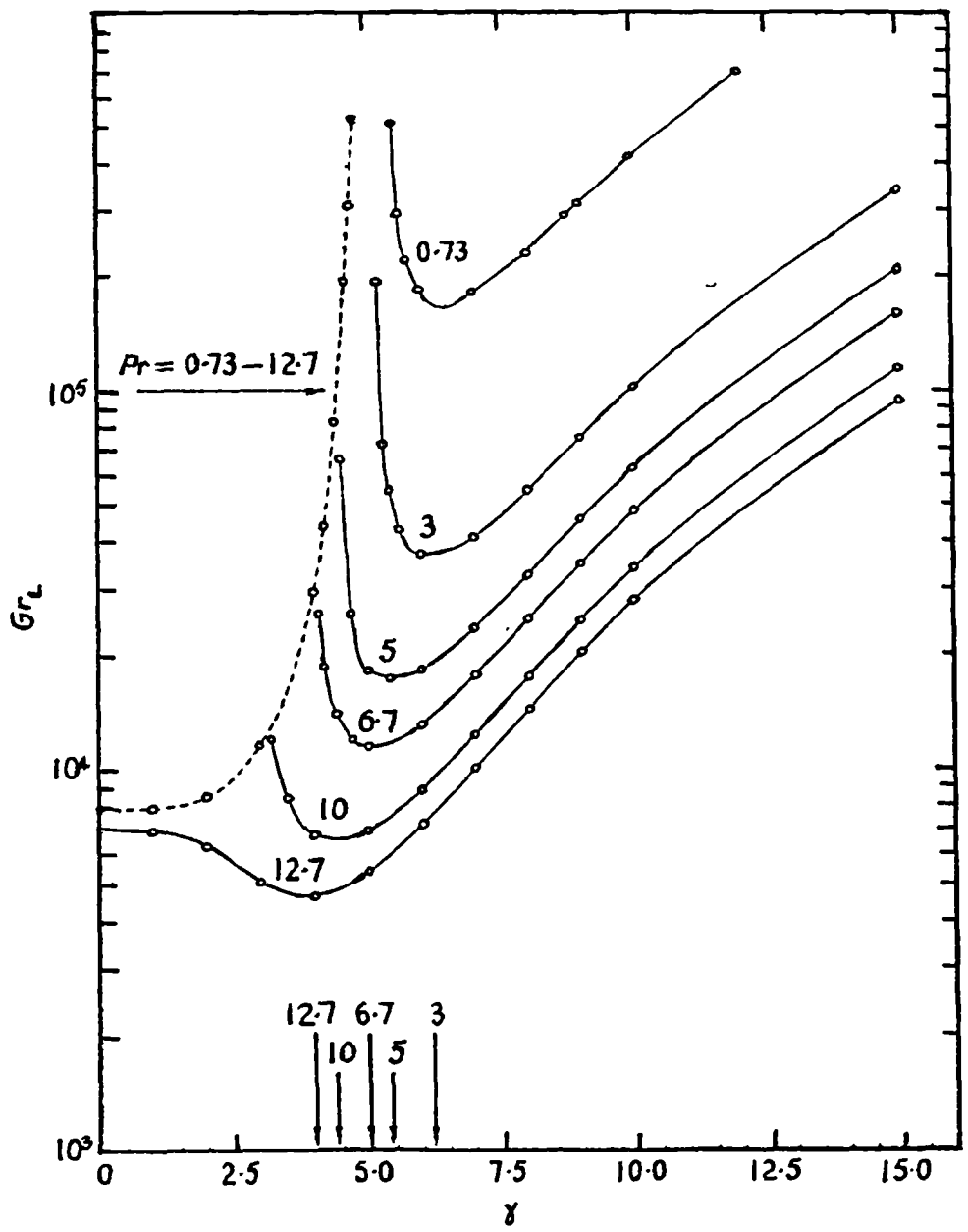

REPRODUCED FROM BERGHOLZ [21]

FIGURE 2.4

THE INFLUENCE OF STRATIFICATION

ON CRITICAL Gr_L FOR Pr > 20

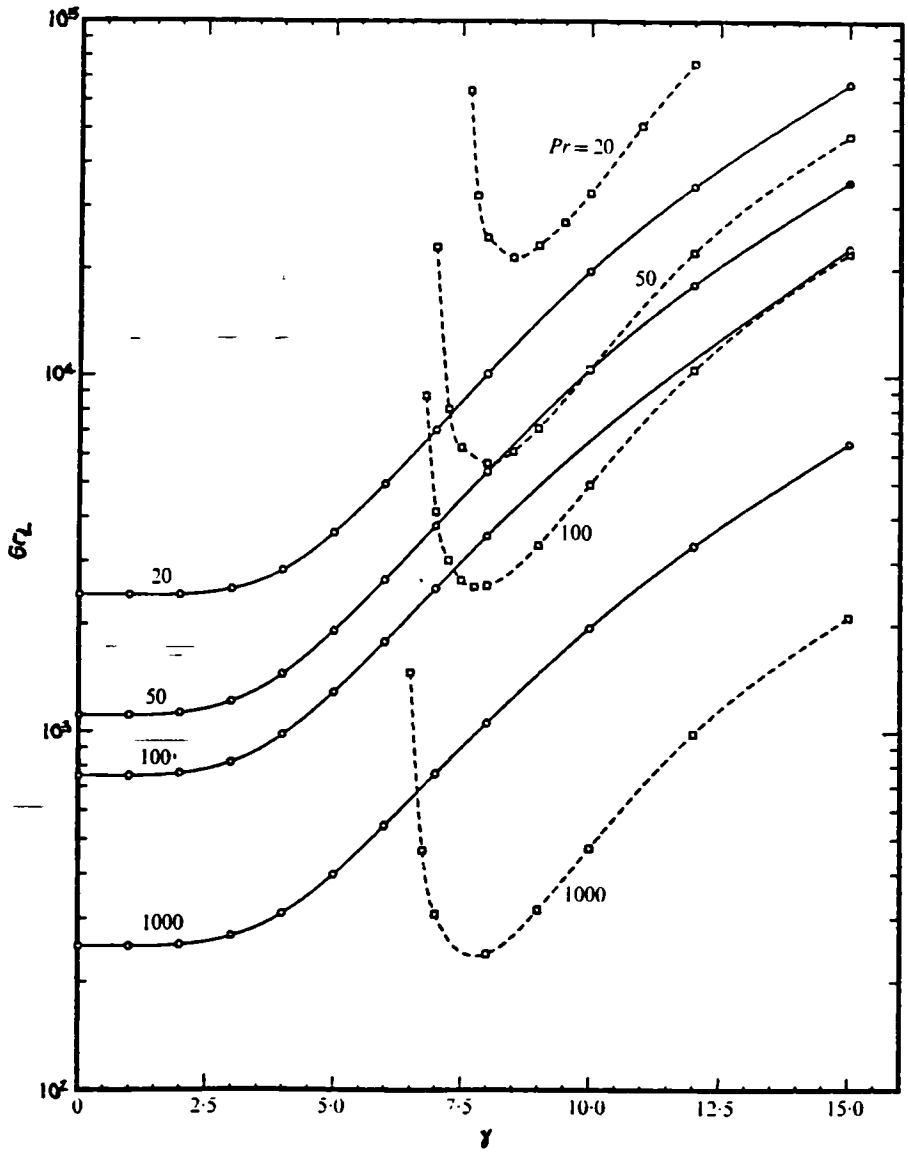

REPRODUCED FROM BERGHOLZ [21]

FIGURE 2.5

THE INFLUENCE OF STRATIFICATION

ON CRITICAL Ra_L FOR $Pr > 0.73$

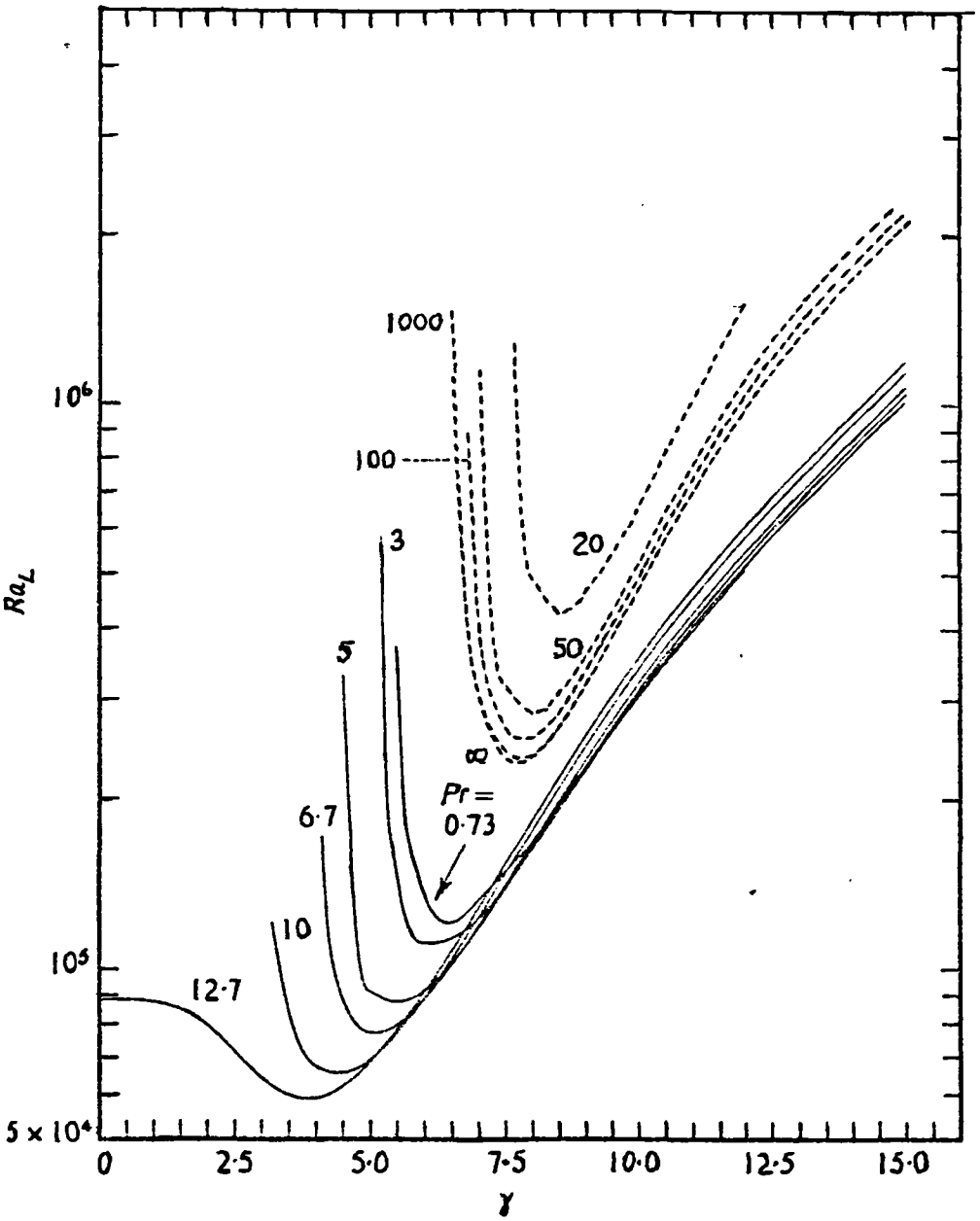

REPRODUCED FROM BERGHOLZ [21]

FIGURE 2.6

VARIATION OF $f/C\dot{Q}^{*0.8}$ WITH $Gr_{x,q*}$

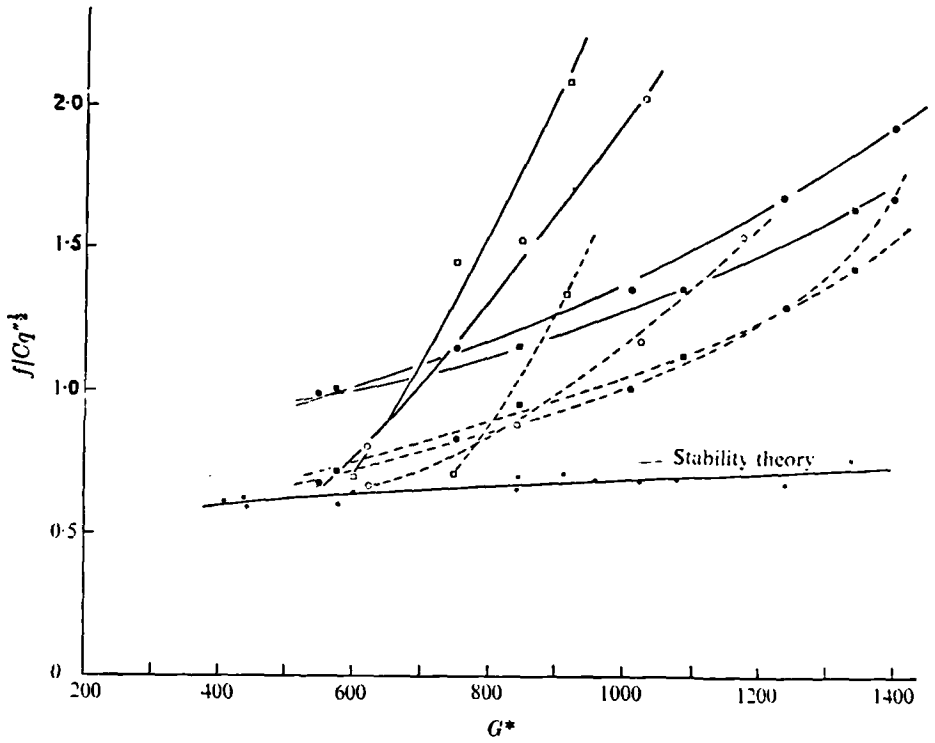

FIGURE 10. Variation of the dominant turbulent disturbance frequency, velocity and temperature, with G^*. ——, velocity; – – – –, temperature; ⊏, $q'' = 67$ B.Th.U./h ft²; ○, $q'' = 120$; ●, $q'' = 300$; ■, $q'' = 415$; ★, during locally laminar flow.

FIGURE 2.7

VARIATION OF DOMINANT TRANSITION FREQUENCY WITH HEIGHT FOR THE VELOCITY FIELD

FIGURE 2.8

VARIATION OF DOMINANT TRANSITION FREQUENCY WITH HEIGHT FOR THE TEMPERATURE FIELD

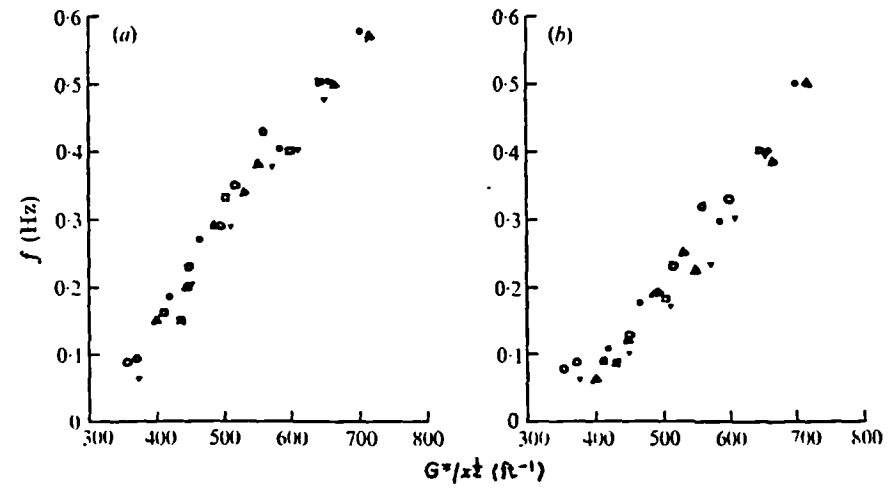

FIGURE 11. Variation of the principal turbulent disturbance frequency with $G^*/x^{\frac{1}{2}}$. The three points on the extreme left are for laminar flow. ○, $x = 15$ in.; □, $x = 24$ in.; ▼, $x = 33$ in.; △, $x = 42$ in.; ●, $x = 48$ in. (*a*) Velocity. (*b*) Temperature.

REPRODUCED FROM JALURIA AND GEBHART [20]

FIGURE 2.9

SKETCH OF THE VELOCITY BOUNDARY LAYER FROM A WATER CAVITY OPERATING IN THE TRANSITIONAL BOUNDARY LAYER REGIME

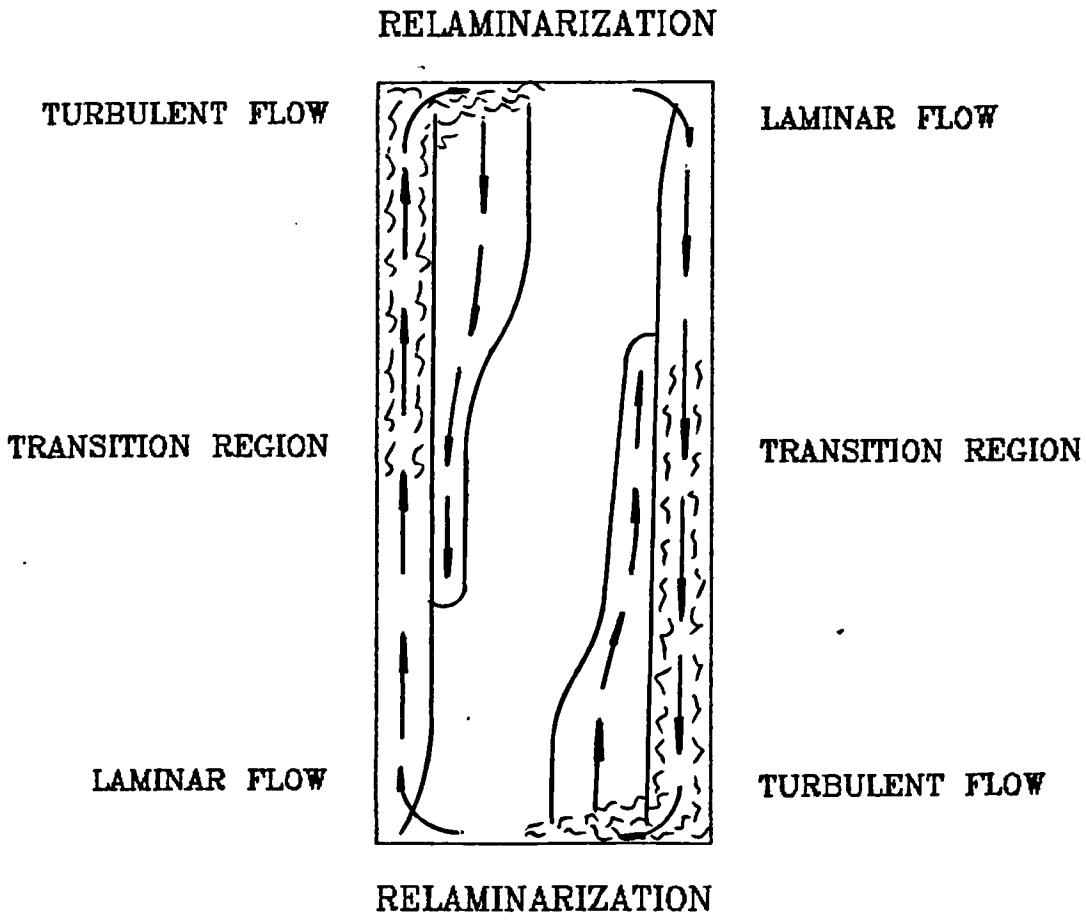

REPRODUCED FROM GIEL AND SCHMIDT [15]

FIGURE 2.10

VELOCITY AND TEMPERATURE PROFILES FROM A WATER CAVITY OPERATING IN THE TRANSITIONAL BOUNDARY LAYER REGIME

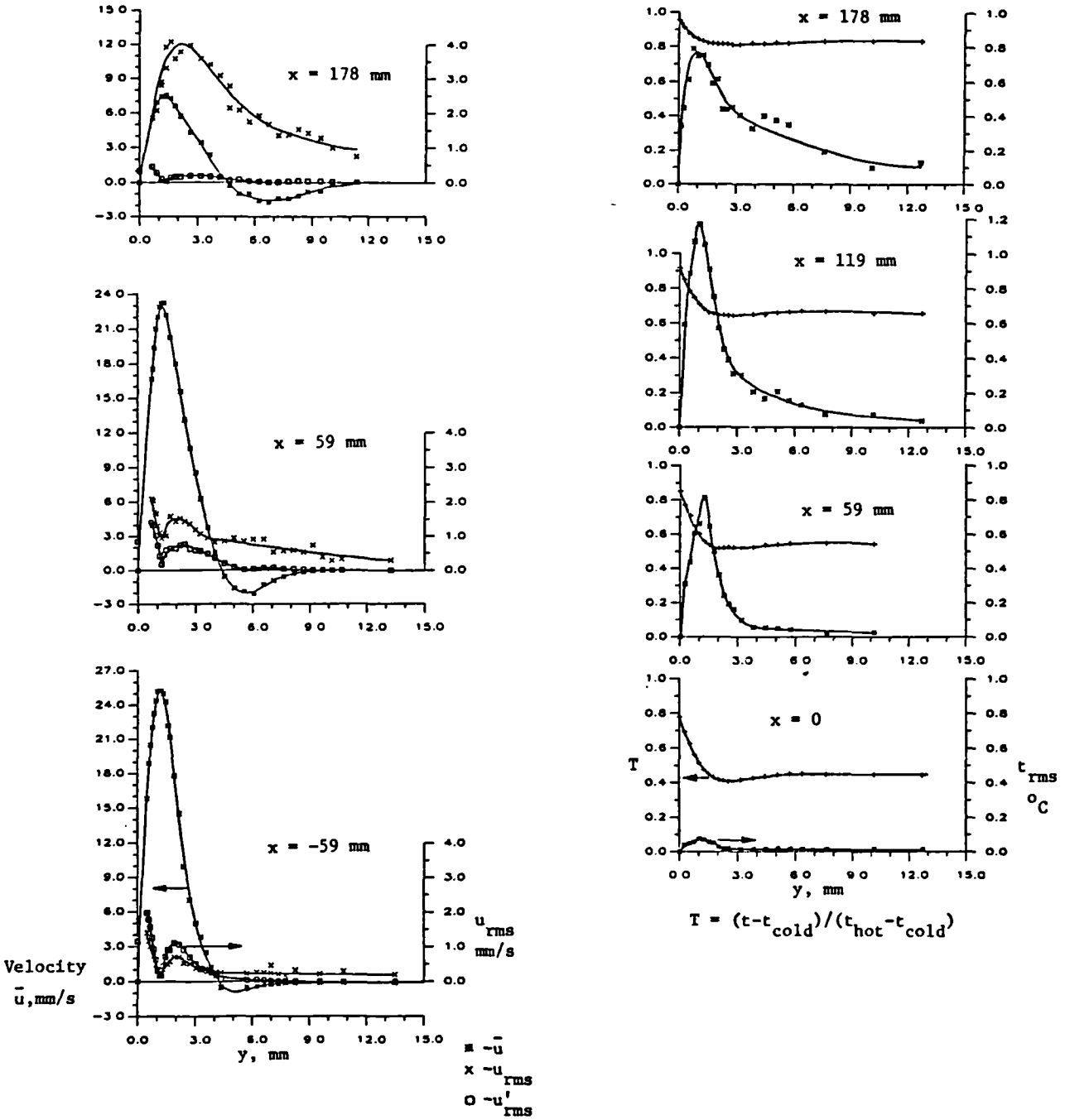

REPRODUCED FROM GIEL AND SCHMIDT [15]

FIGURE 2.11

VELOCITY AND TEMPERATURE PROFILES FROM A RELATIVELY NARROW AIR CAVITY OPERATING IN THE TRANSITIONAL BOUNDARY LAYER REGIME

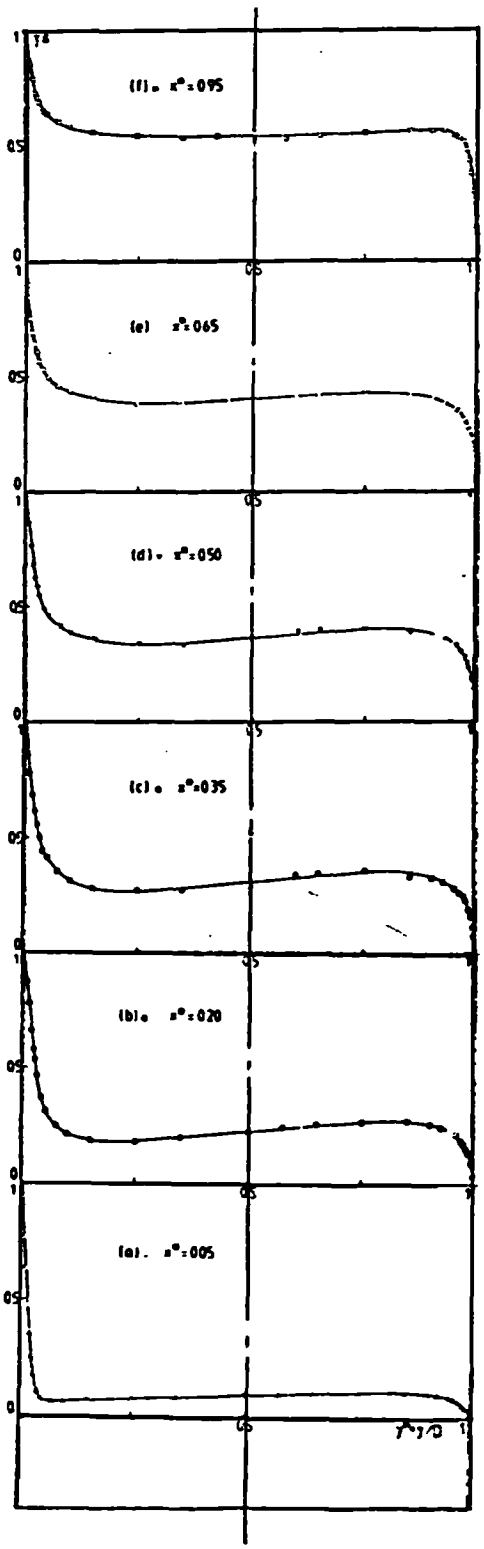

FIG.2
Temperature profiles

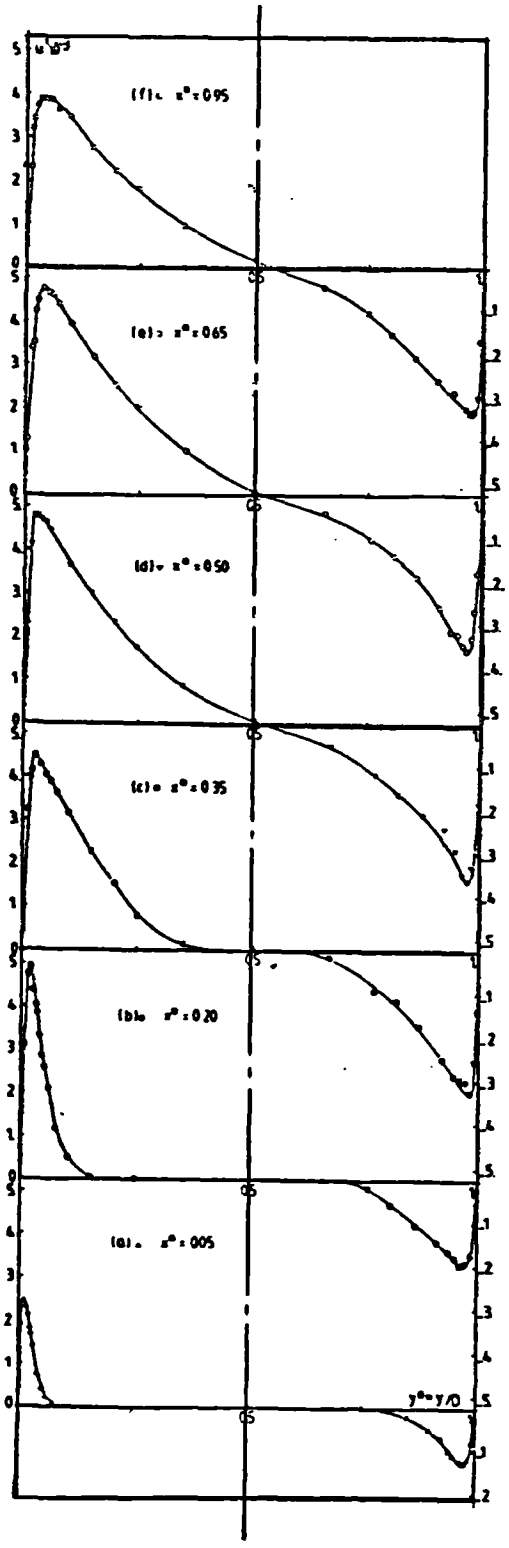

FIG.3
Velocity profiles

REPRODUCED FROM RENAULT AND DOAN-KIM-SON [30]

FIGURE 2.12

OVERALL HEAT TRANSFER IN THE

TRANSITIONAL AND TURBULENT BOUNDARY LAYER REGIMES

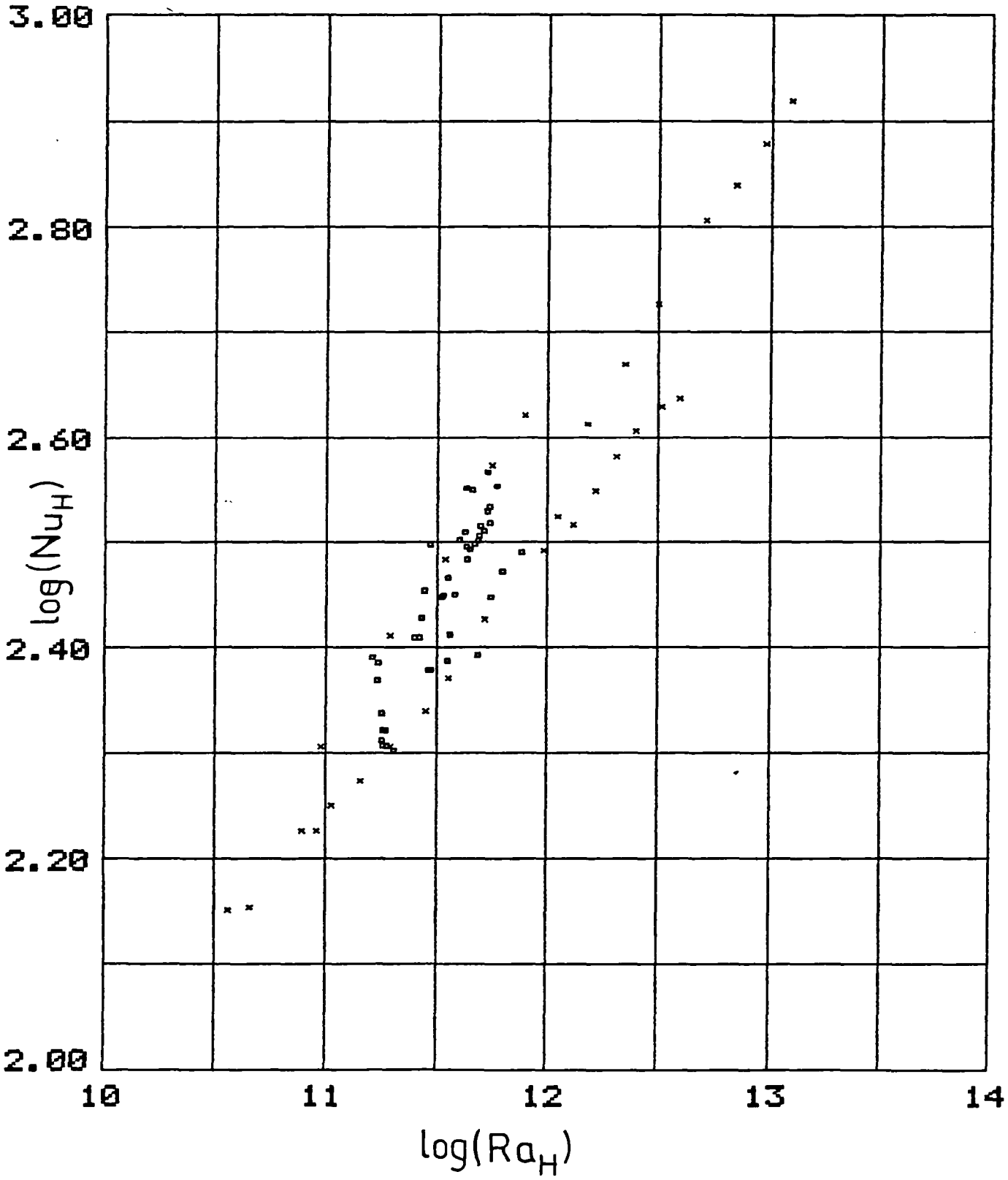

× DATA FROM SEKI ET AL [5]

□ DATA FROM COWAN ET AL [12]

FIGURE 2.13

VELOCITY AND TEMPERATURE PROFILES FROM A WATER CAVITY NOMINALLY OPERATING IN THE TRANSITIONAL BOUNDARY LAYER REGIME

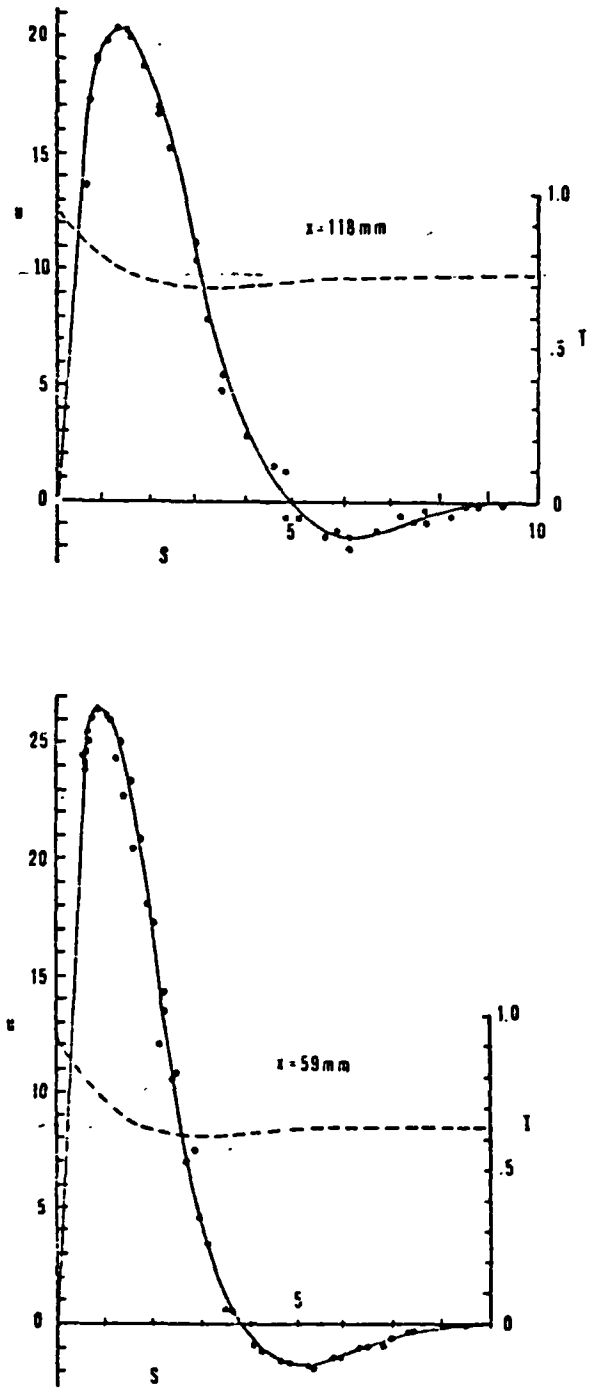

u vertical velocity - mm/s

S distance from wall - mm

$$T = \frac{t - t_c}{t_h - t_c}$$

REPRODUCED FROM SCHMIDT AND WANG [14]

FIGURE 2.14
VARIATION OF REYNOLDS NUMBER AT THE
MEAN VELOCITY PEAK WITH STRATIFICATION

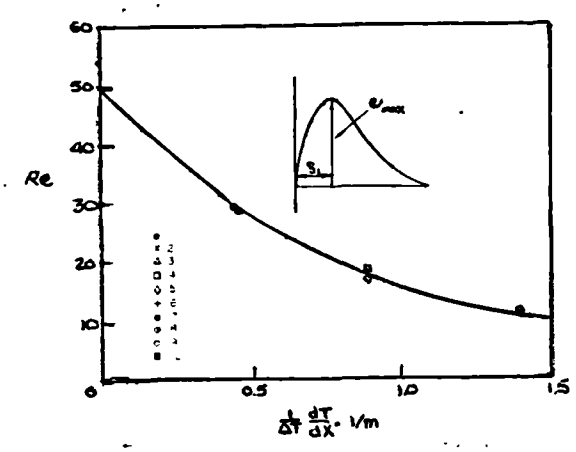

FIGURE 2.15
THE EFFECT ON THE MEAN VELOCITY PROFILE
OF REDUCING THE CAVITY WIDTH AT CONSTANT Ra_H

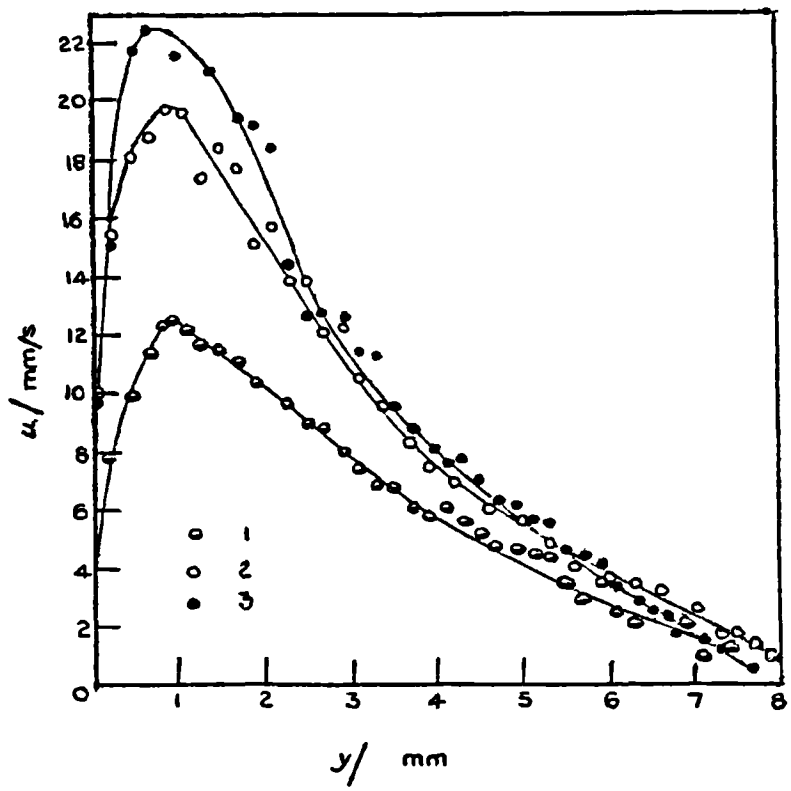

REPRODUCED FROM KUTATELADZE ET AL [35]

FIGURE 2.16A

CORE STRATIFICATIONS FROM CAVITIES

OPERATING IN THE TRANSITIONAL BOUNDARY LAYER REGIME

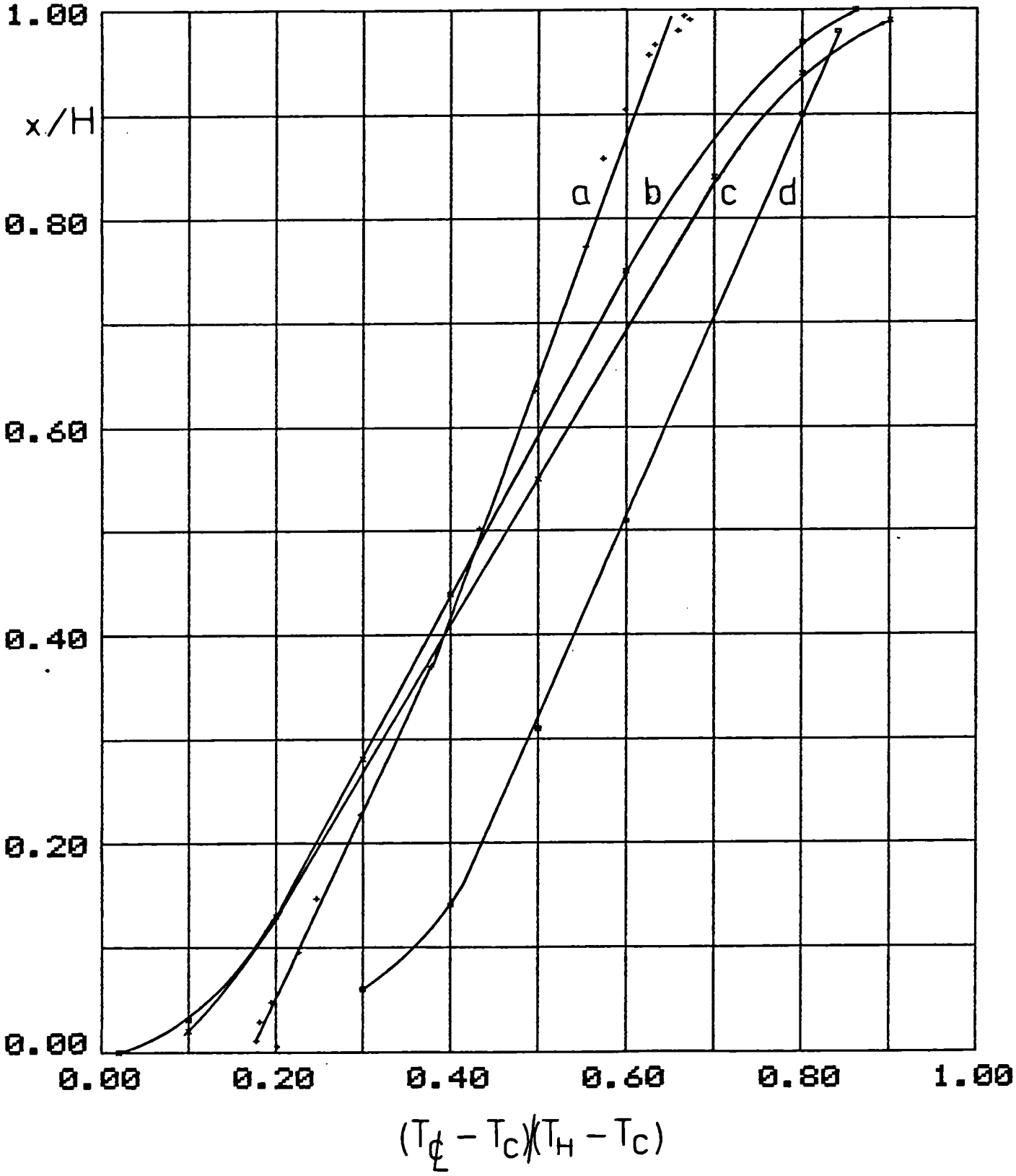

a FROM ZIAI [1]
b FROM GIEL AND SCHMIDT [15]
c FROM SCHMIDT AND WANG [14]
d FROM COWAN ET AL [12]

FIGURE 2.16B

CORE STRATIFICATIONS FROM CAVITIES

OPERATING IN THE TRANSITIONAL BOUNDARY LAYER REGIME

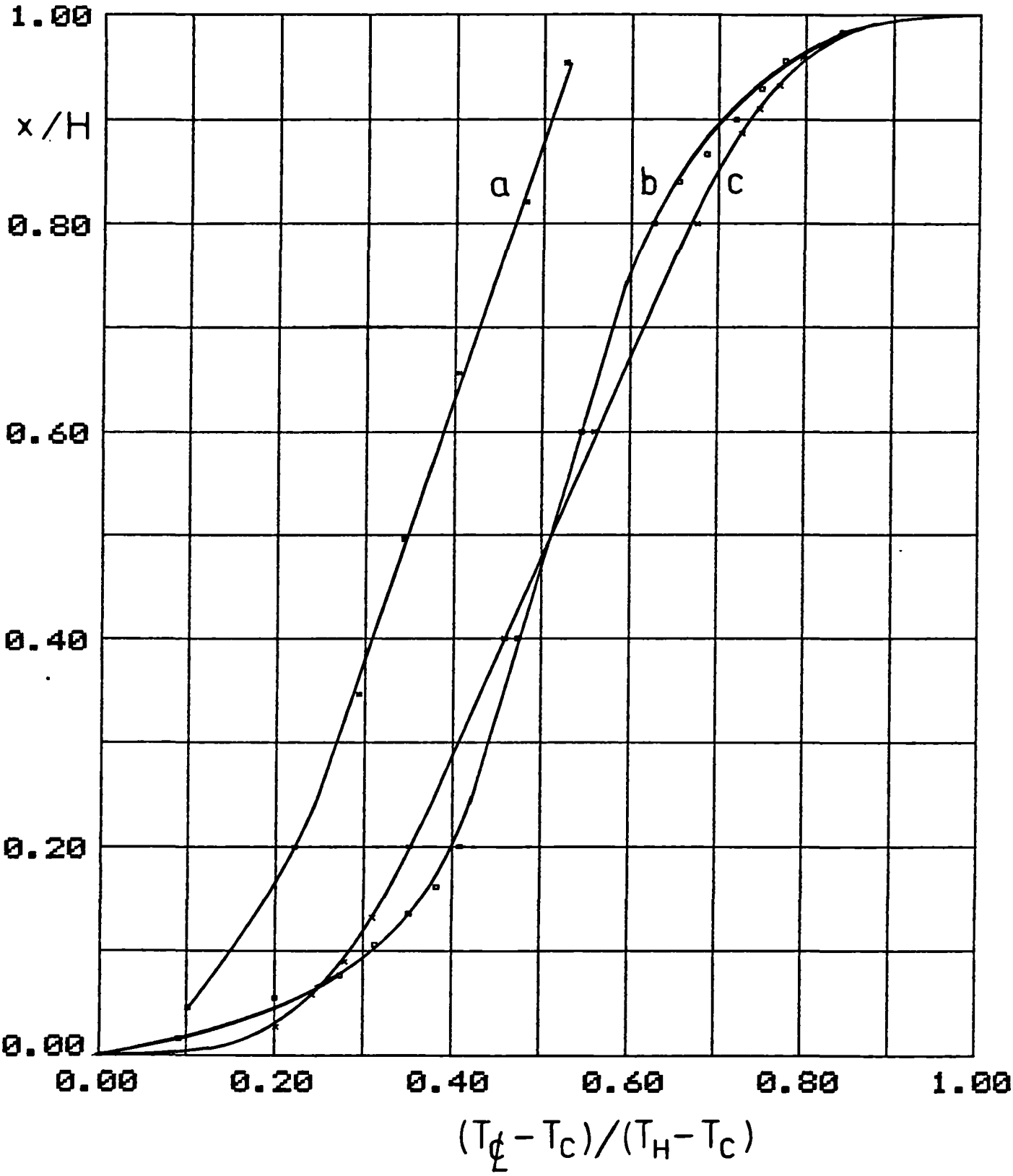

a FROM RENAULT [32]

b FROM KUTATELADZE ET AL [35] H/L = 21.94

c FROM KUTATELADZE ET AL [35] H/L = 8.06

FIGURE 2.17

IDEAL ADIABATIC AND EXPERIMENTAL TEMPERATURE

DISTRIBUTIONS ON THE FLOORS AND CEILINGS OF TWO CAVITIES

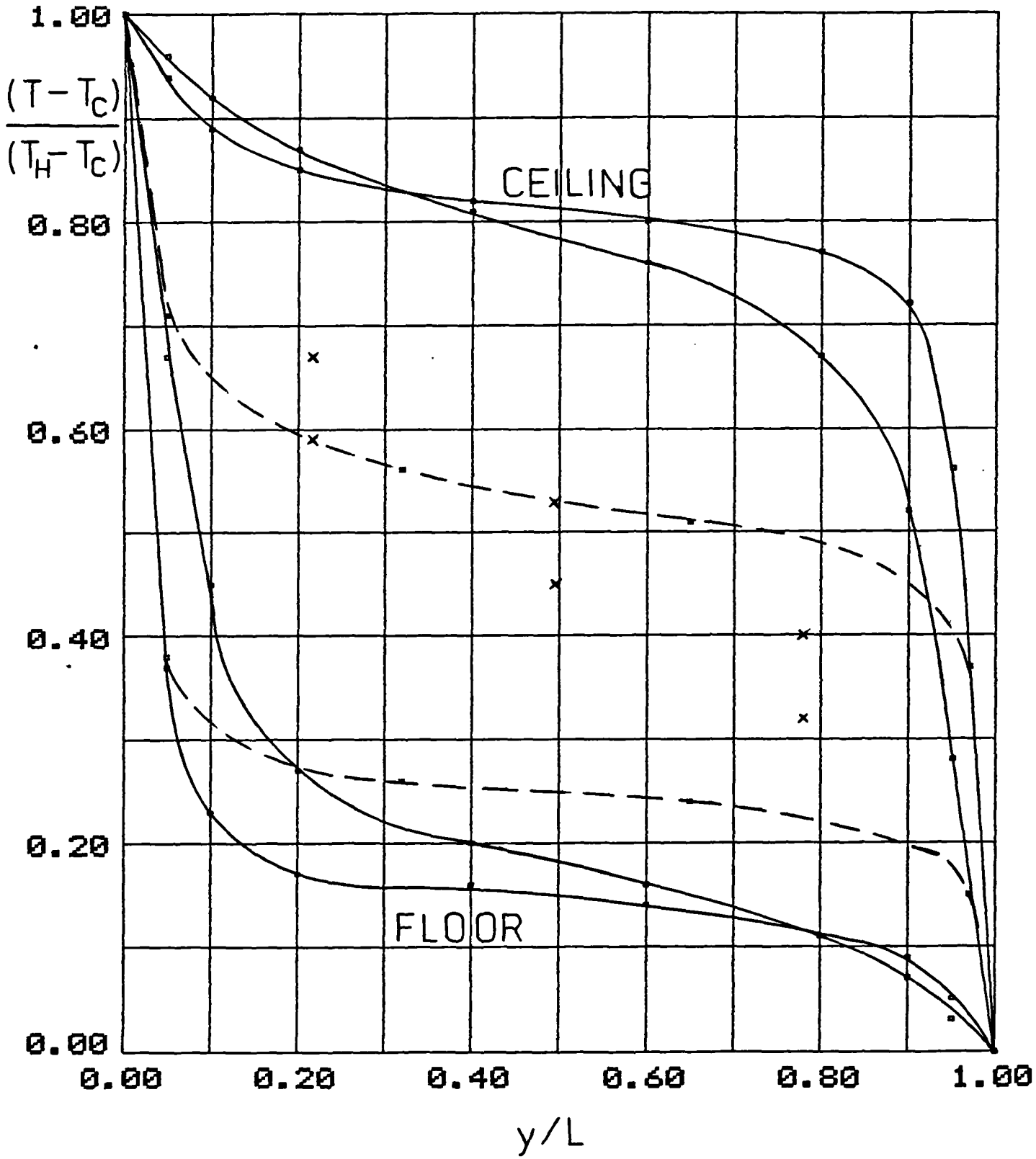

——— BILSKI ET AL [64] ADIABATIC

× BILSKI ET AL [64] EXPERIMENTAL

— — — ZIAI [1] EXPERIMENTAL

CHAPTER 3 - APPARATUS

3.1 THE APPARATUS AT QUEEN MARY COLLEGE

The description of the apparatus at Queen Mary College has been split into four Sections dealing, repectively, with: the cavity; the thermocouple signal processing instrumentation; the laser Doppler anemometry system; and the data logging system.

During the series of experiments a number of modifications were made to the original cavity to reduce heat transfer through the closing boundaries, and to eliminate a leakage through the entry and exit slots of the thermocouple support rod.

The present study was the first at Q.M.C. to use a newly acquired laser Doppler anemometry system. A considerable time was spent in setting up the system and becoming familiar with it, a process which was not aided by the poor quality of the documentation provided by the manufacturer (DANTEC).

To aid future users of the system a comprehensive alternative set of documentation was written. This documentation is available as a separate Appendix and so only a summary of the system is presented in this Chapter.

The data logging system was that used by Ziai [1], but a number of new programs were written, both for the collection and analysis of data.

3.1.1 THE CAVITY

The cavity has been described previously by Ziai and Cheesewright [79] and Ziai [1]. It is shown in sketch form in Figure 3.1.

Only a brief summary is presented here, together with a description of the alterations made during the present study.

The cavity consisted of eight major sub-assemblies.

(a) The base frame.

(b) The A-frame which incorporated probe mountings.

(c) The cooled wall.

(d) The heated wall.

(e) Two vertical side walls.

(f) The ceiling.

(g) The floor.

3.1.1.1 THE BASE FRAME

The base frame consisted of six rectangular steel tubes, welded together to form a 3.4 × 1.85m rectangle, which rested on 20mm thick

vibration damping material. Mounted on the top of the longer tubes, to one end, were two stainless steel shafts upon which the A-frame could traverse.

3.1.1.2 THE A-FRAME

The A-frame was constructed from a number of rectangular steel tubes which formed two triangular 'A' shaped structures joined by three tubes, one at each point of the triangle. A fourth tube was attached at the bottom directly in line with the top one.

A vertical rod was attached between the top and bottom tubes. Along this rod a probe carrier could traverse. It was connected, via a thin wire, to an external block which was moved in order to adjust the position of the probe carrier to within an uncertainty of ±3mm.

The A-frame was traversed by driving a 0.5m worm screw which located in a tapped assembly attached to the underside of the A-frame. Drive to the worm screw was provided by either an electric motor or manually through a hand wheel, both linked to a 100:1 reduction gearbox.

The electric motor was used to move the A-frame through relatively large distances, whilst the hand wheel was used for very small distances.

Displacement of the A-frame was determined using either a 300mm rule and vernier attached to the base frame and A-frame respectively, or by using a dial gauge attached to the base frame with it's plunger impinging on the A-frame. The uncertainty of the rule and vernier arrangement was ±0.1mm, whereas that of the dial gauge was ±0.01mm.

Attached to the probe carrier was a probe block on which were mounted two chromel-alumel thermocouples, two linear voltage displacement transducers and two wall contact probes. The thermocouples were manufactured by Omega Engineering Inc., U.S.A. and were of 25μm diameter with a butt-welded junction of less than 40μm diameter. Ziai [1] had calibrated the thermocouples against N.P.L. thermocouples and had determined the thermo-electric response to be:

$$\theta = 26.1103V + 0.745V^2 - 0.2573V^3 \qquad (3.1)$$

In equation (3.1) the units of θ are °C, and V is in millivolts.

The thermocouple probes were mounted on arms in order to position them at the centre-line of the cavity as the vertical rod was offset 120mm from the cavity centre-line.

The length of the thermocouple probes' prongs had been shown by Ziai [1] not to lead to significant conduction losses. The thermocouple wires were arranged in the shape of a 'V' so that the junction could be brought close to the intersection of the laser beams.

The thermocouple probes were oriented as vertically as possible so as to minimise the uncertainties that could be introduced by the steep thermal gradients near the walls.

An analysis of the frequency response of the 40μm diameter chromel-alumel thermocouple junction was carried out by Ziai [1] to justify it's use in the measurement of turbulent fluctuations.

By assuming that the thermocouple junction was in still air, and by using an unfavourable heat transfer coefficient in his calculations, Ziai [1] calculated the slowest frequency response to be 9Hz. As this value would increase substantially in turbulent flow, and because Smith [27] and Dastbaz [26] had found there to be no significant power at frequencies above 20Hz in their temperature spectra (using data for natural convection along a vertical flat plate) Ziai [1] concluded that the thermocouples would be suitable for use in the cavity flow. His temperature spectra confirmed this by showing no significant power in frequencies above 20Hz.

The linear voltage displacement transducers were AC type Schaevitz 100MHR's. Each had a spring loaded armature which contained a magnetic core. Displacement of the core produced a proportional change in the final DC voltage generated by the associated circuitry. These transducers were used to measure very small steps in distance in the first 2mm from each wall. Each transducer was calibrated by Ziai [1] and the equations relating voltage to distance were:

$$\Delta y = 0.3618\Delta V \qquad \text{(heated wall)} \qquad (3.2)$$

$$\Delta y = 0.3426\Delta V \qquad \text{(cooled wall)} \qquad (3.3)$$

In equations (3.2) and (3.3) the units of Δy are mm, and ΔV is in volts.

Mounted on (but electrically insulated from) each thermocouple probe casing was a wall contact probe. When this came into contact with a wall an LED on the cavity control panel would light up. This indicated the closeness of the thermocouple junction to the wall.

All probes on the probe block had to be aligned outside the cavity on a small jig. This jig consisted of a mounting for the probe block, a screw to advance/retract the probe block, and a plate representing the wall.

When aligning the probes the jig was oriented so that the probe block was in the position it would assume in the cavity. The first probe to be aligned on each side was the thermocouple. It s junction was aligned with two intersecting lines scored on the plate. These represented the vertical centre-line of the cavity and the horizontal centre-line of the probe block.

Next the wall contact probe was set up. A separate multi-pin connector was used to link the probe to the main control panel, and the plate was earthed. A microscope was used to view the junction and a feeler gauge used to estimate it's distance from the plate. The contact probe was set up to touch the plate when the junction was approximately 0.25mm from it.

Finally the L.V.D.T. was positioned so that it registered a voltage within the manufacturer's recommended range of ±8V when the junction was between 0.25 and 2.0mm from the plate.

Unfortunately due to a twist in the vertical rod the settings made on the jig did not always coincide with those found in practice. Generally speaking, the difference in thermocouple junction position, relative to the wall, was small when the probe block was in the top third of the cavity, but the difference increased further down.

A further complication was an excessive clearance between the probe carrier and the keyways in the central region of the rod. This allowed the probe carrier to swing about it's nominal position. This could not be corrected when the cavity was kept closed in the early experiments. Later experiments required the cavity be opened before a run at a new height. In these circumstances two "Jubilee" clips were attached to the rod at the top and bottom of the probe carrier. They were pushed against the carrier and tightened so restricting the angular movement.

Thermocouple lead wires, and wires to the L.V.D.T.'s and wall contact probes, were led through a slot in the floor of the cavity. All these wires were greased to stop them being stretched within their guide tubes as the A-frame was moved. Both the vertical rod and outer vertical beam were also greased to allow easy movement of the probe carrier and external block.

In the latter experiments the vertical rod was lagged with 12mm thick sponge to reduce heat transfer to it (and so conduction of heat to the A-frame).

The A-frame had new structures added to it for the present study to facilitate the use of a laser Doppler anemometer. Two vertically traversing supports were added, one to carry the light transmitting optics and the laser, and the other to carry the photomultiplier. Both were counter balanced and were made as rigid as possible to reduce misalignment between the measuring volume and the photomultiplier when moving the A-frame. The new structures are shown in Figure 3.1

3.1.1.3 THE COOLED WALL

The cooled wall sub-assembly was the only one which was not mobile or easily removed. This was due to the attachment of bulky ducting which carried cooling air.

The wall consisted of a 3000 x 1000 x 8mm aluminium plate with a steel plate located 10mm behind it. Seven, horizontal, right angle sections divided the gap between the two plates into six cooling channels.

The heights of the channels had previously been fixed by Ziai [1] to allow approximately equal heat transfer through each channel. Any variation in practice could be allowed for by varying the flow rate of the coolant through the channels.

To reduce heat transfer from the steel plate, 30mm of fibre glass wool, faced off by 5mm of plywood, was fixed to it s external face.

The coolant, air, was drawn from an adjacent large laboratory by a two-stage axial-flow fan. To prevent damage to the fan, or clogging of the cooling channels, a large filter was fitted to the air intake.

The air was directed along ducting, insulated with expanded polystyrene and cardboard, until it entered convergent ducts which were attached to flow gates. From there it passed through divergent ducts to the cooling channels.

On the exit side of the cooled wall, convergent ducts directed the air to ducting which carried it back out into the adjacent laboratory, to a position well away from the intake.

Immediately downstream of the fan (some 6m upstream of the cooling channels) was a 3kW heater. Some 4m downstream of this was a 1.5mm bead thermistor which was connected via a control circuit to the heater and a control box.

The control circuit attempted to keep the temperature of the cooling air entering the channels to within ±0.1K of that set at the control box. Unfortunately the control box could not be marked with absolute temperatures and so it s setting was largely a matter of experience.

Fitted in the centre of each channel, on the back of the aluminium plate, was a copper-constantan thermocouple. Each thermocouple could be connected to a common cold junction via a multiway thermocouple selector switch. The cold junction was an ice-water mixture kept in a thermos flask with a 30mm expanded polystyrene cover.

Ziai [1] claimed that the readings from these thermocouples would give a reasonable indication of the temperature distribution over the vertical

centre-line of the cooled wall, and so adjustments to the flow gates and the control box were made using the readings from these thermocouples.

The copper-constantan thermocouple thermo-electric response was quoted by Ziai [1] as:

$$\theta = 25.599V - 0.05127V^2 - 0.11685V^3 \qquad (3.4)$$

In equation (3.4) the units of θ are °C, and V is in millivolts.

Information concerning the channel heights and thermocouple positions for the cavity heights of 2.5 and 2.0m is given in Tables 3.1 and 3.2.

3.1.1.4 THE HEATED WALL

The heated wall was mounted on a platform which could be moved back from the rest of the cavity in order to gain access to remove the probe block, clean the inner walls, etc.

The wall was a 3000 × 1000 × 5.75mm aluminium plate which was mounted in an aluminium frame. Bonded to the rear of the plate were twenty Watlow, silicone rubber based, heaters, all of which extended across the full 1m width of the plate. All but two of the heaters were of the same height.

The heaters were connected in ten groups, each of which was supplied with a constant voltage via a variac. The group connections were made so that there were fewer heaters per variac in regions where the heat transfer rate varied most rapidly with height.

To prevent overheating a trip, set at approximately 100°C, was attached to the plate under each heater group.

A relay switching arrangement allowed a Wattmeter to be connected to each variac, in turn, so that the power supply to each group could be monitored.

The heater group arrangement used by Ziai [1] had to be changed when the cavity height was reduced, first to 2.5m and then to 2.0m, during the course of the present study. In these instances heaters above and below the false floor and ceiling were used as guard heaters. General information concerning the heater connections is given in Table 3.3.

The heaters were insulated at the rear by a 115mm thick layer of fibre glass wool which was faced off by 15mm thick plywood.

Expanded polystyrene was already fixed around the edge of the aluminium frame holding the heated wall, but more was added during the present study to reduce heat loss from the frame.

Rubber draught proofing strips were fixed to the outer edges of the polystyrene to prevent leakage.

The heated wall was firmly butted to the rest of the cavity by two large clamps, spanning the rear platform channel and a cross member on the base frame, and by seven special screws passing through the frame and into the vertical side walls.

Twenty copper-constantan thermocouples were installed in the wall, in positions corresponding to the centres of the heaters. Each thermocouple was seated in a 1mm diameter, 5.5mm deep hole, which placed the thermocouple junction approximately 0.25mm from the plate surface. As for the cooled wall the thermocouples were connected to a common cold junction, and were of the same type. Table 3.4 gives all the height information for the thermocouples in the 2.5 and 2.0m cavities.

3.1.1.5 THE VERTICAL SIDE WALLS

The side walls were each originally constructed from a 15mm thick plywood frame (3000 x 500 x 190mm) and three 6mm sheets of perspex forming two cavities, one 84mm deep and the other 100mm deep. Ziai [1] had calculated the heat loss through these walls (using the recommendations of Jakob [78]) to be of an acceptable level.

Early experiments in the present study indicated that the heat transfer through these walls was unacceptably high and in order to reduce it the middle perspex sheet was removed and the whole 190mm gap was filled with expanded polystyrene.

To provide optical access for the laser beams, sections were cut out of the polystyrene at the heights of interest. Each access slot was 70mm high on the beam output side, and 90mm high on the beam input side. Smaller sections of 50mm width had also to be taken out on the beam output side, to allow for alignment of the laser beams with the thermocouple junctions. These are shown in Figure 3.2 and Plate 3.1.

3.1.1.6 THE FLOOR AND CEILING

The original floor and ceiling were basically perspex boxes which were completely filled with expanded polystyrene. Both had a 300 x 12.5mm slot through which the vertical rod passed.

The decision to use laser Doppler anemometry in the present study meant that a false floor and ceiling had to be installed. This was necessary because the cavity structure did not allow the anemometer access to the upper and lower extremities of the 3.0m high cavity.

Initially the cavity height was reduced to 2.5m with the new ceiling and floor 205mm and 295mm, repectively, from the originals.

At first a structure made from lengths of alumnium angle (with the four vertical supports in the corners of the cavity) was used to support perspex panels which formed the floor and ceiling. The gaps between the panels and the original floor and ceiling were left unfilled.

The results from the first survey showed that this arrangement allowed excessive leakage (and hence heat loss) through the floor and ceiling.

A solution to these problems was found by removing the aluminium frame and building up the floor and ceiling with expanded polystyrene blocks.

For the ceiling, the blocks were cemented to the original ceiling and faced off by hardboard which provided a smooth surface.

In the case of the floor the blocks were just placed in position and the previously used perspex panels laid on top.

Extra sponge seals were installed in both the floor and ceiling slots to reduce leakage.

As a further attempt to reduce leakage, expanded polystyrene blocks were cemented to the cavity around the top and bottom beams of the A-frame as shown in Figure 3.3.

Draught proofing strips and wads of cotton wool at the ends of the polystyrene completed the seal.

When the cavity height was reduced to 2.0m, for the final measurements, a further layer of blocks was added to those at the floor.

In all Series the seeding generator for the laser Doppler anemometer system was housed in a cavity in the blocks supporting the false floor.

The seeding generator was connected to a compressed air supply which was regulated by a needle valve.

The seeding particles were conveyed into the cavity via a polymer tube which passed through the vertical rod access slot (at the position closest to the cooled wall) and protruded approximately 10mm into the cavity.

3.1.2 THE THERMOCOUPLE SIGNAL PROCESSING INSTRUMENTATION

The temperature range of interest within the cavity was 25-80°C which corresponded to an output of 1.0-3.2mV for the chromel-alumel thermocouples.

The data logging system had a range of 0-10V. The thermocouple signals were amplified and zero-shifted to make the best possible use of that range.

The signals were first amplified by DANA high gain DC amplifiers then passed to DISA signal conditioning units which provided zero shift and further amplification.

Previous surveys of natural convection temperature fields (Ziai [1] and Dastbaz [26]) had shown that the power at frequencies above 20Hz was insignificant. Thus, a minimum sampling rate of 40Hz was required to prevent aliasing in the power spectral analysis.

The clock in the data logging system did not permit sampling at less than 100Hz and so this was the sampling rate chosen.

To match the sampling rate, the low pass filters on the DISA signal conditioning units were set to 50Hz.

3.1.3 THE LASER DOPPLER ANEMOMETRY SYSTEM

Laser Doppler anemometry, in relation to natural convection flow, has been reviewed in Chapter 1, the Introduction. The present author has also produced internal reports King [80] and King [81] which respectively described laser Doppler anemometry in general and the present anemometer system in detail.

Therefore it is only necessary to describe the most important details of the system (in this Section) which is illustrated in Figure 3.4 .

The laser Doppler anemometry system was a standard 55X modular optics system manufactured by DISA (now DANTEC) utilizing a 15mW, co-axial He-Ne laser and a frequency tracker. It was operated in the dual beam mode with a Bragg cell to provide the frequency shift necessary for the measurement of negative velocites.

A beam expander, mounted at the front of the transmission optics, was incorporated to reduce the dimensions of the probe volume. A cardboard mask was fixed to the beam expander. This was used to cut out the unwanted beams generated by the Bragg cell. This made the alignment of the probe volume with the thermocouple junctions easier, and increased the signal to noise ratio of the system.

A DISA seeding generator was used to provide particles of corn oil (Mazola corn oil!). The corn oil was not entirely satisfactory as it deposited on the vertical side walls of the cavity necessitating frequent cleaning of these walls.

At the suggestion of DISA, a 50-50 volume mixture of water and glycerine was initially used but it proved to have too short a life within the cavity, showing a significant loss of signal after only five minutes operation.

As will be described later, olive oil was used as the seeding agent in Poitiers. This is now considered to be preferable to corn oil.

The use of a frequency tracker rather than, say, a counter, was dictated by availability of the equipment rather than by any technical reason. This decision led to a requirement for a relatively high level of seeding since the tracker needs an almost continuous Doppler signal.

The frequency tracker was able to monitor signals within discrete frequency ranges which were switch selectable on the front panel. The frequency range chosen was determined by the expected frequency range of the signals, which in turn were determined by the expected velocity range.

Each of the selectable frequency ranges had a quoted accuracy of 1% of the maximum in each range. This limited accuracy initially presented some problems when measuring the relatively small velocities near to the cavity centre, as it was not desirable to change the range during the measurement of any profile.

Tests at the cavity centre showed that the tracker exhibited an uncertainty of +0.02m/s for the frequency range 33.3-333kHz. Further details of the problems caused by the limited accuracy of the tracker were given in a paper presented at the 1st Laser Doppler Users Conference held in Manchester in December 1985 (Cheesewright and King [87]).

The solution to the accuracy problem proved to be the calibration of the tracker against a frequency standard. This enabled the accuracy to be improved to approximately 0.3% of the maximum of the 33.3-333kHz range. This was the best one could expect as the accuracy was limited by the eight bit resolution of a digital stage in the signal path within the tracker.

This tracker accuracy corresponded to a velocity resolution of 0.009m/s when using the 33.3-333kHz range and the 750mm focal length lens.

The calibration graph for the tracker range of 33.3-333kHz is shown in Figure 3.5. It was found to be repeatable from day to day.

Further details of the system parameters are included in Chapter 4, the Experimental Procedure.

3.1.4 THE DATA LOGGING SYSTEM

The data logging system was based on a Digital PDP 11-34/A computer with 256k bytes of memory. The operating system used was RT-11 version 4.

The other modules of the system were: an analogue to digital converter; an SE labs 8000 tape unit; a Winchester disc drive with 80Mb storage capacity; a Datamedia Excel 12 VT100 terminal; and a Sanders Media 12/7 printer.

The twelve bit analogue to digital converter had previously been designed and manufacturered at the College. It was capable of accepting up to nine inputs of which a maximum of four were used: two for the thermocouple signals; one for the Tracker velocity signal; and one for the Tracker lock detector signal.

Both the sampling frequency and the number of channels were set by switches on the front panel of the A/D converter.

When the digital representation of a signal was transferred to the computer it occupied the lower twelve bits of a sixteen bit word. The data were stored on either magnetic tape or the Winchester disc, with the former being used whenever it was intended to process the data on the ICL 2988 mainframe computer.

The tapes were written with E.C.M.A.-13 standard labels (two header standard VOL1 HDR1 HDR2 * DATA * EOF1 EOF2 * HDR1 etc. where * represents a tape mark) with the byte order of the data arranged for direct reading on the ICL 2988 mainframe.

A FORTRAN program had previously been written to put the data and the E.C.M.A.-13 labels on the tape. The subroutines which wrote the labels to the tape were rewritten to improve their readability and to bring them into line with the latest version of E.C.M.A.-13.

The volume identifier of each tape was six characters in length, the first two representing the month, and the second two representing the day, on which the data were recorded. The final pair of characters represented the non-dimensional height at which the data were from. An example is JE1490 where data was recorded on June 14th at $x/H \simeq 0.90$.

Initial processing of the tape data was made using the PDP 11-34/A and yielded the mean and R.M.S. of the fluctuating components. Some of the early results, using the PDP, were subject to uncertainties in the R.M.S. data. This was due to errors in tape reads. A later version of the basic analysis program incorporated checks on the magnitude of the data (always in the range 0-4095). This eliminated the tape read errors (which incidentally did not affect the mean quantities).

The program which writes data to tape has been retained on the PDP system under the name PMTW3V, and the basic analysis program under the name PLATA1 (this program incorporates the tracker calibration corrections). More detailed accounts of the programs are given in King [82].

Several analysis programs were written for the ICL 2988. These were used to calculate $\overline{u'T'}$, $\overline{u'\rho'}$ and power spectral densities, among other quantities, and utilized ICL subroutines which read the data at byte level.

3.2 THE APPARATUS AT POITIERS

The apparatus at Poitiers (which has been described by Renault [32]) differed from that at Q.M.C. in the construction of the cavity, the method of traversing the temperature probe and in some aspects of the laser Doppler anemometry system.

The description is again split into Sections dealing with: the cavity; the temperature measuring system: and the laser Doppler anemometry system.

The final signal processing was performed by a Solartron 7065 microprocessor voltmeter for both the temperature and velocity measuring systems. The in-built programs used in each case are described in the relevant sections.

No alterations were made to the cavity (although if time had permitted additional insulation would have been added to all closing boundaries) but an alteration was made to the temperature measuring system which had been used by Renault [32], because of a fault which developed in it.

3.2.1 THE CAVITY

In view of the decription by Renault [32], only a brief summary is presented here.

The cavity consisted of four major sub-assemblies.

(a) The cooled wall.

(b) The heated wall.

(c) Two vertical side walls walls.

(d) The floor and ceiling.

Views of the cavity heated and cooled walls can be seen in Plates 3.2 and 3.3 respectively. These also show associated instrumentation.

3.2.1.1 THE COOLED WALL

The cooled wall was a single plate, 2.0m high by 0.6m wide, which was cooled by the circulation of Freon R502 refrigerant. The system consisted of four separate units regulated by a flow gates.

Each unit occupied one quarter of the plate height and was comprised of loops of copper tubing attached to the rear of the plate. The copper tube was covered with insulation and four chromel-alumel thermocouples were attached to the rear of the plate, one in the middle of each cooling unit, to monitor the plate temperature.

The motivation behind the use of this type of cooling system was to achieve a greater temperature difference across the cavity, and more importantly, to ensure that the average cavity temperature was close to the

ambient, so reducing heat transfer through the vertical closing walls. Unfortunately this lead to condensation on the cooled wall during the commissioning experiments reported by Renault [32], and so the lowest usable cooled wall temperature was dictated by the need to avoid condensation and was usually 5-10°C.

3.2.1.2 THE HEATED WALL

The heated plate was comprised of five "layers". The first was made from five duralinox A63 plates each 0.4m high by 0.6m wide and 20mm thick. These plates formed the inner face of the wall and were carefully fitted together to ensure a plane surface. Each plate had a chromel-alumel thermocouple installed in it (at 0.5mm from the surface) connected to a common cold junction (of ice-water) via a selector switch.

The second "layer" was a 0.3mm sheet of samicanite which acted as an electrical insulator to the third "layer" which consisted of a carbon ribbon heater, again in five sections corresponding to the five duralinox plates.

Each ribbon was connected to a variable current control supplied from a stabilised power supply. Large variations in plate temperature were made by adjusting the power supply, with finer temperature adjustments being made with the variable current control.

The fourth "layer" was a 12mm kerlane plate which acted both as a thermal and an electrical insulator.

The fifth "layer" was a wall support structure.

The wooden frame which supported the duralinox plates extended approximately 10mm above and below the plates within the cavity, so that the heated wall stood out from the frame. This meant that the heated wall had what might be termed a "leading edge". This is illustrated in Figure 3.6.

The temperature of the heated plate could be varied from room temperature to a maximum of approximately 150°C.

3.2.1.3 THE VERTICAL SIDE WALLS

Unlike the Q.M.C. cavity, the Poitiers cavity was designed to be easily dismantled to allow for changes to the vertical and horizontal walls to alter the cavity width. All vertical walls were of the same construction. They consisted of a wooden frame which housed two 10mm plates of plexiglass separated by a 6mm air gap. A foam seal was incorporated to prevent leakage.

3.2.1.4 THE FLOOR AND CEILING

The floor and ceiling were both comprised of an outer construction based on a 10mm plate of plexiglass and an inner construction consisting of planks of unsanded wood. When condensation ran off the cooled wall it soaked into the wood.

3.2.2 THE TEMPERATURE MEASURING EQUIPMENT

The temperature measuring equipment used by Renault [32] was based on resistance thermometry. This system required calibration before use and was found by the present author to be faulty. Many attempts to locate the problem finally pointed to some problems in the power supply which could not easily be rectified. Thus an alternative system was constructed using 25μm diameter chromel-alumel thermocouple wires of the type used in the Q.M.C. cavity.

Use was made of the existing temperature probe holder and traversing unit which was inserted into holes in the cooled wall. Once the main unit was located the probe was traversed into the cavity. The probe was housed in a thin walled tube and consisted of standard chromel-alumel thermocouple lead wires which were separated into a 'V' at the end, to form two short prongs which were bent downwards to make them vertical. The thermocouple wires were soldered onto these in the form of another 'V' (so that a diamond pattern was formed) and were parallel with the prongs.

In order to measure close to the heated wall the prongs were bent slightly forward so that the measuring junction could touch the wall first. The orientation of the measuring junction at the heated wall was such that it pointed upstream. In the case of the cooled wall the prongs were bent back slightly so that the measuring junction could touch the wall first. The main unit and probe holder were rotated 180°, relative to the position used for measurements at the heated wall, so that the junction again pointed upstream (above the top of the access hole).

This new method of temperature measurement has allowed the heat transfer to the cooled wall of this cavity to be estimated for the first time.

The thermocouple was connected to a common cold junction and its signals fed to a Solartron 7065 microprocessor voltmeter. Two in-built programs were utilized to analyse the incoming signals. Program 8 (devised for all types of chromel-alumel thermocouples) was used to convert the signal to temperature values in °C. Program 7 was used to calculate the mean and the R.M.S. of the fluctuations.

The sampling frequency of the voltmeter was dependent on the number of programs being run. When both programs 7 and 8 were being run the sampling rate was approximately 4Hz. Previous researchers at Poitiers had considered 3 mins to be a sufficient sample time, but, having previously analysed the Q.M.C. data, the author chose 4.5 mins. Justification for this choice is given in Chapter 6.

3.2.3 THE LASER DOPPLER ANEMOMETRY SYSTEM

The laser Doppler anemometry system was based on a 35mW Spectra Physics He-Ne laser, with DISA light transmission, and collection, 55X optical units. These included: a Bragg cell, to provide frequency shift to enable the measurement of negative velocities; a photomultiplier; but no beam expander. The system could measure only one component of velocity at a time, and operated in the dual beam mode.

The laser and light transmission optics were mounted on a milling machine table which provided accurate traversing of the laser beams across the cavity. The photomultiplier was mounted on a separate stand and had to be re-aligned with the measuring volume each time the laser was moved.

Vertical movement of the laser was achieved by traverse of a large vertical column on which the milling machine table was mounted. The photomultiplier could also be easily moved up and down a vertical shaft on it s stand. However, the laser and transmission optics had to be moved to another support for heights below x/H = 0.3. This support is not shown in Plates 3.2 and 3.3.

The signal processor was a DISA 55L96 Counter. This device is normally used when the density of seeding particles is very low and substantial dropout exists. In such a case a Counter is interfaced with other equipment (a buffer and a computer) which are required for intermittent signal analysis.

However, a DISA 55L93 digital to analogue converter had been fitted which provided continuous output to the Solartron 7065 voltmeter running Program 7.

The high seeding density in the cavity meant that dropout was low, and also resulted in a data rate far in excess of the frequencies expected within natural convection (i.e. up to 20Hz). Chapter 6 presents results from the re-sampling of the Q.M.C. data which confirms that the sampling rate of 4Hz yields accurate data.

An oscilloscope was used to monitor the Doppler bursts, this greatly aided alignment of the measuring volume and photomultiplier.

The seeding agent was sunflower oil which was atomised in the same manner as the corn oil of the Q.M.C. experiments. The particles were introduced via a hole at the base of the cooled wall.

FIGURE 3.1

THE Q.M.C. CAVITY

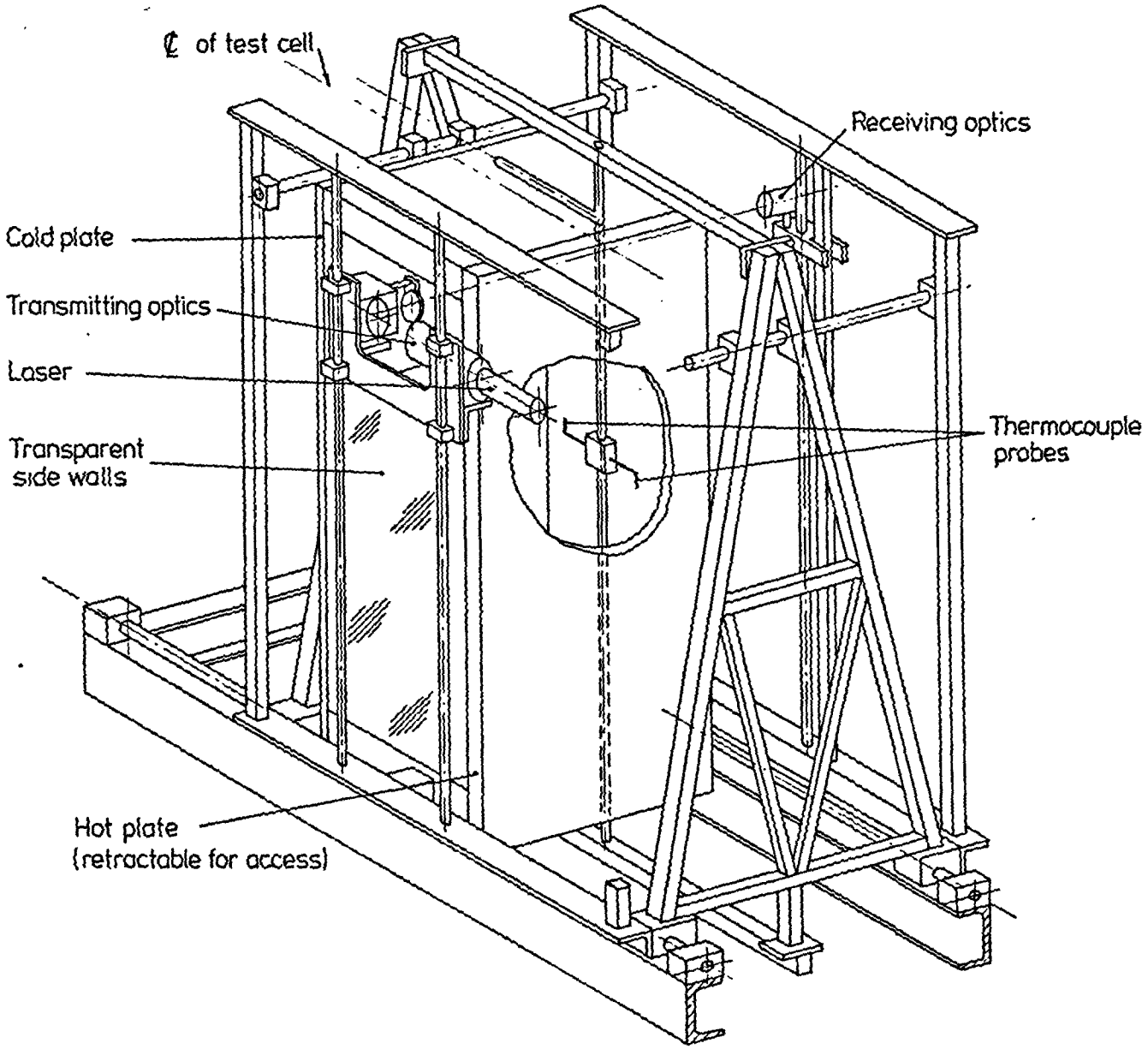

FIGURE 3.2

SKETCH SHOWING THE OPTICAL ACCESS BLOCKS REMOVED

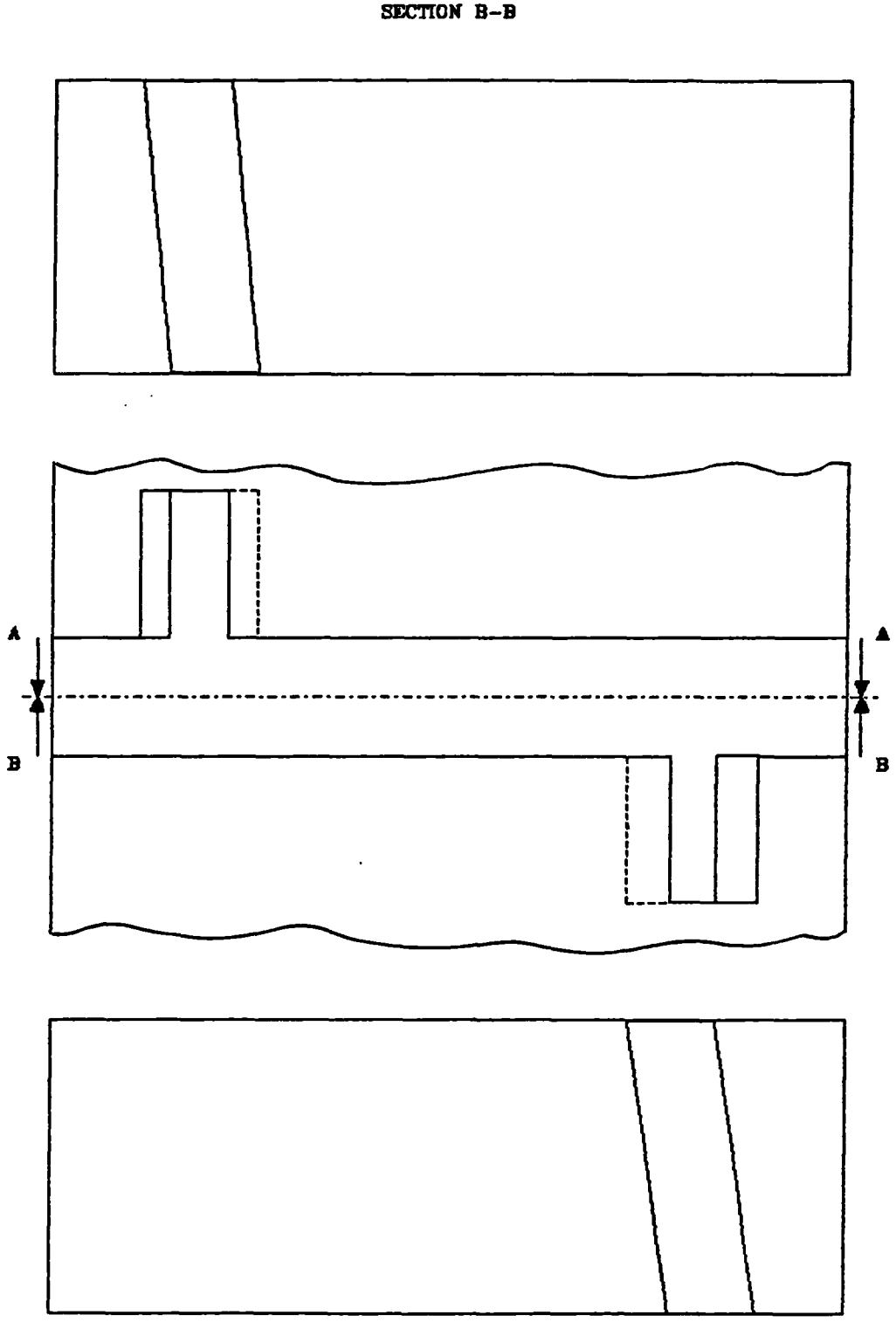

FIGURE 3.3
ADDITIONAL SEALS AT THE TOP
AND BOTTOM OF THE Q.M.C CAVITY

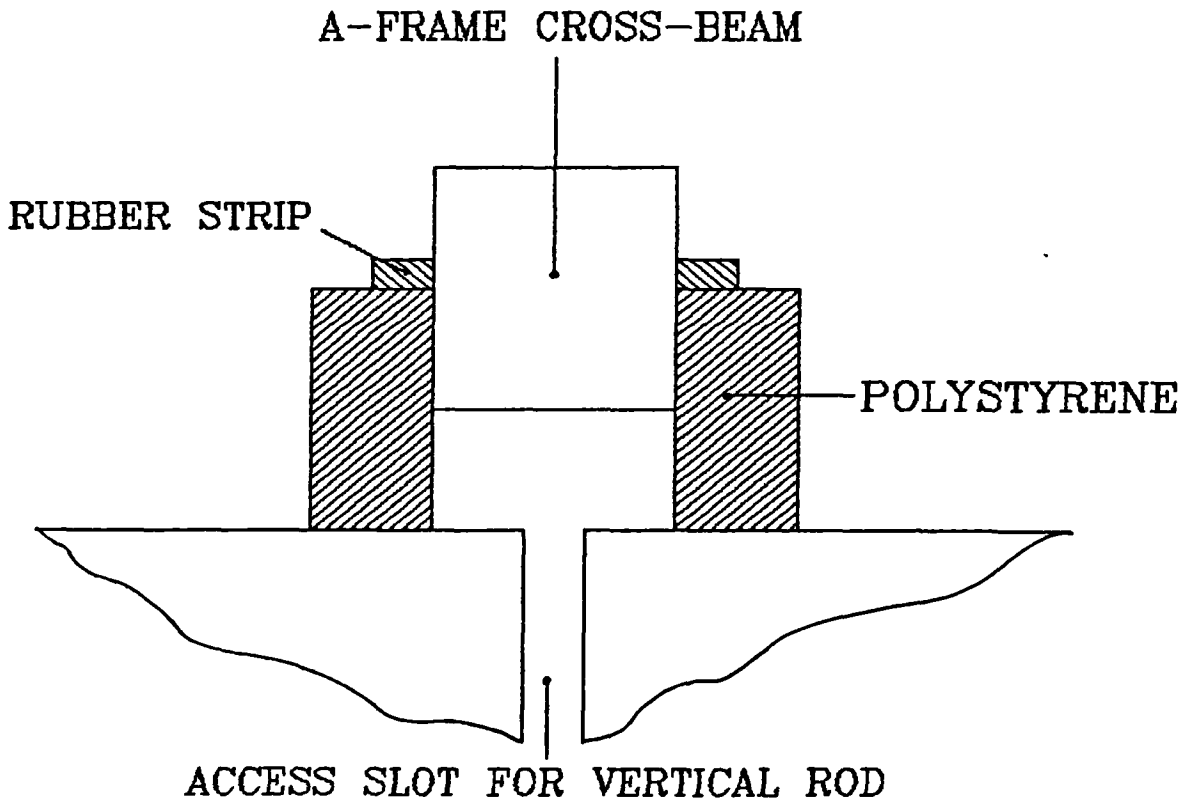

SECTIONAL VIEW LOOKING IN y DIRECTION

FIGURE 3.4

UNITS OF THE Q.M.C. LASER DOPPLER ANEMOMETRY SYSTEM

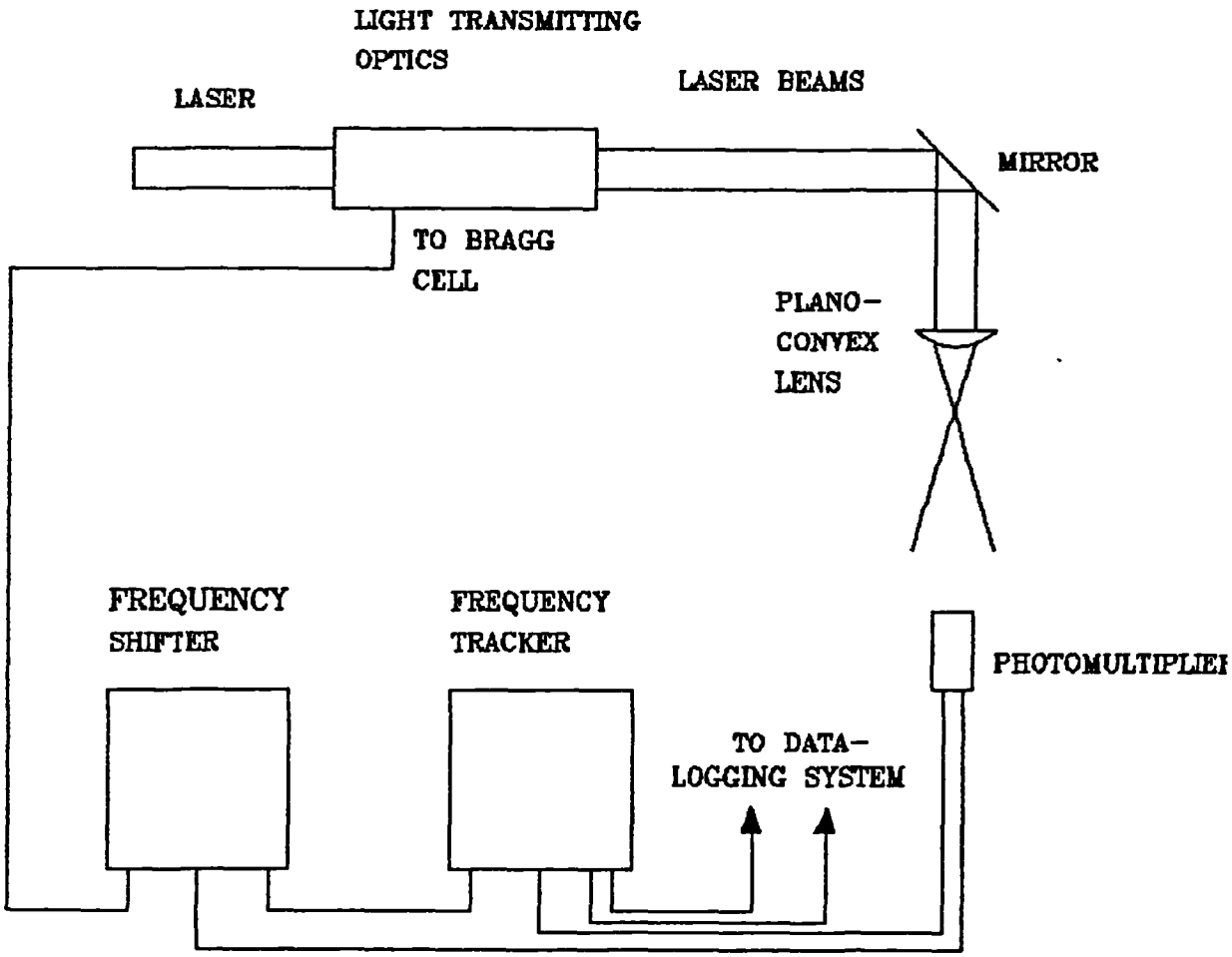


DISA TRACKER CALIBRATION GRAPH
(output - input)/kHz
-.5
0
.5
1.0
1.5
2.0
2.5
3.0
20
40
60
80
100
120
140
160
180
200
220
240
260
280
300
320
input/kHz

FIGURE 3.5

FIGURE 3.6

THE POITIERS CAVITY HEATED WALL

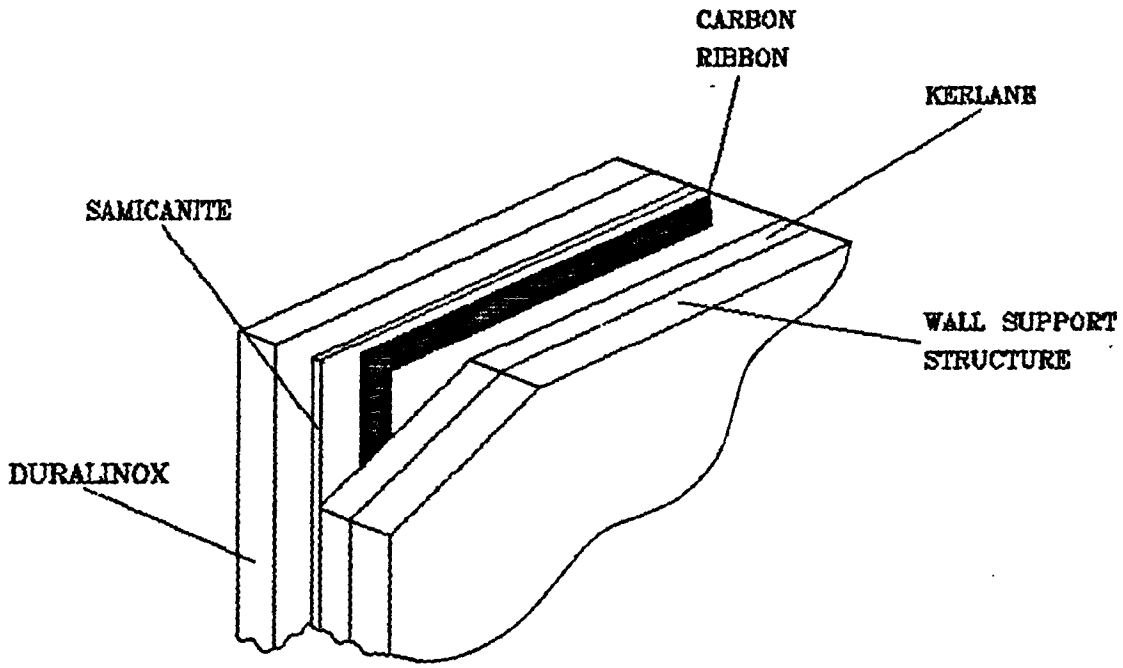

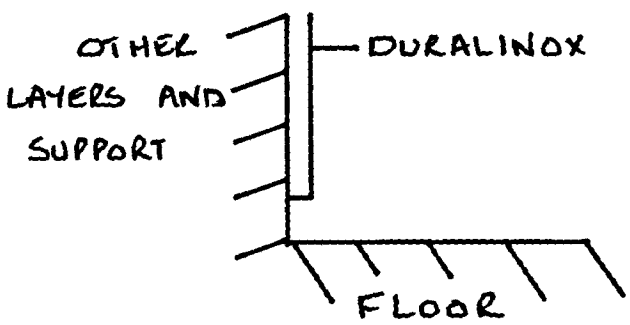

TABLE 3.1

COOLED WALL CHANNEL & THERMOCOUPLE

HEIGHTS FOR ORIGINAL 3.0m HIGH Q.M.C. CAVITY

CHANNEL	HEIGHT/m	THERMOCOUPLE	x/m
1	0.40	1	0.200
2	0.70	2	0.750
3	0.80	3	1.500
4	0.45	4	2.125
5	0.35	5	2.525
6	0.30	6	2.850

TABLE 3.2

COOLED WALL THERMOCOUPLE POSITIONS RELATIVE TO

FALSE FLOOR FOR Q.M.C. CAVITY HEIGHTS OF 2.5 & 2.0m

THERMOCOUPLE	x/m *	x/m **
1	-0.095	-0.595
2	0.455	-0.045
3	1.205	0.705
4	1.830	1.330
5	2.230	1.730
6	2.555	2.055

SUPERSCRIPTS

* H = 2.5m

** H = 2.0m

TABLE 3.3

HEATER DATA FOR Q.M.C. CAVITY HEIGHTS OF 2.5 & 2.0m

HEATER	HEIGHT/m	VARIAC *	VARIAC **
1	0.1524	-	-
2	0.127	1	-
3	0.127	1	-
4	0.1524	2	1
5	0.1524	3	1
6	0.1524	4	2
7	0.1524	4	3
8	0.1524	5	4
9	0.1524	5	5
10	0.1524	5	5
11	0.1524	6	6
12	0.1524	6	6
13	0.1524	7	7
14	0.1524	7	7
15	0.1524	8	8
16	0.1524	8	8
17	0.1524	9	9
18	0.1524	9	9
19	0.1524	10	10
20	0.1524	10	10

SUPERSCRIPTS

* H = 2.5m

** H = 2.0m

TABLE 3.4

HEATED WALL THERMOCOUPLE POSITIONS RELATIVE TO FALSE FLOOR FOR Q.M.C. CAVITY HEIGHTS OF 2.5 & 2.0m

THERMOCOUPLE	x/m *	x/m **
1	-0.185	-0.685
2	-0.035	-0.535
3	0.080	-0.420
4	0.170	-0.330
5	0.355	-0.145
6	0.530	0.030
7	0.690	0.190
8	0.830	0.330
9	0.945	0.445
10	1.145	0.645
11	1.335	0.835
12	1.450	0.950
13	1.575	1.075
14	1.700	1.200
15	1.955	1.455
16	2.025	1.525
17	2.175	1.675
18	2.375	1.875
19	2.485	1.985
20	2.615	2.115

SUPERSCRIPTS

* H = 2.5m

** H = 2.0m

PLATE 3.1

QMC CAVITY SIDE WALL WITH OPTICAL ACCESS

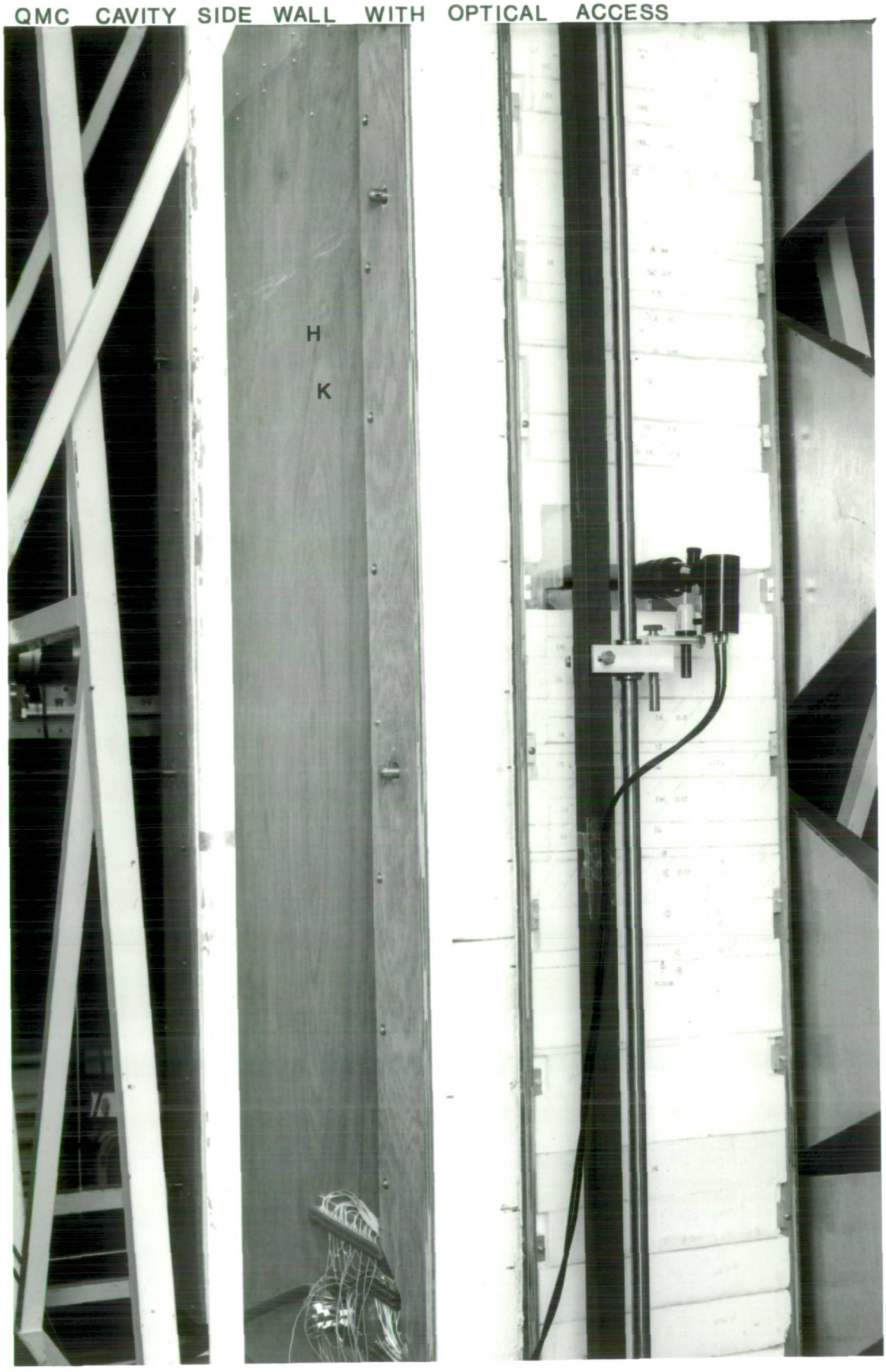

PLATE 3.2

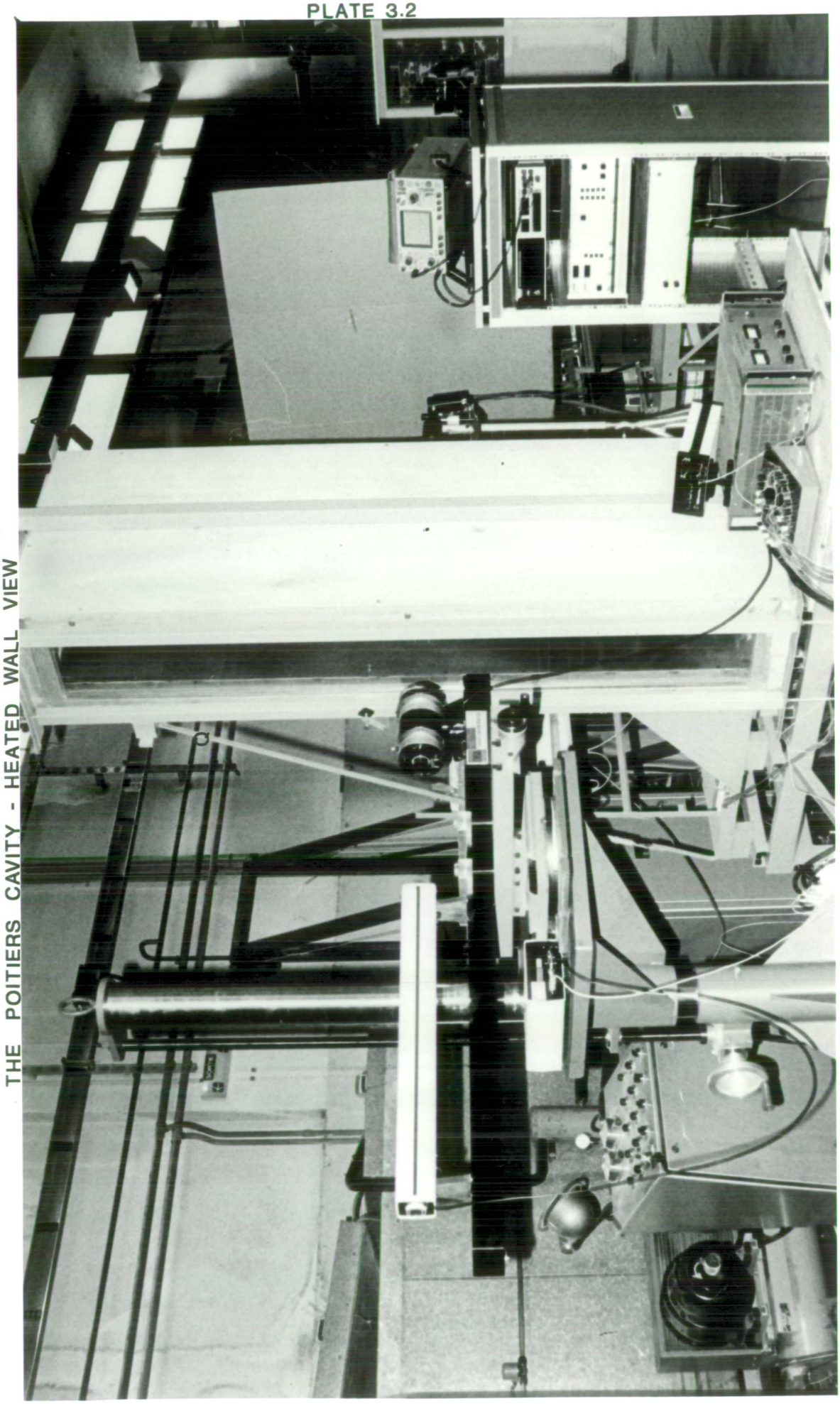

THE POITIERS CAVITY - HEATED WALL VIEW

PLATE 3.3

THE POITIERS CAVITY - COOLED WALL VIEW

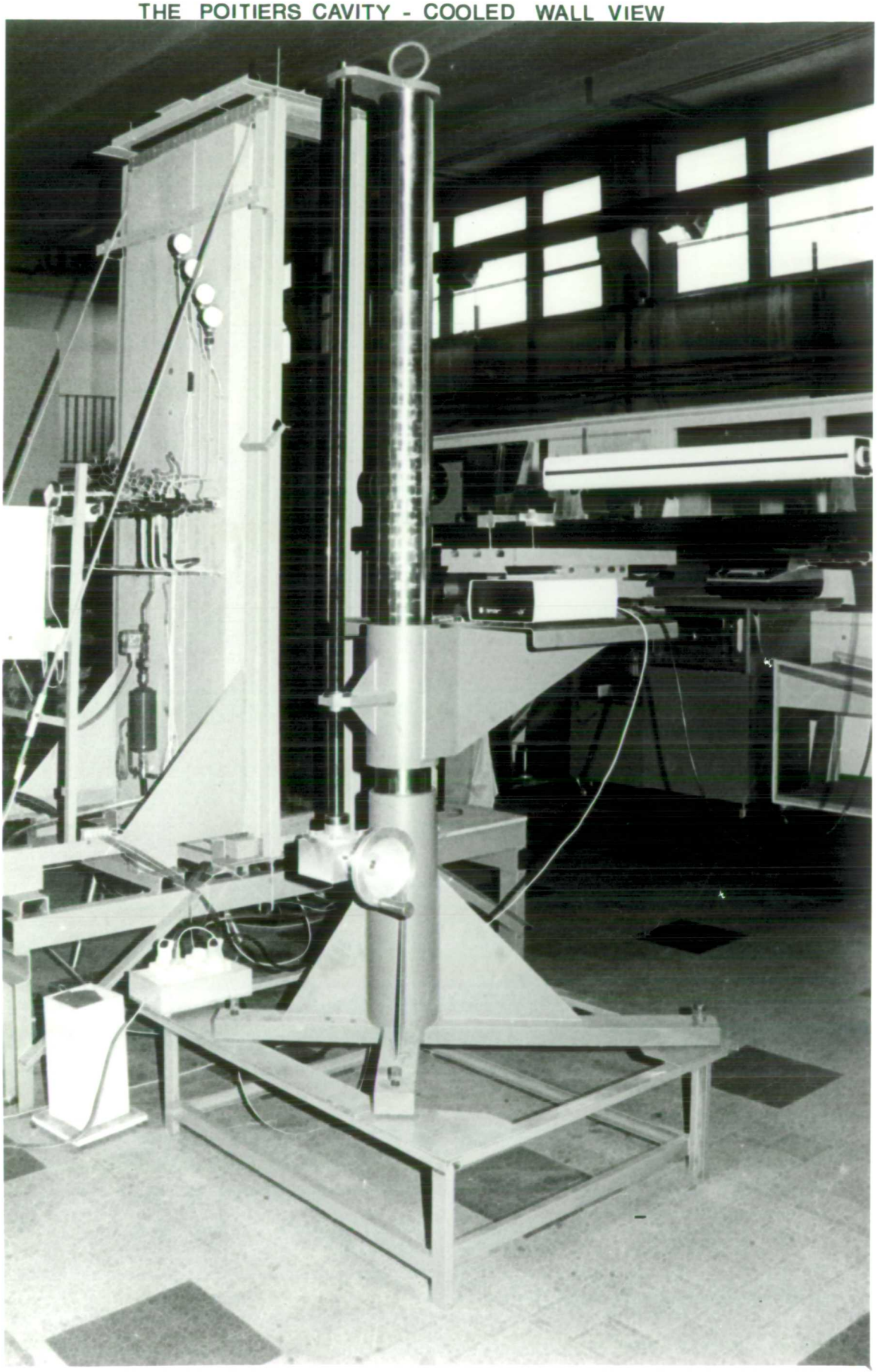

CHAPTER 4 - EXPERIMENTAL PROCEDURE

4.1 INTRODUCTION

Both the experimental procedures for the Q.M.C. and Poitiers cavities are described.

For the two surveys of the Poitiers cavity (Series 6 and 7) the experimental procedures were identical, but the procedure for the Q.M.C. cavity varied slightly between Series 1, 2, 3 and 5.

The procedures for Series 3 and 4 were the same, there being only a difference in sampling time between the procedures of Series 4 and 5.

The procedure followed in Series 3 was a refinement of that used for Series 1 and 2.

4.2 PROCEDURE FOR SERIES 1

The procedure developed for Series 1 formed the basis for all Series on the Q.M.C. cavity. The description has been subdivided into a number of topics, namely: probe preparation; laser Doppler anemometer preparation and parameters; initial cavity preparation; and run procedure.

4.2.1 PROBE PREPARATION

The probes on the probe block were set up as previously described in Chapter 3, the Apparatus, but beforehand the thermocouple wires had to be soldered onto their probe prongs. There were problems associated with this. Firstly, it had to be carried out whilst looking through a microscope, and, secondly, it was not easy to solder the chromel and alumel wires onto their prongs.

It has been recommended, by past researchers, that the process of soldering would be eased by wiping the prongs with phosphoric acid then cleaning them with water and acetone, but this did not significantly aid soldering. The best method was to wash and clean the prongs as descibed and then to "Emery" them. After wiping the dust away with cotton wool, this provided a surface onto which the wires could be soldered with relative ease.

To check that the wires were attached correctly, each thermocouple was connected to the main control panel by a length of lead wire and dipped up to the base of it's prongs in a beaker of water. The position of the thermocouple was maintained by mounting it in a laboratory clamp. The water had previously been allowed to stand, undisturbed in the laboratory, for half an hour to reach a stable temperature. It was easy to ascertain

whether the wires had been attached correctly, and whether the electrical contact between the wires and prongs was good, by measuring the water temperature with a thermometer and comparing this to the thermocouple output signal.

During all such tests (accidental breakage meant that two thermocouples were replaced) it was found that the readings from each thermocouple were never different by more than ±0.005mV which is approximately equal to 0.13K.

Once the probe block had been mounted on the probe carrier, and the cavity closed, the settings of the L.V.D.T.'s and the wall contact probes were checked.

Within the first 2mm from each wall previous researchers (Ziai [1], Dastbaz [26] and Smith [27]) had shown that, for air, the R.M.S. of the fluctuating components of temperature is directly proportional to y.

By using the On-Line program POLDAB it was possible to quickly obtain a value for $T'_{R.M.S.}$. A plot of this against y gave the wall position. If the wall contact probes indicated contact at between 0.0-0.3mm from the wall then their settings were considered acceptable.

The voltage output from the L.V.D.T.'s sometimes exceeded the ±8V range quoted by the manufacturers. As resetting of these devices was time consuming, and insignificant uncertainty was introduced into the value of y beyond 3mm from the wall (where ±8V would be exceeded) the practical range of use was extended to ±11.0V.

4.2.2 LASER DOPPLER ANEMOMETER PREPARATION AND PARAMETERS

Before each experimental series the anemometer was set up in accordance with the detailed procedure given by King [81]. This involved: checking the Bragg cell setting to ensure that the intensities of the shifted and non-shifted beams were approximately equal; checking that the beams were parallel; and measuring the distance between the two beams.

The distance between the beams was found by using internal calipers to measure the distance between the centres of the beams. Obviously the accuracy of this measurement was dependent on the present author's ability to judge the position of the centre of each beam (whilst they were projected onto a vertical white card) and so the technique was checked.

The laser and optics were taken into a larger laboratory and a 750mm focal length converging lens placed in front of them. The beams were projected some 5m down the laboratory onto a vertical surface. By measuring the distance between the surface and the lens, and the distance between the

two beam centres, the uncertainty in the multiplying parameter (used in the equation relating tracker output frequency to velocity) calculated using the beam separation and lens focal length, was found to be 0.05%, i.e. insignificant. However, this only represented a one-off measurement and a more realistic uncertainty may be found by considering an uncertainty of ±0.5mm in the measurement of the distance between the beams. This would result in a ±0.6% uncertainty in the multiplying parameter, $2\sin(\theta/2)$.

Prior to the commencement of some of the daily runs the laser was inadvertently knocked. Each time this occurred the laser and optical units were taken off their support and the beam settings checked. Every time the settings were found to be unaltered. This reflects the robust nature of the construction, and fixings, of the laser and optical units.

For Series 1 the anemometer parameters were as follows.

λ = 632.8nm $2\sin(\theta/2)$ = 0.09506 f_s = 100kHz

Tracker range 33-333kHz Tracker filter BW1

Probe volume: height = 0.284mm, width = 0.284mm, length = 5.970mm

In $2\sin(\theta/2)$, the multiplying parameter referred to previously, θ is the angle between the beams which are brought to intersection by a converging lens. During all the Q.M.G. Series a 750mm focal length lens was used for this purpose, except when off-centre measurements were made for two-dimensionality checks, where a 600mm focal length lens was used.

The tracker frequency range and the frequency shift were selected to allow the measurements of velocities in the range -0.4 to 1.3m/s. These values were similar to the minimum and maximum found by Ierokipiotis [42] and Smith [27] from work on vertical flat plates, and Ziai [1] from work on the 3.0m high version of the present cavity, using hot-wire anemometry.

The tracker low-pass filter was set to it's lowest value, represented by BW1, of 59Hz, which was suitable as Smith [27] and Ziai [1] had not found significant power levels at frequencies greater than 20Hz in velocity spectra.

The appropriate theory regarding the equation relating the velocity component and anemometer parameters is given by King [80]. Thus it is only necessary to quote here, the equation, incorporating frequency shift, together with a description of the anemometer co-ordinate system. Figure 4.1 depicts the laser beams as they cross, with the initially uppermost beam being subject to a positive frequency shift. The component of velocity to be measured is perpendicular to the bisector of the beams.

The equation relating tracker frequency output to velocity is:

$$f_D = f_s + [2\sin(\theta/2)]U/\lambda \qquad (4.1)$$

4.2.3 INITIAL CAVITY PREPARATION

Before each run it was necessary to clean the inner side walls, using acetone, at the appropriate height. This was to remove corn oil which had deposited there from the previous run.

Each run took about 14hrs (minimum) and the flow was seeded thirty times for approximately 5secs each time. This amount of oil, depositing on the vertical side walls, would have caused a reduction in the signal-to-noise ratio of the photomultiplier output. This in turn would have increased the dropout typically by 30% from the end of one run to another. The use of so much oil also necessitated the topping up of the seeding generator.

During this preparation the cavity heating and cooling systems were kept on. After closing the cavity at approximately 2pm the cavity had nearly attained the required temperature at each wall by 7am the next day. Although the variac settings were always left unaltered after each run, the wall temperatures were dependent on the time taken for the cavity to heat up and the temperature of the cooling air in the adjacent laboratory.

The time between 7am and 9am was spent adjusting the wall temperatures to bring them up or down to the required levels. To do this the variac settings were altered by monitoring the heater power output via a Wattmeter. Typically, the power output had to be raised by less than 3%.

The first hour of wall temperature adjustment was taken up in reaching the required temperatures, and the second hour in gradually reducing the variac settings to achieve a stable temperature at each wall.

4.2.4 RUN PROCEDURE

The run was split into two halves, each being completed on the same day. During the first half the probes were brought up to the heated wall and traversed to the cavity centre, and similarly, during the second half, the probes were brought up to the cooled wall and traversed to the centre.

The maximum recommended warm up time of all the instruments used was one hour. Typically the time allowed in practice was one and a half to two hours. The instruments requiring the longest warm up period were the DISA signal conditioning units and, curiously, the DISA frequency tracker.

Whilst the cavity temperatures were being monitored for stability the heated wall thermocouple junction was aligned with the intersection of the laser beams. They had to be as close as possible without creating significant "glare" from the junction. The alignment could only be made when the cavity was seeded so making the beams visible. A small telescope was used to view the position of the junction, it incorporated a graticule which

allowed the measurement of the separation of the junction and beams. (One graticule division being equal to 0.3mm).

The junction was positioned within 0.75mm of the intersection on the upstream side; within ±0.25mm in the traverse direction, y; and within ±0.5mm in the spanwise direction, z. Alignment in the traverse direction was achieved by looking down onto the thermocouple and viewing it against the background of the beams. Care was taken to ensure that the beam width seen was a minimum so reducing any uncertainty in alignment. In the cases of the vertical and spanwise alignments the A-frame was moved so that the beams were directed into the cavity corner to the left of the photomultiplier. In this position the beams could not reflect from the active walls into the author's eyes. Vertical movement was achieved by moving the laser and optics. This option, rather than moving the thermocouple, allowed closer control over the vertical gap between the junction and intersection. To reduce uncertainty in the spanwise alignment the angle of view was kept as near perpendicular to the plane of the beams as possible.

With the junction and intersection aligned, the thermocouple was brought to within 50mm of the heated wall. Here the photomultiplier was aligned with, and focused on, the probe volume. To prevent misalignment, during movement of the A-frame, parts of the photomultiplier connecting leads were "Sellotaped" to the A-frame. This prevented a pull being exerted on the photomultiplier tube via the connecting leads.

The photomultiplier had been supplied with a standard pinhole through which the probe volume was viewed. It's size meant that the area of projection of the measuring volume was approximately twice that of the probe volume.

After alignment of the photomultiplier the probes were moved further towards the heated wall, with a watch being kept on the lock detector output to make sure the photomultiplier stayed in alignment with the probe volume. Whilst bringing the thermocouple close into the wall care was taken not to let the photomultiplier current exceed the manufacturers specified limit of 100μA. This was achieved by reducing the supply voltage to the photomultiplier when the current became too high.

Movement of the probes within 2mm of the wall was achieved by using the hand wheel. Relative position information was taken from the L.V.D.T. output, and extra special care taken in bringing the probes close to the wall until the wall contact LED came on. The hand wheel was then wound backwards until the LED went off and the L.V.D.T. output began to change.

Unfortunately, due to the construction of the cavity, the beams could not be brought parallel to the wall. Instead they arrived at an angle of approximately 6°. This caused substantial glare from the wall which swamped the scattered light, entering the photomultiplier, which formed the signal. This was the case out to at least 0.6mm from the wall, beyond which velocity measurements were possible.

With the thermocouple in position the next step was to calibrate the thermocouple and the data logging systems. Using a 9V battery, connected to resistance boxes, known millivolt signals were input in place of the thermocouple signals. Three values were input to each thermocouple system, these provided enough data to calculate a linear relationship between the thermocouple signal, in millivolts, and the digital computer number.

All data were recorded on magnetic tape using the data collection program PMTW3V. Each data block consisted of 4096 bytes which was 2048 words. There were four channels of input (channel 1 heated wall thermocouple, channel 2 cooled wall thermocouple, channel 3 tracker frequency output, and channel 4 tracker lock detector output) thus each block contained 512 samples from each channel. The sampling rate was 100Hz. Four blocks of calibration data were recorded for each discrete input.

To utilize the maximum range of the analogue to digital converter the thermocouple signals were zero shifted by different amounts. The amount being decided upon by using the data of Ziai [1] to estimate the temperature range which each thermocouple had to cover. Fortunately the tracker frequency output was in the range of 1-10V which coincided with the A/D converter's range.

Channel 3 was calibrated using voltage outputs from a signal conditioning unit, but it was not necessary to calibrate channel 4 as the difference between the lock detector output of 0.1 and 5V was so large. In the analysis program, PLATAI, a computer number over 2000 was considered to be indicative of the 5V signal.

The reason for taking readings from both thermocouples, when only one was really relevant, was to examine the change, if any, of the cavity centre temperature during a run. (When one thermocouple was at a wall the other would be in the cavity centre). Unfortunately one of the signal conditioners had a transient fault which meant that it's output was not always reliable. ← Naturally, only the good unit was used for the most relevant thermocouple during each half of the run, the thermocouple inputs being switched around at the half-way point.

Once the calibration data had been recorded the "run proper" could begin. The photomultiplier voltage was adjusted so that the anode current meter needle was in the lower third of it s scale, and the tracker gain control adjusted so that it s indicator light just blinked.

In normal use, away from the wall, the photomultiplier voltage would be set to 1.75kV, and the gain control adjusted accordingly. The recommended nominal voltage was 1.25kV but the present author found the higher voltage, and lower gain, improved the S.N.R. In such a case the anode current meter needle would only be in the first tenth of it's scale.

The sampling program allowed the number of data blocks to be changed from the calibration requirement of four to the experimental requirement of one hundred (a duration of approximately eight and a half minutes resulting in 51,200 samples from each channel). After the data had been collected the terminal bell would sound and a new position would be moved to.

Data were recorded at thirty positions for each half of the run. The nominal positions are given in Table 4.1. Seeding was undertaken at every two positions.

The duration of the seeding was a matter of experience, as was the setting of the needle valve controlling the compressed air supply. Data collection was not resumed until five minutes had passed after each seeding. The lock detector reading at this time, as seen on a multimeter, was typically 4.8V, indicating a low dropout.

For positions out to 20mm from the wall, movement of the probes was via the hand wheel. The relative position was read from the L.V.D.T output for the first 2mm and then from a dial gauge out to 20mm. Data were collected at eight positions within the first 2mm from the wall to provide a good estimate of the local wall heat transfer rate. Progression after this was in steps of 1mm, out to 10mm, to allow the accurate location of the velocity peak.

Beyond 20mm changes in probe positions were measured using a rule and vernier arrangement, and motive power was provided by the electric motor. The alignment of the photomultiplier and probe volume was checked for these latter positions as the motor tended to induce a "jerky" start to the A-frame's motion.

At every position the temperatures of the wall thermocouples were recorded. The range of millivolts centred around the mean value was kept at ±0.010mV which represented ±0.22K. Alterations were made to the heater outputs using the Wattmeter as previously described, and to the cooled wall

temperature by adjustments at the control box and, rarely, the flow gates. For Series 1 the nominal wall thermocouple values were 3.130mV and 1.095mV.

When the half-way point was reached the laser and optical units were rotated through 180° so that the velocity of the downward flow near the cooled wall could be measured. The beams were then aligned with the cooled wall thermocouple junction as previously descibed for the heated wall thermocouple, and the remaining procedure of the first half followed after the thermocouple inputs to the signal conditioning units had been swapped around.

This Section is completed by providing information on the records which have been kept for each run.

Every run had a code allocated to it which formed the Volume Identifier in the E.C.M.A.-13 label VOL1. This comprised six characters: two letters indicating the month; two numbers indicating the day; and two numbers indicating the non-dimensional height at which the data were recorded. An example is JY1690. This shows that the date was July 16TH, and that the non-dimensional height was approximately 0.90.

A lab book was used to record all relevant information which included the exact non-dimensional height, the value of $2\sin(\theta/2)$, the atmospheric pressure during each half of the run, the relative positions, and the calibration data. A separate file was used to record the readings from the wall thermocouples and the readings of the L.V.D.T.'s and dial gauge.

The data collection program PMTV3V also produced output which showed the number of blocks on the tape and at which block position each reading began.

The data analysis program PLATAI output the calibration values input to it and the resulting linear relationships between: thermocouple millivolt signal and computer number; and tracker voltage output (representing frequency) and computer number.

Different analysis programs on the ICL 2988 have utilized these values instead of recalculating them. All such outputs were kept and stored in the lab books or files.

As Series 1 was very much a pioneering survey, only three of the original data tapes have been kept in storage for any future use.

4.3 PROCEDURE FOR SERIES 2

The readings taken for Series 2 were for heat transfer calculations only. The initial analysis of Series 1 data had shown that the heat

transfer through the cavity closing boundaries was unacceptably high, and so all closing boundaries were filled with expanded polystyrene.

The probes were prepared in the same manner as for Series 1, but the cavity preparation was slightly different in that the walls did not need to be cleaned as the laser Doppler anemometer was not to be used. All the polystyrene insulation was left in the vertical side walls and the cavity closed, and kept closed, for the duration of Series 2.

Temperature data were recorded over three days at the same eleven heights studied in Series 1. However, the only positions at which readings were taken were those within 2mm of each wall and at the cavity centre.

The vertical rod, supporting the probe carrier, was left uninsulated, as in Series 1. This allowed the height of the probes to be adjusted from outside the cavity. Care was taken to ensure that the probes were well away from either wall when the height was changed, thus preventing any damage to them.

Regrettably the present author made a mistake when adjusting the cavity wall temperatures. The heaters were set so that the heated wall thermocouples read the same as for Series 1, i.e. 3.130mV, but the cooled wall thermocouples read 1.015mV instead of 1.095mV. This effectively reduced the cooled wall temperature by approximately 4K.

Only the resulting mean temperature and R.M.S. of temperature fluctuations have been kept in the author's files, the original data being overwritten during Series 3.

4.4 PROCEDURE FOR SERIES 3

In order to make full use of the results of Series 2, the heated and cooled wall thermocouple readings were adjusted to the same values of 3.130mV and 1.015mV for Series 3. There were only minor differences in procedure from Series 1 to Series 3. These arose from the need to remove blocks of polystyrene from the vertical side walls; the insulating of the vertical rod carrying the probe block; the improvements in sealing against leakage; and off-centre measurements.

4.4.1 PROBE PREPARATION

The probes were checked to ensure that they were in good condition and set up as for Series 2. However, they had to be reset when off-centre measurements (to check for two-dimensionality of the flow) were made. The supports, on which the thermocouples and the L.V.D.T.'s were mounted, were increased by screwing on additional lengths. The additonal lengths were

calculated to allow the thermocouples to be positioned 150mm off the cavity centre. The wall contact probe connecting wires also had to be lengthened.

4.4.2 LASER DOPPLER ANEMOMETER PARAMETERS

For all runs at the cavity centre-line (z/B = 0.5) the only parameter different from Series 1 was 2sin(θ/2) which was 0.09634. Three runs were carried out 150mm from the centre-line (z/B = 0.65) for which a converging lens of 600mm focal length was used. For these runs 2sin(θ/2) was 0.12035.

4.4.3 INITIAL CAVITY PREPARATION

Before each run the cavity was opened to allow the cleaning of the inner walls and to remove, and replace, appropriate polystyrene blocks to allow optical access. First of all the outer sheet of perspex was removed from each vertical wall. The blocks which had been previously removed were replaced and different ones removed for the new height. This aided the cleaning of the inner walls, in that, the area to be cleaned could be clearly seen and no guesswork was involved.

This activity had taken a considerable time during Series 1 as it was inevitable that too large an area was cleaned each time. The act of rubbing the perspex generated a static charge on it, this resulted in small pieces of polystyrene clinging to the outer surface of the inner wall. This surface was wiped with a damp cloth to remove the pieces after first taking away some additional blocks to provide better access. Before replacing these blocks the perspex was checked for smears and the blocks dusted down. They were replaced with great care together with thin supports at either end which took the place of the main block which had been removed. The outer perspex sheet was cleaned and replaced carefully.

Attention was then focussed on the height of the thermocouples. Insulation around the vertical rod was taken away and the probe carrier roughly positioned at the new height. The laser and optics were remounted and positioned so that the beams entered the cavity centrally through the access area. The probe carrier was then positioned so that the junction of the thermocouple impinged on the intersection of the beams. "Jubilee" clips were then tightened above and below the probe carrier, to prevent movement in both vertical and angular directions.

The vertical rod was then reinsulated and the heights, from the cavity floor, of the thermocouple junctions were measured. Finally the cavity seals at the top and bottom were checked and the cavity closed.

4.4.4 RUN PROCEDURE

The run procedure was basically the same as for Series 1 but with the notable exception of the time between seedings. The improved seals meant that the oil particles in the cavity stayed there for a much longer time. Typically reseeding was only required every six or eight readings, instead of the previous two.

The seeding times were also found to be shorter than for Series 1, with the seeding generator only requiring one refill during the whole Series.

All the data tapes for Series 3 have been kept in store at Q.M.C. for any future analysis that may be desired.

4.5 PROCEDURE FOR SERIES 4

The procedure for Series 4 was the same as that for Series 3, as were the laser Doppler anemometer parameters. The only difference was in the the values at which the wall thermocouple outputs were kept. The values were 2.555mV and 1.095mV. Whilst the thermocouples in the cooled wall were kept at a higher value than for Series 3, the temperature of the cooled wall was almost the same as that for Series 3. This setting had been determined by trial and error.

The reason for having to increase the temperature of the coolant was the decrease in the heated wall temperature which initially led to a reduction in the cooled wall temperature.

All the data tapes for Series 4 have been kept in store.

4.6 PROCEDURE FOR SERIES 5

The run procedure for Series 5 was basically the same as for Series 3, but there were some significant changes. The changes were those of: the non-dimensional heights at which data were collected; the media on which data were recorded; the number of data blocks recorded; and the parameter $2\sin(\theta/2)$ which was 0.09432.

The cavity height was reduced to 2.0m for this Series where data were collected at eight heights instead of eleven. The top four non-dimensional heights were chosen to match those which Renault [32] had used for his 2.0m high cavity which was to be used for Series 6 and 7. The bottom four non-dimensional heights were selected so that their dimensional heights matched those at which data were collected for Series 3. The intention was that the data collected at these heights would serve to show the effect of H on the onset of transition and the velocity and mass flow profiles.

The magnetic tape unit had developed a fault and the necessary repair work was deemed too expensive, therefore data were stored in files on the Winchester disc using a program which had been written by another researcher. The block size was 512 bytes, 256 words, one eigthth of that for the magnetic tape.

To conserve space on the Winchester only three channels of data were recorded. Channel 1 carried the relevant wall thermocouple output, channel 2 the tracker frequency output and channel 3 the tracker lock detector output.

An analysis of the Series 3 data had shown that by the time half of the samples had been taken the mean values of temperature and velocity had become reasonably stable. Therefore the number of samples was reduced for this Series.

Twenty four blocks of data were recorded for each calibration value and three hundred and four at each position. This resulted in 25,840 samples which is just in excess of 25,600, i.e. half of 51,200.

Only a few data files were kept for subsequent power spectral analysis. These selected files were at heights at which the transition phenomenon was expected to be seen.

4.7 PROCEDURE FOR SERIES 6

Series 6 was the first Series undertaken on the Poitiers cavity. The most outstanding difference between the facilties at Q.M.C. and Poitiers was the lack, at the latter, of a data logging system which enabled recording of each individual sample. Instead the R.M.S. of fluctuating components and the mean were calcuated in real time by a microprocessor voltmeter. This prevented the subsequent calculation of power spectral densities and the turbulence quantities $\overline{u'T'}$ and $\overline{u'\rho'}$, as velocity and temperature measurements could not be taken simultaneously.

4.7.1 PROBE PREPARATION

The resistance thermometry system was found to be faulty and so was replaced with one based on a chromel-alumel thermocouple, as previously described. The only adjustment that had to be made to the probe, before placing it in the cavity, was to slightly angle the thermocouple prongs so that the junction would touch the relevant wall before any other part of the probe.

4.7.2 LASER DOPPLER ANEMOMETER PREPARATION AND PARAMETERS

The laser Doppler anemometer had previously been set up by other researchers at Poitiers. It s setting was checked and found to be correct.

Sunflower oil was used as the seeding agent and it s duration in the cavity, and the effect this had on the mean velocity registered by the Counter, were investigated before the Series commenced.

The present author found that by opening the compressed air supply valve to the seeding generator; for approximately one second, enough oil particles would enter the cavity to provide reliable data for up to nine minutes. (This, of course, was the time period after an initial five minutes had elapsed which allowed for the flow to settle down after seeding). The mean velocity registered by the anemometer stayed constant for this period (when variations of three and four minute sample times were used) but started to increase after this time. It was presumed that after nine minutes a bias effect came into being as the particle population decreased.

The seeding time could have been increased but there were two very good reasons for not doing this, both relating to the time available for the experiments. Firstly, an excess of oil particles might have necessitated the cavity being opened up, during a Series, to clean the inner walls, and secondly; more extensive initial trials would have been required to ascertain when the anemometer would be likely to register a biased velocity.

The counter was a DISA 55L90a type. The front panel incorporated four modules: a 55L97 high voltage supply; a 55L91 data rate indicator; a 55L93 digital to analogue converter; and a 55L96 L.D.A. counter. The signal output was taken from the D/A converter and was different to that from the tracker at Q.M.C. The output voltage from the D/A converter was in the range 0-1.25V. This output represented a frequency, the exact value being dependent on the gain set at the D/A converter. The equation relating D/A output to velocity was:

$$u = 6.34(100V/2^A) - f_s) \qquad (4.2)$$

In equation (4.2) the multiplying constant was derived from the angle between the beams and the wavelength of the laser light, 632.8nm; V was the D/A output in volts, A was representative of the D/A gain setting, and f_s, the frequency shift, was in MHz. The value of A for all runs was 10 (i.e. the 48dB and 12dB buttons were depressed).

Based on the expected frequency range of the photomultiplier signal, the counter high-pass filter was set to 4kHz and the low-pass filter to 256MHz. The counter mode of operation was fixed 5/8 fringe count mode with

a computational accuracy of 1.5%. In addition the threshold window was set → to the maximum possible and the counter amplifier gain to 7db. ←

4.7.3 INITIAL CAVITY PREPARATION

The author did not need to prepare the cavity as this had been done by staff at Poitiers who fully assembled it after cleaning the side walls. Fortunately a combination of the small amount of oil input to the cavity, and it's relative "unwillingness" to deposit on the cavity side walls, meant that the cavity remained closed for Series 6 and 7.

4.7.4 RUN PROCEDURE FOR VELOCITY MEASUREMENTS

The cavity was seeded to make the beams visible and the laser and optics traversed so that the beams touched the heated wall at some point. This position was, usually, at the wall edge furthest from the side through which the beams entered. The laser and optics were then traversed so that the beam intersection impinged on the wall. This was taken as the approximate zero position of y.

The handle on the traversing mechanism was then turned back, typically by 0.5mm, so that the glare from the wall was reduced enough to allow the photomultiplier to be aligned with, and focussed on, the probe volume. The cavity was then seeded again and the flow allowed five minutes to settle.

Data were then sampled and analysed for approximately four minutes. The data analysis program used in the voltmeter was number 7 which sampled the data at approximately 5Hz. Records of the wall thermocouple readings; the data rate; and the validation rate were made. The data rate from the D/A converter was always far greater than the sampling rate.

After recording the values calculated by the voltmeter, the laser and optics were traversed to the next position, the photomultiplier realigned and another reading taken.

The majority of positions at which data were sampled were common to all runs. However, close to the wall the start position did vary, as the local surface conditions dictated the position at which the glare from the wall was reduced sufficiently for successful alignment of the photomultiplier to take place.

It was known, from the work of Renault [32], that only a small frequency shift would be required out to approximately 30mm from the wall (the cavity width being 200mm). Therefore a shift of 20kHz was used in this region. For the region 30-100mm a shift of 50kHz was used.

At the half-way point of the run the optics were rotated through 180° and, together with the laser, were traversed to the cooled wall. The initial positioning of the beams relative to the wall was somewhat easier due to the fact that the cooled wall was slightly convex. The procedure for the first half was then repeated.

Typically, two heights were investigated in one day.

4.7.5 RUN PROCEDURE FOR TEMPERATURE MEASUREMENTS

In order to assimilate as much relevant data as possible, in the time available, most of the temperature data were taken from the regions close to each wall and the cavity centre. Only some temperature profiles were investigated fully from the heated wall to the centre in order to determine whether temperature inversions were present.

The non-dimensional heights at which temperature readings could be taken were limited by the cavity construction. Of those available, six were chosen which would yield the most relevant data. The non-dimensional heights at which full profiles were recorded were 0.22, 0.47, 0.66, 0.79 and 0.91. Each profile was from the heated wall to the cavity centre, except for those at 0.22 and 0.66 which extended to within 10mm of the cooled wall.

The temperature difference between the two walls was close to that of Series 5, i.e. 46K, but the absolute wall temperatures were not the same.

The procedure was very simple. A plug was removed from a hole in the cooled wall and the probe holder inserted. The probe was then pushed into the cavity and positioned close to the relevant wall. Fifteen minutes were then allowed to stabilize the temperature of the probe casing and to let the flow settle. The probe was then carefully moved to as near to the wall as possible. This action was helped by monitoring the R.M.S. of the fluctuating components of temperature on the voltmeter.

Data were then sampled for approximately three and a half minutes by the voltmeter with two programs running. These programs were number 8 which converted the thermocouple signal to temperature, and program 7 the basic statistical analysis program. The combination of the two reduced the sampling rate to approximately 4Hz. The sample time of three and a half minutes had previously been determined by the present author to be quite adequate for accurate temperature data.

Whilst the data were being sampled all wall thermocouple outputs were monitored and any necessary adjustments made.

Traverse of the thermocouple was achieved by a screw arrangement, with the distance being read off from a dial gauge with an uncertainty of

0.01mm. Due to the limited range of the screw, spacers had to be used to move the thermocouple beyond 30mm from each wall.

Data from at least four heights, at one of the walls, were recorded in one day. The capablity for controlling the wall temperatures, from day to day, was not as good as that at Q.M.C., but the variation in local wall temperatures was kept within a range of ±0.5K.

4.8 PROCEDURE FOR SERIES 7

The procedure for Series 7 was exactly the same as that for Series 6, except that no full temperature profiles were recorded. The only other difference between the two series was the wall temperatures. The difference between the two walls for series 7 was approximately 62K, with the heated wall temperature being close to that of Series 5.

FIGURE 4.1

CO-ORDINATE SYSTEM FOR THE LASER DOPPLER ANEMOMETER

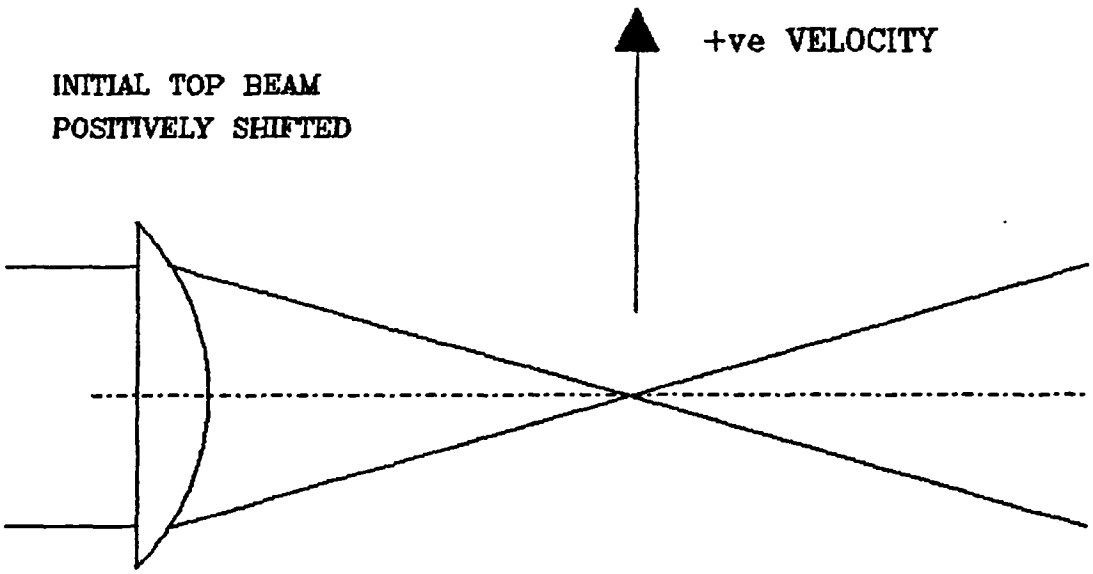

TABLE 4.1

NOMINAL POSITIONS FOR DATA COLLECTION - Q.M.C. CAVITY

POSITION	y/mm	POSITION	y/mm
1	0.0	16	9.0
2	0.2	17	10.0
3	0.4	18	12.5
4	0.6	19	15.0
5	0.8	20	17.5
6	1.0	21	20
7	1.2	22	30
8	1.4	23	40
9	2.0	24	50
10	3.0	25	60
11	4.0	26	70
12	5.0	27	100
13	6.0	28	150
14	7.0	29	200
15	8.0	30	250

CHAPTER 5 - SUMMARY OF THE EXPERIMENTAL SERIES

5.1 INTRODUCTION

This Chapter is split into several Sections. The first details the overall data for the seven series of experiments which were undertaken. The reader can thus appreciate how variables were changed so that their effect on the temperature and velocity fields could be studied.

5.2 EXPERIMENTAL SERIES DESCRIPTION

Seven series of experiments were carried out, each one being designated by a Series number.

This Section details the basic data for each Series and describes the differences between each as regards levels of insulation, the quantities measured, the cavity dimensions and the wall temperatures.

A graphical summary is presented in Figure 5.1 which shows more clearly how each Series followed a logical progression of variable changes.

The wall temperatures which have been quoted are subject to uncertainties as the wall temperatures at different heights were recorded on different days.

The average wall temperatures were calculated by plotting a graph of height versus temperature, integrating the area underneath the curve and dividing through by the cavity height.

In calculating the average wall temperature in this manner a number of sources of uncertainty arose. Firstly, the variation of wall temperature during the day, and from day to day.

The maximum variation of wall temperature, both during the day and from day to day, was kept to within ±0.25K.

The largest, and most important source of uncertainty, was the variation of wall temperature with height. As will be seen the heated wall temperature did vary slightly with height, whereas the cooled wall temperature was significantly lower in temperature in it's lower region.

5.2.1 SERIES 1

The first series carried out on the Q.M.C. cavity utilized a false floor and ceiling supported by an aluminium framework. The vertical side walls were of a double cavity arrangement. Both velocity and temperature fields were surveyed.

H = 2.5m	L = 0.5m	H/L = 5
T_H = 77.5°C	T_C = 35.0°C	(T_H-T_C) = 42.5K
Ra_H = 4.04×10^{10}	Pr = 0.7	Gr_H = 5.77×10^{10}

5.2.2 SERIES 2

The second series carried out on the Q.M.C. cavity utilized a false floor and ceiling constructed from blocks of expanded polystyrene. The vertical side walls were filled with expanded polystyrene.

This series was special in that only heat transfer measurements were taken with no polystyrene sections taken out for optical access. The reason behind this was to examine the effect of the removal of these blocks in later series.

H = 2.5m	L = 0.5m	H/L = 5
T_H = 77.8°C	T_C = 31.6°C	(T_H-T_C) = 46.2K
Ra_H = 4.49×10^{10}	Pr = 0.7	Gr_H = 6.41×10^{10}

5.2.3 SERIES 3

The third series involved the surveying of both velocity and temperature fields. Polystyrene blocks were removed for optical access.

H = 2.5m	L = 0.5m	H/L = 5
T_H = 77.2°C	T_C = 31.4°C	(T_H-T_C) = 45.8K
Ra_H = 4.48×10^{10}	Pr = 0.7	Gr_H = 6.40×10^{10}

5.2.4 SERIES 4

The fourth series on the Q.M.C. cavity differed from Series 3 in the use of a lower temperature difference.

H = 2.5m	L = 0.5m	H/L = 5
T_H = 64.9°C	T_C = 32.2°C	(T_H-T_C) = 32.7K
Ra_H = 3.40×10^{10}	Pr = 0.7	Gr_H = 4.86×10^{10}

5.2.5 SERIES 5

The fifth and final series on the Q.M.C. cavity reverted back to, approximately, the temperature difference of Series 3, but the height was reduced to 2.0m.

H = 2.0m	L = 0.5m	H/L = 4
T_H = 77.4°C	T_C = 32.0°C	(T_H-T_C) = 45.4K
Ra_H = 2.26×10^{10}	Pr = 0.7	Gr_H = 3.23×10^{10}

5.2.6 SERIES 6

This was the first series from the Poitiers cavity whose width was smaller than that of the Q.M.C. cavity.

The temperature difference was chosen to match that of Series 3 and 5.

H = 2.0m	L = 0.2m	H/L = 10
T_H = 51.9°C	T_C = 9.4°C	(T_H-T_C) = 42.5K
Ra_H = 2.99×10^{10}	Pr = 0.7	Gr_H = 4.27×10^{10}

5.2.7 SERIES 7

The seventh series was basically the same as the sixth series except that the temperature difference was increased.

H = 2.0m	L = 0.2m	H/L = 10
T_H = 74.5°C	T_C = 13.2°C	(T_H-T_C) = 61.3K
Ra_H = 3.55×10^{10}	Pr = 0.7	Gr_H = 5.07×10^{10}

FIGURE 5.1

SUMMARY OF THE EXPERIMENTAL SERIES

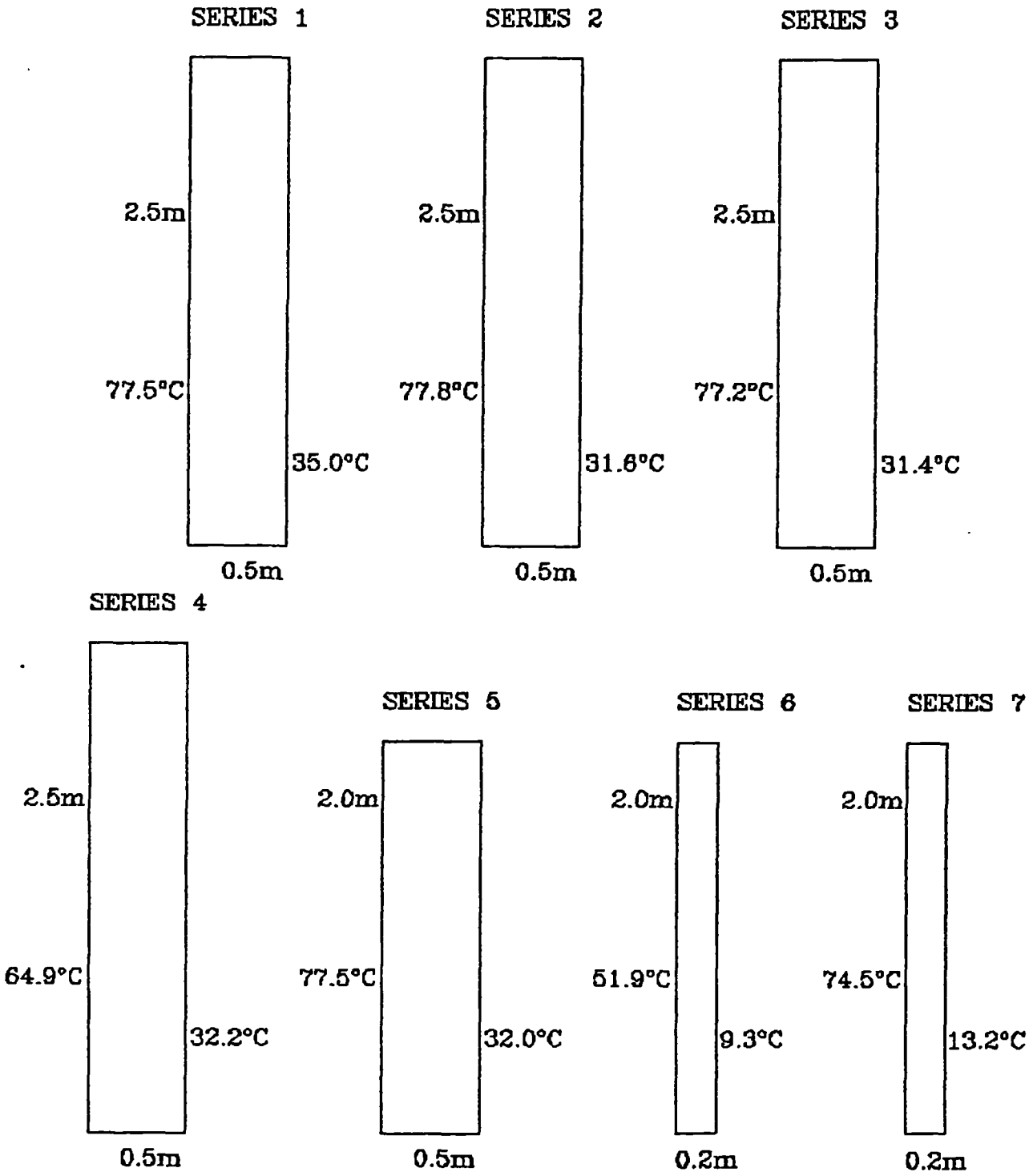

CHAPTER 6 - UNCERTAINTY ESTIMATIONS

6.1 INTRODUCTION

In order to be able to refine computer codes correctly one must have access to reliable data. Within all data there are uncertainties which must be identified and assigned a magnitude. This Chapter reports the results of tests carried out to estimate the level of uncertainties in the data which will be presented in Chapter 7.

The tests, which were carried out to determine the uncertainties in the velocity and temperature data, mainly dealt with the repeatability of data during a run and from day to day.

Those tests which did not deal with repeatability of data were concerned with the effect of the presence of the thermocouple junction on local velocity.

Sections 6.2-6.5 deal with the uncertainties in the Q.M.C. cavity data, and Section 6.6 deals with the uncertainties in the Poitiers cavity data.

6.2. CONSECUTIVE REPEATABILITY OF DATA

This Section investigates the ability of the instrumentation to repeat data readings within a short timescale of approximately 20mins.

6.2.1 VELOCITY DATA

The ability to repeat readings of the mean velocity and the R.M.S. of velocity fluctuations, at any position, was dependent on: the calibration curve of the tracker and its consistent applicability to a specific frequency range; the stability of the frequency shift; and the stationary statistical nature of the flow.

As mentioned in Chapter 3 the calibration of the tracker was found to be essentially repeatable with negligible uncertainty.

A 0.1% uncertainty in a shift of 100kHz would have resulted in a velocity difference of 0.001m/s (to three significant figures) for the present study. DISA quoted the uncertainty of the frequency shift to be less than 0.1%.

As for the statistical nature of the flow, this has always been assumed to be stationary, with the timescale over which repeatable readings can be achieved being considered to be eight minutes for the case of a vertical flat plate in air. However, the cavity data have shown that the mean velocity becomes reasonably stable after approximately four minutes. The variation of the R.M.S. of velocity fluctuations and mean velocity, with

time, is shown in Table 6.1 for different positions across the boundary layer.

Table 6.2 shows velocity data which were recorded at the same position in space for 4mins and 18.4s in consecutive samples 1-5 (the equivalent of 8mins and 36.8s sample times are also shown). The samples were taken at $y/\delta \simeq 0.154$ where the average of the mean velocities was 0.107m/s. Using this value, the minimum and maximum uncertainties of the 4min samples were 1.9 and 6.5% respectively (corresponding to 0.002 and 0.007m/s). For the 8min samples the uncertainties were 0.9 and 1.9% (corresponding to 0.001 and 0.002m/s).

The average R.M.S. of velocity fluctuations (from Table 6.2) was 0.077m/s leading to minimum and maximum uncertainties of 0 and 6.5% for 4min samples (corresponding to 0 and 0.005m/s) and 1.3 and 2.6% for 8min samples (corresponding to 0.001 and 0.002m/s).

From the data in Tables 6.1 and 6.2 it is clearly demonstrated that a sample time of 8mins is better than that of 4mins, but that 4mins still gives quite reasonable results.

Additional tests, for boundary layer positions with different mean velocities, showed that the uncertainties quoted above were typical of all readings, when considered in units of m/s. This meant that there appeared to be, on average, a constant absolute uncertainty in the readings. Obviously, the uncertainty in percentage terms varied because of this.

6.2.2 TEMPERATURE DATA

Temperature data were recorded at the same time as the velocity data presented in Section 6.2.1. They have been presented in Tables 6.3 and 6.4 in a similar manner to the velocity data of Tables 6.1 and 6.2.

The average of the mean temperatures was 46.46°C. Using this value, the minimum and maximum uncertainties of the 4min samples were 0.03 and 0.3% respectively (corresponding to 0.01 and 0.16K). For the 8min samples the uncertainties were 0.07 and 0.14% (corresponding to 0.03 and 0.07K).

The average R.M.S. of temperature fluctuations was 2.071K leading to minimum and maximum uncertainties of 0.6 and 6.7% for 4min samples (corresponding to 0.013 and 0.139K) and 2.0 and 3.0% for 8min samples (corresponding to 0.042 and 0.062K). However, one notes that the value of $T'_{R.M.S.}$ for Sample 2 does appear to have distorted the average value somewhat.

The temperature data again show that a sample time of 8mins is better than that of 4mins, but that 4mins still gives quite reasonable results.

As before, additional tests were carried out which showed that the data quoted in this Section exhibit the largest uncertainty levels found, both in absolute and percentage terms.

6.3 DAY TO DAY REPEATABILITY OF DATA

The previous Section dealt with the repeatability of readings within a timespan of some 20mins, during which the temperature and velocity fields would not have altered. Now one considers the ability of the present author to reproduce the velocity and temperature fields from day to day.

The reproduction of velocity and temperature fields from day to day could be achieved by reproducing: the same wall temperatures; the same leakage flow; and by allowing enough time, between closing the cavity and taking readings, for the flow to stabilize.

Velocity and temperature profiles are presented for both the R.M.S of fluctuations and mean quantities. The velocity data are presented in Figures 6.1-6.4, and the temperature data in Figures 6.5-6.8.

The temperature profiles have also provided a chance to examine the repeatability of the measurement of heat transfer rates at each wall.

Please note that because of the considerable time taken to record data for one full profile, the data were restricted to one height and two profiles.

6.3.1 VELOCITY PROFILES

The profiles which have been compared were those of JE1490 and JY2290, both taken from Series 3 at x/H = 0.898, and recorded approximately 5 weeks apart.

The profiles, presented in Figures 6.1-6.4, have not been corrected in the manner to be described in Section 6.4, as such an exercise was not necessary here.

The Figures show that the profiles of the R.M.S. of velocity fluctuations and mean velocity were repeatable.

The mean velocity profiles exhibited maximum differences of 0.008m/s on the wall side of the peak, 0.004m/s at the peak, and 0.006m/s beyond the peak. Typical differences, at any position, compared well with the maximum difference of 0.004m/s between consecutive samples found in Section 6.2.1.

As for the R.M.S. of velocity fluctuations, the two profiles were generally in closer agreement than those of the mean quantities. The maximum difference, at any position, was 0.003m/s, which compared very well to the 0.004m/s found in 6.2.1.

Velocity data were also available from Series 1 runs, namely JE1995 and JE2595, taken at x/H = 0.95, with a time delay of 6 days. The agreement between these profiles was just as good as that between JY2290 and JE1490. The data from the Series 1 runs are not presented here as they would essentially be repeating Figures 6.1-6.4.

6.3.2 TEMPERATURE PROFILES

Temperature data from the same runs as the velocity data have been compared. The profiles are presented in Figures 6.5-6.8.

The mean temperature profiles showed repeatability with the wall temperatures being 77.861°C and 32.978°C for JY2290 and 77.434°C and 32.834°C for JE1490.

Whilst the differences between profiles were generally greater than that of the 0.13K found in 6.2.1., they were of an acceptable magnitude, typically being less than 0.5K.

The data for the R.M.S. of the temperature fluctuations were also repeatable, with all differences between profiles again being less than 0.5K.

In the case of the Series 1 data, the wall temperatures were 77.884°C and 36.748°C for JE1995, and 77.682°C and 36.106°C for JE2595.

Both the velocity and temperature data have been shown to be repeatable. This has validated the cavity preparation technique devised by the present author.

6.3.3 WALL HEAT TRANSFER RATES

The heat transfer rates for JY2290 were 78.9W/m² and -109.5W/m², and 76.7W/m² and -112.1W/m² for JE1490.

For JE1995 the heat transfer rates were 79.0W/m² and -135.9W/m², and 75.2W/m² and -136.4W/m² for JE2595.

The heat transfer rates showed good repeatability with a minimum and a maximum uncertainty of 0.2% and 2.4% when compared to the average values. These percentage levels corresponded to absolute uncertainties of 0.2 and 1.9W/m².

Whilst the values quoted in this Section show good agreement, one must note that in statistical terms not enough data were available to yield indisputable uncertainty levels. Therefore it is recommended that future researchers investigate the repeatability of wall heat transfer rates in more detail than time has allowed for the present study.

6.4 THE EFFECT OF THE THERMOCOUPLE ON VELOCITY

During his work on the natural convection of air along a vertical flat plate, Ierokipiotis [43] presented an energy balance to within ±5%. This discrepancy was quoted as being within experimental uncertainty. The sources of this uncertainty could only have arisen in either the velocity or temperature data, or the method of calculation.

Ierokipiotis investigated the effect of the laser beams impinging on the thermocouple junction and found there to be no detectable change in the temperature, registered by the thermocouple, when the beams were directed onto it. Therefore, providing that his thermocouple was registering a correct absolute temperature, and that his experimental conditions were constant, one is led to believe that the largest uncertainty must have arisen in either the velocity data, or the method of calculation.

One is unable to comment on any uncertainties arising from the method of calculation and so only uncertainties in the velocity data can be considered.

Ierokipiotis [43] took velocity readings using a counter based L.D.A. system. He found that, for his experimental conditions, there was no bias in the velocity data, which compared favourably with those from a tracker.

Regretably Ierokipiotis [43] did not specify any sources of uncertainty in his velocity data, and so one is led to speculate that either he considered them to be present in the counter data when compared to tracker data, or in repeatability of readings at any position.

There was no evidence of the latter being investigated, nor was there an investigation of the effect of the nearness of the thermocouple junction, to the probe volume, on the velocity recorded by the anemometer. Therefore, for this study, both of these points were investigated, the former having already been dealt with.

The effect of the nearness of the thermocouple junction, to the probe volume, was investigated in four ways.

A crude analytical approach was the first to be used, to attempt to predict creeping flow around the thermocouple junction, and so determine the field of influence it may have.

An equation for the prediction of two-dimensional creeping flow around a sphere was taken from Schlicting [84]. This equation was applicable only for an an approaching laminar flow. As far as the present author is aware no equivalent equation exists for an approaching turbulent, and so three-dimensional, flow. No attempt to derive any such equation was made as such

a task falls well outside the scope of the present study. The equation used was:

$$u = u_\infty \left\{ \frac{3Rx^2}{4r^3} \left[\frac{R^2}{r^2} - 1 \right] - \frac{R}{4r} \left[3 + \frac{R^2}{r^2} \right] + 1 \right\} \qquad (6.1)$$

Where $r^2 = x^2 + y^2 + z^2$, u_∞ is the approach velocity, and R the radius of the sphere. The co-ordinates x, y and z are defined in Figure 6.9.

Calculations were performed for three positions from the sphere vertical centre-line, namely y = 0.0, 0.5 and 1.0mm.

The influence of the 40μm diameter junction on the velocity field is shown in Table 6.5 for the x direction only. One notes that the region of significant influence is small.

If only the thermocouple junction has an influence on the flow, then considering the typical vertical separation of the probe volume and junction (of approximately 0.75mm) one would expect a correction of 1.017-1.04 to be necessary in laminar flow (the correction being the multiplier applied to the recorded data) . However, there may be an effect due to the presence of the probe block and the analysis could very well be inadequate for the actual situation.

The actual situation involves turbulent flow, the attachment of side wires to the junction, the probability that the junction is not a true sphere, and the variation of junction size. Therfore experiments were necessary to confirm the effect, if any, of the junction.

The first experiment was concerned with taking measurements at one position and gradually moving the junction further away from the probe volume. This produced an unexpectedly large effect (as can be seen in Table 6.6).

Confirmation of these results was sought in different regions of the boundary layer at a vertical separation used typically in the experiments. The results are given in Table 6.7.

The inconsistency of the velocity data of Table 6.7 was speculated to be due to either repeatability uncertainty or to position within the boundary layer. Therefore a full traverse was carried out with, and without, the thermocouple in position. The resulting velocity profiles are shown in Figures 6.10-6.14, for the heated wall, and Figures 6.15-6.19, for the cooled wall.

The results indicated that the percentage difference between the velocities measured with and without the thermocouple varied across the

boundary layer, and with the horizontal separation between the probe volume and the thermocouple (as would be expected).

Firstly one may consider the variation of the percentage difference across the boundary layer and speculate that it is either the local turbulence intensity or the local mean velocity gradient which has this effect. As the mean velocity gradient was relatively steep near the wall, but the correction in this region smaller than for y>20mm, one may assume that it was probably the former.

To check the effect of the local turbulence intensity, it, and the correction necessary to convert the junction influenced velocities to their true values were plotted against each other in Figure 6.20. This Figure shows some support for the proposal of correction dependence on turbulence intensity.

A decision was taken to classify each part of the boundary layer with a correcting factor, but this correction would be dependent on the horizontal separation between the probe volume and the thermocouple.

It has been shown by the data in Table 6.5 that any velocity correction would be dependent on the horizontal separation of the probe volume and the thermocouple.

The horizontal separations for the data with the thermocouple present have been calculated to be 0.53mm for the heated wall data and 1.41mm for the cooled wall data. One may use this together with the data from Table 6.6 (taken with a horizontal separation of approximately zero) to investigate the variation of correction with separation for y>20mm (the data in Table 6.6 were taken at y>20mm).

The corrections at y>20mm for the heated and cooled wall data have been estimated to be 1.11 and 1.07, respectively. In plotting these in Figure 6.21, together with the data from Table 6.6 at a vertical separation of 0.75mm, one sees that an approximately linear relationship exists between horizontal separation and correction.

It will be shown (in Chapter 7) that all the horizontal separations in Series 3, 4 and 5 were centred around 0.5 and 1.4mm, for the heated and cooled walls respectively, with a range about these average values of ±0.4mm. This means that an uncertainty in velocity correction of ±2% would be expected if a standard set of velocity correction factors were selected to cover all runs.

For the heated wall a correction of 1.06 was applied to the measured velocities in the region from the wall to the velocity peak. A correction of

1.07 was applied to the measured velocities in the region from the peak to y = 20mm, and finally, a correction of 1.11 was applied to data for y>20mm.

For the cooled wall, a correction of 1.02 was applied to the region from the wall to the velocity peak. From the peak to y = 20mm a correction of 1.03 was applied, and for y>20mm a correction of 1.07 was applied.

The selection of corrections for the viscous sub-layer regions was not easy as it was critically dependent on locating the wall position correctly.

In all the velocity profiles presented in this thesis the wall position was originally unknown because the probe volume could not be guaranteed to stay in complete alignment with the thermocouple junction, due to angular movement of the probe block on the vertical support rod.

The location of the wall was determined in the calculation of the wall shear stress, which will be described in Chapter 7.

As the wall shear stress, velocity correction and wall position were initially unknowns estimates of all three had to be made from manual extrapolations of graphs. Through trial and error, the best velocity correction was found to be 1.06 for the heated wall, which is in keeping with the value predicted by Figure 6.20, and 1.02 for the cooled wall.

When the R.M.S. of the velocity fluctuations was examined, one saw that a correction in a manner similar to that of the mean velocity was not possible. Instead one notes that the effect of the thermocouple was to reduce the R.M.S. value by a constant amount for y>10mm and to have little effect when y<10mm. A suitable correction to the R.M.S. data for both the heated and cooled wall boundary layers is +0.004m/s. By assuming an uncertainty of ±0.002m/s, with this correction, virtually all differences between the profiles in Figures 6.14 and 6.18 can be accounted for.

6.5 SUMMARY OF UNCERTAINTIES IN THE Q.M.C. DATA

When considering the uncertainties one is concerned with two aspects. Firstly the uncertainty of data in individual runs which will eventually be scaled non-dimensionally and compared, and secondly, the uncertainty of the data in relation to a specific set of cavity boundary conditions.

In the first case the important points are the ability to repeat data consecutively, the ability to measure the separation between the laser beams correctly, and the ability to assign a suitable correction to the velocity data (to account for the presence of the thermocouple).

In the second case, a fourth aspect is introduced which is the ability to repeat data from day to day.

The usual manner in which uncertainties are compounded to give an overall value is by considering the parameter in question as a function of a number of variables. One may then write an equation linking a small change in the parameter to a function of small changes in the variables. Rearrangement of the equation links a percentage uncertainty in the parameter with percentage uncertainties in the variables.

It is not easy to represent the uncertainties of the variables which go towards the final velocity and temperature data in percentage form, as the absolute uncertainties appear to remain the same for different values of the variables. Therefore the direction taken here is to present absolute uncertainties in the measured data. Only in the case of velocity is there a percentage uncertainty which is associated with the correction (for the presence of the thermocouple) and the evaluation of the parameter $2\sin(\theta/2)$.

6.5.1 UNCERTAINTIES IN INDIVIDUAL RUNS

Uncertainties are quoted for 4 and 8min samples of temperature and velocity.

In the case of mean temperature these are ±0.16K and ±0.07K, for 4 and 8min samples respectively. For the R.M.S. of temperature fluctuations the uncertainties are ±0.14K and ±0.06K for 4 and 8min samples, respectively. These values do not take into account any uncertainty in the calibration of the thermocouples by Ziai [1].

For mean velocity the absolute uncertainties are ±0.007m/s and ±0.002m/s for 4 and 8min samples repectively. The uncertainty in the velocity correction has been quoted as ±2%, and in the calculation of the parameter $2\sin(\theta/2)$ (for the laser Doppler anemometer) the maximum uncertainty was ±0.6%. One may combine the velocity correction with this to give an overall uncertainty of ±2.6%. As for the R.M.S. of velocity fluctuations the uncertainties are ±0.007m/s and ±0.004m/s for 4 and 8min samples respectively.

It is useful to look at these uncertainties in relation to a typical peak velocity of 0.35m/s. The overall uncertainty for this velocity would be ±4.6% for 4min samples and ±3.2% for 8min samples.

There remains only two further points to comment on which concern the resolution of the tracker and the A/D converter. The resolution of the tracker was 1/256 of the full velocity range, which corresponded to 0.0085m/s. That of the A/D converter was 1/4096, which corresponded to 0.0005m/s.

As the sample size approaches infinity, so the uncertainty in the mean velocity approaches zero for turbulent flow. In practical terms, both the mean velocity and the R.M.S. of the velocity fluctuations will have been unaffected by the uncertainties in individual readings, as the typical sample size was over 45000.

In order to confirm this the data were re-sampled at 3.125Hz and 6.25Hz to see if there was any change in the velocity data. If there was little or no change then one could assume negligible uncertainty in the velocity data, due to uncertainties in individual readings. Table 6.8 lists the re-sampled data which showed little change in the data re-sampled at 3.125Hz and virtually no change in the data re-sampled at 6.25Hz.

One must remember that when assessing any velocity or temperature scales there will be uncertainties within those scales, therefore one would not expect scaled velocities and temperatures to necessarily be within the uncertainties quoted in this Section.

6.5.2 UNCERTAINTIES IN RELATION TO SPECIFIC CAVITY CONDITIONS

The maximum uncertainties for mean temperature are ±0.66K and ±0.57K for 4 and 8min samples, respectively. In the case of the R.M.S. of temperature fluctuations the uncertainties are ±0.33K and ±0.25K for 4 and 8min samples, respectively.

In the case of mean velocity the maximum uncertainties are ±0.011m/s for 4min samples and ±0.006m/s for 8min samples. For the R.M.S. of velocity fluctuations the maximum uncertainties are ±0.009m/s for 4min samples and ±0.006m/s for 8min samples. The percentage uncertainties associated with the parameter $2\sin(\theta/2)$ and the velocity correction remain at ±2.6%.

When considering a typical peak velocity of 0.35m/s the uncertainties are ±5.7% for 4min samples and ±4.3% for 8min samples.

6.6 UNCERTAINTIES IN THE POITIERS CAVITY DATA

Table 6.9 shows four pairs of consecutive 3.5min samples taken from the Poitiers cavity at different positions. The repeatability of the mean velocity was generally excellent with the maximum uncertainty being ±0.002m/s.

The accuracy of the digital output from the counter was 1/256 of the selected range. The settings used in all experiments covered a velocity range of 1.6m/s which means that the uncertainty of the digital output of the Counter was 0.006m/s. In addition, the output resolution of the D/A

module was 0.2% of the selected range which means that the uncertainty of the output of the D/A was 0.003m/s.

It is known that these uncertainties will become negligible in the final mean quantity as the number of samples tends towards infinity. It has already been shown that by re-sampling the Q.M.C. data at 3.125Hz and 6.25Hz the change in mean velocity was generally very small, but one may assign an uncertainty of ±0.001m/s to account for the low sampling rate used in the Poitiers experiments.

Therefore, as no velocity correction was required in the Poitiers data, the value of ±0.003m/s can be considered to be the maximum uncertainty in the mean velocity.

The maximum uncertainty in the R.M.S. of the velocity fluctuations was ±0.003m/s. The re-sampled data in Table 6.8 indicate that uncertainties in the R.M.S. data, due to counter resolution, were negligible, therefore one can consider the R.M.S. data to have a maximum uncertainty of ±0.003m/s.

Unfortunately time did not allow the author to carry out any evaluation of the uncertainties of the Poitiers data in relation to specific cavity conditions. One must therefore assume the same uncertainty levels found in the 4min sample Q.M.C. data apply to the Poitiers data. These are ±0.011m/s for mean velocity and ±0.007m/s for the R.M.S. of velocity fluctuations.

As the type of thermocouple in each cavity was the same, one may consider the 4min sample uncertainties in the Q.M.C. data to apply to the Poitiers data. These were ±0.16K and ±0.14K for the mean temperature and the R.M.S. of temperature fluctuations, respectively, in individual runs, and ±0.66K and ±0.33k for the mean temperature and the R.M.S. of temperature fluctuations, respectively, for specific cavity conditions.

FIGURE 6.1

REPEATABILITY OF MEAN VELOCITY - HEATED WALL

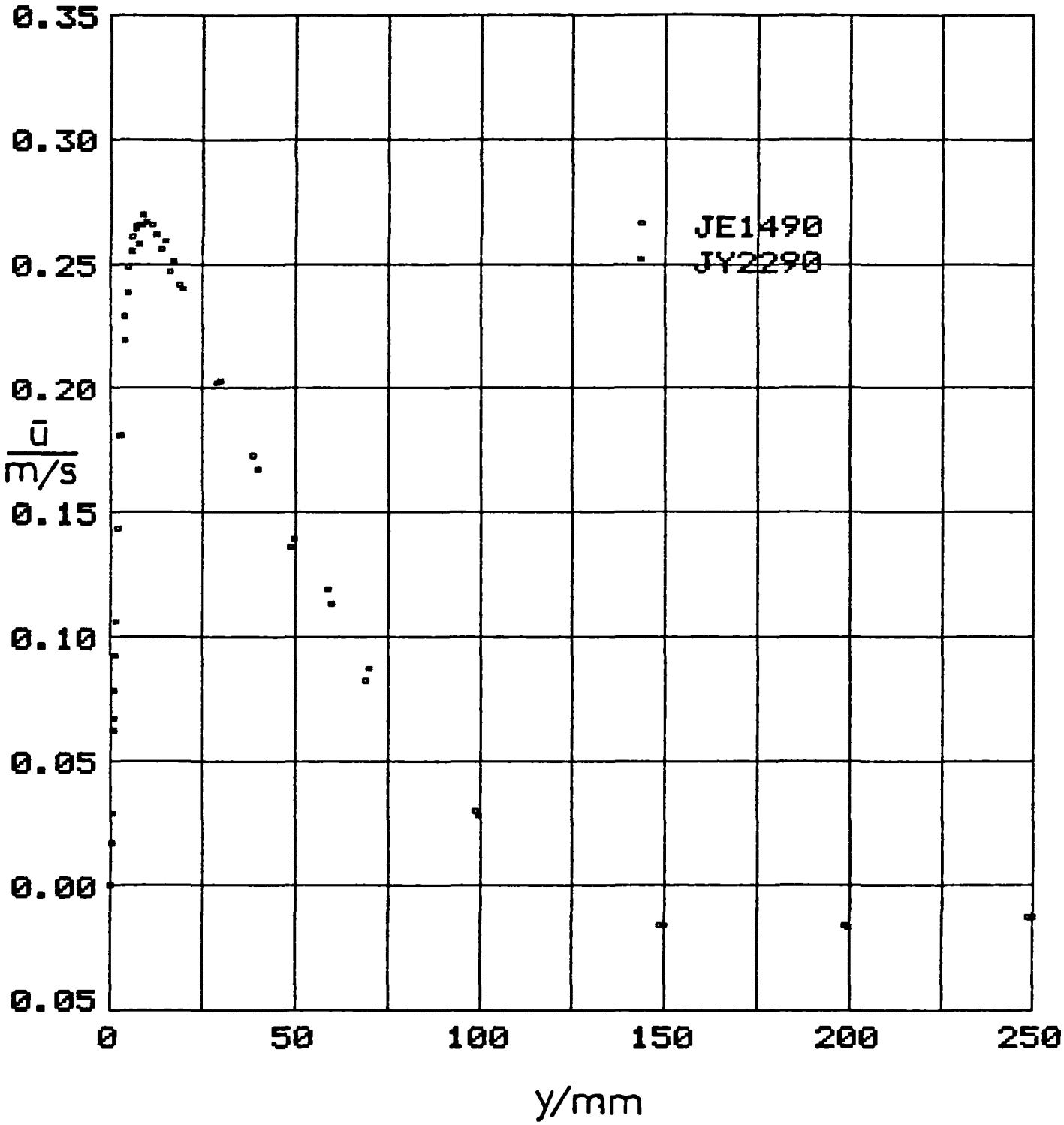

FIGURE 6.2

REPEATABILITY OF R.M.S. OF

VELOCITY FLUCTUATIONS - HEATED WALL

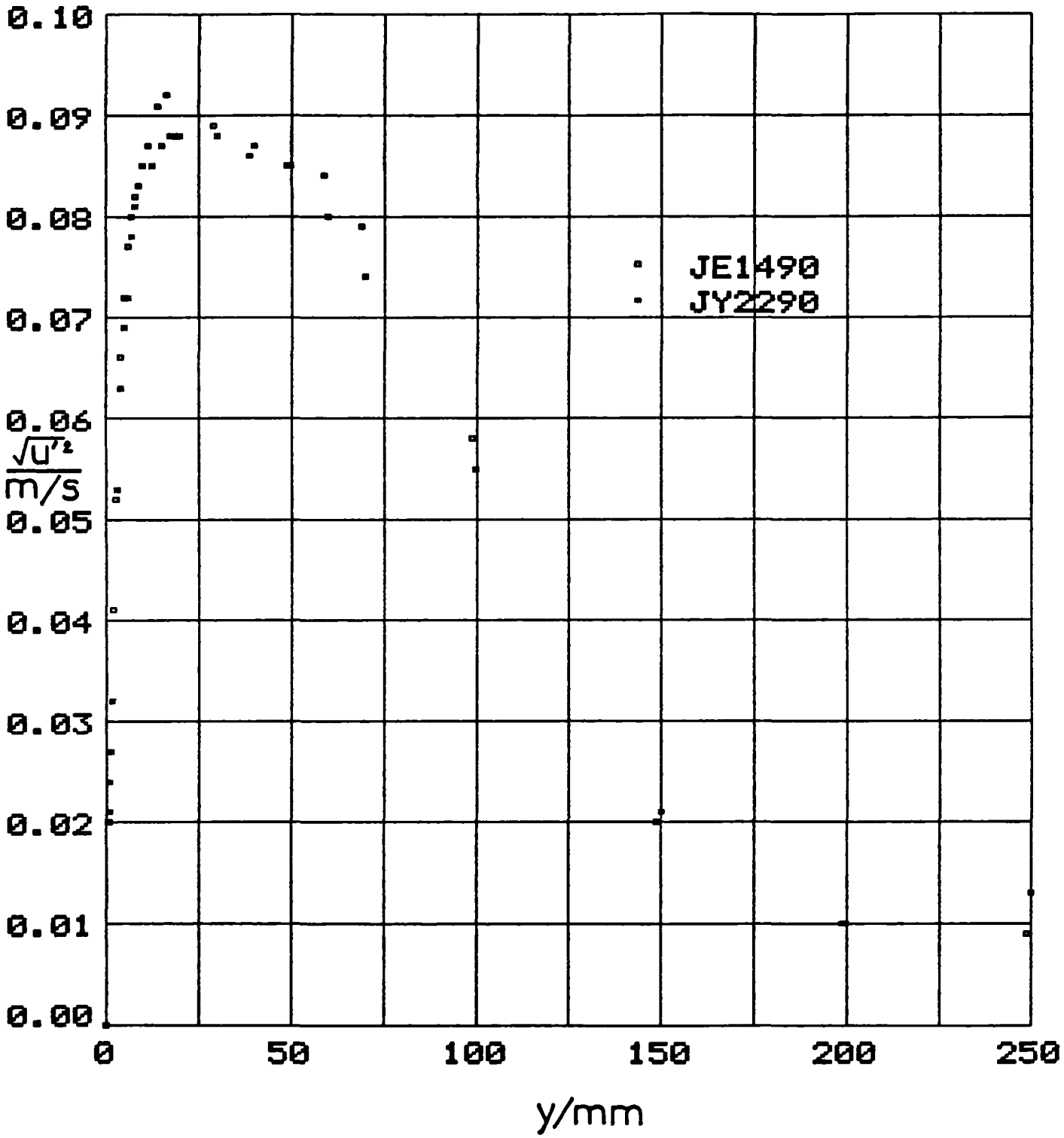

FIGURE 6.3

REPEATABILITY OF MEAN VELOCITY - COOLED WALL

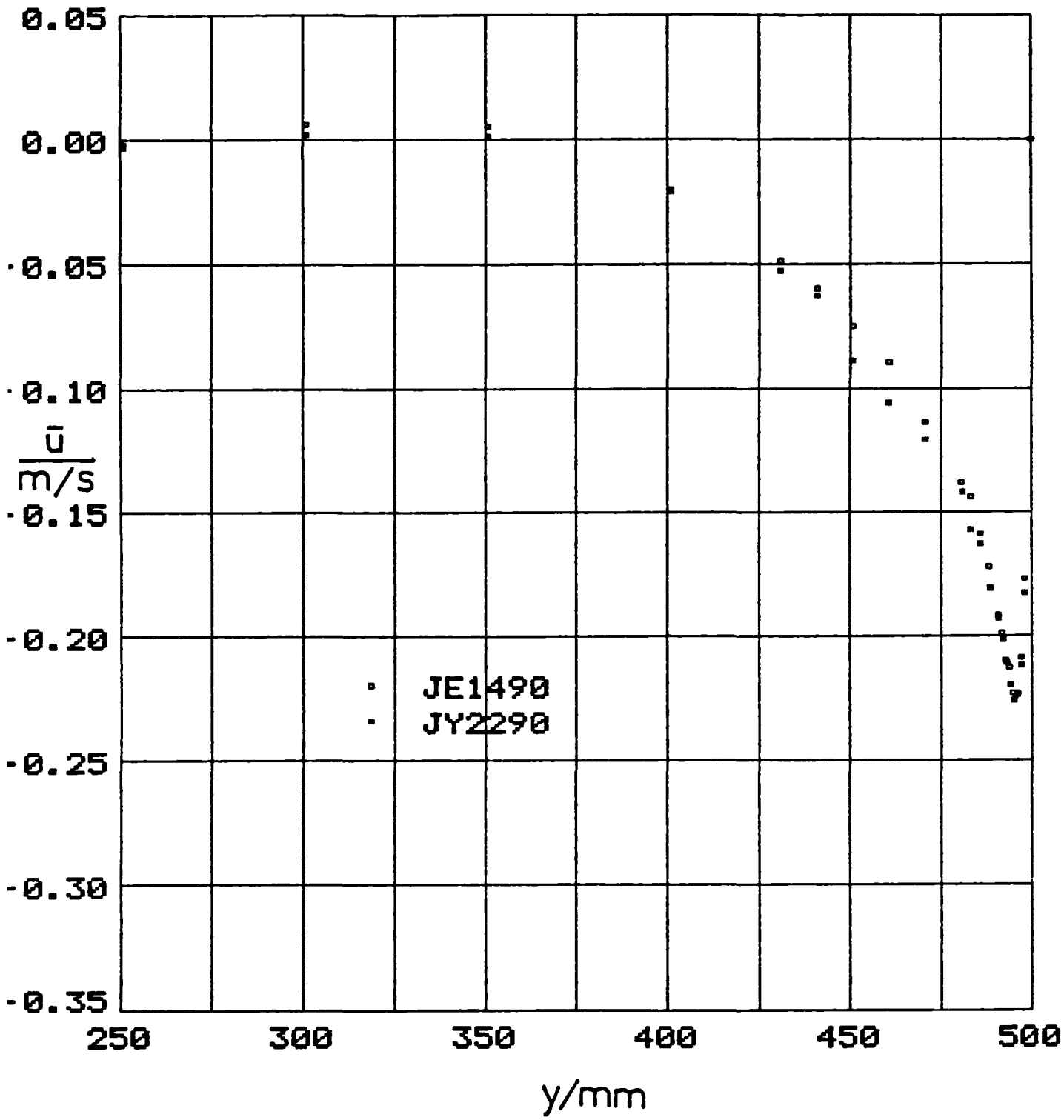

FIGURE 6.4

REPEATABILITY OF R.M.S. OF

VELOCITY FLUCTUATIONS - COOLED WALL

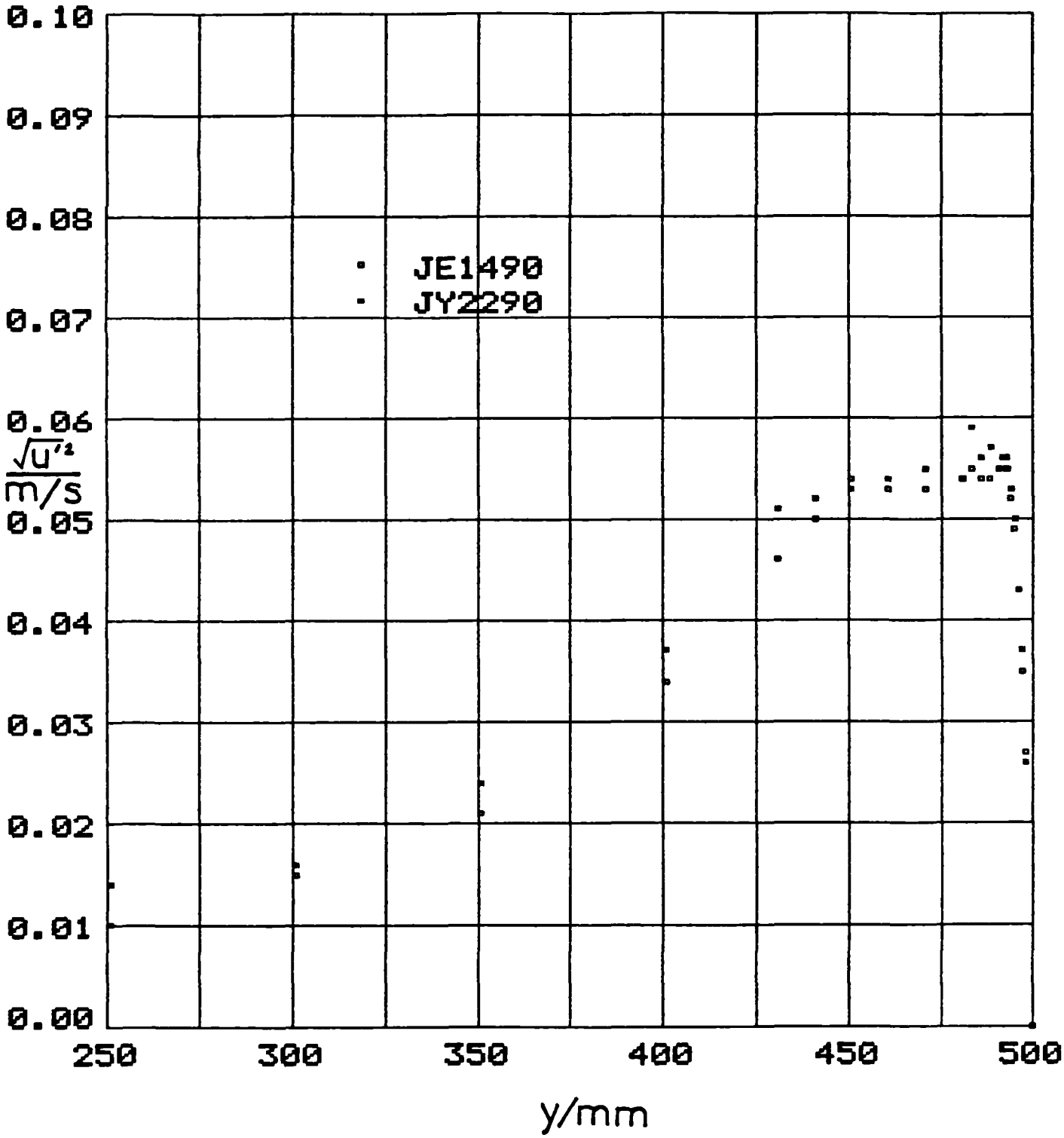

FIGURE 6.5

REPEATABILITY OF MEAN TEMPERATURE - HEATED WALL

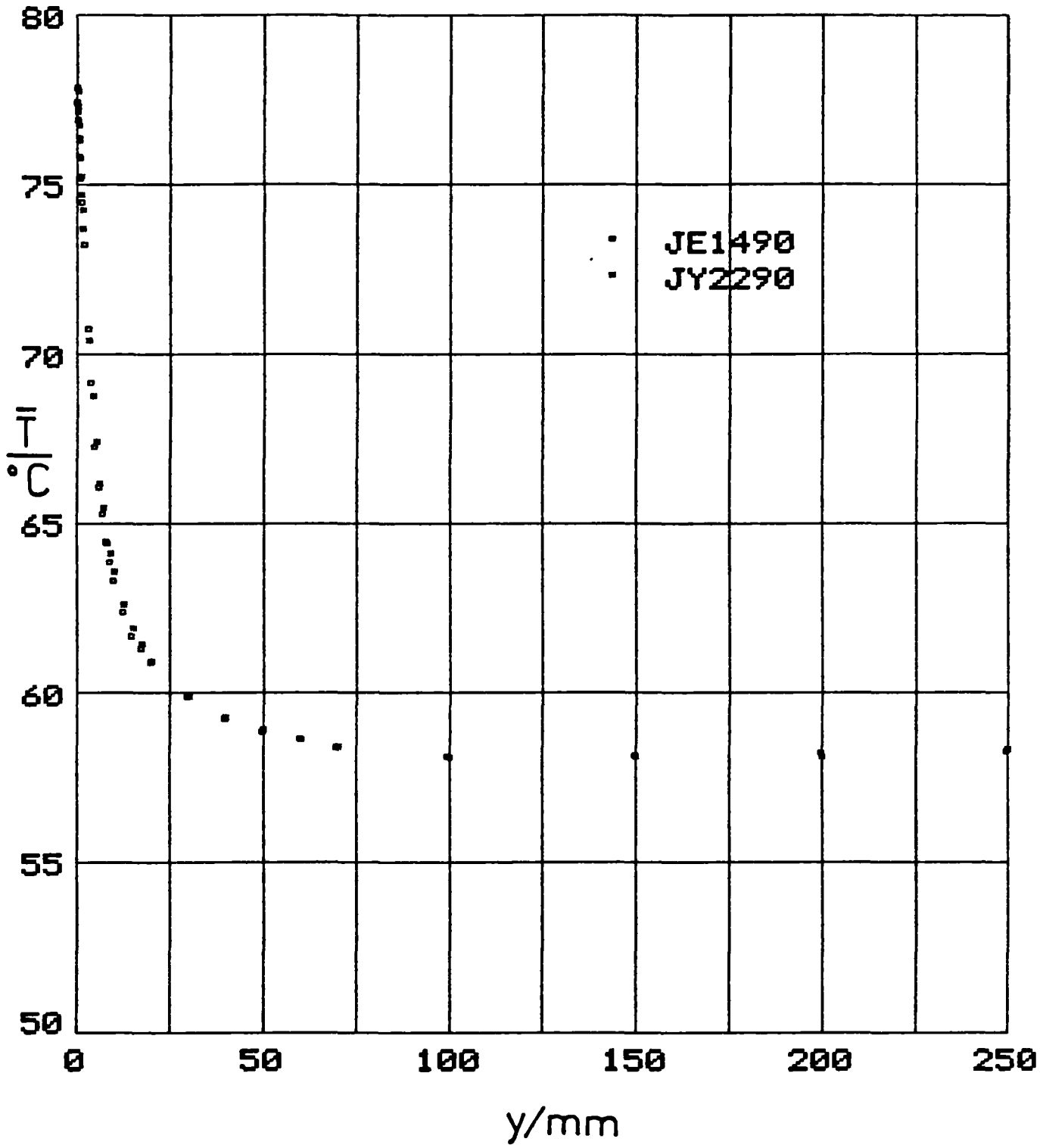

FIGURE 6.6

REPEATABILITY OF R.M.S. OF

TEMPERATURE FLUCTUATIONS - HEATED WALL

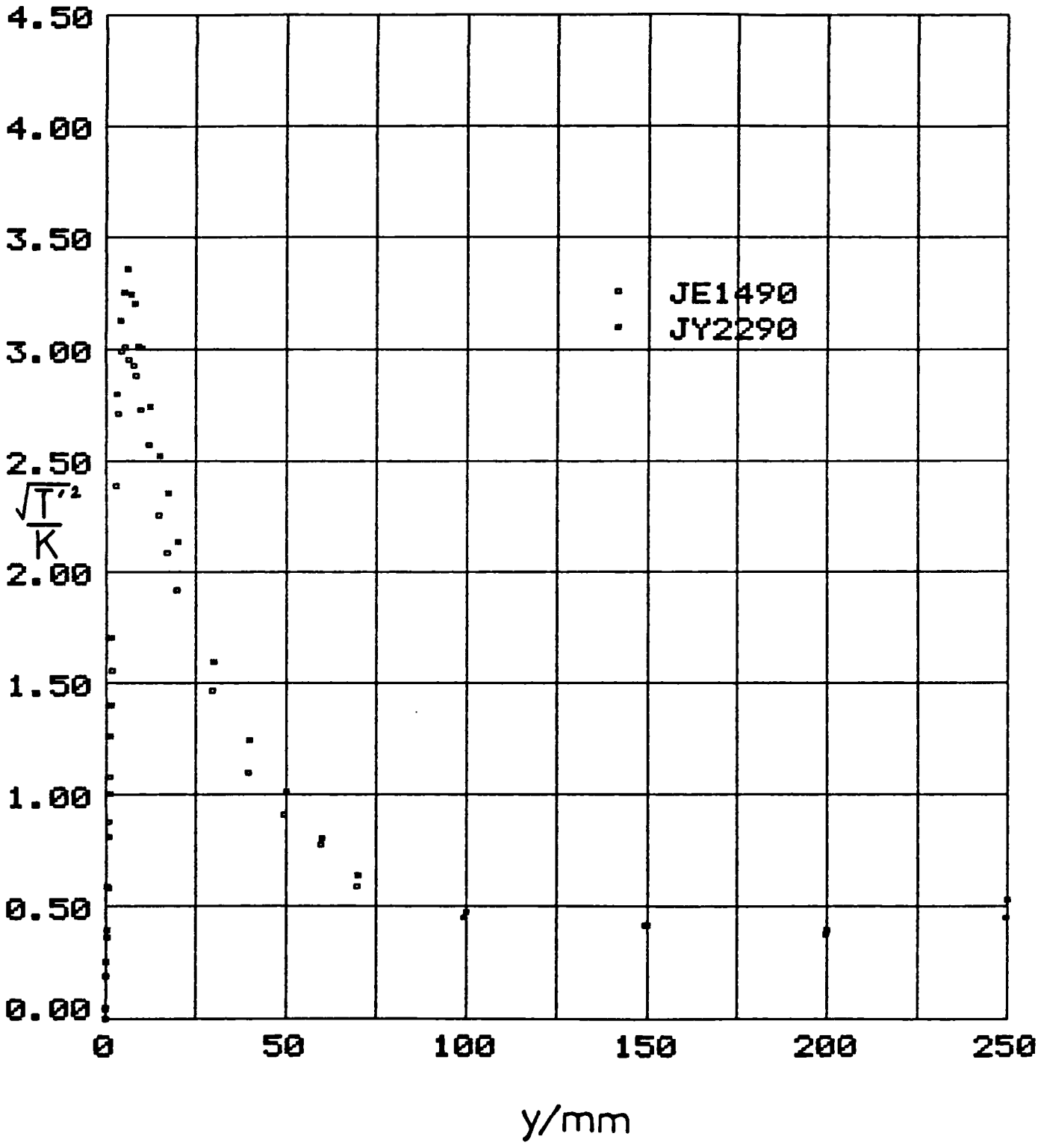

FIGURE 6.7

REPEATABILITY OF MEAN TEMPERATURE - COOLED WALL

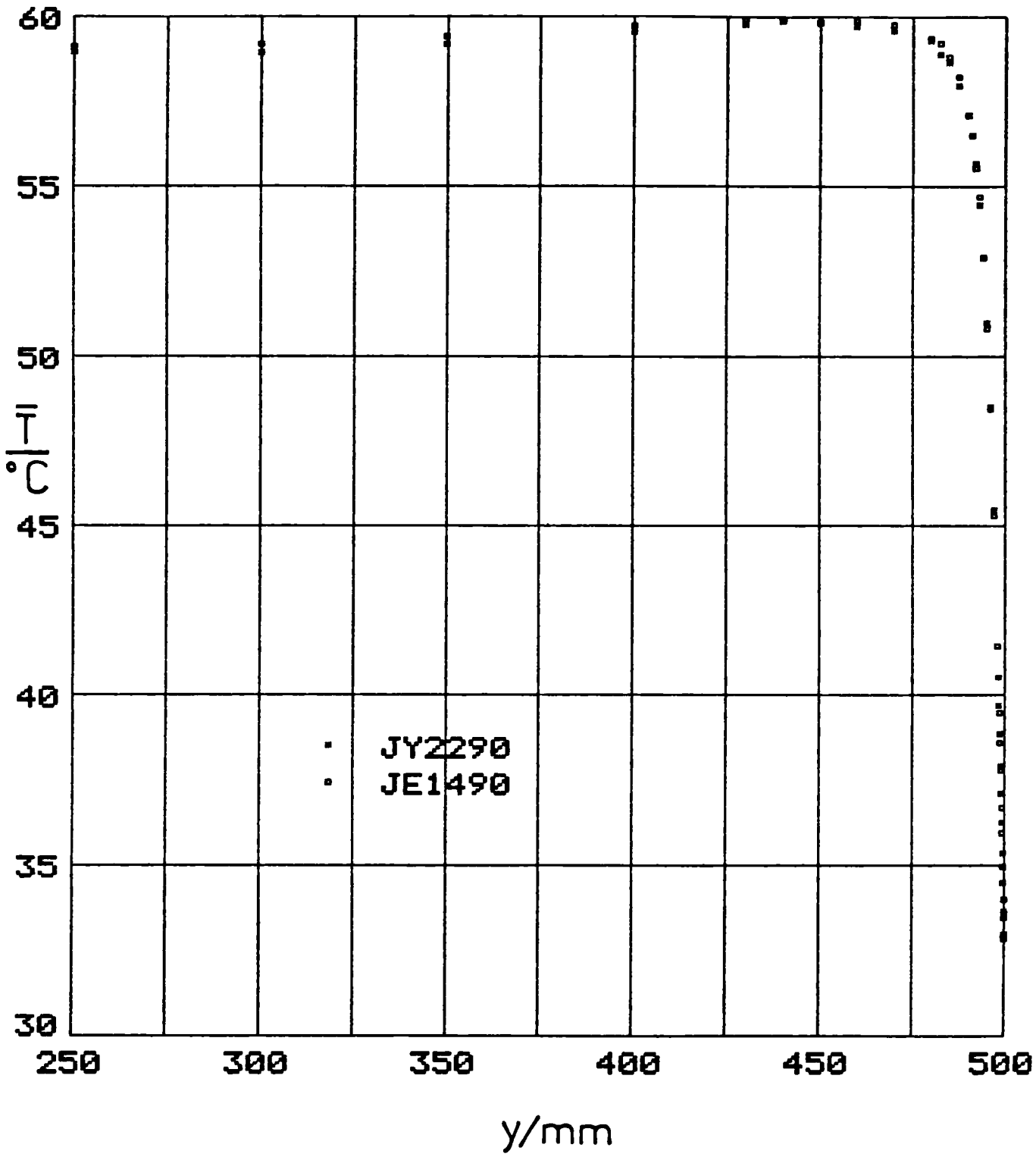

FIGURE 6.8

REPEATABILITY OF R.M.S. OF

TEMPERATURE FLUCTUATIONS - COOLED WALL

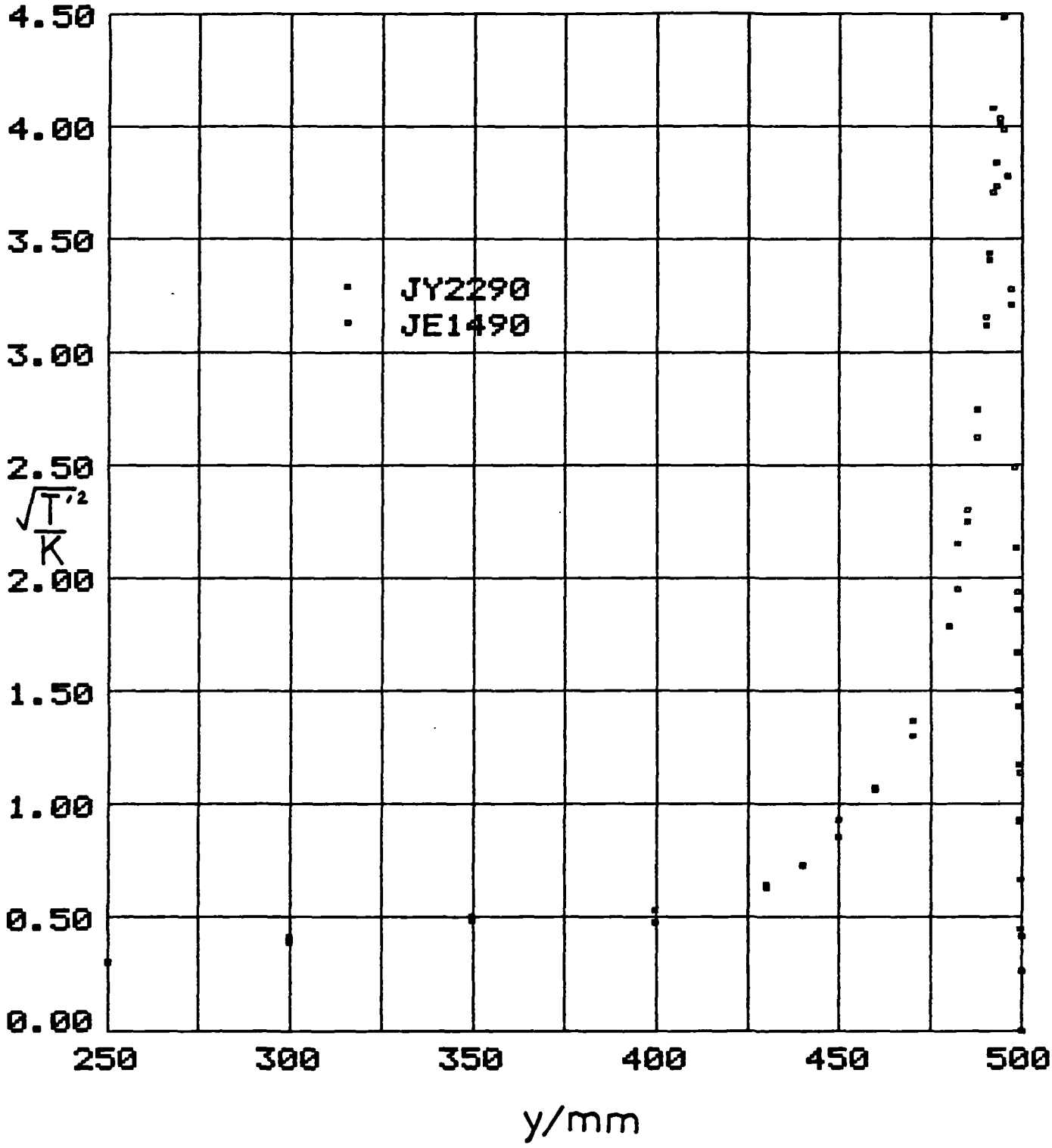

FIGURE 6.9

CO-ORDINATE SYSTEM FOR CREEPING FLOW AROUND A SPHERE

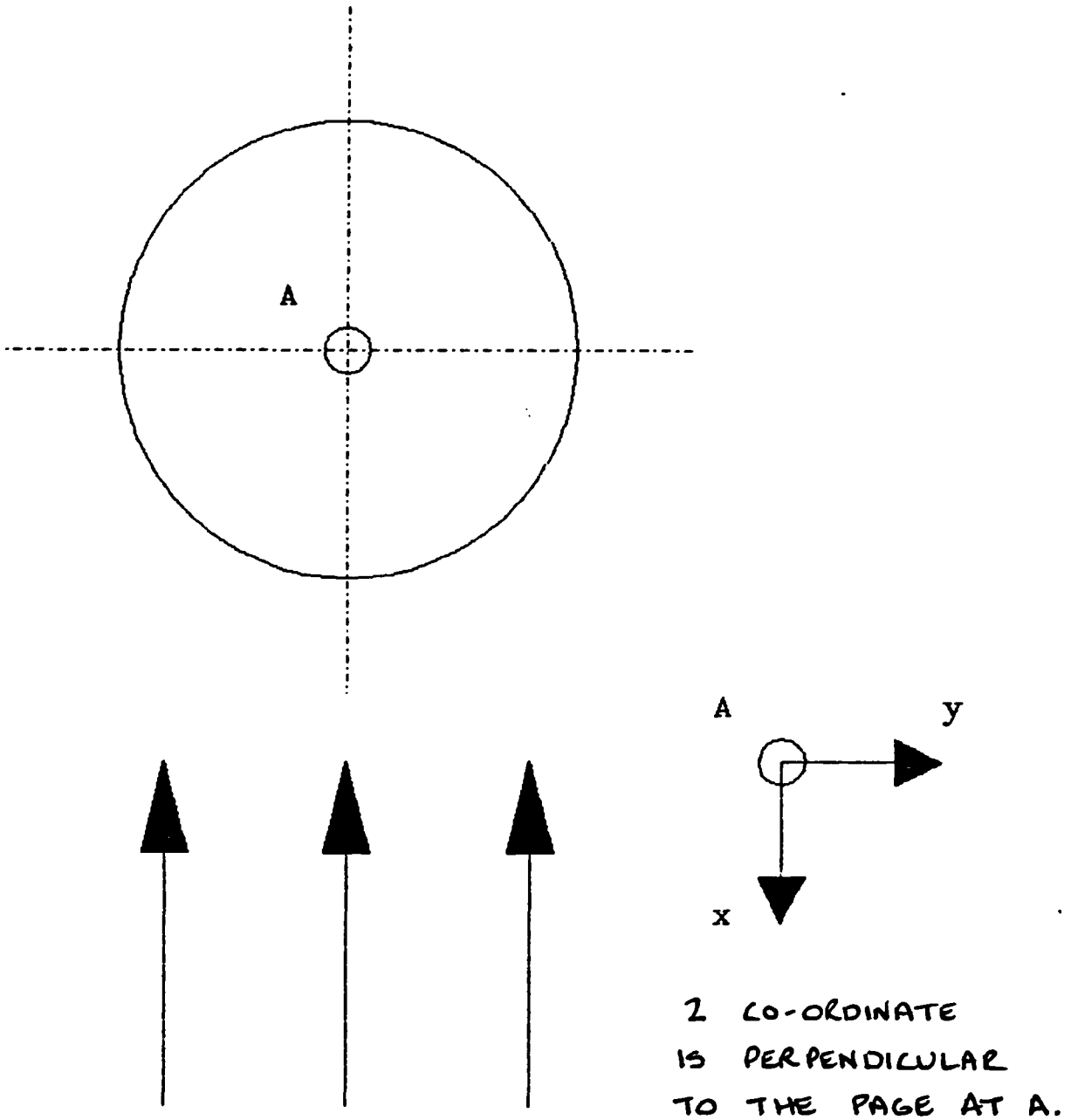

FIGURE 6.10

THERMOCOUPLE EFFECT ON

MEAN VELOCITY - HEATED WALL - FULL BOUNDARY LAYER

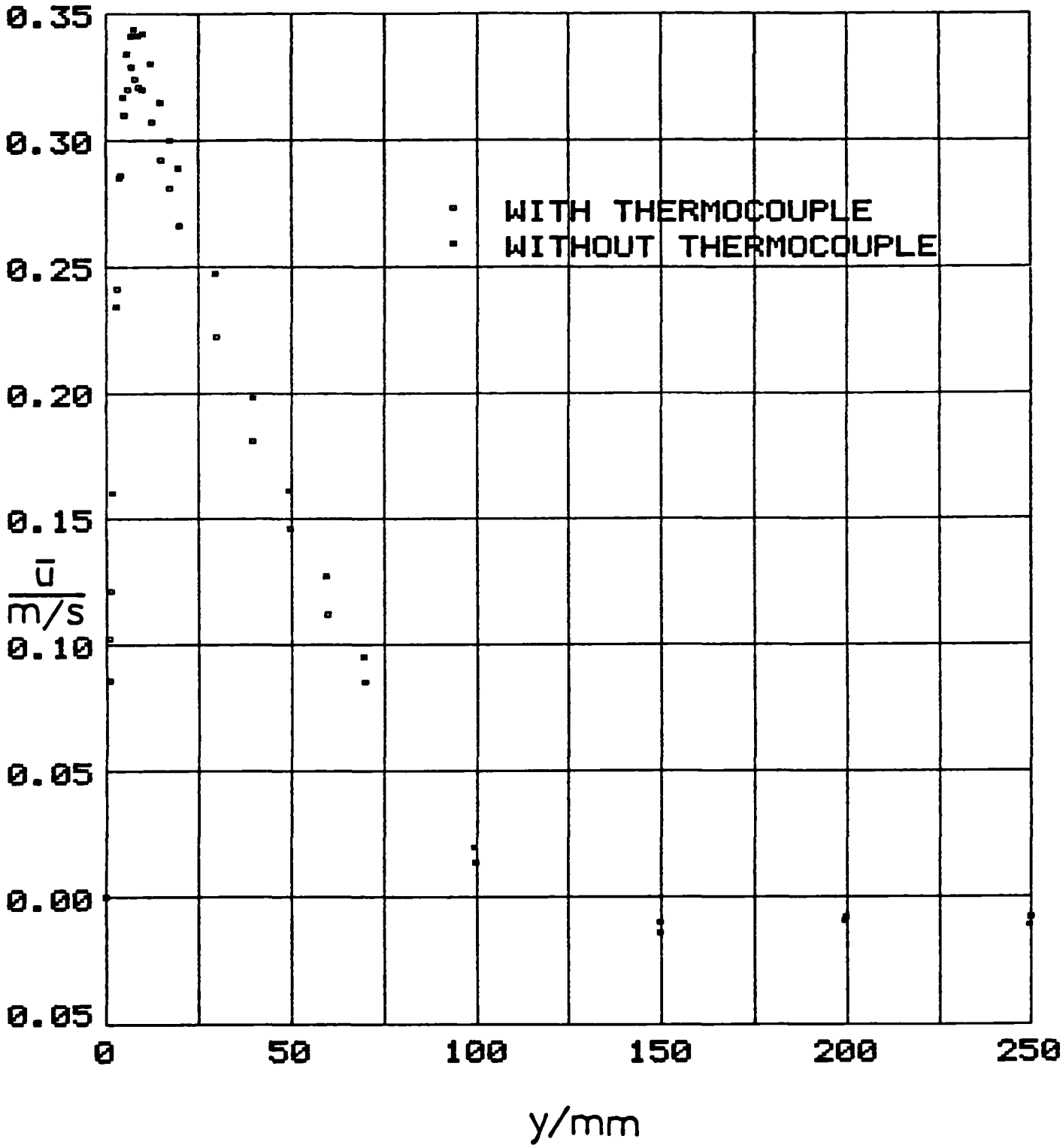

FIGURE 6.11

THERMOCOUPLE EFFECT ON

MEAN VELOCITY - HEATED WALL - FROM WALL TO y = 20mm

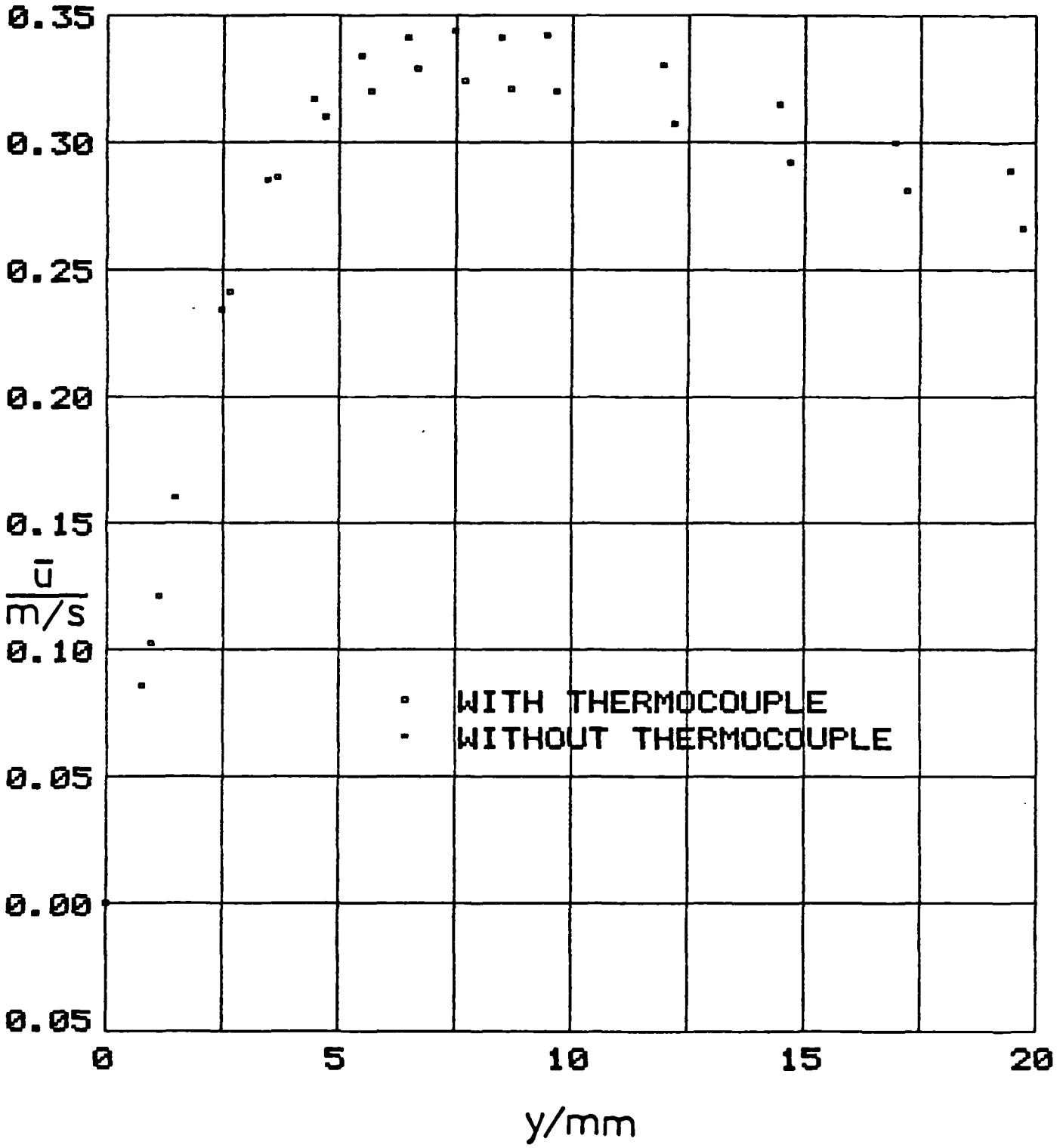

FIGURE 6.12

THERMOCOUPLE EFFECT ON

MEAN VELOCITY - HEATED WALL - FROM WALL TO y = 5mm

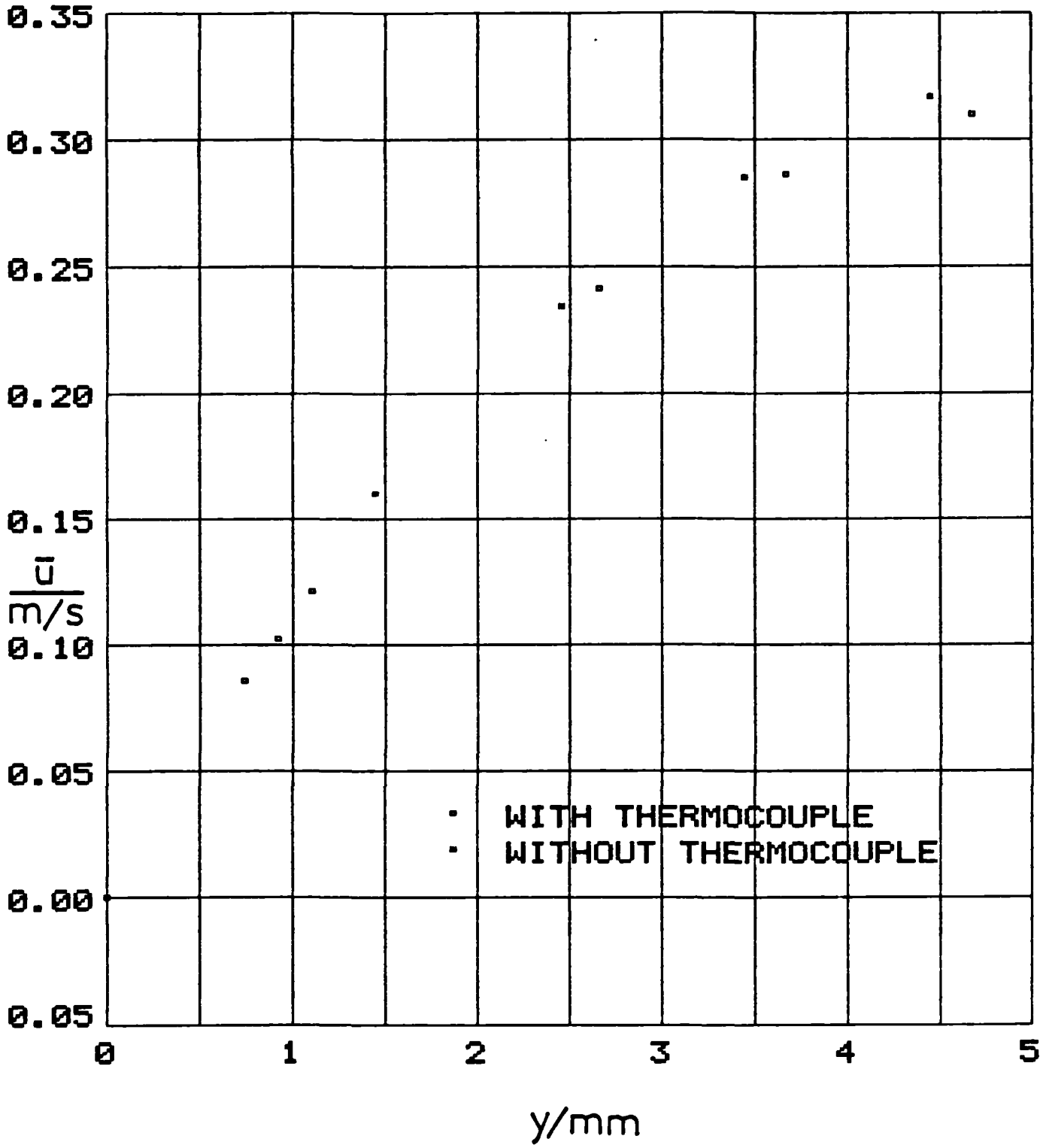

FIGURE 6.13

THERMOCOUPLE EFFECT ON R.M.S. OF

VELOCITY FLUCTUATIONS - HEATED WALL - FULL BOUNDARY LAYER

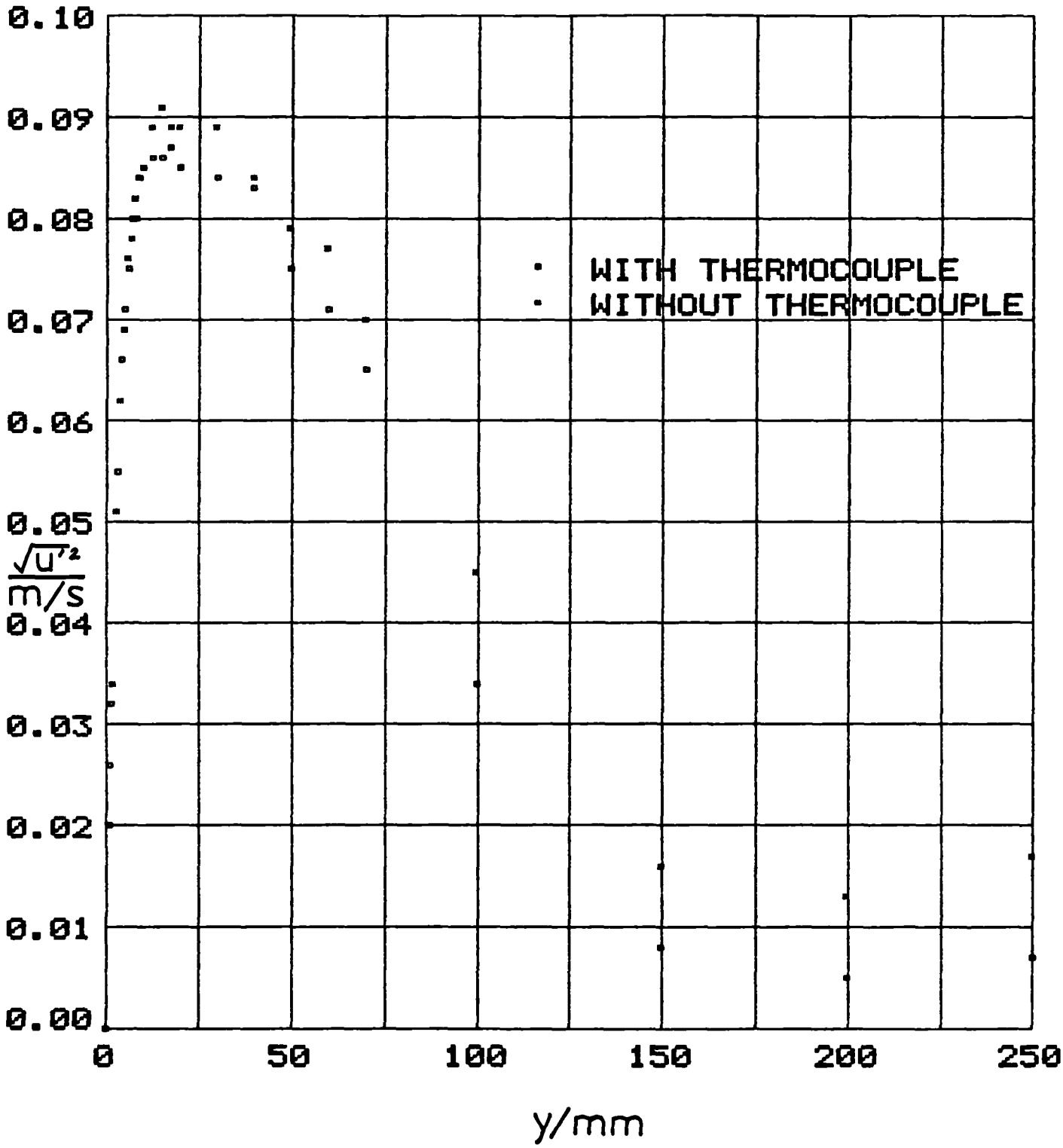

FIGURE 6.14

THERMOCOUPLE EFFECT ON R.M.S. OF

VELOCITY FLUCTUATIONS - HEATED WALL - FROM WALL TO y = 20mm

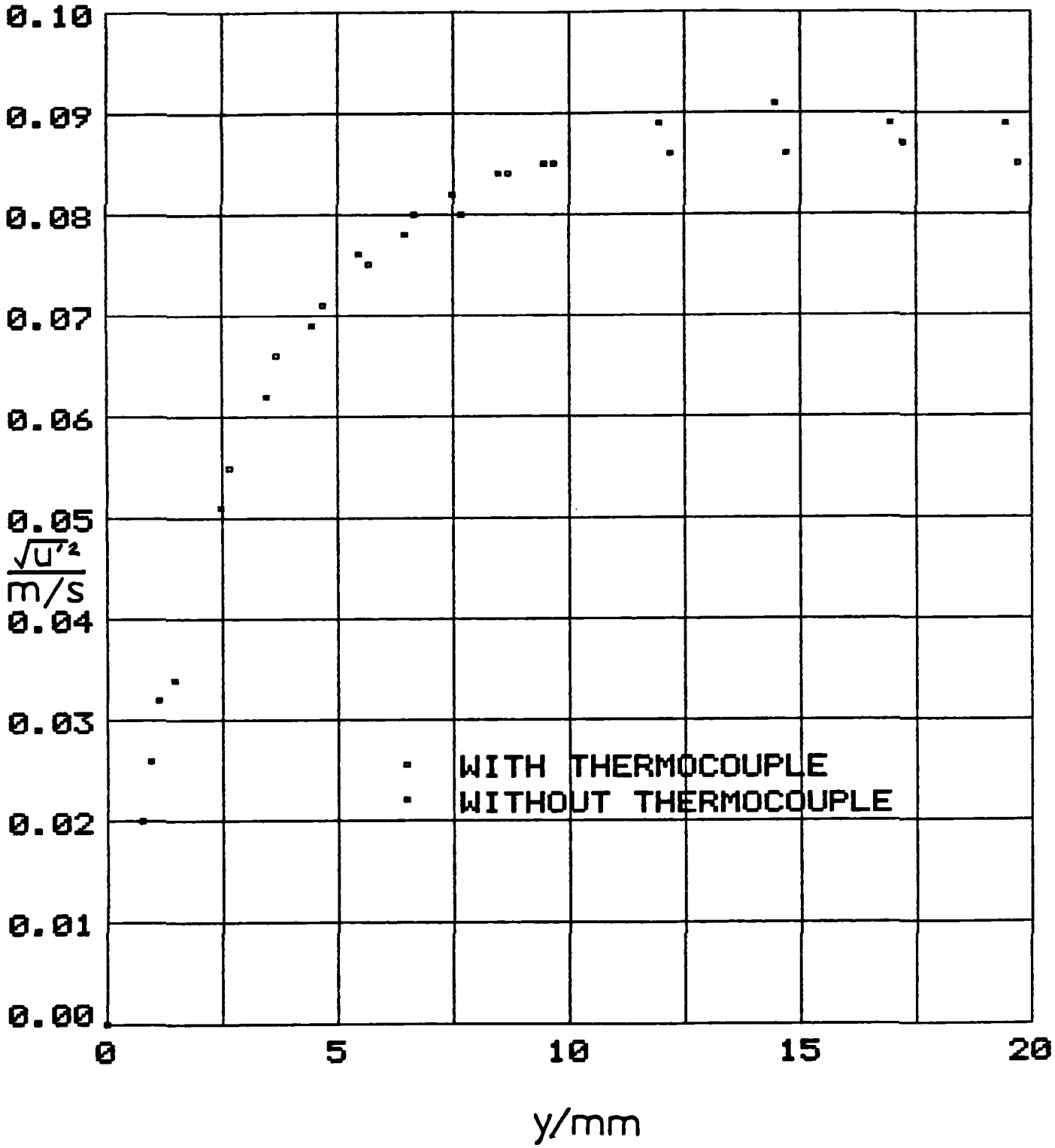

FIGURE 6.15

THERMOCOUPLE EFFECT ON

MEAN VELOCITY - COOLED WALL - FULL BOUNDARY LAYER

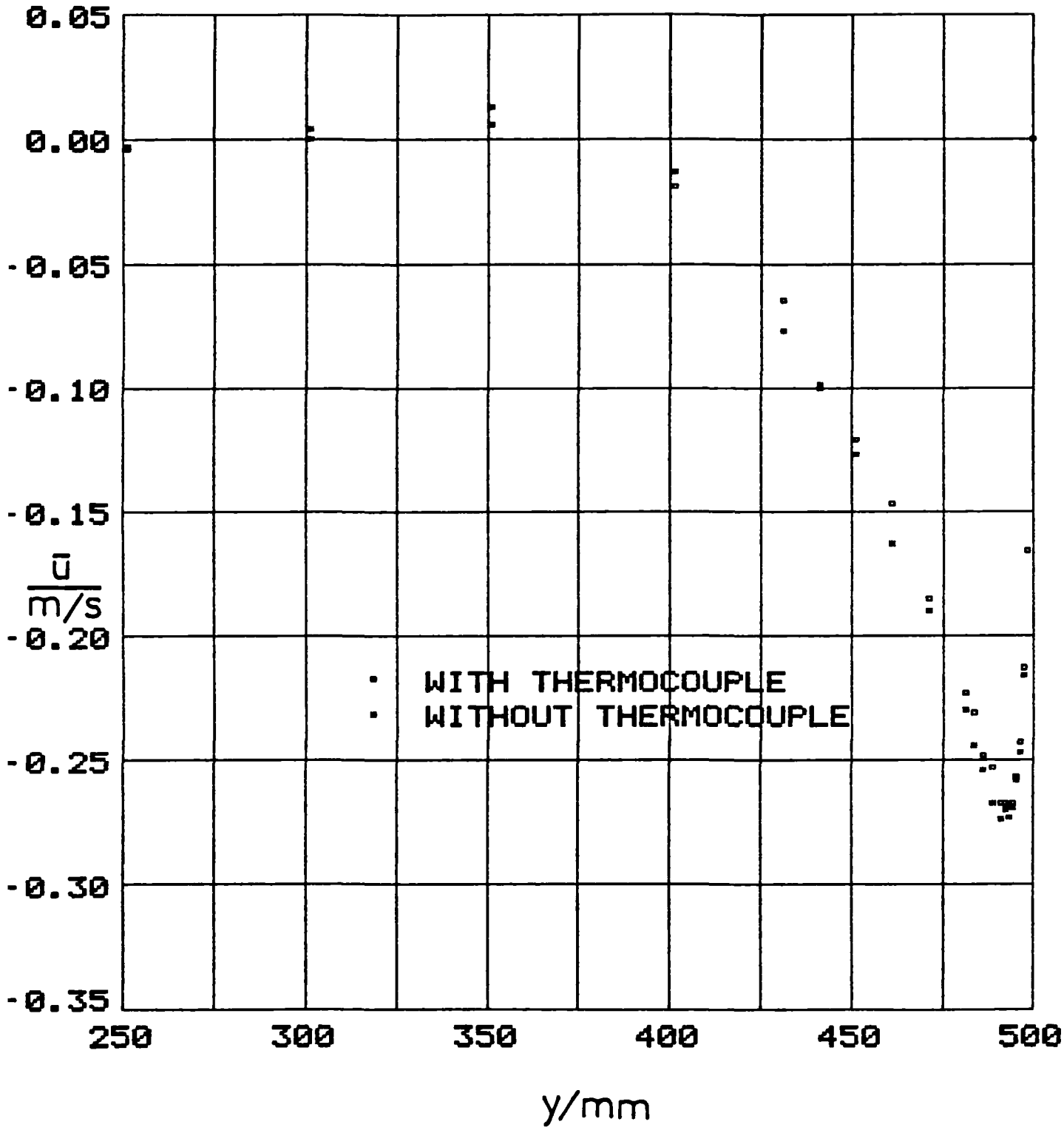

FIGURE 6.16

THERMOCOUPLE EFFECT ON

MEAN VELOCITY - COOLED WALL - FIRST 20mm FROM WALL

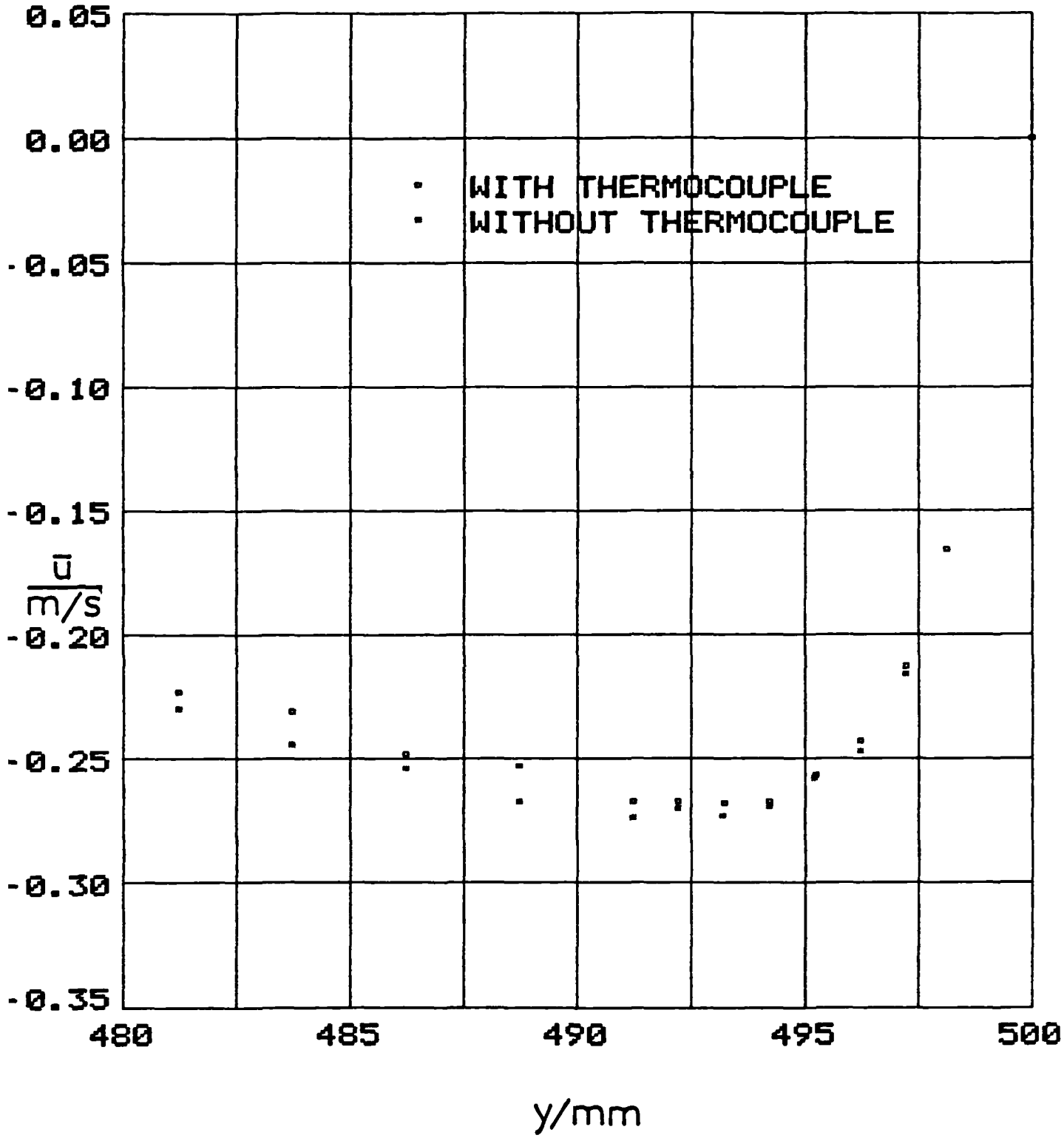

FIGURE 6.17

THERMOCOUPLE EFFECT ON

MEAN VELOCITY - COOLED WALL - FIRST 5mm FROM WALL

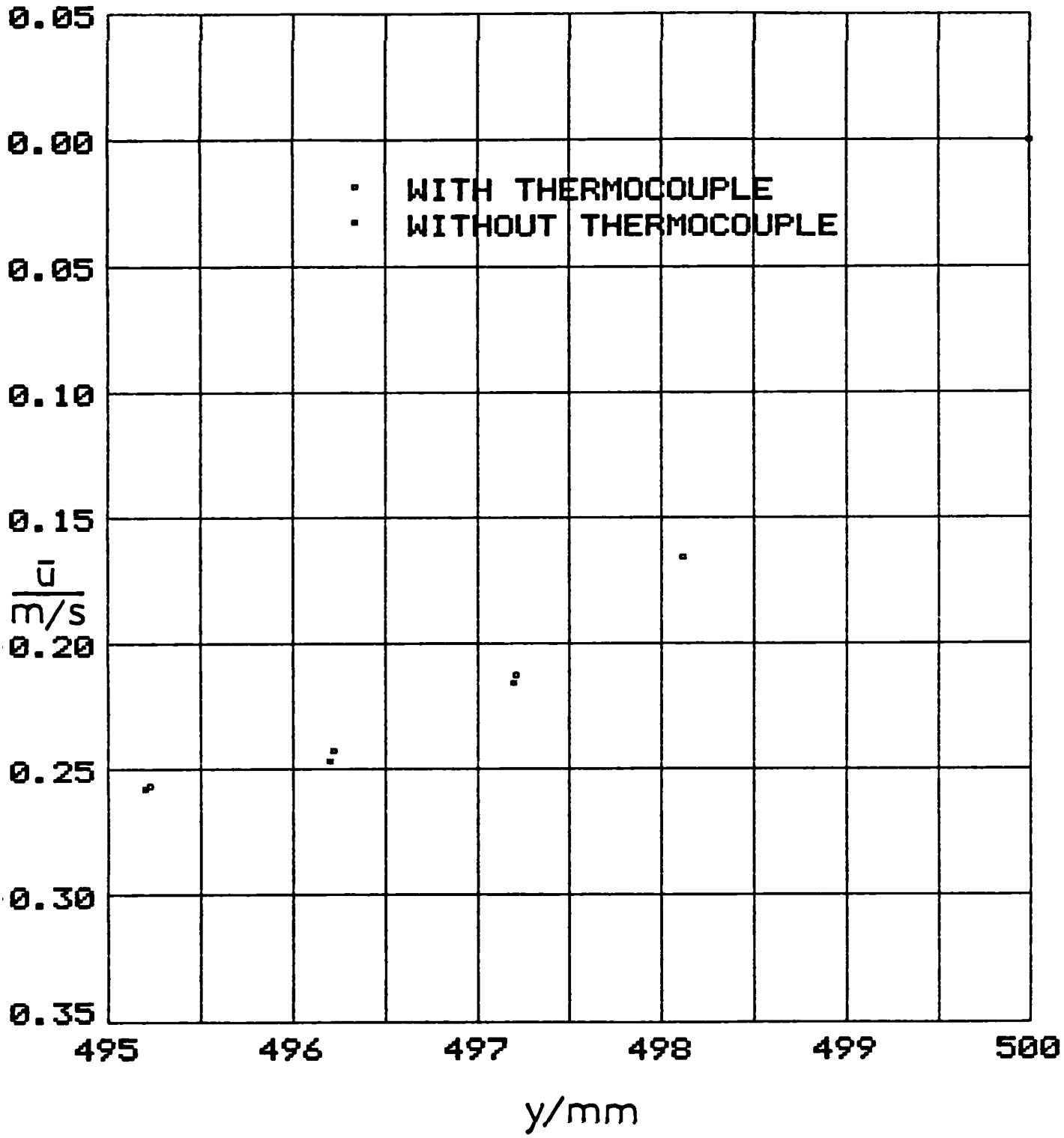

FIGURE 6.18

THERMOCOUPLE EFFECT ON R.M.S. OF

VELOCITY FLUCTUATIONS - COOLED WALL - FULL BOUNDARY LAYER

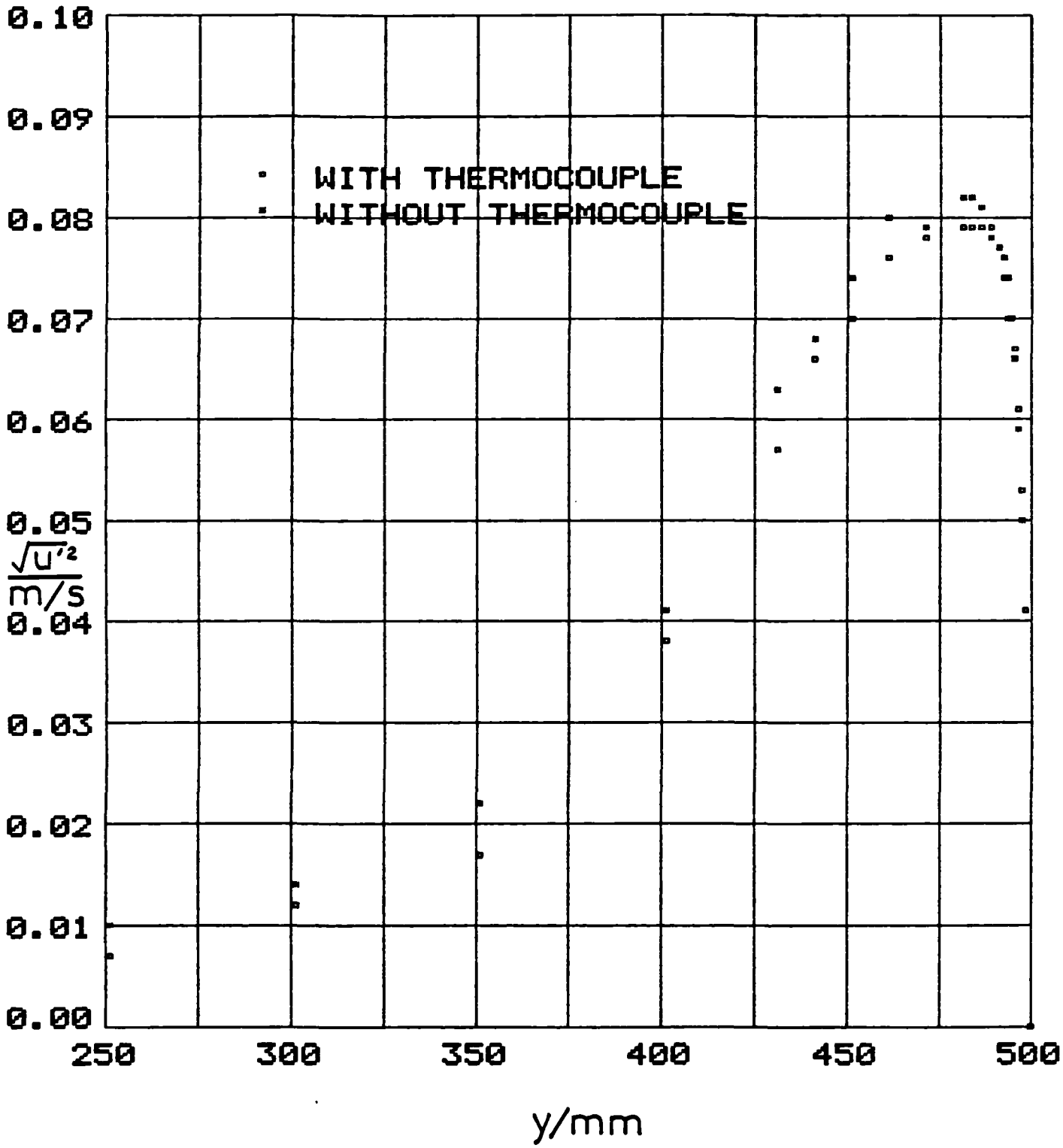

FIGURE 6.19

THERMOCOUPLE EFFECT ON R.M.S. OF

VELOCITY FLUCTUATIONS - COOLED WALL - FIRST 20mm FROM WALL

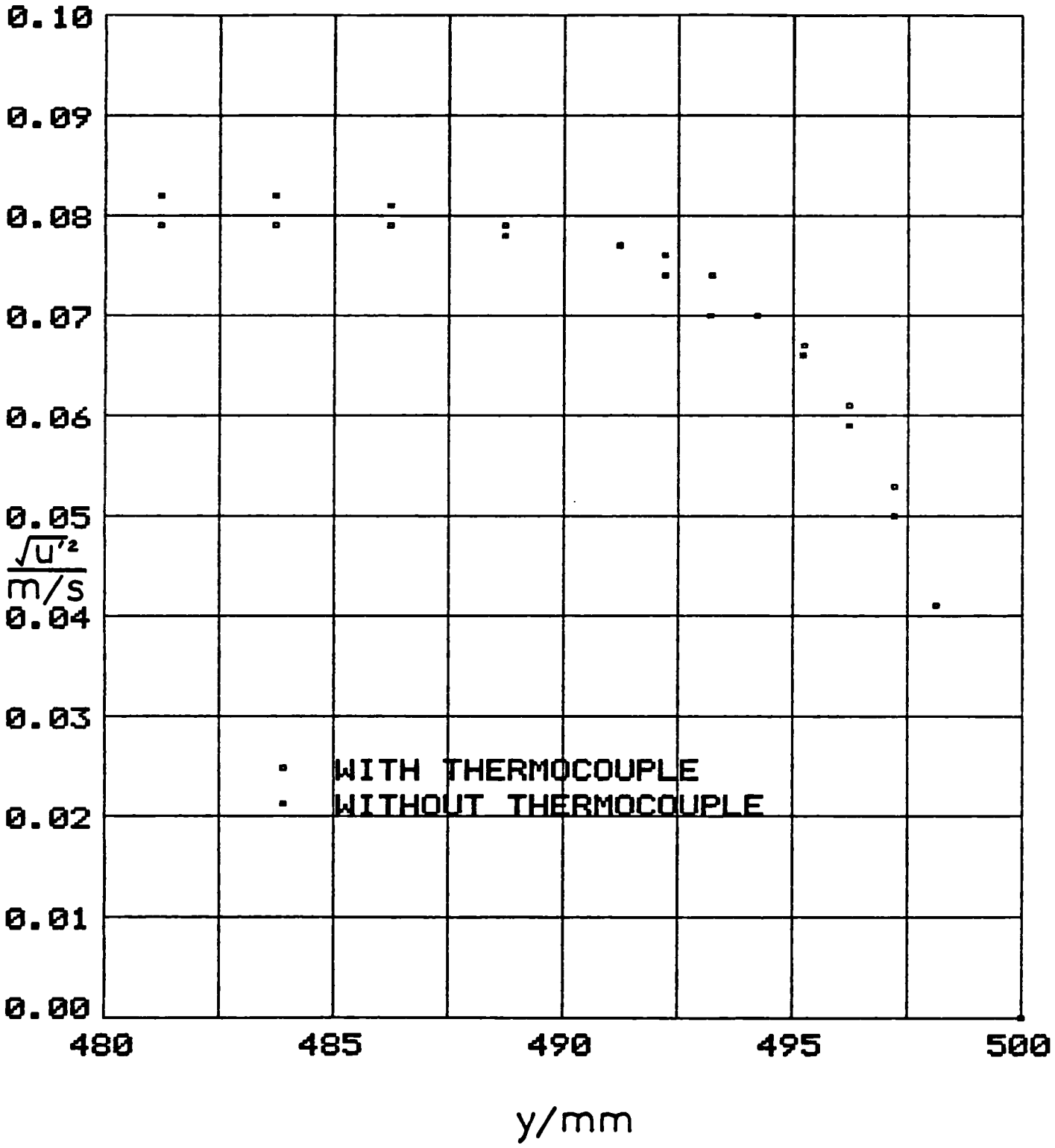

FIGURE 6.20

VARIATION OF VELOCITY CORRECTION WITH TURBULENCE INTENSITY

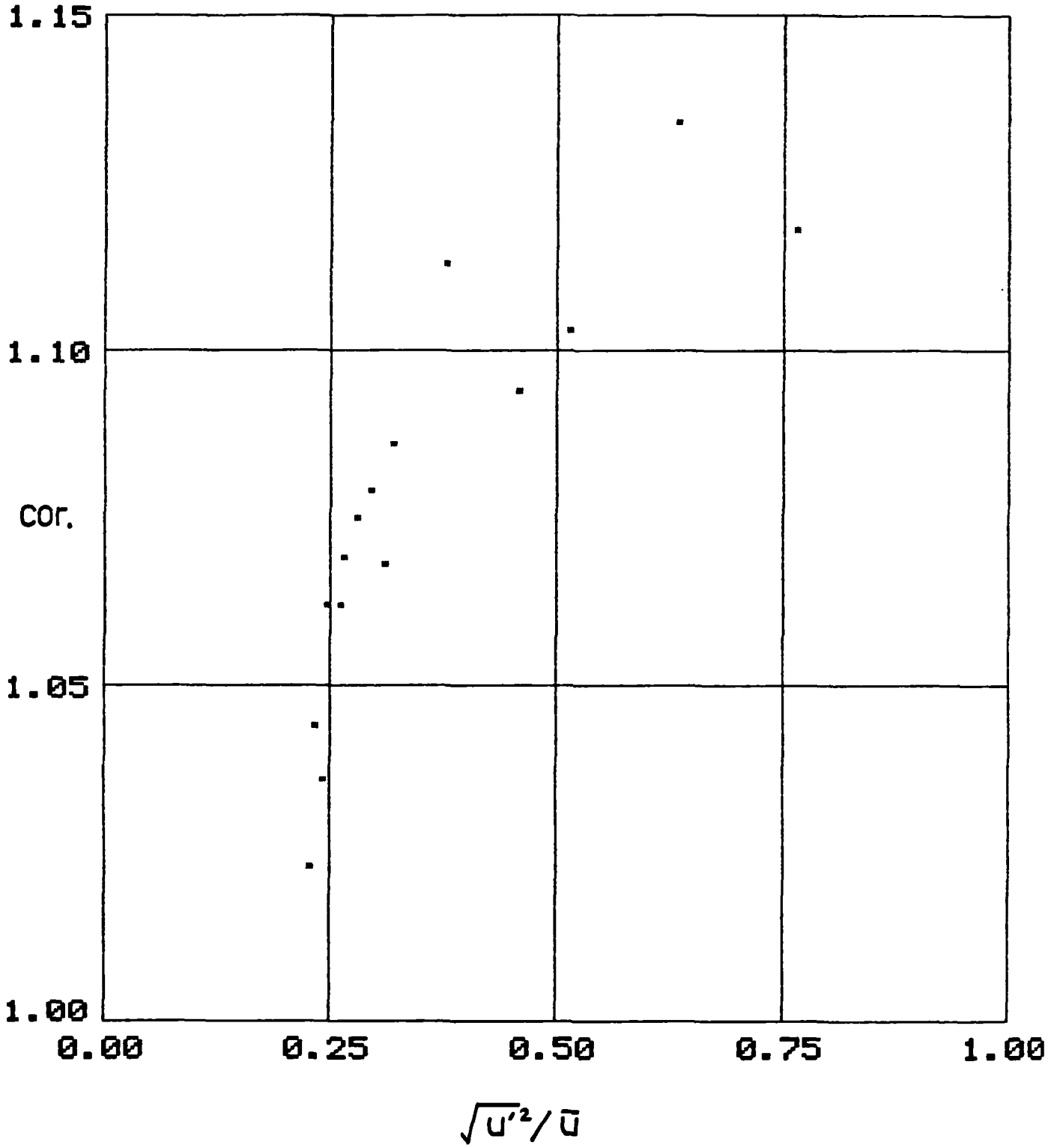

FIGURE 6.21

VARIATION OF VELOCITY CORRECTION WITH HORIZONTAL SEPARATION OF THERMOCOUPLE JUNCTION AND PROBE VOLUME

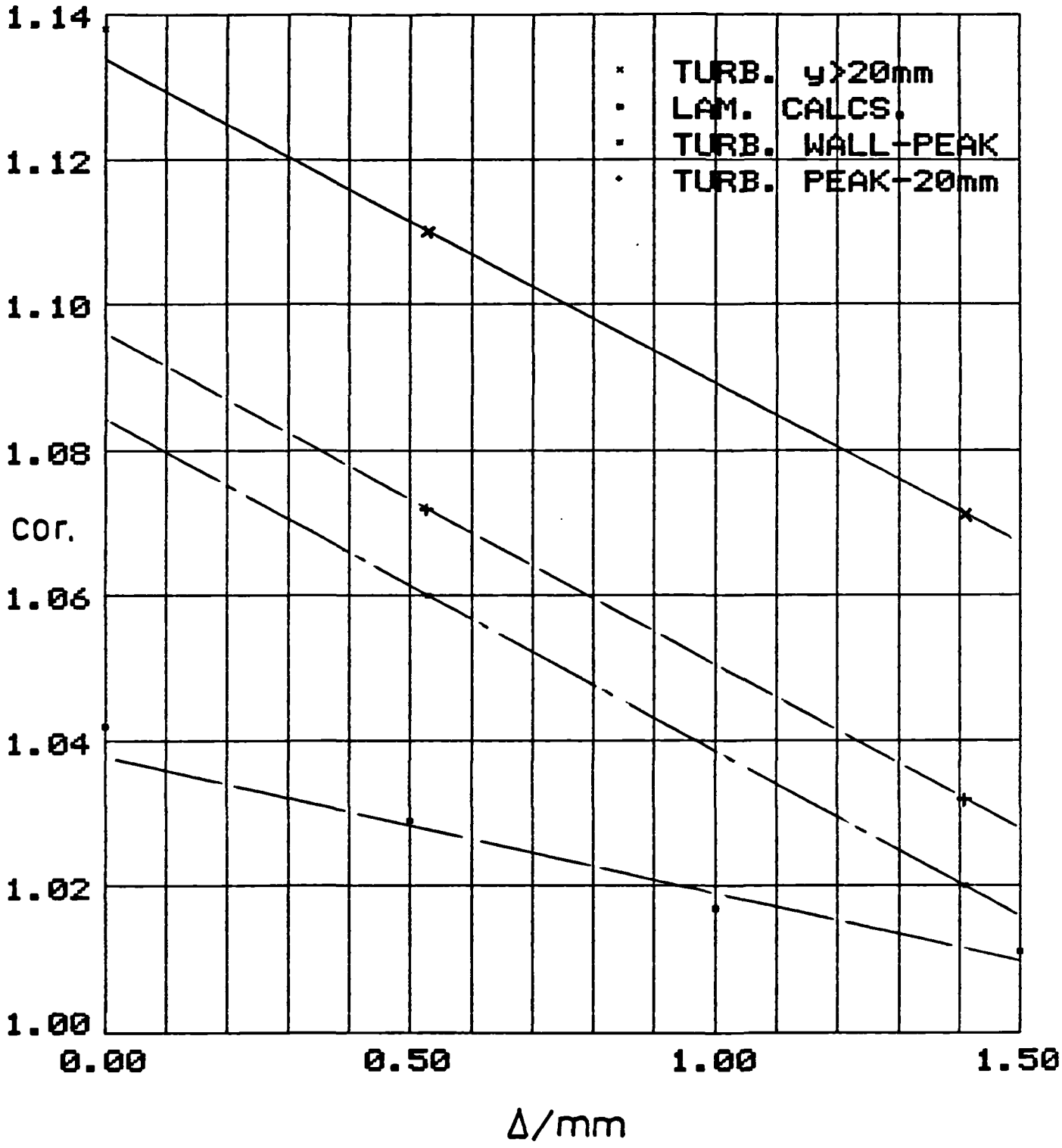

TABLE 6.1

VARIATION OF MEAN VELOCITY

AND R.M.S OF VELOCITY FLUCTUATIONS WITH TIME

	$y/\delta \approx 0.045$		$y/\delta \approx 0.141$		$y/\delta \approx 0.574$	
$\frac{t}{s}$	$\frac{u}{m/s}$	$\frac{u'_{rms}}{m/s}$	$\frac{u}{m/s}$	$\frac{u'_{rms}}{m/s}$	$\frac{u}{m/s}$	$\frac{u'_{rms}}{m/s}$
51.2	0.223	0.064	0.215	0.082	0.087	0.064
102.4	0.222	0.060	0.220	0.080	0.079	0.069
153.6	0.224	0.061	0.217	0.081	0.076	0.068
204.8	0.222	0.062	0.221	0.079	0.080	0.068
256.0	0.221	0.062	0.220	0.079	0.078	0.068
307.2	0.222	0.063	0.222	0.079	0.078	0.068
358.4	0.221	0.063	0.222	0.079	0.075	0.067
409.6	0.221	0.063	0.223	0.079	0.077	0.068
460.8	0.220	0.063	0.221	0.079	0.077	0.068
512.0	0.221	0.062	0.221	0.079	0.078	0.069

TABLE 6.2

REPEATABILITY OF MEAN VELOCITY AND R.M.S.

OF VELOCITY FLUCTUATIONS FOR THE Q.M.C. CAVITY

SAMPLE	$\frac{u}{m/s}$	$\frac{u'_{rms}}{m/s}$	SAMPLE	$\frac{u}{m/s}$	$\frac{u'_{rms}}{m/s}$
1	0.110	0.078			
2	0.101	0.072	(1+2)	0.106	0.075
3	0.114	0.079			
4	0.104	0.077	(3+4)	0.109	0.078
5	0.105	0.078			

TABLE 6.3

VARIATION OF MEAN TEMPERATURE

AND R.M.S OF TEMPERATURE FLUCTUATIONS WITH TIME

	$y/\delta \simeq 0.045$		$y/\delta \simeq 0.141$		$y/\delta \simeq 0.574$	
$\frac{t}{s}$	$\frac{T}{°C}$	$\frac{T'_{r.m.s.}}{K}$	$\frac{T}{°C}$	$\frac{T'_{r.m.s.}}{K}$	$\frac{T}{°C}$	$\frac{T'_{r.m.s.}}{K}$
51.2	56.19	2.621	52.71	1.893	50.34	0.575
102.4	56.25	2.606	52.79	1.877	50.30	0.549
153.6	56.52	2.553	52.72	1.818	50.30	0.532
204.8	56.45	2.526	52.74	1.843	50.32	0.553
256.0	56.44	2.520	52.72	1.844	50.32	0.547
307.2	56.50	2.508	52.74	1.851	50.32	0.528
358.4	56.49	2.491	52.73	1.852	50.31	0.526
409.6	56.51	2.492	52.73	1.857	50.32	0.537
460.8	56.52	2.499	52.71	1.851	50.32	0.537
512.0	56.55	2.499	52.68	1.845	50.32	0.539

TABLE 6.4

REPEATABILITY OF MEAN TEMPERATURE

AND R.M.S. OF TEMPERATURE FLUCTUATIONS

SAMPLE	$\frac{T}{°C}$	$\frac{T'_{r.m.s.}}{K}$	SAMPLE	$\frac{T}{°C}$	$\frac{T'_{r.m.s.}}{K}$
1	46.49	2.084			
2	46.30	1.932	(1+2)	46.39	2.009
3	46.51	2.120			
4	46.47	2.107	(3+4)	46.49	2.113
5	46.53	2.106			

TABLE 6.5

VARIATION OF VELOCITY CORRECTION

WITH UPSTREAM DISTANCE x FOR LAMINAR FLOW

y = 0.0mm		y = 0.5mm		y = 1.0mm	
x mm	CORRECTION	x mm	CORRECTION	x mm	CORRECTION
0.3	1.111	0.3	1.034	0.3	1.016
0.4	1.081	0.4	1.034	0.4	1.016
0.5	1.064	0.5	1.033	0.5	1.016
0.6	1.053	0.6	1.031	0.6	1.017
0.7	1.045	0.7	1.030	0.7	1.017
0.8	1.039	0.8	1.028	0.8	1.017
0.9	1.034	0.9	1.026	0.9	1.016
1.0	1.031	1.0	1.025	1.0	1.016
3.0	1.010	3.0	1.010	3.0	1.009
5.0	1.006	5.0	1.006	5.0	1.006

TABLE 6.6

EXPERIMENTALLY DETERMINED EFFECT

OF THERMOCOUPLE JUNCTION ON VELOCITY

x mm	u m/s	CORRECTION
0.75	0.152	1.138
1.20	0.154	1.123
2.25	0.164	1.055
3.0	0.159	1.088
4.2	0.166	1.042
5.7	0.174	1.000
9.9	0.168	1.000
70.0	0.173	1.000

TABLE 6.7

VELOCITY MEASUREMENTS WITH AND WITHOUT A THERMOCOUPLE IN BOTH WALL BOUNDARY LAYERS

$y_H \simeq 6.5$mm			$y_H \simeq 18.5$mm		
$\frac{u^T}{m/s}$	$\frac{u}{m/s}$	CORRECTION	$\frac{u^T}{m/s}$	$\frac{u}{m/s}$	CORRECTION
0.312	0.346	1.109	0.125	0.136	1.088

$y_H \simeq 140.5$mm		
$\frac{u^T}{m/s}$	$\frac{u}{m/s}$	CORRECTION
-0.002	0.000	-

$y_C \simeq 15.0$mm			$y_C \simeq 27.0$mm		
$\frac{u^T}{m/s}$	$\frac{u}{m/s}$	CORRECTION	$\frac{u^T}{m/s}$	$\frac{u}{m/s}$	CORRECTION
0.161	0.178	1.106	0.116	0.131	1.129

TABLE 6.8

RE-SAMPLING OF Q.M.C. DATA AT 3.125Hz AND 6.25Hz

100Hz		3.125Hz		6.25Hz	
$\frac{u}{m/s}$	$\frac{u'_{RMS}}{m/s}$	$\frac{u}{m/s}$	$\frac{u'_{RMS}}{m/s}$	$\frac{u}{m/s}$	$\frac{u'_{RMS}}{m/s}$
0.221	0.062	0.221	0.062	0.221	0.062
0.235	0.066	0.234	0.066	0.235	0.066
0.237	0.073	0.235	0.072	0.236	0.073
0.226	0.076	0.225	0.076	0.226	0.076
0.217	0.077	0.215	0.076	0.217	0.077
0.154	0.077	0.153	0.076	0.153	0.077
0.099	0.072	0.097	0.072	0.098	0.072
0.078	0.069	0.078	0.069	0.078	0.069

TABLE 6.9

REPEATABILITY OF MEAN VELOCITY AND R.M.S. OF VELOCITY FLUCTUATIONS FOR THE POITIERS CAVITY

SAMPLE	$\frac{U}{m/s}$	$\frac{u'_{RMS}}{m/s}$	SAMPLE	$\frac{U}{m/s}$	$\frac{u'_{RMS}}{m/s}$
1A	0.556	0.125	3A	0.228	0.055
1B	0.556	0.129	3B	0.227	0.057
2A	0.560	0.130	4A	0.242	0.049
2B	0.561	0.124	4B	0.239	0.054

CHAPTER 7 - RESULTS AND DISCUSSION

7.1 INTRODUCTION

In the present study the two major subjects of investigation were the temperature and velocity fields. Within the study there were many sub-topics, e.g. the local heat transfer, the local wall shear stress and the turbulence quantities. Not all of the sub-topics could be classified as being applicable to either of the two major subjects, as in the case of the two component turbulence quantities $\overline{u'T'}$, $\overline{u'\rho'}$ and $\overline{v'T'}$, where both velocity and temperature data were utilized. This has lead to the present author choosing to present the results in more than two major Sections.

The Sections in which the results are to be presented deal with the temperature field, the velocity field, the turbulence quantities (involving both velocity and temperature data) and, finally, the P.S.D. calculations.

The P.S.D. calculations have been included in a separate Section because they were undertaken on the initiative of the present author. It has been noted in Chapter 2 that there is very little information, either theoretical or experimental, which covers this subject and, as the present author found the subject interesting, a decision was made to carry out extensive P.S.D. calculations.

The results are not presented in Series order, but rather in Sections dealing with specific sub-topics which incorporate the results of all Series. The most basic results (i.e. mean and standard deviation data) are presented first, followed by quantities which were caloulated directly from the basic data (e.g. heat transfer rates). Finally, those quantities which have been calculated by graphical interpretation (e.g. the turbulence quantity $\overline{u'v'}$) or by other manipulation of the basic data, are presented.

It is worthwhile to inform the reader, now, of a few of the general characteristics of the cavity flow which should be borne in mind when reviewing the results. Most important of all is that the turbulence underwent near total collapse in the flow over the floor of each cavity, but only partial collapse in the flow over the ceilings. This gave rise to a fully recognisable transition process in the heated wall boundary layer, but only a limited transition process, in the near wall fluid, in the cooled wall boundary layer.

As a consequence of the difference in the extent of the collapse of the turbulence in the flow over the floor and ceiling, the flow at the heated wall became "dominant" over that at the cooled wall, leading to a departure of the cooled wall thermal and velocity boundary layer

characteristics from those of true natural convection. The term "dominant" is used in the context where fluid flows from one boundary layer to another to accommodate a transition process in the latter.

Another important feature was the limitation of the lateral extent of the thermal and velocity boundary layers brought about by the cavity width. In the Poitiers cavity the boundary layers on each wall met at the cavity centre. This was not the case in the Q.M.C. cavity.

7.2 THE TEMPERATURE FIELD

A full set of temperature profiles are presented in non-dimensional form for Series 3 and 6 (one Series each for the Q.M.C. and Poitiers cavities). These profiles use (T_H-T_C) as the temperature scale and L for the length scale. The profiles are of mean temperature and root mean square of fluctuating components of temperature.

Also, several local profiles of mean temperature are presented in two non-dimensional forms, using different local temperature drops as the temperature scale and a local Nusselt number as the non-dimensional length.

The quantities which have been calculated directly from the temperature data are the wall heat transfer rates, the heat transfer coefficients, the vertical centre-line temperature distributions and the local Nusselt and Grashof numbers.

7.2.1 THE MEAN AND FLUCTUATING COMPONENTS OF TEMPERATURE

The temperature data from Series 1 were important because they showed the effect on the temperature field of significant heat transfer through the vertical side walls when they were compared to the data of Series 2. In this respect only the total heat transfer and vertical centre-line temperature data from Series 1 are presented in later Sections, as the full temperature profiles from Series 3, 4, 5 and 6 are quite sufficient for the present analysis.

The mean temperature data are tabulated in Appendix A which lists all relevant data recorded during the present study.

The form of presentation in this Section is of y/L against non-dimensional temperature $\theta = (T-T_C)/(T_H-T_C)$.

Consider the mean temperature distribution for Series 3 presented in Figure 7.1, where the centre-line temperatures have been corrected in the manner to be described in Section 7.2.4. One notes that the general characteristics of the Series 3 mean temperature field were the same as

those found by Ziai [1] for the 3m high version of the Q.M.C. cavity, with a similar wall temperature difference.

At the heated wall those profiles below x/H = 0.360 showed that the thermal boundary layer was much thinner than that further up the wall. A similar characteristic was seen at the top of the cooled wall. Such observations are normally linked with an intially laminar flow which undergoes transition to a turbulent one.

It was expected that the majority of the boundary layer flow would be turbulent and that a region of flow, exhibiting laminar characteristics, would, at least, be observed at the bottom of the heated wall. This prediction was based on the graphical summary of previous work which was presented in Figure 2.2.

However, the observations of the thickness of the thermal boundary layer do not, by themselves, indicate that the flow had a laminar nature in the upstream region of each wall. Confirmation has to be sought from the distributions of $T'_{R.M.S.}$, $u'_{R.M.S.}$, mean velocity, and, most importantly, from power spectral density calculations.

In (what will be seen to be) the fully developed turbulence regions of Series 3 (above x/H = 0.360 for the heated wall and below x/H = 0.630 for the cooled wall) all mean temperature profiles exhibited a horizontal inversion which will be seen later to coincide with regions of velocity reversal.

There were horizontal inversions in the cooled wall thermal boundary layer above x/H = 0.630 but these were not as large as those below x/H = 0.630. In all cases inversions occurred when turbulent flow was present.

The mean temperature distributions of Series 4 and 5 were very similar in nature to those of Series 3 and, therefore, are not presented in graphical form. However, the change in cavity width from 0.5m to 0.2m (Q.M.C. cavity to Poitiers cavity) resulted in some significant differences in the temperature field between Series 3 and 6.

The mean temperature profiles of Series 6 are shown in Figure 7.2 from which it was clearly seen that for x/H = 0.47, and above, the mean temperature profiles did not show a horizontal inversion.

The lateral position of maximum inversion in Series 3 was 100mm from each wall, which, for Series 6, was the position of the cavity centre-line. Thus, the first point to be noted is that there was insufficient lateral space in Series 6 to accomodate the inversion seen in Series 3, providing that the thermal boundary layer developed in a similar manner in both Series 3 and 6.

One also notes that a reduction in the cavity width will lead to a reduction in the cavity "core". As the core normally exerts a damping effect on the turbulence, a reduction in the core size would be expected to lead to a lateral extension of the region of influence of the turbulence. Increased turbulence in the region of the cavity centre would tend to "smear out" any horizontal temperature inversion.

Below x/H = 0.47 one sees that there were horizontal temperature inversions in Series 6. The velocity field will show, later, that in this region the boundary layers did not meet as they did for x/H = 0.47 and above. Whilst a "core" may be considered to have occurred in this lower region it will also be seen that velocity reversal took place at the two heights studied. As previously stated, velocity reversals are associated with temperature inversions.

One of the reasons for recording the data of Series 5 and 6 was to see how the temperature field changed with changing cavity width, at constant wall temperature difference. Unfortunately, a direct comparison of temperature profiles, at identical heights, was not possible as the heat transfer through the vertical side walls was of each cavity was considerably different, resulting in different centre-line values of $(T-T_C)/(T_H-T_C)$. But, comparison of the non-dimensional mean temperature profiles, using the θ - Nu_V presentation, will be made later. Before this is done the distributions of $T'_{R.M.S.}$ in Series 3-6 will be considered.

Figure 7.3 shows the distribution of $T'_{R.M.S.}$ for Series 3. It was noted that the peak values of $T'_{R.M.S.}$, at the bottom of the heated wall, initially decreased with height up to x/H = 0.096. This must have been due to the effect of the wall in damping fluctuations.

The fluctuations must have resulted from disturbances introduced into the flow as it turned through the corner region between the wall and the floor, and also from any turbulence in the floor boundary layer that did not totally collapse. The reduction of peak $T'_{R.M.S.}$, with height, was seen more clearly in the Series 4 $T'_{R.M.S.}$ data which continued to decrease up to x/H = 0.143.

The trends in the $T'_{R.M.S.}$ data at the top of the cooled wall were similar, but the absolute values were quite different. Initially, the peak value of $T'_{R.M.S.}$ was quite considerable, it being greater at x/H = 0.949 than at any other height, for either wall. This was due to both the flow turning the corner and the failure of the turbulence to collapse to anywhere near the extent that it did in the flow across the floor. However, there was a reduction in peak $T'_{R.M.S.}$ down to x/H = 0.849 in both Series 3 and 4.

The T'r.m.s. data of Series 3 indicated that a transition process started to occur in the heated wall thermal boundary layer at approximately x/H = 0.229 (Gr_x = 4.46×10⁸ and Ra_x = 3.12×10⁹). It was at this height, and that of x/H = 0.360 (Gr_x = 1.52×10⁹ and Ra_x = 1.06×10¹⁰) at which the maximum peak value of T'r.m.s. occurred in Series 3. This was accompanied by an increase in the width of the thermal boundary layer.

A transition process also occurred in the heated wall boundary layer of Series 4, but because the wall temperature difference was lower, the process was seen to occur at a greater absolute height than Series 3. This was shown by the maximum peak in T'r.m.s. occurring at x/H = 0.360 (Gr_x = 1.27×10⁹ and Ra_x = 8.91×10⁹).

With the reduction in cavity height in Series 5, one sees that the maximum peak in T'r.m.s. was at x/H = 0.283 (Gr_x = 4.27×10⁸ and Ra_x = 2.99×10⁹) with that at x/H = 0.482 (Gr_x = 1.75×10⁹ and Ra_x = 1.22×10¹⁰) being almost the same.

The absolute heights in Series 5 corresponding to x/H = 0.283 and 0.482 were 0.566m and 0.964m, respectively. In Series 3 the absolute heights corresponding to x/H = 0.229 and 0.360 were 0.573m and 0.9m. With a reduction in cavity height, but constant wall temperature difference, it was expected that the absolute height at which the transition process would occur, would increase. This assumption was based primarily on the fact that the local Grashof number would be lower in Series 5 at the same absolute height, but also on the idea that the total heat transfer to the flow would have been lower (it has been proposed by Godeaux and Gebhart [19] that the thermal energy input to the flow has an effect on the start of the transition process). The results did not disprove this, but they were insufficient to confirm it.

In the Poitiers cavity a transition process was also seen in the heated wall boundary layer. Figure 7.4 shows the profiles of T'r.m.s. for Series 6, where the maximum peak in T'r.m.s. at the heated wall, was seen at x/H = 0.22 (Gr_x = 2.80×10⁸ and Ra_x = 1.96×10⁹). Regrettably, the interval between heights was too large to comment properly on even the approximate position at which the transition process could be said to have started or finished.

No T'r.m.s. data were available for the Poitiers cavity cooled wall, except those within 1mm of the wall which came from the heat transfer measurements. Therefore one cannot comment on any possible transition process in the fluid close to the cooled wall, with regard to the temperature field.

Turning now to the $T'_{R.M.S.}$ data associated with the "limited" transition process in the cooled wall thermal boundary layer of Series 3, one notes that the peak value of $T'_{R.M.S.}$ increased when going from x/H = 0.849 (Gr_x = 1.59x10^8 and Ra_x = 1.11x10^8) to 0.765 (Gr_x = 6.01x10^8 and Ra_x = 4.21x10^8). Now, while this is indicative of a transition process, it does not mean that the flow was exactly similar to that at the bottom of the heated wall.

In the case of the heated wall the values of $T'_{R.M.S.}$ increased over the whole of the thermal boundary layer, but this did not happen in the cooled wall thermal boundary layer. Only those data close to the peak in $T'_{R.M.S.}$ showed a significant change. This leads one to consider the possibility that, with the outer flow essentially already turbulent, a transition process only occurred in the near wall fluid.

In Series 4 the values of $T'_{R.M.S.}$ peaked in the cooled wall flow at x/H = 0.765 (Gr_x = 4.22x10^8 and Ra_x = 2.95x10^8).

As for Series 5-7, there were insufficient data to establish the position where $T'_{R.M.S.}$ peaked in the cooled wall flow.

The observations on the transition process at the heated wall have indicated that for the range Ra_H = 2.263x10^{10} - 4.486x10^{10}, the position at which the thermal fluctuation data indicate that it starts is not easily determined. A separate investigation dealing specifically with the transition process would be necessary, but from the present $T'_{R.M.S.}$ results one can quote a range of Gr_x and Ra_x over which one might expect a transition process to have started. For the heated wall this was 2.80x10^8 < Gr_x < 1.75x10^9 and 1.96x10^8 < Ra_x < 1.22x10^9, and for the cooled wall this was 1.59x10^8 < Gr_x < 6.01x10^8 and 1.11x10^8 < Ra_x < 4.21x10^8.

With the available temperature data it could easily be considered that the non-dimensional height at which transition occurred at the heated wall, in all Series, was 0.25. This was the value quoted by Seki et al [5] when they employed manual observation techniques to determine the onset of transition. As previously stated, there is no reason why transition should occur at a constant non-dimensional height.

This study, and that of Seki et al [5], have shown that if one wants to identify the position at which a transition process starts, then data must be collected at several heights with relatively small, and preferably constant, separations. Furthermore, manual observation cannot be considered to be a suitable method, neither can the variation of the root mean square quantities, as will be shown later by power spectral density calculations.

There were further interesting variations of $T'_{R.M.S.}$ in Series 3 which appear to have been associated with either regions of mean velocity reversal or regions of cross-flow between the boundary layers (or both).

In the cooled wall thermal boundary layer one notes a second peak in $T'_{R.M.S.}$ at approximately y = 400mm for all heights except x/H = 0.630, 0.898 and 0.949. Those heights below x/H = 0.630 exhibited regions of mean velocity reversal, and since the heated wall boundary layer was undergoing a transition process between x/H = 0.229 and 0.497, there must have been cross-flow there as well, as one would expect the increase in mass flow within the heated wall boundary layer to be accommodated by the loss of fluid from the cooled wall boundary layer.

The heated wall data did not show a secondary peak in $T'_{R.M.S.}$ at any height. This indicated that the secondary peak could be independent of mean velocity reversal. As there was only a relatively "minor" transition process at the cooled wall one would not have expected as much cross-flow at x/H = 0.765 as one would have at x/H = 0.229, but some would have been expected.

If then, one is to conclude that, because the heated wall data did not show a secondary peak in $T'_{R.M.S.}$, there was no connection between the secondary peak in the cooled wall thermal boundary layer and mean velocity reversal, one is left with only the link to cross-flow. If the proposed link is correct, then the really interesting aspect concerns the secondary peaks at x/H = 0.765 and 0.849. Whilst there were small mean velocity reversals in this region, the magnitude of the secondary $T'_{R.M.S.}$ peak did not correspond with them in the manner in which it did below x/H = 0.630. One may speculate that there was some cross-flow at x/H = 0.765 and 0.849 which contributed to the magnitude of the secondary peak. All these speculations, as regards cross-flow, will be checked with the graphical calculations of the lateral mean velocity, v, the results of which are presented in Section 7.3.9.

7.2.2 THE MEAN TEMPERATURE IN θ AND Nu_v FORMAT

In this Section the presentation of mean temperature data is of Nu_v against $\theta = (T-T_{REF})/(T_w-T_{REF})$ where T_{REF} has been taken to be either the centre-line temperature or T_{MIN} (T_{MIN} is the temperature in either boundary layer, between the wall and the centre-line, where the modulus of (T_w-T_{MIN}) is a maximum). For an isothermal environment the centre-line temperature = T_{MIN}, but in some cavities the latter reference temperature (the result of a horizontal temperature inversion) becomes important as it is this temperature on which the wall heat transfer rate depends.

The evaluation of Nu_y is very important. Most researchers have failed to properly identify the temperature at which the thermal conductivity has been evaluated, and indeed, there have been some manipulations of Nu_y which have subtly altered it from the standard representation of $Q''_w y/[k\Delta T]$. The evaluation of Nu_y for this thesis is based on the work of Cheesewright [57] which is now clarified.

Consider the energy equation as described in equation (1.6), and which is repeated below.

$$u\frac{dT}{dx} + v\frac{dT}{dy} = \alpha_R\frac{d^2T}{dy^2} - \frac{d\overline{v'T'}}{dy} \qquad (7.1)$$

In the thermal sub-layer the turbulence quantity v'T' can be considered to be negligible, as can the inertia terms on the L.H.S. of equation (7.1). Now, as the thermal diffusivity is considered constant (α mormally varies with temperature but is evaluated at a reference temperature in the Boussinesq approximation) the equation may be integrated twice to yield:

$$\alpha_R T = \alpha_R T_w - \frac{\alpha_R \dot{Q}''_w y}{k_w} \qquad (7.2)$$

One may now subtract the product of a reference temperature and α_R from each side of equation (7.2) and divide through by α_R and $(T_w - T_{REF})$ to give:

$$\frac{(T-T_{REF})}{(T_w-T_{REF})} = 1 - \frac{\dot{Q}''_w y}{k_w(T_w-T_{REF})} \qquad (7.3)$$

Equation (7.3) may be represented as $\theta = 1 - Nu_y$ which is exactly the same as proposed by Cheesewright [57] in equation (2.25), but here one sees how Nu_y should be evaluated. Incidentally, this equation also confirms the linear distribution of temperature in the thermal sub-layer, which was not a precondition in the evaluation of equation (7.2).

As Cheesewright [57] has shown significant success in the collapse of full temperature profiles using θ and Nu_y, it is logical to use these two groups in the presentation of the full cavity temperature profiles.

Consider now Figures 7.5-7.14 which depict Nu_y against θ for the heated and cooled walls of Series 3, 4, 5 and 6.

The first point to consider is which reference temperature provides a better basis for the comparison of profiles. One sees from Figures 7.6 and 7.8 (heated wall Series 3 and 4) that the agreement between profiles was reasonable when T_∞ was used. However, the agreement between profiles was better when T_{MIN} was used, as shown by Figures 7.5 and 7.7 (the heated wall

Series 3 and 4). The latter observation was not unexpected as T_∞ was only estimated (the recorded value in each case being unreliable) whereas T_{MIN} was reliable. Therefore one must consider other scenarios in which one of the temperatures may be expected to provide a better basis for comparison, since the current results are inconclusive.

Consider the case where the vertical centre-line temperature gradient is much larger than that of either Series 3 or 4. As a result, the horizontal temperature inversion would also be much larger. In such circumstances the minimum value of θ would be lower than the minimum in either Series 3 or 4. Thus the range of values that θ could assume is seen to be variable if T_∞ were used, but constant if T_{MIN} were used. It is this variation in θ which shows that any comparison of mean temperature profiles would be made easier by using T_{MIN}, especially when considering profiles where $T_\infty = T_{MIN}$.

It is important to note that the choice of T_{MIN} for the comparison of mean temperature profiles does not mean that T_∞ is abandoned in all other analyses. Indeed, it is used far more often than T_{MIN} (e.g. in local heat transfer calculations for Gr_x and Nu_x).

From Figures 7.5, 7.7 and 7.9 one notes that agreement between the profiles at various heights within the turbulent boundary layer of each Series was very good. Figure 7.11 shows that the agreement between the heated wall profiles of different Series (i.e. 3, 4 and 5) was also very good.

Attention is now turned to the mean temperature profiles at the cooled wall. Figures 7.12 and 7.13 show relevant profiles from Series 3 and 4 respectively. One notes that the agreement between the profiles of each graph is markedly less than that of the heated wall profiles. Profiles based on T_∞ were also calculated and showed even less agreement than those of Figures 7.12 and 7.13. These graphs have not been presented as the use of T_{MIN} has already been justified.

When heated and cooled wall profiles (from the turbulent downstream flow) were compared in Figure 7.14 a difference between the thermal boundary layers at each wall became evident.

The general lack of agreement between the heated and cooled wall non-dimensionalised profiles was most probably due to the characteristics of the flow down the cooled wall being significantly altered from natural convection flow (for $x/H < 0.360$) by the loss of cooled wall boundary layer fluid to the heated wall boundary layer, where a transition process was starting at approximately $x/H = 0.229$.

Those cooled wall profiles which most closely matched those from the heated wall were at x/H = 0.630, 0.497 and 0.360 in Series 3 and 0.630 and 0.497 in Series 4, all in the central vertical region. This is as would be expected if the absolute value of the derivative with respect to height of the mass flow, in both boundary layers, was relatively small in the central region, thus indicating a relatively small net cross flow between the boundary layers. Such a situation has been reported in many research papers and evidence to support this will be presented in Section 7.3.9.

Moving on from the Q.M.C. Series data to that of the Poitiers Series, one sees from Figure 7.10 that the heated wall temperature profiles from Series 6 were the most interesting. The Figure shows that the profiles at x/H = 0.66, 0.79 and 0.91 were all identical, but different from those of Series 3-5. Only the profile at x/H = 0.47 was the same as those from Series 3-5. It is clear that the difference between the Poitiers and Q.M.C. profiles must have been due to the reduced cavity width preventing the same lateral development of the thermal boundary layer downstream from x/H = 0.47, as was seen in the Q.M.C. Series.

The final comments on the temperature profiles are connected with the work of Cheeswright [57] and Sibers et al [60] where $\ln(Nu_V)$ was plotted against θ. Both of these works used temperature data from vertical flat plates, and so T_{MIN} was the best choice of reference temperature for comparison between their data and the present. This view was re-inforced when considering the presentation by Cheesewright and Ziai [59], of a comparison of cavity and flat plate mean temperature data using T_∞ as the reference temperature in both cases. The difference between the profiles from each scenario was significant.

Cheesewright [57] found a linear relationship between $\ln(Nu_V)$ and θ, of $\theta = 0.28 - 0.08\ln(Nu_V)$ for $\ln(Nu_V)$ ranging from 0.8 to 3.1. The data presented by Siebers et al [60] also showed a linear relationship between θ and a range of the natural log of a variation of Nu_V.

Figures 7.15 and 7.16 show the present data in the format of Cheesewright [57]. One notes that when $\ln(Nu_V)$ was positive there were three ranges where a linear relationship could be considered to exist, and one range when $\ln(Nu_V)$ was negative. The ranges of $\ln(Nu_V)$ and the equations for each range were as follows:

For $-1.3 \leq \ln(Nu_V) < 0$ $\quad \theta = 0.33 - 0.31\ln(Nu_V)$ (7.4)

For $0 < \ln(Nu_V) < 0.6$ $\quad \theta = 0.34 - 0.24\ln(Nu_V)$ (7.5)

For $0.6 < \ln(Nu_V) < 1.2$ $\quad \theta = 0.29 - 0.16\ln(Nu_V)$ (7.6)

For $1.2 < \ln(Nu_V) < 2.2$ $\quad \theta = 0.21 - 0.09\ln(Nu_V)$ (7.7)

The last range had a gradient of approximately -0.09 which was very close to that found by Cheesewright [57]. However, the y intercept was considerably different at 0.21. This underlines the difference between the present cavity flow and that for a vertical flat plate.

The near wall profile presented in Figure 7.15 was in good agreement with that of Ziai [1] who had shown that the thermal sub-layer (for air) in both cavity and flat plate flows is very similar. The $T'_{R.M.S.}$ data indicated that in the present study the thickness of the thermal sub-layer was 1.6mm which was very close to the 1.6-2.0mm put forward by Ziai [1].

7.2.3 THE VERTICAL CENTRE-LINE TEMPERATURE DISTRIBUTION

The non-dimensional vertical centre-line temperature distributions are shown in Figure 7.17 for Series 1-4, and Figure 7.18 for Series 5-7. In all but Series 2 there were two centre-line temperatures which could be used to calculate $\theta = (T-T_C)/(T_H-T_C)$. These two temperatures were always different by at least 0.3K indicating that either the wall temperatures had changed slightly from one half of the run to the other, or that the thermocouples were not reading the same absolute value. To compensate for either of these effects a compromise was made in calculating the non-dimensional value, θ. The formula used to calculate θ at the centre-line was:

$$\theta_{CL} = \frac{\Delta T_C/\Delta T_H}{(1 + \Delta T_C/\Delta T_H)} \qquad (7.8)$$

Where ΔT_H is the difference between the heated wall temperature and that of the centre-line fluid for the first half of the run, and ΔT_C the difference between the temperature of the cooled wall and the centre-line fluid for the second half of the run.

From Figure 7.17 one notes the substantial difference in centre-line temperature between Series 1 and 2, the temperature of the centre-line fluid being higher in the latter Series at all heights. This shows conclusively that the effect of an increase in heat transfer through the vertical side walls is a reduction in the temperature of the fluid at the centre-line.

The centre-line temperatures for Series 3 have been corrected for an effect which became apparent in the calculation of the turbulence quantity $\overline{u'v'}$. The corrected values showed good agreement with the data of Series 2, but were generally higher. This was not expected as the local removal of blocks of polystyrene should have led to a small reduction in the non-dimensional temperatures of Series 3 compared to those of Series 2. However, one can easily explain the observation.

Figure 7.19 compares the non-dimensional centre-line temperature for Series 3 (before and after the corrections were applied) to those of Series 2 and 5. One sees that the corrected data were generally higher than the uncorrected data. If one could apply the same correction to the Series 2 data then they would increase. One would then expect to see little difference between the Series 2 and 3 data.

The non-dimensional temperature data of Series 4 were lower than those of Series 3 which were for a higher wall temperature difference. This trend was reversed in the comparison between Series 6 and 7 where the latter, with the higher wall temperature difference, showed a lower non-dimensional centre-line temperature than the former. The reason for the reversed trends is not clear.

The two main factors which would be expected to influence the non-dimensional centre-line temperature are the difference between the ambient temperature and the average of the wall temperatures, and, the extent (and characteristics) of the flow down the vertical side walls which is determined by the difference in wall temperatures and the effectiveness of the insulation on the side walls.

One may have expected the non-dimensional temperature data of those cavities with the higher wall temperature differences to have exhibited lower non-dimensional centre-line temperatures due to an increase in the heat transfer coefficient at the vertical side walls. This would have arisen because the local temperature drop between the external ambient temperature and the average of the wall temperatures would be higher (the local heat transfer coefficient being expected to increase with increasing local temperature drop). Such a variation of heat transfer coefficient with temperature drop is also linked to the trend necessary for Nu_v to be a constant at the velocity peak within a cavity.

As has been shown in Tables 7.1-7.4, the heat transfer coefficient is dependent on the characteristics of the flow (i.e. is the flow laminar or turbulent). When the flow has a "laminar aspect" to it the heat transfer coefficient is lower. A flow down the vertical side walls which exhibits a laminar aspect would be more likely at lower wall temperature differences and so higher non-dimensional centre-line temperatures would be expected in such cases.

Both of the effects which have been mentioned only support the observations of the non-dimensional centre-line temperatures of Series 6 and 7. The observations from Series 3 and 4 still remain unexplained. One

can only speculate that it is something to do with the cavity structure which has led to the unexpected results.

There were differences between the Q.M.C. and Poitiers cavity structures, most notably in the inclusion of the vertical rod and probe block in the former and a higher breadth to width ratio (B/L) in the latter.

The ratio of breadth to width has been shown by Morrison and Tran [73] to affect the extent of the central region in the cavity which exhibits uniform profiles of velocity and temperature, in the z co-ordinate direction. They recommended a ratio of 5 be used in any cavity construction. This is larger than the ratios of 2 and 3 employed in the Q.M.C. and Poitiers cavities, respectively.

Generally, there was good agreement between the data of Series 3 and 5 which showed that the decrease in height from 2.5 to 2.0m did not have a significant effect on the non-dimensional centre-line temperature.

Turning now to the equation which describes the non-dimensional centre-line temperature distributions, one notes that in all the Q.M.C. Series the distributions can be approximated as linear. Strictly speaking this was not the case for the Poitiers data but they have been approximated as linear for the sake of a complete, consistent, set of data. The resulting equations are given below:

Series 1	$\theta = 0.449(x/H) + 0.131$	(7.9)
Series 2	$\theta = 0.495(x/H) + 0.158$	(7.10)
Series 3*	$\theta = 0.463(x/H) + 0.179$	(7.11)
Series 3	$\theta = 0.473(x/H) + 0.180$	(7.12)
Series 4	$\theta = 0.464(x/H) + 0.153$	(7.13)
Series 5	$\theta = 0.469(x/H) + 0.169$	(7.14)
Series 6	$\theta = 0.411(x/H) + 0.184$	(7.15)
Series 7	$\theta = 0.443(x/H) + 0.137$	(7.16)

* original uncorrected data.

Ziai [1] reported the gradient and intercept to be 0.50 and 0.19, respectively. The closest agreement, in terms of the gradient, comes from the data of Series 2. One would have expected a closer agreement to have come from the Series 1, 3, 4 and 5 data, where the local levels of insulation were closer to that used by Ziai. It may be that Ziai [1] did not take all his data into account when forming his equation, but if one selects only the fully turbulent data in Series 1 and 3 the agreement becomes worse.

It appears that Ziai [1] imposed a line with 0.5 gradient on his data, as this was the value that his Literature Survey found to be the most common. Certainly, one can tell by visual inspection, that if all his data had been taken into account a different line would have resulted.

As the differences between the data for Series 3 and 5 are not significant, one would have expected little difference between the data of Ziai [1] and those for Series 3, as there was only a difference of height (3.0m for Ziai [1] and 2.5mm for Series 3) between the two cavities. Ziai [1] did have one triple glazed vertical side wall which would have been expected to reduce the non-dimensional centre-line temperature but there is no indication of this happening.

From these observations one is faced with two explanations as to why there was a difference between the data of Ziai [1] and those of Series 1-5. The first is that the difference may be attributed to experimental uncertainty. This is unlikely as the equipment used by Ziai was identical to that used in the present study. The second reason is that the technique used by Ziai to calculate the non-dimensional values was not accurate enough (i.e. it did not take into account the variation of wall temperatures during the experiment). Such a mistake is easily made and must not be made by future researchers.

In Chapter 2 a trend was noted of decreasing non-dimensional temperature gradient with increasing aspect ratio. This is again seen when comparing the data from Series 3 and 4 (H/L = 5) and Series 6 and 7 (H/L = 10). This trend is most strikingly seen when one considers only the data for x/H $\geq$ 0.47 from Series 5, 6 and 7. The equations for this region were:

Series 5 $\theta = 0.404(x/H) + 0.219$ (7.17)

Series 6 $\theta = 0.389(x/H) + 0.200$ (7.18)

Series 7 $\theta = 0.355(x/H) + 0.203$ (7.19)

The data from Series 6 and 7 were best represented by two regions, those above and below x/H = 0.47. The equations for the lower regions were:

Series 5 $\theta = 0.372(x/H) + 0.180$ (7.20)

Series 6 $\theta = 0.474(x/H) + 0.175$ (7.21)

Series 7 $\theta = 0.484(x/H) + 0.124$ (7.22)

In the work of Renault [32] the lower region was said to exhibit a "laminar aspect". This, together with other work reviewed in the Literature Survey has indicated that (in the transitional boundary layer regime) the region exhibiting a "laminar aspect" displays a slightly different non-dimensional temperature gradient than that found in the fully developed

turbulent flow region. The same trend has been shown to occur in all Series, but there were differences between them.

In Series 1-5 the non-dimensional temperature gradient in the lower region was smaller than that in the fully developed turbulence region. This was reversed in Series 6 and 7, which reflected the temperature distribution found by Renault [32].

It is possible that the derivative of mass flow with height is associated with the non-dimensional temperature gradient. If this were the case then in all Series the lower region would be expected to show a similar gradient. But, in the fully developed flow regions of Series 6 and 7 (where the derivative of mass flow was expected to be quite small in comparison with Series 1-5) one would expect some difference in the gradient to that found in Series 1-5.

7.2.4 THE HEAT TRANSFER COEFFICIENTS

The heat transfer coefficients for Series 1-7 are presented in Tables 7.1-7.4. These data provide information which give some limited help in determining the position of the transition process at the heated wall, and the height at which the flow can be considered to be fully developed. They also show up differences between the flow characteristics of the heated and cooled wall boundary layers.

Consider first the data for Series 1, 2 and 3. One immediately notes that the coefficients for the heated walls at x/H = 0.050 were much higher than those at x/H = 0.100. This was due to the fluctuations in the flow (introduced when the flow turned the corner) enhancing the heat transfer.

Beyond x/H = 0.050 the heat transfer coefficient decreased up to and including x/H = 0.150. This was representative of a damping of fluctuations by the wall. The coefficient then increased with height as a transition process took place and was approximately constant from x/H = 0.366 upwards. One may therefore assume that the flow above x/H = 0.366 was fully developed.

The trend of the heat transfer coefficient for the cooled wall flow was the same as that for the heated wall flow. An initially high value at x/H = 0.950 decreased with distance downstream until x/H = 0.850 after which it increased to an approximately constant value from x/H = 0.766 downwards.

The indication from the heat transfer coefficient is that a transition process started at approximately x/H = 0.233 and finished at approximately x/H = 0.366 for the heated wall, and similarly at x/H = 0.850 and 0.766 for

the cooled wall. These observations do not quite coincide with those of the $T'_{R.M.S.}$ data, but are very similar.

The fully developed regions of both wall boundary layers exhibited approximately the same value for the heat transfer coefficient. Therefore the coefficient did not show up any significant difference between the flow characteristics of the heated and cooled wall flows. Neither was there any indication of a trend of decreasing coefficient with increasing height, as would be expected if the position of the peak mean velocity was characterised by a constant value of Nu_V.

The data from Series 5 were very similar in magnitude to those of Series 1-3, whereas those from Series 4 were smaller than those from Series 1-3. This showed that the coefficient was generally dependent on the wall temperature difference, an observation which was confirmed by the data from Series 6 and 7.

However, the data from Series 6 (which had the same wall temperature difference as Series 5) were significantly larger than those of Series 5, thus showing that the reduction in cavity width had an effect on the heat transfer. The difference in heat transfer coefficient must have been linked to an increase in the turbulence level brought about by the elimination of the core.

The data from Series 6 and 7 were also different in that the heat transfer coefficients for the cooled wall flow were significantly lower than those for the heated wall. The only reasonable explanation for this is the relatively poor side wall insulation of the Poitiers cavity. This would have promoted a substantial flow down the vertical side walls thus causing a significant difference between the flows down each wall. Such an effect would have been less noticeable in the Q.M.C. Series as the side wall insulation was considerably more effective, although one might have expected to have seen this in the Series 1 data.

The effects of the insulation on the vertical side walls will be shown in later Sections with regard to overall heat transfer, and mass flow at the cavity mid-height.

In respect of the difference between the mean temperature profile of θ against Nu_V for Series 6 at $x/H = 0.47$ and those for the heights beyond this, one notes that there was no indication from the heat transfer coefficient that the flow was different at $x/H = 0.47$ from that at the other three heights.

Some expected trends in the heat transfer coefficient have not been observed (e.g. reduction in coefficient with height). There are two

expalanations for this, either the accuracy of the heat transfer coefficients was poor or the expected trends were not present. The former explanation is certainly possible as an uncertainty of only 3% would be responsible for the largest difference between expected and experimental trends.

7.2.5 THE LOCAL HEAT TRANSFER

The local heat transfer relationship between Nu_x and Gr_x, or Nu_x and Ra_x, will vary with the stratification at the cavity centre-line for any local temperature drop. However, since the variation in the centre-line temperature stratification was reasonably small over all Series, one would expect the relationships for Series 2, 3 and 4 to be very similar, and that for Series 5, 6 and 7 to be similar also (providing that in the latter two Series no substantial effect was brought about by the relatively small cavity width).

Local Nu_x, Gr_x and Ra_x have been calculated and are presented in Tables 7.5-7.10. The choice of the reference temperature at which the three numbers were calculated was very important. Such a choice has been commented upon by Zhong et al [58] and Siebers et al [60].

Zhong et al [58] merely pointed out that the use of different reference temperatures makes comparison of experimental data difficult, and that there appeared to be no concensus on which temperature to use. Siebers et al [60] went further by trying to introduce a correction to air data when they were all evaluated at the environmental temperature (T_∞).

It appears that most researchers have failed to take into account the fact that the equations which describe natural convection flow are subject to the Boussinesq approximation, and it is these equations which yield the commonly accepted relationship $Nu_x = Nu_x(Gr_x,Pr)$ for a vertical flat plate (this is the relationship which is of interest in the local heat transfer within the cavity). It should be remembered that if the Boussinesq approximation fails in any particular scenario then the relationship $Nu_x = Nu_x(Gr_x,Pr)$ would also be expected to fail as this is derived as a result of the approximation. In this respect, work by Gray and Giorgini [83] has indicated that the approximation is acceptable for a cavity when $(T_H-T_C)/T_C < 0.2$. This was the case for all Series, and, in terms of local heat transfer, the ratio $(T_w-T_\infty)/T_\infty$ was always less than 0.1 for all Series.

Now, the term $\beta_T(T_w-T_\infty)$ in the Grashof number comes from the quotient $-(\rho_w-\rho_\infty)/\rho_{REF}$. Previously, in Section 7.2.2, it was shown that a suitable temperature at which to calculate the thermal conductivity in the Nusselt

number was the wall temperature. To ensure a consistent approach to the problem it is best to use the wall temperature as the reference temperature in the density quotient. The quotient results directly from the Boussinesq approximation and so it should be manipulated in the most accurate manner possible. This means using the formula for an ideal gas to convert the density quotient to the desired temperature quotient. This results in the coefficient of thermal expansion in Gr_x as being the reciprocal of the environmental temperature. So the expression used for Gr_x was:

$$Gr_x = \frac{g\beta_T(T_w-T_\infty)x^3}{(\mu/\rho)\omega^2} \qquad \text{where } \beta_T \equiv 1/T_\infty \qquad (7.23)$$

By using the wall temperature as a reference temperature, and so deriving β_T as the reciprocal of the environmental temperature, one can expect to see some minor differences between any existing air data, from a stratified environment, and the present data. The difference will be least when comparing data which were calculated by evaluating both β_T and (μ/ρ) at the film temperature.

The local heat transfer data are presented graphically in Figures 7.20-7.23 for the heated and cooled walls. It is seen that the data from Series 2, 3, 4 and 5 were grouped very closely, as were the data from Series 6 and 7. However, the heated wall data from Series 5 and Series 6 were different at the lower values of Gr_x. The increase of Nu_x for a given value of Gr_x (from Series 5 to 6) was indicative of the higher levels of turbulence at the bottom of the heated wall in the Poitiers cavity.

The relationship between Nu_x and Gr_x has been calculated for two regions at each wall. The first is associated with the flow displaying a laminar aspect, whilst the second is the region associated with the fully turbulent flow. The demarcation, in terms of Gr_x, between each region has been chosen arbitrarily as insufficient data exist to fix it absolutely. The local heat transfer relationships for Series 2, 3, 4 and 5 were:

$$Nu_x = 0.305Gr_x^{0.261} \quad Gr_x < 2.35\times10^8 \quad \text{heated wall} \qquad (7.24)$$

$$Nu_x = 0.030Gr_x^{0.395} \quad Gr_x > 2.35\times10^8 \quad \text{heated wall} \qquad (7.25)$$

$$Nu_x = 0.635Gr_x^{0.235} \quad Gr_x < 5.05\times10^8 \quad \text{cooled wall} \qquad (7.26)$$

$$Nu_x = 0.006Gr_x^{0.474} \quad Gr_x > 5.05\times10^8 \quad \text{cooled wall} \qquad (7.27)$$

The local heat transfer relationships for Series 6 and 7 were:

$$Nu_x = 0.196Gr_x^{0.304} \quad Gr_x < 3.60\times10^8 \quad \text{heated wall} \qquad (7.27)$$

$$Nu_x = 0.050Gr_x^{0.376} \quad Gr_x > 3.60\times10^8 \quad \text{heated wall} \qquad (7.28)$$

$$Nu_x = 0.144Gr_x^{0.322} \quad Gr_x < 1.00\times10^8 \quad \text{cooled wall} \qquad (7.29)$$

$$Nu_x = 0.120Gr_x^{0.336} \quad Gr_x > 1.00\times10^8 \quad \text{cooled wall} \qquad (7.30)$$

There was no distinct trend in the relationships for each individual Series, indicating that the local heat transfer relationship was not significantly affected by the range of dT/dx at the centre-lines of the cavities. For natural convection in an isothermal environment the powers on the Grashof number for laminar and turbulent flow are generally accepted as 0.25 and 0.333, respectively. In all of the relationships shown above, the powers were greater than those for an isothermal environment.

The only other local heat transfer data available are those of Cowan et al [12] from the heated wall of a water cavity. Their data are shown in Figure 7.24 together with lines representing the current data. The agreement between the air and water data was poor, with the water cavity data exhibiting the larger value of Nu_x at all experimental values of Gr_x.

It was thought that the use of Ra_x might improve the agreement between the water and air data, and so Figure 7.25 was produced. This Figure shows the local heat transfer data from the present study together with those from Cowan et al [12] using Ra_x instead of Gr_x. In this case it was the air data which exhibited the larger values of Nu_x at all experimental values of Ra_x, a reverse of the situation in Figure 7.24. Therefore, the data in Figures 7.24 and 7.25 further demonstrate that there is a Prandtl number dependency in the local heat transfer function.

The present local heat transfer data can be used in an attempt to predict the centre-line temperature distribution for the theoretical case of zero heat transfer through the vertical side walls. This would mean equal heat transfer at each active wall, but little change in the heat transfer through the floor and ceiling.

To predict the centre-line temperature distribution one must first select an appropriate gradient. For the Q.M.C. cavity this was 0.495, the gradient from the Series 2 data which matches closely the gradient most frequently found by Ziai [1] in his Literature Survey. The resulting distribution was:

$$\theta = 0.495(x/H) + 0.21 \qquad (7.31)$$

The gradient chosen for the Poitiers cavity was 0.411 (from Series 6) which was very close to that found by Renault [32].

$$\theta = 0.411(x/H) + 0.28 \qquad (7.32)$$

The two equations above predict θ at $x/H = 0.5$ to be 0.46 and 0.48 respectively, which compare favourably to $\theta = 0.46$, at mid-height, reported by Schmidt and Wang [14] and $\theta = 0.44$ by Giel and Schmidt [15], for a reasonably well insulated water cavity. However, when all closing boundaries

are adiabatic the arguments presented in Section 2.8 predicted $\theta > 0.5$ at mid-height.

Neither equation (7.31) or (7.32) come close to the reported centre-line temperature distribution in the well insulated water cavity of Cowan et al [12], but equation (7.31) is similar to the reported distribution in the ethyl-alcohol cavity of Kutateladze et al [35].

7.2.6 OVERALL HEAT TRANSFER

The overall heat transfer rates at each wall for Series 1-7 are given in Table 7.11.

It is seen that the improvement in the vertical side wall insulation from Series 1 to 2 resulted in a reduction in heat transfer through these walls, such that the percentage loss dropped from 37.4% to 22.8% (this was for wall temperature differences of approximately 42.5K for Series 1 and 46.2K for Series 2).

In order to validate the quantitative nature of the overall heat transfer data one must be able to adequately account for $\Delta\dot{Q}'_{\omega}$ in all Series, and, most especially, for the dissimilar trends in percentage loss between Series 3 and 4 and Series 6 and 7. (It will be seen that $\Delta\dot{Q}'_{\omega}$ can be accounted for by heat transfer to the cavity structure and through all closing walls).

Most striking is the rise in percentage loss from Series 3 to Series 4. This may be explained in two ways, either the heat transfer to the cavity structure in both Series was approximately constant, or that the heat transfer through the vertical side walls in both Series was approximately constant.

One may attempt to examine the first explanation by estimating the heat transfer through the closing walls. By considering the outer wall temperature to be approximately 20°C and the average temperature of the inner walls to be that of the centre-line fluid at $x/H = 0.497$, it was estimated that the heat transfer through the closing walls would account for 40-45W/m in Series 3 and 33-37W/m in Series 4, of $\Delta\dot{Q}'_{\omega}$. This left deficits of 27.4-32.4W/m and 29.7-33.7W/m in Series 3 and 4, respectively, which are approximately equal. (It is recognized that the deficit for Series 4, as calculated here is higher than that for Series 3, but as temperature measurements of the internal and external closing wall temperatures were not made, the calculations presented here can only be considered to be valid to approximately ±20% at best).

In further support of the first explanation is the fact that the vertical probe support rod passed through the Q.M.C. cavity. This would have provided a ready path for heat transfer to the remainder of the cavity structure.

Now, one may compare the variation in $\Delta\dot{Q}'_w$ between Series 7 and 6, to that between Series 3 and 4. In Series 3 and 4 the value of $\Delta\dot{Q}'_w$ only dropped from 72.4W/m to 66.7W/m, whereas in Series 7 and 6 it dropped from 198.1W/m to 118.1W/m. In the Poitiers cavity there was no internal structure which could provide a path to the bulk of the cavity structure and so the ratio of $\Delta\dot{Q}'_w$ between Series 6 and 7 would be expected to be close to that of the ratio of the heat transfer through the closing walls in both Series. The ratio of $\Delta\dot{Q}'_w$ from Series 6 to that of Series 7 was approximately 0.6, and the ratio of the heat transfer through the closing walls (assuming an external wall temperature of 16°C) was calculated to be 0.5. The closeness of these two ratios definitely suggests that the heat transfer to the cavity structure was approximately the same in Series 3 and 4.

Going back to the second explanation, one sees that if it were to be valid then the difference between the inner and outer side wall temperatures would have had to be approximately equal in both Series 3 and 4. This would have been unlikely given the values of $\Delta\dot{Q}'_w$ in Series 6 and 7.

If one accepts the reasoning that the first explanation is probably correct, then the observation of the variation in non-dimensional centre-line temperature between Series 3 and 4 (Section 7.2.4) may be accounted for. The non-dimensional centre-line temperatures of Series 4 were lower than those of Series 3 which could have been brought about by the disproportionate heat transfer, in Series 4, to the cavity structure.

Of course, the heat transfer rate where the measurements were taken need not have been constant over the entire breadth of the active walls. From measurements taken at a 150mm offset from wall centre-lines the heat transfer rates were seen to be the same as those at the wall centre-line, but the remaining 70% of the wall area was not investigated.

Ziai [11] undertook experiments which gave an estimate of the heat transfer from each active wall as a percentage of the heat transfer at the wall centre-lines. This estimate was 90%. Therefore it is possible that the true values of $\Delta\dot{Q}'_w$ for Series 3 and 4 were 65.2W/m and 60.0W/m, thus reducing the deficits by 7.2W/m and 6.7Wm respectively.

In attempting to explicitly account for $\Delta\dot{Q}'_w$ in Series 3, one may estimate a best and worst case of 7% and 14% of $\Delta\dot{Q}'_w$ being attributed to heat transfer to the cavity structure.

Now, the object of these calculations was to verify the validity of the heat transfer rates calculated from the near wall mean temperature data. This was necessary as Ziai [1] had expressed some doubts as to the validity of his heat transfer rates calculated from data gathered using the same equipment used in the present study. With a range of 7-14% of the total heat transfer from the heated wall being attributed to heat transfer to the cavity structure, the present heat transfer data would appear to be validated.

7.2.7 TWO-DIMENSIONAL CHECKS

In both Series 3 and 4 a number of runs were made at an offset of 150mm from the wall centre-lines (z = 650mm). These checks, at x/H ≈ 0.229, 0.497 and 0.949, showed the mean temperature profiles to be identical to those at the wall centre-lines (z = 500mm). All differences between profiles fell within the range of uncertainties estimated in Chapter 6.

This means that the central 30% of the cavity (at least) exhibited a uniform mean temperature distribution, and consequently, uniform wall heat flux. This resulted from a breadth to width ratio of 2, which was significantly less than the ratio of 5 proposed by Morrison and Tran [73], to ensure uniform profiles of velocity and temperature in the central cavity region.

7.2.8 SUMMARY OF THE FINDINGS FROM THE TEMPERATURE RESULTS

Horizontal temperature inversions were seen, as in other previously presented data, but were found to be associated with regions of turbulent flow. However, the existence of turbulent flow was no guarantee of a horizontal inversion as the cavity width also had a considerable influence. The effects of a smaller cavity width tended to eliminate the horizontal inversion.

The distribution of T'_{RMS} was a reasonable indicator of the onset of transition within the boundary layers at each wall. For the range $Ra_H = 2.263\times10^{10} - 4.486\times10^{10}$, the range of Gr_x and Ra_x at which the onset of transition was seen was $2.80\times10^{8} < Gr_x < 1.75\times10^{9}$ and $1.96\times10^{8} < Ra_x < 1.22\times10^{9}$ for the heated wall, and $1.59\times10^{8} < Gr_x < 6.01\times10^{8}$ and $1.11\times10^{8} < Ra_x < 4.21\times10^{8}$ for the cooled wall.

In order to compare mean temperature profiles from different scenarios the presentation of θ against Nu_y should be made using the thermal

conductivity evaluated at the wall temperature and T_{MIN} as the outer temperature.

Using θ against Nu_V has shown that the cooled wall thermal boundary layer did not develop in the same manner as the heated wall thermal boundary layer. It was proposed that the substantial cross-flow induced by the transition process at the heated wall was responsible for this.

The θ against Nu_V presentation has also shown that the development of the heated wall thermal boundary layer differed between Series 3 and 6, the difference being promoted by the change in cavity width.

The heat transfer coefficient indicated which regions in the cavity were applicable to fully developed flow, as in these regions it was approximately constant. It also showed the effect of a change in cavity width for constant Ra_H. A decrease in cavity width increased the heat transfer coefficient.

The non-dimensional vertical temperature gradient varied within the cavities depending on whether the local region featured a flow with "laminar" aspects, or fully developed turbulence. It also varied with the aspect ratio, decreasing as H/L increased.

The vertical centre-line temperature was also affected by the level of insulation on the vertical side walls. The centre-line temperature increased as the side wall insulation increased, with all other parameters constant.

The local heat transfer calculations showed that the power on the Grashof number, in both the "laminar aspect" and fully developed turbulence regions, was greater than that previously found in flat plate flow.

The thickness of the thermal sub-layer in the present study has been found to be 1.6mm which compares very favourably with that found by previous researchers.

7.3 THE VELOCITY FIELD

A full set of velocity profiles are presented in dimensional form for Series 3 and 6 (one Series each for the Q.M.C. and Poitiers cavities).

The velocity corrections proposed in Chapter 6 have been applied to all the Q.M.C. data presented in this Chapter. However, Appendix A contains the original, uncorrected, data.

Local wall shear stresses have been calculated directly from the data, and subsequently used in the calculations of the distributions of $\overline{u'v'}$ across the velocity boundary layers. From these distributions of $\overline{u'v'}$ an estimate of the thickness of the viscous sub-layer became possible.

A discussion of the various velocity scales proposed by other researchers has been undertaken. This has been supplemented by an attempt by the present author to derive a suitable scale for the near wall region.

Mass flow data have been calculated which show the effects of the dominant transition process at the heated wall, and of heat loss through the vertical side walls.

An attempt has been made to estimate the velocity profiles of Series 3 for adiabatic vertical side walls. This attempt was based on predicting local Gr_x for such a condition, when given a predicted centre-line temperature distribution, and extrapolating profiles from Series 3 and 4 at values close to the predicted Gr_x.

Lateral mean velocities have also been calculated graphically. They are compared to those measured by another Q.M.C. researcher.

7.3.1 THE MEAN AND FLUCTUATING COMPONENTS OF VELOCITY

Consider the mean velocity profiles of Series 3, presented in Figure 7.26. The profiles were similar to those of Ziai [1] apart from the central cavity region, where he could not satisfactorily measure the fluid velocity using hot-wire anemometry.

The development of the flow, starting at the bottom of the heated wall, will now be discussed.

The thickness of the velocity boundary layer was at it's smallest at the bottom of the heated wall, only increasing in thickness by a relatively small amount when going from x/H = 0.046 to 0.143. In contrast the peak mean velocity increased significantly over this height from 0.205 to 0.340m/s.

The most noticeable aspect of the boundary layer, at the bottom of the heated wall, was at the outer edge of the boundary layer at x/H = 0.046. Here, there was a significant region of upward flow which was not present at the two heights immediately above. This upward flow could have arisen in two ways. Firstly, it could have occurred as a result of the flow turning the corner, or secondly, it could have been due to heat transfer to the fluid, from the floor, resulting in a local upward flow.

A significant change in the boundary layer occurred at x/H = 0.229 where the thickness increased substantially and the peak mean velocity reached a maximum of 0.364m/s. The development of the boundary layer up to this height was very similar to that observed in a laminar boundary layer which then starts to undergo transition.

The peak mean velocity dropped when going from x/H = 0.229 to 0.360, but rose again to 0.352m/s at x/H = 0.497, the thickness increasing at each height.

Contrary to the previous observations of Schmidt and Wang [14] and Giel and Schmidt [15], the maximum peak velocity was not observed at mid-height but at x/H = 0.229, where a transition process is predicted to have just started. Indeed, a similar state of affairs existed in Series 4 where the maximum peak velocity of 0.337m/s was at x/H = 0.229, with the peak velocity at x/H = 0.497 being 0.295m/s, and Series 5 with the maximum of 0.363m/s at x/H = 0.283 and the peak velocity at x/H = 0.634 being 0.305m/s.

The present author appreciates that a more detailed survey would be necessary to locate the position of the maximum peak velocity, but also notes that there is no guarantee that it would be close to mid-height rather than close to the height where transition has started.

With respect to the last point of the possibility of the maximum peak mean velocity being associated with the region where transition occurs, one notes that such a trend was present in the numerical calculations of Ozoe et al [33].

It was at x/H = 0.229 that the first velocity reversal was seen at the edge of the heated wall boundary layer. This was associated with a substantial increase in mass flow coupled with the onset of transition (the mass flow is discussed in more detail in Section 7.3.8).

The magnitude of the peak reversed velocity increased until x/H = 0.849 after which it decreased slightly.

The peak mean velocity decreased with height after x/H = 0.497. Associated with this was a gradual "flattening" of the peak velocity region, and an increase in the value of y at which the first position of zero velocity was noted. For x/H = 0.497 to 0.949 the first lateral position of zero velocity varied from y = 112.5 to 134.5mm.

The position of the peak mean velocity, at all heights above x/H = 0.360, was difficult to establish. Therefore the observation of Kutateladze et al [35], of the increase of lateral position of the peak mean velocity with height could not be confirmed.

Following the flow across the ceiling to the top of the cooled wall one notes that the mean velocity profile at x/H = 0.949 was quite different from that diagonally opposite at the bottom of the heated wall.

The boundary layer at the top of the cooled wall was much thicker than that already described at the bottom of the heated wall. The

difference can be attributed to a number of factors resulting from the failure of the turbulence within the flow across the ceiling to collapse to anywhere near the extent that it did within the flow across the floor.

The collapse of the turbulence within the flow along the floor of the cavity meant that an almost full transition process could occur within the heated wall boundary layer.

Associated with the transition process at the heated wall, will have been a cross-flow to the heated wall boundary layer within the bottom third of the cavity (to accomodate the increase in mass flow brought about by the transition process).

However, with less collapse of the turbulence within the flow across the ceiling, a much less prominant transition would be expected, which would not be associated with such a large increase in mass flow as that at the heated wall.

The reduced cross-flow in the upper third of the cavity, as compared to that in the lower third, meant that the mass flow at the top of the cooled wall was much greater than that at the bottom of the heated wall, thus resulting in a much thicker boundary layer.

One does note that the mean velocity profile at the top of the cooled wall was not as smooth as any at the heated wall, there being a well defined "kink" in the profile. It appears that fluid close to the wall was behaving in a similar manner to the fluid at the bottom of the heated wall. One could extrapolate the near wall mean velocity profile to show a much thinner boundary layer, although still thicker than that at the bottom of the heated wall.

The same phenomenon was evident at x/H = 0.898, only more pronounced. It seems that the near wall fluid was affected by the wall so that it behaved in a manner similar to the "laminar-like" flow at the bottom of the heated wall. The effect was still present at x/H = 0.849 and 0.765. Only at x/H = 0.630 did the mean velocity profile become smooth again, thus indicating that a transition process may have occurred in the near wall fluid, causing the boundary layer to become turbulent across it's entire width.

No velocity reversal was found at the outer edge of the cooled wall boundary layer at x/H = 0.949, 0.765 or 0.630, although such a reversal was present at all other heights. The reversal was at a maximum at x/H = 0.229.

Because of the difference between the extent of collapse of the turbulence in the floor and ceiling boundary layers, and the predicted result in difference between cross-flow, there was a substantial difference

in the overall development of the cooled wall boundary layer compared to that of the heated wall boundary layer.

The peak mean velocity in the cooled wall boundary layer increased with distance downstream until, at x/H = 0.849, it was 0.258m/s. The peak mean velocity then decreased at x/H = 0.765, but then increased again to a maximum of 0.276m/s at x/H = 0.497. Thus the maximum peak mean velocity, of the cooled wall boundary layer, was observed at mid-height. (The stations at which the maximum peak mean velocity occurred in Series 4 and 5 were x/H = 0.631 and 0.482 respectively).

The peak mean velocity decreased with distance downstream after x/H = 0.497. Associated with this were a decrease in mass flow and a decrease in the first lateral position of the zero mean velocity, from y = 121.5 to 66.5mm.

Consider now the mean velocity distribution of Series 6 shown in Figure 7.27.

Starting again at the bottom of the heated wall one immediately notes that the boundary layer was at its thinnest at x/H = 0.12.

The boundary layer thickness increased with distance downstream with a substantial increase occurring when going from x/H = 0.25 to 0.50. At the same time the peak mean velocity increased reaching a maximum of 0.351m/s at x/H = 0.50.

The description of the development of the heated wall boundary layer so far is very similar to that in Series 3, although a more meaningful direct comparison may be made between Series 5 and 6 as the cavity heights were identical, and the wall temperature differences almost the same.

When comparing the Series 5 and 6 mean velocity data at x/H = 0.12 in Series 6 and x/H = 0.118 in Series 5 one notes that the thickness of each boundary layer was almost the same, but the peak mean velocity was greatest in Series 6. This was not surprising as the relatively poor level of insulation of the Poitiers cavity was expected to result in higher peak velocities in the heated wall boundary layer of the Poitiers cavity, when both cavities were subject to the same wall temperatures.

Now, although the wall temperature difference in Series 5 and 6 was almost the same, the absolute wall temperatures were not. The wall temperatures in Series 6 were lower than in Series 5. With the same level of insulation for both cavities one might have expected a lower peak mean velocity in Series 6 because the local density would have been lower, and so to keep mass flow constant the mean velocity across a profile would have to have been lower. Therefore the occurrence of the greater peak mean

velocity in Series 6 underlines the difference in effectiveness between the insulation used in each cavity.

Returning to the development of the heated wall boundary layer in Series 6 one sees that the boundary layer had not fully developed by x/H = 0.50, as the profile changed significantly when going from x/H = 0.50 to 0.65. At the latter height the profile from the peak to the cavity centre was more like a straight line, as compared to the definite curve at x/H = 0.50.

One other very important feature was noted at x/H = 0.50. This was the meeting of the heated and cooled wall boundary layers in the centre of the cavity. This aspect was also noted at all heights above mid-height.

The peak mean velocity decreased with height after x/H = 0.50, as did the mass flow. These decreases in peak mean velocity and mass flow, which were also seen in Series 7, did not support the previous observation of Renault and Doan-Kim-Son [30] who claimed that each mean velocity profile was similar, and so exhibited "self-preservation".

So far no mention has been made of any region, at the outer edge of the heated wall boundary layer, where regions of reversed velocity were seen. This is because none were seen for the heated wall boundary layer. This was one of the major differences between the Q.M.C. and Poitiers cavity data.

It has already been mentioned previously, that the reduction in cavity width prevented a horizontal temperature inversion. It would also seem that the reduction in cavity width has prevented any occurence of a region of reversed velocity at the edge of the heated wall boundary layer.

The data from Series 5 showed an increase in the first position of zero velocity from y ≈ 86mm at x/H = 0.482, to y ≈ 100mm at x/H = 0.634 and 0.784, and y ≈ 130mm at x/H = 0.931.

The position of the first zero velocity showed that there was insufficient lateral distance to allow a region of reversed velocity to exist, providing that the heated wall boundary layer of Series 6 developed in a similar manner to that of Series 5. One must also remember that with a less effective level of insulation, the resulting increase of boundary layer thickness of Series 6 (as compared to Series 5) would have contributed to the non-existence of a region of reversed velocity.

One other point arising from the boundary layer thickness of Series 5 is it's increase between the heights of x/H = 0.482 and 0.634. This indicated that the boundary layer was not fully developed at x/H = 0.482.

The development of the cooled wall boundary layer will now be examined.

At the top of the cooled wall (x/H = 0.95) the mean velocity profile was very similar to those in the fully developed region of the heated wall, but further down the wall at x/H = 0.80 the profile showed a distinct difference in the near wall fluid. This was similar to that found in Series 3 where it was proposed that the influence of the wall promoted a reduction in the turbulence of the fluid close to it, but left the fluid further out unaffected.

With increasing distance downstream the peak mean velocity continued to increase until a maximum of 0.289m/s was reached at x/H = 0.50. Below x/H = 0.50 the peak mean velocity decreased as in Series 3.

The most interesting aspect of Series 6 and 7 was the presence of regions of reversed velocity at the edge of the cooled wall boundary layer at the two lowest heights of x/H = 0.25 and 0.12. These regions merged with the heated wall boundary layer so that a position of zero velocity did not occur between the heated wall and the cavity centre.

In Series 3 it was noted that regions of reversed velocity were found when the boundary layer was turbulent. The merging of the reversed velocity region with the heated wall boundary layer would therefore be expected to have an effect on the heated wall boundary layer.

Renault and Doan-Kim-Son [30] reported that the heated wall boundary layer at the bottom of the heated wall displayed a "laminar" aspect. If the boundary layer at the bottom of the heated wall in the Q.M.C. Series was laminar in nature then the reduction in cavity width, in the Poitiers cavity, has led to an increase in turbulence in the region at the bottom of the heated wall.

Consider Figure 7.28 which shows the profiles of $u'_{R.M.S.}$ from Series 3. Starting at the bottom of the heated wall one sees that the peak value of $u'_{R.M.S.}$ increased downstream to a maximum at x/H = 0.898.

Unlike the temperature R.M.S. data there was no reduction in the peak value of $u'_{R.M.S.}$ when moving from x/H = 0.046 to 0.096, however the Series 4 data did show that the peak values of $u'_{R.M.S.}$ at x/H = 0.096 and 0.145 were the same, indicating that the wall had an influence which resulted in the damping of fluctuations.

Most striking was the lack of a local maximum in peak $u'_{R.M.S.}$ to indicate a transition process, however, Series 4 and 5 did exhibit different characteristics.

In Series 4 the peak value of $u'_{R.M.S.}$ decreased going from x/H = 0.360 to 0.496, but then increased to a maximum at x/H = 0.849. In Series 5 the maximum in peak $u'_{R.M.S.}$ was at x/H = 0.283. By taking the data from Series 3, 4 and 5 one is able to propose that a maximum in peak $u'_{R.M.S.}$ does exist somewhere in the transitional region, but that it's location can only be determined by detailed study.

In the cooled wall boundary layer the peak value of $u'_{R.M.S.}$ increased downstream from x/H = 0.949 to 0.765 after which it decreased, although the difference between the peak values of $u'_{R.M.S.}$ for the heights x/H = 0.630 to 0.360 was minimal. Exactly the same trend was shown by the Series 4 data, and a similar trend was shown by the Series 5 data where the maximum peak value of $u'_{R.M.S.}$ occurred at x/H = 0.634.

Hence, there was no indication of transition in the near wall fluid (of the cooled wall boundary layer) from the trend of the peak values of $u'_{R.M.S.}$, but there was from the lateral distribution of $u'_{R.M.S.}$.

The near wall profiles of $u'_{R.M.S.}$ at x/H = 0.949 and 0.898 were not a smooth curve as would be expected, but were essentially a straight line, the value being constant. Only at x/H = 0.849 and beyond were the profiles again smooth, showing a well defined peak. Had the outer profile been extrapolated at either x/H = 0.949 or 0.898, then a higher value of $u'_{R.M.S.}$ would have been observed. This indicates that the flow was not fully turbulent across the entire width of the cooled wall boundary layer. Presumably, a limited transition process took place in the near wall fluid to result in a smooth distribution of $u'_{R.M.S.}$ across the boundary layer.

Unlike the downstream trend of increasing $u'_{R.M.S.}$ in the heated wall boundary layer, the decrease in $u'_{R.M.S.}$ beyond x/H = 0.360 was associated with substantially decreasing mass flow.

The two extreme heights are worthy of further mention with regards to the distribution of $u'_{R.M.S.}$.

At x/H = 0.046 one notes that $u'_{R.M.S.}$ decreased as the flow went towards the heated wall until y/L = 0.6, after which it remained constant (at approximately 0.009m/s) until y/L = 0.12. A small increase in $u'_{R.M.S.}$ then occurred which must have been linked to the upward flow seen in the mean velocity profile. The trend in the Series 4 data was the same except that the reduction continued to y/L = 0.5.

At x/H = 0.949 the value of $u'_{R.M.S.}$ dcreased until y/L = 0.5 (the minumum being 0.024m/s) after which it increased slightly until y/L = 0.88 when it became constant, except for a significant increase near to the wall.

The same trend was observed in Series 4 except that $u'_{R.M.S.}$ reached a minimum at y/L = 0.4.

The $u'_{R.M.S.}$ data at the two extreme heights gave a good indication of what happened to the turbulence in the floor and ceiling boundary layers.

It is apparent that the turbulence within the floor and ceiling boundary layers underwent collapse which was then arrested. The point to which the turbulence collapsed being greater in the floor boundary layer.

The difference in the point to which the turbulence collapsed in the floor and ceiling boundary layers was due mainly to the thermal boundary conditions on the floor and ceiling, but was also influenced by the mass flow in each of the boundary layers. This was important because one would expect the thermal boundary conditions to have only a finite region of influence on the turbulence, and so the thicker ceiling boundary layer would impose fluctuations on the flow nearer to the ceiling whose turbulence was being reduced.

Moving on, one may now consider Figure 7.29 which shows the distribution of $u'_{R.M.S.}$ for Series 6.

Starting with the heated wall boundary layer one sees that initially the peak value of $u'_{R.M.S.}$ increased when going from x/H = 0.12 to 0.25. After this height the value remained the same at x/H = 0.50 but increased slightly at x/H = 0.65. The peak value at x/H = 0.80 was the same as that at x/H = 0.65, but it dropped slightly at x/H = 0.95 to the value seen at x/H = 0.50. One therefore sees that the range of the peak value was only 0.075-0.085m/s.

The reason for the relatively small range of peak $u'_{R.M.S.}$ was due to the fact that only six heights could be examined because of the limitations of the Poitiers cavity. If heights below x/H = 0.12 could have been examined then it is certain that a smaller peak value of $u'_{R.M.S.}$ would have been recorded. This proposal is supported by the $u'_{R.M.S.}$ from the cooled wall boundary layer.

In the cooled wall boundary layer the lowest peak value of $u'_{R.M.S.}$ was noted at x/H = 0.95, it was 0.037m/s. This was the lowest peak value recorded in Series 6. Obviously one would expect a lower value, at a diagonally similar height of x/H = 0.05, at the heated wall.

Tracing the development of the peak in $u'_{R.M.S.}$ in the cooled wall boundary layer, one sees that it increased when going from x/H = 0.95 to x/H = 0.80, after which it remained approximately constant until it decreased when going from x/H = 0.25 to x/H = 0.12.

The distribution of $u'_{R.M.S.}$ within the cavity for Series 7 was very similar, there being no height at which a local maximum in the peak value of $u'_{R.M.S.}$ indicated the presence of a transition process at either wall.

In general, the profiles of $u'_{R.M.S.}$ in Series 7 exhibited larger values than the profiles from Series 6, although the profiles at x/H = 0.12 in both Series were almost identical, indicating that the conditions at this height were similar in both Series.

Most interesting is the comparison of the distribution of $u'_{R.M.S.}$ in Series 6 with that from Series 5. At $x/H \simeq 0.50$, and above, the profiles of $u'_{R.M.S.}$ in Series 5 exhibited larger values of $u'_{R.M.S.}$ than those from Series 6. This must mean that the reduction in cavity width had a damping effect on the turbulence in the boundary layers of Series 6 for $x/H \simeq 0.50$, and above. However, at the lowest two heights the reverse was true, thus indicating that the reduction in cavity width had increased the turbulence level in the boundary layers at the lowest heights. This evidence supports the proposal made in Chapter 2 that the non-existence of a steady laminar region in the cavity of Ralph et al [31] was due to the influence of surrounding turbulent regions.

7.3.2 COMMENTS ARISING OUT OF THE USE OF THE LASER DOPPLER ANEMOMETER

The circumstances in which the laser Doppler anemometer was used were not ideal, but nonetheless good results were obtained.

The signal-to-noise ratio observed on the oscilloscope was quite poor when compared to that seen when using the same anemometer on a flat plate rig. The reasons for this were: the reduction in laser power brought about by reflection from optical surfaces (the mirror, lens and perspex walls); the attenuation of the signal by particles within the cavity and the perspex walls; and the relatively long optical paths.

In order for the beam waist to coincide with the point of focus of the converging lens, the distance from the laser to the lens should be the same as the focal length of the lens. The focal length of the lens was 0.75m, but due to the restrictions of the cavity structure, the distance from the laser to the lens was only approximately 0.35m. This meant that the beam waist occurred approximately 7mm before the point of focus of the converging lens. The difference in radius between the two positions was only 0.00035mm.

The number of fringes within the probe volume was approximately 42 which was enough to yield reasonable signals.

Most of the calculations regarding uncertainty have been presented in Chapter 6. However, as one of the important features of the current research has been the use of a laser Doppler anemometer, it was felt that a separate discussion devoted to uncertainties brought about by the anemometer, should be included within the text describing the velocity results.

Uncertainties were possible in both the mean velocity and the R.M.S. of the velocity fluctuations.

It was possible for the mean velocity to be affected by the mean velocity gradient within the probe volume.

Giel and Schmidt [15] presented two equations which described the corrected mean velocity and the uncertainty in the R.M.S. of the fluctuating component of velocity. These equations were simplified versions of other researchers' work. The assumptions they made to arrive at the equations were that the following quantities should be uniform within the probe volume: the number of particles per unit vol. ; the fluid density; and the v and w components of velocity. All these assumptions were reasonable in the present circumstances.

By assuming a maximum mean velocity gradient of $170s^{-1}$, the present author calculated that the difference between the arithmetic mean (already calculated for the present study) and the corrected mean velocity (indicated by the equation of Giel and Schmidt [15]) was negligible.

As a further check a program was written to simulate the sampling of velocity readings from a probe volume across which there existed a mean velocity gradient. In this case the particle density was also assumed constant.

The program examined the probe volume to see if any particles were in it, and if so the arithmetic mean of the velocity of those particles present was taken to be the sample value. The results of this program confirmed the previous calculations, indicating that the mean velocity gradients encountered within the cavity were not sufficient to affect the arithmetic mean.

There are a number of sources associated with a frequency tracker which can give rise to an increase in the value of the R.M.S. of the velocity fluctuations. However, in the present study these were all insignificant when compared to the uncertainties which could be introduced by the presence of a mean velocity gradient.

Using the appropriate equation from Giel and Schmidt [15] the uncertainty in the value of $\bar{u}'_{R.M.S.}$ has been calculated at several heights and lateral positions. The results of these calculations showed that the

uncertainties due to the mean velocity gradient were negligible for y > 6mm.

The uncertainties for y < 6mm were at a maximum close to the wall and were typically 0.005m/s at y = 1mm; 0.003m/s at y = 3mm; and 0.001m/s at y = 6mm. In percentage terms, the uncertainties were only significant for y < 3mm

In order for a frequency tracker to function efficiently the percentage dropout should be as low as possible. During Series 3, 4 and 5 the dropout was typically less than 8%, although it was a little higher very close to the walls.

Data from Series 5 were used to construct a graph of % dropout against time. The data, presented in Figure 7.30, show how the dropout increased gradually over the time period required for four readings. The apparent steps in % dropout were due to adjustment of the tracker between readings.

The Series 5 data in Figure 7.30 represent a "worst case" whereby the % dropout increased from 6 to 12% over four readings.

7.3.3 THE WALL SHEAR STRESS

One of the velocity scales which has been proposed for the near wall region is that of the shear velocity. Therefore before presenting any data regarding velocity scales it is first necessary to present the calculations for the wall shear stresses.

Calculation of the wall shear stresses was made difficult because the absolute position of the probe volume from each cavity wall was unknown and, furthermore, the probe volume and the thermocouple junction could not be considered to be at the same lateral position, because angular movement of the probe block occurred when the L.V.D.T.'s impinged on the walls.

The present author faced two choices when estimating the zero position. Firstly one could use a curve fitting routine, as Ierokipiotis [43] had done, or, by assuming that the turbulence quantity $\overline{u'v'}$ was negligible very close to the wall, a trial and error routine could be used to find the best combination of velocity gradient at the wall, and zero position, using the sub-layer equation.

The sub-layer equation is derived by integrating equation (1.2) after assuming that the terms on the L.H.S. are negligible and considering μ/ρ to be constant and evaluated at a suitable reference temperature in keeping with the Boussinesq approximation. The sub-layer equation is given below,

$$u = \frac{\tau_w y}{\mu_w} - \frac{g\beta_T(T_w-T_\infty)y^2}{2(\mu/\rho)_R} + \frac{g\beta_T\dot{Q}''_w y^3}{6(\mu/\rho)_R k_w} \qquad (7.33)$$

The second option was selected after intial trials were carried out, to see how well the predicted velocities agreed with the experimental values. These trials showed that the agreement between the predicted and experimental velocities was excellent, provided that two practices were adhered to.

Firstly, the local temperature was used to calculate the kinematic viscosity instead of assuming a constant reference temperature to be applicable to the entire sub-layer. Secondly, the full equation resulting from the integration of equation (1.2) was used. This introduced the integrals of the terms on the L.H.S. of equation (1.2) which had been calculated from graphical interpretation primarily for the estimation of the turbulence quantity $\overline{u'v'}$.

Examples of the agreement between predicted and experimental velocities are given in Table 7.12. Note that the technique was only valid out to $y \approx 4$mm, beyond which $\overline{u'v'}$ was not negligible.

The trial and error technique looked for the smallest sum of the differences between the predicted and experimental velocities, both in terms of the sum of the moduli of the differences, and the sum of the absolute differences.

Where different combinations of the wall shear stress and zero position were given for the minimum of each sum, the predicted and experimental data were inspected visually and an appropriate judgement made.

Of course, all experimental data were corrected for the presence of the thermocouple junction before estimation of the shear stress and the zero position.

Figure 7.31 shows the near wall velocity profile from Series 3 at x/H = 0.765, together with the predicted data which have been supplemented at various positions to show the full near wall curve.

The values of the wall shear stresses and the squares of the shear velocities are given in Tables 7.13-7.17. Also included are the corrections to the thermocouple positions (for Series 3, 4 and 5) which locate the lateral position of the probe volume, and the corrections to the relative positions of the probe volume for Series 6 and 7. The corrections at the heated and cooled walls were consistent for Series 3 and 4 which gives some confidence in the technique used to determine them.

7.3.3.1 THE WALL SHEAR STRESS AT THE HEATED WALL

The variations of wall shear stress with absolute and non-dimensional height, are shown in Figures 7.32 and 7.33 which compare Series 3, 4 and 5, and Series 5, 6 and 7, respectively. There was an almost linear variation of wall shear stress with height in the turbulent regions.

One sees that the flow at the bottom of the heated wall, which exhibited "laminar aspects", showed an increase of wall shear stress with height. This was as expected.

A drop in wall shear stress occurred when the flow underwent a transition process. As the wall temperature difference of Series 3 was greater than that of Series 4, one would have expected the former to undergo a transition process at a lower absolute height. This expectation does have support from the shear stress data which appears to peak at a greater height in Series 4.

Surprisingly, the wall shear stresses of Series 3 and 5 (identical wall temperature differences) are very similar at heights up to 0.9m, i.e. before full transition. One would not have expected this as the reduction in cavity height should have reduced the mass flow at any dimensional height, so reducing the wall shear stress. However, the differences in the wall shear stresses, between Series 3 and 5, are as expected in the turbulent region.

The wall shear stress data in Series 5 and 6 were different, even though the wall temperature differences were very similar. This was due to heat transfer through the vertical side walls which reduced the centre-line temperature in Series 6 below that of Series 5, and so increased the mass flow and wall shear stress along the heated wall in Series 6.

The most interesting difference between Series 5 and 6 was the magnitude of the wall shear stresses at the base of the heated wall. The incresed level of disturbance in the heated wall boundary layer of Series 6 was shown up by a lower value of the wall shear stress.

The general trend of the wall shear stress, with height, was the same for Series 6 and 7. A transition process was expected at a lower height for Series 7, but insufficient data prevented any confirmation of this.

7.3.3.2 THE WALL SHEAR STRESS AT THE COOLED WALL

Figures 7.32 and 7.33 show the cooled wall shear stress data for Series 3, 4 and 5 and Series 5, 6 and 7, respectively. The cooled wall shear stress data for Series 3, 4 and 5 exhibited the same trends as those for the heated wall.

There was an initial increase in wall shear stress at the top of the cooled wall which was associated with a "laminar aspect" to the flow near to the wall. (It must be emphasised that it is only the near wall flow which exhibited this "laminar aspect").

The fluid beyond 20mm from the wall was turbulent. This was shown by a marked deviation from a smooth mean velocity profile at x/H = 0.949, 0.898 and 0.849.

The near wall fluid underwent a transition process in the region of x/H = 0.765, after which the wall shear stress decreased with distance down the wall. No difference in height could be seen, between Series 3 and 4, regarding the onset of this transition process.

Even in the cases of the poorly insulated cavities of Series 6 and 7 a transition process in the near wall fluid was indicated by the wall shear stresses at the cooled wall. Series 6 and 7 data again exhibited the same general trends as those of Series 3, 4 and 5.

7.3.3.3 REPEATABILITY, VELOCITY CORRECTION AND UNCERTAINTY ESTIMATION WITH REGARD TO THE WALL SHEAR STRESS

In Table 7.13 there is one example of the repeatabilty of wall shear stress data and one of the accuracy of the velocity correction. At x/H = 0.898 the uncertainty of the wall shear stresses was a maximum of ±1.2%, and at x/H = 0.497 the maximum uncertainty due to velocity correction was ±0.6%.

Several calculations of the cooled wall shear stresses at different heights were made using velocity correction multipliers of 1.06 and 1.02. The maximum uncertainty introduced by the use of the larger, incorrect, multiplier was 2%.

Taking into account the excellent agreement of predicted and experimental velocity profiles (which indicates very small uncertainty in the velocity data and validation of the technique to determine the lateral zero position and wall velocity gradient) one may consider the wall shear stress data to exhibit a maximum uncertainty of ±2.8% (this is a very high degree of accuracy and is dependent on the author's assessment of the validity of the technique for establishing the lateral zero position and the wall velocity gradient).

7.3.4 VELOCITY SCALES

The three velocity scales which have been proposed for the near wall region (normally taken to be from the wall to the peak in mean velocity) are:

(i) $(\tau_w/\rho_w)^{1/2}$ (ii) $(g\beta_T\Delta T(\mu/\rho))^{1/3}$ (iii) $\dot{Q}''/(\rho Cp\Delta T)$

The mean velocity data from Series 3, 4, 5, 6 and 7 have all been plotted in non-dimensional form using each of these scales, in conjunction with Nu_v as the non-dimensional length.

First consider Figures 7.34-7.38 which show the mean velocity non-dimensionalised with respect to group (i), the shear velocity u_τ.

The agreement between the profiles of each Series was generally very good with the variation being within ±4.7% at the peak (typically much better than this). When considering all Series the agreement was quite good with the variation being within ±6%. This compares very favourably with the estimated uncertainty range of ±2.6% (zero velocity) to ±4.3% (0.35m/s peak velocity) determined in Chapter 6.

The limits which have been quoted do not account for all the profiles which have been presented. Those profiles which are not considered to be in a region of fully developed flow have been ignored. Typically these were the profiles at x/H = 0.95, and in the case of Series 5, x/H = 0.482.

It was previously suggested that the flow at x/H = 0.482 in Series 5 was not fully developed and the profiles in Figure 7.36 certainly support this.

Figures 7.34-7.38 definitely suggest that shear velocity is a suitable velocity scale, and that Nu_v is a suitable non-dimensional length to be used in conjunction with it.

Moving on to the buoyancy velocity scale, group (ii) one sees from Figures 7.39-7.43 that there was reasonable agreement between the profiles within each Series, although there was a slightly larger variation at ±6.3% or better. The same variation of ±6.3% also applied to all Series, this was virtually the same as for the shear velocity scale.

Whilst the buoyancy velocity scale has provided as good an overall collapse of the data as has the shear velocity, it must be remembered that only a small range of stratification has occurred within the cavities. The problem associated with the variation of stratification has been discussed in Chapter 2 and can be summarised by saying that different velocity profiles would be expected when the stratification varies but ΔT remains the same. Therefore one would not expect the buoyancy velocity scale to be applicable to data over a large range of stratification.

Before finishing the discussion of the buoyancy velocity scale, it is worth especially noting the data from Series 5 in Figure 7.41. Here the profile at x/H = 0.482 matched those at x/H = 0.634 and 0.764, this was unexpected and again indicates that this velocity scale is not valid by itself.

The poorest collapse of data was provided by the thermal velocity scale, group (iii). This can be seen from Figures 7.44-7.48.

The variation within the data of each Series was ±7.7% or better, and the variation overall was ±13%. Clearly the thermal velocity scale cannot be applicable by itself.

The argument for the inapplicablity of the thermal velocity scale is the same as that for the buoyancy velocity scale.

Note also that the profile at x/H = 0.482 from Series 5 agrees with the other profiles below x/H = 0.931, which as for the buoyancy velocity scale was not expected.

The fourth, and final, velocity scale proposed by Cheesewright [57] for the near wall region was for the outer part of this region. Here he argued that du/dy was not independent of α, but could be independent of (μ/ρ). The velocity scale he proposed was $\propto (g\beta_T \Delta T)(\rho C_p \Delta T)^2/\dot{Q}''_w{}^2$. This has been plotted against the natural log of Nu_Y as this representation of the non-dimensional length comes directly from equation (2.29).

Figures 7.49 and 7.50 show the fourth non-dimensionalised velocity against $\ln(Nu_Y)$ for Series 3 and 4. The profiles appear to follow two distinct curves, which between them show a variation of ±10% at the peak which is clearly unacceptable in the light of the reasonable agreement shown by alternative velocity scales.

Bayley [36] proposed the following mean velocity profile.

$$u = u_1 (y/\delta)^{1/7}(1-y/\delta)^4 \qquad (7.34)$$

The quotient u_{MAX}/u_1 was said to be 0.537, i.e. u_1 varied depending on the individual profile.

Substitution of the present data into equation (7.34) showed that it was not applicable to the mean velocity profiles from any Series.

Three velocity scales have been proposed for the entire boundary layer by Cheesewright [57]. These were:

(i) $(\tau_w/\rho_w)^{1/2}$ (ii) $[g\beta_T \Delta T \delta]^{1/2}$ (iii) $[k g\beta_T \Delta T^2/\dot{Q}''_w]^{1/2}$

In association with these scales the length scale was proposed as the boundary layer length which has been taken to be the lateral distance to the first position of zero velocity.

Figures 7.51-7.54 show the entire boundary layer scaled using δ and group (i), the shear velocity. The data from all Series (including Series 5 which is not shown) showed good agreement between profiles in all the fully developed regions, thus indicating that the shear velocity and the boundary layer length are potentially valid velocity and length scales for the entire boundary layer (the word potentially has been used because data from fluids of different Pr are required to verify the universal applicability of the scales).

In all Series a change in the curvature of the graph was seen between y/δ = 0.5 to 0.6. In the case of Series 3, 4 and 5 this occurred approximately 20mm beyond the position at which the local temperature first matched that at the cavity centre-line. As a horizontal temperature inversion did not arise in the Series 6 and 7 data one is not left with an obvious explanation for this change in curvature. However, it is likely that the change may have been associated with a change from a predominantly buoyancy induced flow to a flow predominantly induced by shearing action.

Figures 7.57-7.58 also show that group (ii) was a good choice for the scaling of the present mean velocity data in the outer region. However, one notes that at the peak the agreement between profiles was generally poor. The same observations also applied to the mean velocity data when they were scaled with group (iii), as can be seen in Figures 7.59-7.62.

From the preceeding work on velocity scales, for both the inner and outer regions of the boundary layer, one can select a suitable velocity and length scale with which to compare the cooled wall velocity profiles to those from the heated wall.

For both the inner and outer regions the best velocity scale was the shear velocity. This may be used in conjunction with Nu_y as the dimensionless length in the inner (near wall) region, and with δ as the length scale for the outer region of the boundary layer.

As a difference between heated and cooled wall mean temperature profiles has been previously noted in Section 7.1, it is wise to compare only selected mean velocity profiles from the cooled wall to those of the heated wall. Those cooled wall velocity profiles which were expected to most closely match those of the heated wall were at x/H = 0.360 and 0.497 from Series 3 and 4, and at x/H = 0.50 from Series 6 and 7.

Figure 7.63 shows the near wall scaled velocity profiles at the cooled wall from Series 3, 4, 6 and 7. The closest match with the heated wall profiles was provided by those profiles of Series 6 and 7 at x/H = 0.50.

They matched the lower curves found at x/H = 0.898 and 0.949 shown in Figures 7.34 and 7.35.

The scatter over the cooled wall profiles of Series 3 and 4 in Figure 7.63 was reasonable at ±5.4%, but the profiles were quite removed from those of the heated wall in Figures 7.34 and 7.35. The average peak value of the cooled wall profiles were at -13% from the average peak value of the heated wall profiles.

Such a difference between the heated and cooled wall scaled velocities could not be considered to be a result of the different corrections applied to the velocities (1.11 and 1.06 to the heated wall profiles and 1.07 and 1.02 to the cooled wall profiles in the vicinities of the peak and the wall respectively). One is therefore forced to conclude that the difference must have been due to different characteristics in the heated and cooled wall flows bought about by the thermal boundary conditions on the floor and ceiling.

Most interesting was the reasonable agreement between the heated and cooled wall profiles of Series 6 and 7. One might initially think that because there was no thermocouple present, then the Series 3 and 4 corrections were wrong, but this has been disproved as not being feasible. Therefore, some other characteristic of the Poitiers cavity must be responsible for the similarity between the fully developed heated and cooled wall profiles at mid-height. The most obvious factor was the smaller cavity width which eliminated the core and allowed substantial turbulent mixing of the fluid. This might have promoted a similar flow development down each wall.

A simlilar state of affairs applied to the whole boundary layer profiles shown in Figure 7.64. The cooled wall profiles of Series 6 and 7 were similar to those of the heated wall at the two uppermost heights in Series 3 and 4, with the cooled wall profiles of Series 3 and 4 being lower than any observed at the heated wall.

7.3.5 PROBABILITY DISTRIBUTIONS OF VELOCITY

This Section is concerned with a brief description of the probability distributions of velocity and how these change with lateral position within the boundary layer. A brief mention is also made of minimum and maximum velocity envelopes.

The heights chosen to show the probability distributions of velocity at selected lateral positions were x/H = 0.229 and 0.497, both of which were from Series 3.

The group width selected was 0.025m/s and the velocity range covered was -0.2 to 0.7m/s. This meant that there were 36 groups, with groups 8 and 9 being immediately either side of zero. If values of velocity were to be plotted on the x axis the presentation would be confusing, therefore the group numbers have been used. The position of each group number on the plots represents the centre of each group. (The groups and their associated velocity ranges are given in Table 7.18).

Firstly consider the three distributions from x/H = 0.229 at positions of y = 4.977, 9.961 and 70mm shown in Figure 7.65. The first plot at y = 4.977mm shows a distribution (of the Gaussian type) skewed towards the higher velocities. This lateral position coincided with the position of peak velocity.

The second plot at y = 9.961mm showed an approximately even distribution (of the normal type) with just a little skew towards the lower velocities. This lateral position coincided with the peak in $u'_{R.M.S.}$.

The third plot at y = 70mm was mostly resticted to two groups which was as expected because this position was approximately 20mm beyond the edge of the boundary layer.

The relatively larger thickness of the boundary layer at x/H = 0.497 has allowed a more detailed study of the frequency distributions across the boundary layer.

Consider Figure 7.66 which shows the frequency distributions at y = 0.7, 2.611, 6.625 and 17.157mm. The range of velocities at y = 0.7mm was restricted to a narrow band with an approximately normal distribution The distributions at the other three lateral positions (which included the position of peak mean velocity at y = 6.625mm and peak $u'_{R.M.S.}$ at y 17.157mm) were almost perfect normal distributions of velocity.

Further out in the boundary layer the distributions changed. Figure 7.67 shows the frequency distributions at y = 49.7, 99.7, 149.7 and 249.7mm. The distributions at y = 49.7 and 99.7mm were skewed towards the lower velocities which is to be expected close to the edge of a boundary layer. The two distributions at y = 149.7 and 249.7mm in the region of reversed velocity were restricted to a very narrow range of velocities as one would expect.

The frequency distributions from both heights have shown that towards the edge of the boundary layer there is a skew towards the lower velocities. The distributions at the peak in mean velocity were different in that a normal distribution was seen at x/H = 0.497 and a skewed distribution (towards the higher velocities) was seen at x/H = 0.229. The

lack of a position close to the heated wall (at x/H = 0.497) with a noticeable skew towards the higher velocities was interesting and unexpected, as was the considerable range over which the frequency distributions were of a normal type.

This Section is completed by an examination of the minimum and maximum velocity envelopes at x/H = 0.497 from Series 3. The profiles are shown in Figure 7.68 and show the velocity range at each lateral position much more clearly than the frequency distributions.

Whilst the general shape of the three profiles (minimum, mean and maximum) are the same, one does note that there was more scatter in the maximum velocity profile in the region where the velocity profile has been noted to change it's curvature.

The range of the velocities in the outer part of the boundary layer was approximately constant. This range was dependent on the resolution of the laser Doppler anemometer which accounted for approximately half of the range shown.

.

7.3.6 THE RATIO u'_{RMS}/v'_{RMS}.

With the v'_{RMS}. data supplied by Mr. A. Bowles it was possible to calculate the ratio u'_{RMS}/v'_{RMS}. and so examine where the flow was isotropic and where it was anisotropic.

Figure 7.69 shows the data at all heights for which the v'_{RMS}. data existed for Series 3. One notes that for the region y = 100-400mm the ratio was approximately one and so the flow can be considered to have been isotropic in this region. However, for most of the width of the boundary layers the flow was quite clearly anisotropic, with the ratio decreasing with distance away from each wall.

One may explain the trend towards isotropy with distance from each wall as follows. The vertical stratification generally increased with distance away from the wall thus helping to reduce the value of u'_{RMS}. which will have also been reduced by a decrease in buoyancy force.

This explanation shows why the flow became less anisotropic with distance from each wall, but does not explain why the flow was anisotropic near the walls. The anisotropy must arise because of the buoyancy force promoting the fluctuations in the vertical direction.

The variation of the anisotropic nature of the flow was not as predicted by Bolgiano [51] who had proposed that stratification would increase anisotropy.

7.3.7 MASS FLOW CALCULATIONS

The mass flow has been calculated for Series 1, 3 and 4 where the velocity and temperature were measured simultaneously. As temperature was not measured simultaneously with velocity in Series 6, it was only possible to estimate the mass flow, and so calculations were not carried out. The data for Series 1, 3 and 4 are tabulated in Tables 7.19, 7.20 and 7.21.

The method used to calculate the mass flow was to plot the profiles of ρu and then to planimeter the areas under the curves which were drawn by hand. For each area six readings were taken and the average calculated. As a check, a plot whose axes lengths were increased by a magnitude of ten, was used to calculate the areas under the curves. This revealed an uncertainty in planimeter results of only 0.5-0.7%.

It has been proposed that as the flow traversed the ceiling, some of the fluid flowed down the vertical side walls, thus creating a mass imbalance at mid-height. One may attempt to link the mass imbalance at mid-height to that at $x/H \simeq 0.95$. In Series 1 the mass imbalance at $x/H = 0.50$ was 3.0kg/m.s (16.4% with reference to the heated wall mass flow) and at $x/H = 0.95$ it was 2.2kg/m.s. In Series 3 the mass imbalance at $x/H = 0.497$ was 1.91kg/m.s (12.8%) and at $x/H = 0.949$ it was 1.92kg/m.s. In Series 4 the mass imbalance at $x/H = 0.496$ was 1.872kg/m.s (14.7%) and at $x/H = 0.947$ it was 1.677kg/m.s.

One notes that the mass imbalance at the two heights concerned in each Series were of the same magnitude, although the difference between the two values did vary. For Series 1 the difference was 27%, for Series 3 it was negligible, and for Series 4 it was 10%.

The relatively high difference between the mass imbalance at $x/H = 0.50$ and 0.95 in Series 1 can be explained by the existence of a leakage flow which was substantially reduced for Series 3 and 4 as described in Chapter 3.

The larger difference between mass imbalance at $x/H \simeq 0.50$ and 0.95 for Series 4, as compared to that of Series 3 could not have arisen due to uncertainties arising in the calculation of mass flow, but it may have arisen from uncertainties in the velocity data (see Chapter 6).

The mass flow imbalance at mid-height has also shown the effects of heat transfer through the vertical side walls and via the remainder of the cavity structure. The large difference in mass imbalance at mid-height between Series 1 and 3 was due to both a leakage current and the difference in heat transfer through the vertical side walls. Whereas the large

difference between the mass imbalance at mid-height in Series 3 and 4 showed the effect of heat transfer via the cavity structure.

The general variation of mass flow was as expected in the lower half of the cavity, with a substantial increase in the mass flow at the heated wall associated with the transition process taking place there, and a consequent decrease in the mass flow at the cooled wall.

The mass flow at the heated wall continued to increase from x/H ≈ 0.497 to 0.630 in each of the three Series thus indicating that the maximum peak mean velocity was located somewhere between these two heights, or just above x/H ≈ 0.630.

Beyond x/H ≈ 0.630 the mass flow decreased at the heated wall as was expected, but then increased when going from x/H ≈ 0.849 to 0.949. A complementary trend in the mass flow at the cooled wall was also noted, such that it appears that in the upper region of the cavity there was a cross-flow from the cooled wall to the heated wall. This is confirmed by the calculations for the lateral mean velocity discussed in Section 7.3.10.

7.3.8 COMPARISON OF PROFILES AT SIMILAR Ra_x

Schmidt and Wang [14] have suggested that profiles of mean velocity in a water cavity are similar at similar values of Ra_x. If this is so, then by using the data of Series 3 and 4 one should be able to predict the mean velocity profiles for the nominal Series 3 cavity conditions when there is equal heat transfer at each wall (zero heat transfer through the vertical side walls) but still heat transfer through the floor and ceiling.

The centre-line temperature for such conditions has already been calculated as equation (7.31). From this equation and that of the local heat transfer the local values of Ra_x were calculated. By using the values of Ra_x for each of the velocity profiles of Series 3 and 4 new profiles can be extrapolated.

Such an extrapolation was performed for all the heights in Series 3. Perhaps the most interesting result was the prediction of the mass flow at mid-height where the imbalance was seen to reduce to 3%, with more mass flow down than up.

An attempt at the same procedure on Series 6 data resulted in a new mass imbalance of 12.5% which was a considerable improvement on the original estimated value. The value of 12.% is very large but it does not automatically invalidate the technique, proposed to eliminate the effects of heat transfer through the vertical side walls, because of the difficulties in calculating mass flow in Series 6.

The estimation of mass flow in Series 6 was made difficult by the fact that the temperature and velocity fields were not measured simultaneously. Instead they were measured on different days, with slightly differing wall temperatures and at slightly different heights. Significant uncertainties must have been introduced into the data by the need to estimate the temperature profiles for both Series 6 and 7 at the correct heights, using the wall thermocouple readings as a guide to the wall temperature. The present author also had to assume that the temperature profiles for the heated and cooled wall sides were the same.

Calculations have indicated that for the prediction of the mass flow at mid-height in Series 6, the level of uncertainty introduced into the calculation of the local Rayleigh number was ±7%, and for the local density it was ±1%. If then, an uncertainty of ±8% is assumed then the existing 12.5% mass flow imbalance could be reduced to 4.5% which compares favourably with the 3% predicted for the Series 3 data.

This Section is completed with a look at the proposal made in Section 2.7 that horizontal temperature inversions may be associated with dm/dx. In the regions of fully developed turbulence of Series 3 the present data have indicated that this might be so. At x/H = 0.630 and 0.765 dm/dx and the horizontal inversion were both constant, whereas as the horizontal temperature inversion was zero at x/H = 0.849 where dm/dx was also close to zero. However, much more research would be needed to investigate the link.

7.3.9 THE LATERAL MEAN VELOCITY

The lateral velocity, v, was calculated primarily for use in the estimation of the Reynolds stress, $\rho\overline{u'v'}$, for Series 3. It was calculated, using graphical interpretation, from an integrated form of the differential equation describing the conservation of mass, namely equation (1.1) repeated below.

$$\frac{du}{dx} + \frac{dv}{dy} = 0 \qquad (7.35)$$

By integrating once and rearranging, equation (7.35) becomes:

$$v = -1 \frac{d}{dx} \int_0^y u \, dy \qquad (7.36)$$

In having applied the Boussinesq approximation, whereby density is considered a constant, equation (7.36) is seen to be quite valid. However, it

is best if one considers the variable density form of equation (7.36) which is:

$$\frac{d(\rho u)}{dx} + \frac{d(\rho v)}{dy} = 0 \qquad (7.37)$$

This may be integrated to give:

$$v = \frac{-1}{\rho} \frac{d}{dx} \int_0^y \rho u \, dy \qquad (7.38)$$

This, more usual, representation is more accurate and so has been used to calculate v. The uncertainties in the values of v maybe quite significant in statistical terms, as the graphical interpretation was very much dependent on the authors ability to accurately take gradient data from the relevant graphs. It was very difficult to assess the uncertainties so an overall one of ±10% has been assumed. When one considers that a typical value of v was 0.010m/s the absolute uncertainty is seen to be quite small.

One must bear in mind that, when considering only v, it is the trends in the velocity distribution which are of more importance than the absolute values, although the absolute values obviously become important when calculating $\rho\overline{u'v'}$.

The values of v are presented in Tables 7.63-7.73, where a positive value of v is towards the cooled wall. The distribution of v gives important information on cross-flow within the cavity which has been previously speculated as being linked to a secondary peak in $T_{r.m.s.}$.

The data from the lower half of the cavity showed that the lateral velocity was towards the heated wall at all heights, with the largest velocities occurring at x/H = 0.360. As there was a lateral velocity towards the heated wall at x/H = 0.497 one may assume that the heated wall boundary layer was still growing at this height and so the peak values of u and mass flow, at the heated wall, can be said to have occurred somewhere between x/H = 0.497 and 0.630. Previous researchers have claimed that the peak value of u has occurred at mid-height.

For x/H = 0.497-0.765 the lateral velocity was towards the cooled wall for the entire cavity width, but this changed for the remaining three heights. Going from y = 0 to 500mm, the lateral velocity was initially towards the cooled wall but changed direction towards the heated wall at y ≈ 150mm and then back again towards the cooled wall at y ≈ 450mm. This was quite unexpected. It indicated that there was a vortex in the central region of the cavity, between x/H = 0.630 and 0.949, which rotated towards the heated wall in it's lower region, and towards the cooled wall in it's

upper region. The flow is now seen to have departed even further from the ideal anti-symmetric flow expected in a cavity with adiabatic closing boundaries.

Confirmation of the trends exhibited by the calculated data have come from measurements of v undertaken by Mr. A. Bowles (research student) from the Q.M.C. cavity with conditions similar to those of Series 3. As his data will form part of his thesis only four of the most relevant profiles are presented here in Figure 7.70.

For the majority of the cavity width the sign and magnitude of the calculated and measured velocities were in agreement. When measuring the velocities in the region of agreement, the laser beams were input to the cavity so that the direction of measurement was perpendicular to the active cavity walls. In the regions close to the walls, where differences between the two sets of data were considerable, the laser beams had to be input at an angle of approximately 15°. It may be that this introduced additional uncertainties into the measured data, even after they were corrected.

There is a remarkably small amount of data available concerning the lateral velocity, none of which can support either the calculated or measured velocities in the regions close to each wall. Those data which are available mostly concern L.D.A. measurements at the vertical centre-line of the cavity (which have not shown the vortex present in the upper half of the Q.M.C. cavity) or come from hot-wire measurements. Ierokipiotis [42] did attempt measurements of v for the case of a vertical flat plate but they were considered to be unrelaible in the region of interest.

The data presented in Figure 7.70 for x/H = 0.229 and 0.765 are at the two heights were the transition process on each wall may be considered to have just started. In both profiles one notes an increase in v at y ≈ 60mm from the relevant wall where the transition process was taking place (i.e very close to the edge of the boundary layers). The peaks show the entrainment of fluid caused by the transition processes.

Measurements of v were taken in the central region of the Poitiers cavity during Series 7. The results are presented in Tables 7.22-7.24. The magnitude of the velocities were similar to those calculated for Series 3. For the heights x/H = 0.65 and 0.80 the velocities were always towards the cooled wall. The v velocities at x/H = 0.50 were close to zero, as in the Q.M.C. cavity.

This Section is ended by referring back to Section 7.2.1 which proposed that there may have been a link between cross-flow and a secondary peak in the $T'_{R.M.S.}$ profiles at the cooled wall. As cross-flow of

a similar magnitude has been seen to exist at all heights above mid-height this link would not seem to exist. Thus, the reason for the existence of a secondary peak in T'_{RMS} remains unknown.

7.3.10 COMPARISON WITH HOT WIRE DATA ON A QUALITATIVE BASIS

One may take the Series 1, 3, 4 and 5 data and non-dimensionalise the mean velocity profile at mid-height with respect to the peak velocity and plot them with the data produced by Ziai [1] when he used hot-wire anemometry. This will show whether or not he was able to produce data which are correct from a qualitative point of view.

The data have been non-dimensionalised and are presented in Figure 7.71. This Figure shows that the data of Ziai [1] were qualitative and that, if necessary, one may use appropriately calibrated hot-wires within a cavity to gain an indication of the velocity profile.

7.3.11 HEATED CEILING

In order to attempt to control the thermal boundary conditions on the cavity ceiling, it was covered with heater elements normally used to heat the rear windows of cars. The idea was to prevent heat transfer through the ceiling and so yield a local Richardson number high enough to promote re-laminarization along the ceiling.

The increases in ceiling temperature (monitored by two centrally positioned thermocouples) which were achieved were 0.95 and 2.28K. The resulting cooled wall profiles of mean velocity and u'_{RMS} are presented in Figures 7.72 and 7.73 respectively.

In Figure 7.72 it can be seen that there was very little change in the mean velocity profile. What change there was, was not consistent with each increase in ceiling temperature.

The resulting u'_{RMS} data shown in Figure 7.73 did indicate some change in the level of u'_{RMS}, but only in the region y = 250-400mm. In this region the level of u'_{RMS} did decrease as ΔT increased, thus indicating that the increase in ceiling temperature did have some effect.

Clearly a higher increase in temperature would be needed to yield the appropriate value of the local Richardson number which would result in a similar collapse of the flow along the ceiling as occurred for that across the floor. However, this would have required heater elements of a much higher Wattage to be installed. Unfortunately time and money did not allow this line of investigation to continue further.

7.3.12 FLOW VISUALISATION

An attempt was made to visualise the flow at the centre-line of the cavity. This was to be achieved by generating a sheet of laser light and injecting incense smoke into the cavity.

The sheet of laser light was generated by a rotating mirror onto which the laser beam from a 35mW laser was impinging. The beam reached the rotating mirror after reflection from two static mirrors and passage through three perspex walls. Two of the perspex walls formed one of the vertical side walls of the cavity, and the third was part of the housing separating the rotating mirror from the rest of the cavity.

The motor on which the mirror was mounted was connected to a variable power supply so that slow and fast scans of the cavity centre-line could be made.

Unfortunately the arrangement did not work very well because of reflections from the perspex walls and the mirrors reducing the intensity of the laser light which eventually formed the sheet. Only marginal success was achieved within a radius of 50cm from the rotating mirror when it was rotating slowly.

Improvements to the arrangements used could have been brought about by the use of a more powerful laser, or the application of an anti-reflective coating to all relevant perspex and mirror surfaces. Unfortunately a more powerful laser was not available, and the anti-reflective coating would have required more finance than was available.

7.3.13 SUMMARY OF THE FINDINGS FROM THE VELOCITY RESULTS

In all Series the velocity profiles were seen to be anti-symmetric. This was caused by the non-adiabatic thermal boundary conditions on the floor and ceiling. The boundary conditions at the floor promoted an almost total collapse of the turbulence within the floor boundary layer, but those at the ceiling only promoted a partial collapse of the turbulence within the ceiling boundary layer. As a direct consequence of this an easily identifiable transition process took place at the heated wall, whilst only a very limited transition process occurred at the cooled wall (restricted to the region of fluid between the peak and the wall). The associated local variations of mass flow emphasised the anti-symmetric nature of the flow.

The velocity profiles in the Q.M.C. and Poitiers cavities differed at the edge of the boundary layers because of the difference in cavity width. In the region above mid-height the profiles in the Q.M.C. cavity generally

showed regions of reversed velocity at the edge of the boundary layers which merged at the cavity centre. In the case of the Poitiers cavity there were no regions of reversed flow above mid-height as the two boundary layers merged at the cavity centre.

In the Q.M.C. Series, the regions of reversed velocity were noted at the edge of the heated wall and cooled wall boundary layers where the local flow was turbulent. The only exceptions to this were in the region of x/H = 0.765 where no velocity reversal was noted at the edge of the cooled wall boundary layer. This was associated with a large vortex which was shown to exist by the calculated lateral mean velocity. The general rotation of the vortex was such that it promoted the region of reversed velocity on the heated wall side, but negated the region of reversed velocity on the cooled wall side.

Regions of reversed velocity did occur below mid-height in the Poitiers cavity, but only at the edge of the cooled wall boundary layer. This was possible because the heated wall boundary layer thickness in this lower region was comparatively small. The regions of reversed velocity were also seen to coincide with regions of horizontal temperature inversion, this was also seen in the Q.M.C. Series.

The general development of the velocity profile with regard to the peak in mean velocity was similar in all Series. The maximum peak velocity in the heated wall boundary layer was not noted at mid-height, but in the region where transition was just starting (the maximum in $u'_{R.M.S.}$ was also deduced as occurring at the start of transition). With an increase in height the peak mean velocity reduced and the region at the peak flattened out thus making the determination of the position of the peak difficult.

The development of the heated wall boundary layer width in all the Q.M.C. Series was similar, with the boundary layer width increasing with height.

Comparison of Series 5 and 6 results showed that the velocity profiles were affected by the effectiveness of the insulation on the vertical side walls. The effect of decreasing the level of insulation (with all other parameters constant) is to increase the velocity profile and so the mass flow, at any height in the regions of fully developed turbulence. The Series 5 and 6 results also showed that in the region of fully developed turbulence the reduced cavity width affected the level of the velocity fluctuations. In the region of fully developed turbulence the effect was to reduce the velocity fluctuations, but in the lower region of the cavity the level of the velocity fluctuations was increased.

The laser Doppler anemometer yielded valid mean velocity data which were not subject to significant uncertainty in the regions of high mean velocity gradient. The mean velocity gradient only had a significant effect on the $u'_{R.M.S.}$ data in the region $y \leq 3mm$.

Whilst calculating the wall shear stress it was found that $\overline{u'v'}$ was negligible out to $y = 4mm$. One may therefore consider the viscous sub-layer to be 4mm thick.

The trend of the wall shear stress with distance downstream was similar in both the heated and cooled wall boundary layers. At first the wall shear stress increased with distance downstream, but then decreased with distance downstream after the transition process took place.

All velocity scales proposed to-date were used to scale the heated wall profiles, both in the near wall region and across the full boundary layer. It was seen that the shear velocity was a good velocity scale for both the near wall region and the entire boundary layer width. It was used successfully in conjunction with Nu_y in the near wall region, and with y/δ for the entire boundary layer width.

The other velocity scales which were investigated were shown to be less suitable for the present data. Arguements were put forward which showed that the near wall velocity scales would be even less suitable for data with a much greater range of environmental stratification. The investigation of velocity scales also included that proposed by Bayley [36]. This was shown to be quite inappropriate.

Using the shear velocity the mean velocity profiles from the cooled wall were seen to be different from those of the heated wall, thus indicating differences in flow characteristics.

In the fully developed turbulence region of Series 3 at $x/H = 0.497$ the probability distributions of velocity indicated that the distributions were of a normal type out to the position where $u'_{R.M.S.}$ was a maximum. Beyond this position the distributions became skewed towards the lower velocities.

Within the boundary layers the flow was seen to be anisotropic, whereas in the central region it was isotropic. Thus the suggestion of Bolgiano [51] that stratification introduced anisotropy was not supported.

The mass flow imbalance at mid-height was seen to be approximately the same as that at $x/H \simeq 0.95$ for both Series 3 and 4. Extrapolation of mean velocity profiles was used to predict those profiles which would exist for equal heat transfer at each active wall. The resulting mass flow imbalance at mid-height was significantly reduced.

In an attempt to control the collapse of turbulence in the ceiling boundary layer a heated ceiling was used with a maximum temperature increase of 2.28K. This was insufficient to provide the control which was desired. Heaters able to provide a higher temperature difference would be required.

7.4 TURBULENCE QUANTITIES

The data from Series 3 have been used to calculate a number of turbulence quantities which are based upon two component correlations.

The whole process of calculation for each two component correlation was very time consuming and so only one complete set of each was produced for Series 3. No two component correlations were calculated for the Poitiers cavity as the data were not sufficient to produce meaningful results.

Those correlations which were calculated directly from the data were $\overline{u'T'}$ and $\overline{u'\rho'}$. However, these correlations are subject to uncertainties due to the separation (ranging from 0.5 - 1.5mm) between the thermocouple and the probe volume which inevitably occurred in practice.

The two component correlations which were calculated graphically were $\overline{u'v'}$ and $\overline{v'T'}$. These correlations will have been subject to uncertainties arising from the subjective interpretation of the numerous graphs which were necessary for their calculation.

Whilst one must bear in mind that the quantitative nature of the data presented in this Section cannot be assessed properly, one can nevertheless derive useful information from the qualitative nature of the data.

As well as calculating the two component correlations, two quantities based on $\overline{u'\rho'}$ and $\overline{u'v'}$ were also calculated. These were Q the production of turbulence kinetic energy due to buoyancy, and P the production of turbulence kinetic energy due to shear.

The two component correlation $\overline{u'v'}$ has also been used to calculate one other quantity, the total shear stress at any lateral position.

7.4.1 THE VERTICAL TURBULENCE HEAT FLUX

The vertical turbulence heat flux $\rho C_p \overline{u'T'}$ (the turbulent transport of heat downstream) can be examined by looking at the trend of the two component correlation $\overline{u'T'}$.

Firstly consider Figure 7.74 which shows the distribution of $\overline{u'T'}$ within the Q.M.C. cavity for Series 3. The corresponding data are tabulated in Tables 7.25-7.35.

Starting with the data at x/H = 0.046 one notes that, by taking the boundary layers as a whole, the lowest values of $\overline{u'T'}$ occurred at this height. This was not surprising as the flow down the cooled wall had transferred most of it's thermal energy to the cooled wall, and the flow at the bottom of the heated wall would not have received much thermal energy.

Using the data of Ziai [1] one may estimate that the sign of the vertical temperature gradient close to the floor changed at y/L ≈ 0.7, with a stable gradient near to the cooled wall. The heat transfer to the flow, resulting from the unstable temperature gradient near to the heated wall, will have been partially responsible for the relatively higher level of u'T' in the heated wall boundary layer.

Generally the value of $\overline{u'T'}$ at this, and other heights, was positive, with regions of negative $\overline{u'T'}$ in the central region of the cavity. This means that within both boundary layers most of the turbulent transport of heat was in the positive vertical direction.

Negative values of $\overline{u'T'}$ were mostly confined to regions of reversed velocity, indicating that the motion in these regions was not purely due to buoyancy forces.

At all heights the moduli of the peak negative values were higher in the cooled wall boundary layer.

Moving up in height to x/H = 0.143 did not show any reduction in the level of u'T' at the heated wall, instead it increased. Thus no evidence of a wall damping effect was seen, as was the case in the $T'_{R.M.S.}$ and $u'_{R.M.S.}$ data. This obviously implies that the $\overline{u'T'}$ correlation coefficient changes at this height.

Now, the convection of thermal energy downstream is the sum of $\rho C_p uT$ and $\rho C_p \overline{u'T'}$ integrated across the boundary layer. Therefore any reduction in u near the wall during transition can be compensated by either an increase in the boundary layer width or an increase in $\overline{u'T'}$.

A four fold increase of $\overline{u'T'}$ occurred at the heated wall when moving from x/H = 0.143 to 0.229 where the maximum peak velocity occurred. However, the values of $\overline{u'T'}$ across the boundary layer dropped when going from x/H = 0.229 to 0.360 thus indicating that the corresponding reduction in peak velocity was offset by the increase in the width of the boundary layer.

The peak value of $\overline{u'T'}$ decreased from x/H = 0.360 upwards, as did the values across the boundary layer, thus indicating that the vertical convection of thermal energy was not constant with height.

Before examining the data for the cooled wall boundary layer it is interesting to look at a typical distribution of the correlation coefficient for $\overline{u'T'}$ across the heated wall boundary layer. One expects the correlation coefficient to be higher nearer the wall so denoting a coupling of the temperature and velocity fields through buoyancy.

Figure 7.75 shows the correlation coefficient across the heated wall boundary layer for x/H = 0.497. It is seen that the correlation coefficient reaches a maximum at y ≈ 15mm, with a small range of values over the range y ≈ 7-40mm. The lateral position of 40mm was approximately the position at which the local temperature matched that at the cavity centre, for most heights.

To and Humphrey [47] and Miyamoto et al [45] reported the correlation coefficient to be approximately constant at 0.6 for Nu_y > 3.5. In the example shown in Figure 7.75 the maximum was just under 0.6. However, the value of Nu_y at which the plateau of values started was approximately 1.5, considerably less than that observed previously.

When comparing the correlation coefficient of $\overline{u'T'}$ between flat plate and cavity flow, one must remember that there was a separation of approximatley 0.5mm between the thermocouple junction and the probe volume in the heated wall flow of the present study, although this would not be expected to show a significant effect.

The increase in correlation coefficient at the cavity centre was also a feature at other heights, the reason for this is unknown. Such a phenomenon does not occur in vertical flat plate natural convection.

Looking now at the data for x/H = 0.949 one sees that the values of $\overline{u'T'}$ were much higher than they were at x/H = 0.046, with the cooled wall boundary layer exhibiting a higher peak value than the heated wall boundary layer.

Along the ceiling the data of Ziai [1] indicated that the sign of the vertical temperature gradient changed sign at y/L ≈ 0.54 with an unstable temperature gradient close to the cooled wall which will have been partially responsible for the higher peak values.

The values of $\overline{u'T'}$ increased across the cooled wall boundary layer with distance downstream until x/H = 0.765 after which they decreased.

7.4.2 THE LATERAL TURBULENCE HEAT FLUX

The lateral turbulence heat flux $\rho Cp\overline{v'T'}$ (the turbulent transport of heat from the inner to the outer region) can be examined by looking at the two component correlation $\overline{v'T'}$.

By integrating equation (1.6) one obtains equation (7.39) given below.

$$\overline{v'T'} = \alpha_R \frac{dT}{dy} + \alpha_R \frac{\dot{Q}''_\omega}{k_\omega} - \int_0^y u\frac{dT}{dx}\,dy - \int_0^y v\frac{dT}{dy}\,dy \qquad (7.39)$$

The choice of reference temperature for the evaluation of α is important, one can argue that it ought to be a constant value for all lateral positions across the boundary layer, or that it ought to be evaluated at the local temperature for each lateral position.

By evaluating α at the local temperature, the centre-line values (evaluated from both walls) at most heights showed a substantial disagreement, only when $\alpha_R = \alpha_\omega$ was used at all heights was the agreement between centre-line values improved.

Unfortunately, the agreement between the centre-line values at x/H = 0.229 and 0.360 was still extremely poor thus rendering a graphical presentation very confusing, therefore only the tabulated data in Tables 7.36-7.46 will be considered.

The major reason for the discrepancy between the centre-line values at x/H = 0.229 and 0.360 was the relatively large variation of dT/dx at these heights. The estimates of dT/dx made from the data were clearly incorrect, but insufficient data were available to even attempt a correction procedure.

Apart from the two previously mentioned heights, agreement between the centre-line values was generally reasonable considering the uncertainties that the data were subject to. However, a check on expected values of $\overline{v'T'}$ at the centre-line, assuming a correlation coefficient of one, showed that most of the data could not be considered to be quantitative, therefore the present data can only be considered from a qualitative point of view.

In order to establish the validity of the present data for a qualitative analysis one may compare them with the data produced by Mr. A. Bowles [89] using the 2.5m high Q.M.C. cavity. Figure 7.76 shows examples from four heights: x/H = 0.046, 0.497, 0.765 and 0.949.

The qualitative nature of the calculated values of $\overline{v'T'}$ was seen to be proved by the comparison, although the calculated data for x/H = 0.046 showed a large, but constant, offset from the experimental data in the central cavity region. In all cases the peak values of calculated $\overline{v'T'}$ were larger than those found by experimentation.

The general observations resulting from the present $\overline{v'T'}$ data are that within the main part of each boundary layer the sign of $\overline{v'T'}$ is always

positive, i.e. turbulent heat transport occurs from the heated wall and to the cooled wall as would be expected.

A substantial increase in $\overline{v'T'}$ was seen to occur in the region of the heated wall at x/H = 0.229 and 0.360 where a transition process was taking place. Such an increase, although on a smaller scale, took place at the cooled wall at x/H = 0.765.

The experimental data indicated little turbulent transport of heat within the boundary layer along the floor, whereas there was some within the boundary layer along the ceiling. This was as expected.

The data available from To and Humphrey [47], Ierokipiotis [42] and Miyamoto et al [45] showed a peak in $\overline{v'T'}$ at $Nu_Y \approx 2.4$, whereas in the present study it was $Nu_Y \approx 1.3$.

The final point of interest was the existence of regions of negative $\overline{v'T'}$ in the central region of the cavity, associated with regions of reversed velocity and entrainment. These were more prominent in the calculated data.

7.4.3 THE REYNOLDS STRESS $\rho\overline{u'v'}$

The turbulence quantity $\overline{u'v'}$ was not measured directly but calculated by using the first integral, between y and y = 0, of equation (1.5) as shown below.

$$\overline{u'v'} = \frac{(\mu)}{(\rho)_R}\frac{du}{dy} - \frac{(\mu)}{(\rho)_R}\tau_w + \int_0^y g\beta_T(T-T_\infty)\,dy - \int_0^y u\frac{du}{dx}\,dy - \int_0^y v\frac{du}{dy}\,dy \quad (7.40)$$

$$\overline{u'v'} = \quad A \quad - \quad B \quad + \quad C \quad - \quad D \quad - \quad E$$

The calculation of the wall shear stress, in term B, has been described previously in Section 7.3.3. The same equation used in those calculations was used to determine du/dy for y < 4mm. Otherwise, all other quantities and integrals were calculated from graphical interpretation.

In order to provide a consistent approach to the calculation of two component correlations $(\mu/\rho)_\omega$ was chosen as $(\mu/\rho)_R$.

The values of $\overline{u'v'}$ for Series 3 are given in Tables 7.47-7.57. The five groups on the R.H.S. of equation (7.40) have each been assigned an identification letter which has acted as a column head in Tables 7.47-7.57. In this way the presentation is clearer and one is able to see the contribution of each group. Note that the cooled wall values were calculated using local co-ordinates and the final values of $\overline{u'v'}$ are converted to the heated wall (overall) co-ordinates in the final column.

The calculation of $\overline{u'v'}$ was hampered by an apparent error in the centre-line temperature at all heights. Initial calculations indicated extremely high discrepancies between the two calculated values of $\overline{u'v'}$ at the cavity centre-line for most heights. Even when there was good agreement the centre-line values were far too high, as the correlation coefficient derived from these centre-line values was of the order of ten whereas it is impossible for it to go above one.

Using the experimental data, and the turbulence energy equation, the likely values of $\overline{u'v'}$ at the centre-line were calculated. These are presented in Table 7.58.

From Table 7.58 one sees that the values at x/H = 0.046 and 0.096 were virtually zero, as would be expected in a flow which is re-laminarizing. The values at x/H = 0.229 and 0.765 were associated with the regions of greatest cross-flow from one boundary layer to the other. The high value at x/H = 0.949 was not unexpected, as the horizontal flow here was not re-laminarizing, and was also being disturbed by the downflow of fluid which had lost thermal energy through the ceiling.

Further evidence for the magnitude of $\overline{u'v'}$, at the centre-line, comes from the correlation coefficient (non-dimensionalisation of $\overline{u'v'}$ with respect to $u'_{R.M.S.}$ and $v'_{R.M.S.}$) when assuming a possible maximum of one. These data are given in Table 7.59.

It can be seen that the values of $\overline{u'v'}$ in Tables 7.58 and 7.59 match quite well.

In order to correct the $\overline{u'v'}$ profiles so that the centre-line values matched the order of magnitude given by the turbulence kinetic energy equation, one could only feasibly alter group C, the integral of $(T-T_\infty)$ with respect to y. This was achieved by changing the centre-line temperature. In doing this the present author assumed that all the remaining terms in the equation for $\overline{u'v'}$ had been correctly calculated (all the terms involving velocity had been corrected to allow for the presence of the thermocouple, and there were relatively low levels of uncertainty in the values of the wall shear stress and term B).

Now consider an example of a correction in the centre-line temperature. The example height is x/H = 0.765, which was thought to be one of the more accurate profiles as regards temperature. The centre-line temperature measured from the heated wall was 56.39°C and from the cooled wall 57.14°C. These had to be altered to 56.65°C and 56.91°C, respectively.

The values of $\overline{u'v'}$ resulting from the temperature correction at x/H = 0.765 are presented, together with the previous values, in Table 7.60. The

centre-line value of $\overline{u'v'}$ was reduced from an average of 1.70 to 0.07. This was achieved with corrections to the centre-line temperatures of 0.26K and 0.23K for the heated and cooled wall values respectively (0.5% of the temperature in Celsius).

All centre-line temperatures were adjusted to yield the centre-line values of $\overline{u'v'}$ indicated by the turbulence kinetic energy equation. The new centre-line temperatures are presented in Table 7.61. By changing the centre-line temperature it was assumed that all other temperatures were correct, although some changes were required at y = 200mm at three heights.

The new temperatures were used to recalculate the wall shear stresses. The difference between the previous wall shear stresses and the new ones were minimal in the majority of cases. A recalculation of the non-dimensional centre-line temperature showed little change, although the non-dimensional gradient changed slightly, increasing from 0.463 to 0.473.

An interesting observation has arisen from the temperature correction. It was found that the difference between the centre-line temperatures was generally smaller than before. In addition it was noted that a velocity reversal did not occur unless it was accompanied by a temperature reversal, and that the ratio of velocity reversal to temperature inversion was approximately constant (see Table 7.62).

It is not enough to state that a centre-line temperature correction was necessary, without an attempt to provide an explanation as to why the error may have occurred.

The error could have been due to the relatively large distance travelled by the probes in the cavity centre. This movement may have disturbed the flow, requiring some time for it to re-establish. No specific time was allowed for any disturbance of the flow in the central region to subside. The only time in which the flow could settle was the delay between readings. This was approximately 1min. The sample time was 8mins and so one would expect the temperature to have settled during this time. But it appears that it did not. This may be associated with the low level of turbulence in the cavity centre.

The turbulence is the only mechanism by which externally imposed variations of mean temperature can be "ironed out". Certainly, for the positions where the horizontal movement was quite small, and the turbulence intensity high, a very smooth mean temperature curve resulted.

One other possibilty is that both of the thermocouple connections could have been loose. Any influence of a loose connection may be accentuated by the larger movements in the cavity centre, so resulting in

the last three readings being in error. The last three readings started from y = 100mm, where the trough in the mean temperature profile occurred.

Disruption of the flow due to seeding is highly unlikely as the final seeding took place approximately six positions before the end of each half of a run.

Looking back at the work of Ziai [1] one notes that his mean temperature profiles exhibited the same error. As an error due to faulty thermocouple connections is unlikely in both thermocouples, and in both Ziai's and the present work, one is forced to conclude that it must be the disturbance of the flow in the cavity centre, by the probe block, which has resulted in false centre-line temperatures.

Having established the values of $\overline{u'v'}$ one can now comment on the distribution of $\overline{u'v'}$ within the cavity and, in particular, in the near wall region.

Firstly, consider the near wall profile at the heated and cooled walls. The works of Miyamoto et al [45] and Ierokipiotis [42] have shown regions of negative $\overline{u'v'}$ up to $Nu_y \simeq 0.8-1.1$. This has not generally been found in the data calculated for Series 3.

The equation used to calculate the wall shear stress was derived by assuming that the values of $\overline{u'v'}$ were negligible in the near wall region (over which experimental velocities were used to determine du/dy at the wall). One therefore expected the calculated values of $\overline{u'v'}$ over this region to be either zero or very close to it, especially as the agreement between the experimental and theoretically predicted velocities was excellent. Thus the non-existence of a negative region of $\overline{u'v'}$ was not unexpected from the present calculations.

If a similar situation to that found by Miyamoto et al [45] and Ierokipiotis [42] were to have existed in the cavity, then the position at which $\overline{u'v'}$ changed sign ($Nu_y \simeq 0.8-1.1$) would have been just before, or at, the position of peak velocity ($y \simeq 5.5-8.5$mm). For $\overline{u'v'}$ to have been near to zero for the range of Nu_y being considered, then there would have to have been either: a 12% increase in term B; a 12% decrease in term C; or some combination of an increase in term B and decrease in term C.

A change in term B of 12% would not appear to be a feasible proposition as the profiles generated by the near wall sub-layer equation matched the experimental profiles very closely, and any such change would require a relocation of the wall position leading to an unrealistic mean velocity profile very close to the wall (i.e. within 0.5mm of the wall).

It is acknowledged that the lack of an initial precise location of the wall will have introduced a level of uncertainty into the calculated wall shear stress, but not enough to change term B to bring about the difference in distribution of $\overline{u'v'}$ between the present data and those of Miyamoto et al [45] and Ierokipiotis [42].

Similarly a change to term C of 12% would not be considered feasible as there is no variable within the term which may be subject to a high enough level of uncertainty which could result in such a change.

If a region of negative $\overline{u'v'}$ did exist then the only possibility remaining is the combination of uncertainties in both terms. However, given the excellent agreement between predicted and experimental mean velocities, and the reliability of the temperature data, one cannot comment on this further except to explain why one might expect to see a region of negative $\overline{u'v'}$.

If one considers the equation for turbulence kinetic energy in a near wall forced flow situation, one sees that the production of turbulence kinetic energy is due to the term $-\overline{u'v'}du/dy$. This is known as P, the production of turbulence kinetic energy due to shear. As it is the only term which is responsible for the input of energy to the turbulence, it must be positive in sign. Now as du/dy is positive close to the wall, then $\overline{u'v'}$ must be negative for the production term to be positive.

Whilst local regions of positive $\overline{u'v'}$ may occur on the wall side of the peak mean velocity in forced flow, they cannot occupy the majority of this region as the turbulence could not be maintained. However, this need not necessarily be true for a system which comprises other turbulence kinetic energy generating terms, such as a buoyancy term. In this respect the production of turbulence kinetic energy due to buoyancy, G, has been calculated and is compared to P in Section 7.4.5.

Obviously, the only way to resolve the problem of the sign of $\overline{u'v'}$ in the near wall region is to measure $\overline{u'v'}$ directly.

With respect to the heated wall data, the position of peak $\overline{u'v'}$ occurred at $Nu_y \approx 5.7$-7.7 which was less than that reported by Miyamoto et al [45] and Ierokipiotis [42] (10 and 17 respectively). This shows that there is a significant difference in the distribution of $\overline{u'v'}$ within cavity and flat plate boundary layers.

Now consider the overall distribution of $\overline{u'v'}$ within the cavity, shown in Figure 7.77.

Starting at $x/H = 0.046$, one sees that the value of $\overline{u'v'}$ was non-zero across the entire profile.

As one follows the development of the flow up the heated wall the level of $\overline{u'v'}$ remained relatively small until x/H = 0.229 where a substantial increase occurred. The peak value of u'v' then increased with x for all heights.

As the flow progressed along the ceiling $\overline{u'v'}$ changed sign, such that the change was noted at y/L = 0.62 at x/H = 0.949. This height exhibited the largest region where $\overline{u'v'}$ was negative. Such regions did exist at the outer edge of the cooled wall boundary layer where velocity reversals took place, but they were much smaller.

The peak value of $\overline{u'v'}$ within the cooled wall boundary layer increased with distance downstream until x/H = 0.765, after which it was constant until it started to decrease again at x/H = 0.229.

Now the distribution of $\overline{u'v'}$ is important not only in being able to determine P, but also in being able to determine the local shear stress. As $\overline{u'v'}$ represents a transfer of momentum so $-\rho\overline{u'v'}$ describes a turbulence shear stress. This quantity is looked at in the next Section.

The final point to be raised concerning $\overline{u'v'}$ is the distribution of it's correlation coefficient at the two extreme heights of x/H = 0.046 and 0.949. The correlation coefficient is of interest in these regions because of it's behaviour in other systems where re-laminarization takes place.

In the present system re-laminarization is promoted by a stable temperature gradient. But there are other examples where re-laminarization might occur, promoted by a favourable pressure gradient or by a change in geometry such as a diverging channel. In the latter case it has been found that the correlation coefficient of $\overline{u'v'}$ decreases during re-laminarization as the structure of the turbulence changes. Therefore a study of the $\overline{u'v'}$ correlation coefficient may show up a similar state of affairs.

The correlation coeffiecient has been calculated for three heights: x/H = 0.046, 0.497 and 0.949. The second height has been included as a reference for the other two. The results are shown in Figure 7.78.

No trends were visible in the data of Figure 7.78 at x/H = 0.046, so suggesting that the structure of the turbulence in the region of re-laminarization at x/H = 0.046 was not the same as has been observed in diverging channel flow.

The only point of note from Figure 7.78 was that the correlation coefficients at x/H = 0.497 and 0.949 were generally one or less, whilst those at x/H = 0.046 were considerably higher. This indicates either some difference in the turbulence structure between the flow at x/H = 0.046 and the rest of the cavity, or that the available $v'_{r.m.s.}$ data at x/H = 0.046

were subject to high levels of uncertainty. A combination of the two is the most likely.

7.4.4 THE TOTAL SHEAR STRESS

The total shear stress $\tau = \mu du/dy - \rho\overline{u'v'}$ has been calculated for Series 3 at all heights. The resulting data are tabulated in Tables 7.63-7.73 and sample graphs at x/H = 0.046, 0.497 and 0.949 are presented in Figure 7.79.

The general shape of the graphs in Figure 7.79 applied to all heights. Working from the heated to the cooled wall one notes that there was an initially large positive shear stress which then dropped sharply to a negative value, the change of sign occurring between y = 5-6mm at most heights in the regions of fully developed flow. This position was between the wall and the position of peak velocity, occurring at approximately two thirds of this distance.

A minimum in τ occurred between y = 40-60mm (approximately coinciding with the first lateral position at which $T = T_\infty$) after which the value rose to become positive at y ≈ 300mm it's sign then reversing again to become negative, then increasing sharply close to the cooled wall to a relatively high positive value.

The point at which the total shear stress changed sign close to the cooled wall was similar (in relation to the position of local peak velocity) to that near the heated wall, as was the position of the near wall trough in relation to the first lateral position where $T = T_\infty$.

From the description of the distribution of τ one immediately notes that there was no region of constant stress as one finds in forced flows. This has been known for some time in respect of vertical flat plate natural convection and is now confirmed for cavity natural convection.

7.4.5 TURBULENCE KINETIC ENERGY

The two quantities discussed in this Section are the production of turbulence kinetic energy due to buoyancy, $G = -g\overline{u'\rho'}$, and that due to shear, $P = -\overline{u'v'}du/dy$. The former has been calculated directly from the data, whilst the latter term has been calculated by graphical interpretation.

The present experimental data are the first to be published, all other data of this type have come from numerical calculations.

The values of P and G are respectively tabulated in Tables 7.63-7.73 and 7.25-7.35, and are graphically presented for all heights in Figures 7.80 and 7.81. Data at sample heights are also shown in Figures 7.82 and 7.83,

the former showing full profiles and the latter near wall profiles. In all cases a positive value of either P or G indicates the production of turbulence kinetic energy, and obviously a negative value indicates a destruction.

Consider the tabulated data for x/H = 0.046 and the graph in Figure 7.82. Except for the near wall region at the cooled wall the sign of P was positive, with P generally being larger than G. In the central cavity region P was mostly negligible whilst G was small but negative. At all other positions G was positive. A similar profile was seen at x/H = 0.096 and 0.143.

There was a reduction in the peak values of P and G at the heated wall when going from x/H = 0.046 to 0.096 thus showing the influence of heat transfer from the floor at the lower height.

The peak values of P and G at the heated wall increased from x/H = 0.096 to 0.143 after which there was a substantial increase at x/H = 0.229 where both reached a maximum.

Above x/H = 0.229 the value of P in the near wall region at the heated wall became negative thus indicating a destruction of the turbulence due to shearing action. In the same region G was positive and represented the production of turbulence kinetic energy.

The near wall regions are shown in detail in Figure 7.83 for x/H = 0.497 and 0.765. At both walls P was negative and G positive, with the sum of P and G being positive. One therefore notes that confidence in the current calculated values of $\overline{u'v'}$ in the near wall region is increased, because the near wall turbulence could have been sustained by the production of turbulence kinetic energy due to buoyancy. This observation applied to all near wall regions when fully developed flow was present.

As for the whole profile of P and G, the graphs at x/H = 0.497 and 0.765 in Figure 7.82 show that for most of the profile P was larger than G, except in the near wall and central cavity regions (in the central cavity region they were approximately equal and negative).

The peak value of G at the heated wall decreased with height up to, and including, x/H = 0.949, whereas that of P was approximately constant.

At x/H = 0.949 G was mostly positive, except for localized regions at the outer edge of each boundary layer. But P was negative for most of the cooled wall boundary layer.

The development of the profiles of P and G down the cooled wall was similar to that up the heated wall, with the peak values reaching a maximum

at x/H = 0.765, although P was only positive in the near wall region of the cooled wall at x/H = 0.849.

In general one can say that destruction of turbulence kinetic energy by both shear and buoyancy took place in the central cavity region, most notably in the regions of reversed velocity. Production of turbulence kinetic energy due to shear and buoyancy took place in the main part of each boundary layer, with the near wall regions a special case, the sign of G being positive and the sign of P being negative in regions of fully developed flow.

The only numerical data which can be compared to the present results are those of To and Humprey [47]. They also found P to be larger than G for the main part of the boundary layer. They also found that dissipation and convection were the major sink terms of the turbulence kinetic energy. This was also the case in the cavity.

7.4.6 SUMMARY OF THE FINDINGS FROM THE TURBULENCE QUANTITIES RESULTS

Detailed data have been presented for a number of turbulence quantities which are based on two component correlations. All of these have varied with lateral position and in relation to the transition process at the heated wall.

The value of $\overline{u'T'}$ within the boundary layers was always positive, therefore all turbulent transport of heat was in the positive vertical direction. The total amount of thermal energy convected in the vertical direction was not constant with height.

It was seen that the maximum correlation coefficient of $\overline{u'T'}$ matched that reported by other researchers.

The calculated values of $\overline{v'T'}$ have been shown to be qualitative in nature. The value of $\overline{v'T'}$ was always positive in the main part of each boundary layer, thus showing that heat transfer was from the heated wall and to the cooled wall.

A substantial increase in $\overline{v'T'}$ was associated with the transition process at the heated wall.

During the calculation of $\overline{u'v'}$ it was noted that minor corrections to the centre-line temperatures were required.

Unlike the results from flat plate flow presented by other researchers, there was no general region of negative $\overline{u'v'}$ close to either wall.

One other significant difference in the distribution of $\overline{u'v'}$ was found between flat plate and cavity natural convection in relation to the value of Nu_y at which the peak of $\overline{u'v'}$ was found. For cavity natural convection the value of Nu_y was significantly lower.

Unlike the two component correlations associated with the turbulent transport of heat, the value of $\overline{u'v'}$ increased with height along the heated wall.

The distribution of the total shear stress, τ, was presented for the first time for cavity natural convection. Maxima occurred at each wall, and minima occurred, at each position from either wall, where the local temperature first reached that at the centre-line.

Experimentally derived values of P and G were presented for the first time. These two quantities are important, both by themselves and combined together. Each varied across the cavity exhibiting different characteristics in different lateral regions.

Close to each wall P was seen to be negative, thus causing a destruction of turbulence kinetic energy. However, G was positive and large enough such that the sum of P and G was positive in the near wall region. Therefore it was seen that the turbulence could be sustained.

Beyond the near wall region, and up to the edge of the boundary layers, the value of P was positive and larger than the value of G which was also positive.

In the central cavity region, beyond the edge of each boundary layer, the value of P was negligible whilst G was small but negative, thus showing destruction of the turbulence kinetic energy by buoyancy forces.

7.5 POWER SPECTRAL DENSITY CALCULATIONS

Power spectral density (P.S.D.) distributions calculated from time series of either velocity or temperature samples can be considered to be part of a full description of any natural convection flow.

For the present study P.S.D. distributions were useful for three reasons.

Firstly, to help establish the nature of the flow at the bottom of the heated wall, and at the top of the cooled wall. Such an investigation was necessary to find out whether or not a transitional boundary layer regime was present and, if so, what effect the boundary conditions on the floor and ceiling had on the collapse of turbulence within the flow along them.

Secondly, to determine the dominant frequencies in any transition process and to investigate whether the equation, currently available, for

predicting the dominant frequency of transition of natural convection flow along a vertical flat plate, could be used for cavity flow.

Thirdly, to see how the turbulence was affected by stratification in respect of the power law relationship between P.S.D. and frequency (or alternatively wavenumber).

When commenting on the effect of the stratification on the power law relating frequency to P.S.D., previous researchers (e.g Bolgiano [51]) have considered the stratification to have introduced anisotropy into the turbulence thus altering the power within one or more sub-ranges. One must be very careful when using the term anisotropy for one could automatically take it's use to mean that without stratification the turbulence would be isotropic (i.e. the R.M.S. of the fluctuating velocity components would be equal in all three co-ordinate directions, for three and two-dimensional flow).

Miyamoto et al [45] have presented experimental data for the ratio of $u'_{R.M.S.}$ to $v'_{R.M.S.}$ across a turbulent boundary layer flow, for a uniform heat flux vertical wall in an isothermal environment. The ratio was always greater than one with a peak close to the wall, of between six and nine depending on Gr_x, decreasing to approximately two further out.

Miyamoto et al [45] also presented data from another paper which reported experimental data from natural convection flow along an isothermal wall, in an isothermal environment. These data showed the ratio of $u'_{R.M.S.}$ to $v'_{R.M.S.}$ to be between one and two across the boundary layer.

The data of Figure 7.69 show that in the cavity boundary layers the ratio decreased from approximately five, at either wall, to one at the cavity centre.

No other experimental data exist which are able to shed more light on the ratio of $u'_{R.M.S.}$ to $v'_{R.M.S.}$, but one notes that there is no guarantee that it will be one when there is no stratification (i.e. that the turbulence is isotropic). Indeed it has been proposed that the sink terms in the turbulence equations show that scales differ in each co-ordinate direction.

Whilst commenting on the power law relationship between P.S.D. and frequency, wavenumbers (as defined by Taylor for isotropic turbulence) will be quoted for the minimum and maximum frequencies of any sub-range. The reason for doing this was to see if any variation in frequency sub-range limits resulted in constant ranges of wavenumber.

7.5.1 THE MATHEMATICAL TECHNIQUE

There are several mathematical techniques which can be used to calculate P.S.D. The selection of an appropriate technique is dependent on the manner in which data is sampled (random sampling or sampling at discrete time intervals) and the sample time in relation to the sampling frequency.

The cavity data were sampled at constant time intervals for a relatively long time. As the data were stored on magnetic tape in 100 blocks of 2048 words, the most obvious choice of analysis was one based on individual block calculations, culminating in an averaging over the 100 blocks. Each data set in one block contained 512 samples, so leading to a frequency resolution of 0.195Hz in the output.

This, then, was the approach taken in conjunction with the proposals of Otnes and Enochson [86] for such data sets. The general theory is now outlined.

During the calculation of P.S.D. the time history has firstly to be altered to remove the mean value so that one deals only with the fluctuating components. In doing this one also calculates the variance (mean square value) of the data which is commonly used to non-dimensionalise the values of P.S.D.

Once the data have been "mean corrected" then, for a single time history, x(t), a raw estimate of the P.S.D. at any frequency, f, is given by:

$$G_x(f) = \frac{2}{T} |X(f,T)|^2 \qquad (7.41)$$

Where T = Nh, N = total no. of samples, h = time between samples and

$$X(f,T) = h \sum_{0}^{N-1} x_N \exp(-j2\pi fnh) \qquad (7.42)$$

One should note that only an estimate of the P.S.D. can ever be calculated from experimental data, as calculation of the true P.S.D. would require an infinite data series.

Now one can manipulate equation (7.42) by putting f = k/[Nh] where k = 0,1,.....N-1 to give:

$$X(f,T) = h \sum_{0}^{N-1} x_N \exp(-j2\pi[kn/N]) \qquad (7.43)$$

Now, by putting $X_K = X(f,T)/h$ one can write:

$$G_x(f) = \frac{2h}{N} |X_K|^2 \qquad (7.44)$$

The representation of $G_x(f)$ in equation (7.43) is useful as it allows an easy comparison between it and the output of the fast Fourier transform algorithm which has been used to calculate the Fourier transform.

The algorithm used in practice was taken from the NAG library on the Q.M.C. ICL 2988 computer. The name of the routine was C06EAF and it's output was $X_K/N^{0.5}$. Therefore by squaring the output and mutiplying by 2h one obtained $G_x(f)$.

Now, $G_x(f)$ is only a raw estimate which is subject to uncertainties. To compensate for this a "window" has to be applied to the data, either before or after the application of the transform (the transform essentially integrates between $\pm\infty$ and so the window has the effect of making the time history appear as part of an infinite one).

It is much easier to apply a data window after the transform has been carried out, and for this purpose many windows have been proposed. Previous researchers at Q.M.C. have used what is termed the GEO spectral window, but if one is to calculate P.S.D.'s for individual blocks, and then to average the results, a more appropriate window, especially designed for such a use, is the Goodman spectral window.

The Goodman window is applied to the values of X_K, such that:

$$X_K(k) = X_K(k) + \Sigma\ B(i)[X_K(k-1) + X_K(k+1)] \qquad (7.45)$$

Where $B(1) = -0.35$, $B(2) = -0.0875$, $B(3) = -0.0625$

At the begining, and the end of the X_K sequence, one considers the sequence as a continuous loop when selecting $X_K(k\pm1)$.

When the values of $G_x(f)$ have been calculated they must be multiplied by the Goodman factor which is 1.267.

In summary, the technique used by the present author was to subtract the mean value of the data in one block to give $x(t)$ based on fluctuating components only. The modified time history was then fast Fourier transformed to give $X_K/N^{0.5}$. These values were then subjected to the Goodman window, after which they were squared, scaled and multiplied by 2h. This was repeated for the remaining 99 blocks and the resultant values at each frequency averaged over the 100 blocks. No further manipulation of the data was undertaken, although some researchers employ a "smoothing" operation which was considered unnecessary for the present calculations.

The programs used for the P.S.D. calculations were VELPSD and TEMPPSD both in #SRC of the present author's filespace under the username :UGEM117 on the Q.M.C. ICL 2988. The subroutine used by both programs was named GOOD

which was stored in compiled form in *OMF, and in original form on magnetic tape PT1214 under group KEV1.

In preparation for the P.S.D. calculations, checks on the magnitude of the temperature and velocity data were incorporated into the programs to guard against false tape readings. The velocity data did require some extra preparation as dropout in the L.D.A. meant that some readings were not correct.

Each tape was examined using the program DROPOUT, to see which blocks contained sequences of more than 10 consecutive "dropout" readings. These blocks were discarded during the analysis, and, where "acceptable" dropout did occur, the program replaced the incorrect data using a linear interpolation between valid readings, so forming a continuous data sequence.

For the vast majority of the data, it was found that when dropout occurred the number of consecutive samples which were affected was either one or two. Occurrences of five or more consecutive samples affected by dropout were rare.

All the results from DROPOUT, VELPSD and TEMPPSD have been kept on magnetic tape PT1214.

The P.S.D. programs were tested using data derived from simple cosine functions utilizing frequencies of 10 and 20Hz. When the results of these tests were plotted, with normal decimal numbers at each axis, sharp peaks were seen at the two relevant frequencies, and the area under the curve agreed with the mean square value of the data to within 2%. The analysis programs were therefore considered correct.

In most instances P.S.D. data are presented in a log-log format. Indeed, the data from Series 3 and 4 will be presented in log-log format. But, such a representaion of the data can lead to a reduction in the "visual sharpness" of any peaks in a curve of P.S.D. against frequency. This is illustrated quite well by Figure 7.84 which shows the results from cosine test data at a frequency of 10Hz.

P.S.D.'s were also calculated from the data of Series 5 which were stored on the PDP system. In order to be able to do this the fast Fourier transform given in Otnes and Enochson [86] was proposed for use in these calculations.

Test data, identical to that used to test the ICL P.S.D. programs, were used to check the programs on the PDP. A number of errors in the original program listing were shown up, but the eventual results agreed excellently with the ICL calculations when plotted in decimal (or linear) format. However, when plotted in log-log format there were considerable differences

in the results from the PDP and ICL programs which are shown in Figure 7.84.

The differences shown up by Figure 7.84 proved to be significant, so much so that little reliable information could be gleaned from the Series 5 plots of P.S.D. against frequency, especially in relation to estimating the start of transition. It is thought that the smaller word length of the PDP computer was responsible for the differences, and not the algorithmn.

7.5.2 VELOCITY TIME HISTORIES

The flow at the bottom of the heated wall is considered in relation to time histories which were produced from the data recorded on the tapes.

It has previously been noted that the flow at the bottom of the heated wall was predicted to be of a laminar nature for the values of Ra_H studied. Therefore one would expect the "laminar" region to be more extensive in Series 4 than in Series 3, as the value of Ra_H was lower and any transition process would be expected to have started at a greater absolute height in Series 4 than in Series 3.

The onset of transition is shown up best by the time histories from Series 4, at x/H = 0.046-0.229. Those from Series 3 are omitted to conserve space.

Consider Figures 7.85-7.88 which are velocity time histories from Series 4 at x/H = 0.046, 0.095, 0.143 and 0.229 with y ≈ 3mm (the y position corresponds to the peak in mean velocity). These plots can be compared to Figure 7.89 which depicts the time history, at the mean velocity peak, from Series 3 at x/H = 0.497 where the flow was fully turbulent. The difference between the time histories in Figures 7.85-7.87, and that in Figure 7.89, was quite considerable.

In Figures 7.85-7.88 one sees that when the velocity changed it did so relatively slowly and smoothly. Certainly, the nature of the flow at the bottom of the heated wall was quite different from that of the fully developed turbulent flow, it being very close to that of laminar flow, although not strictly so as variations in velocity did occur.

The time segment shown in each Figure is 10.24s out of a total sample time of 512s. Obviously, other sub-samples would show slightly different patterns but one can see that, in general, there were fewest changes in velocity at x/H ≈ 0.096 which reflected the reduction in $u'_{R.M.S.}$ brought about by the damping effect of the wall.

At x/H = 0.096 one also notes that the vertical scatter in the plot decreased to a minimum. This would appear to indicate a lower level of disturbance at this height than at any of the other three.

The minumum scatter at x/H = 0.096 was approximately 0.008m/s which was the resolution of the tracker for the frequency range used.

To check whether the scatter at x/H = 0.096 was purely due to anemometer resolution an investigation was carried out during Series 5. Data were taken at x/H = 0.118 (similar absolute height to x/H = 0.096 of Series 4) for two tracker frequency ranges, namely 33-333kHz and 10-100kHz. The resultant time histories, shown in Figures 7.90 and 7.91, showed that the scatter reduced by one third with a decrease in the frequency range. This is exactly what was expected if the scatter had been due to the anemometer resolution.

The final time history to be examined is that at x/H = 0.229 from Series 4 (Figure 7.88). Here one sees that there were regular sinusoidal variations of velocity, which is a characteristic associated with the initial stages of transition. This time history was the only one, from either Series 3 or 4, to show this feature clearly.

7.5.3 VELOCITY P.S.D. DISTRIBUTIONS

Having examined the time histories one may now turn to the P.S.D. distributions from both Series 3 and 4.

The P.S.D. distributions at all relevant positions within the cavity are discussed.

The discussion begins with the starting corner at the bottom of the heated wall. This is a logical progression from the comments made about the velocity time histories in this region. One then progesses to the other starting corner at the top of the cooled wall to look for any similarities and differences between the characteristics of the two regions.

Following on from this one discusses the P.S.D. distributions at the bottom of the cooled wall and then those of the equivalent region at the top of the heated wall.

Finally, the P.S.D. distributions at mid-height close to the heated wall are discussed

In Figure 7.92 the P.S.D. distributions from Series 3 at x/H = 0.046 and 0.096 (at y ≈ 3.7mm corresponding to the peak in mean velocity) show that there was negligible power in the spectrum above 5Hz. The general shape of the curves were as expected with the largest values of P.S.D. at the lower frequencies.

There was only one identifiable region in Figure 7.92 where a constant power law relation between frequency and P.S.D. could be considered to exist. This was for f ≈ 1-4Hz (wavenumber, n, = 40-144) where the exponent was -5. With an increase in height to x/H = 0.143, a significant increase of P.S.D. occurred in the range 1-10Hz, with peaks at 2.4 and 4.9Hz. So, the transition process in Series 3 is seen to have started by x/H = 0.143, although a very small peak at 2.4Hz was seen in the graph at x/H = 0.096.

For the same heights, but at y ≈ 7.7mm, corresponding to the peak in $u'_{R.M.S.}$, the P.S.D. distributions were slightly different as shown in Figure 7.93. The absolute P.S.D. increased with height at all frequencies, with an additional peak at 7.6Hz shown at x/H = 0.143.

All three frequencies which have been identified so far are multiples of a base frequency. This base frequency is approximately 2.5Hz.

The P.S.D. distribution for x/H = 0.229 from Series 3 at y = 3.95mm (Figure 7.94) shows that the spectral characteristics of the data were those of a nearly fully developed turbulent flow, with only two small peaks at 2.3 and 4.0Hz, and a distinct dissipation sub-range with an exponent of -4.6 (n = 97-∞) relating frequency to P.S.D. (the upper wavenumber limit of ∞ is used merely to show that there was no other sub-range at higher wavenumbers).

At heights above x/H = 0.229 the flow became fully developed with three distinct frequency sub-ranges exhibiting different power law relationships between frequency and P.S.D. (these are discussed later). It was expected that an increase in the base frequency might have occurred as the height increased, as has been observed in vertical flat plate flow, but this has not been observed.

One may compare the P.S.D. distributions of Series 3 and 4 at x/H = 0.229, to show the effect on the start of transition brought about by the reduction in wall temperature difference.

Figure 7.95 shows that, in Series 4 at x/H = 0.229, there were four distinct peaks at 1.9, 3.5, 7.1 and 8.5Hz. These frequencies can be considered to be multiples of a base frequency of 1.8Hz. The differences between Figures 7.94 and 7.95 clearly show that transition started at a greater height in Series 4 than in Series 3. Not only that, but a change in base frequency, from 2.5Hz to 1.8Hz, occurred.

Using equation (2.5) from Gebhart and Mahajan [25] the predicted dominant frequencies for Series 3 at x/H = 0.096 and 0.143 were 2.22 and 2.17Hz, respectively. For Series 4, the frequencies predicted at 0.096, 0.143 and 0.229 were 1.82, 1.78 and 1.72Hz, respectively.

In Series 3 the first small peak in the P.S.D. distributions was seen at x/H = 0.096 with the base frequency being 2.5Hz. This compares favourably with the value of 2.22Hz predicted for this height. In the case of Series 4, the base frequency of 1.8Hz agreed excellently with the predicted frequency of 1.78Hz at x/H = 0.143.

With such reasonable agreement between theory and experimental base frequencies, one sees that, in the stratified cavity flow, there is a decrease in base frequency with decrease in wall temperature difference. In addition one notes that the base frequency remains practically constant with height.

From Chapter 2 one notes that the previously reported dominant frequencies in transition, for the natural convection of air along a vertical flat plate in an isothermal environment, were consistently higher at 3.2-3.6Hz. One is tempted to say that the stratification is responsible for the difference between these and the frequencies found in the cavity flow, but no data are available for flow with a stratified environment, and so it's direct influence on the transition frequency is unknown. One must therefore examine equation (2.5) to see if there is any other possible explanation.

It is seen that the height, x, cancels out overall in equation (2.5) and so it is the wall to environment temperature drop which contributes most significantly to the predicted dominant transition frequency. A lower temperature drop means a lower predicted frequency, a characteristic which has been confirmed in the cavity. Thus the differences between the flat plate and cavity transition frequencies are not so unexpected, as the former frequencies have been noted at higher temperature drops.

Having dealt with the flow at the bottom of the heated wall attention is now turned to the flow at the top of the cooled wall, where the P.S.D. distributions of Series 3 at x/H = 0.849, 0.898 and 0.949 (Figures 7.96 and 7.97) were quite different to those at equivalent heights relating to the flow at the bottom of the heated wall.

At the top of the cooled wall the P.S.D. distributions were essentially those of a turbulent flow (although the absolute values increased slightly with distance down the wall) and small peaks were seen at 2.0, 4.0 and 5.0Hz for x/H = 0.849.

Figures 7.96 and 7.97 show that there were three distinct power law relations between frequency and P.S.D., where the exponents in each relationship varied with distance from the wall. The exponents were -1.3 (n = 22-65), -2.9 (n = 65-160) and -4.8 (n = 160-∞) at y $\simeq$ 4.9mm and -1 (n =

16-48), -2.3 (n = 48-183) and -4.5 (n = 183-∞) at y ≈ 7.9mm, the smaller exponents being applicable to the higher frequencies. The slight change in the power relationship was presumably associated with the change in the vertical temperature gradient, which increased with distance from the wall.

Turning now to the turbulent regions at the top of the heated wall and the bottom of the cooled wall, where the boundary layers were losing fluid, one notes that the power spectra appeared similar.

Consider first the spectra at y ≈ 6.2mm at the bottom of the cooled wall. These spectra consistently showed a relationship with an exponent of -4.6 between frequency and P.S.D. at the higher frequencies. There were two other power relationships discernible (see Figure 7.98) although these did alter with height. At x/H = 0.143 they were -1.8 (n = 35-88) and -2.8 (n = 92-207) and at x/H = 0.046 they were -2.1 (n = 36-120) and -3.4 (n = 126-293).

Further from the wall at y ≈ 11.7mm (Figure 7.99) the exponent applicable to the higher frequencies was -4.0. This was constant for all heights, but at lower frequencies there was only one other clearly discernible sub-range where the exponent decreased, changing from -2.4 (n = 56-209) to -2.8 (n = 71-247) with a decrease in height.

From Figures 7.98 and 7.99 one notes two interesting facts. Firstly, at the lower frequencies the exponent decreased with decreasing height, and secondly, that the exponent of all sub-ranges in the cooled wall flow increased with increasing distance from the wall (this is based on data at the top and bottom of the cooled wall).

The most obvious characteristic which changes with distance from the wall is the vertical temperature gradient, which is zero at the wall, increasing to a maximum somewhere between y = 20 and 50mm from either wall at most heights. It is likely that the increase in stratification contributed significantly to the increase of the exponent of the dissipative sub-range. However, it is unlikely that the exponent is purely a function of the stratification as one expects the exponent to be a function of a dimensionless quantity.

This point can be considered by examining the P.S.D. distributions at the cavity centre for x/H = 0.849, 0.898 and 0.949. These heights were most interesting as the local stratification at the cavity centre was lower than those of the near cooled wall positions already studied.

In the case of Series 3, at x/H = 0.849 and 0.898, the P.S.D. distributions at the cavity centre (Figure 7.100) showed that there was negligible power in the spectrum above 2Hz, and that the exponent relating

frequency to P.S.D. below 2Hz was -3.8. This solitary sub-range must have been a dissipative one. Now the exponent of -3.8 is the highest that has been reported so far. This means that the trend of increasing exponent with increasing stratification was not confirmed.

Further investigation of the variation of exponent with stratification is required to expand on the results at the three top heights. This has been done by bringing together all the available cavity data for velocity P.S.D. distributions and is presented in Section 7.5.4. This investigation deals with the variation of the exponents in all the sub-ranges with the vertical temperature gradient and two forms of the Richardson number.

Staying with Figure 7.100, one notes that the power spectrum at x/H = 0.949 was different at the cavity centre to those at the two lower heights. There were two sub-ranges, as compared to one for the other two heights, with exponents of -2.5 and -3.9 relating frequency to P.S.D. It is presumed that the difference arose because the data at x/H = 0.949 were taken close to the edge of the ceiling boundary layer.

Interestingly two peaks were seen in Figure 7.100 at 2.4Hz and 5.1Hz for x/H = 0.949. These were the dominant frequencies first noted in the heated wall boundary layer at the start of the transition process. The reason for the existence of these peaks is not clear. One may only speculate that by the time the ceiling boundary layer flow had reached the cavity centre-line, heat transfer from the fluid to the ceiling was taking place. This would have caused a downflow of fluid which might have undergone some process which resulted in the two observed peaks.

Ziai [1] showed that heat transfer from the fluid to the ceiling started after the flow had travelled to y/L ≈ 0.57. As the insulation at the ceiling of the present cavity was better than that used by Ziai [1], it was quite possible that heat transfer from the fluid to the ceiling took place before y/L = 0.57. (Whilst the insulation was improved, heat transfer still took place through the ceiling, but the increase in the near ceiling fluid temperature would have meant that heat transfer from the fluid was more likely before the flow reached y/L = 0.57). This gives some limited support to the proposal that there was some downflow of fluid at y/L = 0.5.

Returning to the variation of the exponent with height in the two lower frequency ranges at the bottom of the cooled wall, one may speculate that the decrease in the exponent might be associated with a local variation in a (yet to be properly determined) dimensionless quantity. Such a change would not be unlikely as the flow neared the floor of the cavity. However, one must also seek to explain why the exponent of the dissipative

sub-range did not change. One can only speculate that in this region, the local variation of the dimensionless quantity, whilst significant enough to alter the buoyancy and inertial sub-range exponents, was not significant enough to alter the exponent of the dissipative sub-range.

One point to consider is the effect of potential variables (within any dimensionless quantity) on any sub-range.

The dissipative sub-range is associated with the smallest scale turbulent eddies, which are expected to be less anisotropic than those eddies at the larger scales associated with the lower frequencies. Therefore, any change in stratification could be expected to have less effect on the dissipative sub-range than any other. Indeed, for each lateral position referred to at the bottom of the cooled wall, the local stratification was constant with height (although different at each lateral position).

As the higher frequency sub-range is associated with dissipation, then with a decrease of turbulence intensity with height one might expect this range to become more dominant. This appears to have been the case as the lower frequency limit decreased with decreasing height.

In contrast to the flow at the bottom of the cooled wall, the equivalent heights at the top of the heated wall (x/H = 0.849, 0.898 and 0.949 in Figures 7.101 and 7.102) all basically showed consistently similar P.S.D. distributions, with the absolute values being almost identical at each height, although the exponent of each sub-range again changed with distance from the wall. At y ≃ 8.8mm the exponents of the sub-ranges were -1.5 (n = 20-68), -2.3 (n = 68-161) and -4 (n = 161-∞), whereas at y ≃ 16.4mm the exponents were -1.8 (n = 22-93), -2.8 (n = 93-252) and -4.4 (n = 252-∞). The trend of the exponents, with distance from the wall, was opposite to that which occurred in the cooled wall flow. This evidence gives further support to the idea that the exponent of a sub-range is not dependent on just the local stratification, but also on other local parameters.

Checks made at x/H = 0.497 (Figures 7.103 and 7.104) showed that at y = 2.61mm the exponents were -0.9 (n = 13-70), -2.7 (n = 74-213) and -4.4 (n = 213-∞) whereas at y = 6.63mm the exponents were -0.7 (n = 8-39), -2.1 (n = 40-164) and -4.1 (n = 178-∞). Here, the previously observed trend from the cooled wall data was seen again. Thus, the trends in the data at the top of the heated wall would appear to be due to a local effect.

The most obvious difference between the data at the top of the heated wall and the rest, is that they were taken from a region where a "substantial" flow was turning through a corner (by using the term

"substantial" one seeks to emphasize the differences between this flow and that at the bottom of the cooled wall where the mass flow, heat transfer and boundary layer thickness were all much smaller compared to those at the top of the heated wall). One might therefore expect a region at the top of the heated wall to promote a substantial increase in the lateral mean velocity and $\overline{u'v'}$, as well as some decrease in $\overline{u'T'}$. These quantities have been investigated in earlier Sections which show the expected trends.

7.5.4 COMPARISON OF EXPERIMENTAL AND THEORETICALLY PREDICTED SUB-RANGE EXPONENTS FOR VELOCITY P.S.D. DISTRIBUTIONS

The results regarding the exponents of the sub-ranges identified in the velocity data must now be compared to those predicted in the work reviewed in Chapter 2.

The dissipative sub-range, at the higher frequencies, is the easiest to deal with first. The exponent for this sub-range ranged from -3.8 to -5 with a probable dependence on the local stratification being evident in some cases. For an unstratified flow Corrsin [50] had predicted an exponent of -7 for the dissipative sub-range in a temperature field. (This prediction was unchallenged by the work of Bolgiano [51] for a stratified environment in respect of both temperature and velocity fields). This has been shown to be inapplicable to the present cavity flow.

As regards experimental data, the exponents of the dissipative sub-range observed in natural convection flows with an isothermal environment have been -17/3 by Dastbaz [26] and -5 by Smith [27]. As the environment was nominally isothermal in these two works, one would expect these exponents to form the upper limit for the dissipative sub-range in the natural convection of air, thus casting further doubt on the applicablity of the prediction of Corrsin [50] to velocity data.

Next, one may consider the buoyancy sub-range (at the lowest frequencies) which was predicted by Bolgiano [51] to have an exponent of -11/5. This sub-range was considered to result from the stratification causing anisotropic turbulence, however, the evidence from Figure 7.69 has indicated a trend towards isotropic turbulence (within the cavity) with distance from the wall which was generally associated with an increase in stratification.

As regards the exponent of the buoyancy sub-range, it has varied from -1 to -2.1 in the present study. Typically, previous experimental results have yielded a power of -5/3 for the buoyancy sub-range, which is approximately in the middle of the results of the present study. In relation

to this it must be noted that many researchers have deliberately fitted their data with the -5/3 range, rather than using a "line of best fit", although this does not apply to the results of Smith [27] who found an exponent of -1 to be applicable to the lowest frequencies.

It is pertinent to mention here that the present author produced lines of best fit through his data after initially fixing the range of frequencies over which any line would apply. Such objective decisions were not difficult as the data easily lent themselves to such an approach.

One would expect to see any buoyancy sub-range become more prominent further away from either wall as the stratification increased. Such a trend was not seen at any height with respect to either frequency or wavenumber.

Finally, there is the inertial sub-range, existing at intermediate frequencies. Bolgiano [51] predicted a power of -5/3 for this sub-range, but most experimental evidence points to a power of -3. Only Smith [27] found a power of -5/3 at intermediate frequencies. The present study has shown up a range of powers from -2.4 to -2.8 for the inertial sub-range, which certainly does not support the proposed existence of an inertial sub-range with a power of -5/3.

The final point to be considered in this Section is the variation of exponent (from any range) with stratification and suitable dimensionless groups. In selecting a suitable dimensionless group one must consider those parameters which, from the results presented, may be linked to the variation of the exponents.

The results have indicated that the parameters dT/dx, v, $\overline{u'v'}$ and $\overline{u'T'}$ may be major contributors to any dimensionless group. One may take the comments of Bolgiano [51] as a starting point. He stated that some measurements of the exponent of the dissipative sub-range (in the atmosphere) indicated that it varied with the Richardson number. (A negative correlation between exponent and Richardson number).

Now, the two forms of the Richardson number which were mentioned in Chapter 2 were R_F and R_G. Both of these feature dv/dx in their denominators, v being one of the parameters which the author has proposed as influencing the exponent of a sub-range.

Other proposed parameters are also present in both Richardson numbers, dT/dx being present in R_G and the two turbulence quantities $\overline{u'v'}$ and $\overline{u'T'}$ being present in R_F.

All available data for the three sub-ranges have been plotted. The nature of the plots have been exponent against dT/dx, R_G and R_F. The graphs

are shown in Figures 7.105, 7.106, and 7.107 for the buoyancy, inertial and dissipative sub-ranges, respectively.

First consider Figure 7.105 which depicts the graphs for the buoyancy sub-range. Both the graphs featuring dT/dx and R_G showed considerable scatter, only the graph featuring R_F showed an indication of increasing exponent with increasing R_F. The correlation coefficient for the latter graph was 0.52. It is obvious from the graph that much more data would be required to provide a better indication of any trend.

One must also bear in mind that in all the quantities dT/dx, R_G and R_F, manual interpretation has been used extensively to arrive at the final values. Therefore all values are subject to uncertainties, especially the values of dv/dx.

Substantial improvements in the determination of a trend of exponent with either of dT/dx, R_G or R_F could be made in two ways. Firstly, by the calculation of a large number of P.S.D. distributions from existing tape data, and secondly, by a separate investigation which would measure not only the lateral velocity, v, directly but also the local value of dT/dx with a vertical array of thermocouples, as well as the other parameters measured in the present study.

Pressing on with the variation of exponents with dT/dx, R_G and R_F one can now consider the inertial sub-range using Figure 7.106. None of the graphs showed any trend, which is not unexpected, as the inertial sub-range has been expected to universally exist in stratified and unstratified flows, and so zero correlation would be expected.

Moving on to the dissipative sub-range in Figure 7.107 one notes a possible variation of decreasing exponent with increasing dT/dx or R_F. The correlation coefficients of both these graphs were approximatly the same, at -0.58 and -0.54 respectively. (This is the trend reported by Bolgiano [51]). But, there are two points to bear in mind. Firstly, the removal of a few points on either graph could seriously reduce the modulus of the correlation coefficient, and secondly, the large scatter in the R_G graph shows the effect of uncertainties in dv/dx as this parameter is the major factor in the difference between the graphs using dT/dx and R_G.

Again, it can only be repeated that an in-depth study is required to determine proper trends in the variation of exponents with the Richardson numbers. One must also take note of the fact that a different dimensionless group may affect the exponents, indeed the degree of anisotropy of the flow may have some effect.

7.5.5 TEMPERATURE P.S.D. DISTRIBUTIONS

The sequence of regions discussed in this Section is different from that of Section 7.5.3. The first region discussed is that at the bottom of the heated wall, but then progress is made up the heated wall and then over to the cooled wall.

Consider Figure 7.108 which shows the temperature P.S.D. distribution at the heated wall for Series 3 at x/H = 0.096 for y = 4.24 and 8.24mm. For both lateral positions one can clearly see that there were two distinct frequency sub-ranges. The sub-range at the lower frequencies exhibited an exponent of -2 for both lateral positions, whereas the exponent of the sub-range at the higher frequencies was different at each lateral position. At y ≈ 3.7mm the exponent was -8.6 and at y ≈ 7.7mm it was -6.9.

The sub-ranges with the exponents of -8.6 and -6.9 were clearly dissipative sub-ranges, as for the other sub-ranges with an exponent of -2, it is assumed that these were buoyancy sub-ranges.

From Figure 7.108 one notes that for a given sub-range the increase of the exponent with increasing lateral distance was the same trend as that observed in the velocity P.S.D. distributions at the same height. In addition it is seen that the exponents of the temperature P.S.D. distributions were significantly lower than those of the velocity data.

Now, at the same height and lateral positions of Figure 7.108, the velocity P.S.D. distributions showed a peak at the base transition frequency. Such a peak was not shown in the temperature P.S.D. at y = 4.24mm, but there was a very small peak at 2.4Hz for y = 8.24mm. This is exactly the same frequency as shown in the velocity data.

The lack of a discernible inertial sub-range in Figure 7.108 may possibly be explained by a slight modification of the curve in the region of f = 2.4Hz. As it could be argued that the small peak seen at this frequency (for y = 8.24mm) was due to experimental uncertainty, this explanation does give some support to the proposal that the beginning of the temperature field transition process was seen at x/H = 0.096.

Moving up to x/H = 0.143, for y = 3.99 and 8.03mm, one sees from Figure 7.109 that several peaks were present, these peaks being more prominent than those in the velocity data. The peaks were at 2.3, 4.8, 8.6 and 12.1Hz and can be considered to be multiples of 2.4Hz (compared to 2.5Hz for the velocity field) except for that at 8.6Hz which was approximately 3.6 times the base frequency.

There were substantial peaks in Figure 7.108 at 14.7Hz. These peaks may have been due to a transient fault in the power supply of the signal

conditioning units. Ziai [1] had previously observed peaks at relatively high frequencies which he attributed to an effect of the PDP 11/34A power supply unit. It is unlikely that the same problem arose in the present study, especially as no such peaks were observed in the velocity data.

It may be that the peak in Figure 7.108 at 8.6Hz may also have been due to the same transient fault in the signal conditioning units. Certainly, the present author did have problems with the stability of the output from the signal conditioning units at different times during the study.

The temperature and velocity P.S.D. distributions from Series 3 at x/H = 0.096 and 0.143 have not conclusively shown that transition occurs first in the velocity boundary layer. There is only an indication from Figures 7.92 and 7.108 that this may be so.

Consider Figure 7.110 which depicts P.S.D. data from Series 4 at x/H = 0.229 and y = 4.26 and 8.26mm, with the latter lateral position corresponding to the peak in $T'_{R.M.S.}$. One notes that there were several peaks located at 1.7, 3.5, 5.2, 6.8, 10.6, 12.0, 13.8 and 18.2Hz. These are all multiples of a base frequency of approximately 1.7Hz. This base frequency is very close to that observed in the equivalent velocity P.S.D. distribution although it is slightly lower.

As regards the dominant frequencies during transition for both Series 3 and 4, there was excellent agreement between those present in the temperature and velocity data, although in both Series the base frequency in the temperature data was slightly lower than that in the velocity data by 0.1Hz.

Both Series 3 and 4 P.S.D. distributions have shown that there were no dominant frequencies in the turbulence beyond the height of x/H = 0.229, the distributions at x/H = 0.360 being those of a turbulent flow (see Figure 7.111 for Series 4 temperature P.S.D. distribution at x/H = 0.360).

From Figure 7.111 one notes that there were three distinct frequency sub-ranges in each of the three P.S.D. distributions at y = 4.02, 8.02 and 60mm.

For the dissipative sub-ranges in Figure 7.111 the exponent increased with increasing lateral distance from -6.7 to -5.9 to -5. In the case of the other two sub-ranges there was little difference between the exponents at the two smallest y positions, but there was an increase in exponent at y = 60mm. This observation does not correspond to the proposal in Section 7.5.3 that any change in local stratification may be expected to have less effect on the dissipative sub-range of the velocity data. One may consider the difference to be explained by the fact that the transition process was not

finished at x/H = 0.360, and so some local effect may have been responsible, or that the behaviour of the exponents of the temperature data are basically different from those of the velocity data.

Most interesting was the increase in the range of frequencies applicable to the first sub-ranges (assumed to be buoyancy sub-ranges) of Figure 7.111, which was accompanied by a decrease in the range of frequencies applicable to the intermediate sub-range.

As in the velocity P.S.D. distributions, the range in wavenumbers for the temperature P.S.D. distributions also changed, there being no correlation between wavenumber limits and sub-ranges when using the Taylor definition of wavenumber.

The increase of the exponent with increasing lateral distance was again shown for Series 3 at x/H = 0.497 (see Figure 7.112) at the heated wall. However, here one sees that it was possible to draw in a fourth sub-range. Such a fourth sub-range was also seen in Figures 7.113 and 7.114 which, respectively, show the P.S.D. distributions at constant lateral positions for x/H = 0.849, 0.898 and 0.949 at the heated and cooled walls.

The exponents of the sub-ranges in Figure 7.112 were -1.1, -2.8, -4.6 and -6.1 at y = 4.16mm and -1.1, -2.7, -4.4 and -5.4 at y = 8.15mm. The presence of these four sub-ranges raises the question of which sub-range is which? Clearly the dissipative sub-range must be the one with the lowest exponent at each lateral position. The values of these exponents were similar to those found in Figure 7.111. If one assumes that a relevant local dimensionless quantity was approximately the same at corresponding lateral positions for the data from Figures 7.111 and 7.112, then one would be led to consider that the difference between Figures 7.111 and 7.112, in terms of the sub-ranges, would be an additional sub-range at the lowest frequencies.

The suggestion of a "new" sub-range occurring at the lowest frequencies does not fit in with the expectation that it is the buoyancy sub-range which occurs at the lowest frequencies. One is therefore faced with the possibility that a buoyancy sub-range was not discernible in the previously presented temperature P.S.D. distributions, and so the "new" sub-range is that occurring when the exponent is $\simeq$ -4.5. Further discussion of this point is taken up in Section 7.5.6 when all the temperature data have been presented.

Figure 7.113 shows the P.S.D. distributions at y $\simeq$ 3.5mm from the heated wall, for x/H = 0.849, 0.898 and 0.949. The distributions were virtually the same for each height and showed four sub-ranges with

exponents of -0.9, -3, -4.7 and -6.9. These values were similar to those found in Figure 7.112.

In Figure 7.114 the lateral position was y ≈ 3.4mm from the cooled wall (again for x/H = 0.849, 0.898 and 0.949) and the exponents of the first three sub-ranges were constant at -1.8, -4.6 and -6.7 for each height. The fourth sub-range differed in that the exponent was -7 at x/H = 0.849 and 0.898 and -8.5 at 0.949. The exponents of the two extreme sub-ranges were similar to those at x/H = 0.096 at the heated wall, whilst the middle two were similar to those of the latter two sub-ranges in Figures 7.112 and 7.113.

7.5.6 COMPARISON OF EXPERIMENTAL AND THEORETICALLY PREDICTED SUB-RANGE EXPONENTS FOR TEMPERATURE P.S.D. DISTRIBUTIONS

Only three sub-ranges were anticipated for the temperature data. A dissipative sub-range with an exponent of -7 predicted by Corrsin [50], a buoyancy sub-range with an exponent of -7/5 predicted by Bolgiano [51] and an intermediate inertial sub-range with an exponent of either -5/3 predicted by Corrsin [50] or -3 which has been observed by previous researchers.

The present results are unique in showing four sub-ranges in regions of fully developed turbulent flow.

Each of these four sub-ranges were distinct and did not arise because of visual misinterpretation.

Looking firstly at the dissipative sub-range one notes that the exponent for this has ranged from -8.6 to -5.9 close to the walls to -5 further from the walls.

The exponents applicable to the near wall regions were in reasonable agreement with the -7 power predicted by Corrsin [50] for a non-stratified environment, although the minimum value was less than -7. This exponent, predicted by Corrsin [50], was not challenged by the work of Bolgiano [51] for a stratified environment.

The predicted buoyancy sub-range with an exponent of -7/5 compared favourably with the first sub-range found in the fully developed flow along the heated wall at x/H = 0.497, 0.849, 0.898 and 0.949, as well as that at x/H = 0.849, 0.898 and 0.949 near to the cooled wall. The exponent was found to vary from -0.9 to -1.8. As in the velocity data the predicted exponent was approximately in the middle of the observed exponent range.

An inertial sub-range with an exponent of -3 has consistently been presented for temperature data which is reflected in the presently

identified sub-range showing exponents varying from -2.5 to -3 in near wall regions, except for the flow very close to the top of the cooled wall were it was -4.6.

The final sub-range which has been identified has exhibited exponents varying from -4.3 to -4.7 for the majority of near wall regions, except for the flow very close to the top of the cooled wall where it was -6.7. No explanation for the existence of a fourth sub-range is presently available.

A comparison of the exponents from the velocity and temperature data would be useful in attempting to determine whether or not the present author has designated the sub-ranges correctly.

The exponents of the dissipative sub-range for the temperature data were consistently lower than those for the velocity data. If the same trend were to continue for the buoyancy and inertial sub-ranges then the currently designated sub-ranges would appear to be incorrect, with the "new" sub-range existing at the lowest frequencies. But, such a proposition is countered by the reasonable agreement between predicted values of the exponent and the experimental values. One also has to consider the fact that the buoyancy sub-range is expected to exist at the lowest frequencies.

By assuming that the current designation is correct, one may look at the possibility of the last two sub-ranges at the higher frequencies (where four occur) of being connected in some way. Whilst each of the two sub-ranges are easily identified one may also draw a reasonable straight line through both. In this respect the term reasonable is used to indicate comparison with the data presented by other authors which have not been as detailed as those of the present study. Thus it may be that the dissipative sub-range of the temperature field can be sub-divided into two sub-ranges with an influence of the thermal conductivity being evident.

Assuming then that the first sub-range identified is the buoyancy sub-range, the second the inertial sub-range and the last the dissipative sub-range then the same exercise of plotting exponent against dT/dx, R_G and R_F yields Figures 7.115-7.118, where Figure 7.117 is that of the "new" sub-range. Note that the Series 4 data at x/H = 0.360 are not presented as R_G and R_F could not be calculated for Series 4.

The buoyancy sub-range data of Figure 7.115 showed a negative correlation for all three graphs, the strongest being for the graphs utilizing dT/dx and R_G. This is opposite to that found for the velocity data in the exponent/R_F graph of Figure 7.115.

The inertial sub-range graphs of Figure 7.116 were similar to those of the velocity data in showing little or no correlation.

The "new" sub-range graphs of Figure 7.117 were very similar to those of Figure 7.116 in that there was little or no correlation.

One notes that Bolgiano [51] reported that the magnitude of the exponent exhibited a strong positive correlation with the Richardson number. This means that the exponent would be expected to decrease with increasing Richardson number. The graphs of Figure 7.118 indicate that such a trend may be present in the current data for the dissipative sub-range with respect to dT/dx and R_G. A similar trend was seen in the velocity data of Figure 7.117.

7.5.7 FREQUENCY AND WAVENUMBER RANGES IN RELATION TO THE SUB-RANGES

There was no consistency in either frequency or wavenumber for the limits of any sub-range as the lateral position varied, for either velocity or temperature data.

It was expected that the sub-ranges would be limited by specific wavenumbers. This may be accounted for in two ways. Either the definition of wavenumber used in this study is not applicable, or the results presented here have been incorrect.

The present author is unable to directly comment on the applicability of the wavenumber definition and so must resort to proving the quantitative and qualitative nature of his P.S.D. calculations. This is very important especially in view of the fact that the temperature P.S.D. distributions of the present study are not the same as those of Ziai [1] which were calculated from data gathered using the same equipment.

7.5.8 JUSTIFICATION OF THE VALIDITY OF THE P.S.D. CALCULATIONS

One can argue that the present P.S.D. results are valid in two ways. Firstly, in comparison with the manner in which the P.S.D. distributions of Ziai [1] were analysized, amd secondly in comparison with the results of Giel and Schmidt [15].

As previously stated Ziai [1] did not fit "lines of best fit" to his data, instead he merely superimposed lines with gradients of -5/3 and -3 on his graphs, and, because there was reasonable agreement between these and the experimental data, claimed that the sub-range powers were confirmed.

One may also question the program which was used by Ziai to calculate his P.S.D.'s. The program was an adaptation of one which was written by Dastbaz [26]. As far as the author is aware no test data were utilized by

Ziai to confirm the validity of the program. The only tests carried out on the program appear to be those of Dastbaz [26] who only used a random "white noise" signal to test it.

In contrast, the present author has presented proof of the validity of the present program in accurately detecting a test frequency, and in calculating correct absolute values. It is acknowledged that the output from both the present and past programs would be different in the sense that the spectral "window" in each case was different, but, it is not anticipated that this could cause such differences between the present data and that of Ziai [1].

The second argument for the validity of the present temperature P.S.D. distributions comes from the comparison of the present data with that of Giel and Schmidt [15]. It has been estimated that they found sub-ranges with powers of -3.75 and -6, which agree reasonably with two of the sub-ranges in the present data. In addition, one notes that their experimentally determined dominant transition frequencies were in very close agreement with those predicted by Gebhart and Mahajan [25], as is the case for the present cavity data. In this respect it is interesting to note that Ziai [1] did not comment on any transition frequencies.

Without other cavity, or flat plate, data to compare the present results with, one cannot comment further. But, the present author feels that the present results are quite valid and awaits their confirmation in future publications.

7.5.9 SUMMARY OF THE FINDINGS FROM THE P.S.D. CALCULATIONS

The flow at the bottom of the heated wall in the Q.M.C. Series has been shown to be predominantly laminar. This means that for the values of Ra_H studied in Series 1, 2, 3, 4 and 5 the regime type was transitional boundary layer.

The flow at the top of the cooled wall was turbulent, and so the flow within the cavity was not antisymmetric. This must have been due to different thermal boundary conditions on the floor and ceiling resulting in a near total collapse of the turbulence along the floor but not along the ceiling.

The base frequencies during transition were 2.5 and 2.4Hz for the velocity and temperature fields, respectively, for Series 3 and 1.8 and 1.7Hz for the velocity and temperature fields of Series 4.

The experimental frequencies agreed well with those predicted using equation (2.5). The differences between the dominant frequencies of each Series being applicable to different local temperature drops.

The exponent relating P.S.D. to frequency in any sub-range has been shown to vary. It is proposed that the variation of stratification with lateral distance is partially responsible for this.

Three sub-ranges were found in the velocity data, whilst four were found in the temperature data. The exponents for each corresponding buoyancy and inertial sub-range of the velocity and temperature data were, in general, similar, whereas those of the dissipative sub-range for the temperature data were generally lower than those for the velocity data.

FIGURE 7.1

PROFILES OF NON-DIMENSIONAL MEAN

TEMPERATURE FOR SERIES 3 ($\Delta T \approx 45.8K$)

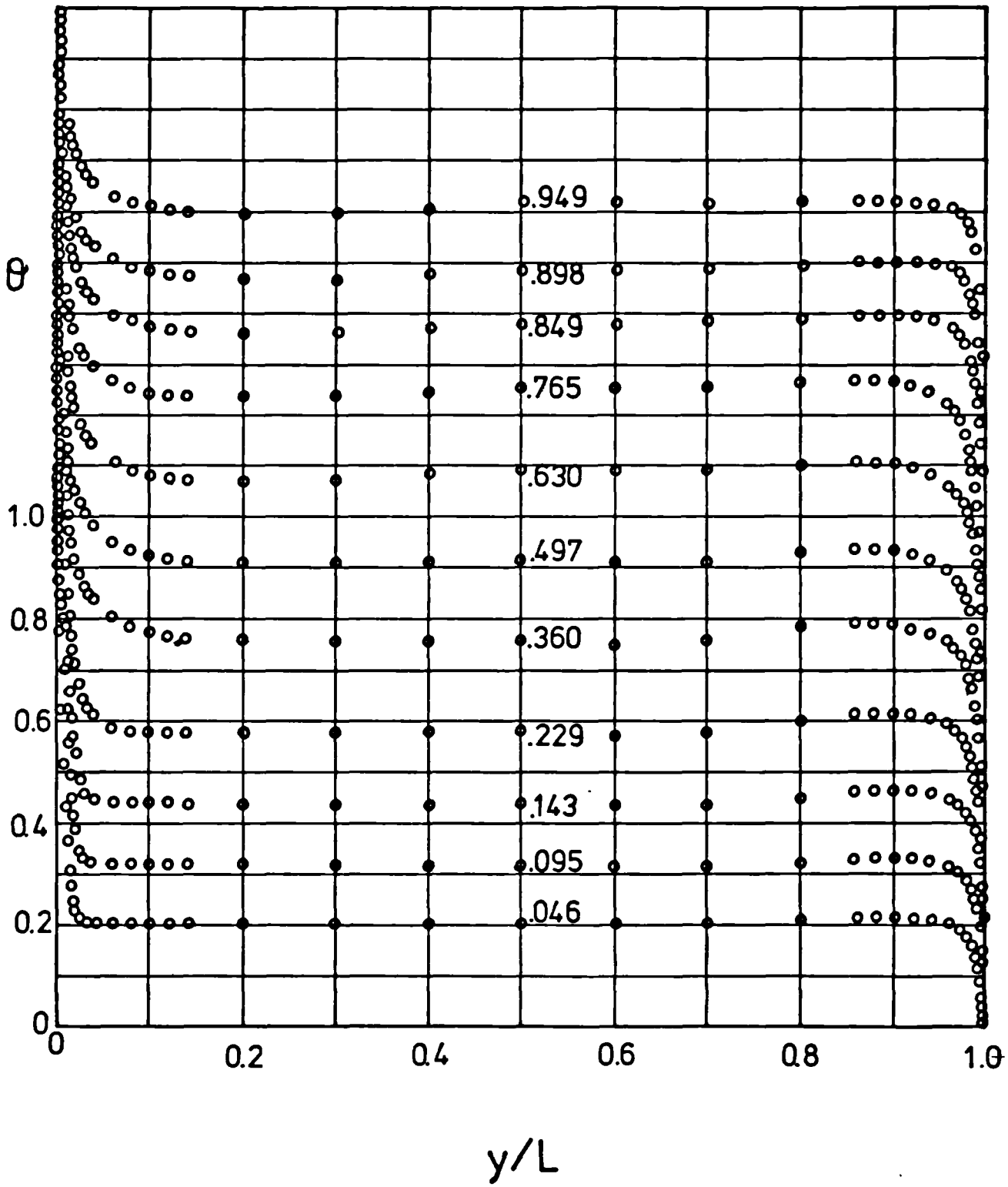

FIGURE 7.2

PROFILES OF NON-DIMENSIONAL MEAN

TEMPERATURE FOR SERIES 6 ($\Delta T \approx 42.5K$)

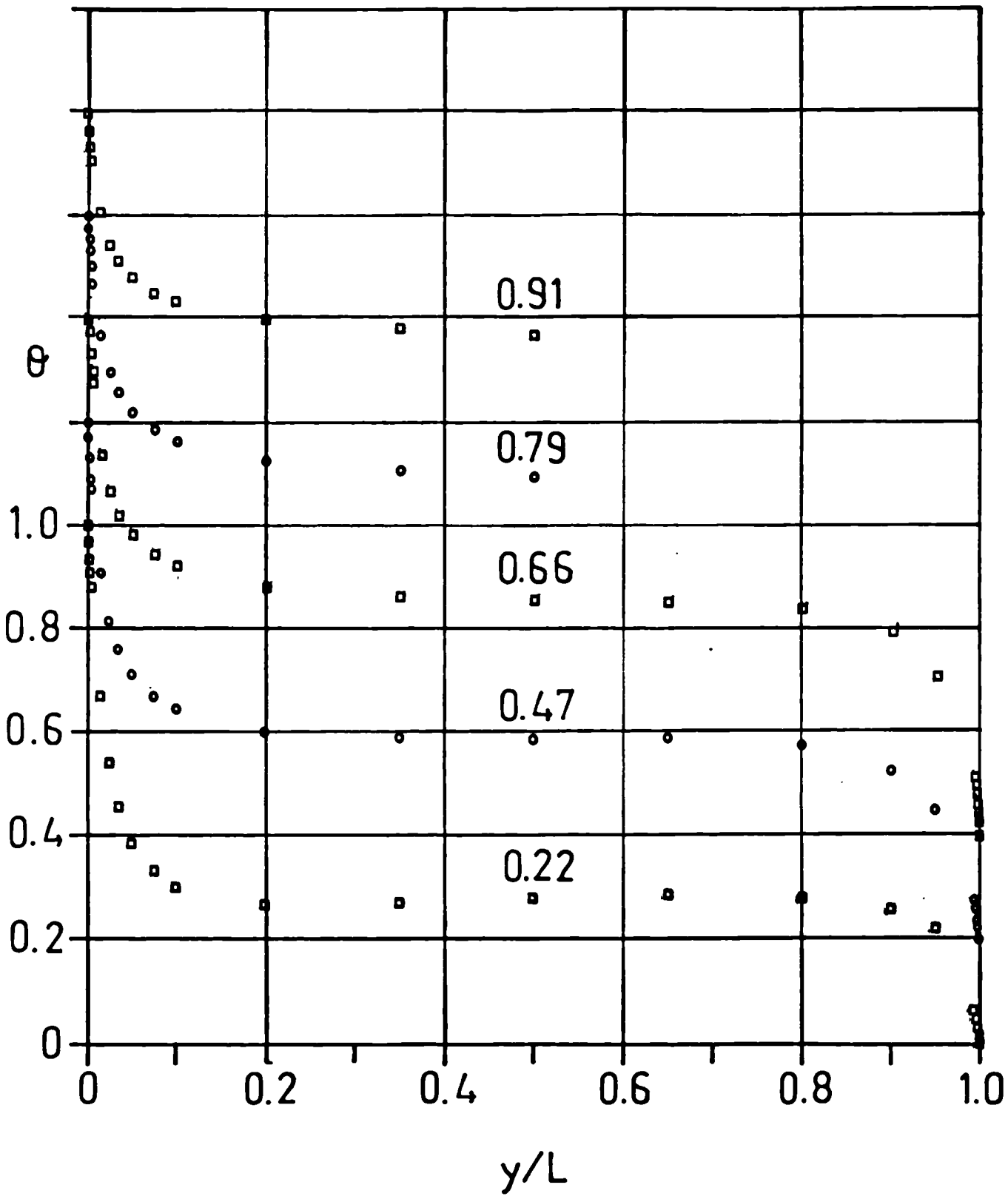

FIGURE 7.3

PROFILES OF NON-DIMENSIONAL

T'R.M.S. FOR SERIES 3 ($\Delta T \approx 45.8K$)

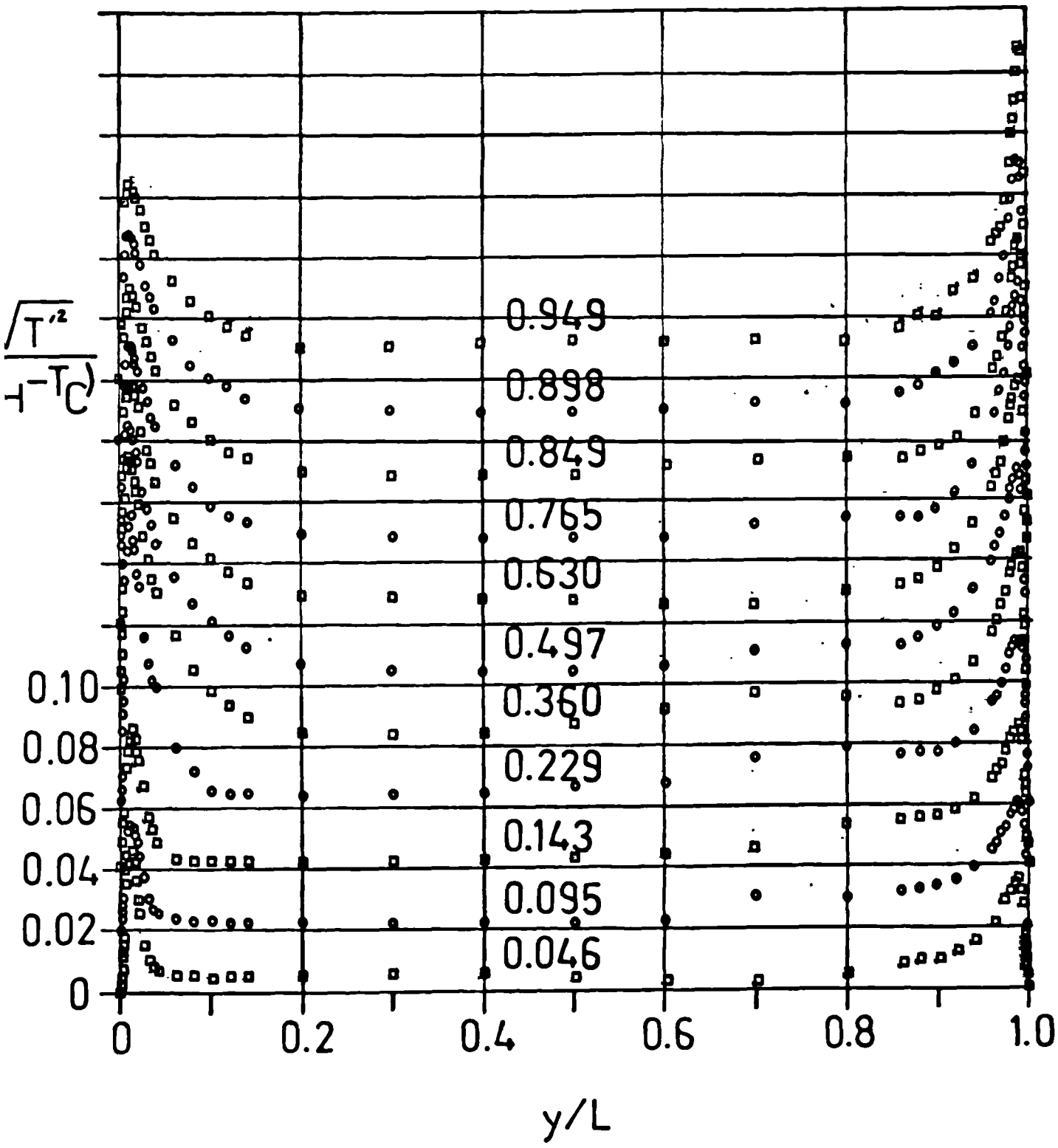

FIGURE 7.4

PROFILES OF NON-DIMENSIONAL

T'R.M.S. FOR SERIES 6 ($\Delta T \simeq 42.5K$)

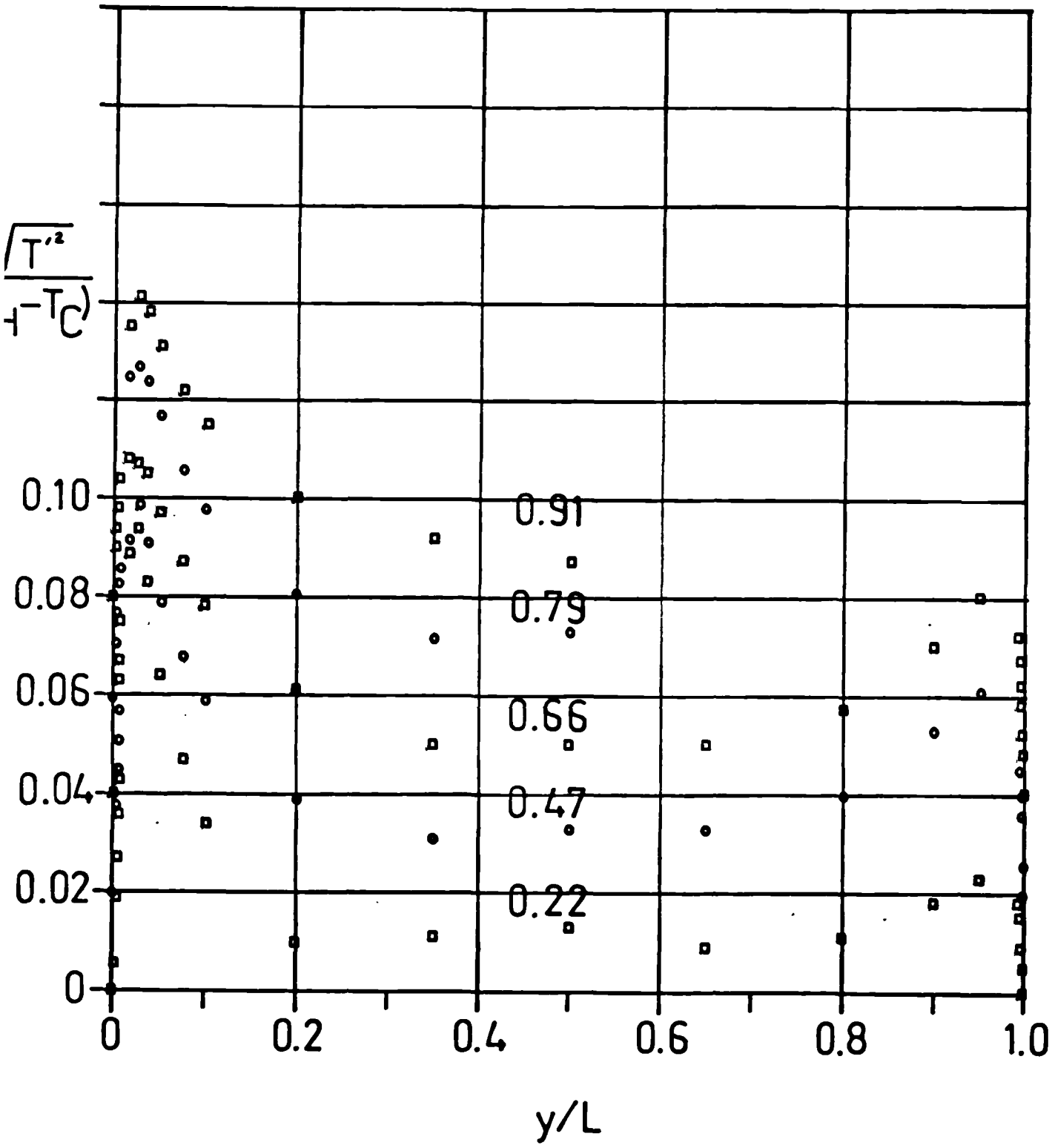

FIGURE 7.5

THETA AGAINST Nu_y AT THE HEATED WALL

OF SERIES 3, WITH T_{MIN} AS THE REFERENCE TEMPERATURE

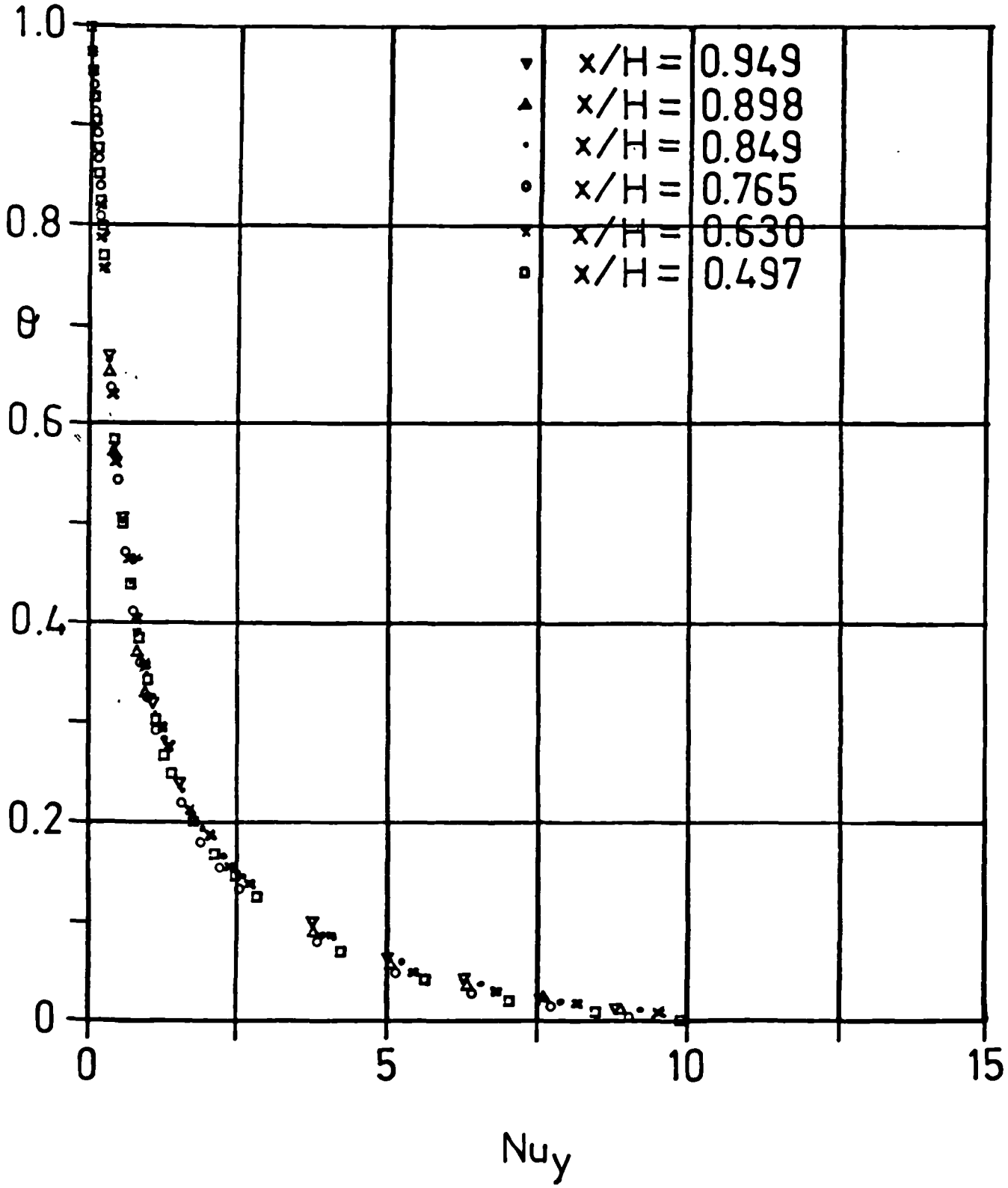

FIGURE 7.6

THETA AGAINST Nu_y AT THE HEATED WALL

OF SERIES 3, WITH T_∞ AS THE REFERENCE TEMPERATURE

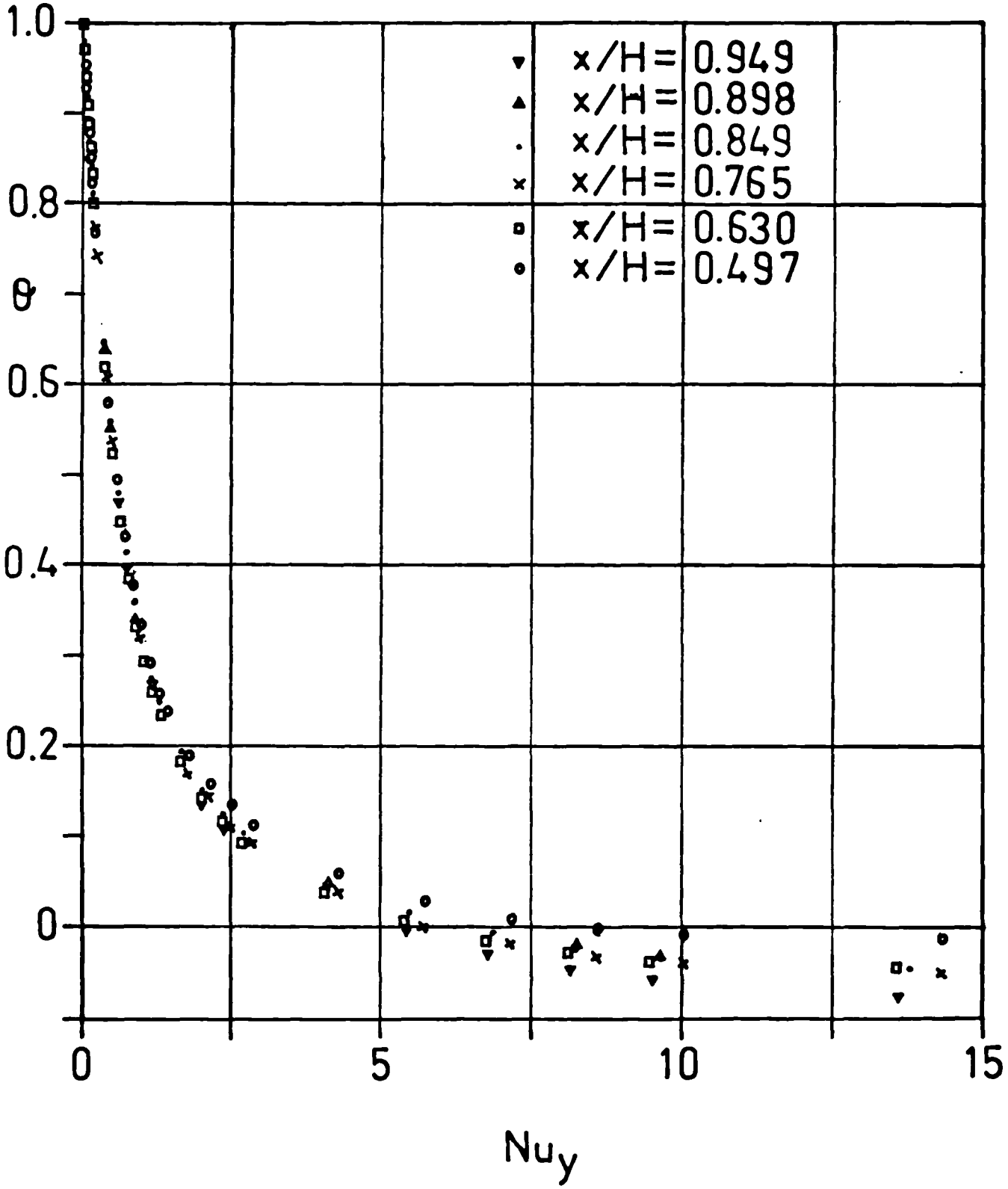

FIGURE 7.7

THETA AGAINST Nu_y AT THE HEATED WALL

OF SERIES 4, WITH T_{MIN} AS THE REFERENCE TEMPERATURE

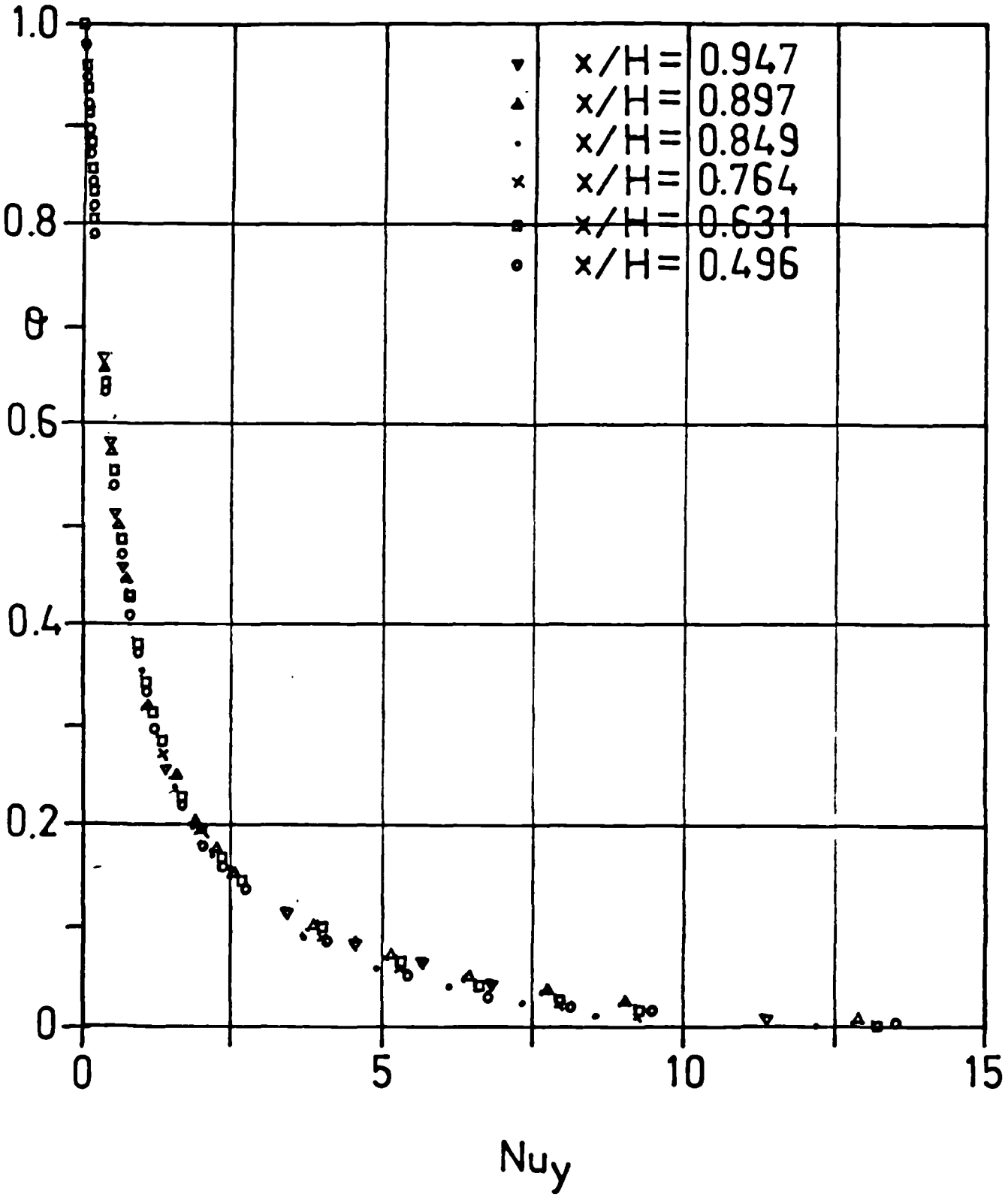

FIGURE 7.8

THETA AGAINST Nu_y AT THE HEATED WALL

OF SERIES 4, WITH T_∞ AS THE REFERENCE TEMPERATURE

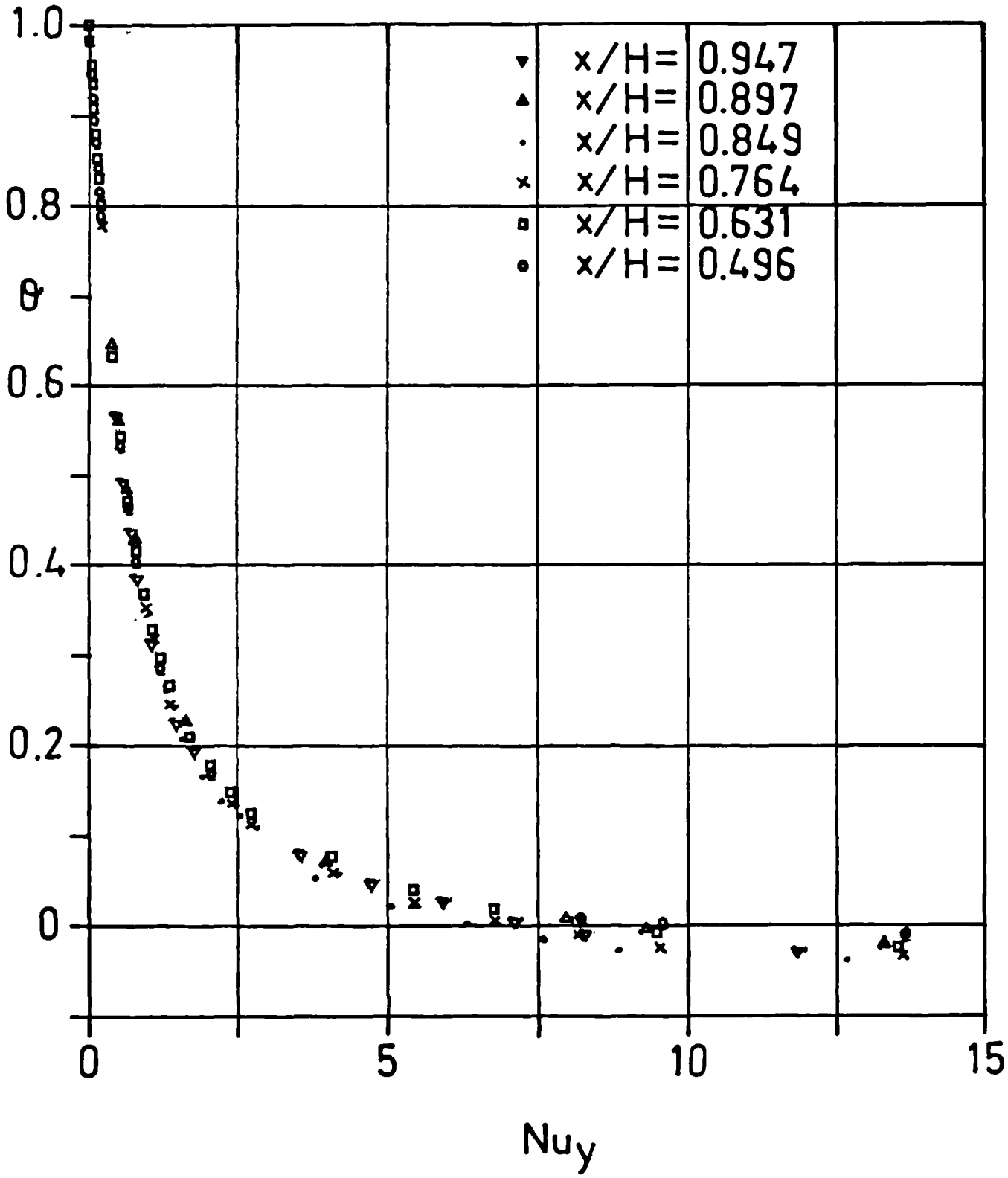

FIGURE 7.9

THETA AGAINST Nu_y AT THE HEATED WALL

OF SERIES 5, WITH T_{MIN} AS THE REFERENCE TEMPERATURE

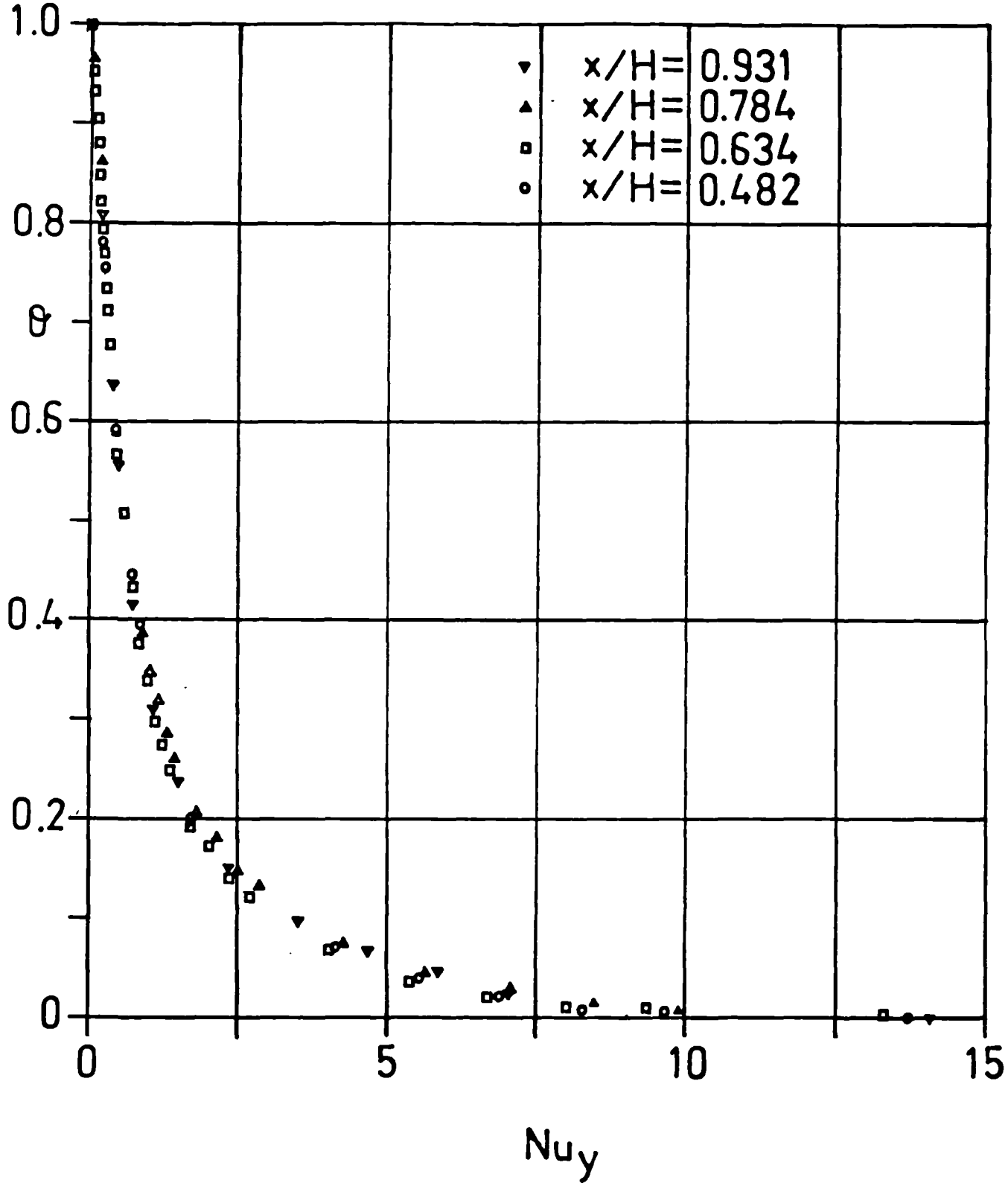

FIGURE 7.10

THETA AGAINST Nu_y AT THE HEATED WALL

OF SERIES 6, WITH T_{MIN} AS THE REFERENCE TEMPERATURE

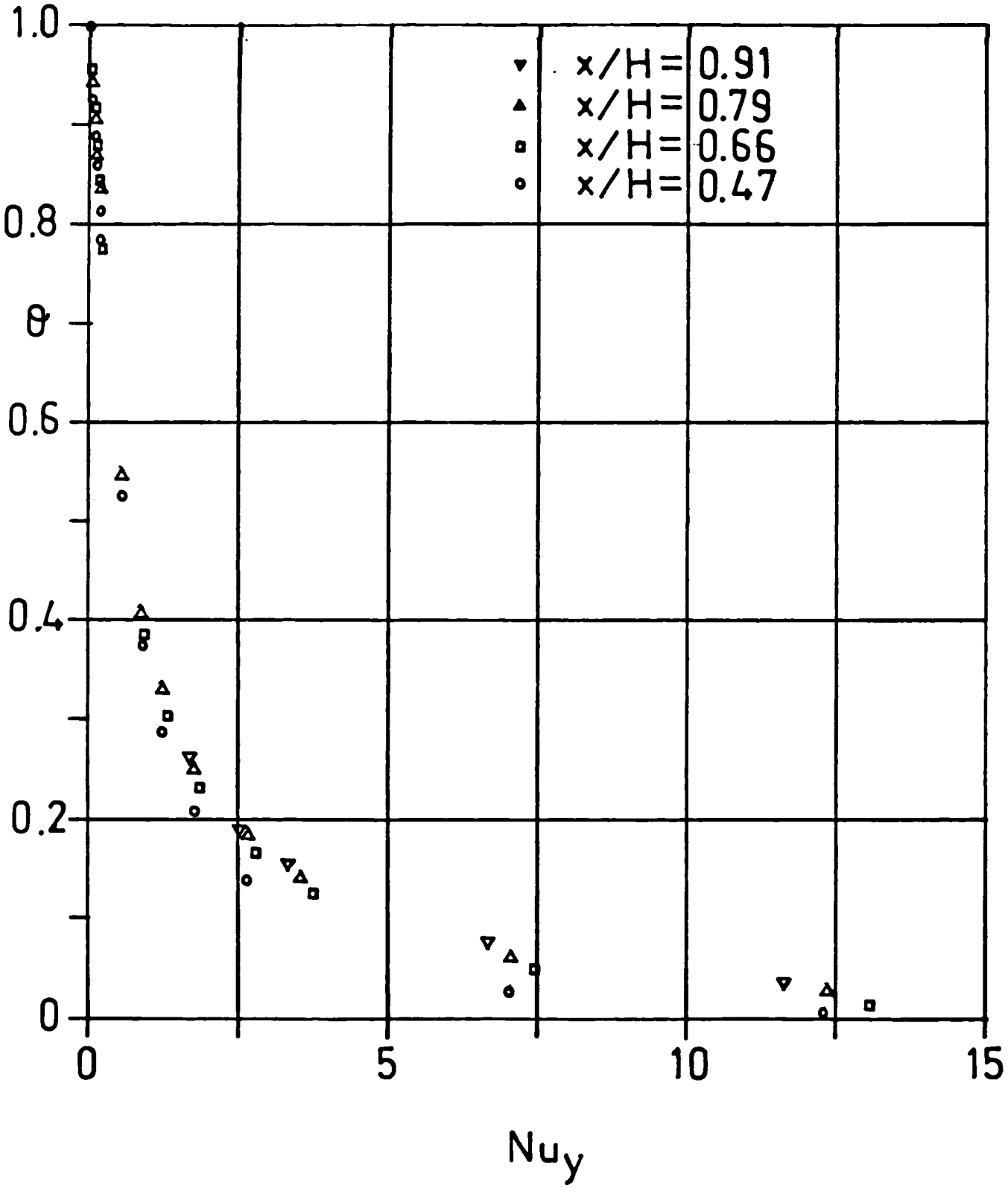

FIGURE 7.11

THETA AGAINST Nu_Y AT THE HEATED WALL

OF SERIES 3, 4, 5 AND 6, WITH T_{MIN} AS THE REFERENCE TEMPERATURE

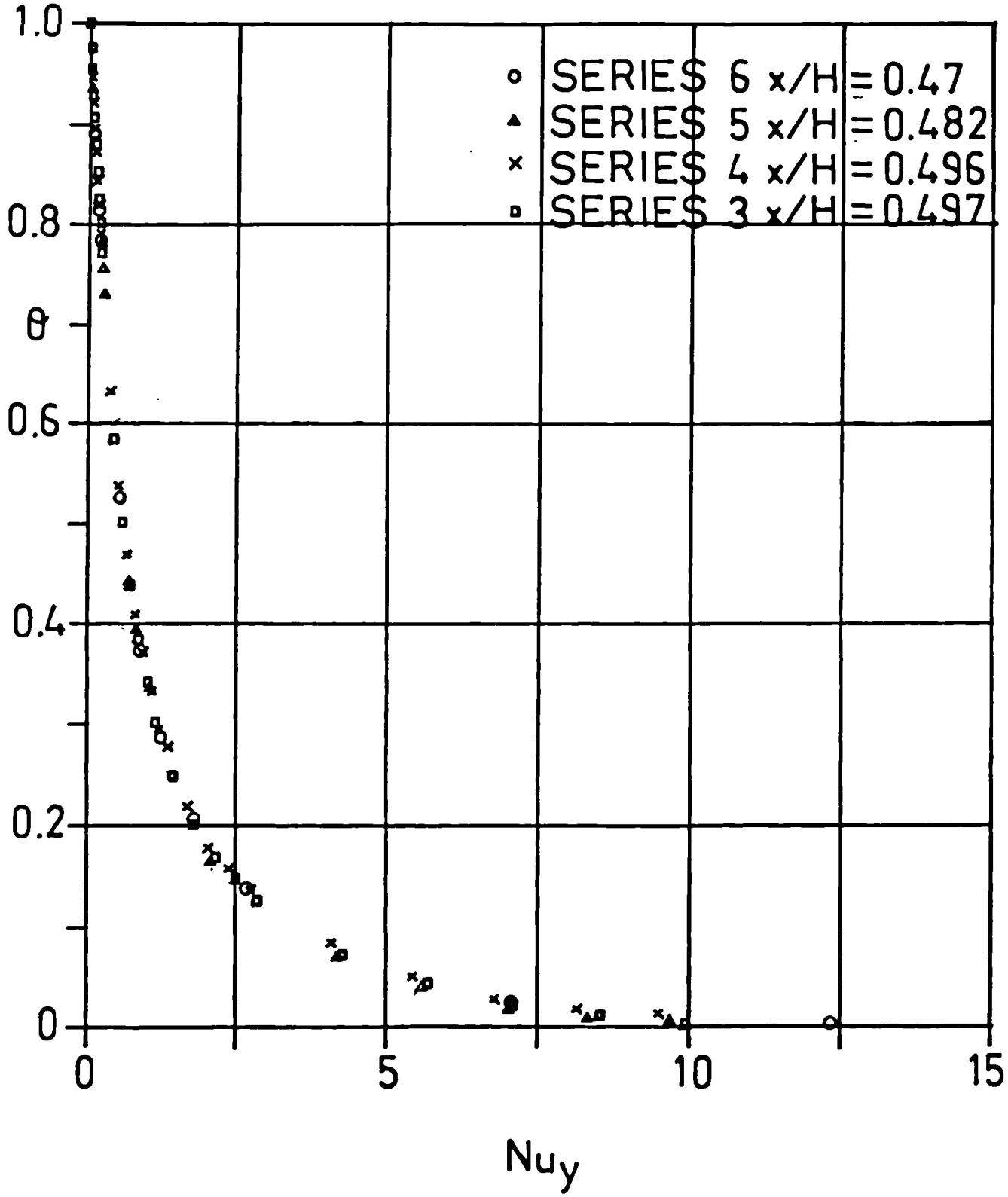

FIGURE 7.12

THETA AGAINST Nu_y AT THE COOLED WALL

OF SERIES 3, WITH T_{MIN} AS THE REFERENCE TEMPERATURE

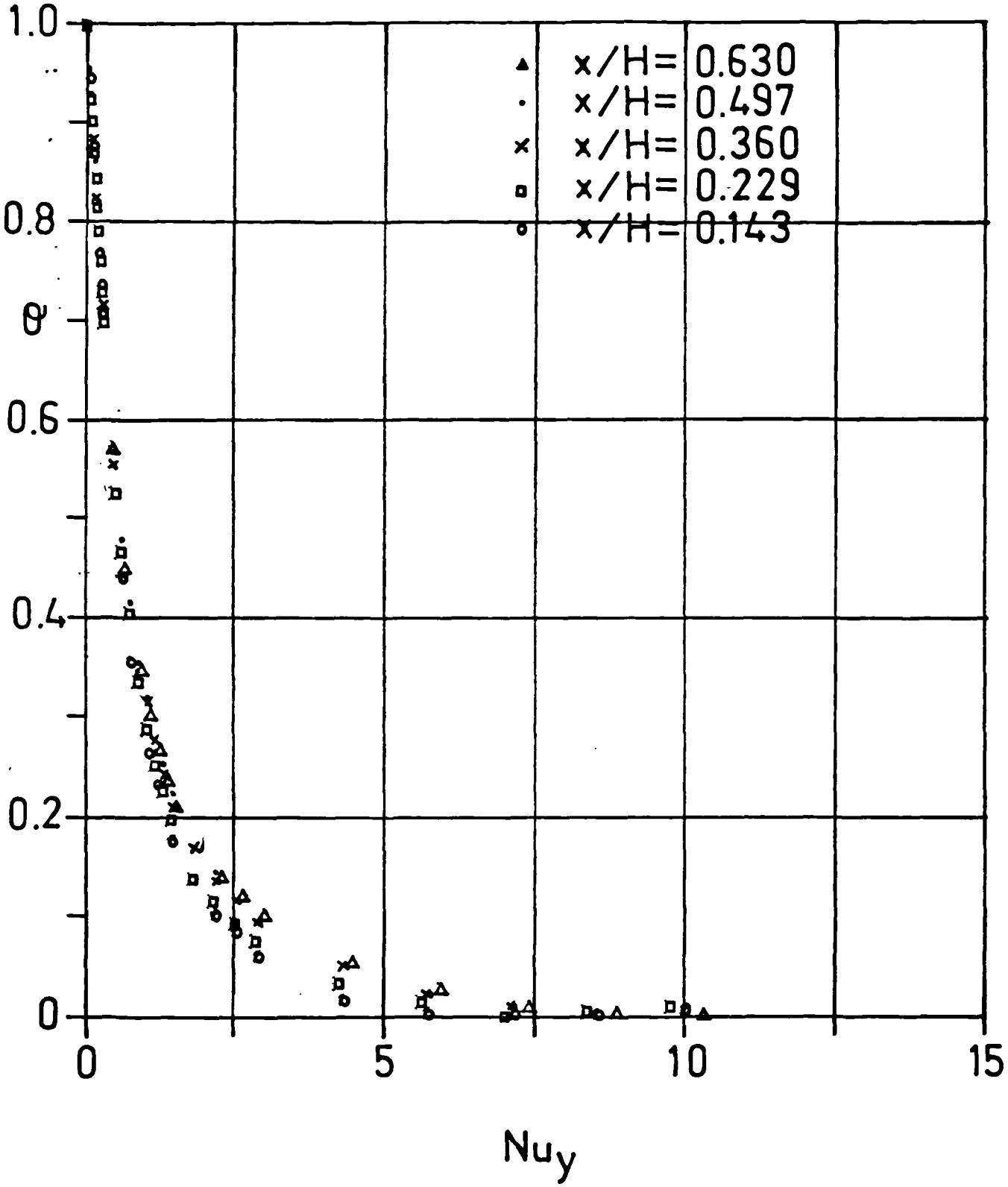

FIGURE 7.13

THETA AGAINST Nu_Y AT THE COOLED WALL

OF SERIES 4, WITH T_{MIN} AS THE REFERENCE TEMPERATURE

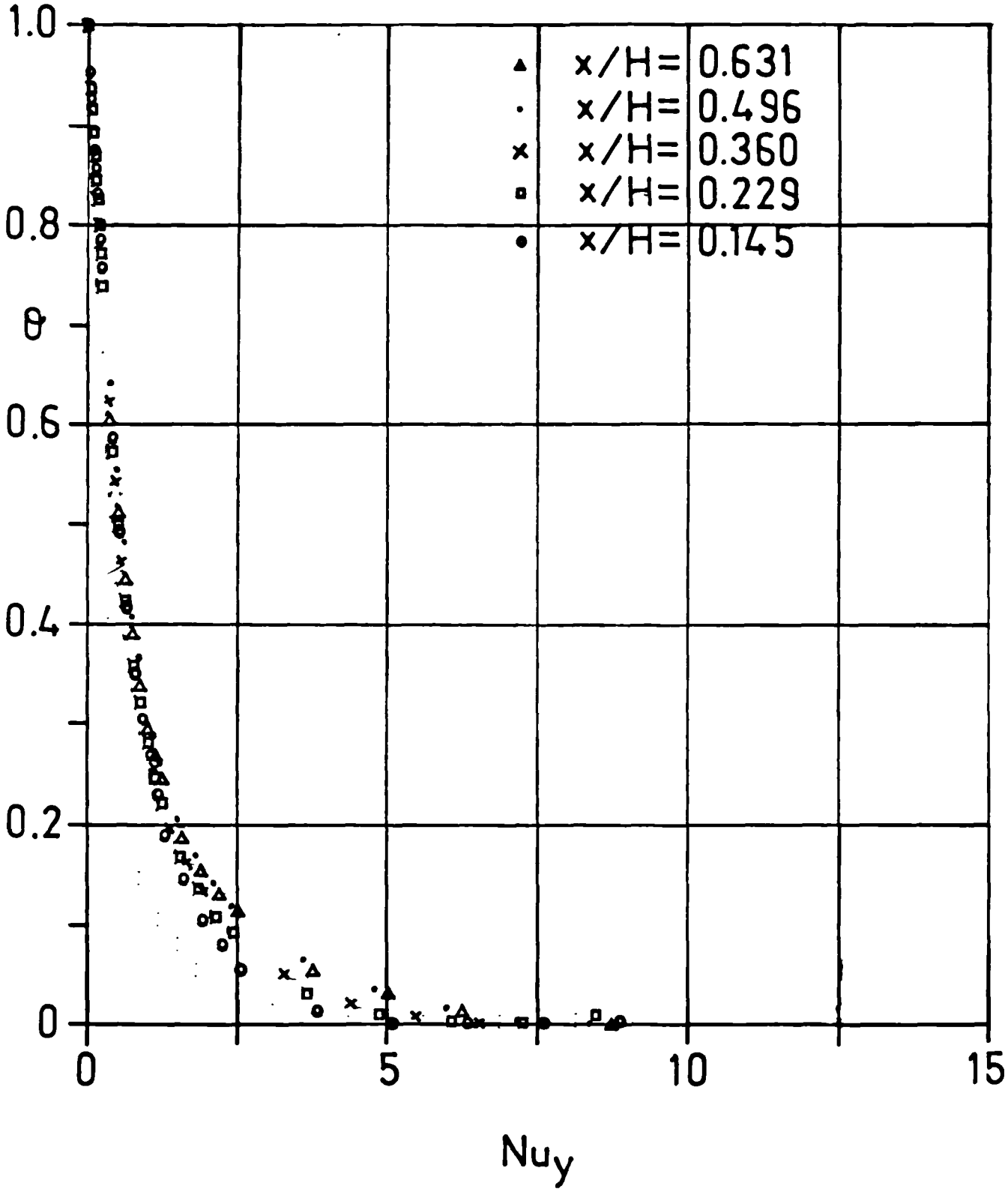

FIGURE 7.14

THETA AGAINST Nu_v AT THE HEATED AND COOLED WALLS

OF SERIES 3 AND 4, WITH T_{MIN} AS THE REFERENCE TEMPERATURE

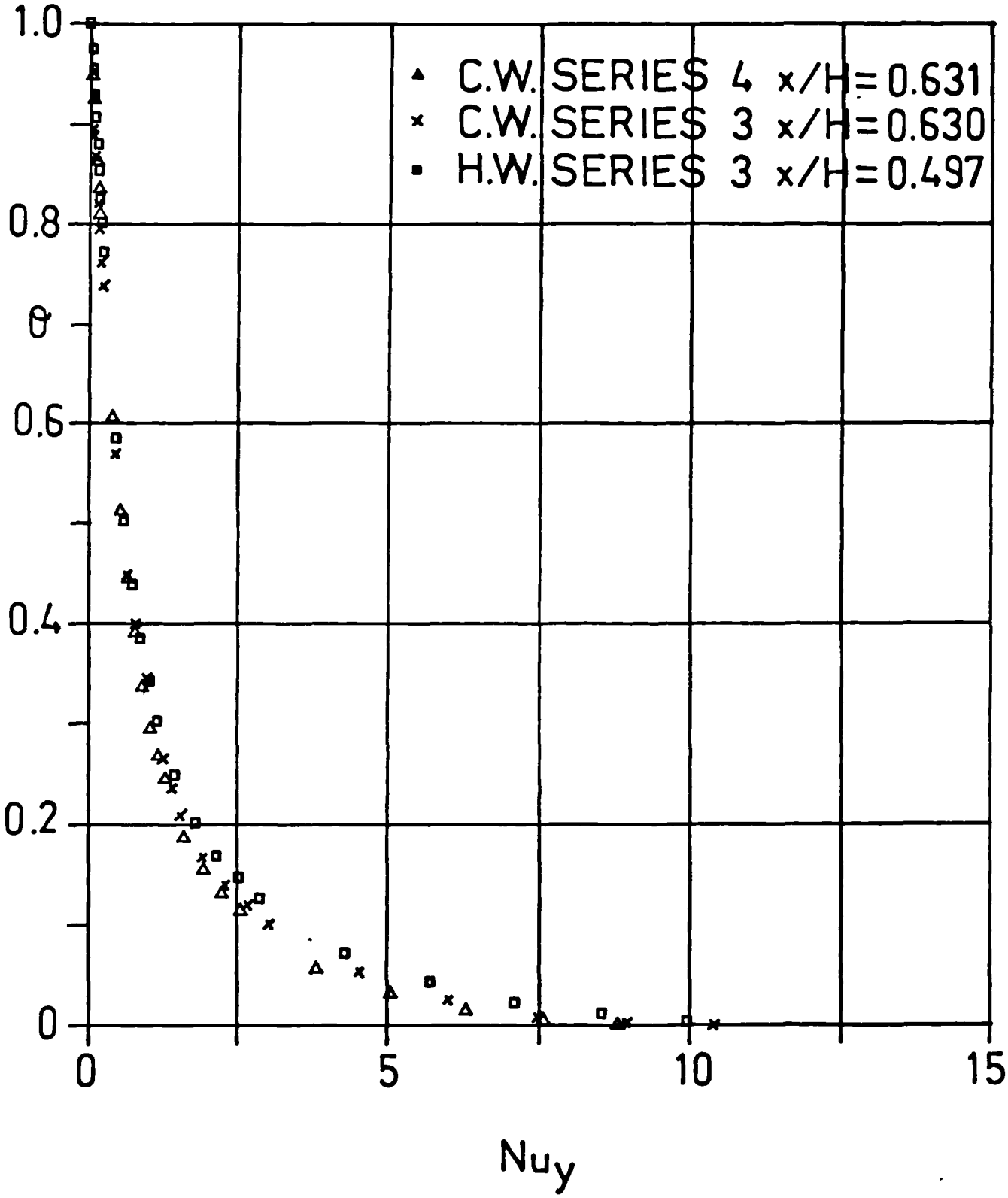

FIGURE 7.15

THETA AGAINST ln(Nu$_Y$) AT THE HEATED WALL

OF SERIES 3, WITH T$_{MIN}$ AS THE REFERENCE TEMPERATURE

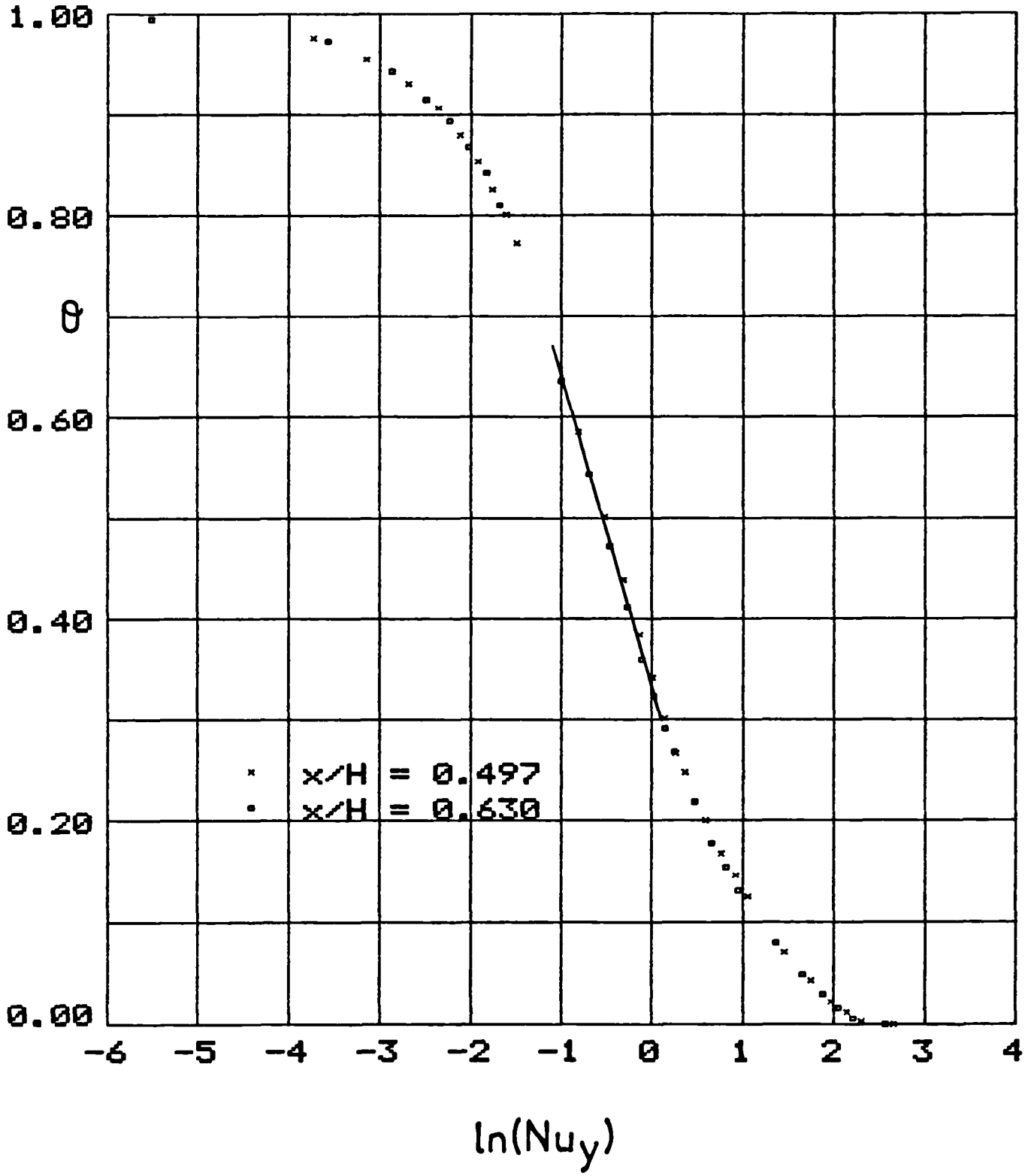

FIGURE 7.16

THETA AGAINST $\ln(Nu_y)$ AT THE HEATED WALL

OF SERIES 3, WITH T_{MIN} AS THE REFERENCE TEMPERATURE

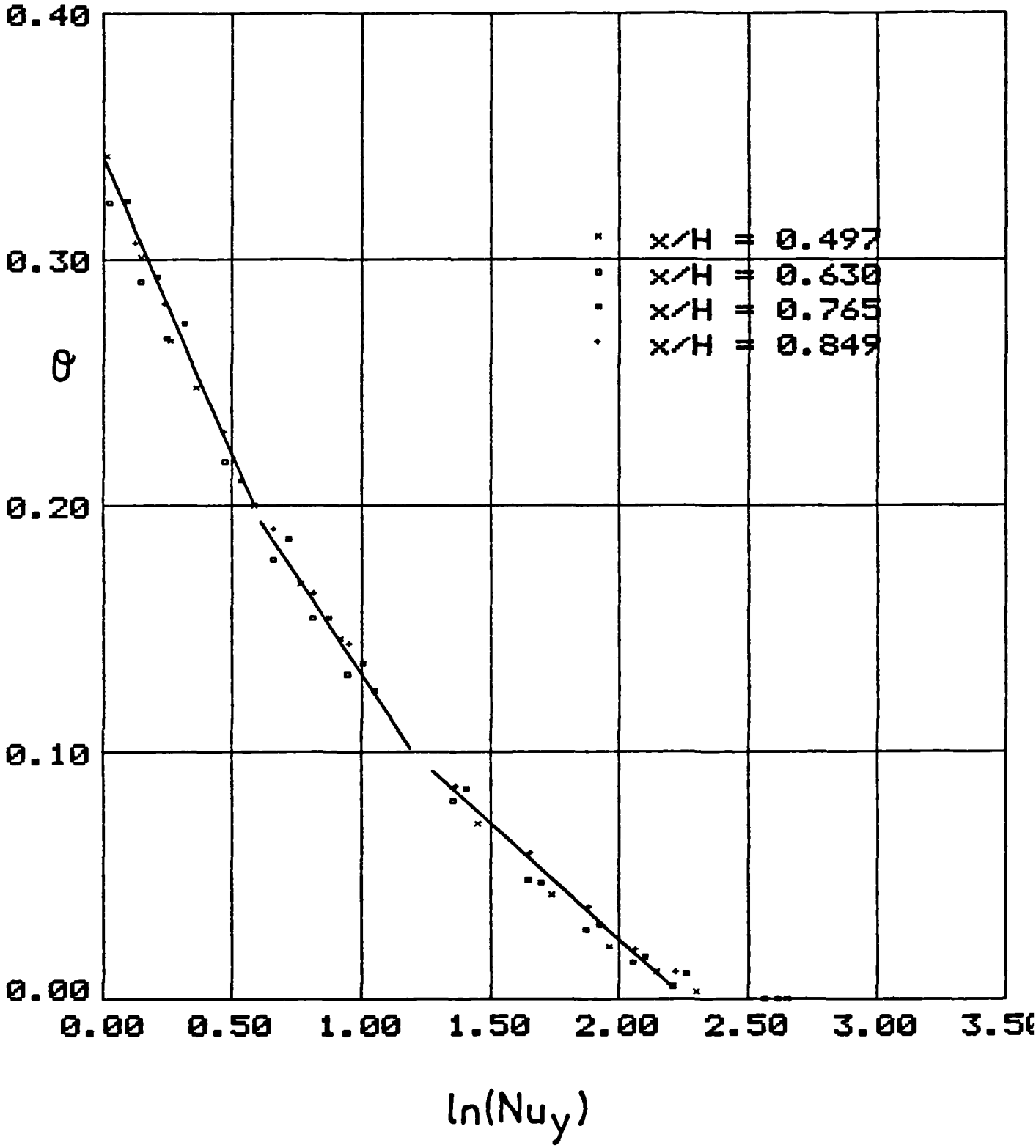

FIGURE 7.17

NON-DIMENSIONAL VERTICAL CENTRE-LINE

TEMPERATURE DISTRIBUTIONS FOR SERIES 1, 2, 3 AND 4

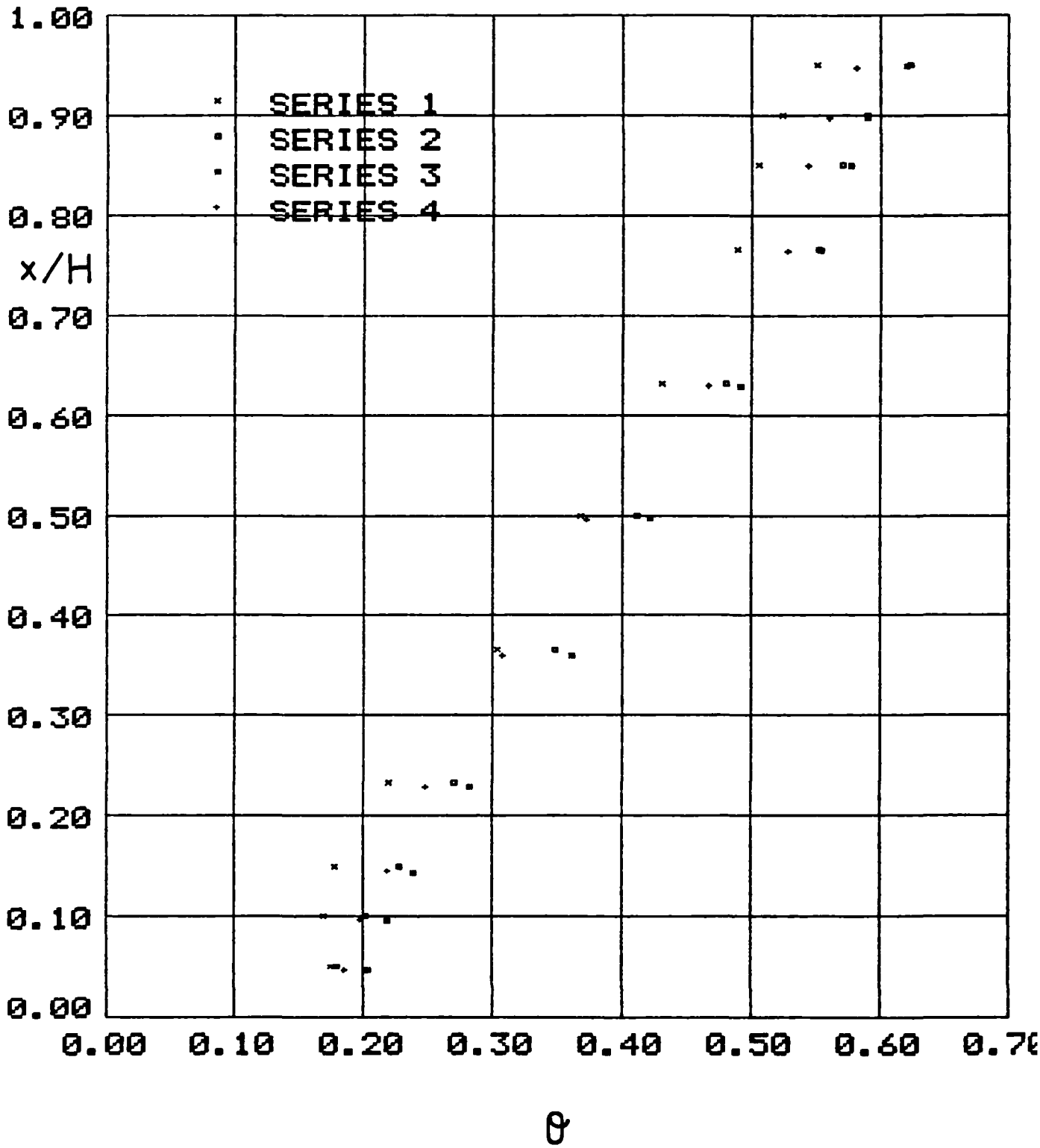

FIGURE 7.18

NON-DIMENSIONAL VERTICAL CENTRE-LINE

TEMPERATURE DISTRIBUTIONS FOR SERIES 5, 6 AND 7

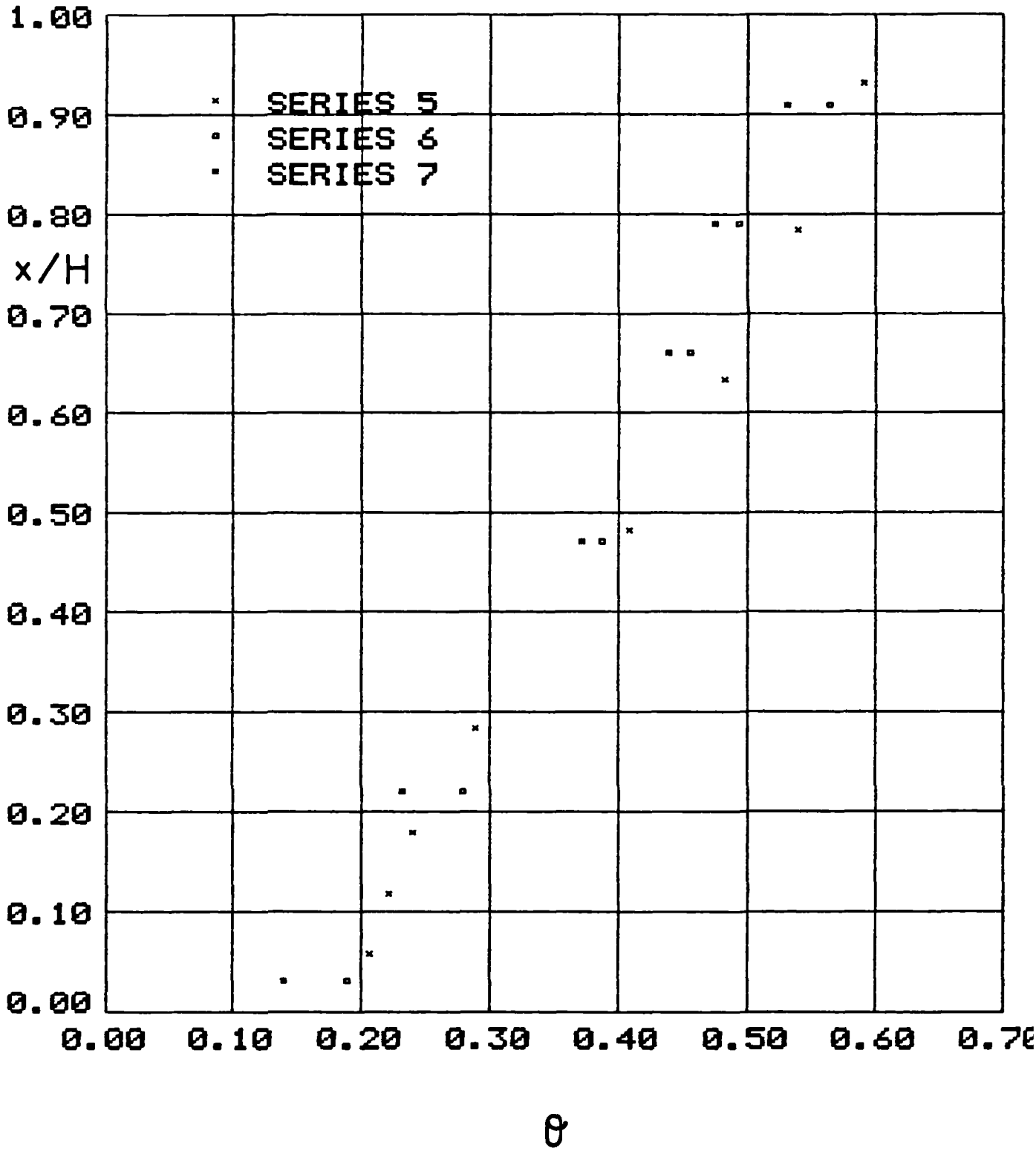

FIGURE 7.19

NON-DIMENSIONAL VERTICAL CENTRE-LINE

TEMPERATURE DISTRIBUTIONS FOR SERIES 2, 3 AND 5

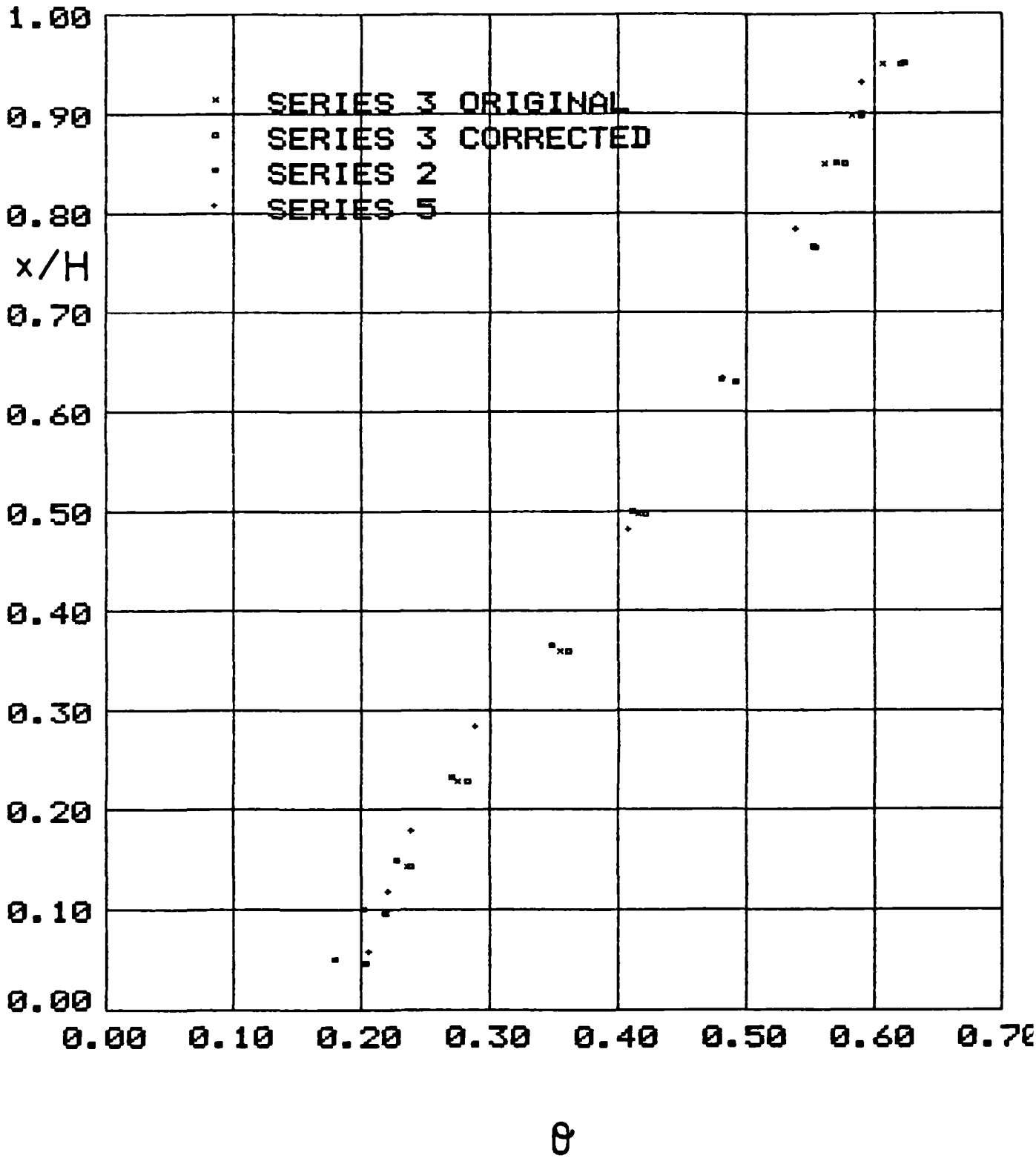

FIGURE 7.20

LOCAL Nu_x AGAINST LOCAL Gr_x AT

THE HEATED WALL FOR SERIES 2, 3, 4 AND 5

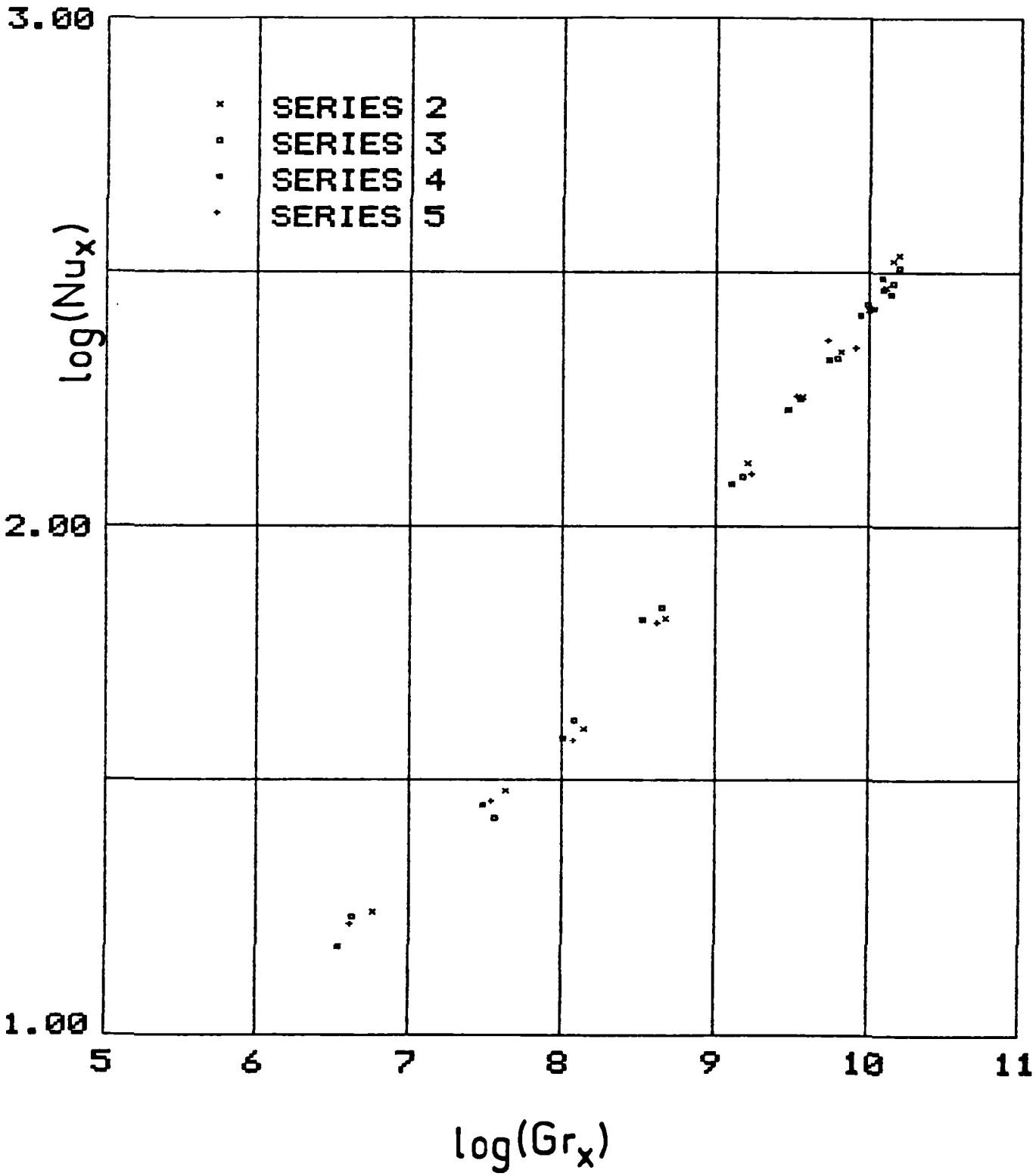

FIGURE 7.21

LOCAL Nu_x AGAINST LOCAL Gr_x AT

THE COOLED WALL FOR SERIES 2, 3, 4 AND 5

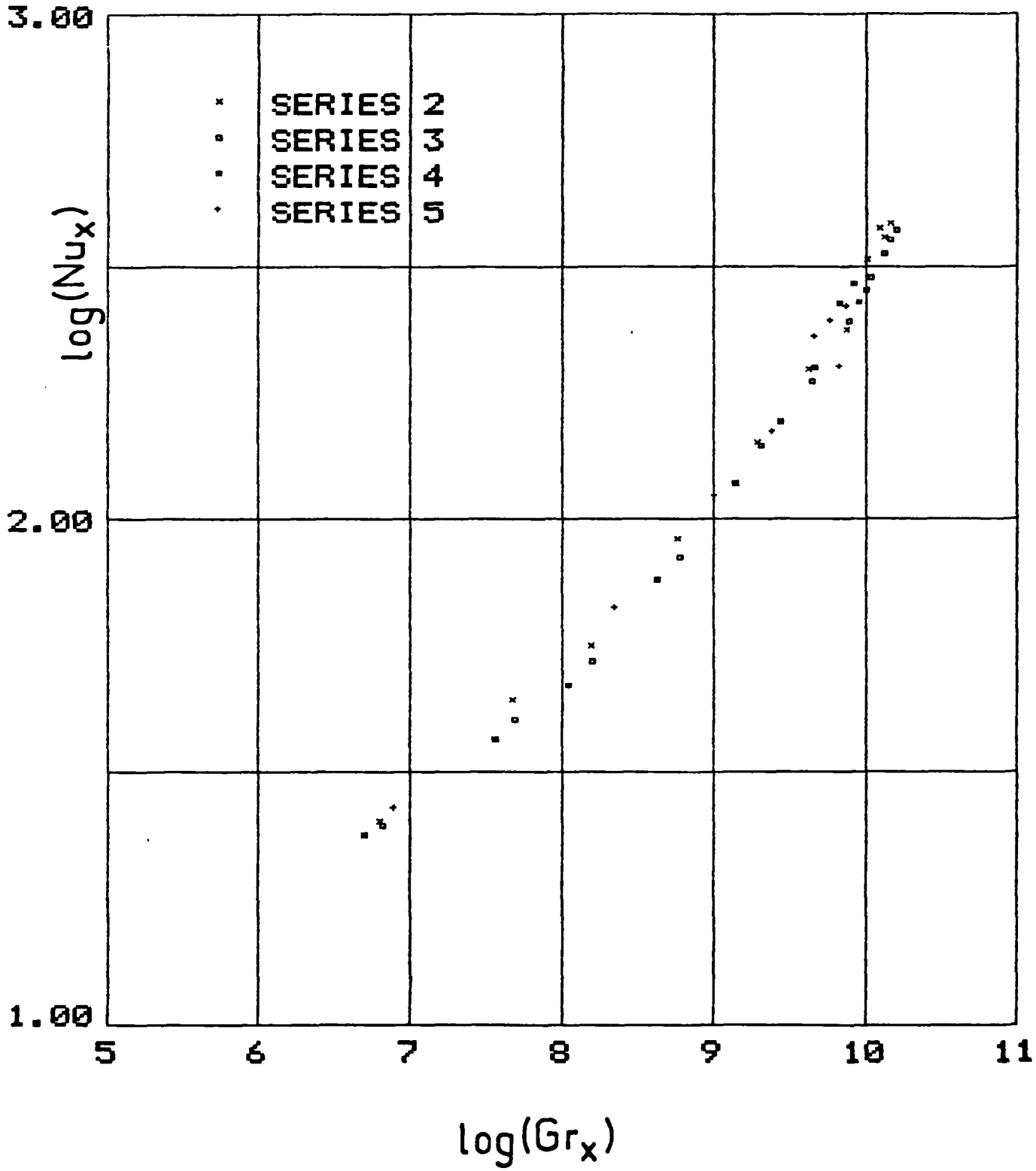

FIGURE 7.22

LOCAL Nu_x AGAINST LOCAL Gr_x AT

THE HEATED WALL FOR SERIES 5, 6 AND 7

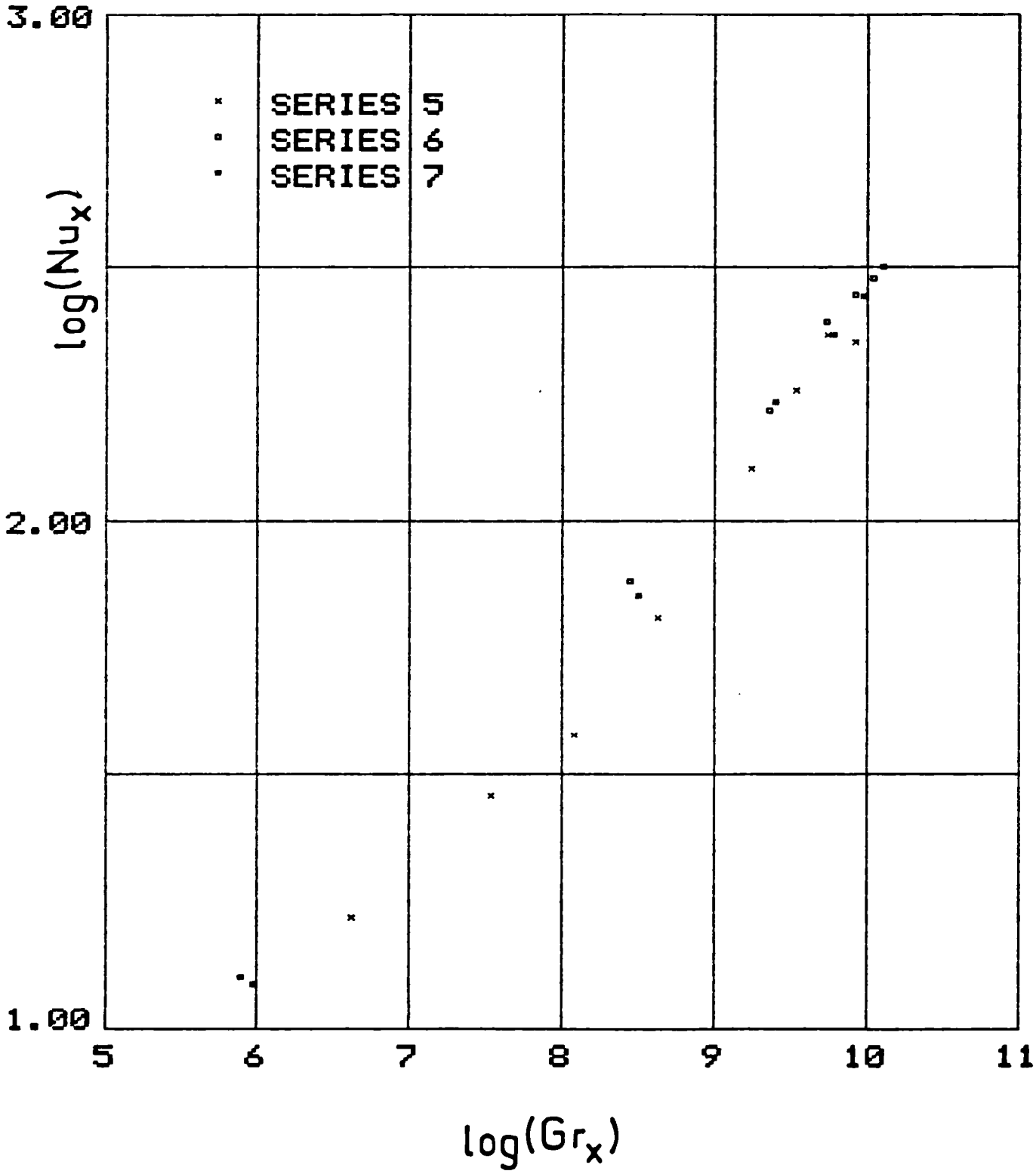

FIGURE 7.23

LOCAL Nu_x AGAINST LOCAL Gr_x AT

THE COOLED WALL FOR SERIES 5, 6 AND 7

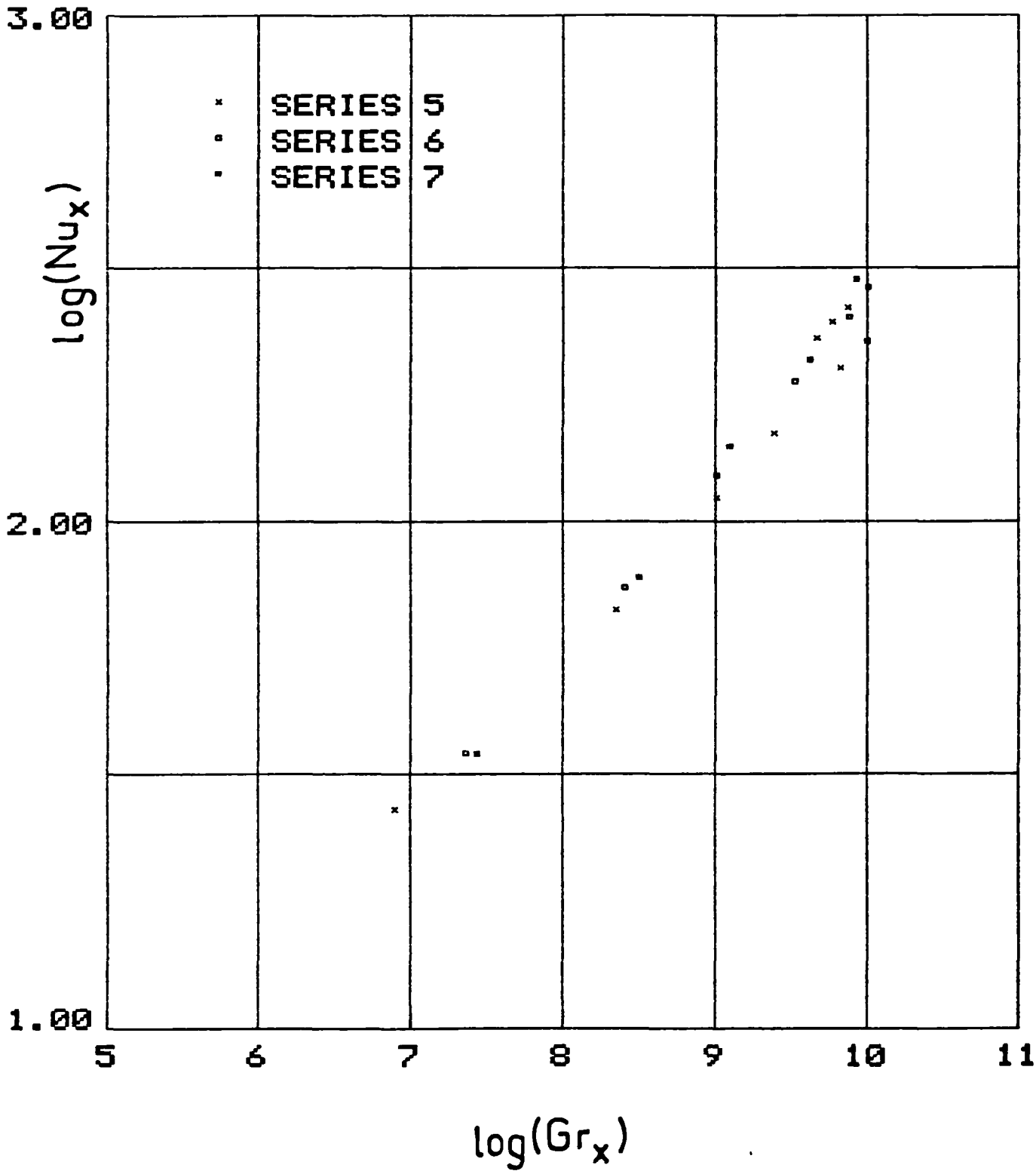

FIGURE 7.24

LOCAL Nu_x AGAINST LOCAL Gr_x AT

THE HEATED WALL FROM COWAN ET AL [12] AND THE PRESENT STUDY

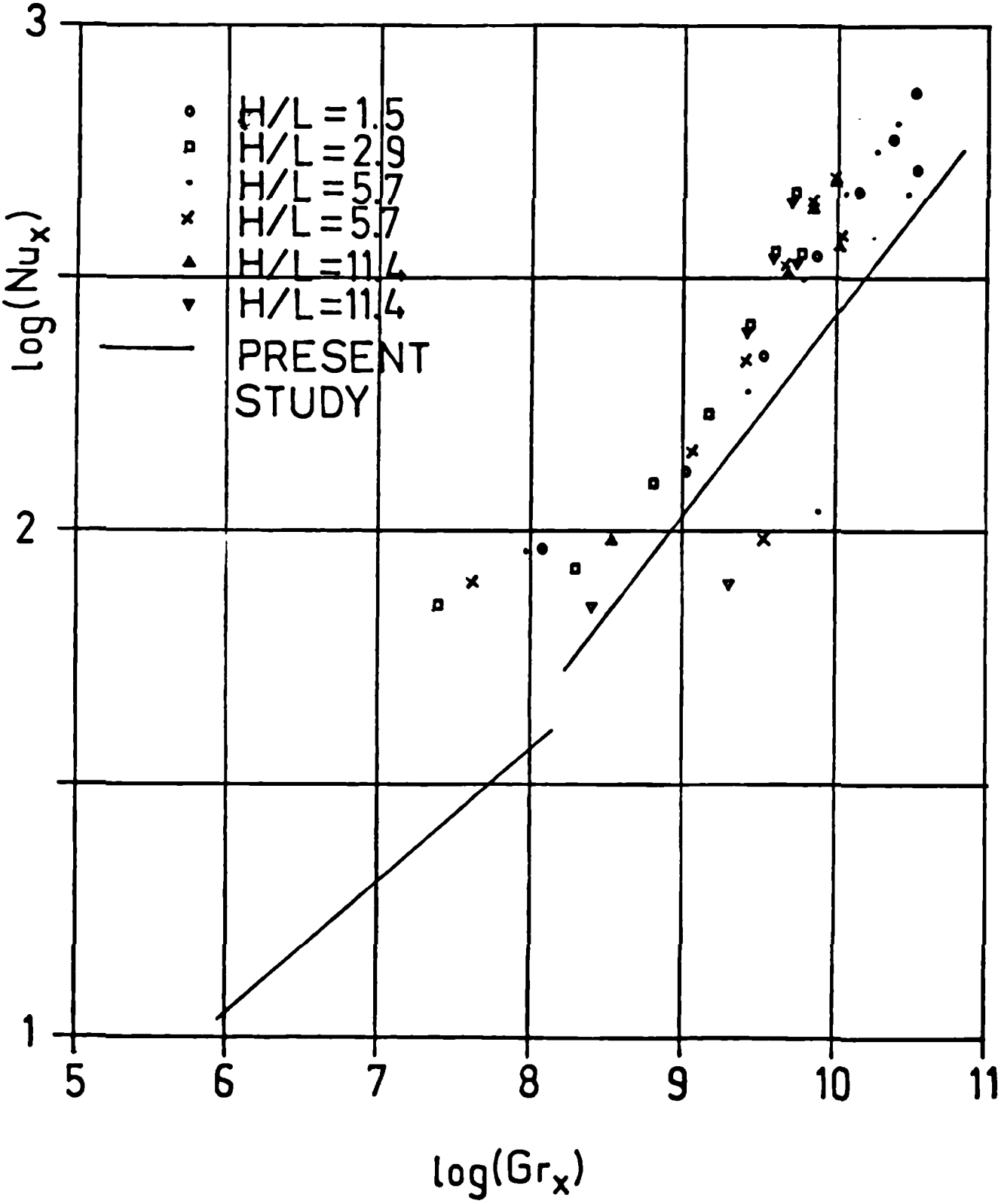

FIGURE 7.25

LOCAL Nu_x AGAINST LOCAL Ra_x AT

THE HEATED WALL FROM COWAN ET AL [12] AND THE PRESENT STUDY

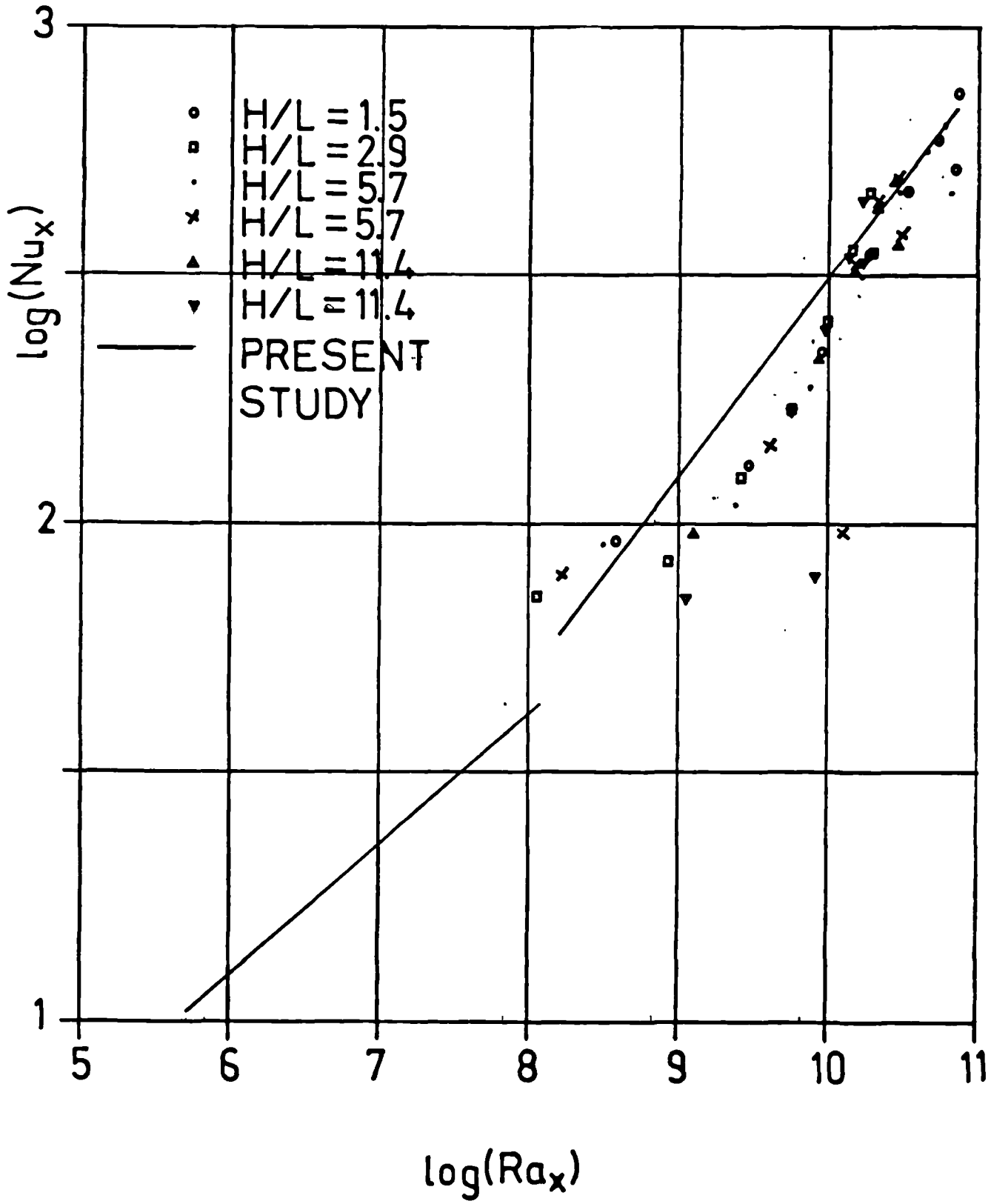

FIGURE 7.26

PROFILES OF MEAN VELOCITY

FOR SERIES 3 ($\Delta T \simeq 45.8K$)

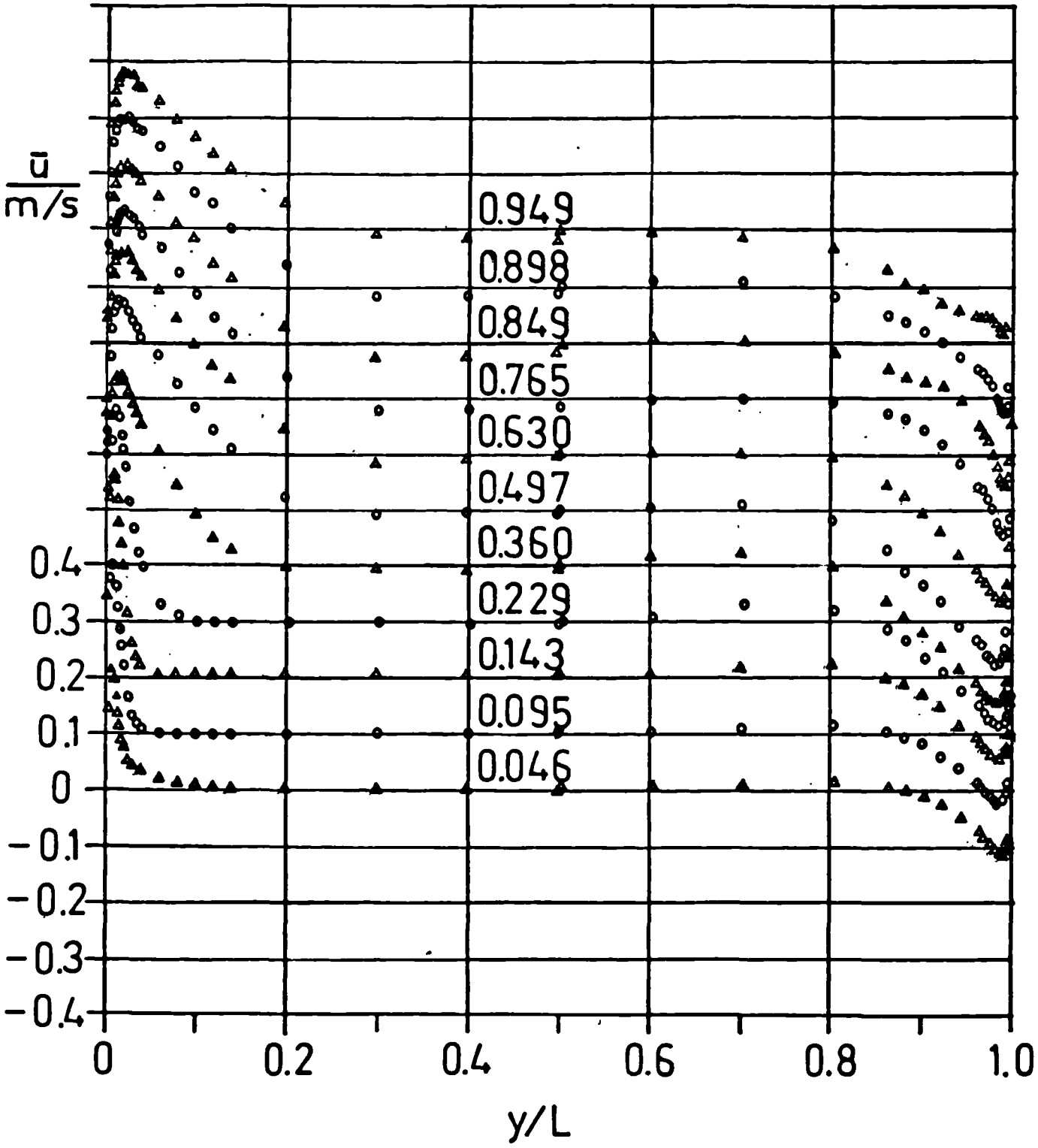

FIGURE 7.27

PROFILES OF MEAN VELOCITY

FOR SERIES 6 ($\Delta T \simeq 42.5K$)

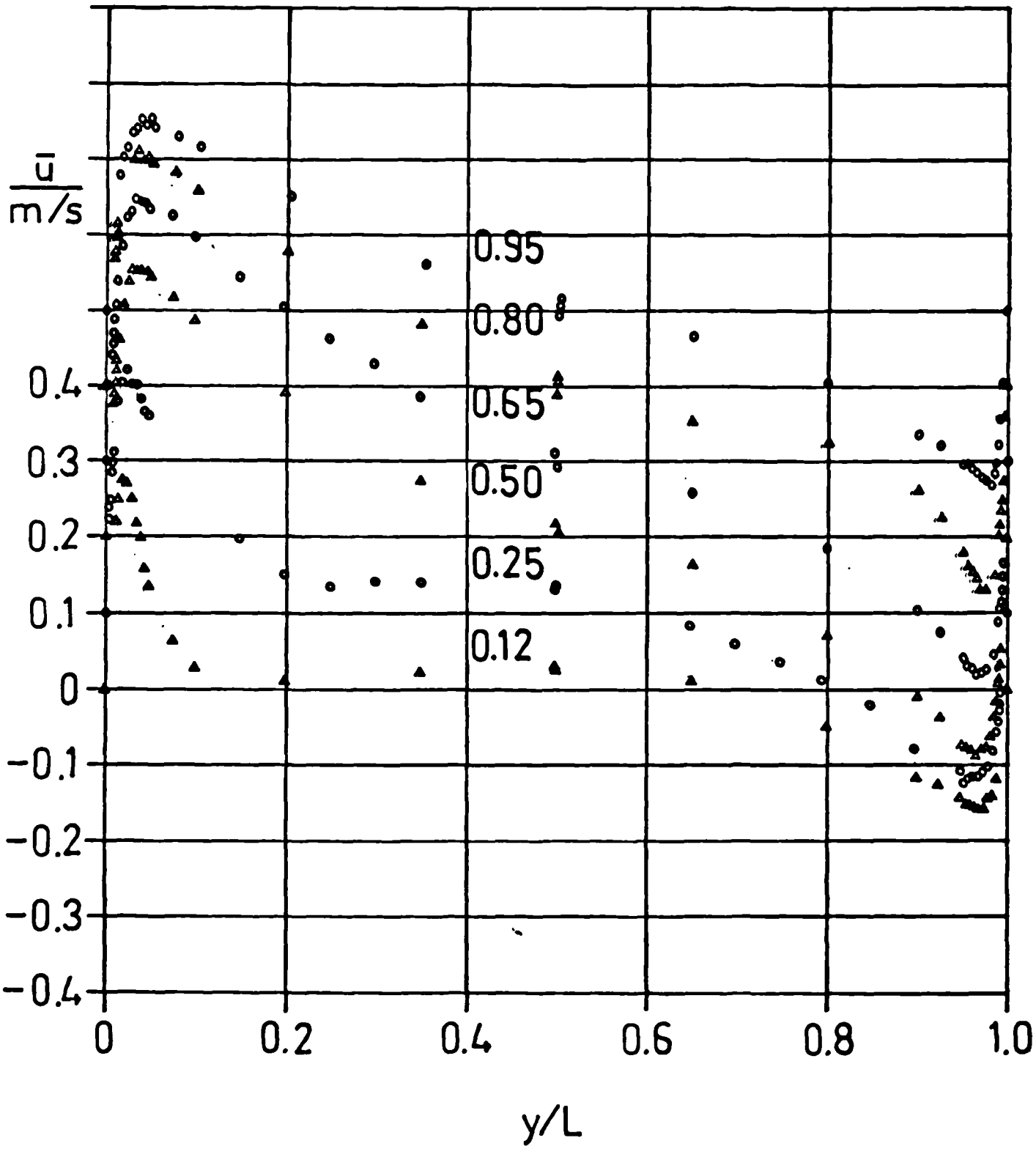

FIGURE 7.28

PROFILES OF u'R.M.S.

FOR SERIES 3 ($\Delta T \approx 45.8K$)

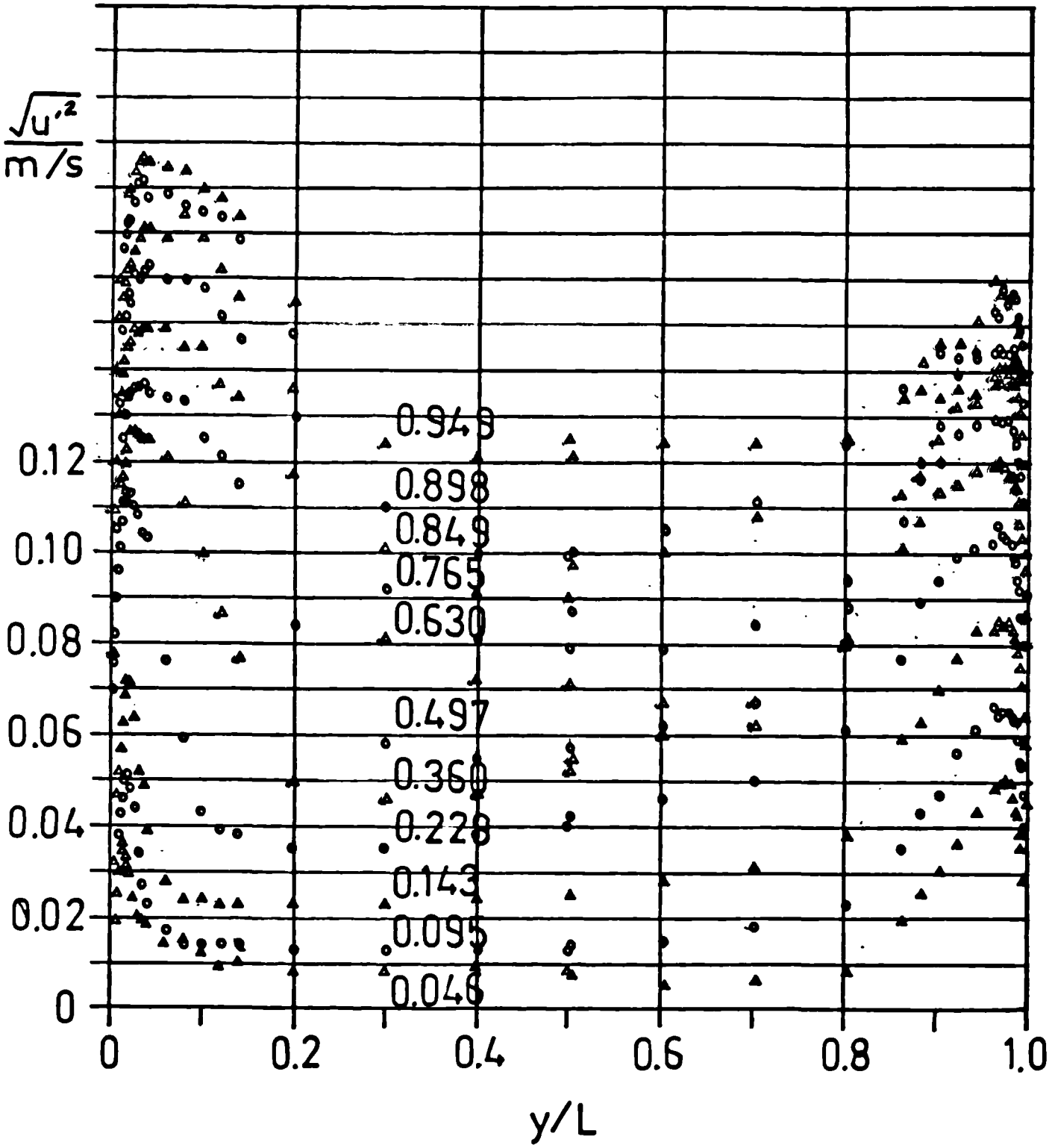

FIGURE 7.29

PROFILES OF $u'_{R.M.S.}$

FOR SERIES 6 ($\Delta T \approx 42.5K$)

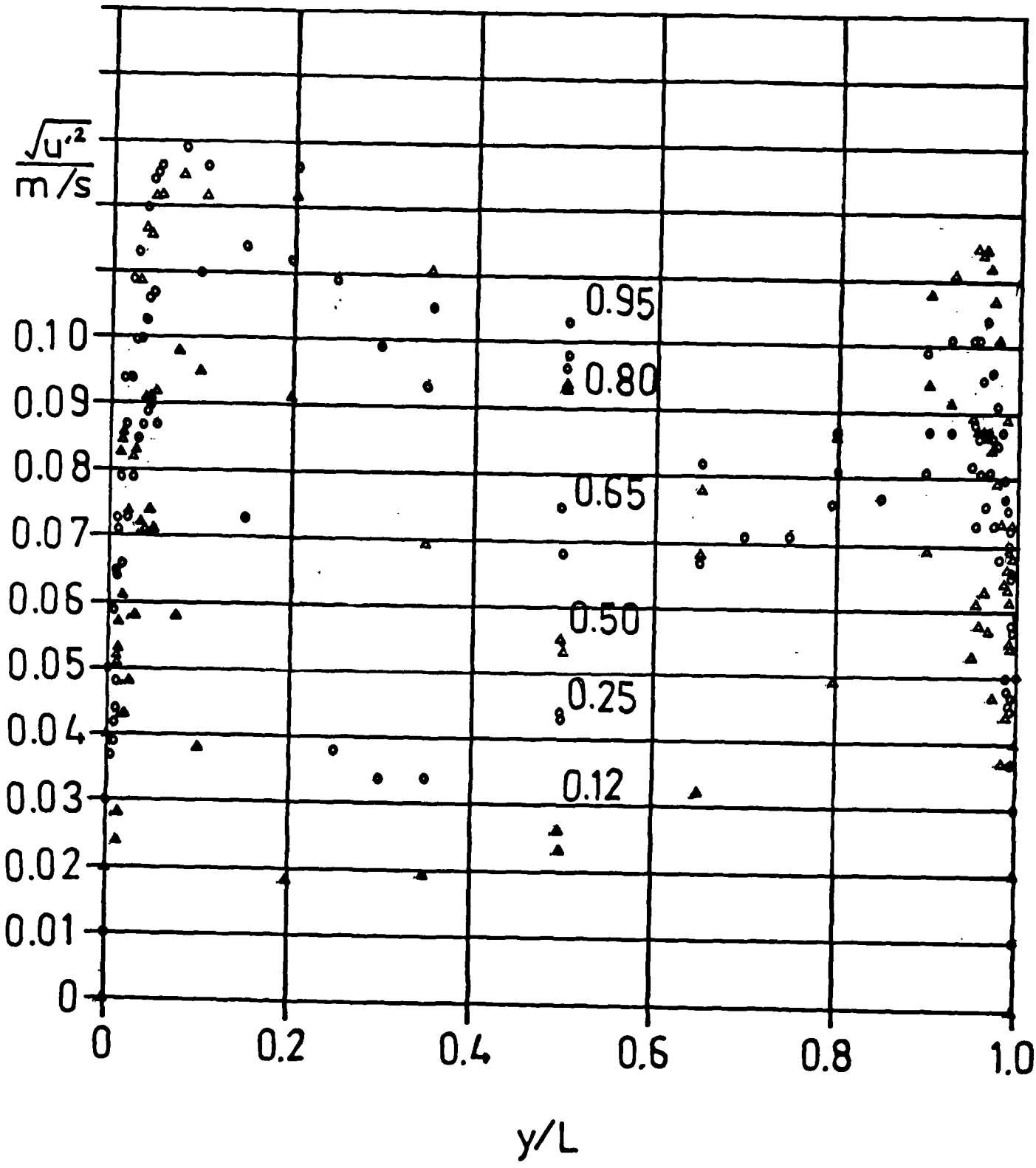

FIGURE 7.30

VARIATION OF % DROPOUT WITH TIME

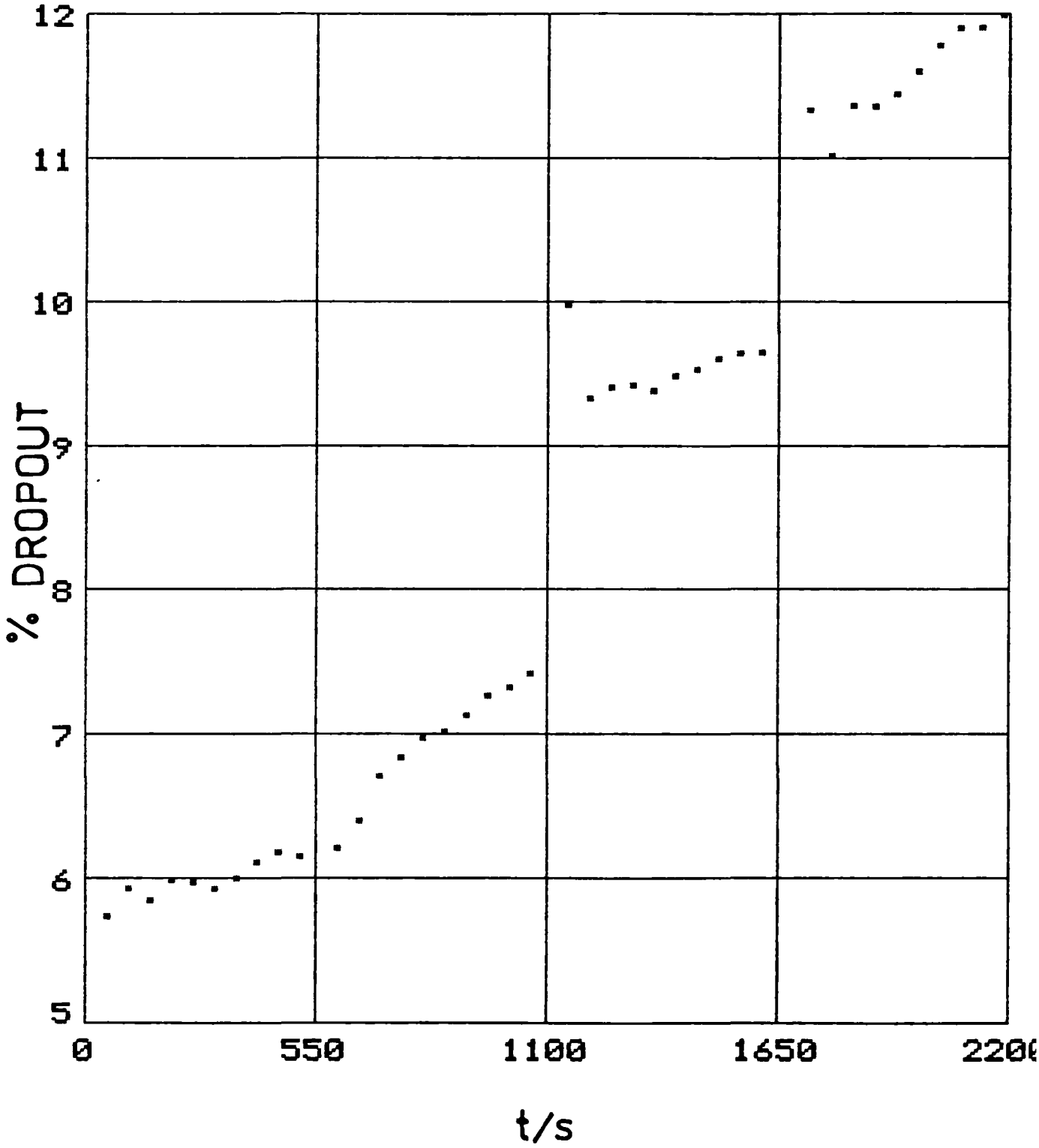

FIGURE 7.31

COMPARISON BETWEEN EXPERIMENTAL AND

PREDICTED MEAN VELOCITY FROM SERIES 3 AT x/H = 0.765

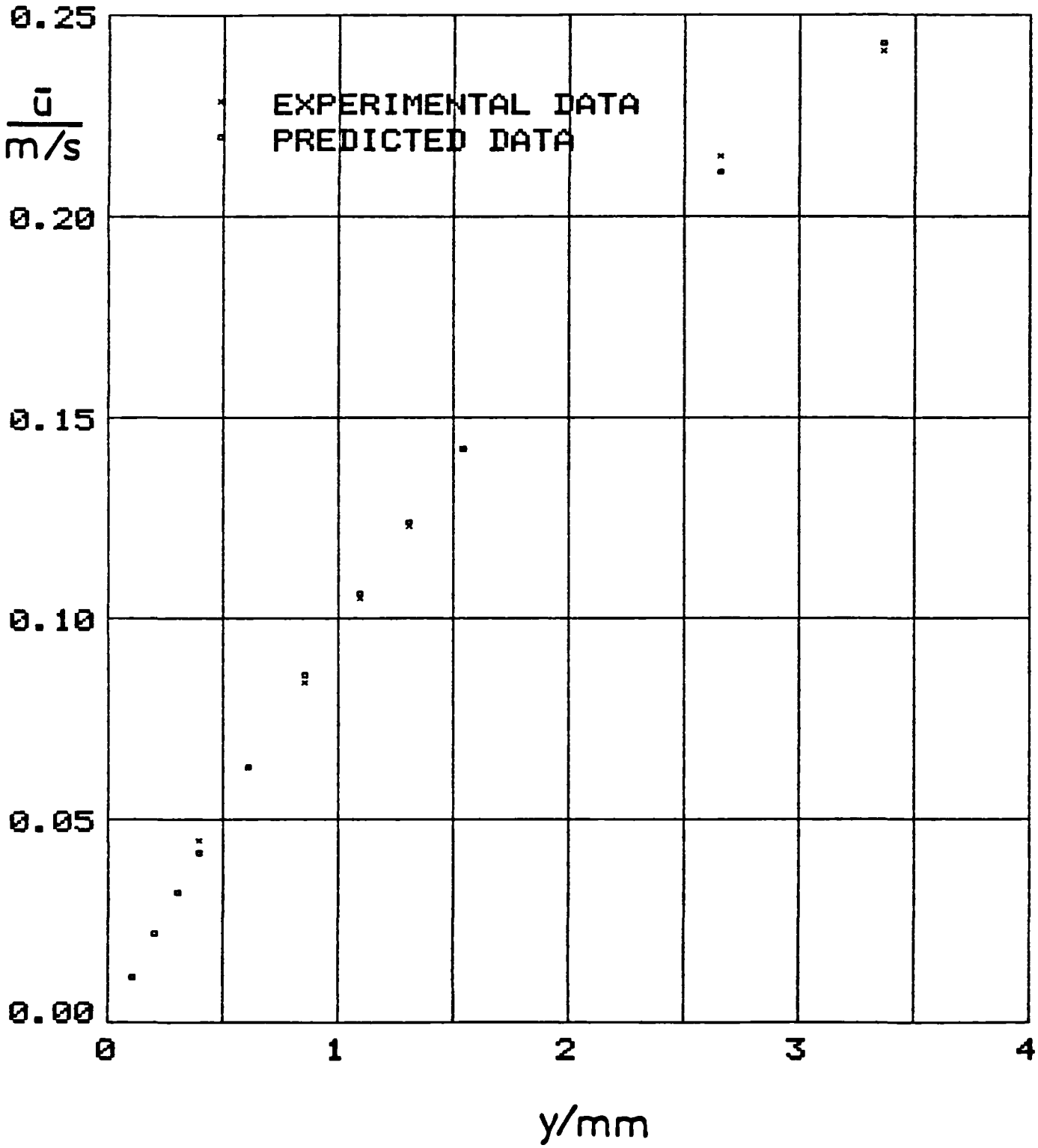

FIGURE 7.32

WALL SHEAR STRESS DATA FOR SERIES 3, 4 AND 5

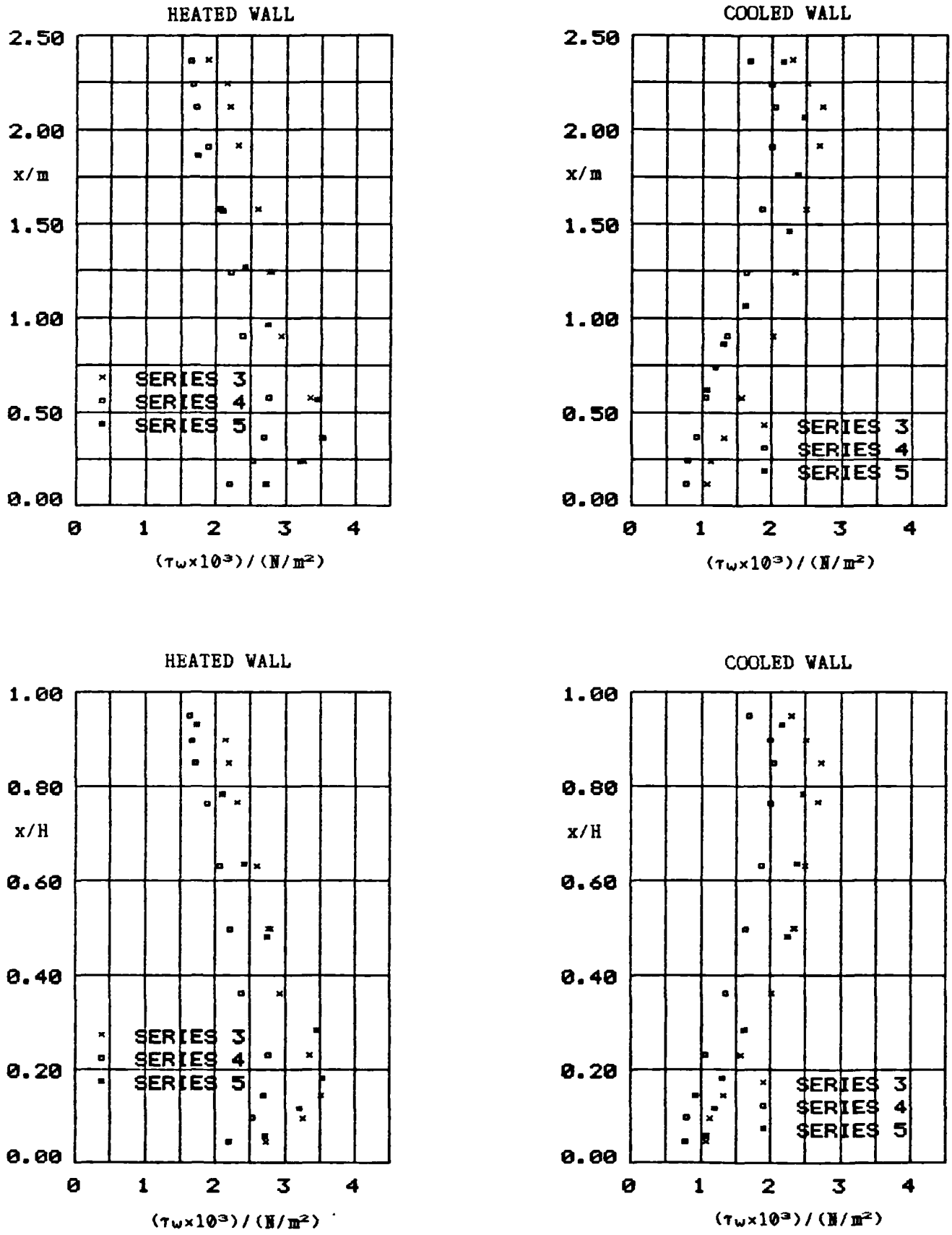

FIGURE 7.33

WALL SHEAR STRESS DATA FOR SERIES 5, 6 AND 7

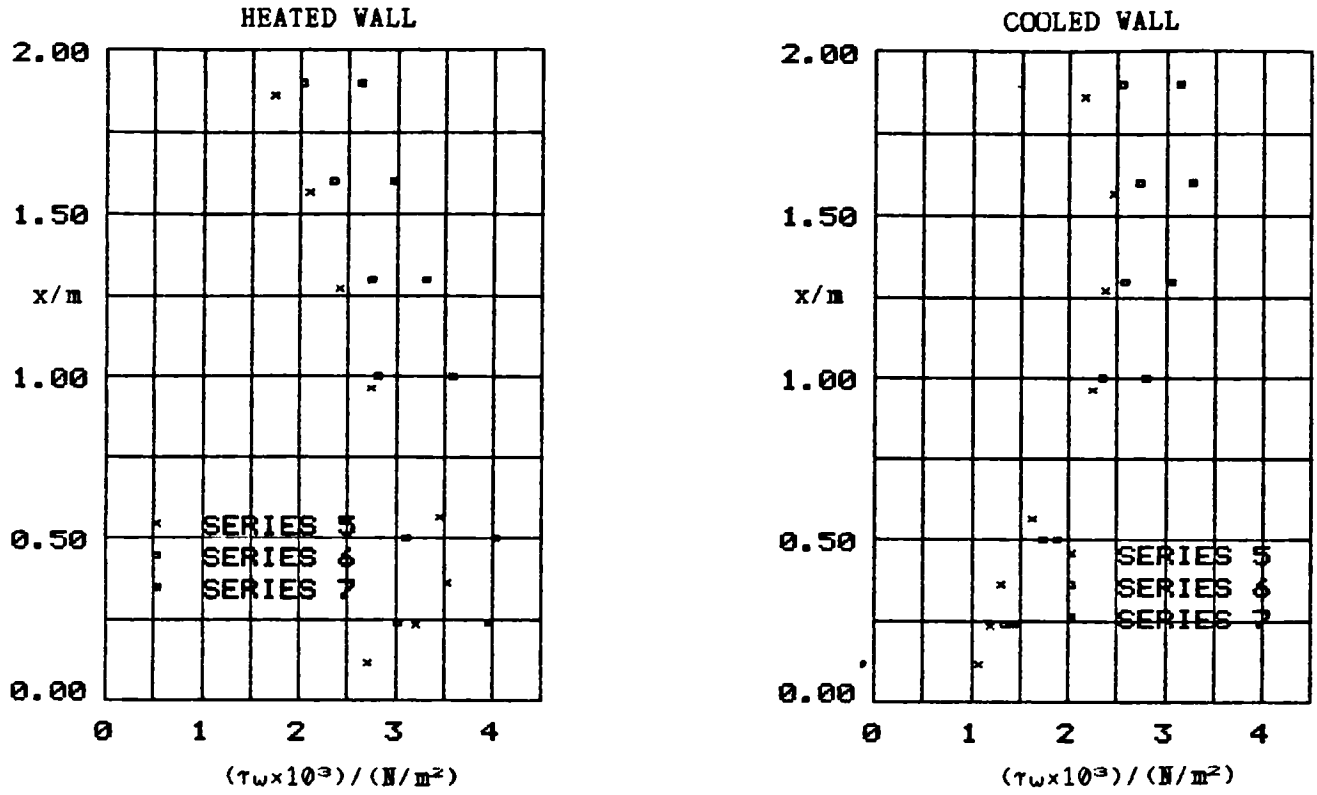

FIGURE 7.34

SERIES 3 MEAN VELOCITY SCALED WITH SHEAR VELOCITY

IN THE NEAR WALL REGION WITH Nu_y AS THE DIMENSIONLESS LENGTH

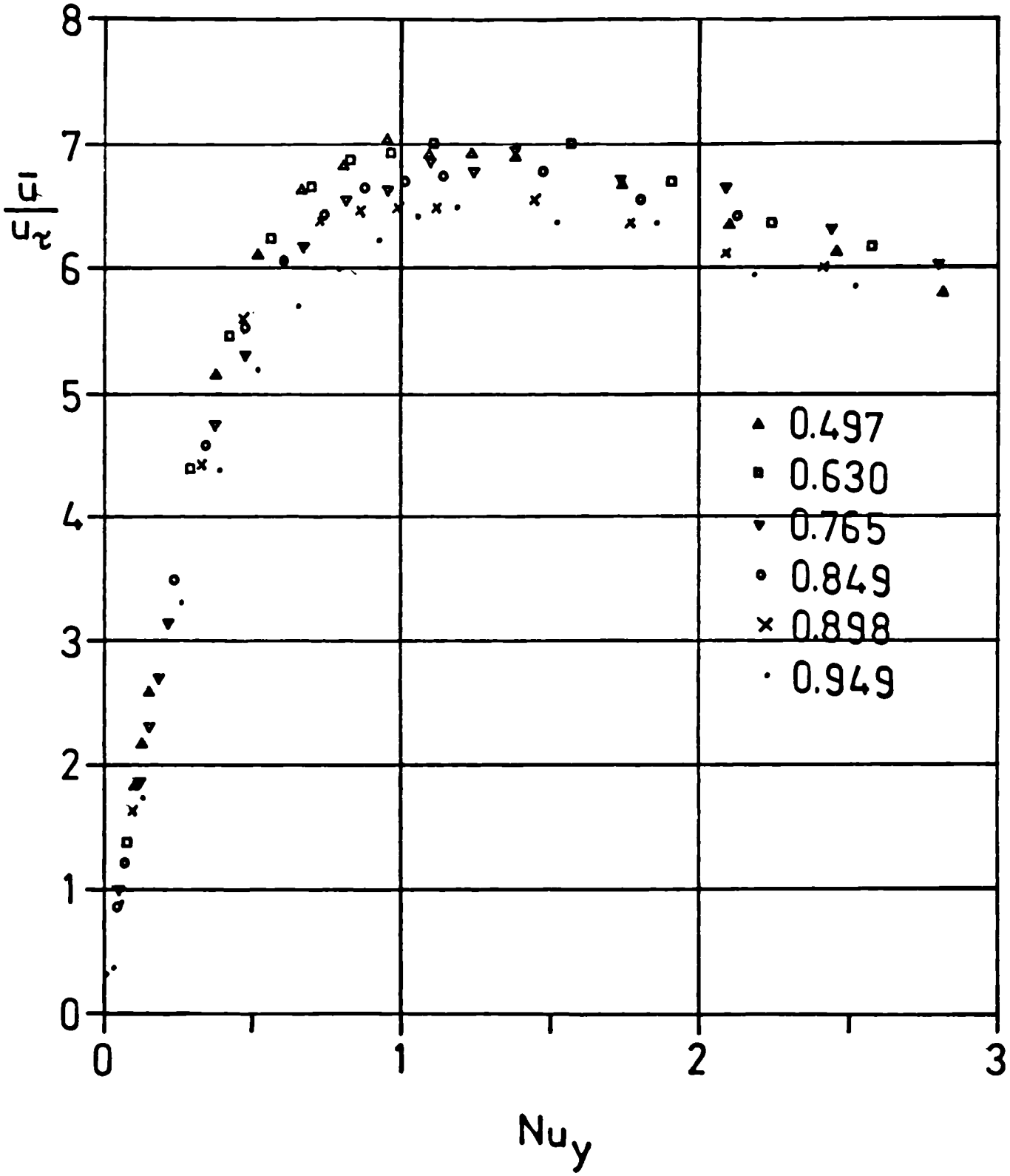

FIGURE 7.35

SERIES 4 MEAN VELOCITY SCALED WITH SHEAR VELOCITY

IN THE NEAR WALL REGION WITH Nu_y AS THE DIMENSIONLESS LENGTH

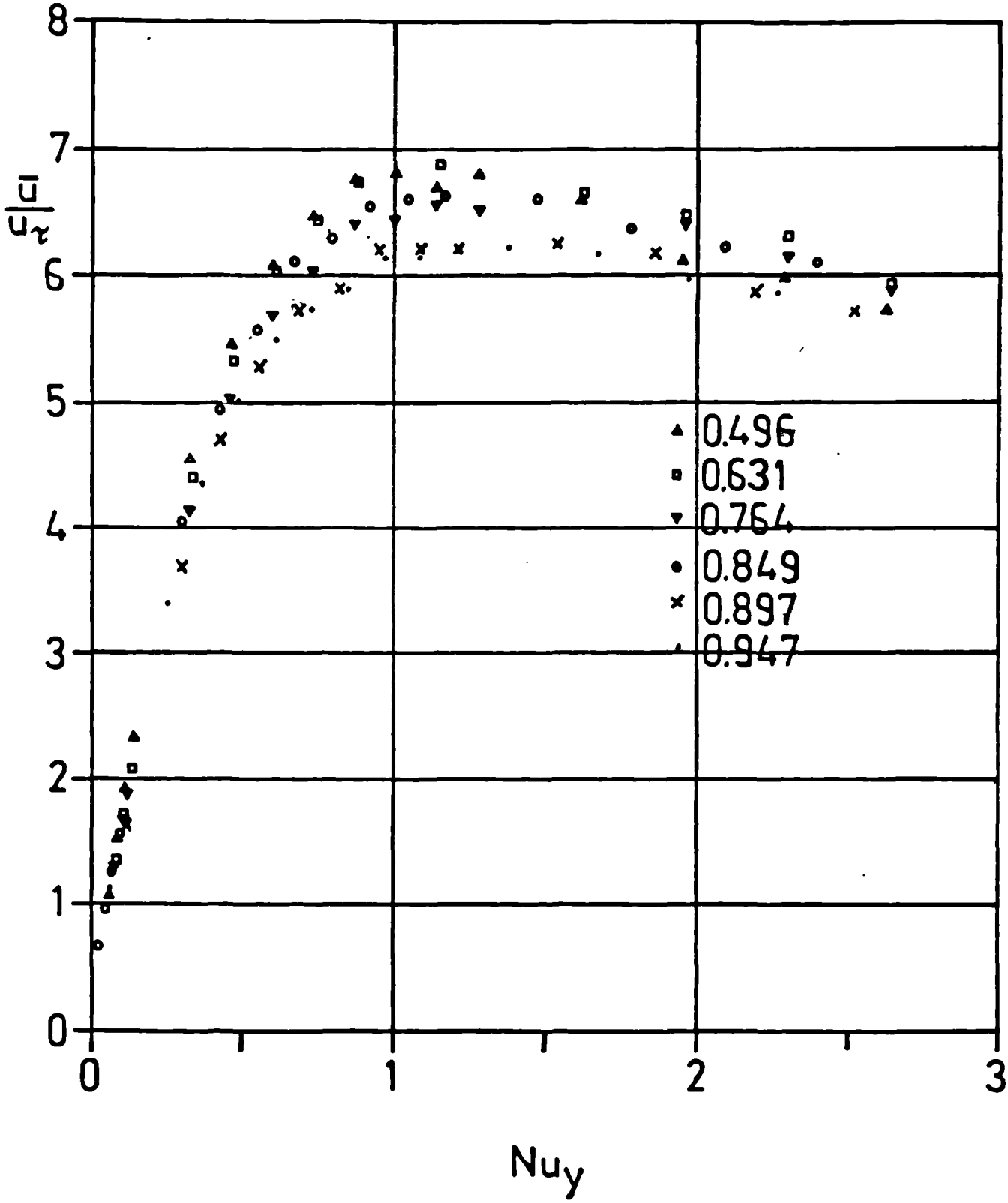

FIGURE 7.36

SERIES 5 MEAN VELOCITY SCALED WITH SHEAR VELOCITY

IN THE NEAR WALL REGION WITH Nu_y AS THE DIMENSIONLESS LENGTH

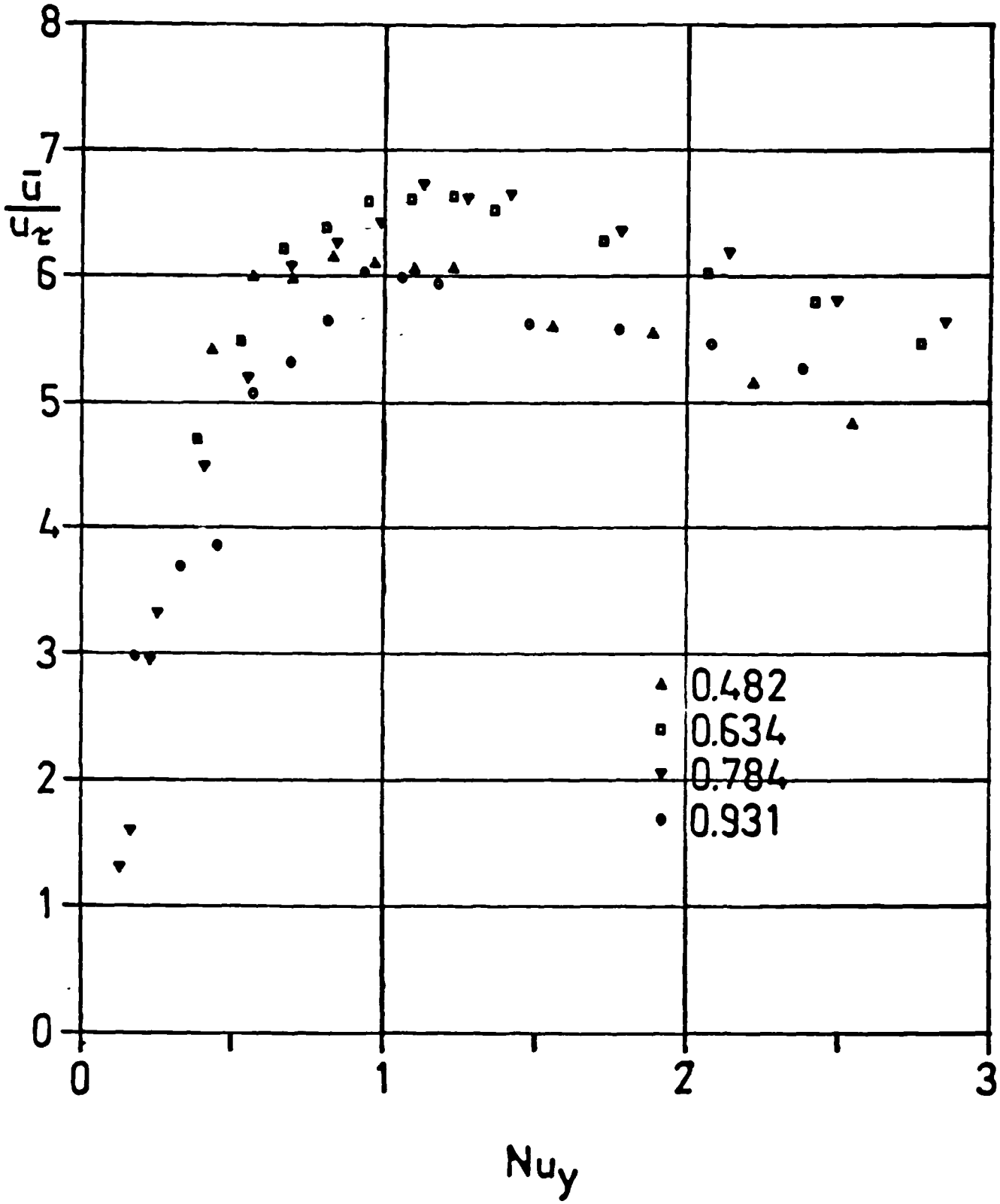

FIGURE 7.37

SERIES 6 MEAN VELOCITY SCALED WITH SHEAR VELOCITY

IN THE NEAR WALL REGION WITH Nu_y AS THE DIMENSIONLESS LENGTH

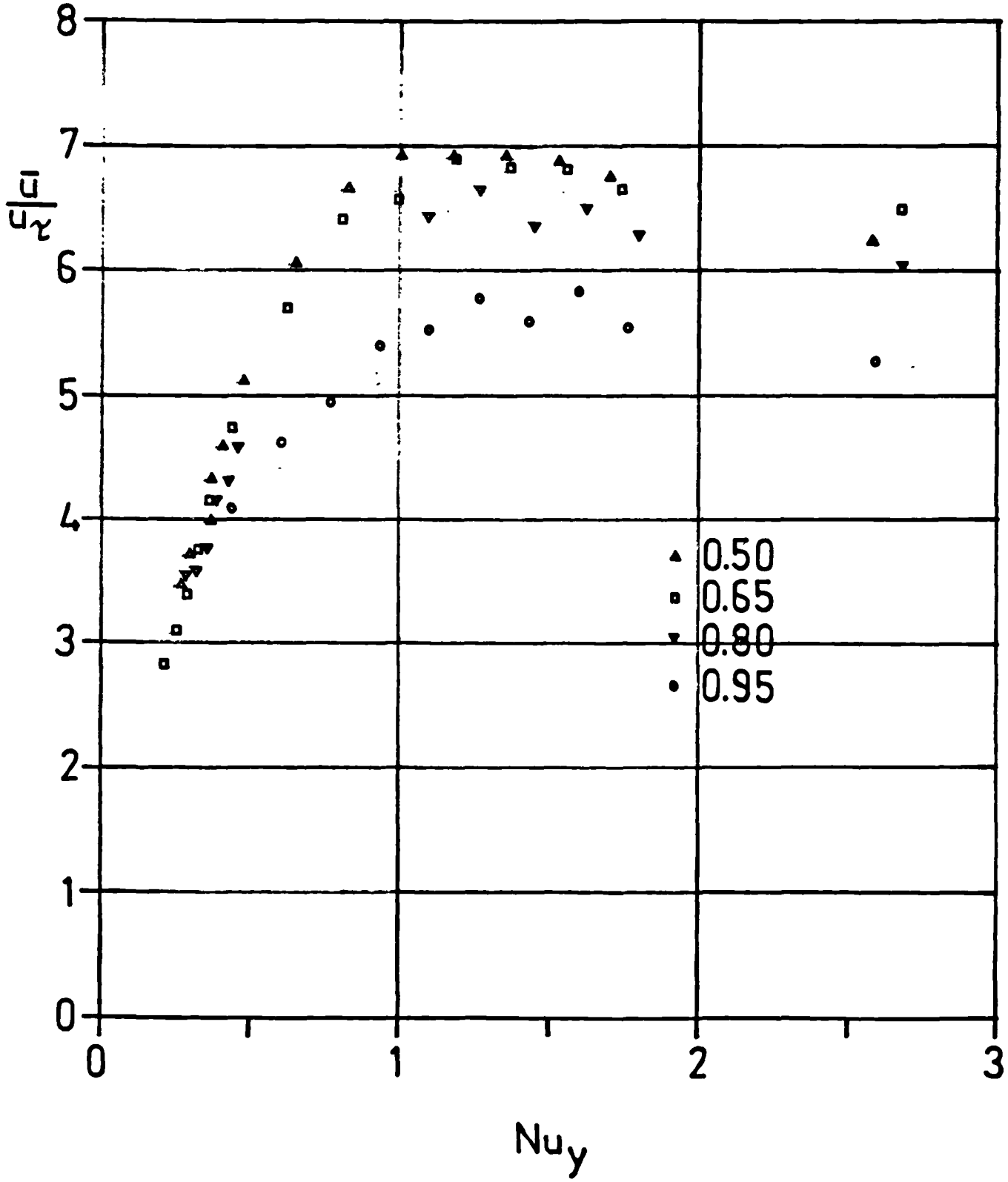

FIGURE 7.38

SERIES 7 MEAN VELOCITY SCALED WITH SHEAR VELOCITY

IN THE NEAR WALL REGION WITH Nu_y AS THE DIMENSIONLESS LENGTH

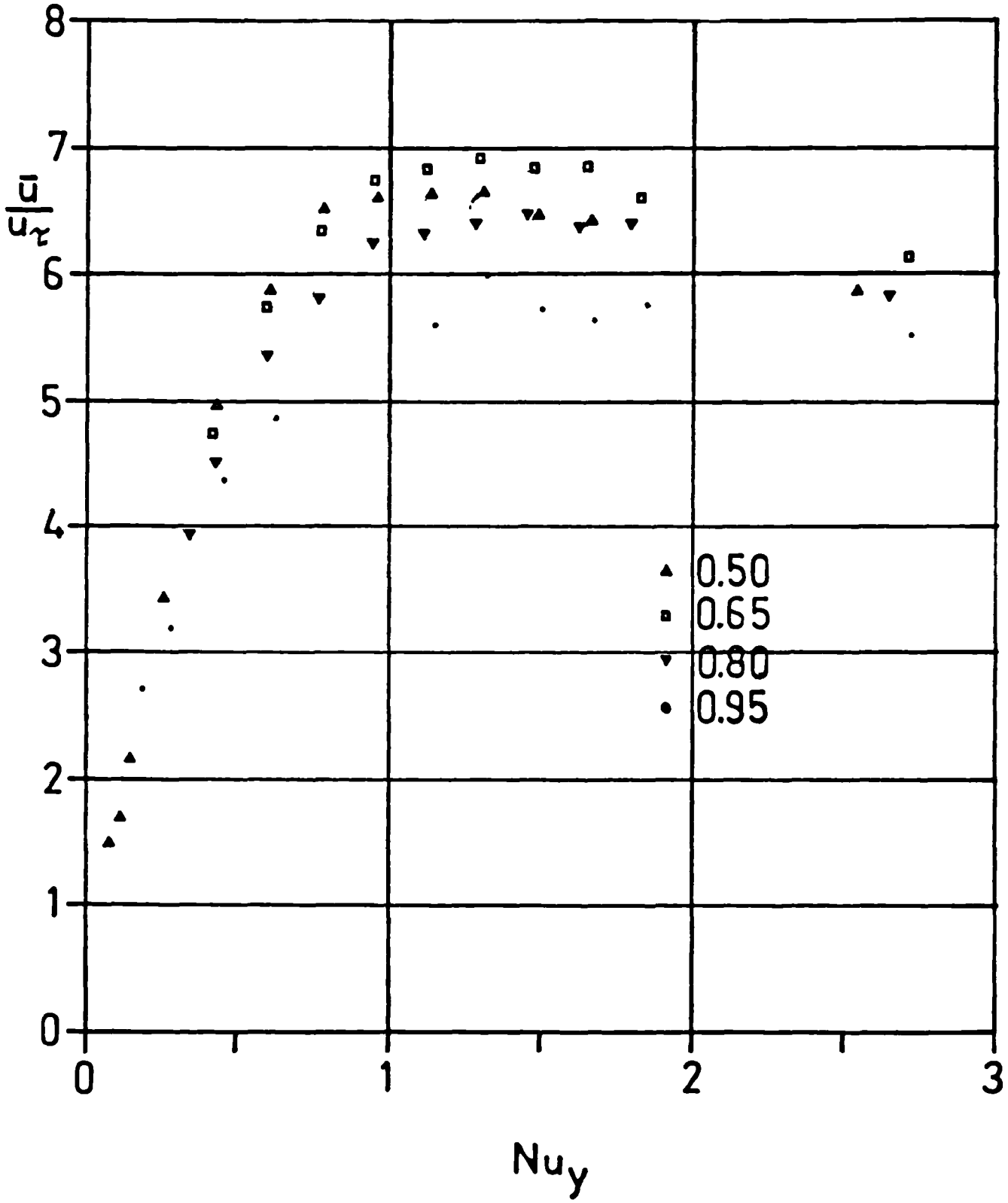

FIGURE 7.39

SERIES 3 MEAN VELOCITY SCALED WITH THE BUOYANCY SCALE

IN THE NEAR WALL REGION WITH Nu_y AS THE DIMENSIONLESS LENGTH

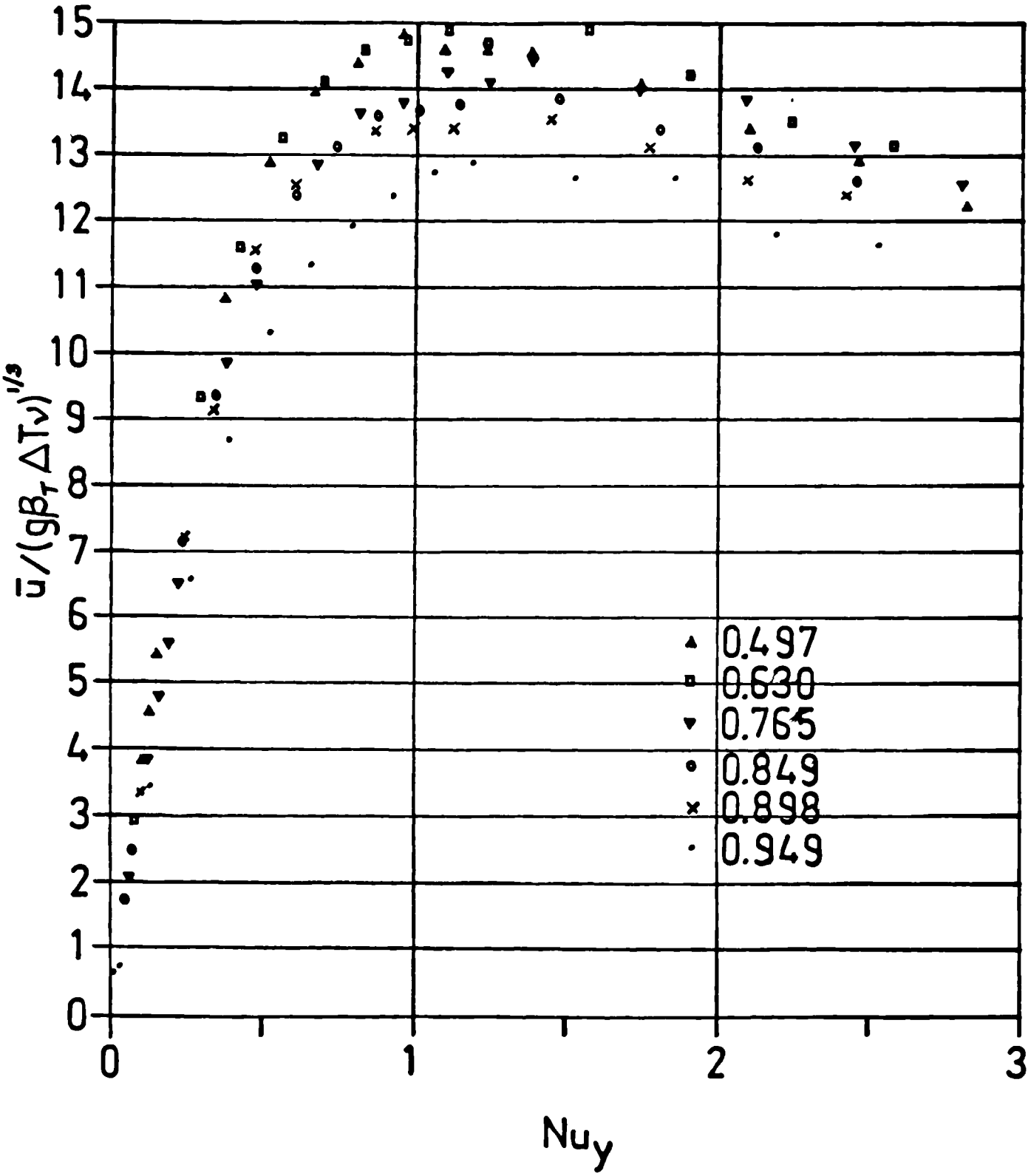

FIGURE 7.40

SERIES 4 MEAN VELOCITY SCALED WITH THE BUOYANCY SCALE

IN THE NEAR WALL REGION WITH Nu_y AS THE DIMENSIONLESS LENGTH

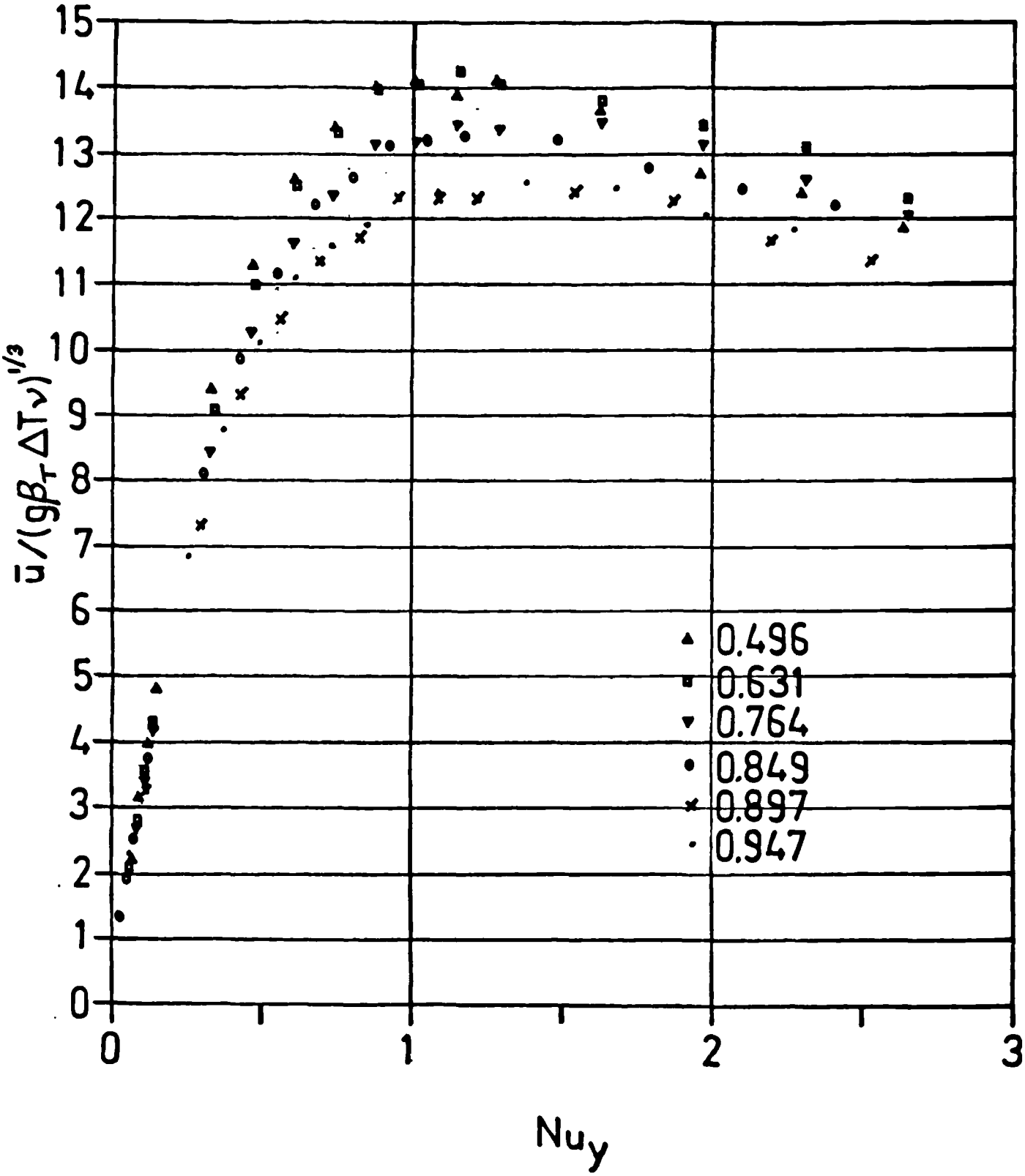

FIGURE 7.41

SERIES 5 MEAN VELOCITY SCALED WITH THE BUOYANCY SCALE

IN THE NEAR WALL REGION WITH Nu_y AS THE DIMENSIONLESS LENGTH

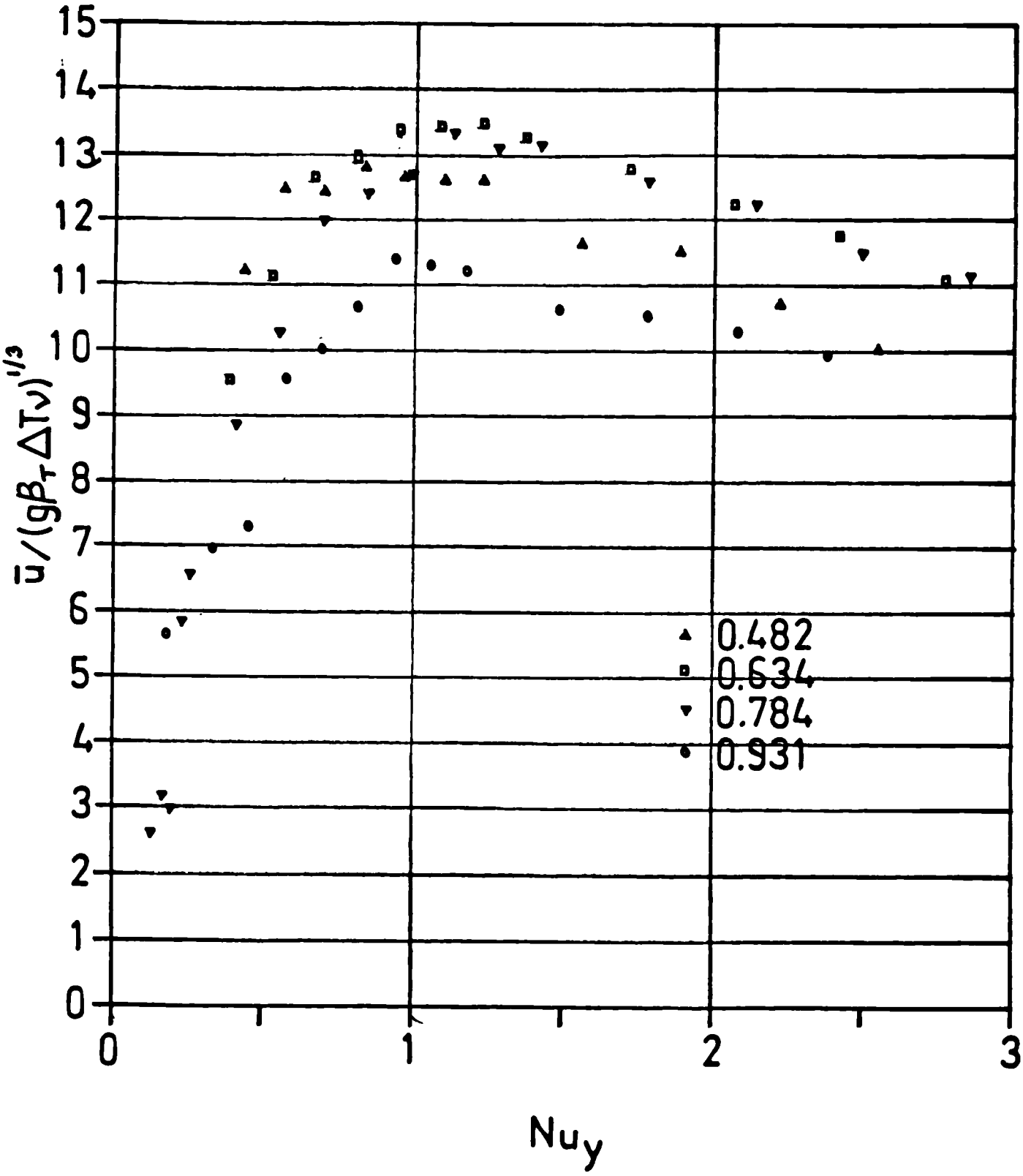

FIGURE 7.42

SERIES 6 MEAN VELOCITY SCALED WITH THE BUOYANCY SCALE

IN THE NEAR WALL REGION WITH Nu_y AS THE DIMENSIONLESS LENGTH

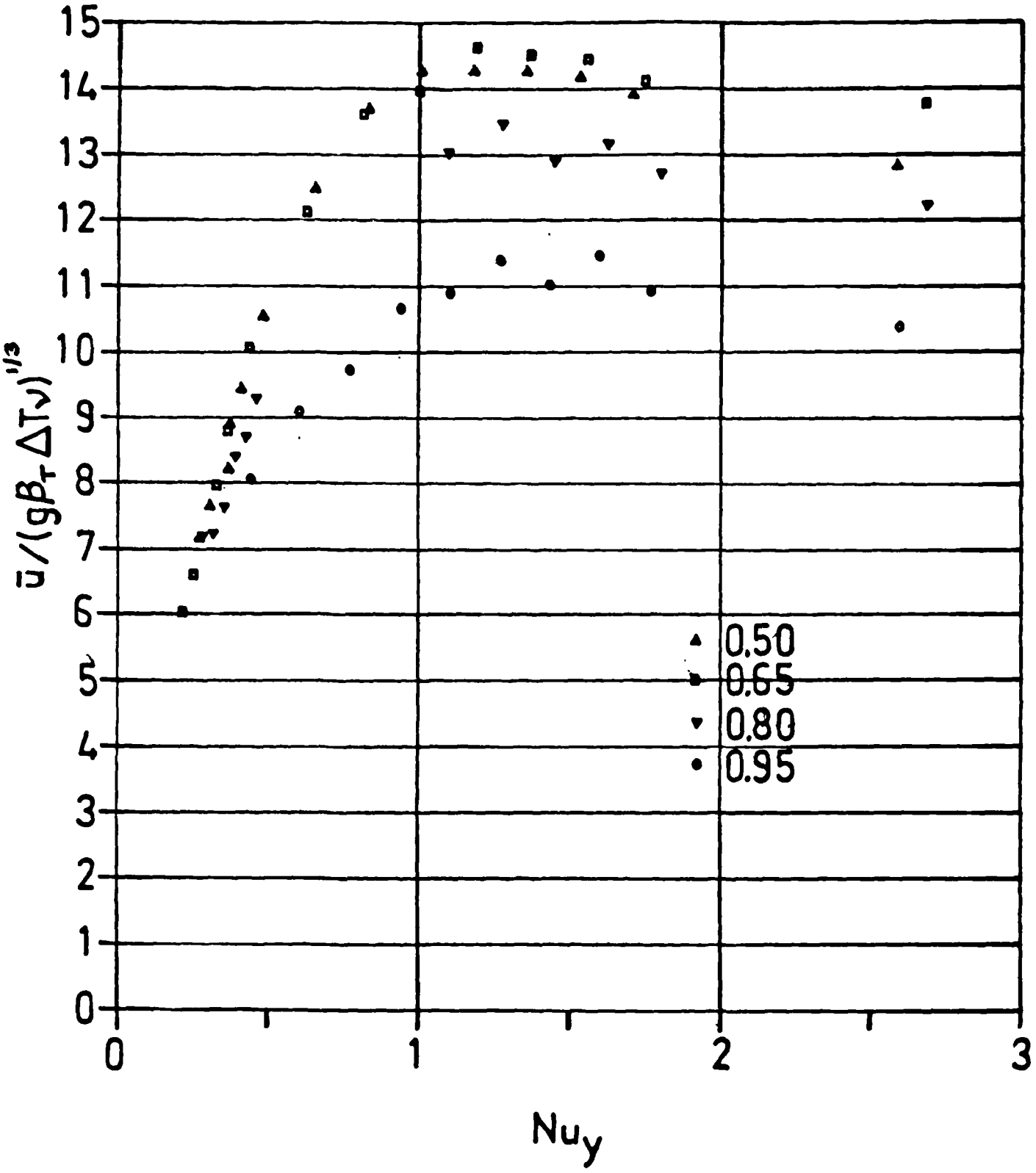

FIGURE 7.43

SERIES 7 MEAN VELOCITY SCALED WITH THE BUOYANCY SCALE

IN THE NEAR WALL REGION WITH Nu_v AS THE DIMENSIONLESS LENGTH

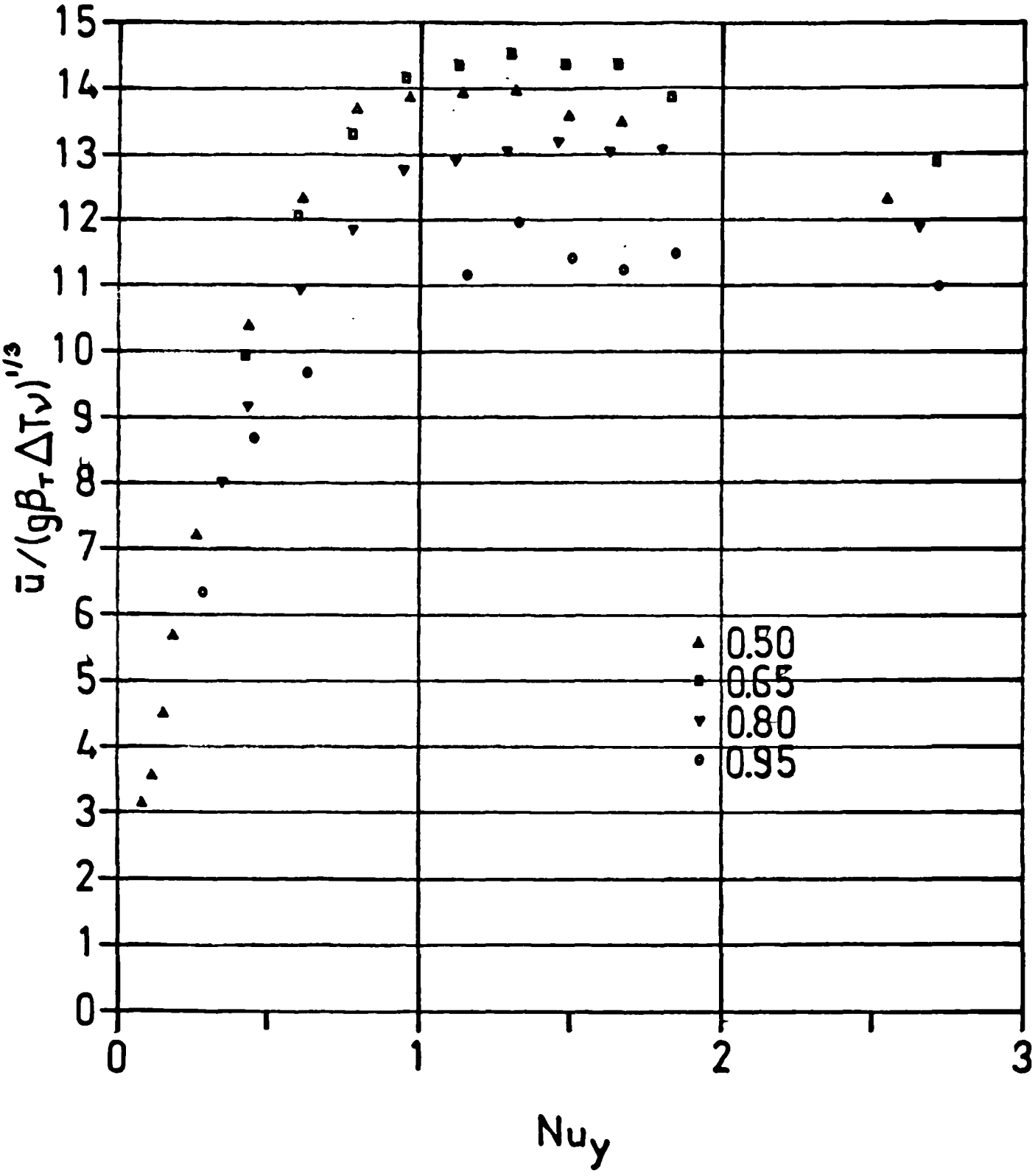

FIGURE 7.44

SERIES 3 MEAN VELOCITY SCALED WITH THE THERMAL SCALE

IN THE NEAR WALL REGION WITH Nu_y AS THE DIMENSIONLESS LENGTH

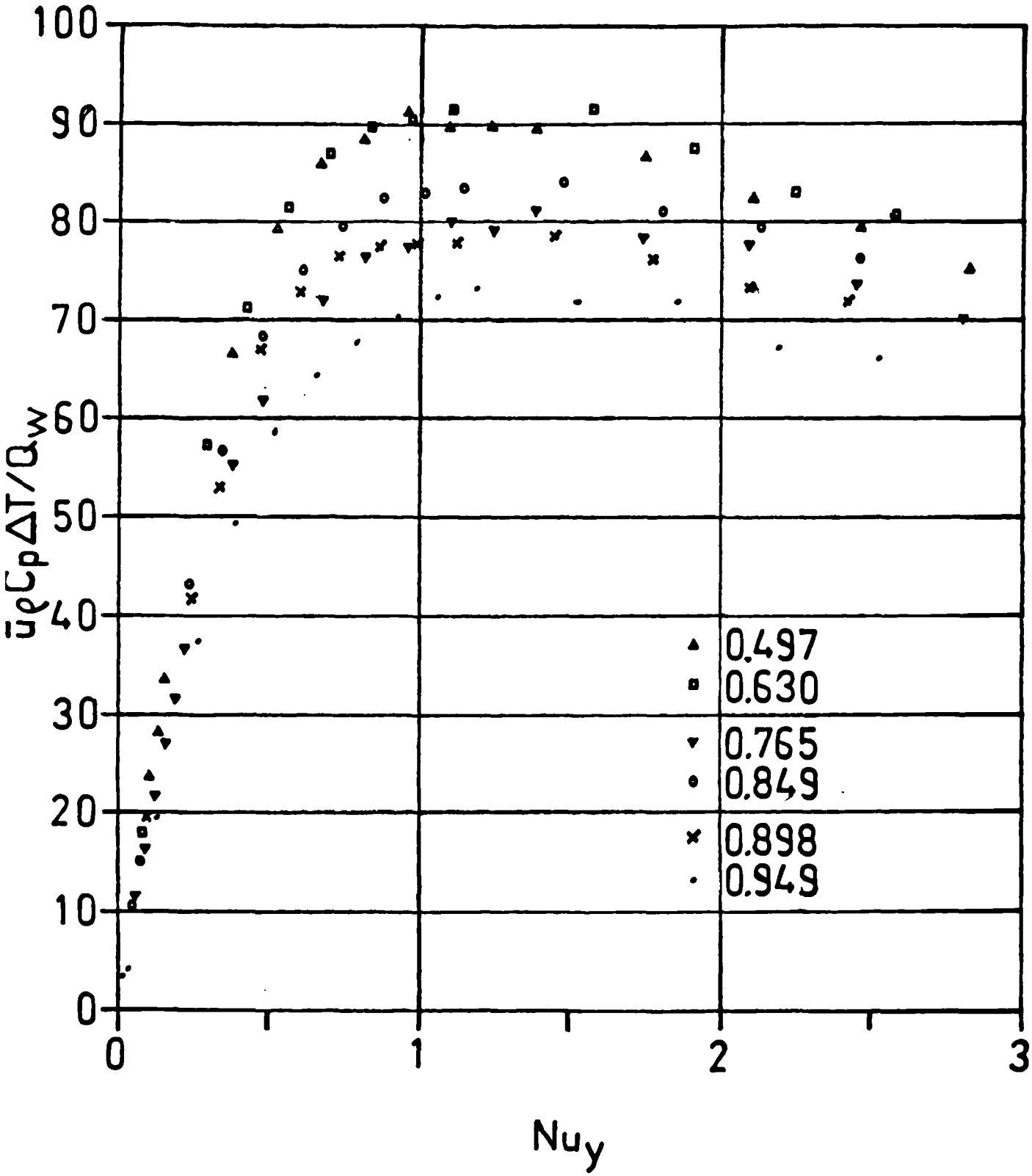

FIGURE 7.45

SERIES 4 MEAN VELOCITY SCALED WITH THE THERMAL SCALE

IN THE NEAR WALL REGION WITH Nu_y AS THE DIMENSIONLESS LENGTH

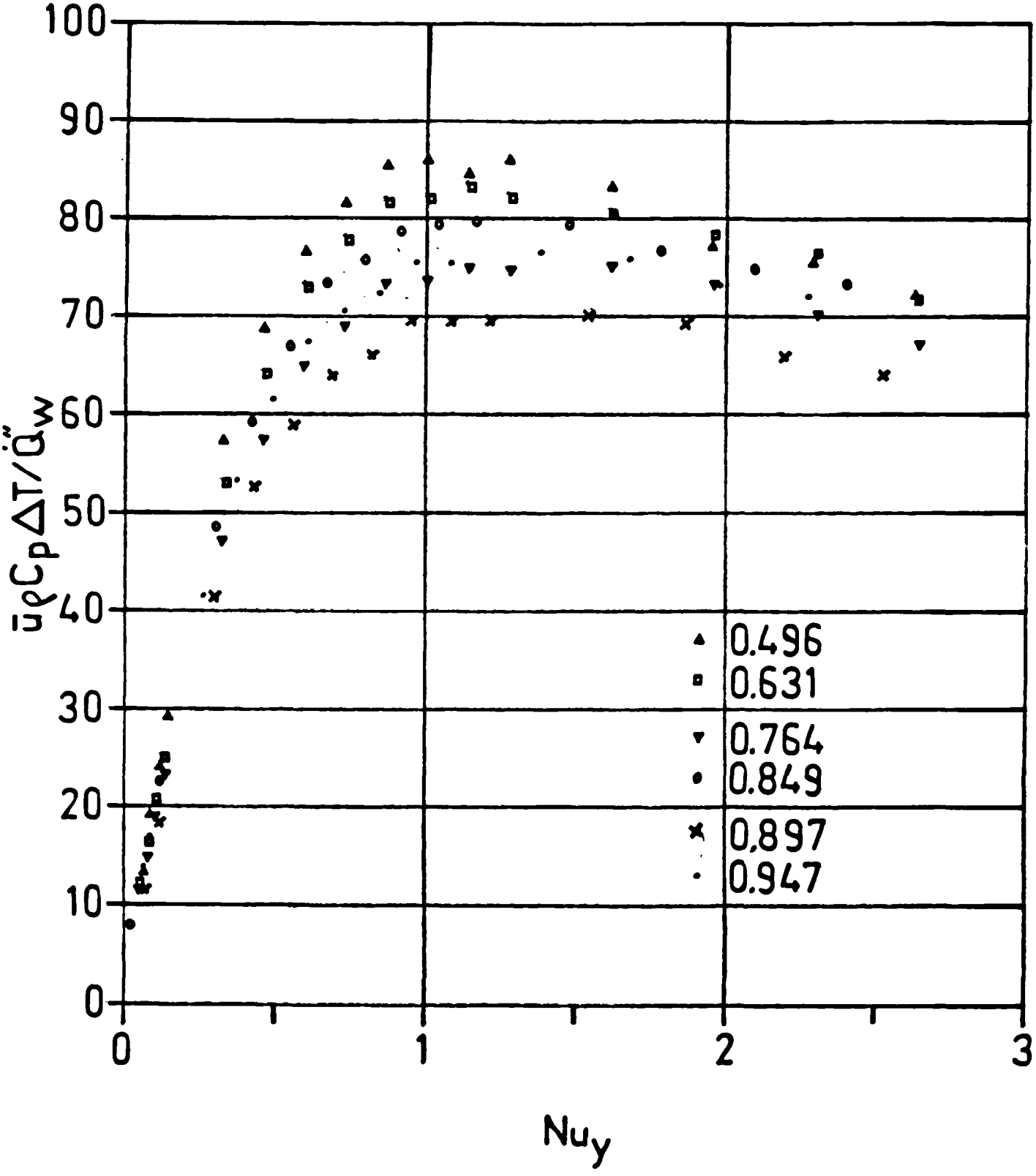

FIGURE 7.46

SERIES 5 MEAN VELOCITY SCALED WITH THE THERMAL SCALE

IN THE NEAR WALL REGION WITH Nu_y AS THE DIMENSIONLESS LENGTH

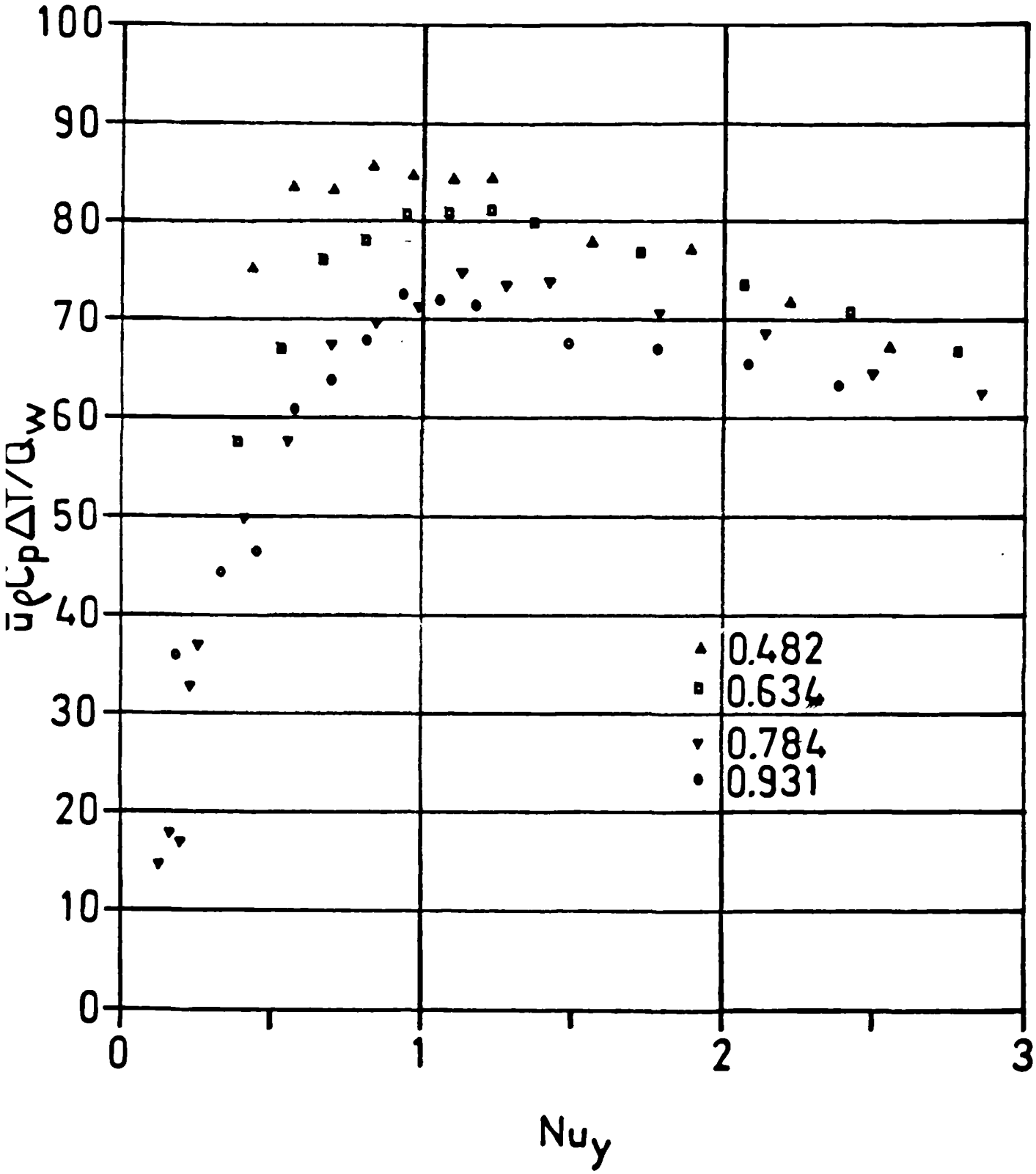

FIGURE 7. 47

SERIES 6 MEAN VELOCITY SCALED WITH THE THERMAL SCALE

IN THE NEAR WALL REGION WITH Nu_y AS THE DIMENSIONLESS LENGTH

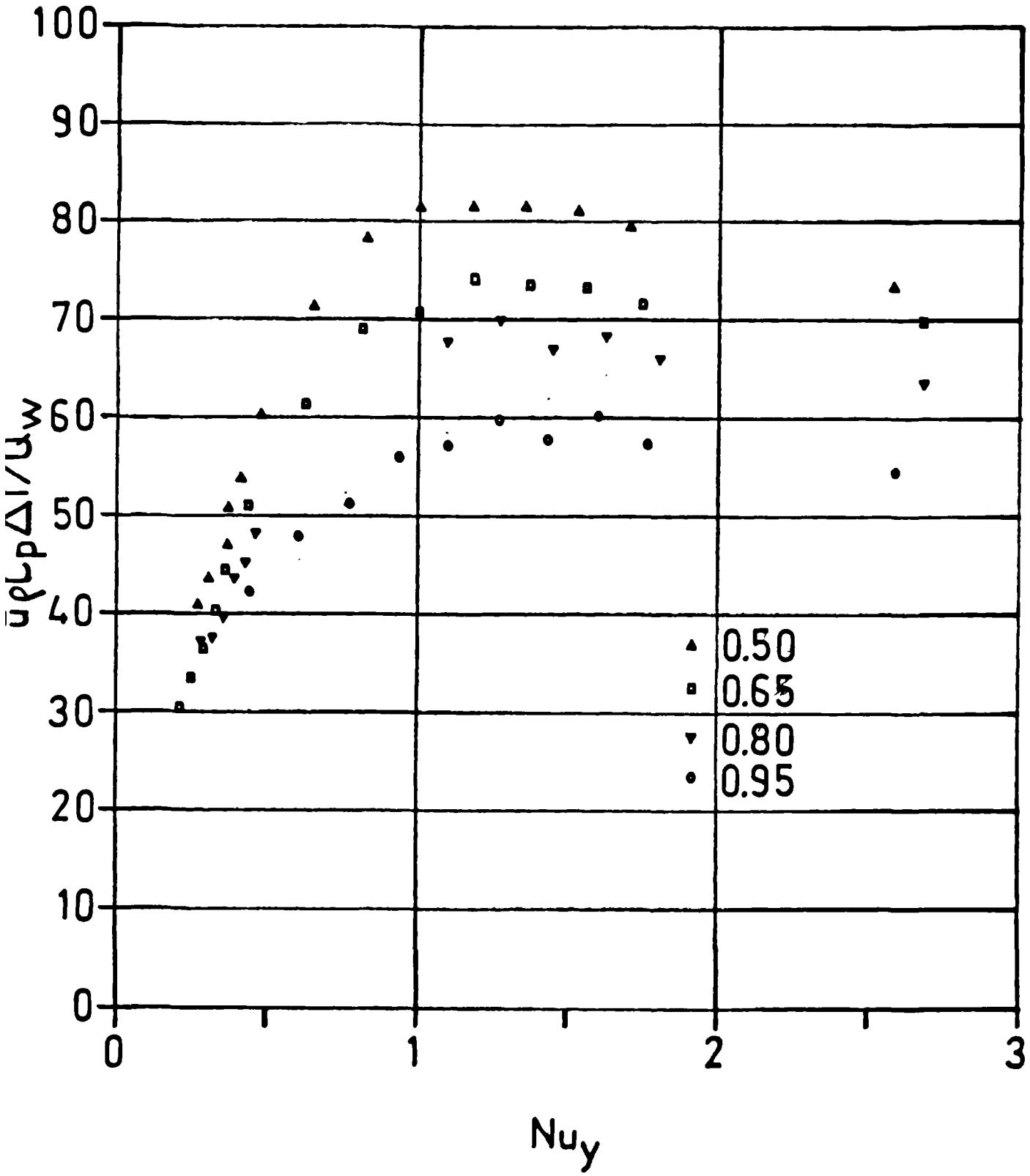

FIGURE 7. 48

SERIES 7 MEAN VELOCITY SCALED WITH THE THERMAL SCALE

IN THE NEAR WALL REGION WITH Nu_y AS THE DIMENSIONLESS LENGTH

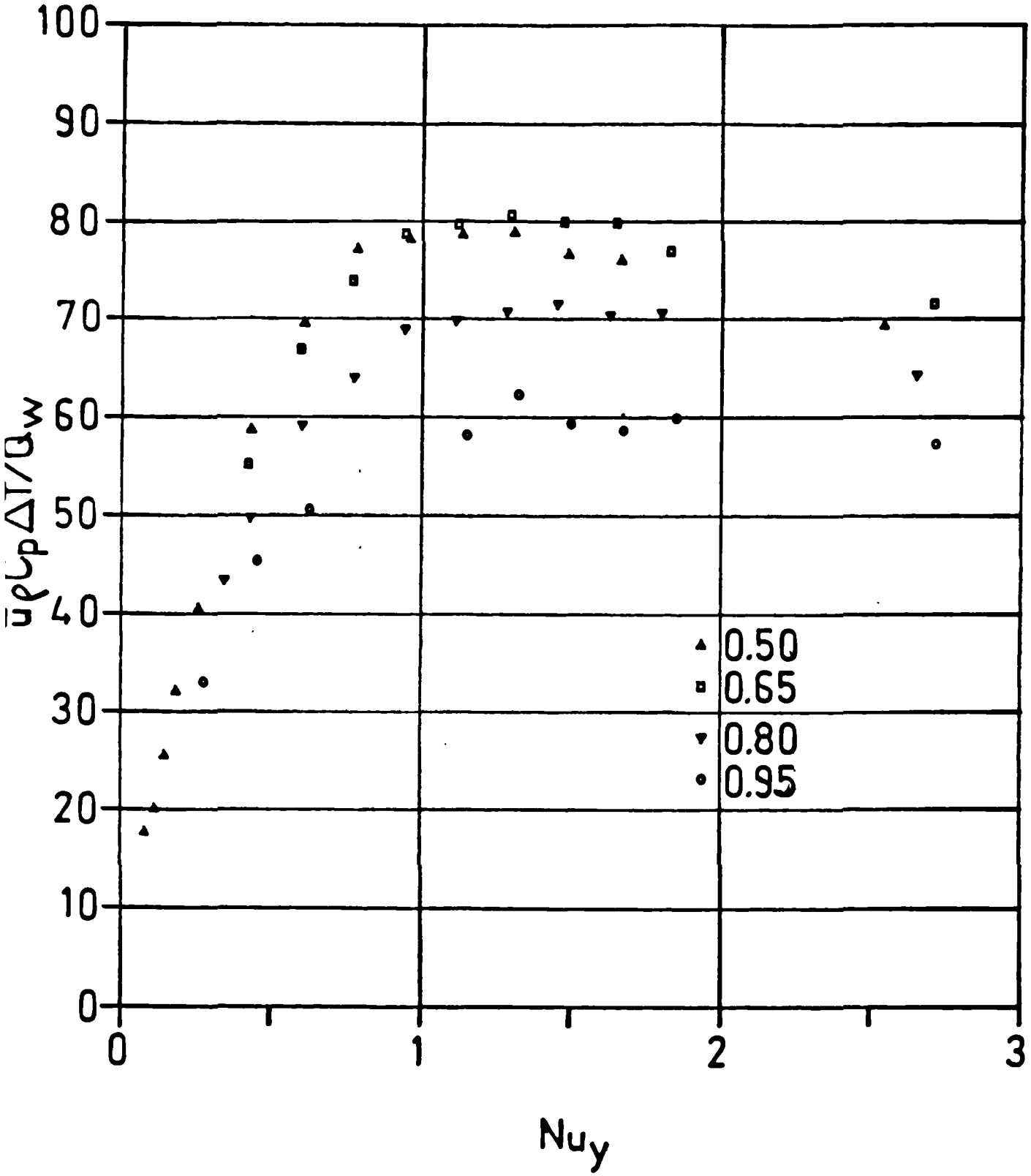

FIGURE 7.49

SERIES 3 MEAN VELOCITY SCALED FOR THE OUTER PART OF THE NEAR WALL REGION WITH Nu_y AS THE DIMENSIONLESS LENGTH

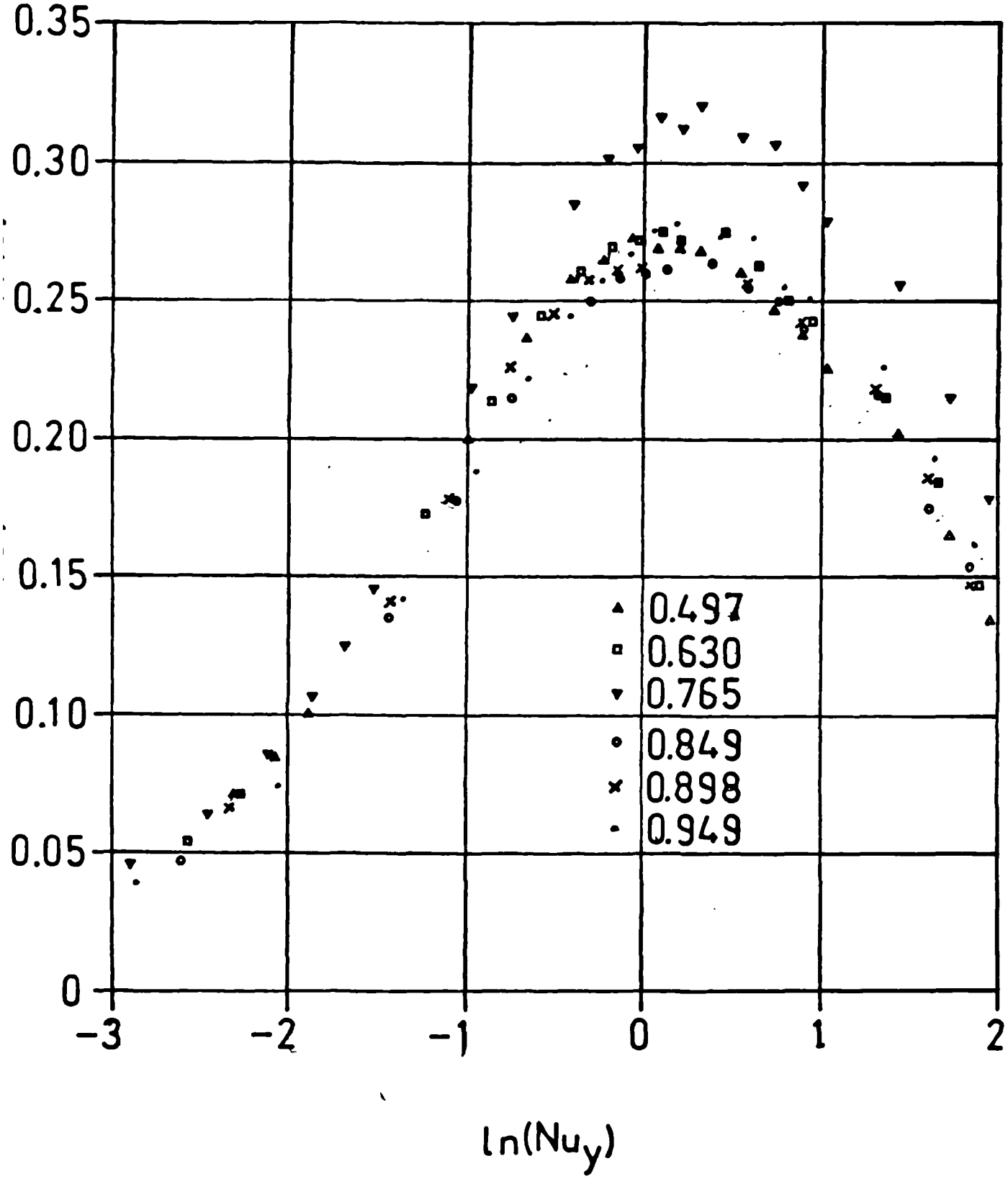

FIGURE 7.50

SERIES 4 MEAN VELOCITY SCALED FOR THE OUTER PART OF THE NEAR WALL REGION WITH Nu_v AS THE DIMENSIONLESS LENGTH

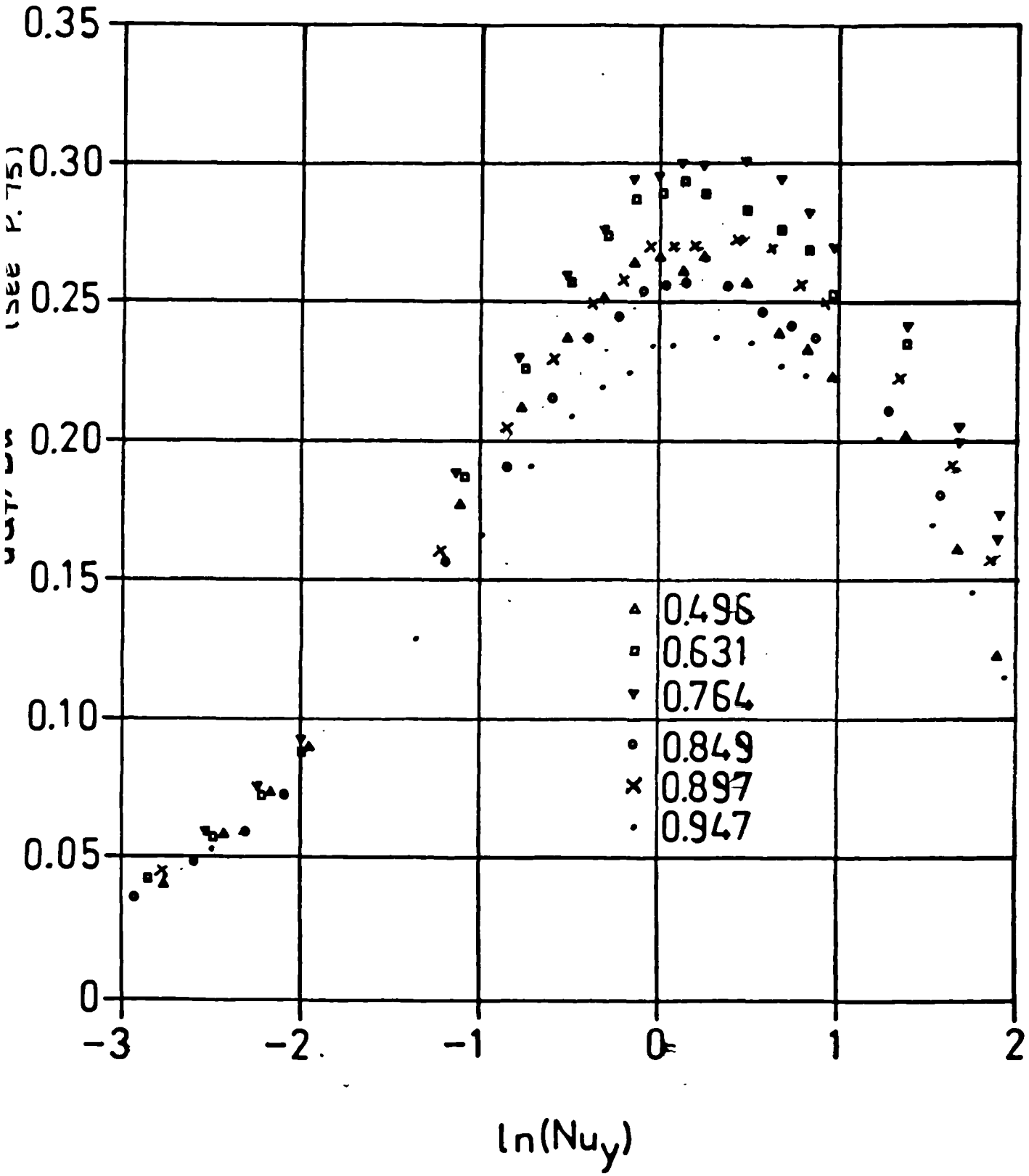

FIGURE 7.51

SERIES 3 MEAN VELOCITY SCALED WITH THE SHEAR VELOCITY AGAINST y SCALED WITH δ

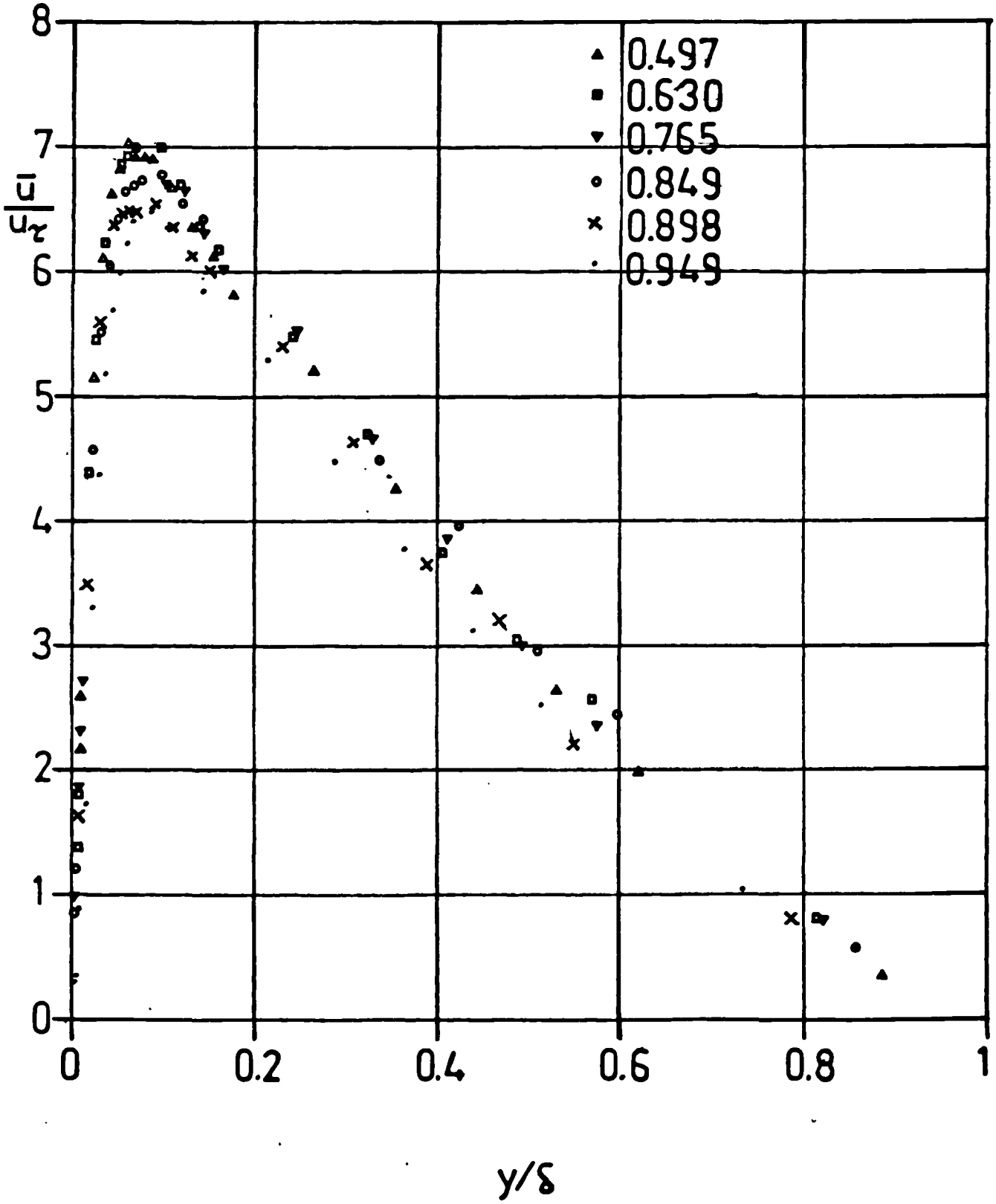

FIGURE 7.52

SERIES 4 MEAN VELOCITY SCALED WITH THE SHEAR VELOCITY AGAINST y SCALED WITH δ

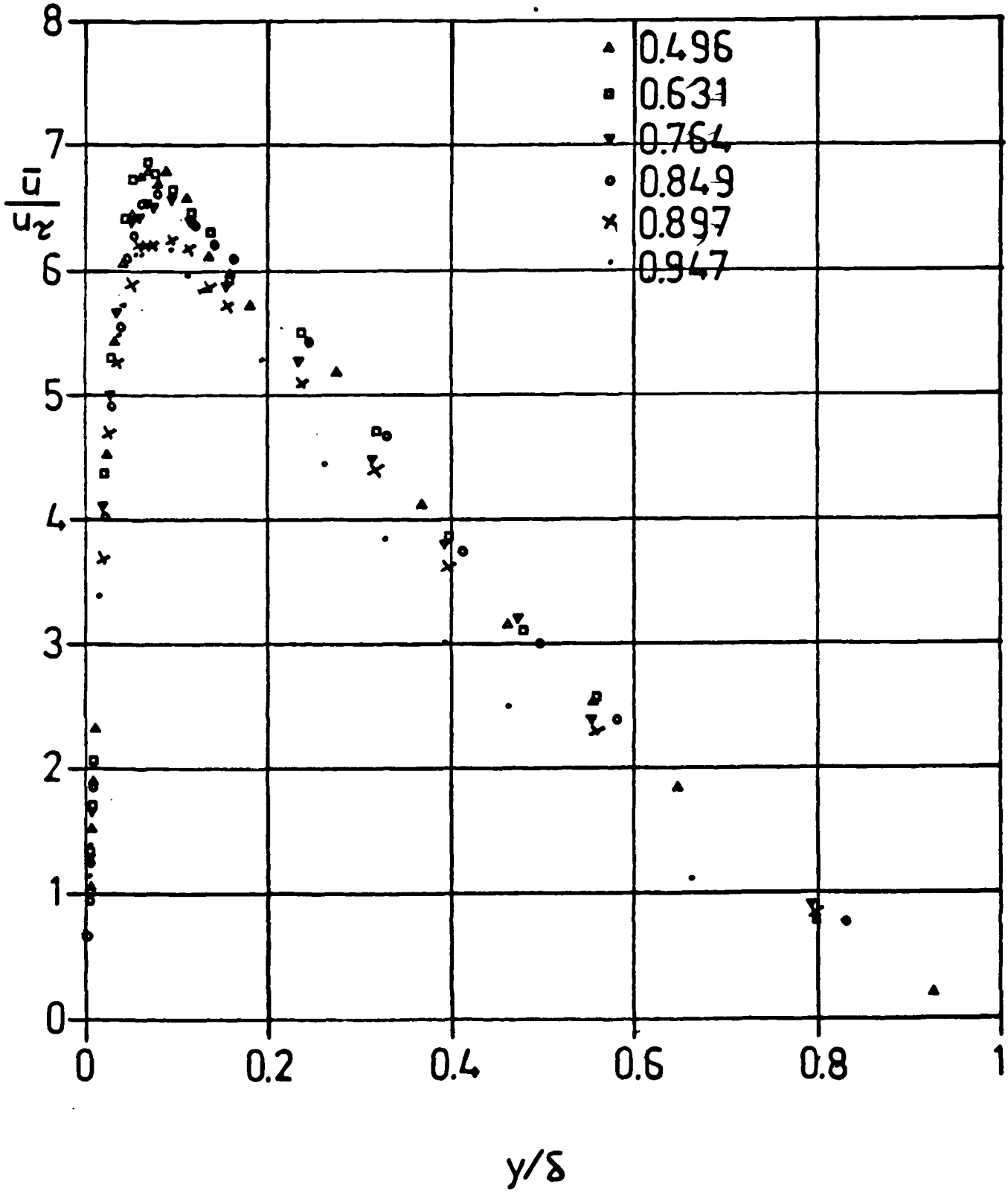

FIGURE 7.53

SERIES 6 MEAN VELOCITY SCALED WITH THE SHEAR VELOCITY AGAINST y SCALED WITH δ

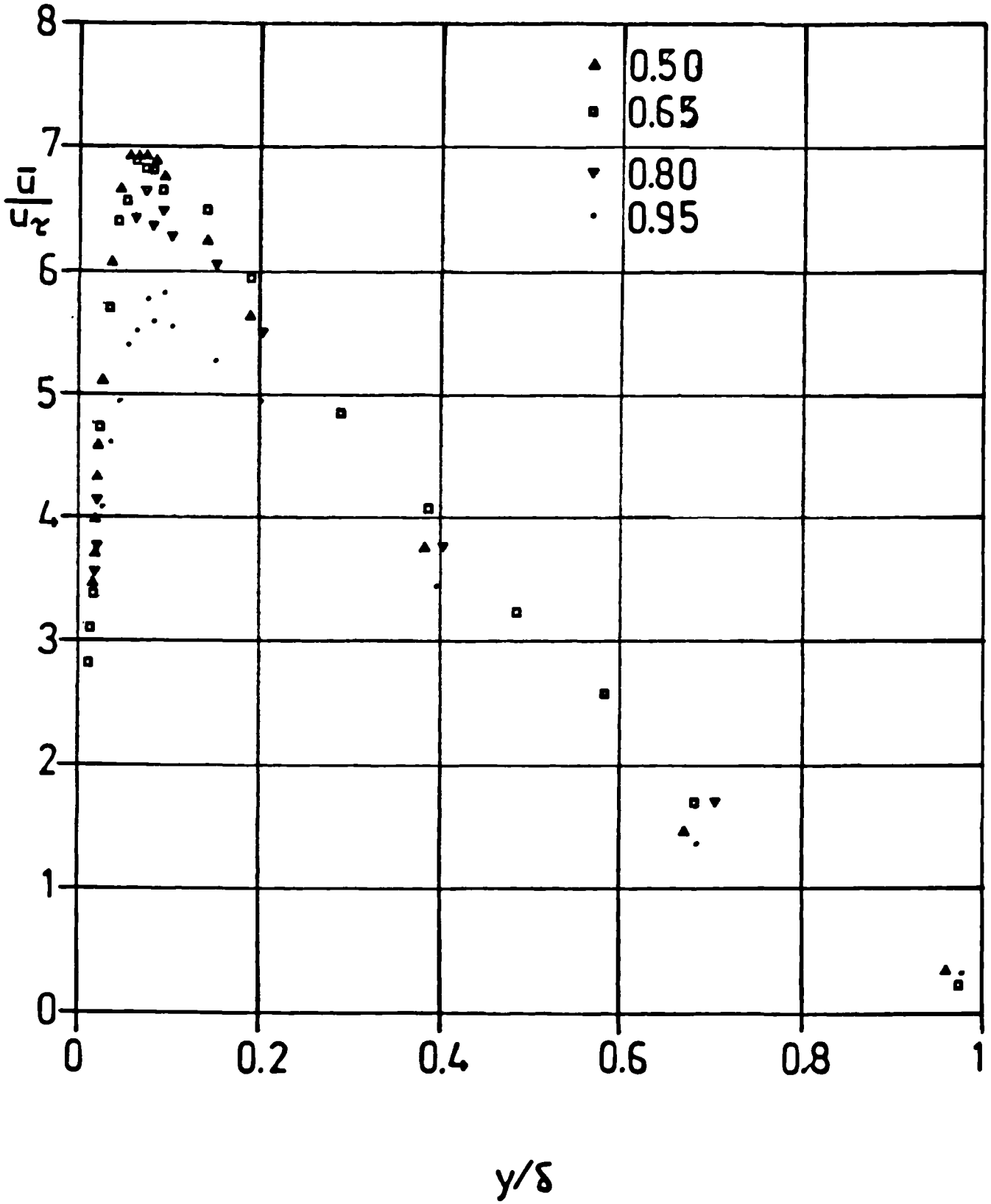

FIGURE 7.54

SERIES 7 MEAN VELOCITY SCALED WITH THE SHEAR VELOCITY AGAINST y SCALED WITH δ

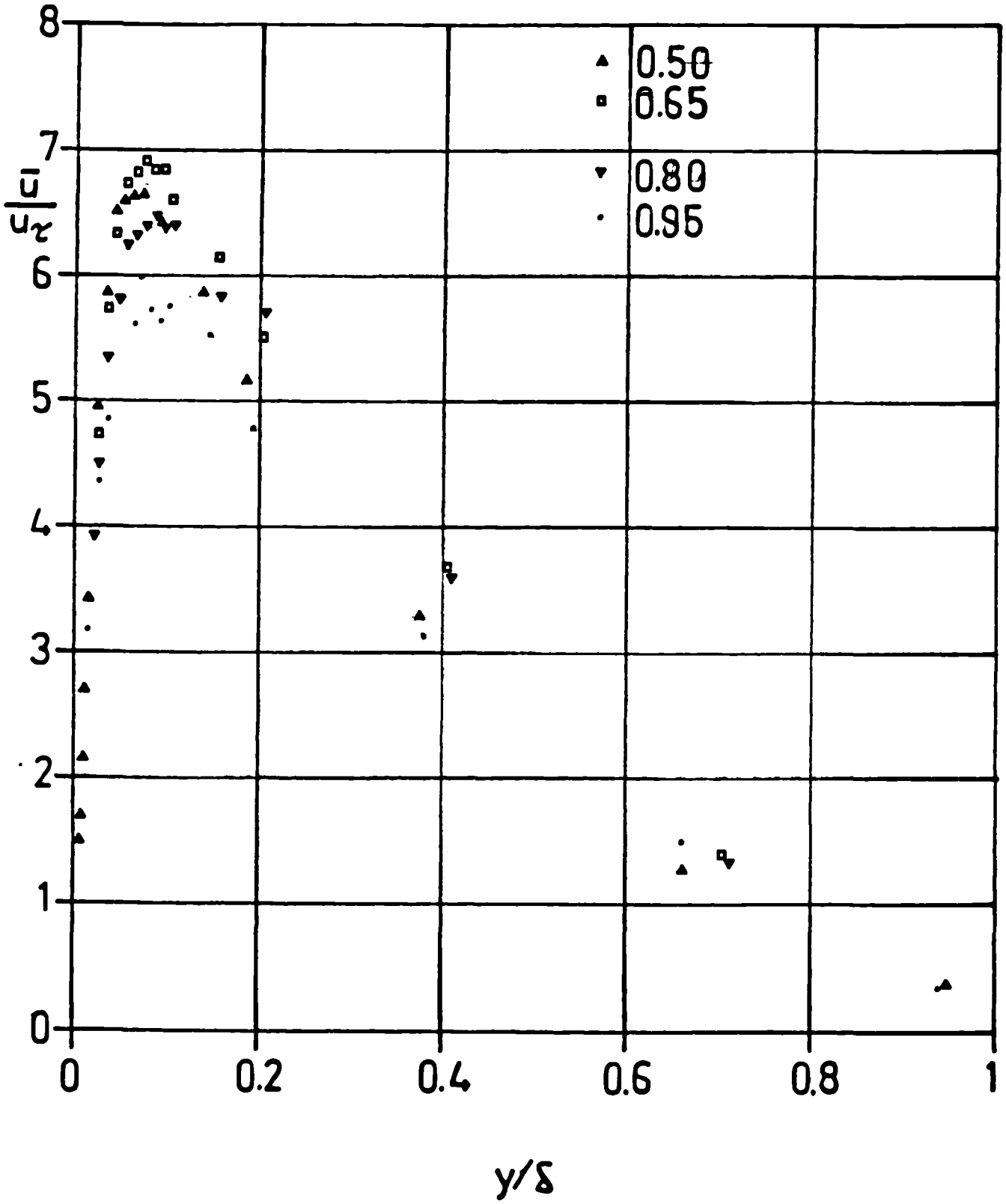

FIGURE 7.55

SERIES 3 MEAN VELOCITY SCALED WITH

$[g\beta_T(T_w-T_\infty)\delta]^{1/2}$ AGAINST y SCALED WITH δ

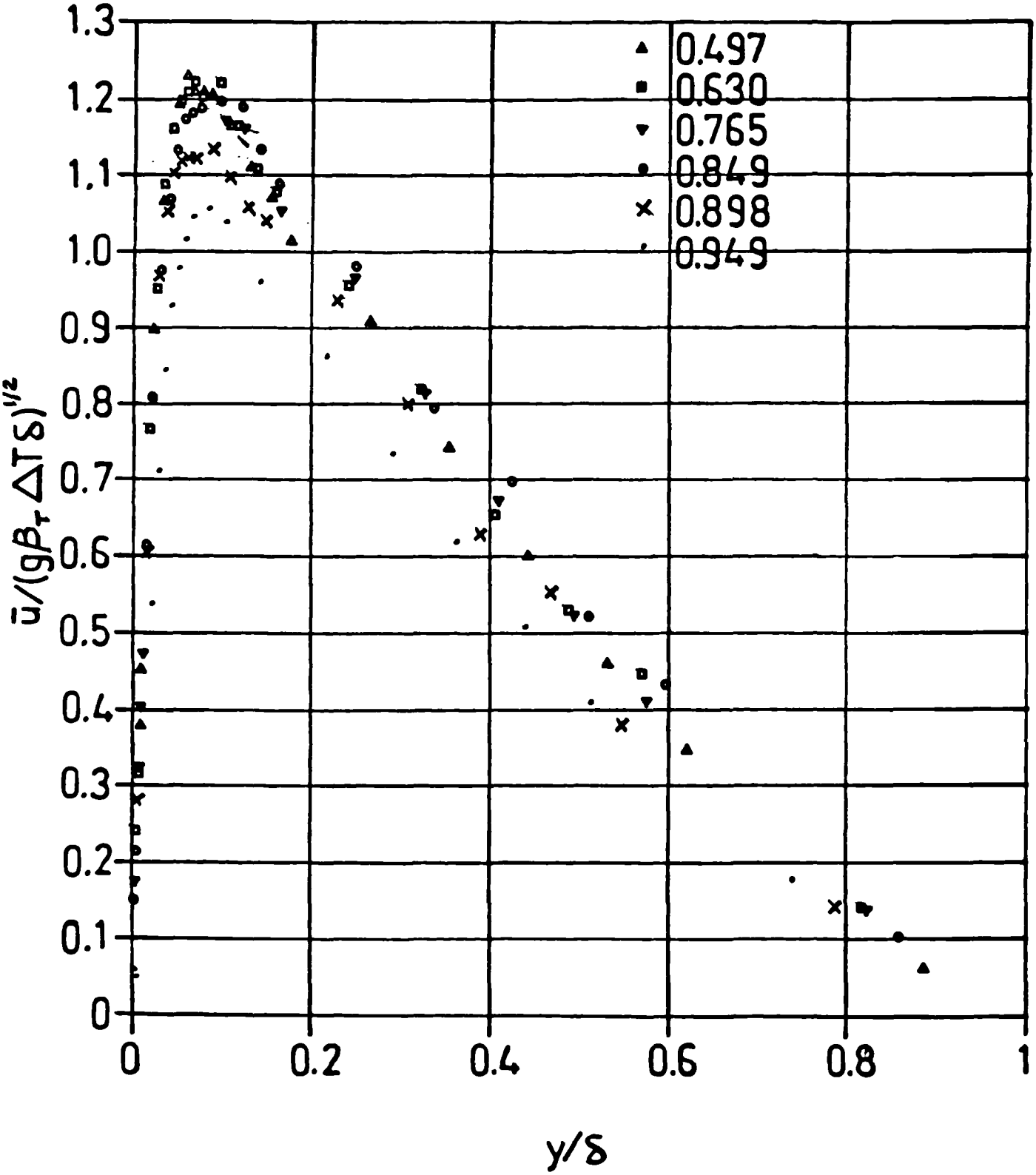

FIGURE 7.56

SERIES 4 MEAN VELOCITY SCALED WITH

$[g\beta_T(T_w-T_\infty)\delta]^{1/2}$ AGAINST y SCALED WITH δ

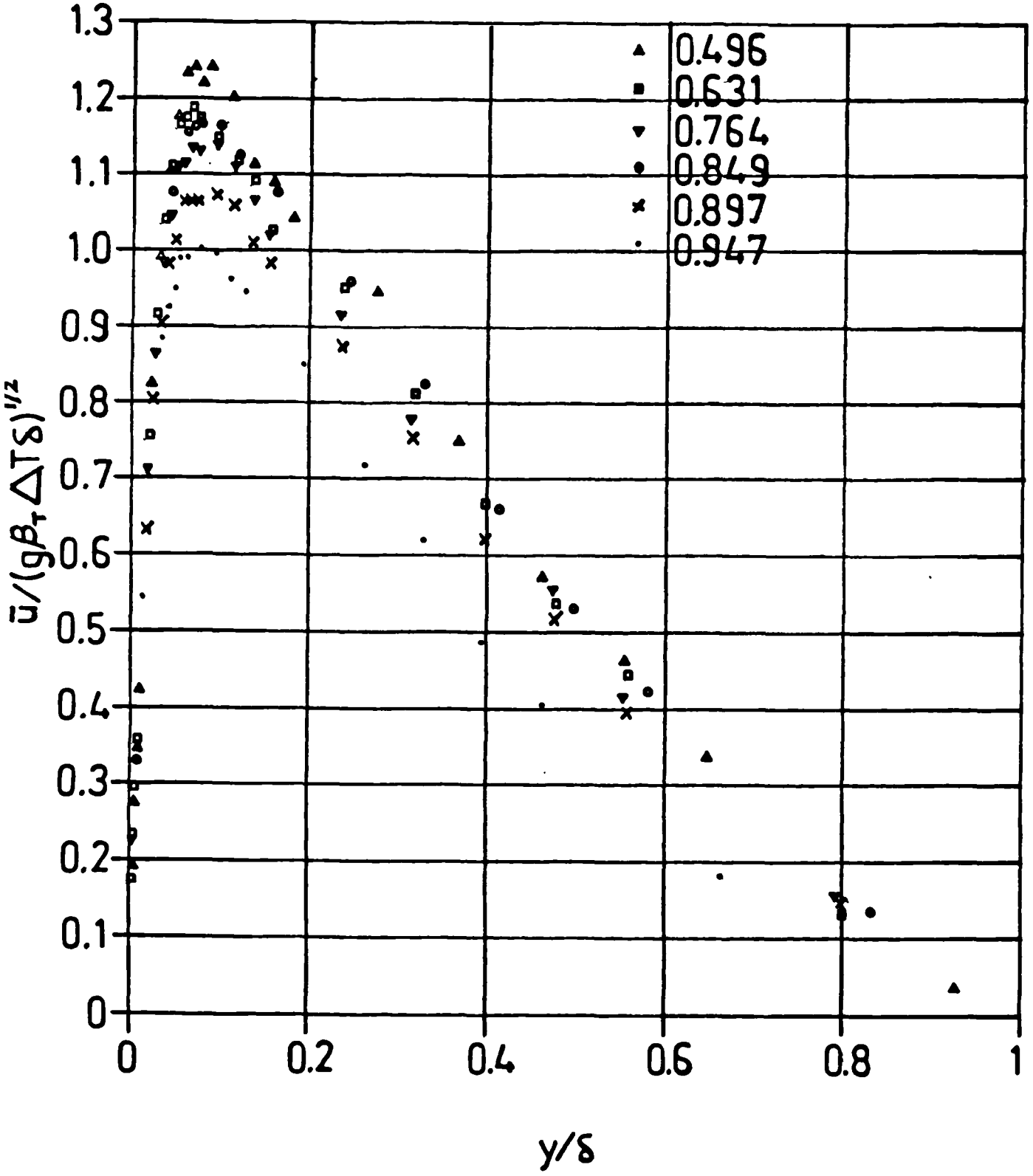

FIGURE 7.57

SERIES 6 MEAN VELOCITY SCALED WITH

$[g\beta_T(T_\omega - T_\infty)\delta]^{1/2}$ AGAINST y SCALED WITH δ

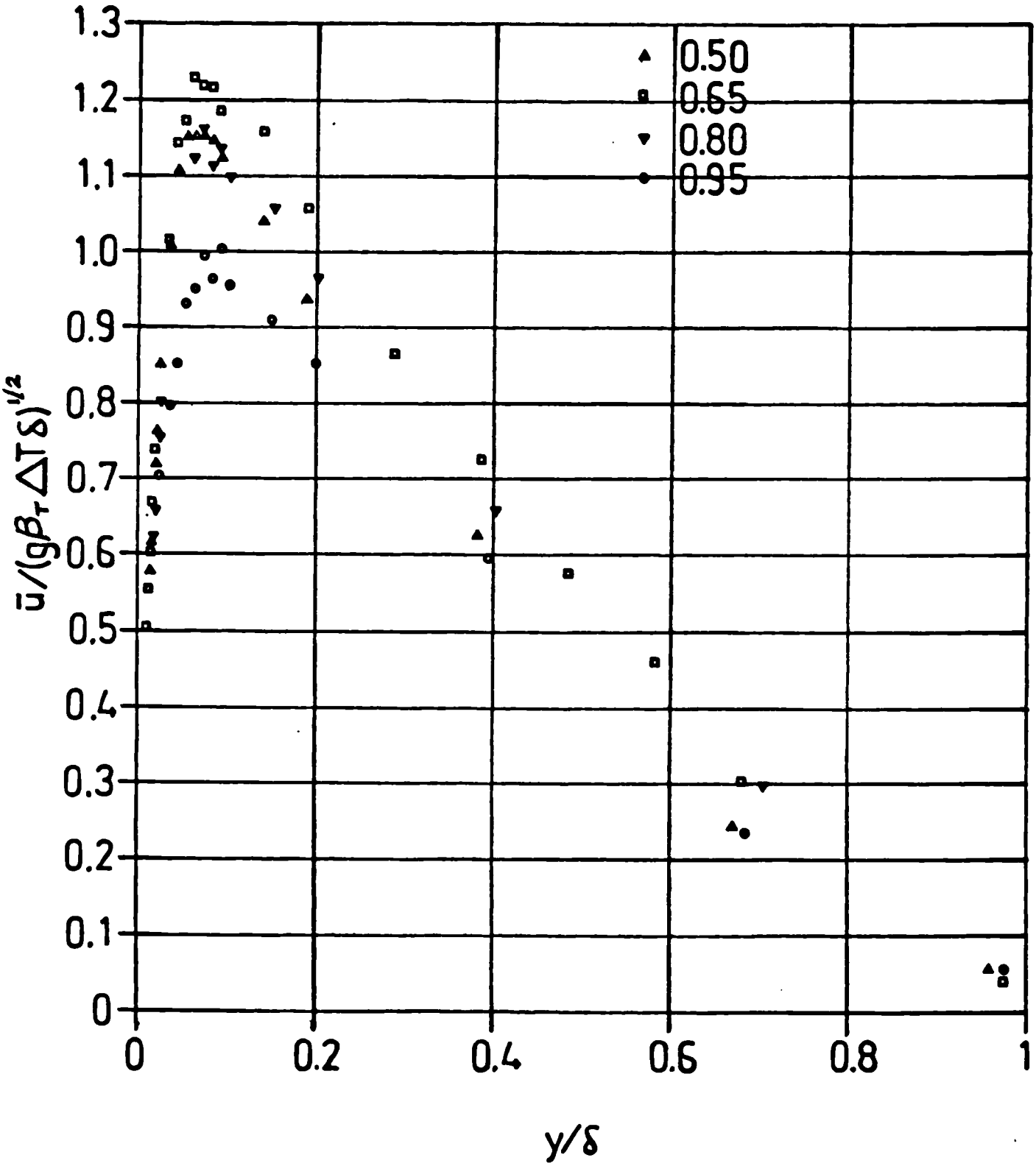

FIGURE 7.58

SERIES 7 MEAN VELOCITY SCALED WITH

$[g\beta_T(T_w-T_\infty)\delta]^{1/2}$ AGAINST y SCALED WITH δ

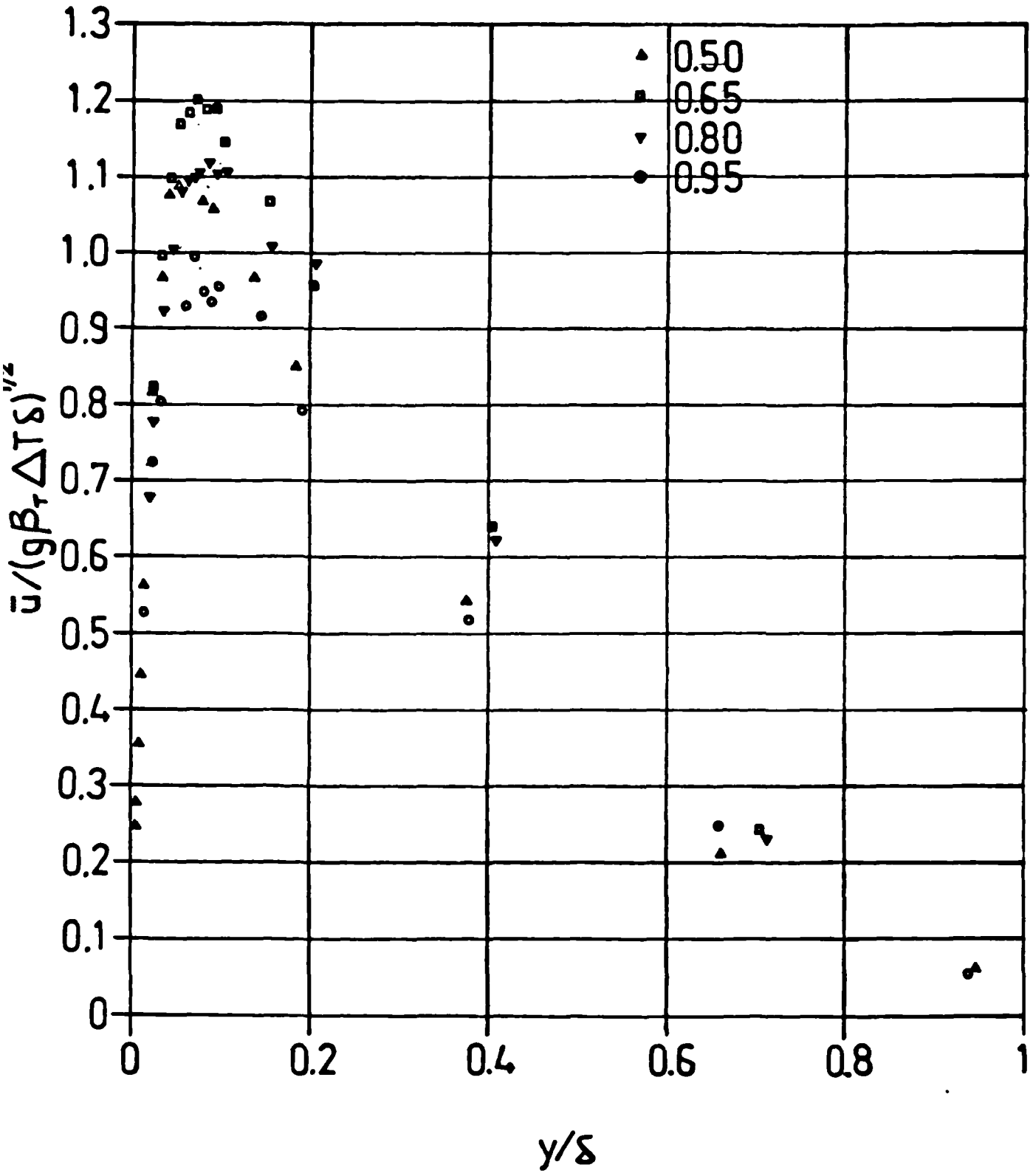

FIGURE 7.59

SERIES 3 MEAN VELOCITY SCALED WITH

$[kg\beta_T(T_w-T_\infty)^2/\dot{Q}''_w]^{1/2}$ AGAINST y SCALED WITH δ

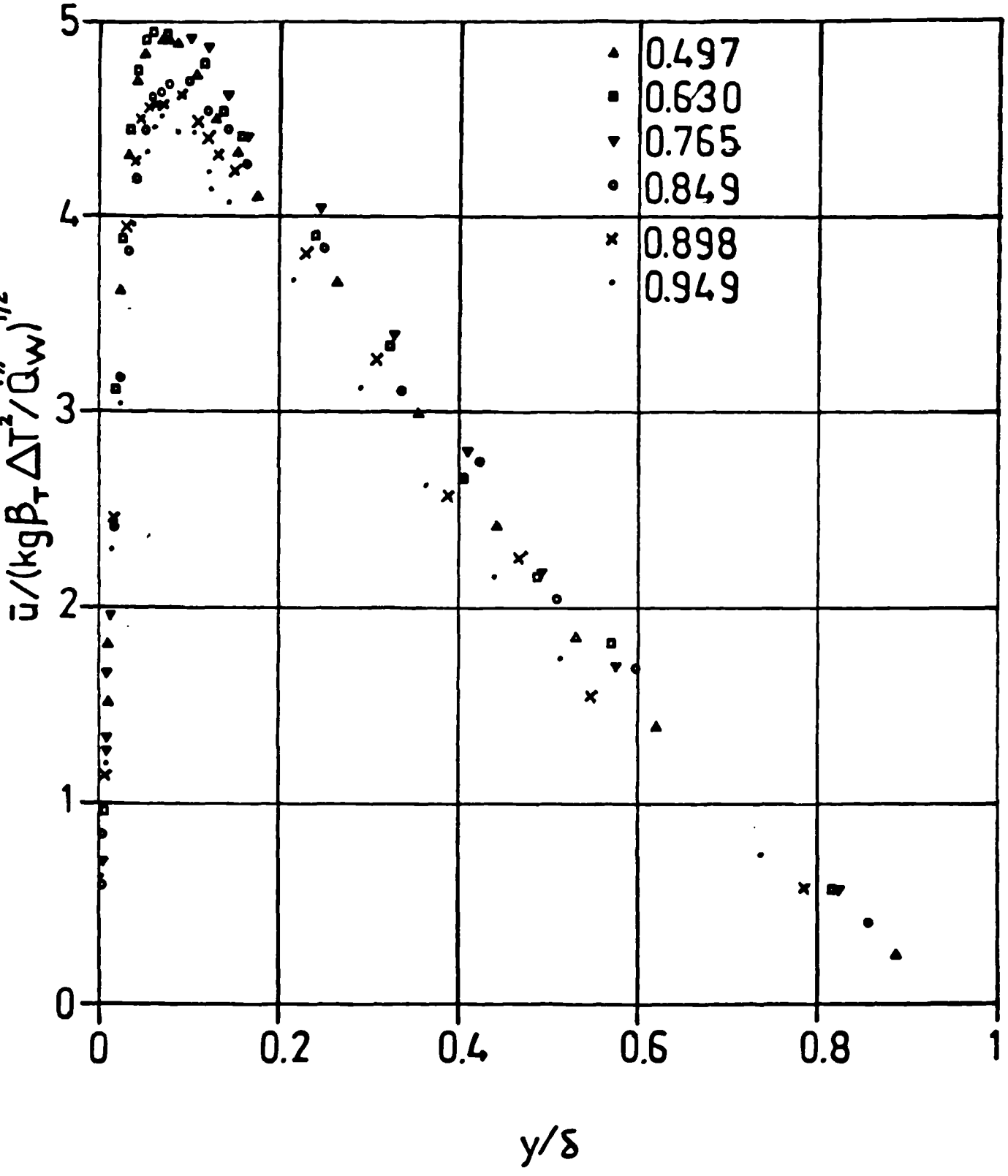

FIGURE 7.60

SERIES 4 MEAN VELOCITY SCALED WITH

$[kg\beta_T(T_w-T_\infty)^2/\dot{Q}''_w]^{1/2}$ AGAINST y SCALED WITH δ

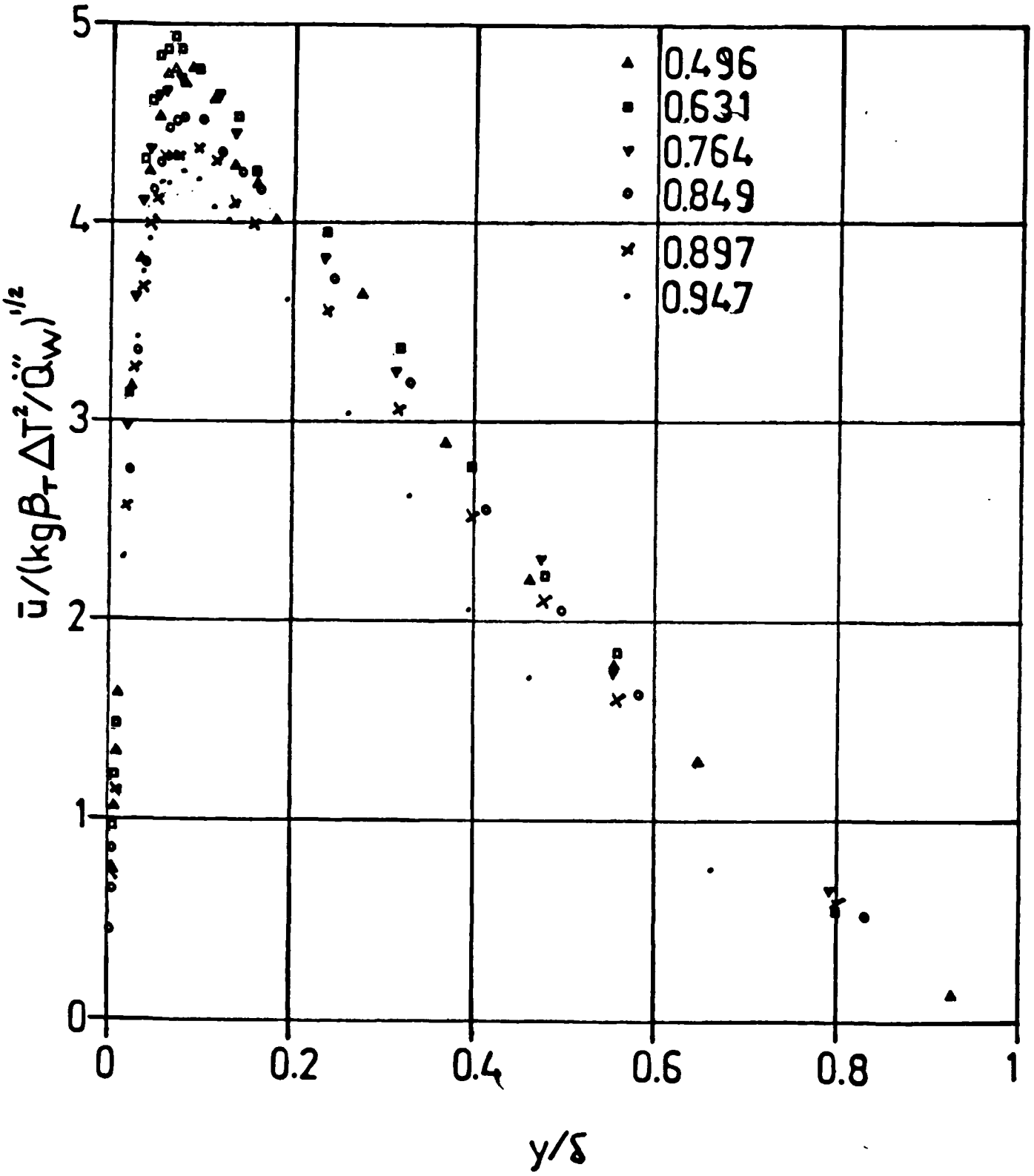

FIGURE 7.61

SERIES 6 MEAN VELOCITY SCALED WITH

$[kg\beta_T(T_w-T_\infty)^2/\dot{Q}''_w]^{1/2}$ AGAINST y SCALED WITH δ

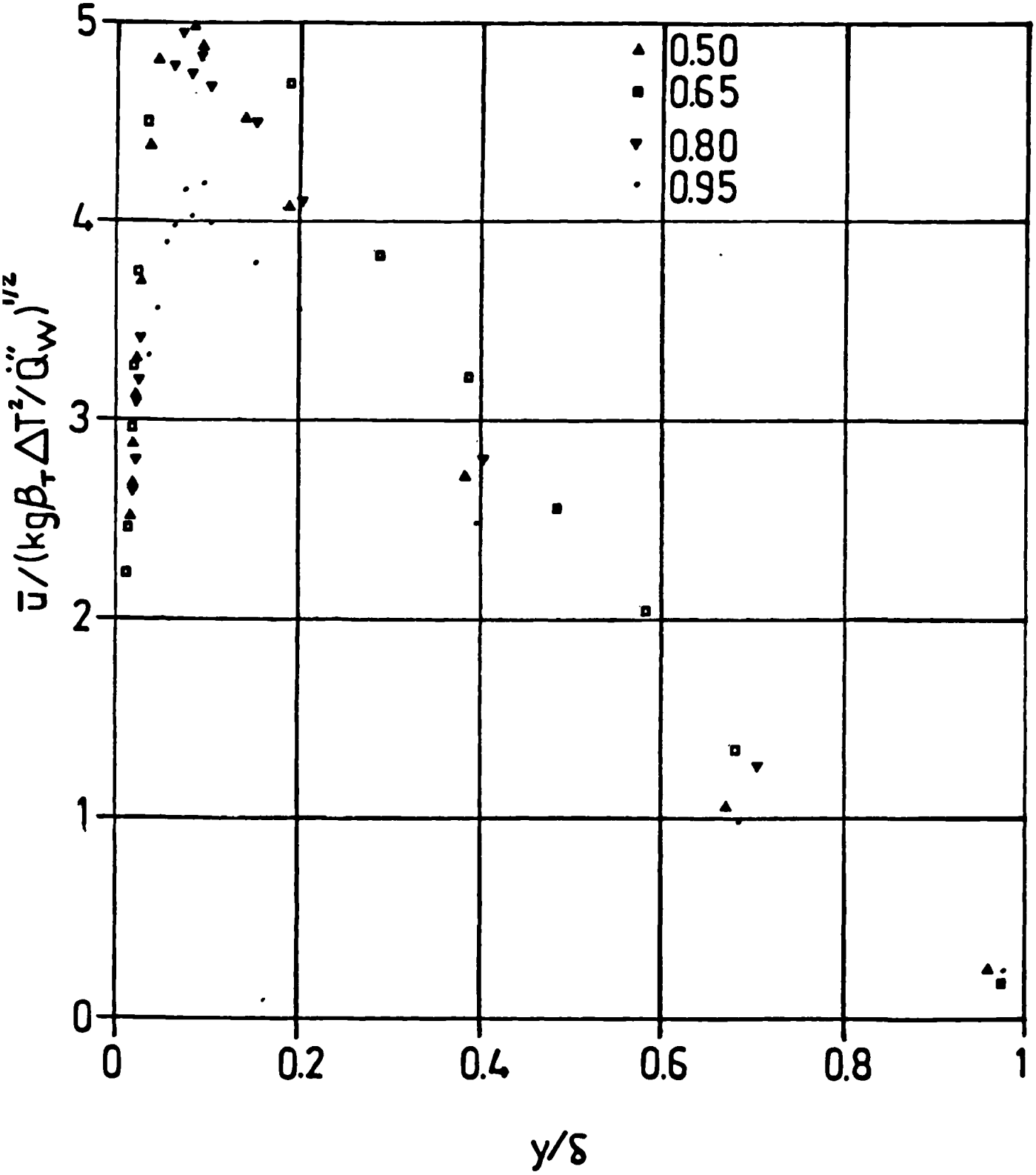

FIGURE 7.62

SERIES 7 MEAN VELOCITY SCALED WITH

$[kg\beta_T(T_\omega-T_\infty)^2/\dot{Q}''_\omega]^{1/2}$ AGAINST y SCALED WITH δ

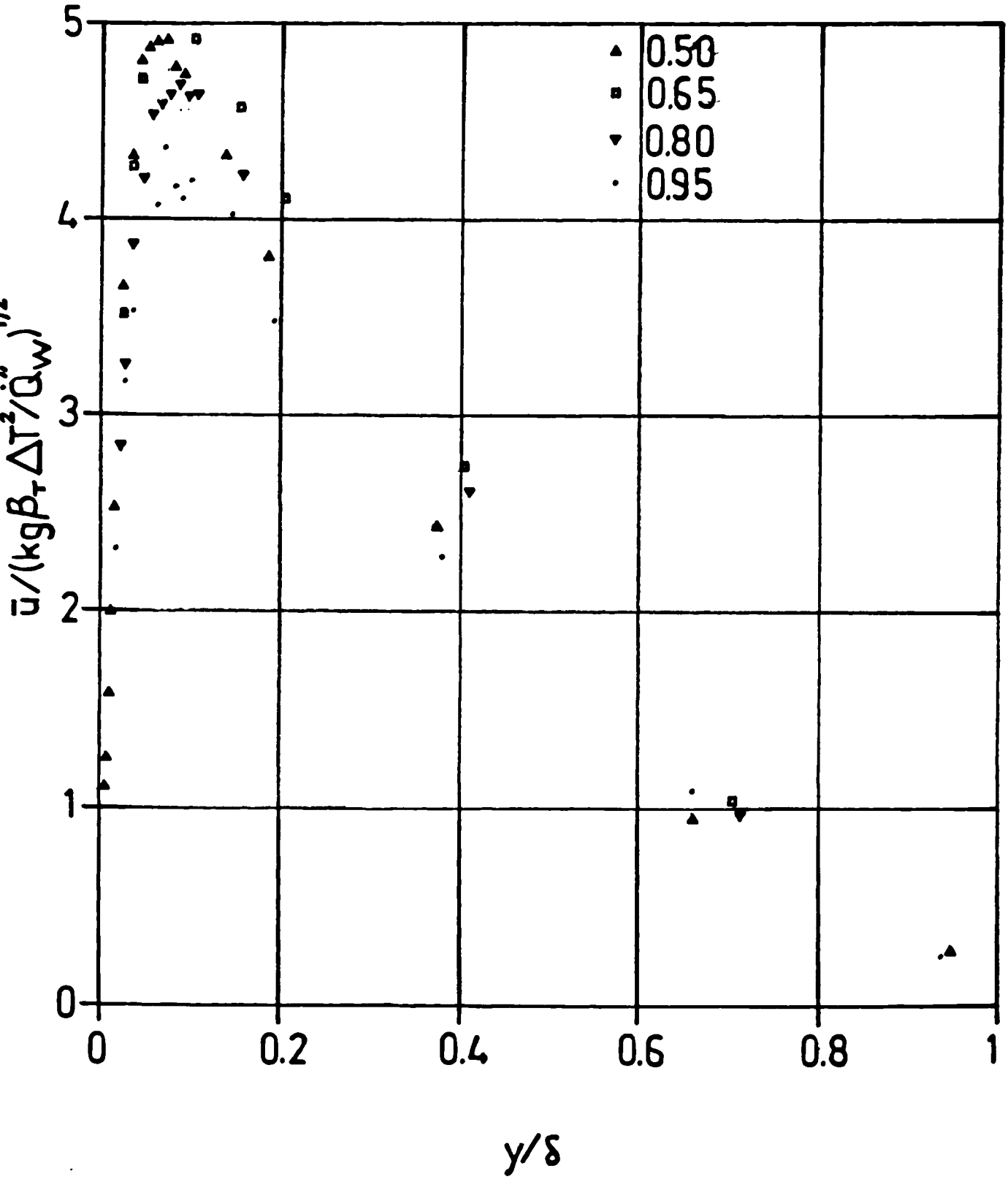

FIGURE 7.63

SERIES 3, 4 AND 6 MEAN VELOCITY SCALED WITH SHEAR VELOCITY

IN THE NEAR WALL REGION WITH Nu_y AS THE DIMENSIONLESS LENGTH

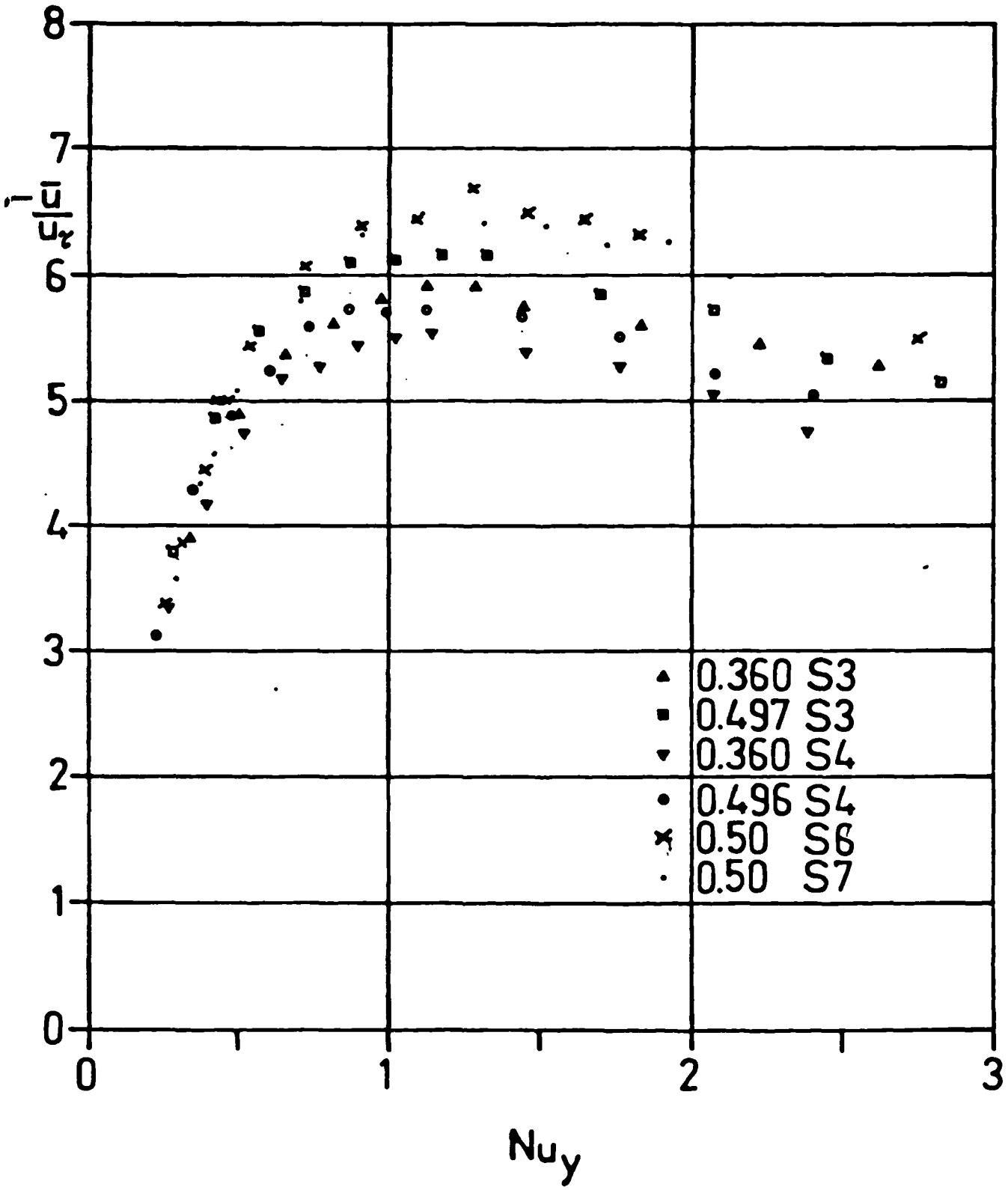

FIGURE 7.64

SERIES 3, 4 AND 6 MEAN VELOCITY SCALED

WITH THE SHEAR VELOCITY AGAINST y SCALED WITH δ

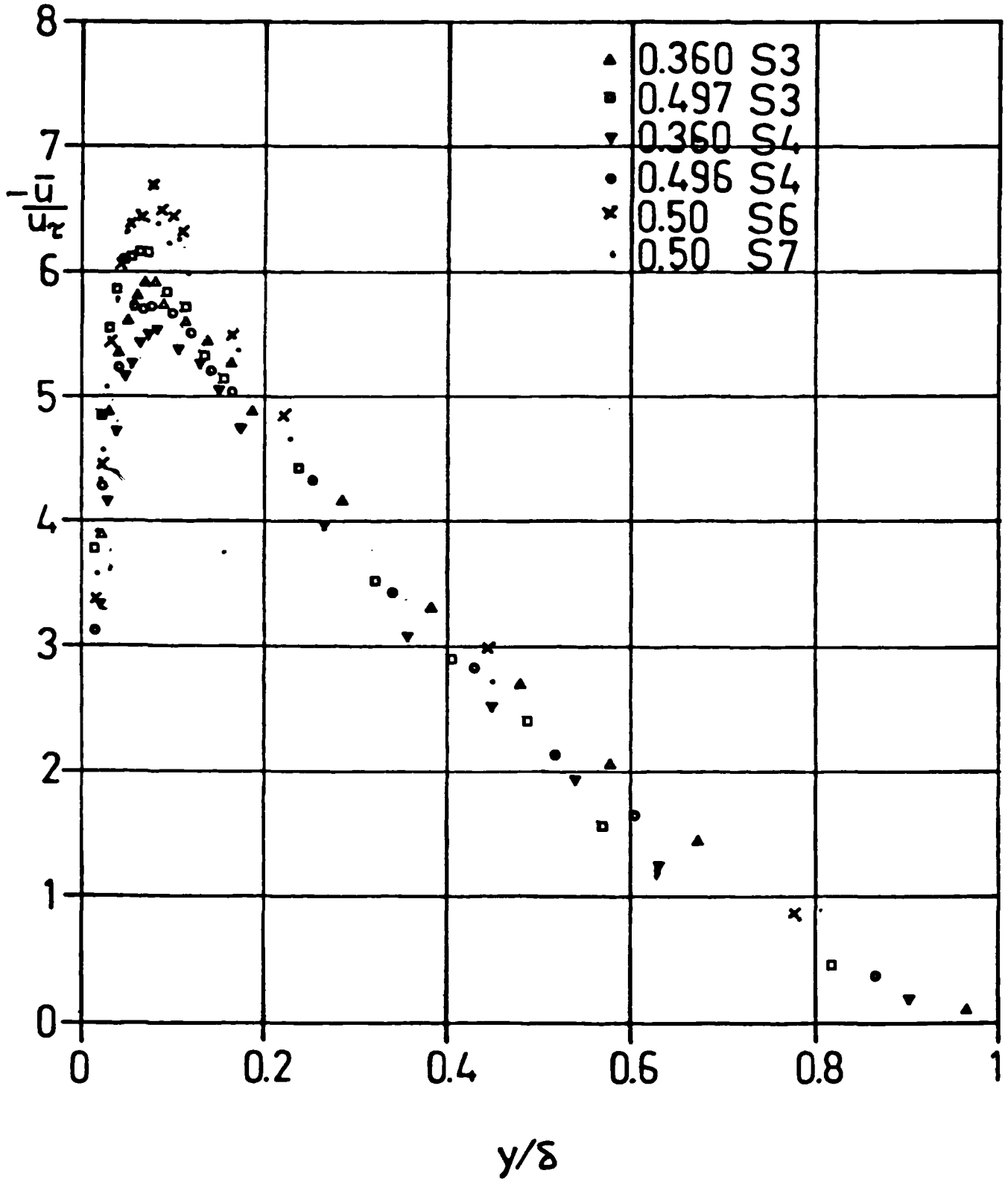

FIGURE 7.65

PROBABILITY DISTRIBUTION OF

VELOCITY FOR SERIES 3 AT x/H = 0.229

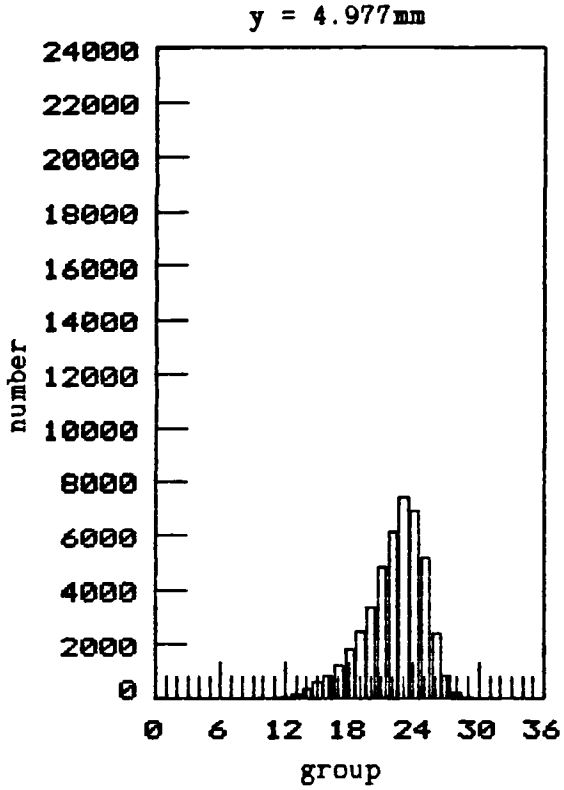

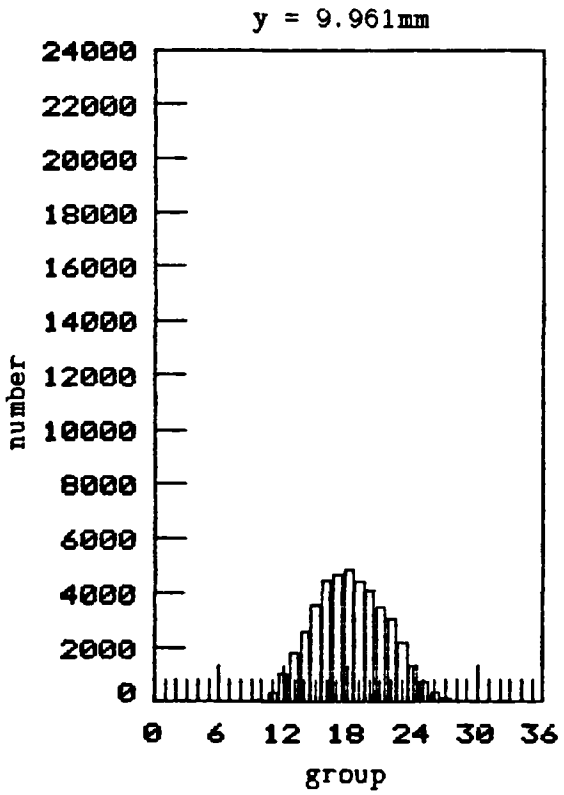

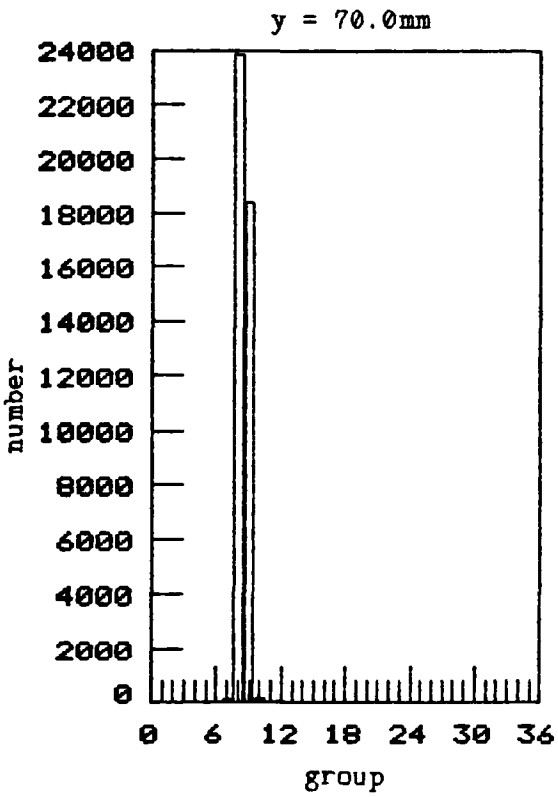

FIGURE 7.66

PROBABILITY DISTRIBUTION OF

VELOCITY FOR SERIES 3 AT x/H = 0.497

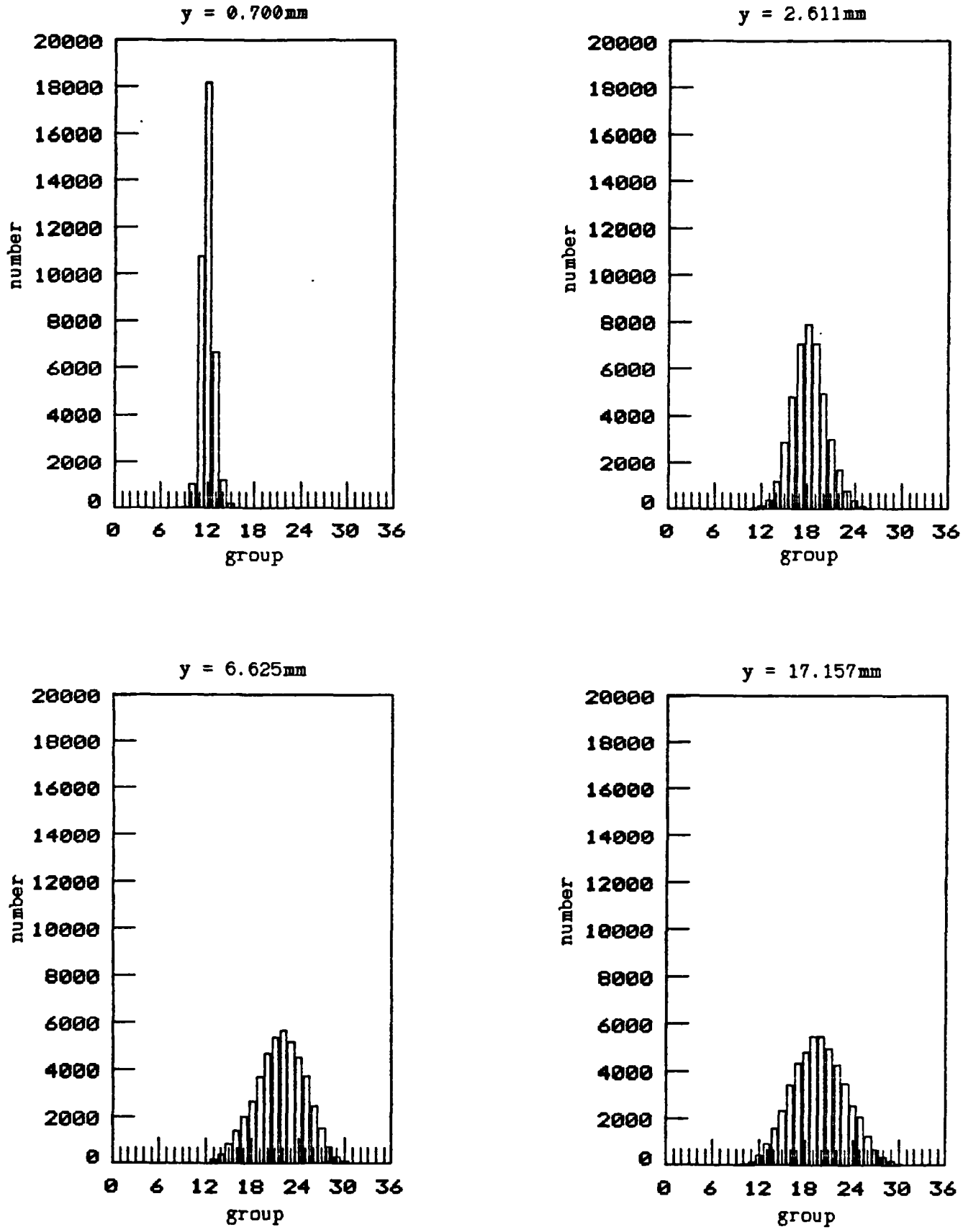

FIGURE 7.67

PROBABILITY DISTRIBUTION OF

VELOCITY FOR SERIES 3 AT x/H = 0.497

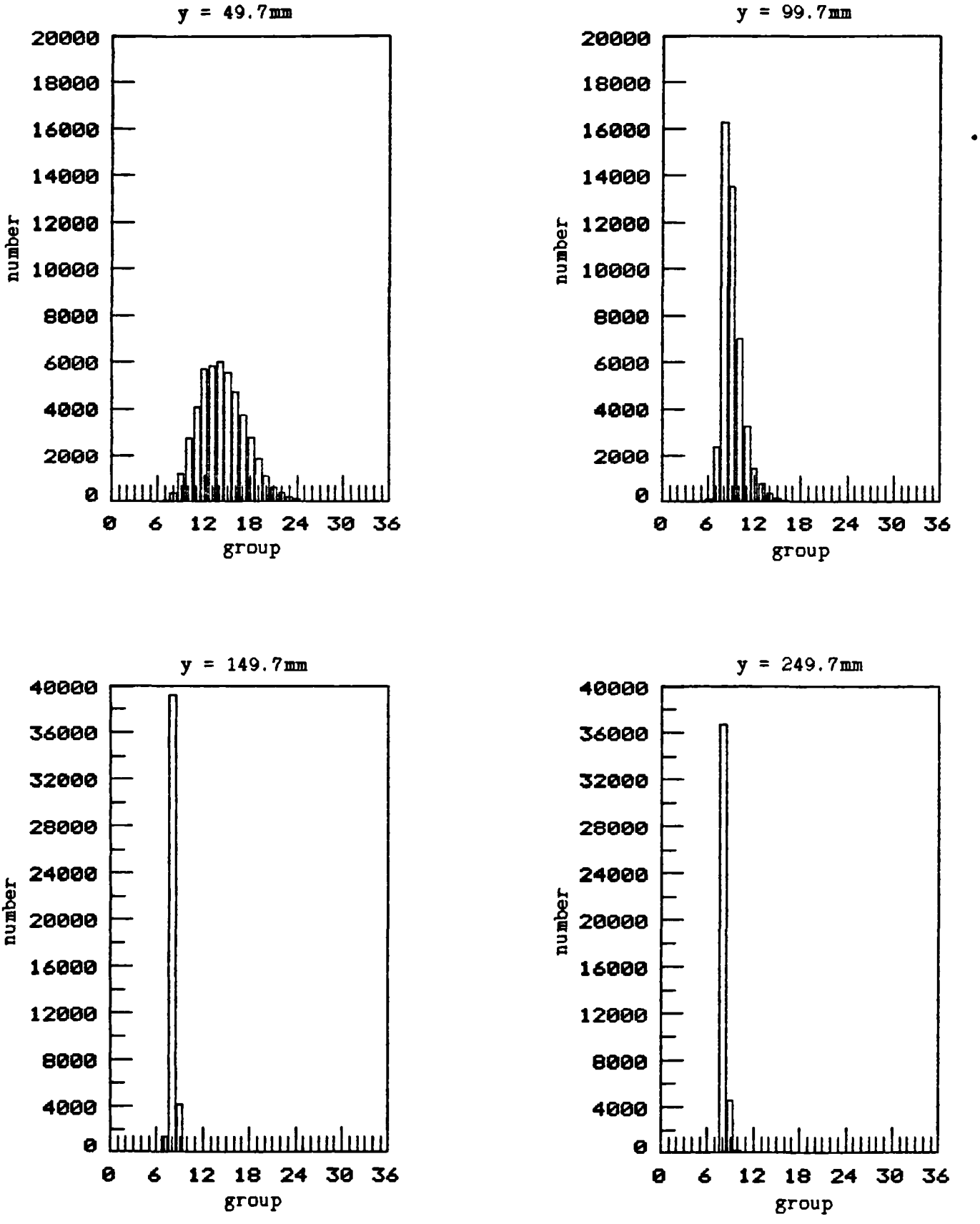

FIGURE 7. 68

MINIMUM, AVERAGE AND MAXIMUM

VELOCITY PROFILES FOR SERIES 3 AT x/H = 0.497

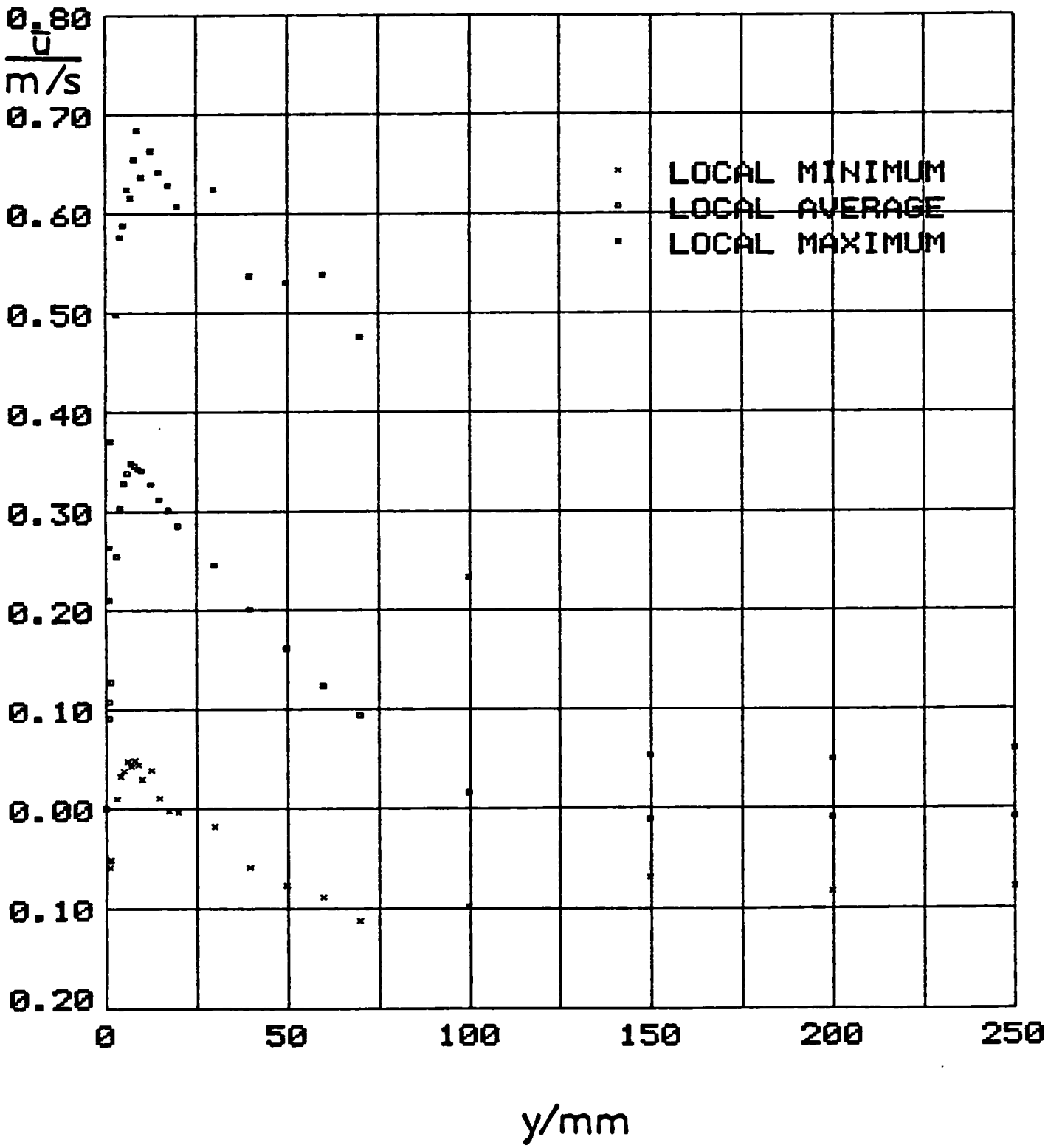

FIGURE 7. 69

SERIES 3 PROFILES OF $u'_{R.M.S.}/v'_{R.M.S.}$

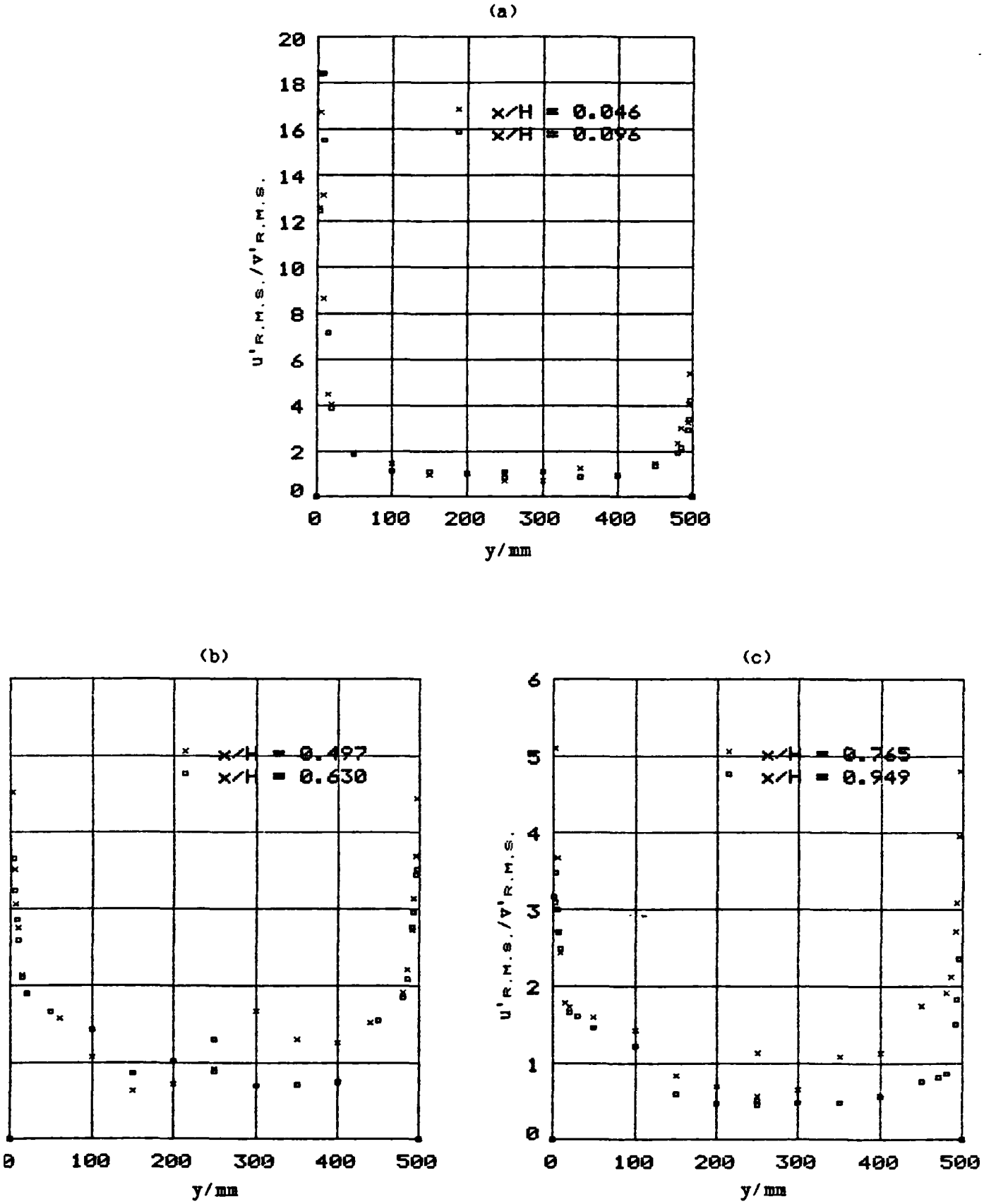

FIGURE 7.70

COMPARISION OF CALCULATED AND

MEASURED MEAN LATERAL VELOCITY FOR SERIES 3

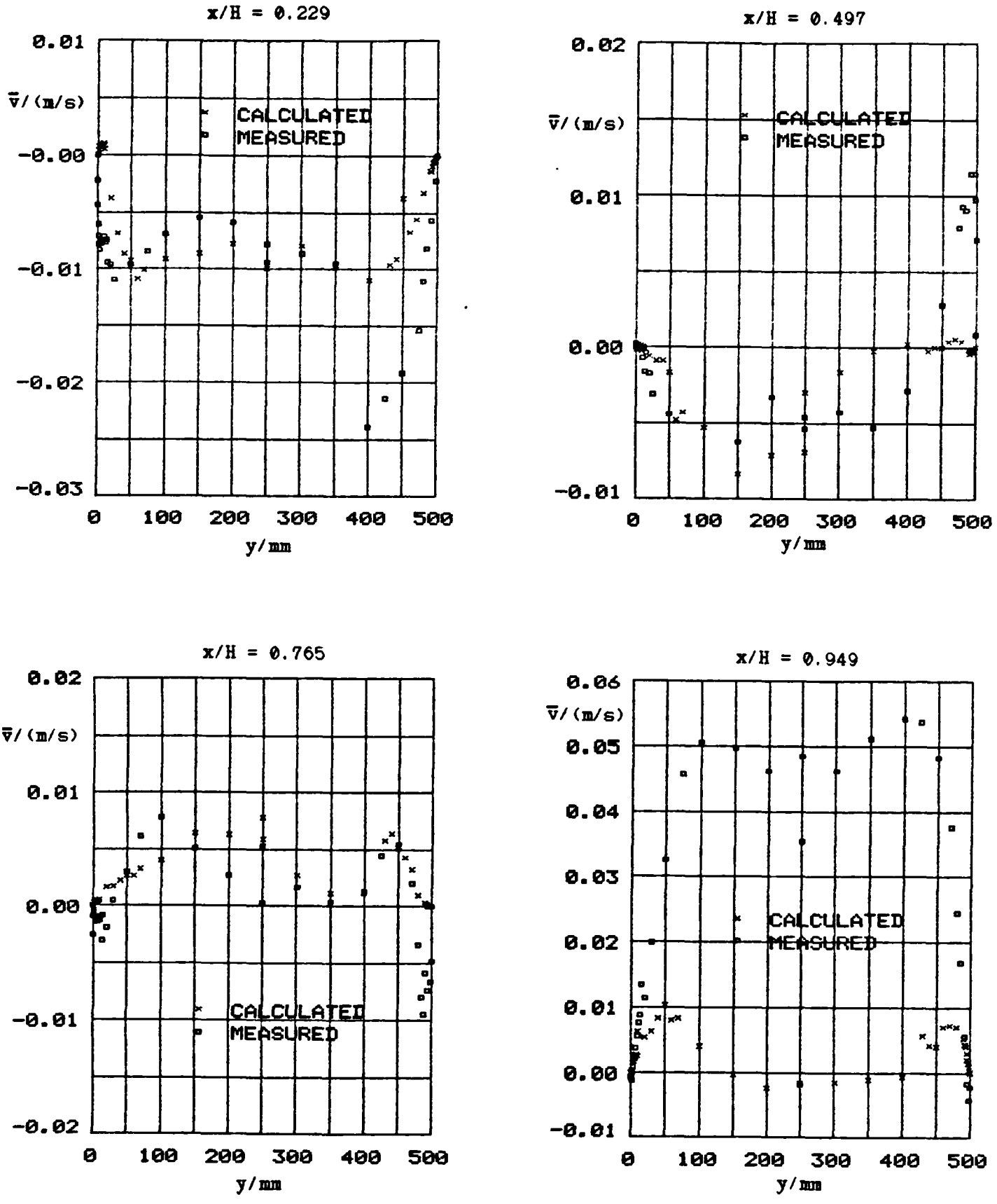

FIGURE 7.71

COMPARISON OF L.D.A. AND HOT-WIRE PROFILES AT MID-HEIGHT

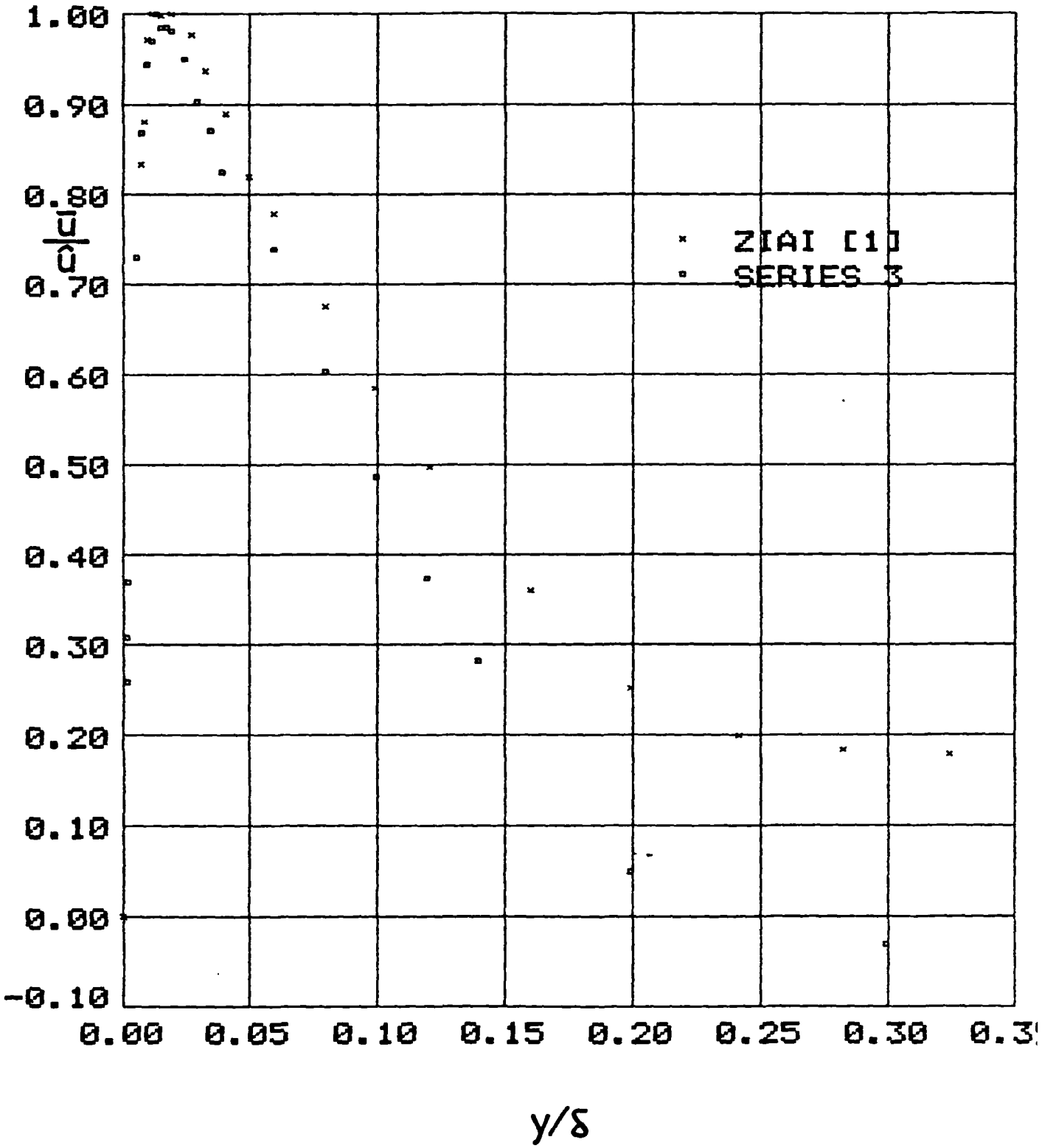

FIGURE 7.72

MEAN VELOCITY PROFILES FOR SERIES 3 AT x/H = 0.949

FOR INCREASES OF CEILING TEMPERATURE OF 0, 0.95 AND 2.28K

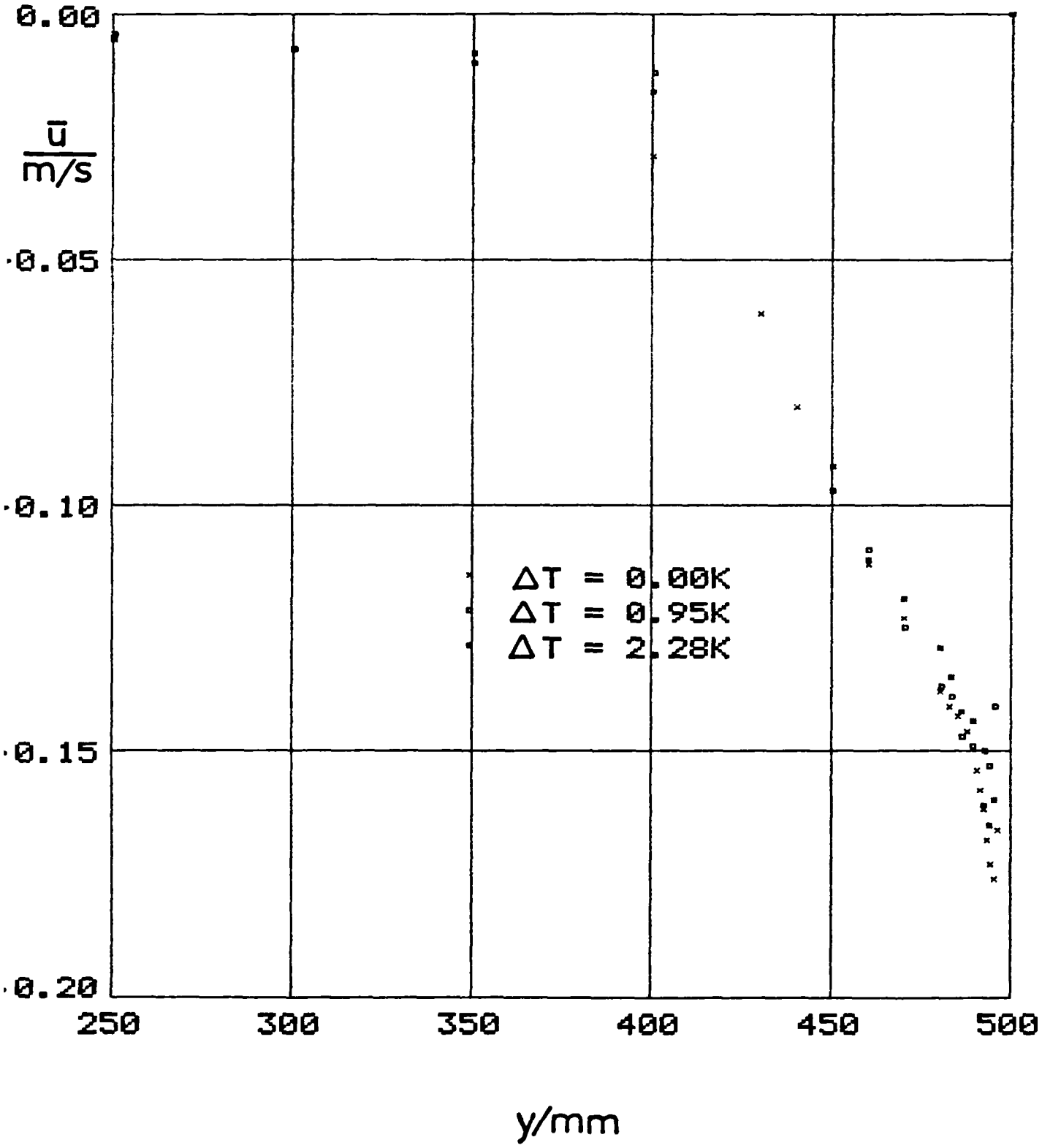

FIGURE 7.73

u'R.M.S. PROFILES FOR SERIES 3 AT x/H = 0.949

FOR INCREASES OF CEILING TEMPERATURE OF 0, 0.95 AND 2.28K

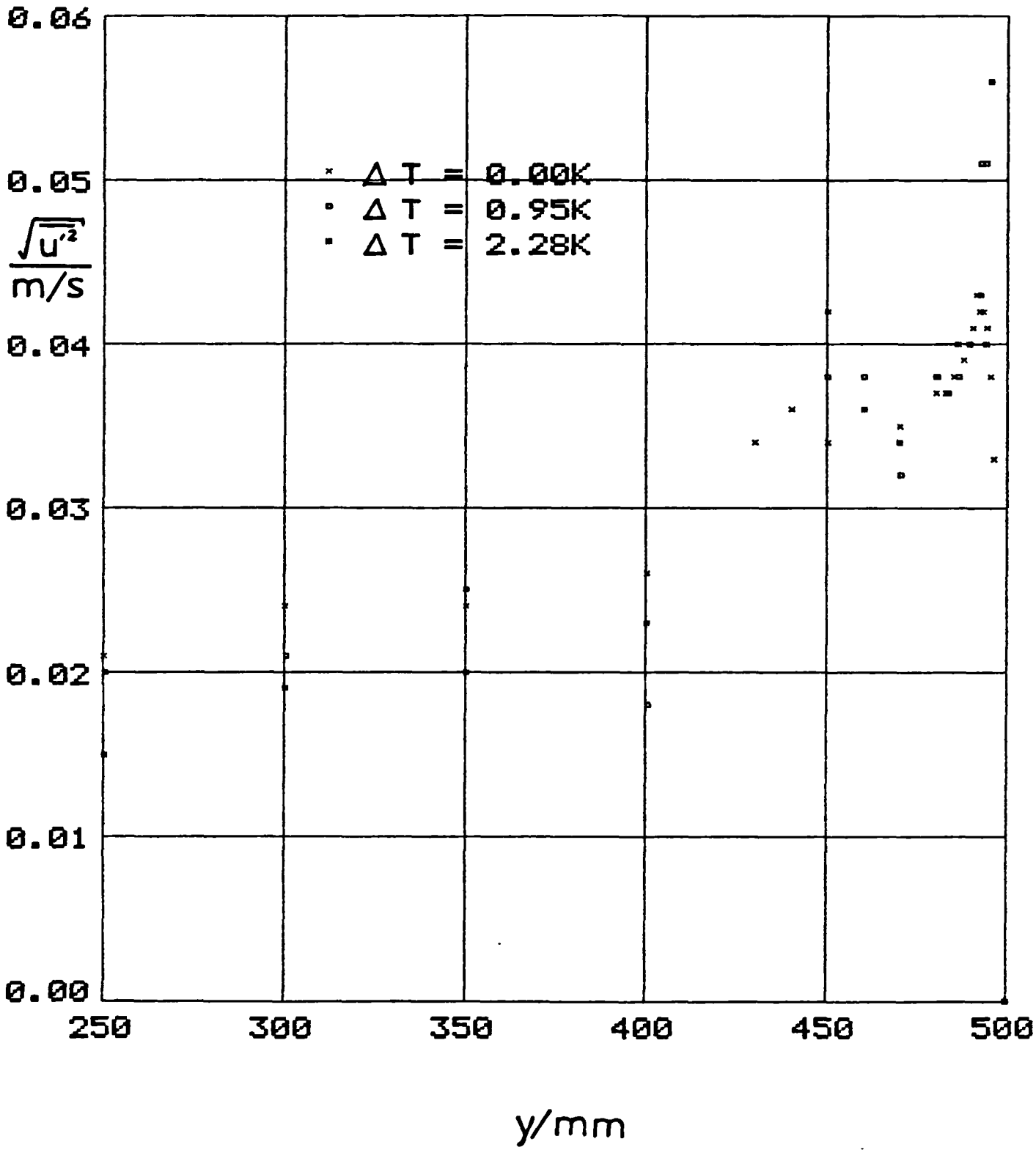

FIGURE 7. 74

PROFILES OF $\overline{u'T'}$ FOR SERIES 3

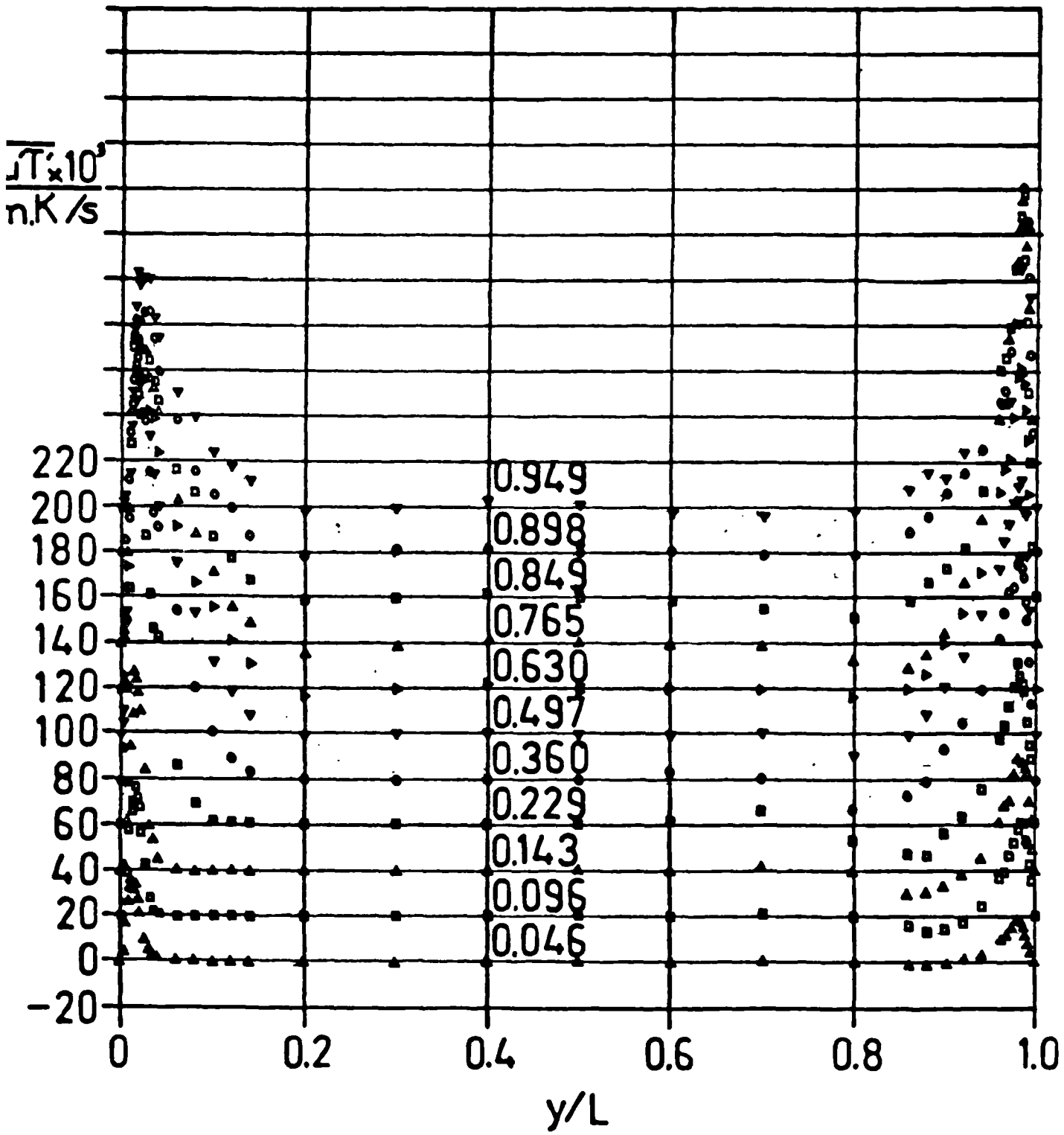

FIGURE 7.75

PROFILE OF $\overline{u'T'}$ CORRELATION COEFFICIENT FOR SERIES 3 AT x/H = 0.497

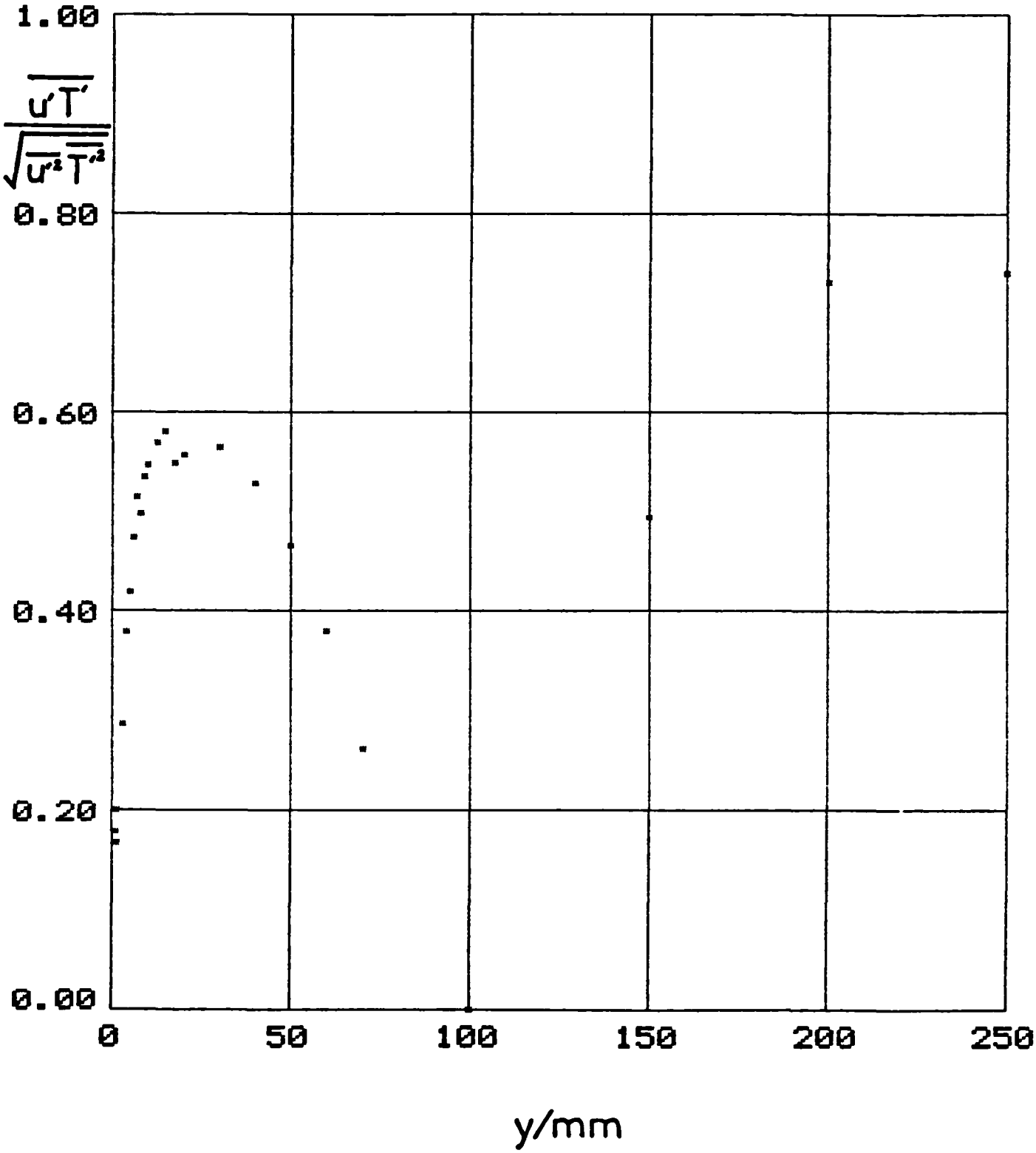

FIGURE 7.76

COMPARISON OF CALCULATED AND

MEASURED VALUES OF $\overline{v'T'}$ FOR SERIES 3

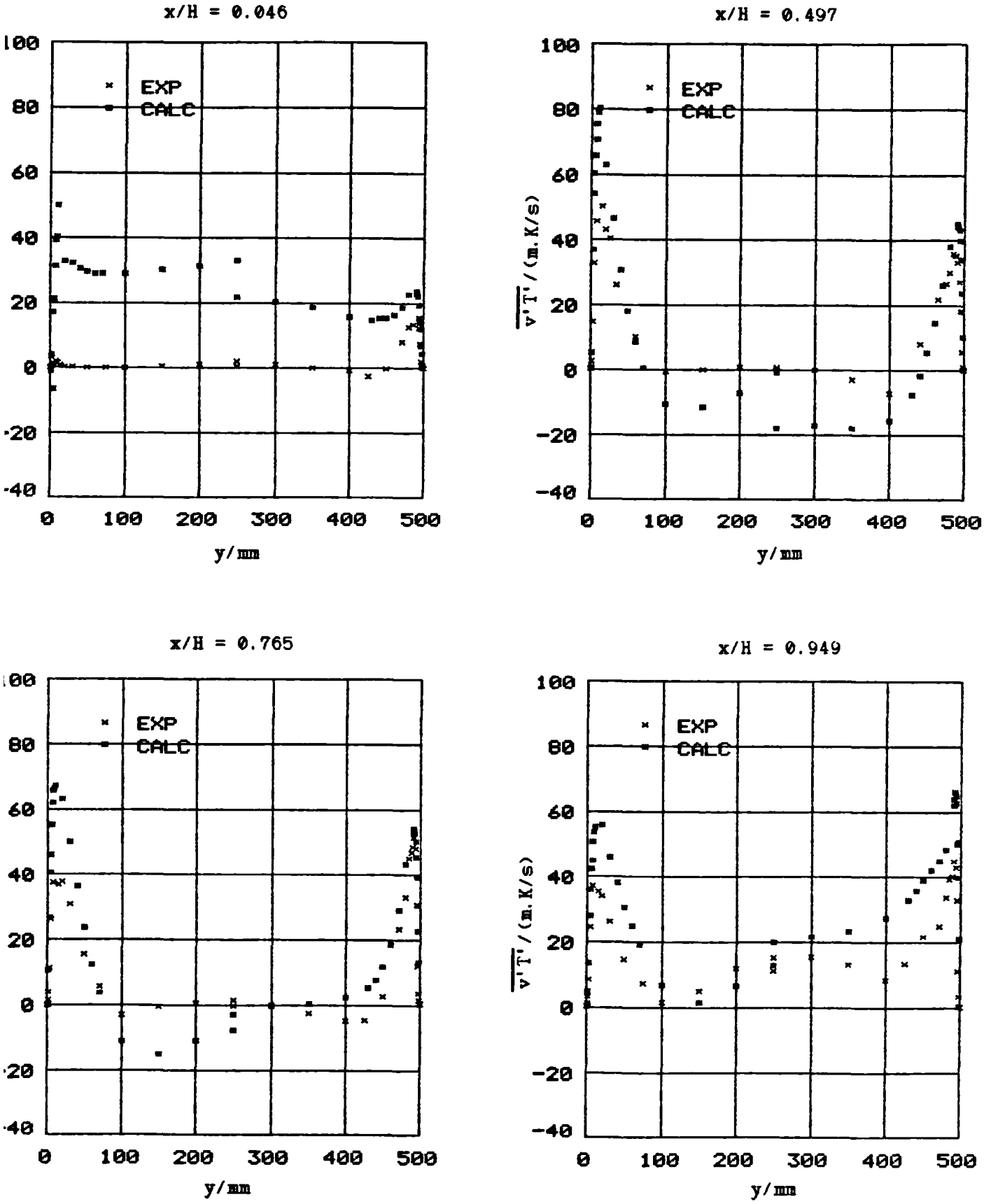

FIGURE 7.77

PROFILES OF $\overline{u'v'}$ FOR SERIES 3

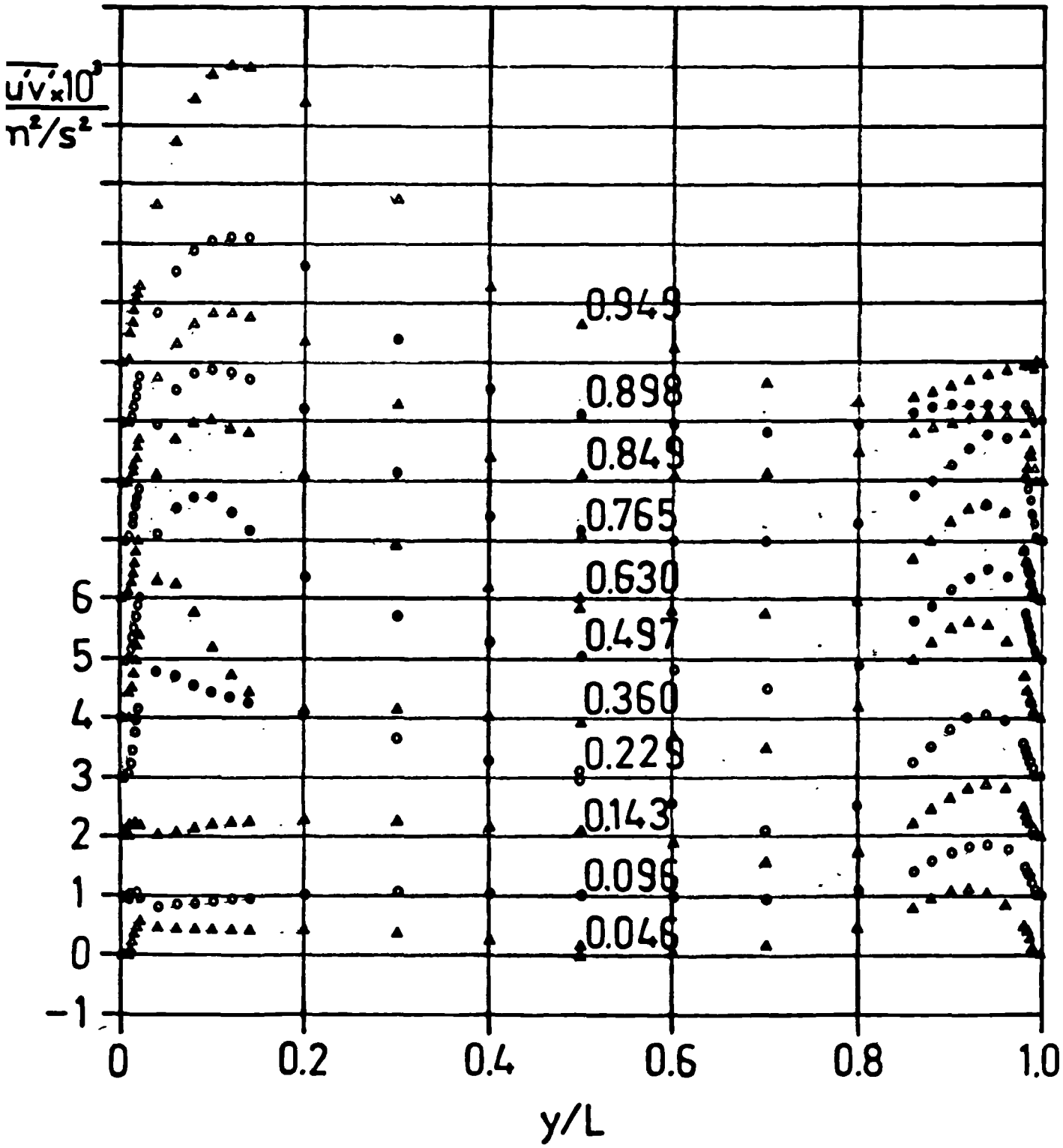

FIGURE 7.78

SAMPLE PROFILES OF $\overline{u'v'}$ CORRELATION COEFFICIENT FOR SERIES 3

x/H = 0.046

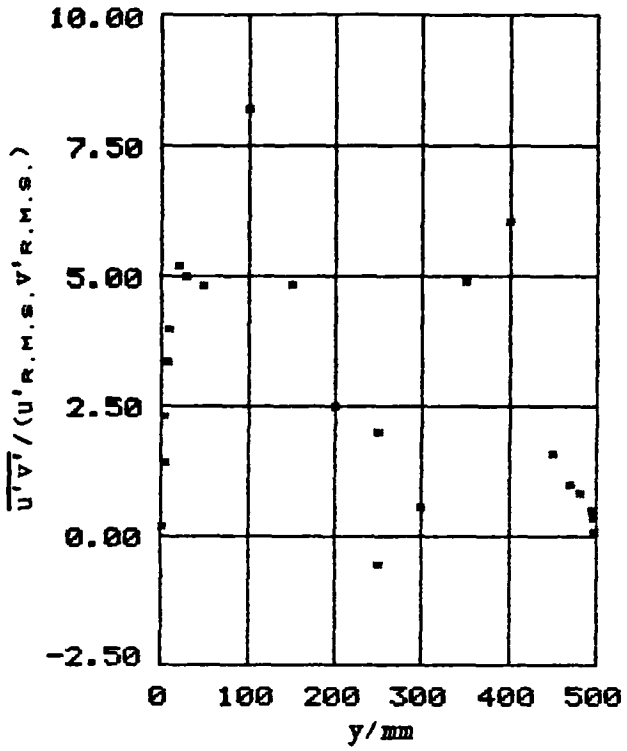

x/H = 0.497

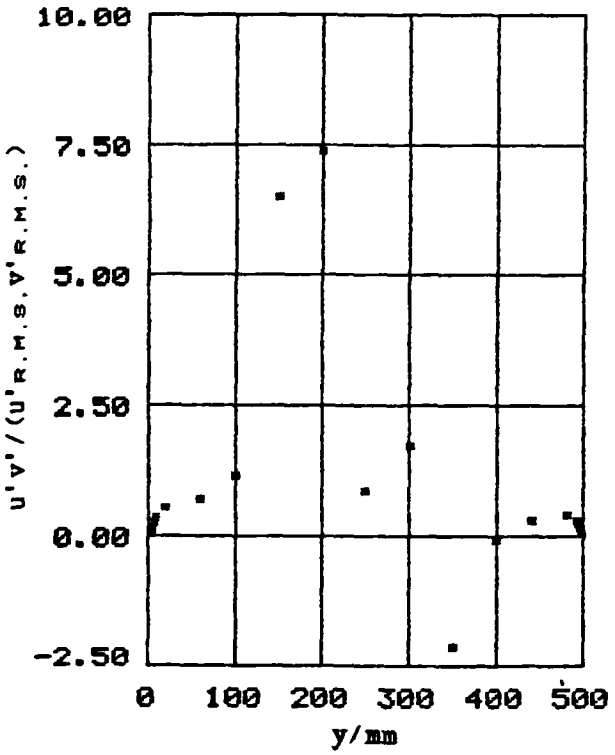

x/H = 0.949

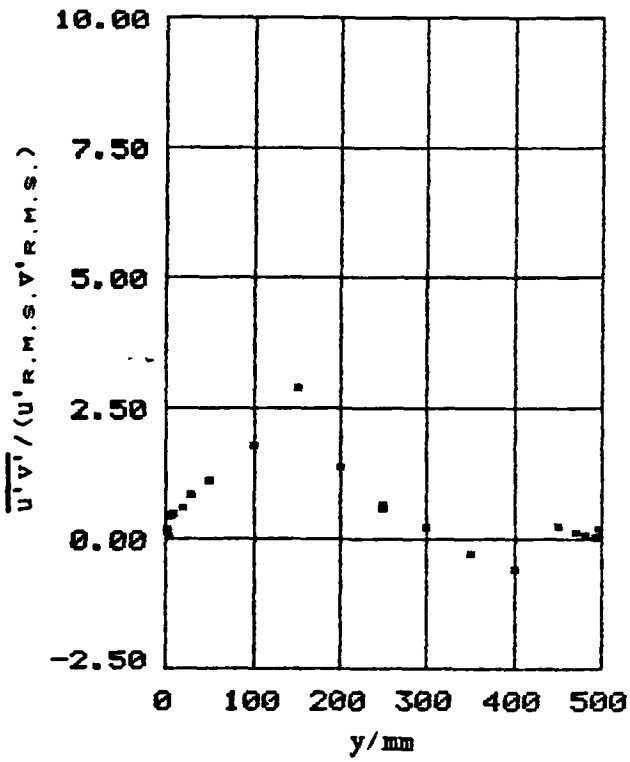

FIGURE 7.79

SAMPLE PROFILES OF τ FOR SERIES 3

x/H = 0.046

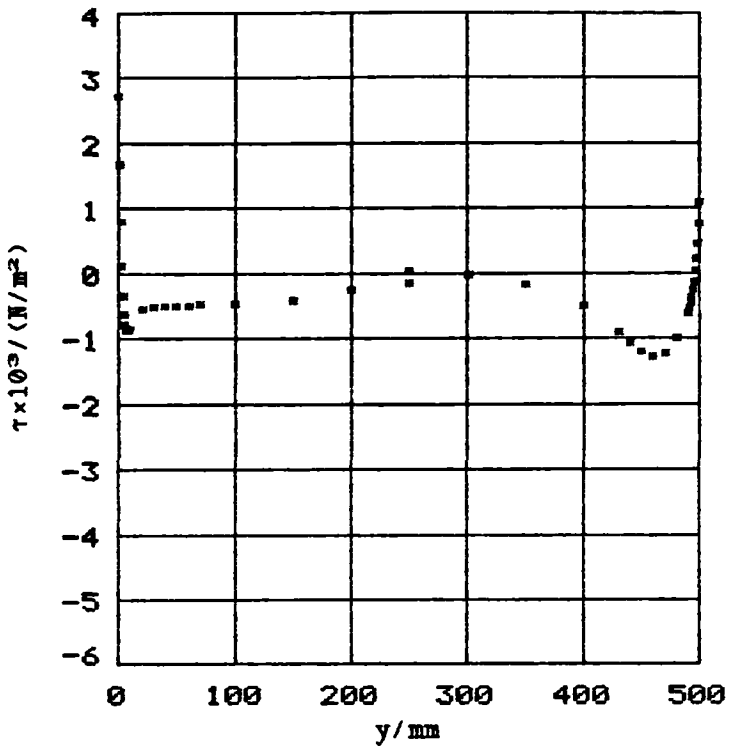

x/H = 0.497

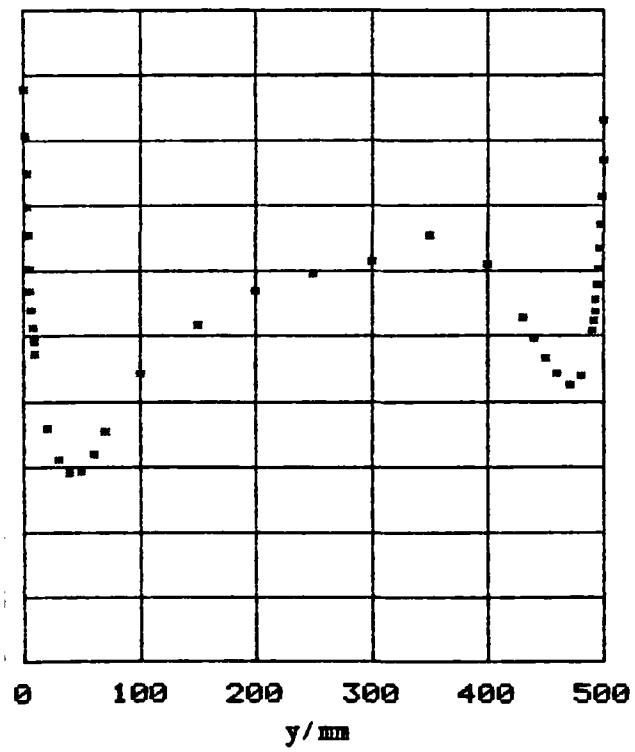

x/H = 0.949

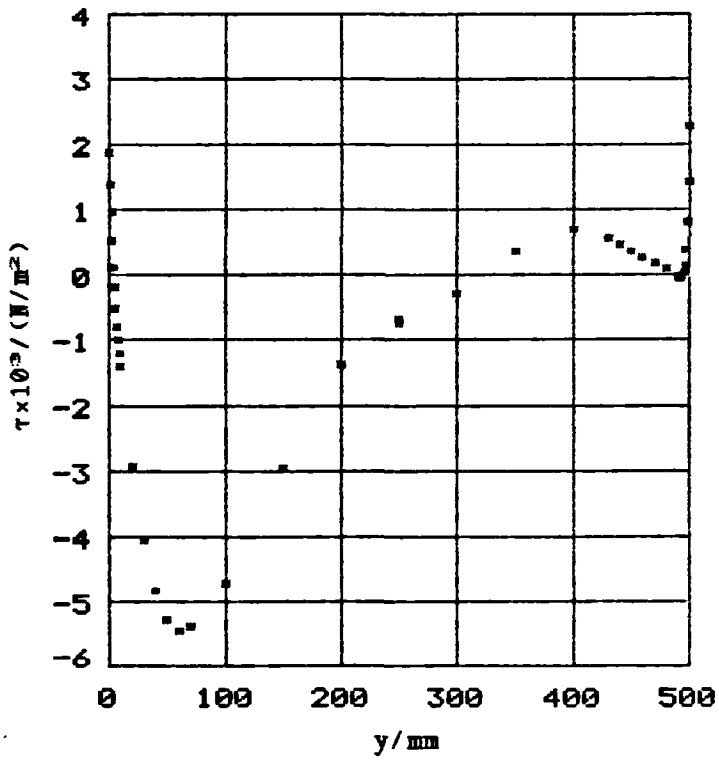

FIGURE 7.80

PROFILES OF P FOR SERIES 3

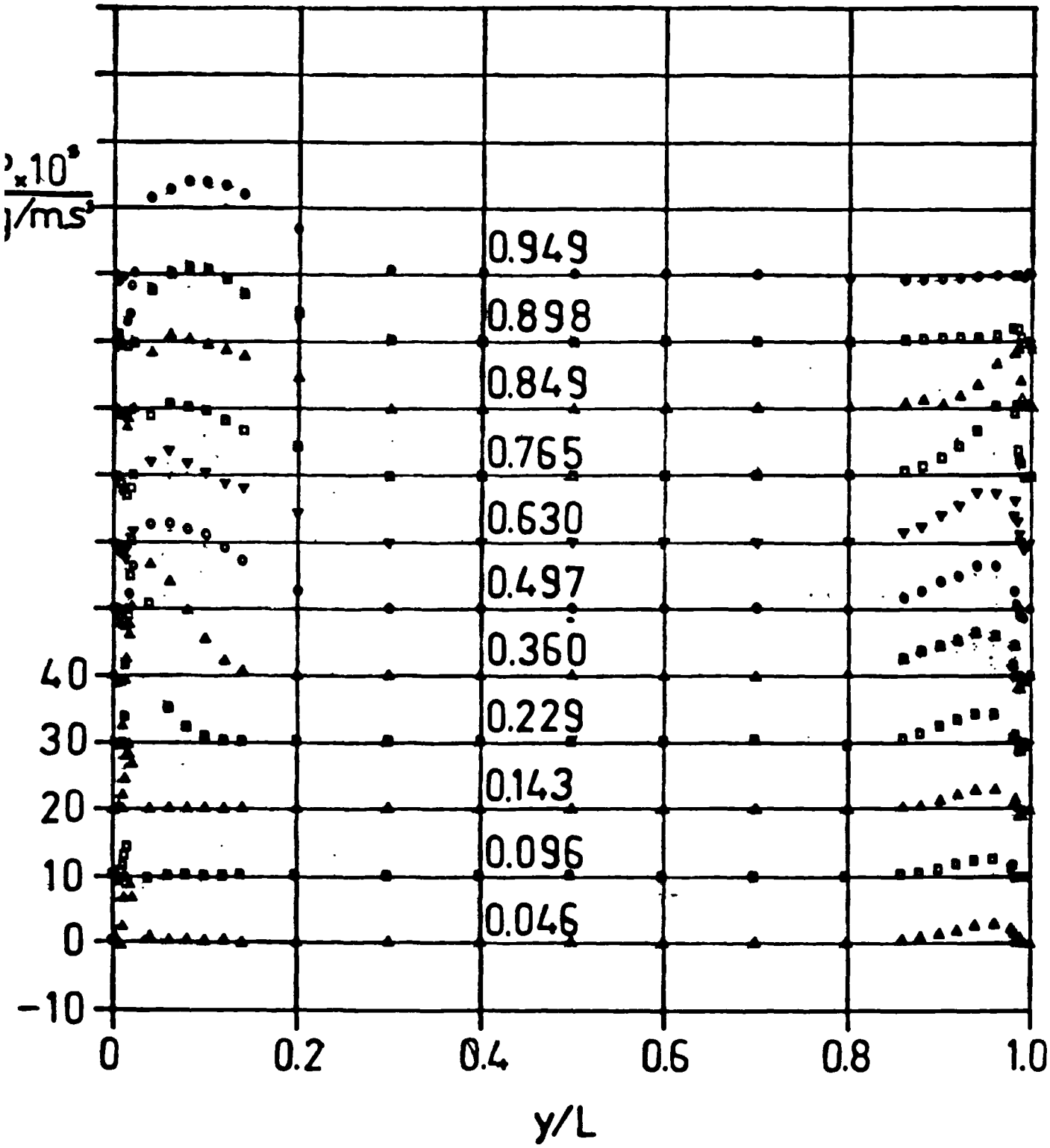

FIGURE 7.81

PROFILES OF G FOR SERIES 3

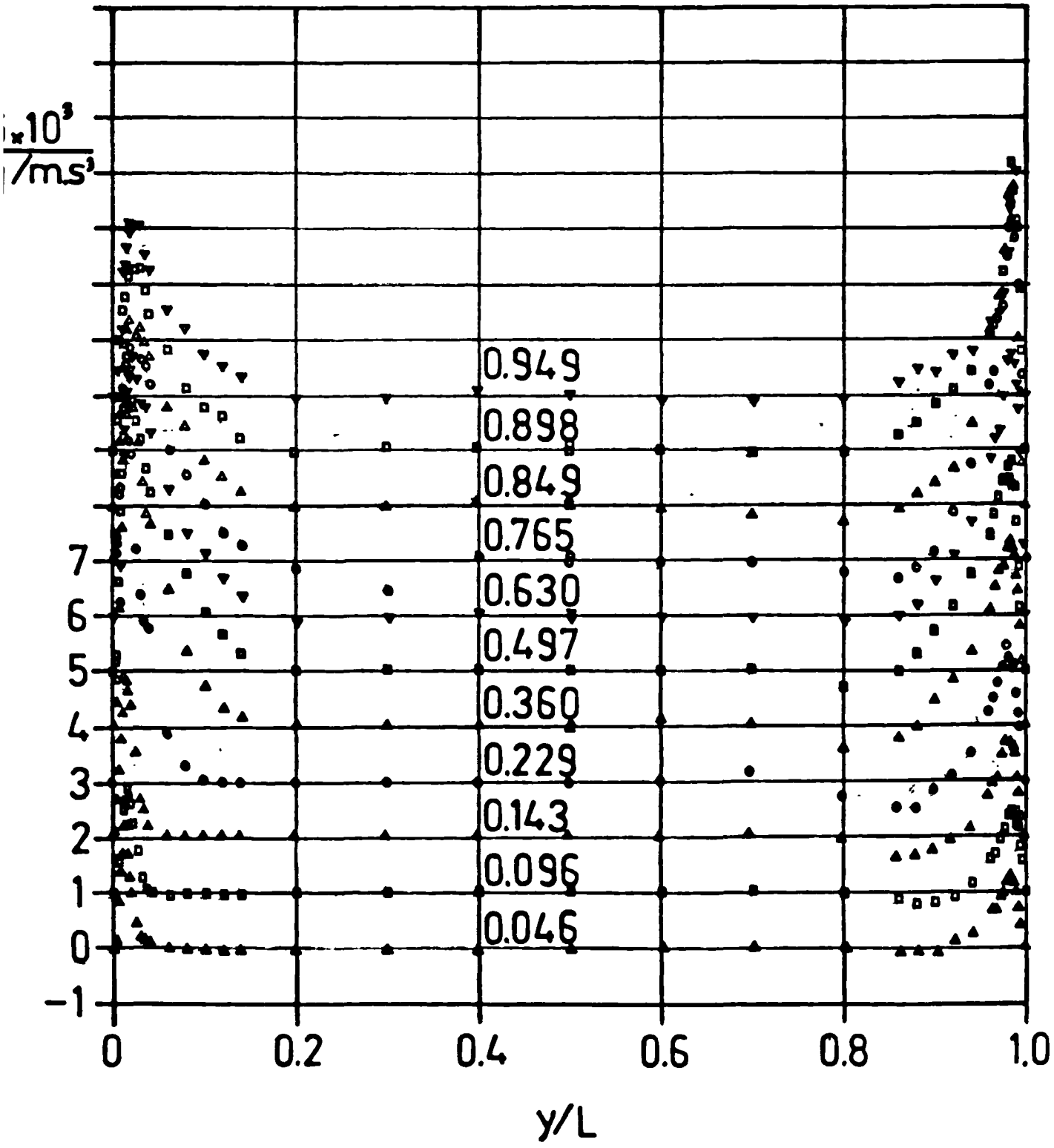

FIGURE 7.82

COMPARISON OF FULL PROFILES OF P AND G FOR SERIES 3

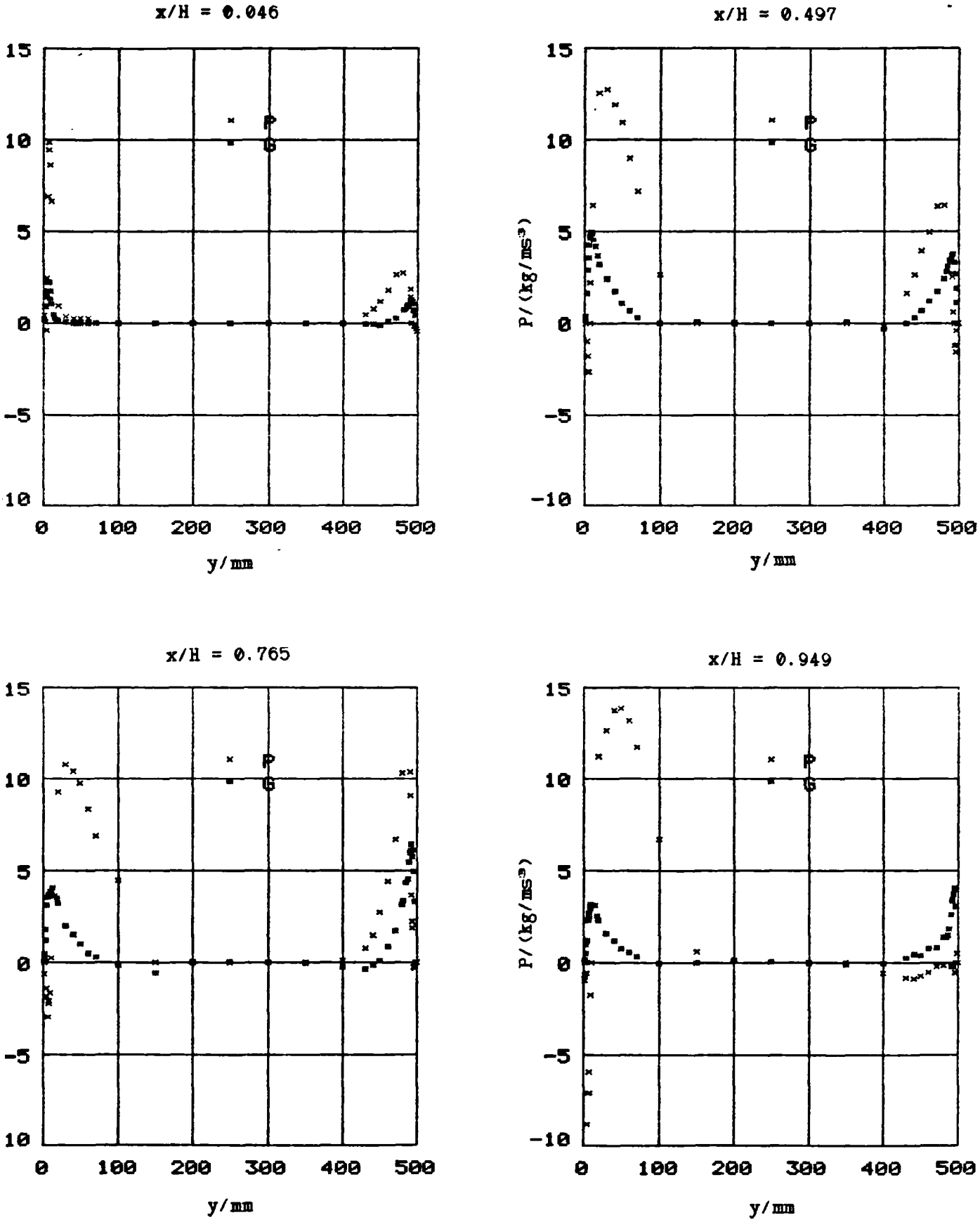

FIGURE 7.83

COMPARISON OF NEAR WALL PROFILES OF P AND G FOR SERIES 3

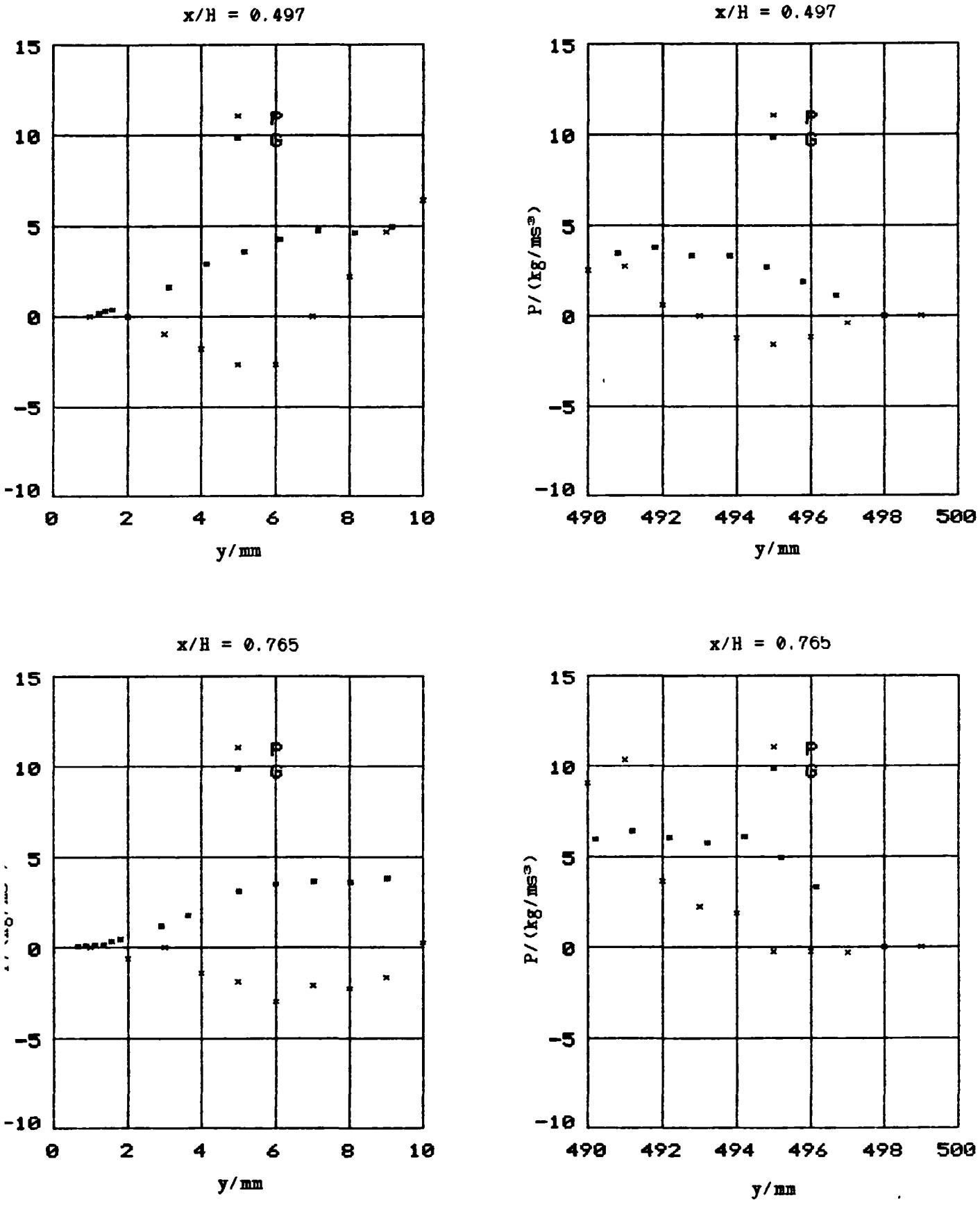

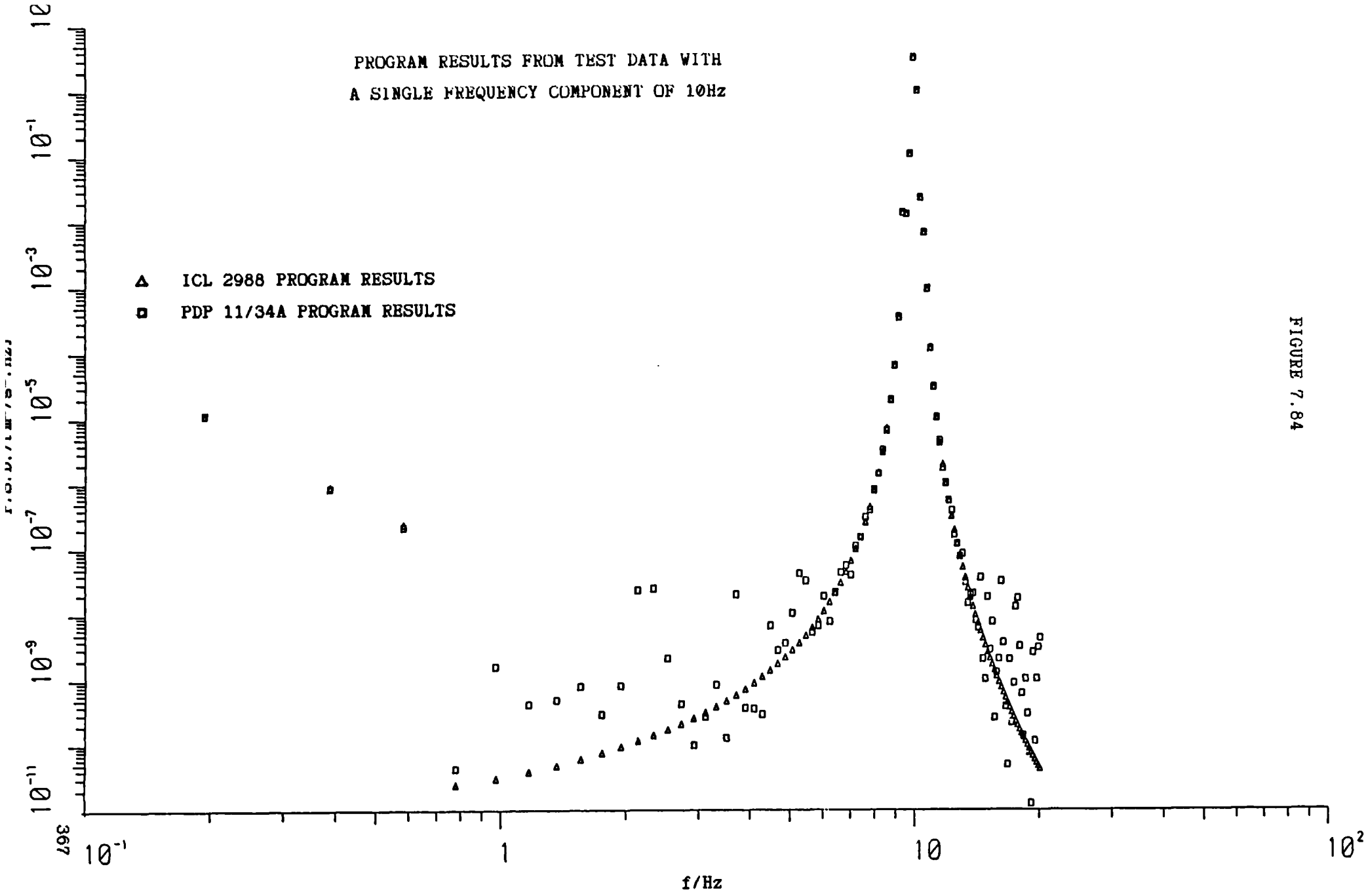
PROGRAM RESULTS FROM TEST DATA WITH
A SINGLE FREQUENCY COMPONENT OF 10Hz
ICL 2988 PROGRAM RESULTS
PDP 11/34A PROGRAM RESULTS
10
10^{-1}
10^{-3}
10^{-5}
10^{-7}
10^{-9}
10^{-11}
10^{-1}
1
10
10^{2}
f/Hz

FIGURE 7.84

FIGURE 7.85

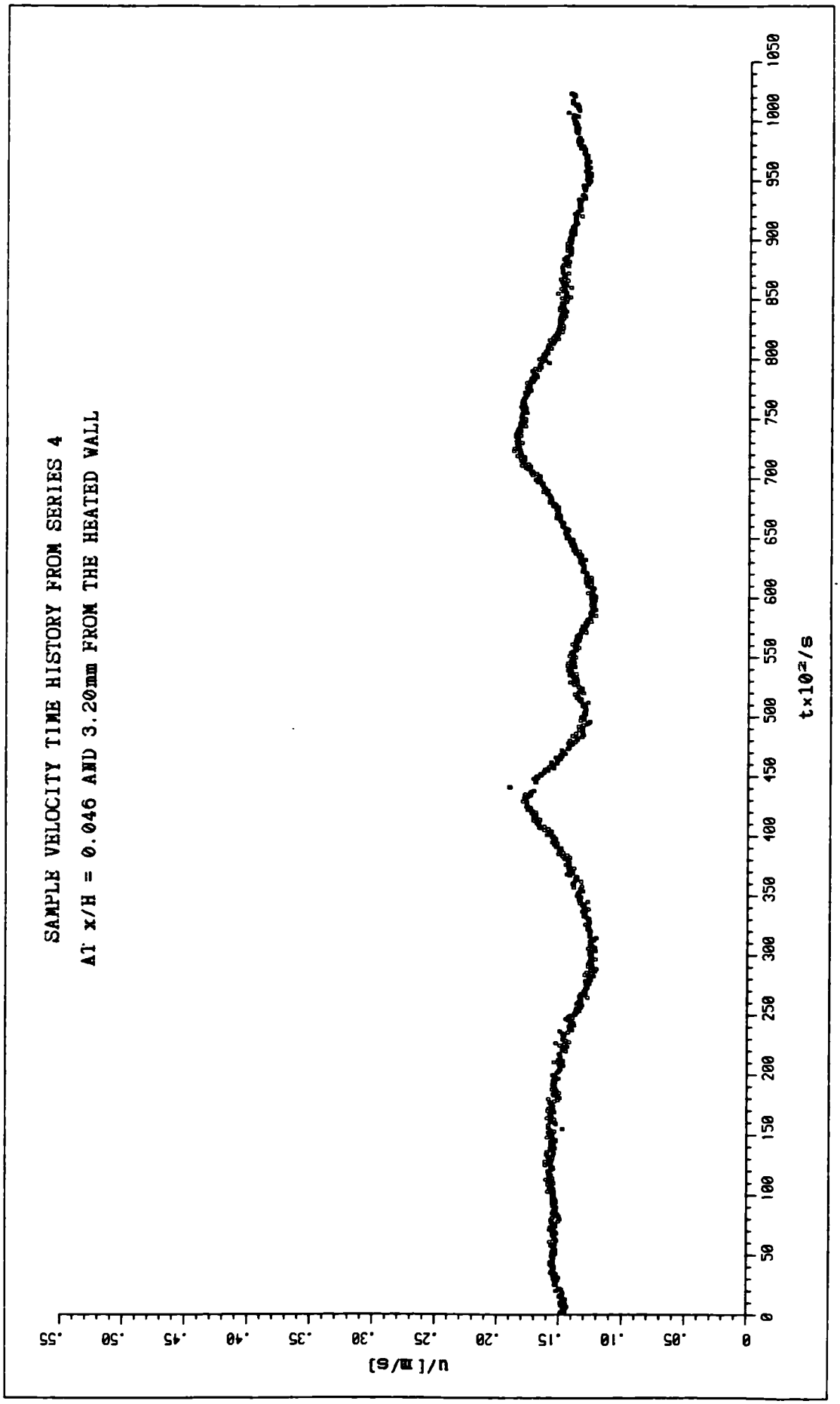
SAMPLE VELOCITY TIME HISTORY FROM SERIES 4
AT x/H = 0.046 AND 3.20mm FROM THE HEATED WALL
u/[m/s]
t x10²/s
0
.05
.10
.15
.20
.25
.30
.35
.40
.45
.50
.55
0
50
100
150
200
250
300
350
400
450
500
550
600
650
700
750
800
850
900
950
1000
1050

FIGURE 7.86

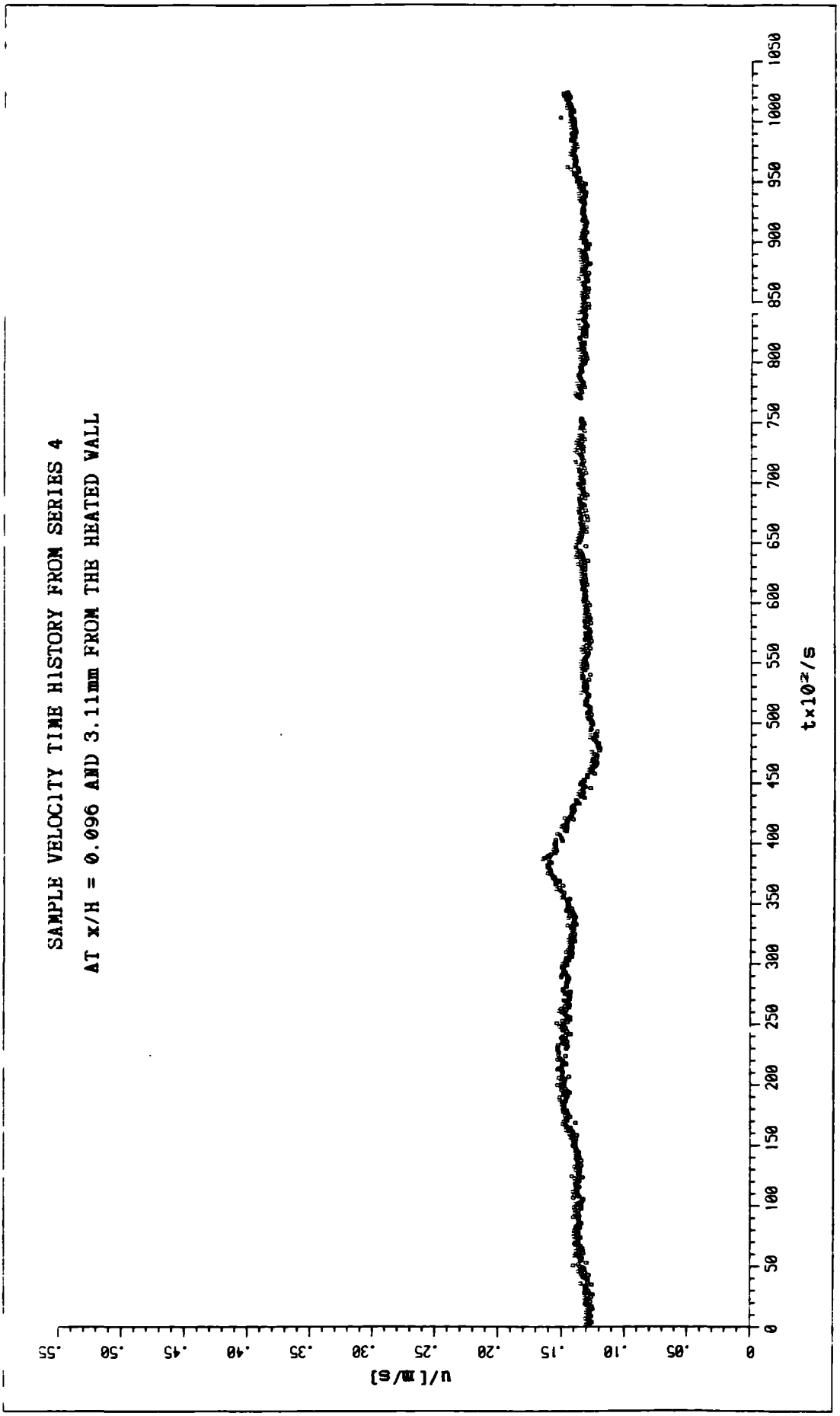
SAMPLE VELOCITY TIME HISTORY FROM SERIES 4
AT x/H = 0.096 AND 3.11mm FROM THE HEATED WALL
u/[m/s]
t×10²/s
0
.05
.10
.15
.20
.25
.30
.35
.40
.45
.50
.55
0
50
100
150
200
250
300
350
400
450
500
550
600
650
700
750
800
850
900
950
1000
1050

FIGURE 7.87

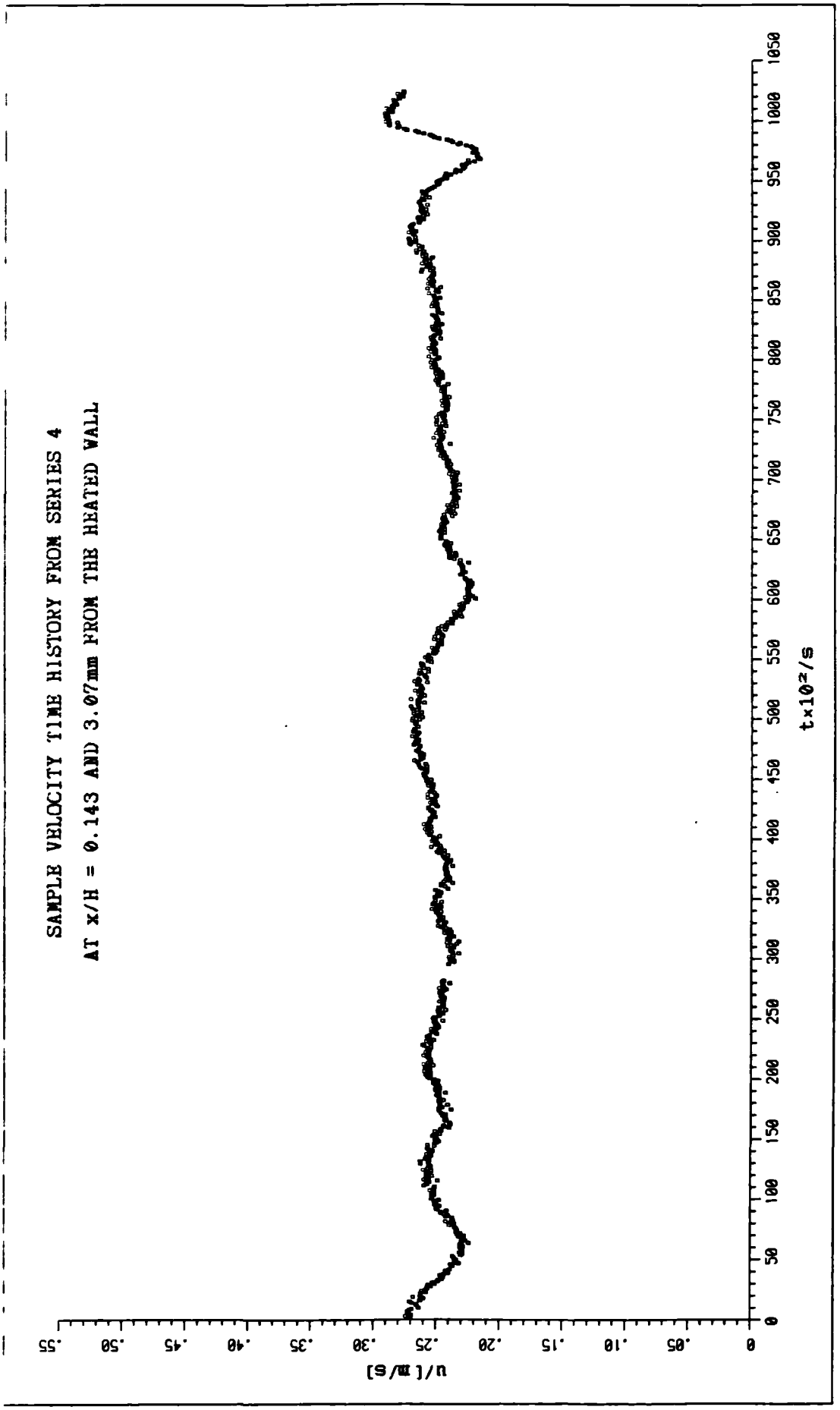
SAMPLE VELOCITY TIME HISTORY FROM SERIES 4
AT x/H = 0.143 AND 3.07mm FROM THE HEATED WALL
u/[m/s]
t×10²/s
0
.05
.10
.15
.20
.25
.30
.35
.40
.45
.50
.55
0
50
100
150
200
250
300
350
400
450
500
550
600
650
700
750
800
850
900
950
1000
1050

FIGURE 7.88

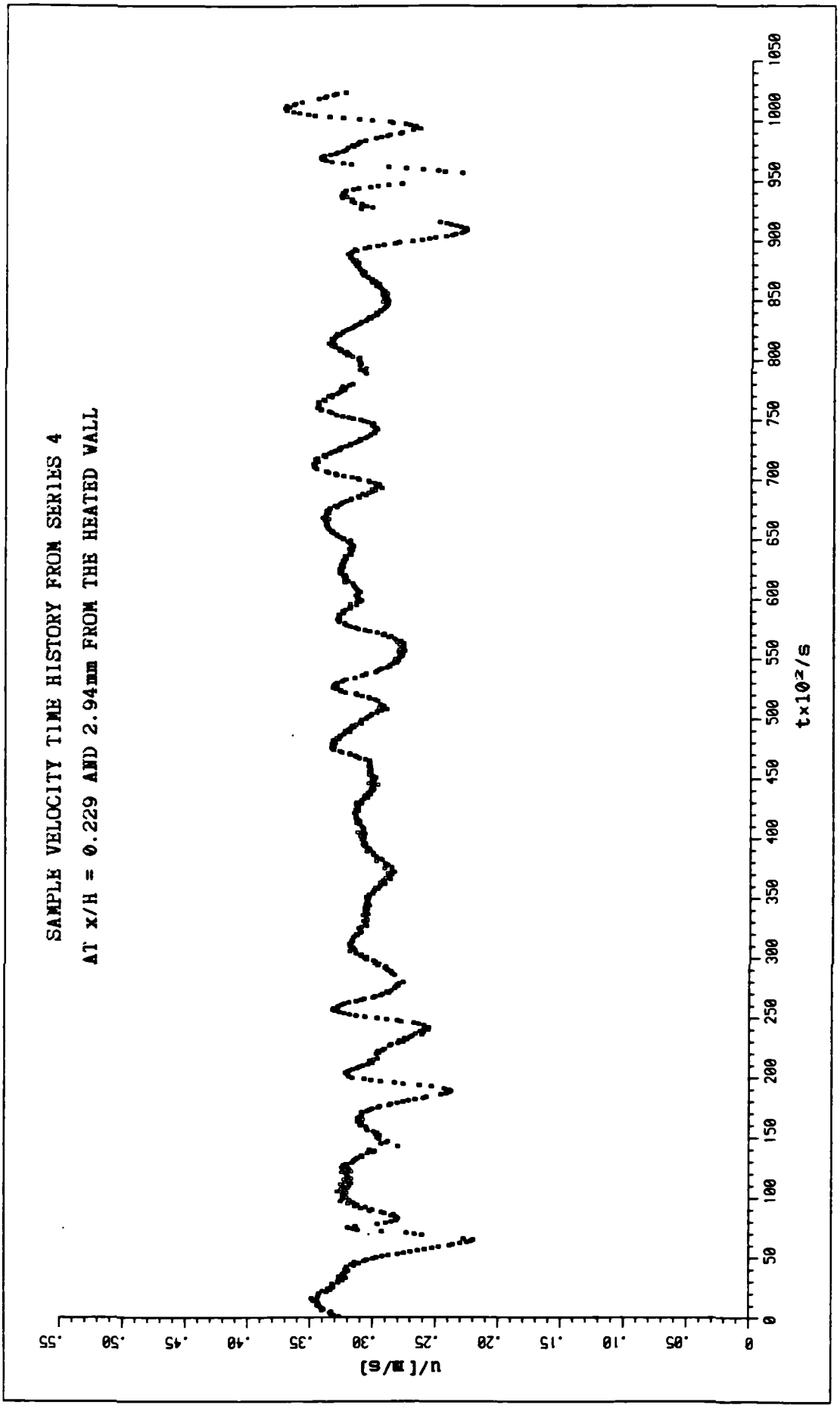
SAMPLE VELOCITY TIME HISTORY FROM SERIES 4
AT x/H = 0.229 AND 2.94mm FROM THE HEATED WALL
u/[m/s]
t×10²/s
0
.05
.10
.15
.20
.25
.30
.35
.40
.45
.50
.55
0
50
100
150
200
250
300
350
400
450
500
550
600
650
700
750
800
850
900
950
1000
1050

FIGURE 7.89

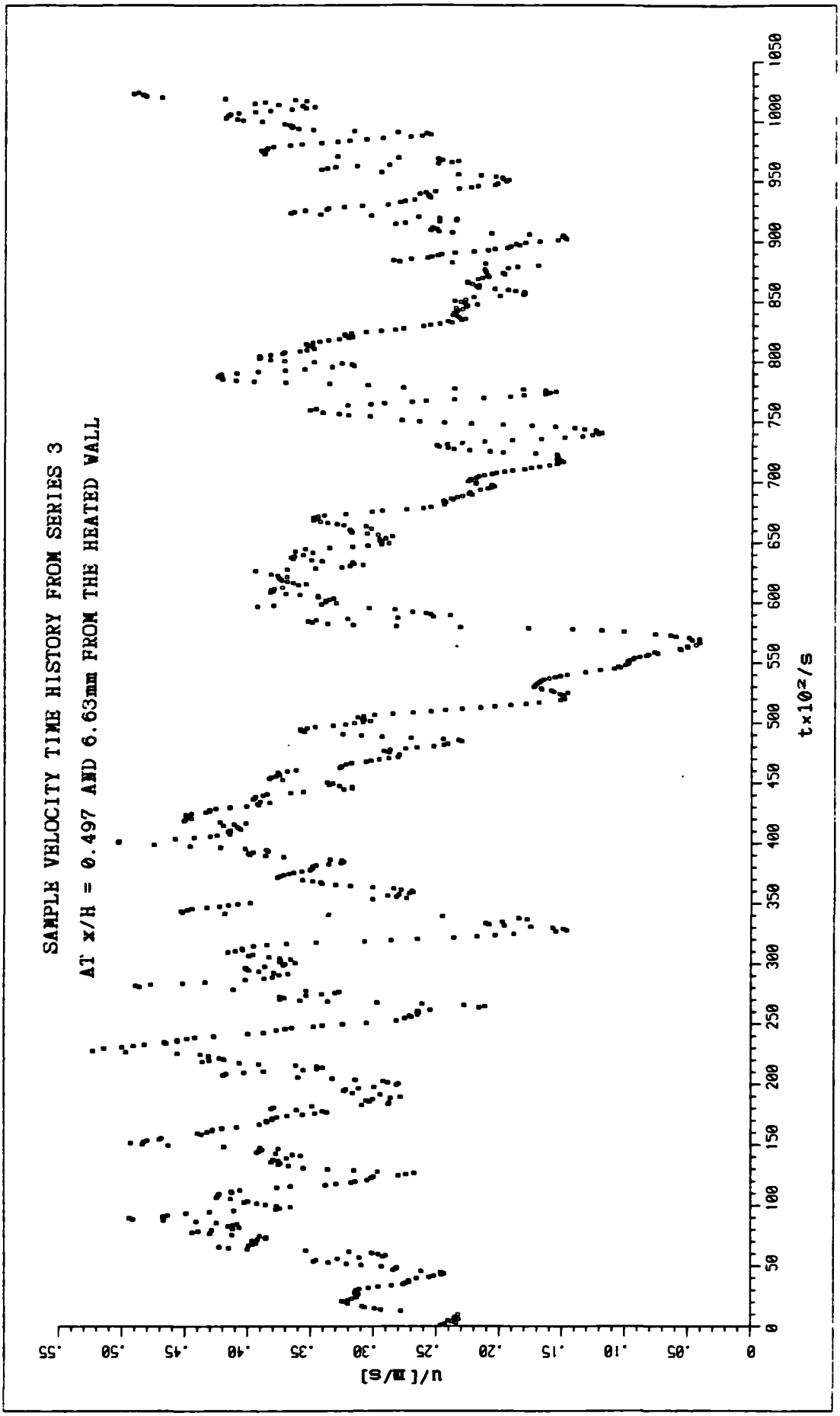
SAMPLE VELOCITY TIME HISTORY FROM SERIES 3
AT x/H = 0.497 AND 6.63mm FROM THE HEATED WALL
u/[m/s]
t x10²/s
0
.05
.10
.15
.20
.25
.30
.35
.40
.45
.50
.55
0
50
100
150
200
250
300
350
400
450
500
550
600
650
700
750
800
850
900
950
1000
1050

FIGURE 7.90

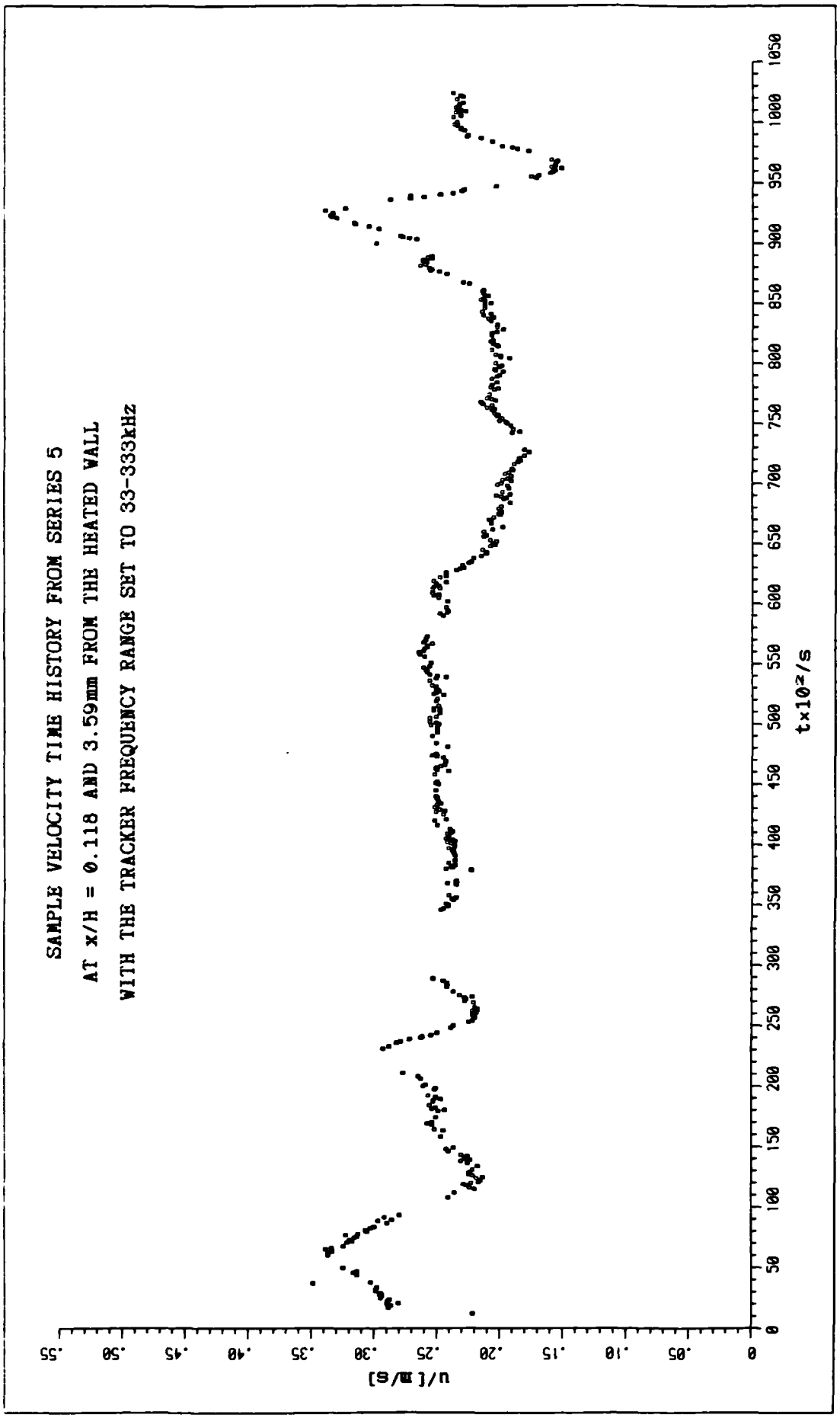
SAMPLE VELOCITY TIME HISTORY FROM SERIES 5
AT x/H = 0.118 AND 3.59mm FROM THE HEATED WALL
WITH THE TRACKER FREQUENCY RANGE SET TO 33-333kHz
u/[m/s]
t x10²/s
0
.05
.10
.15
.20
.25
.30
.35
.40
.45
.50
.55
0
50
100
150
200
250
300
350
400
450
500
550
600
650
700
750
800
850
900
950
1000
1050

FIGURE 7.91

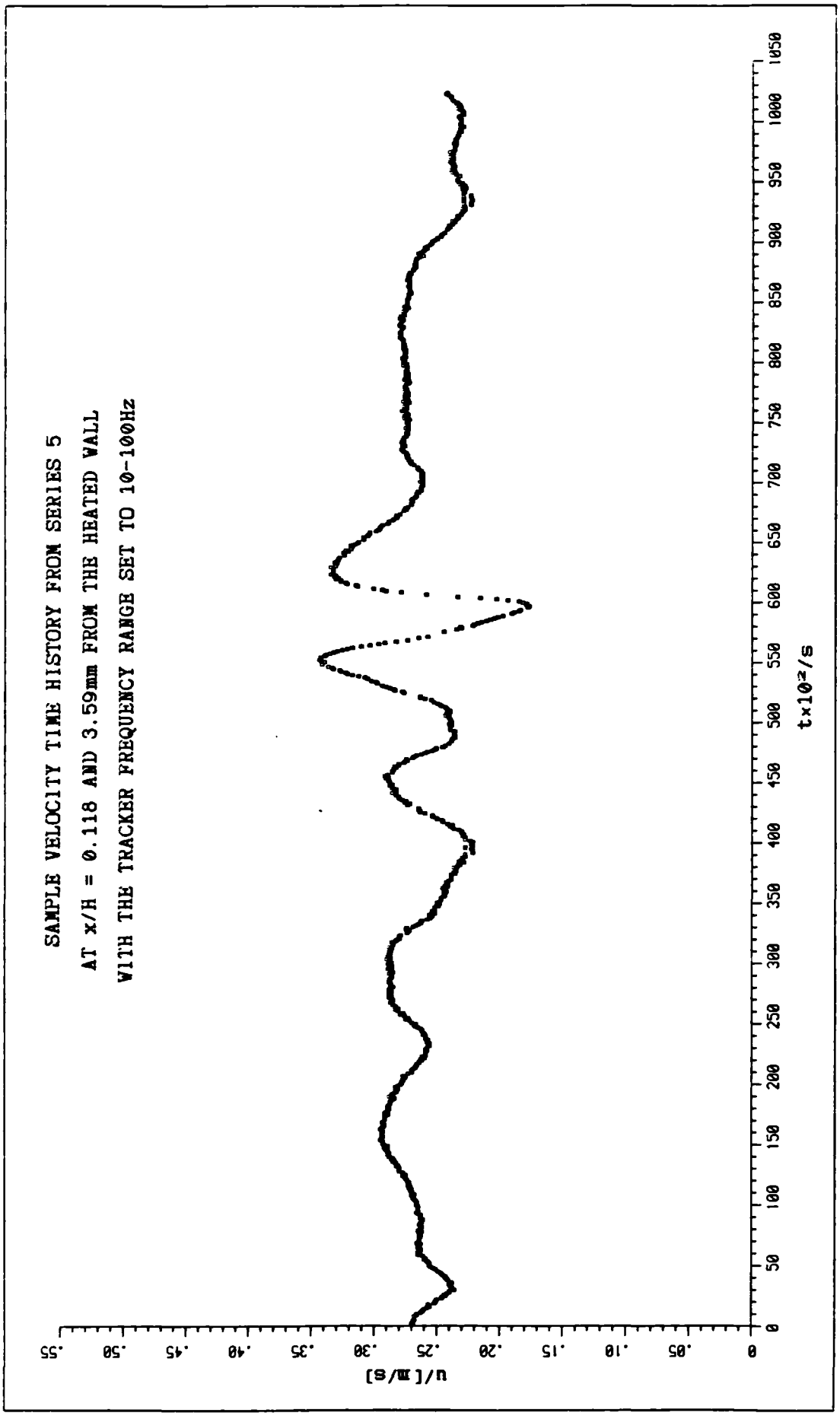
SAMPLE VELOCITY TIME HISTORY FROM SERIES 5
AT x/H = 0.118 AND 3.59mm FROM THE HEATED WALL
WITH THE TRACKER FREQUENCY RANGE SET TO 10-100Hz
u/[m/s]
t×10²/s
0
.05
.10
.15
.20
.25
.30
.35
.40
.45
.50
.55
0
50
100
150
200
250
300
350
400
450
500
550
600
650
700
750
800
850
900
950
1000
1050

FIGURE 7.92

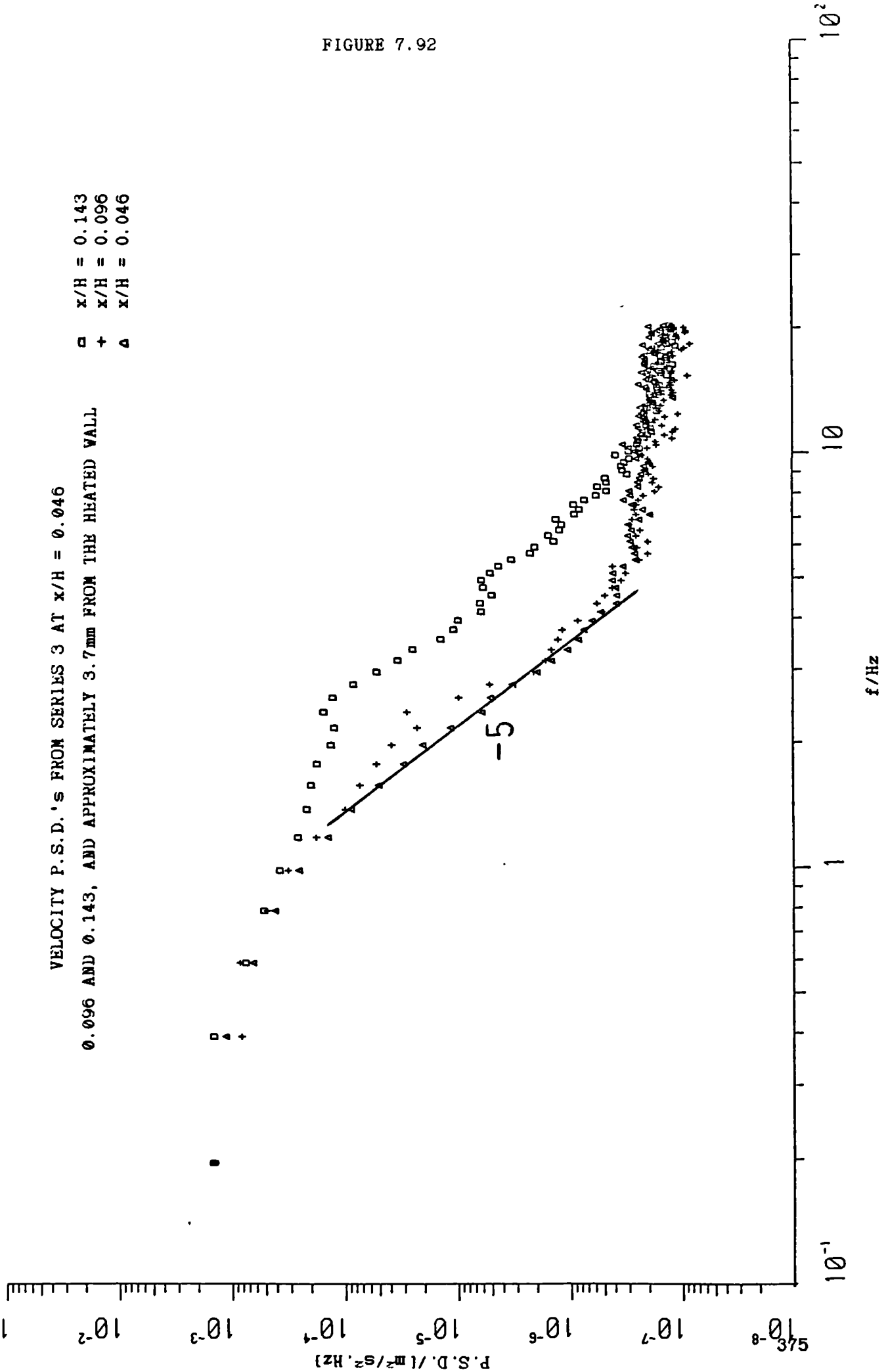
VELOCITY P.S.D.'s FROM SERIES 3 AT x/H = 0.046
0.096 AND 0.143, AND APPROXIMATELY 3.7mm FROM THE HEATED WALL
x/H = 0.143
x/H = 0.096
x/H = 0.046
-5
P.S.D./[m²/s².Hz]
f/Hz

FIGURE 7.93

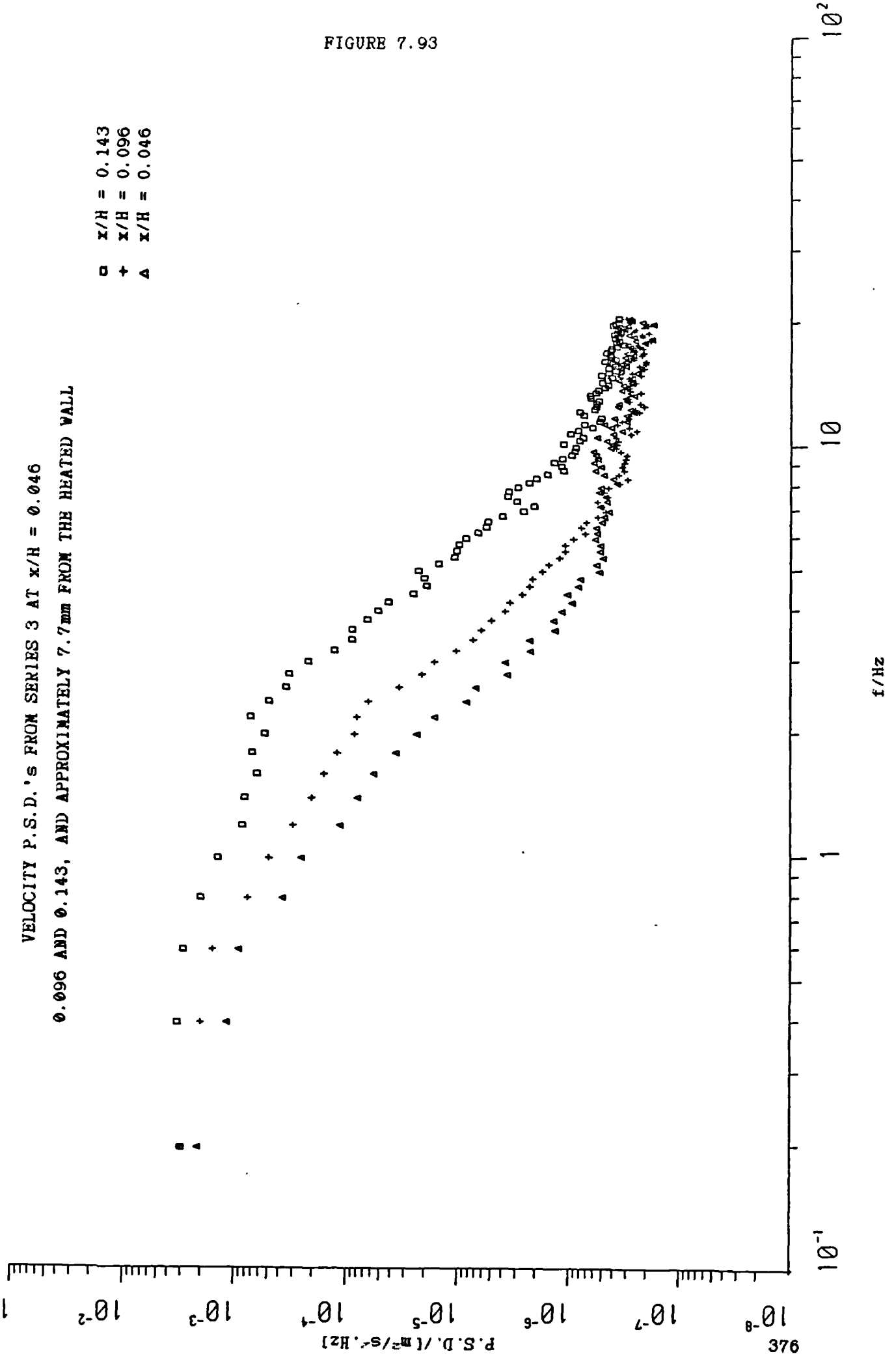
VELOCITY P.S.D.'s FROM SERIES 3 AT x/H = 0.046
0.096 AND 0.143, AND APPROXIMATELY 7.7mm FROM THE HEATED WALL
x/H = 0.143
x/H = 0.096
x/H = 0.046
P.S.D. /[m²/s⁴.Hz]
f/Hz

FIGURE 7.94

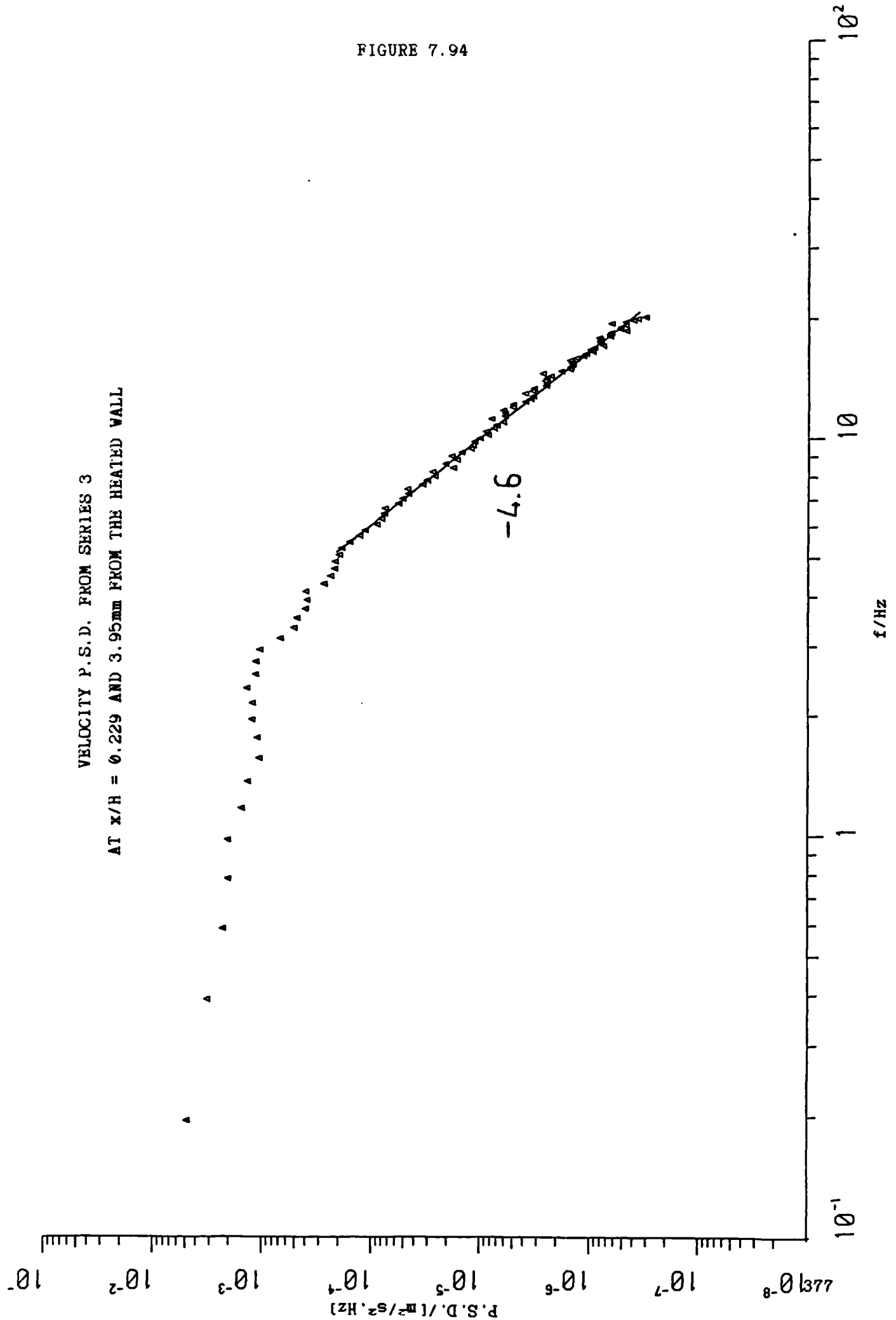
VELOCITY P.S.D. FROM SERIES 3
AT x/H = 0.229 AND 3.95mm FROM THE HEATED WALL
-4.6
P.S.D./[m²/s².Hz]
f/Hz
10⁻¹
1
10
10²
10⁻⁸
10⁻⁷
10⁻⁶
10⁻⁵
10⁻⁴
10⁻³
10⁻²
10⁻
377

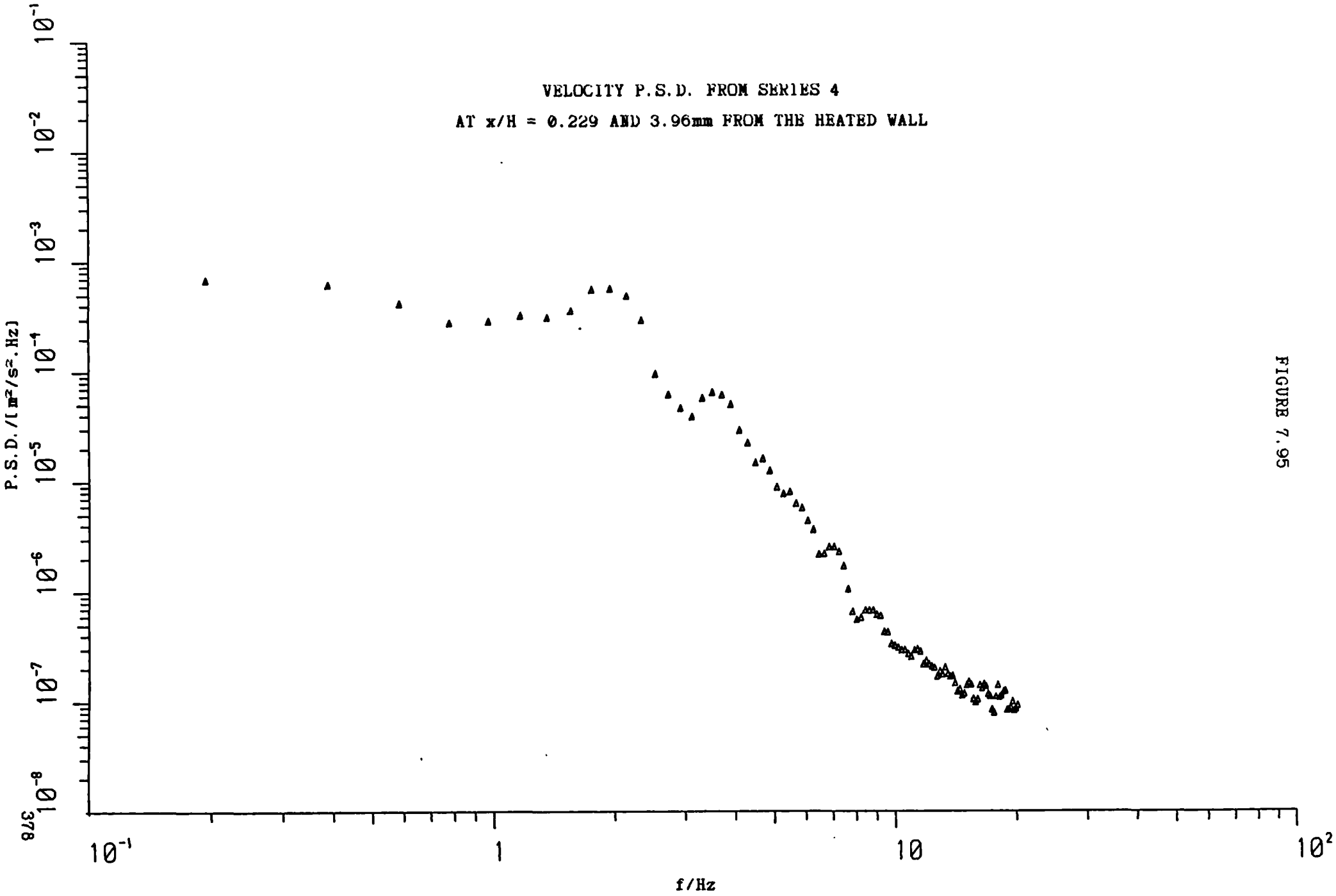
VELOCITY P.S.D. FROM SERIES 4
AT x/H = 0.229 AND 3.96mm FROM THE HEATED WALL
P.S.D./[m²/s².Hz]
10⁻¹
10⁻²
10⁻³
10⁻⁴
10⁻⁵
10⁻⁶
10⁻⁷
10⁻⁸
10⁻¹
1
10
10²
f/Hz

FIGURE 7.95

FIGURE 7.96

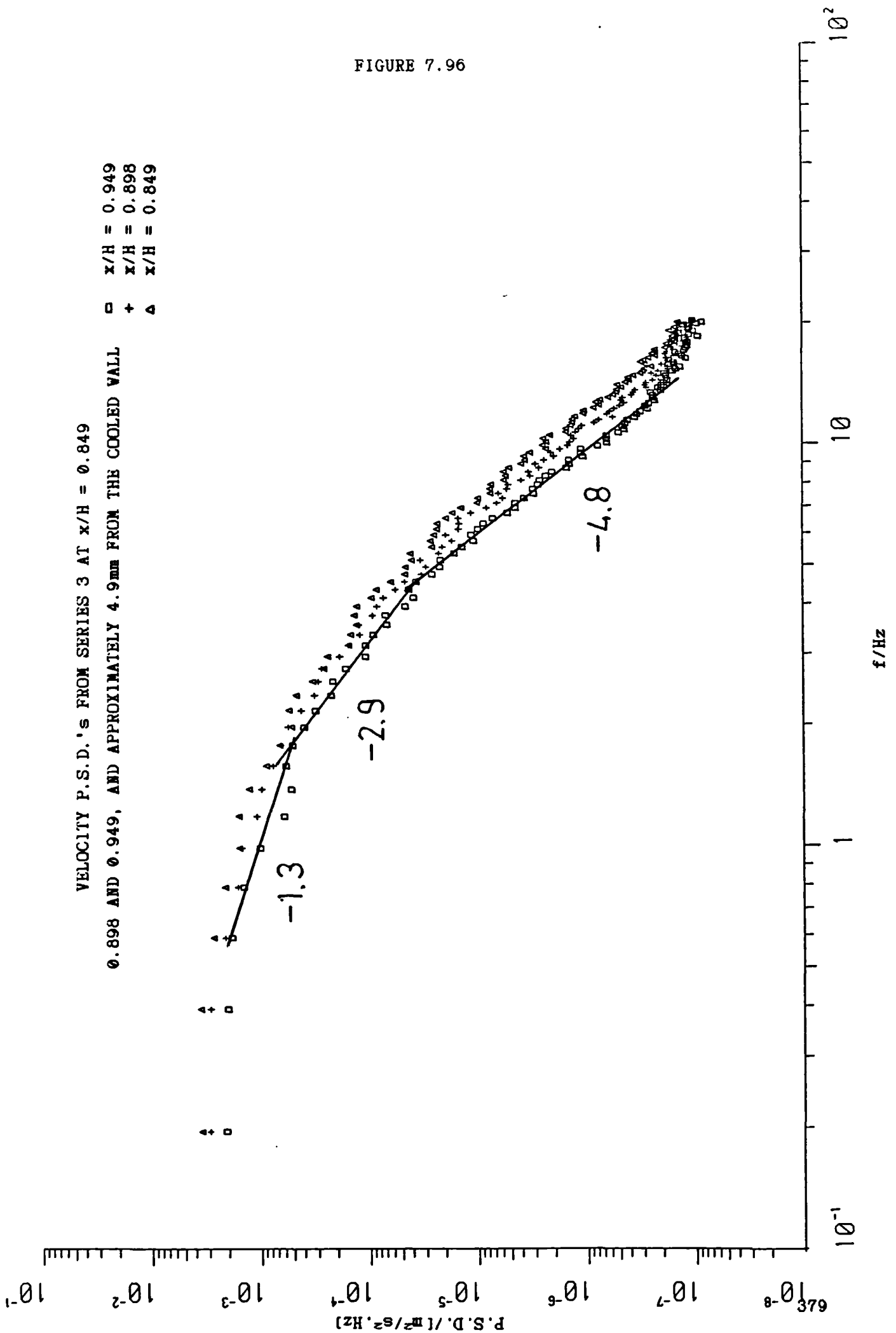
VELOCITY P.S.D.'s FROM SERIES 3 AT x/H = 0.849
0.898 AND 0.949, AND APPROXIMATELY 4.9mm FROM THE COOLED WALL
x/H = 0.949
x/H = 0.898
x/H = 0.849
-1.3
-2.9
-4.8
P.S.D./[m²/s².Hz]
f/Hz
10⁻¹
1
10
10²
10⁻⁸
10⁻⁷
10⁻⁶
10⁻⁵
10⁻⁴
10⁻³
10⁻²
10⁻¹

FIGURE 7.97

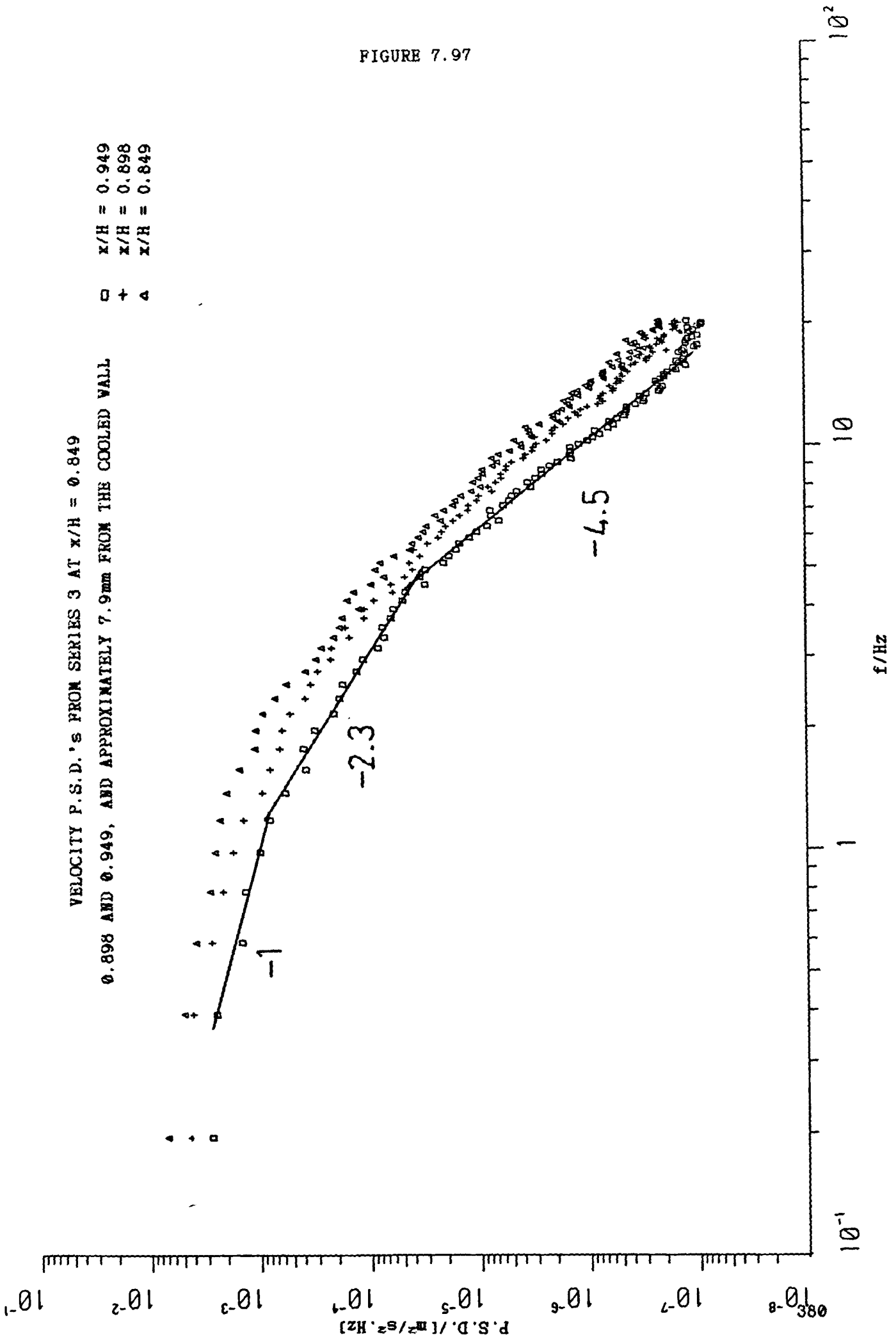
VELOCITY P.S.D.'s FROM SERIES 3 AT x/H = 0.849
0.898 AND 0.949, AND APPROXIMATELY 7.9mm FROM THE COOLED WALL
x/H = 0.949
x/H = 0.898
x/H = 0.849
-1
-2.3
-4.5
P.S.D./[m²/s².Hz]
f/Hz

FIGURE 7.98

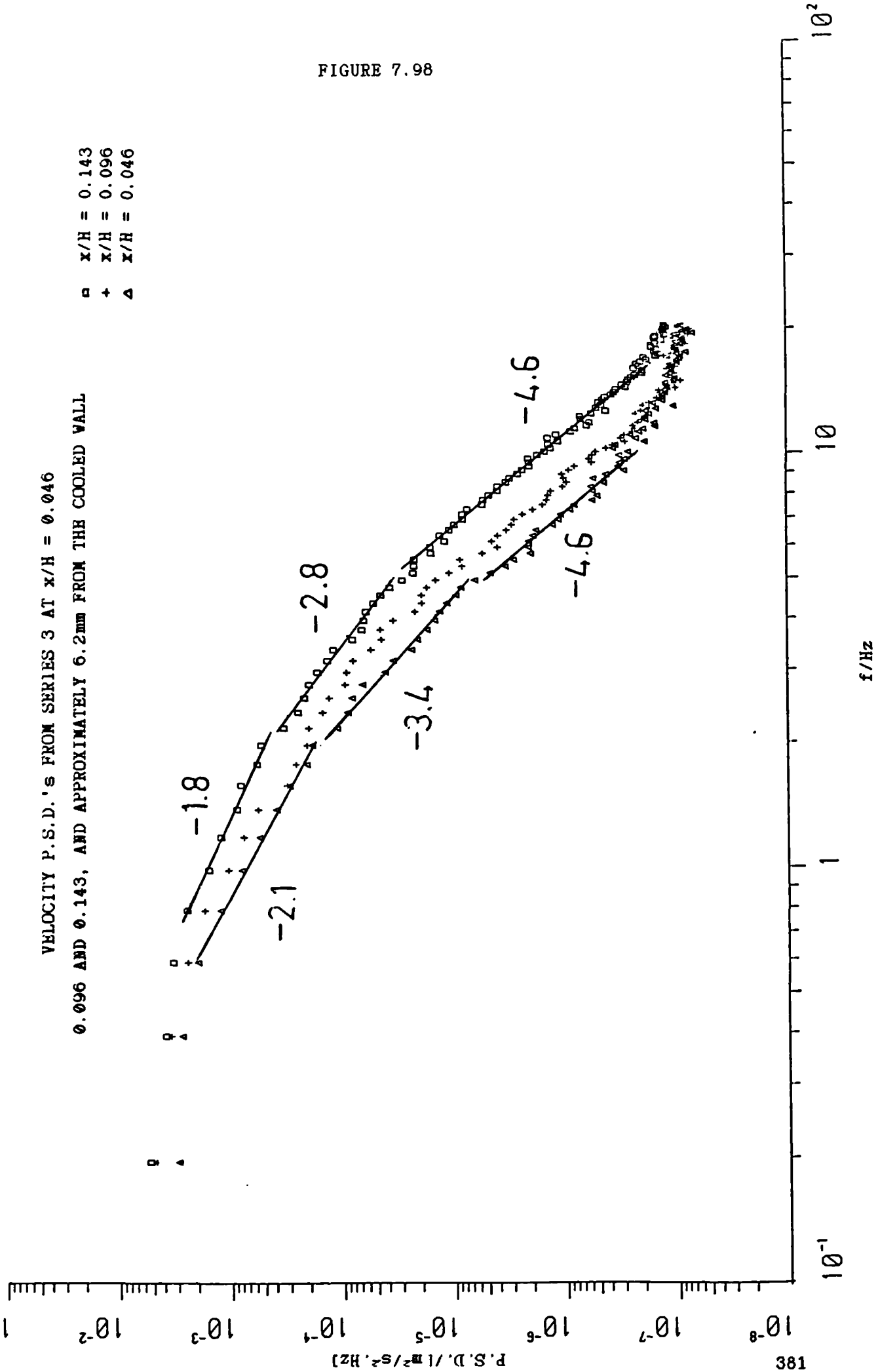
VELOCITY P.S.D.'s FROM SERIES 3 AT x/H = 0.046
0.096 AND 0.143, AND APPROXIMATELY 6.2mm FROM THE COOLED WALL
x/H = 0.143
x/H = 0.096
x/H = 0.046
-1.8
-2.1
-2.8
-3.4
-4.6
-4.6
P.S.D./[m²/s², Hz]
f/Hz

FIGURE 7.99

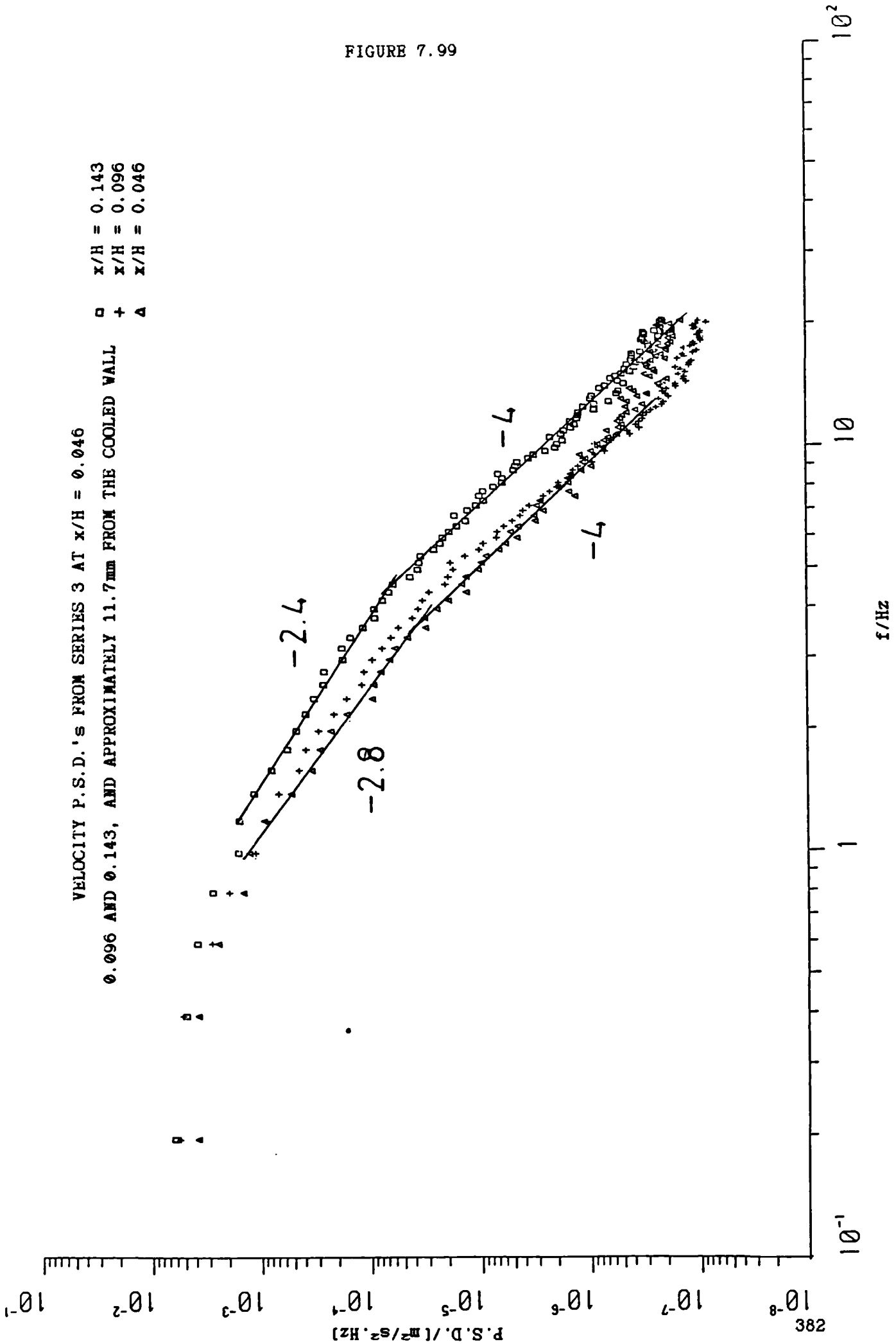
VELOCITY P.S.D.'s FROM SERIES 3 AT x/H = 0.046
0.096 AND 0.143, AND APPROXIMATELY 11.7mm FROM THE COOLED WALL
□ x/H = 0.143
+ x/H = 0.096
△ x/H = 0.046
-2.4
-4
-2.8
-4
P.S.D./[m²/s².Hz]
f/Hz

FIGURE 7.100

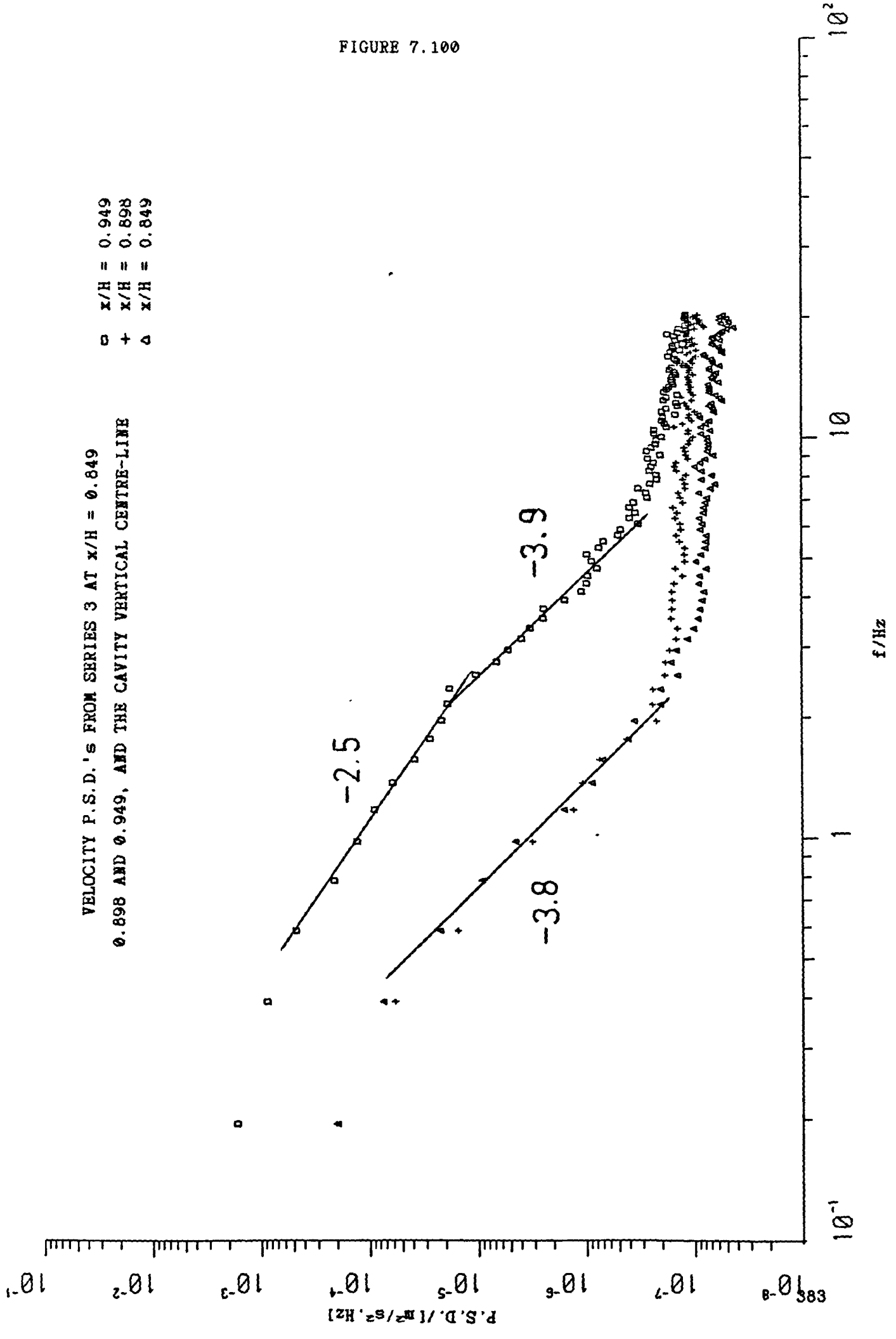
VELOCITY P.S.D.'s FROM SERIES 3 AT x/H = 0.849
0.898 AND 0.949, AND THE CAVITY VERTICAL CENTRE-LINE
□ x/H = 0.949
+ x/H = 0.898
△ x/H = 0.849
-2.5
-3.9
-3.8
P.S.D./[m²/s².Hz]
f/Hz
10⁻¹
1
10
10²
10⁻⁸
10⁻⁷
10⁻⁶
10⁻⁵
10⁻⁴
10⁻³
10⁻²
10⁻¹

FIGURE 7.101

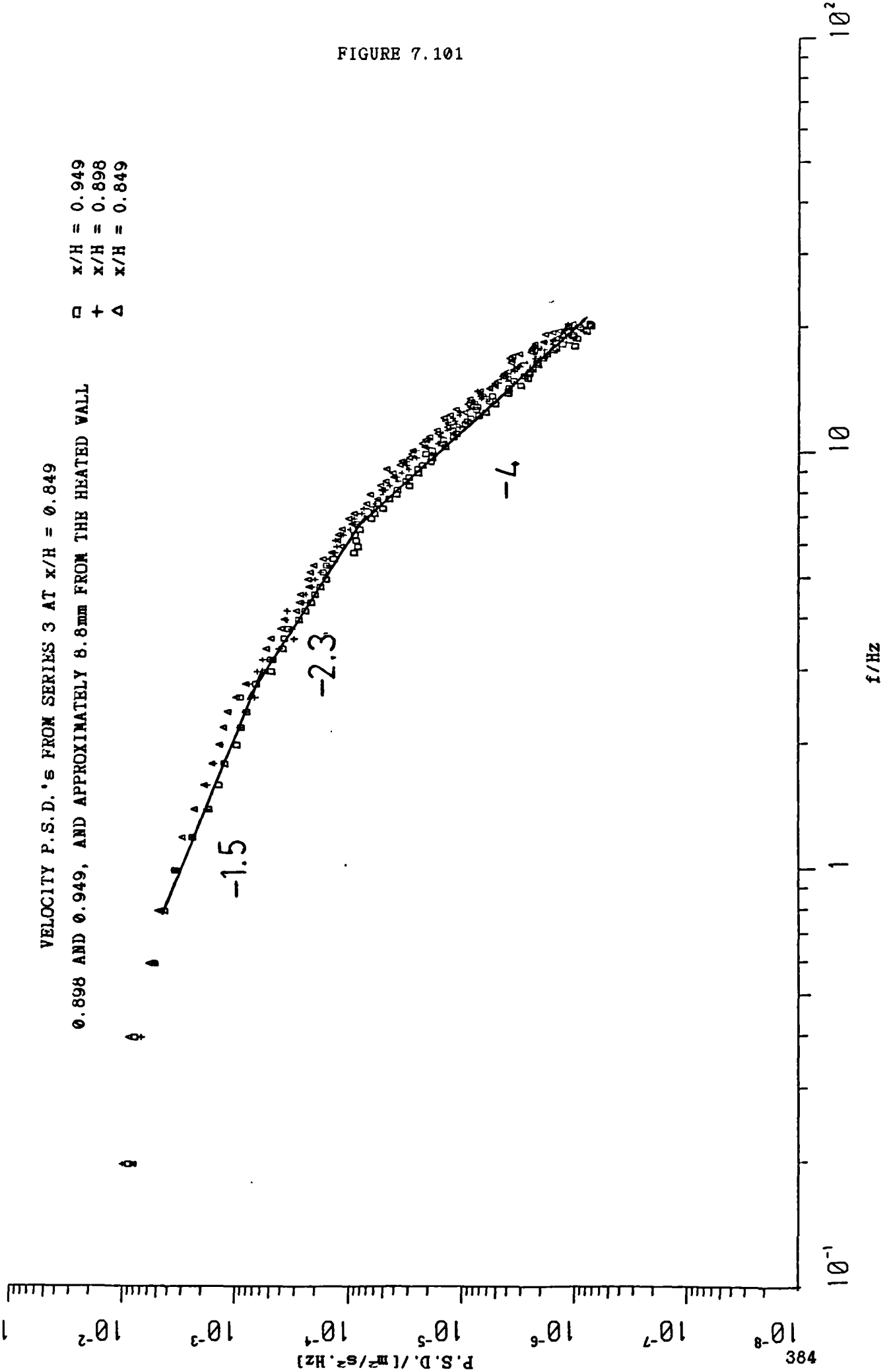
VELOCITY P.S.D.'s FROM SERIES 3 AT x/H = 0.849
0.898 AND 0.949, AND APPROXIMATELY 8.8mm FROM THE HEATED WALL
□ x/H = 0.949
+ x/H = 0.898
Δ x/H = 0.849
-1.5
-2.3
-4
P.S.D./[m²/s².Hz]
f/Hz

FIGURE 7.102

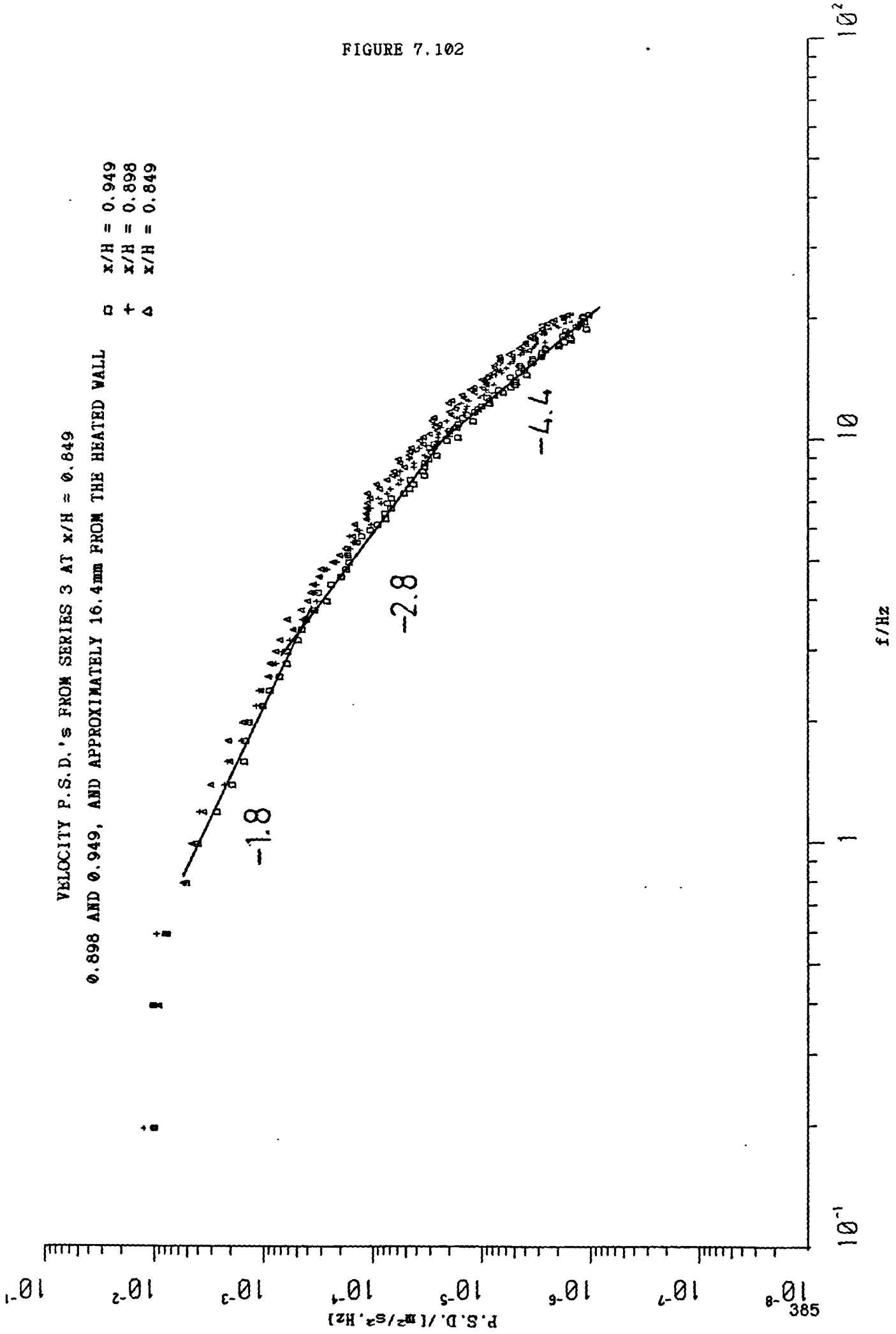
VELOCITY P.S.D.'s FROM SERIES 3 AT x/H = 0.849
0.898 AND 0.949, AND APPROXIMATELY 16.4mm FROM THE HEATED WALL
□ x/H = 0.949
+ x/H = 0.898
△ x/H = 0.849
-1.8
-2.8
-4.4
P.S.D./[m²/s².Hz]
f/Hz

FIGURE 7.103

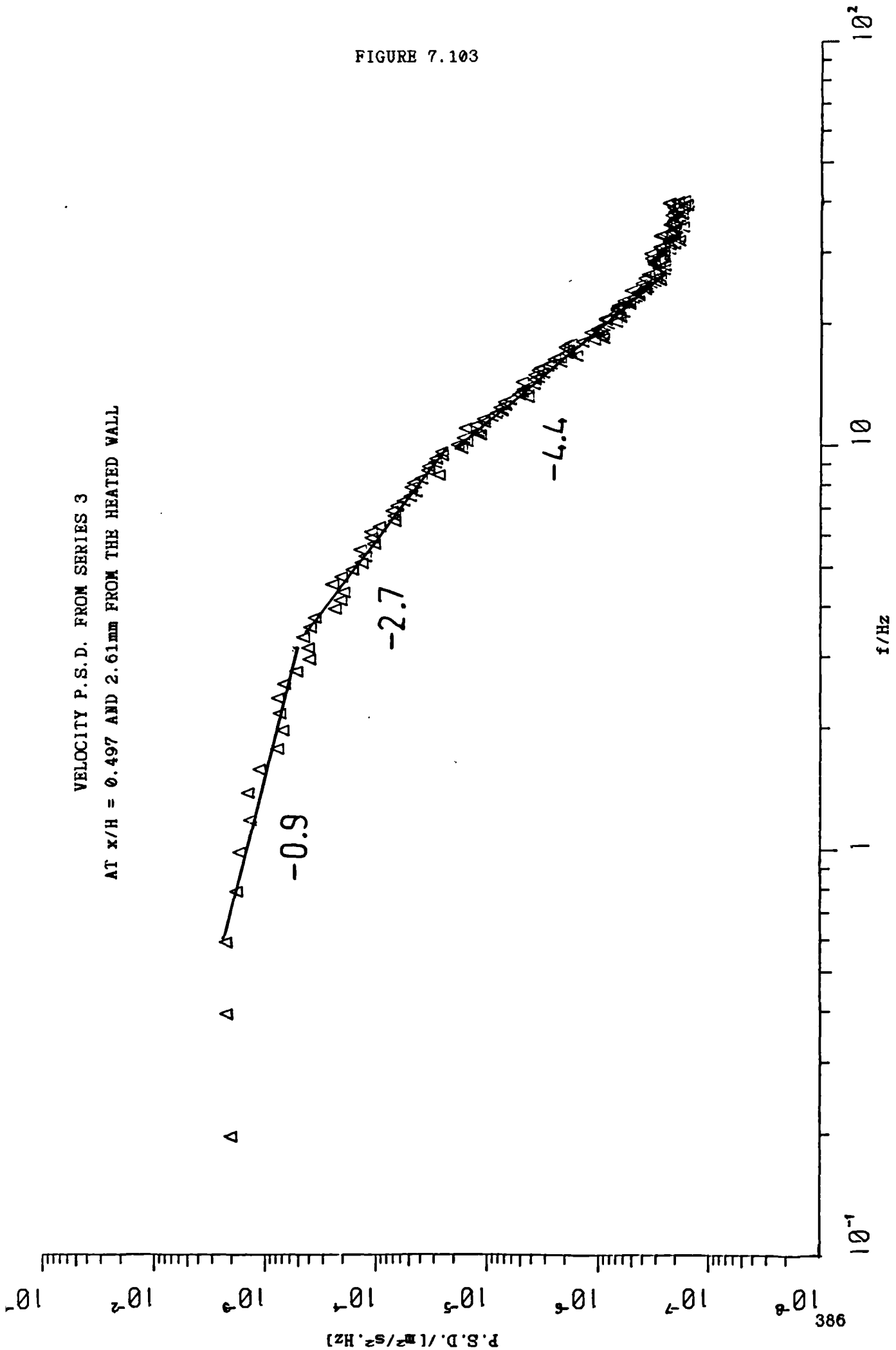
VELOCITY P.S.D. FROM SERIES 3
AT x/H = 0.497 AND 2.61mm FROM THE HEATED WALL
-0.9
-2.7
-4.4
f/Hz
P.S.D./[m²/s².Hz]

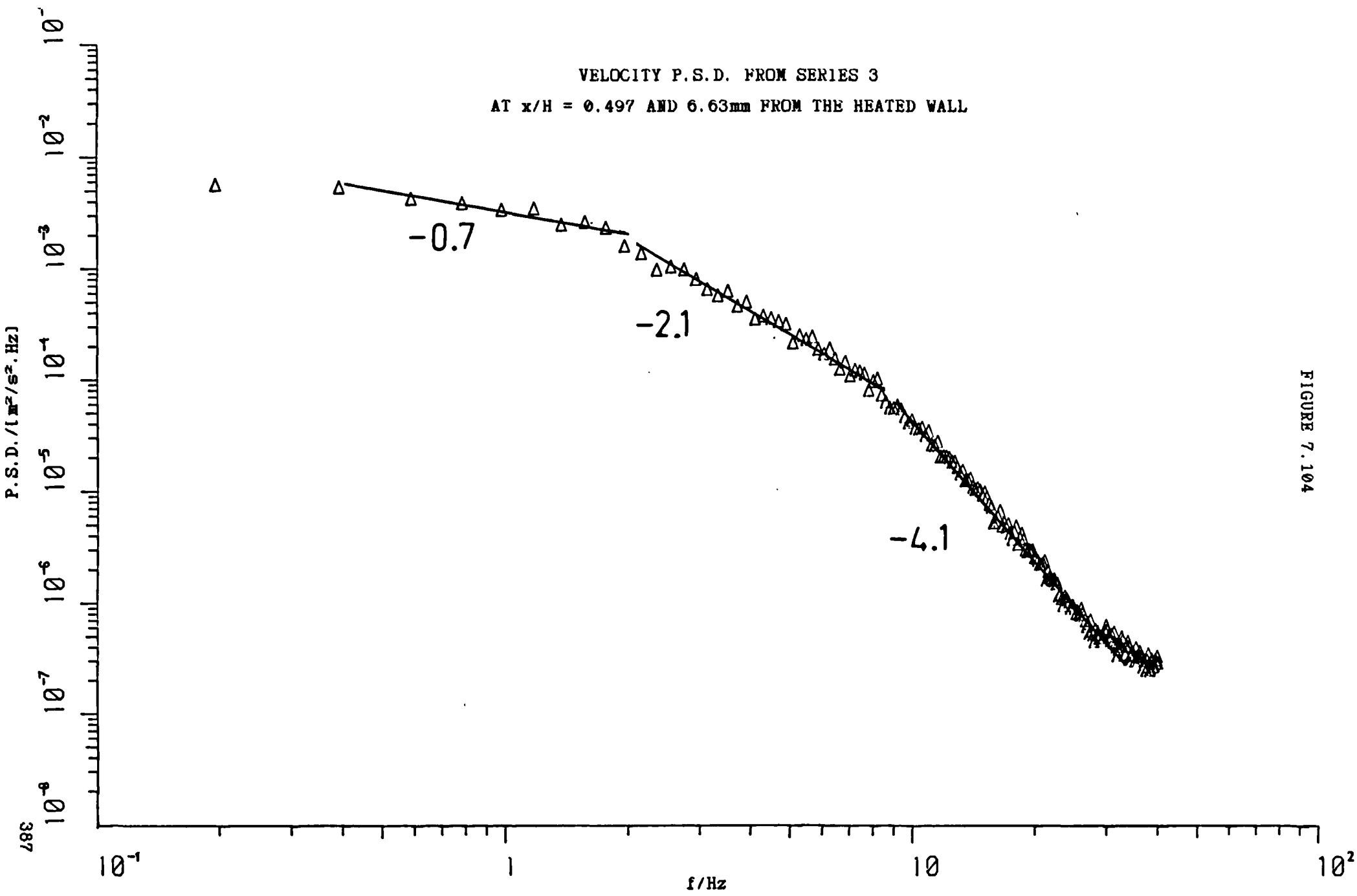
VELOCITY P.S.D. FROM SERIES 3
AT x/H = 0.497 AND 6.63mm FROM THE HEATED WALL
-0.7
-2.1
-4.1
P.S.D./(m²/s².Hz)
f/Hz
10⁻¹
1
10
10²

FIGURE 7.104

FIGURE 7.105

VELOCITY BUOYANCY SUB-RANGE

INDEX AGAINST dT/dx, R_G AND R_F

(a)

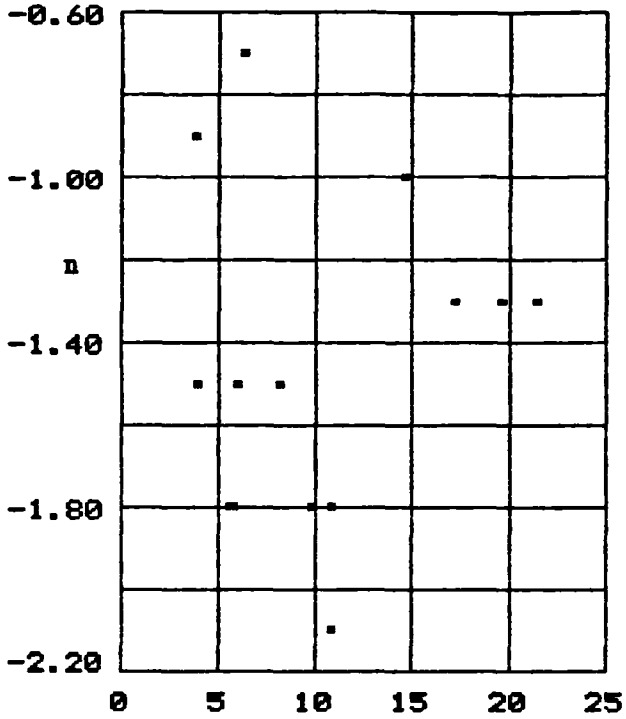

(b)

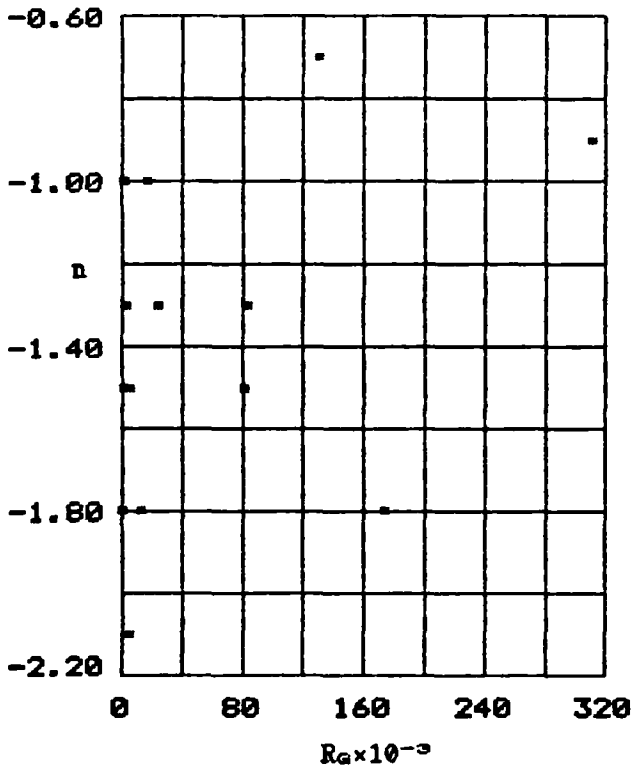

(c)

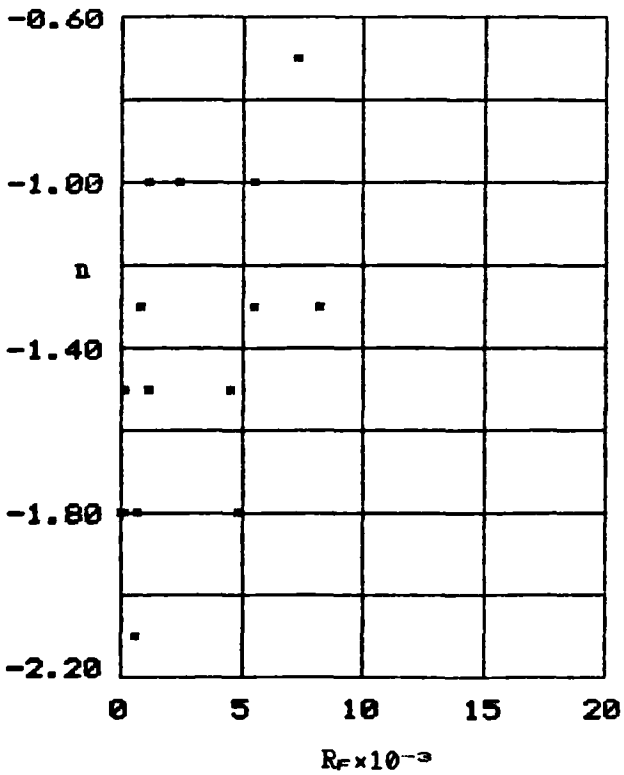

FIGURE 7.106

VELOCITY INERTIAL SUB-RANGE

INDEX AGAINST dT/dx, R_G AND R_F

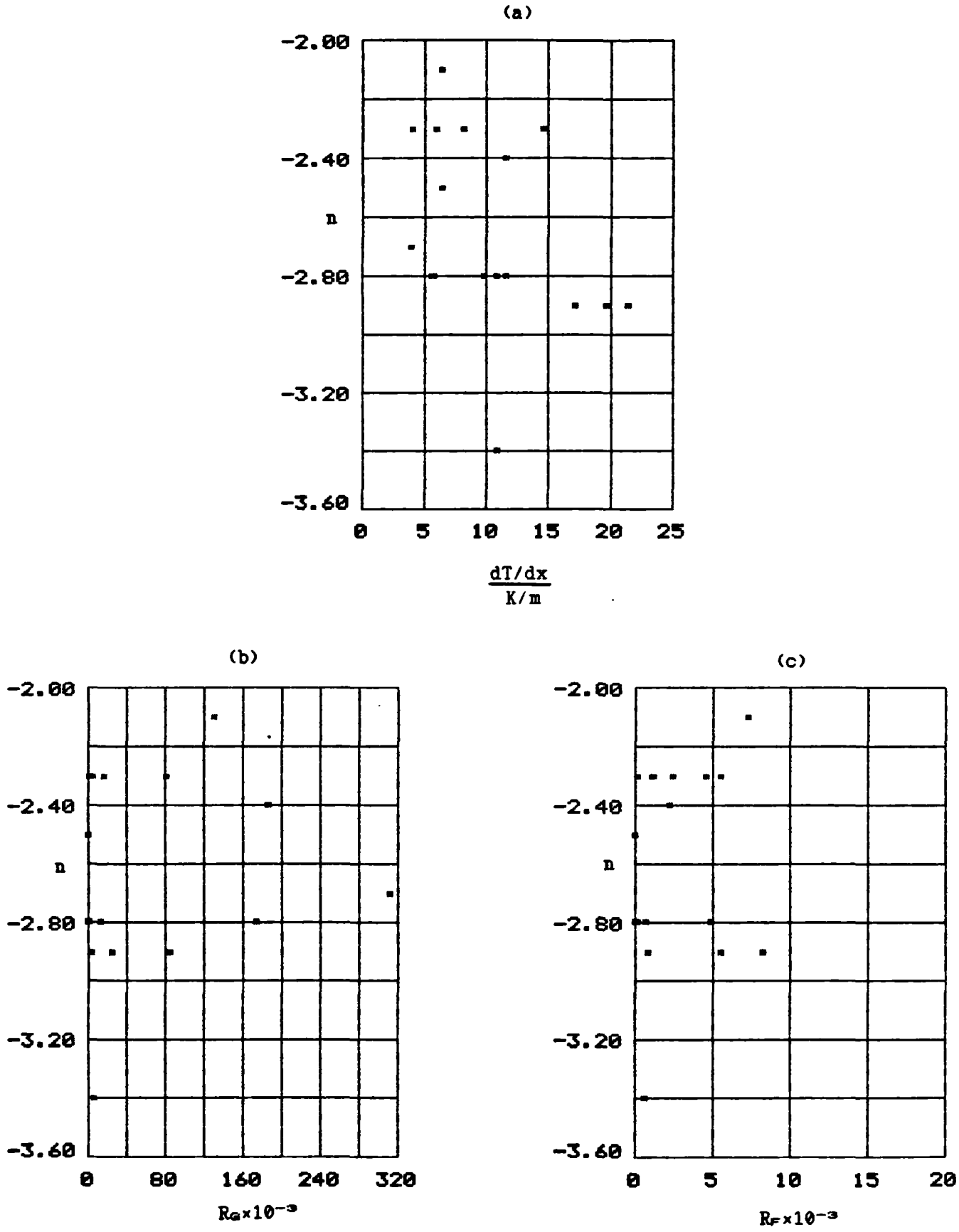

FIGURE 7.107

VELOCITY DISSIPATION SUB-RANGE

INDEX AGAINST dT/dx, R_G AND R_F

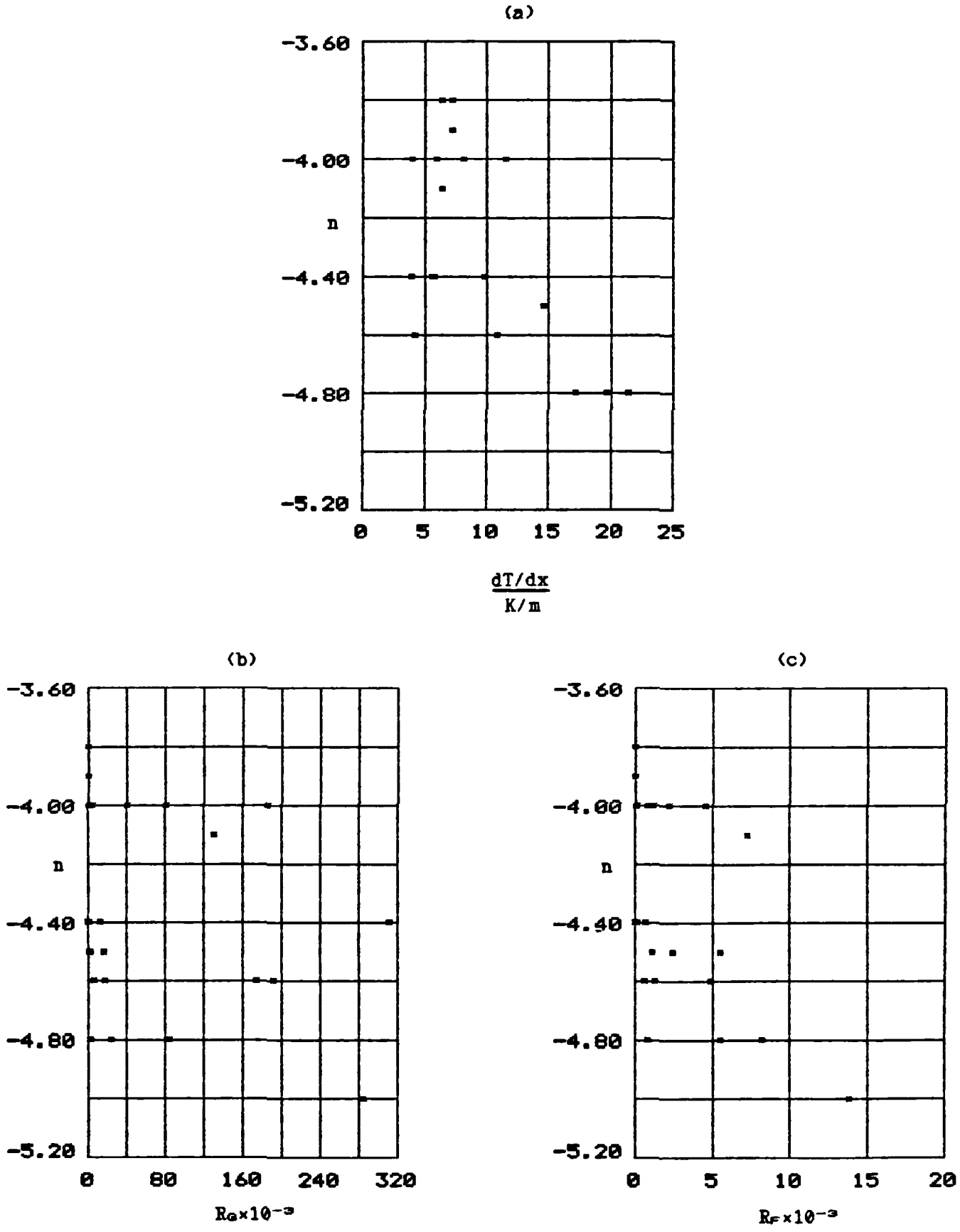

FIGURE 7.108

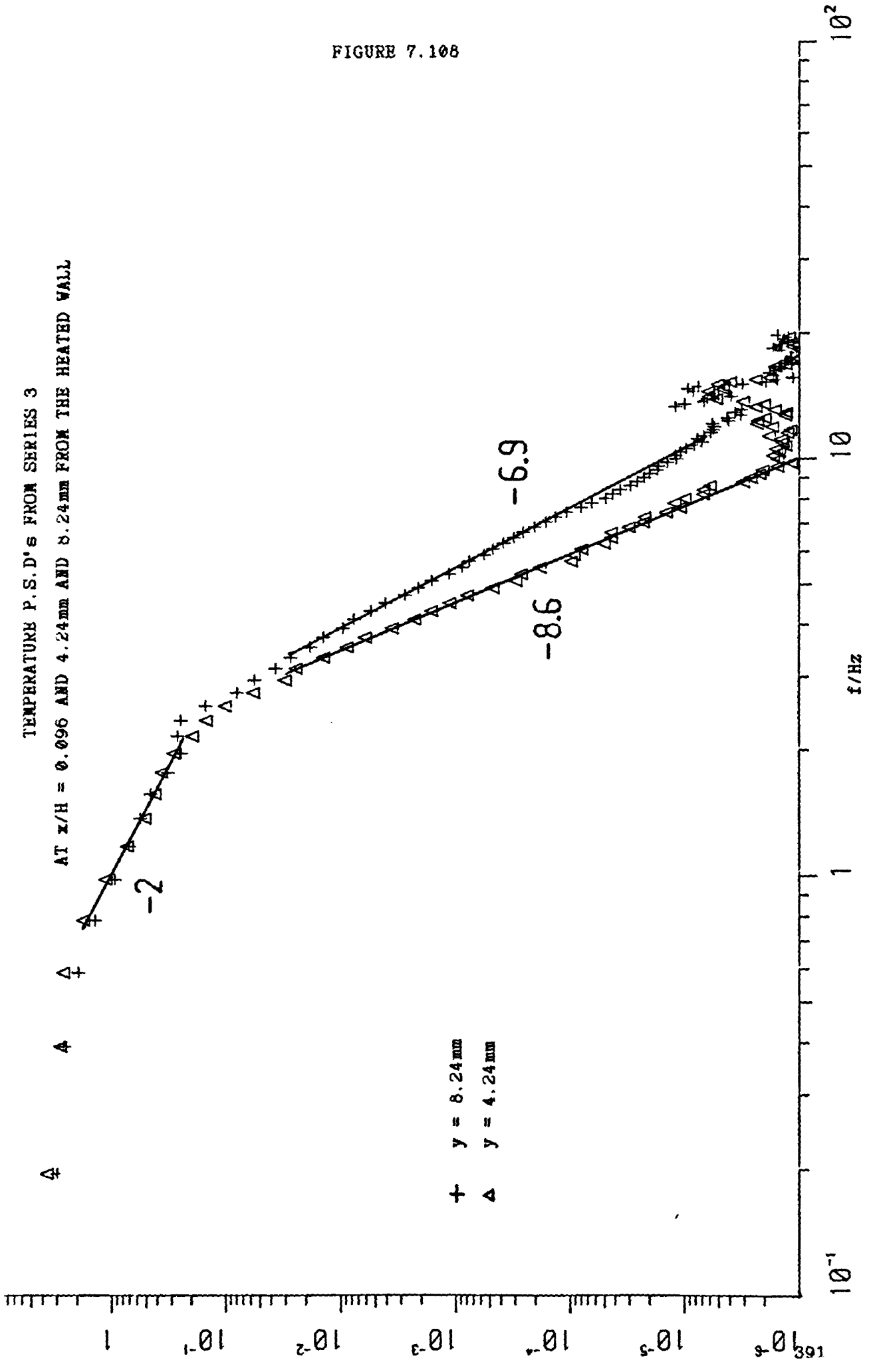
TEMPERATURE P.S.D's FROM SERIES 3
AT z/H = 0.096 AND 4.24mm AND 8.24mm FROM THE HEATED WALL
-2
-6.9
-8.6
y = 8.24mm
y = 4.24mm
f/Hz
P.S.D./(K²/S², Hz)

FIGURE 7.109

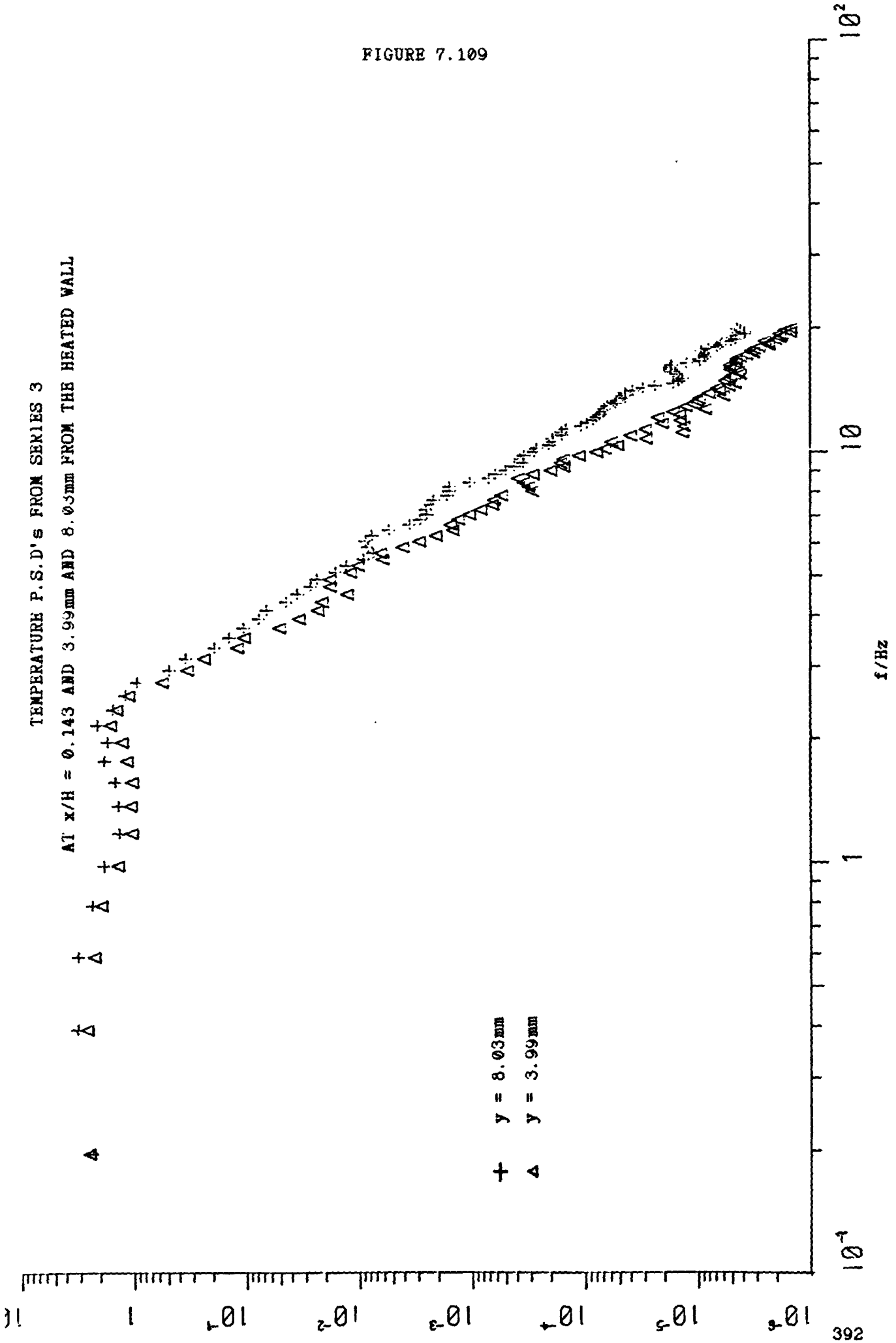
TEMPERATURE P.S.D's FROM SERIES 3
AT x/H = 0.143 AND 3.99mm AND 8.03mm FROM THE HEATED WALL
y = 8.03mm
y = 3.99mm
P.S.D./[m²/s².Hz]
f/Hz
10⁻⁶
10⁻⁵
10⁻⁴
10⁻³
10⁻²
10⁻¹
1
10
10²

FIGURE 7.110

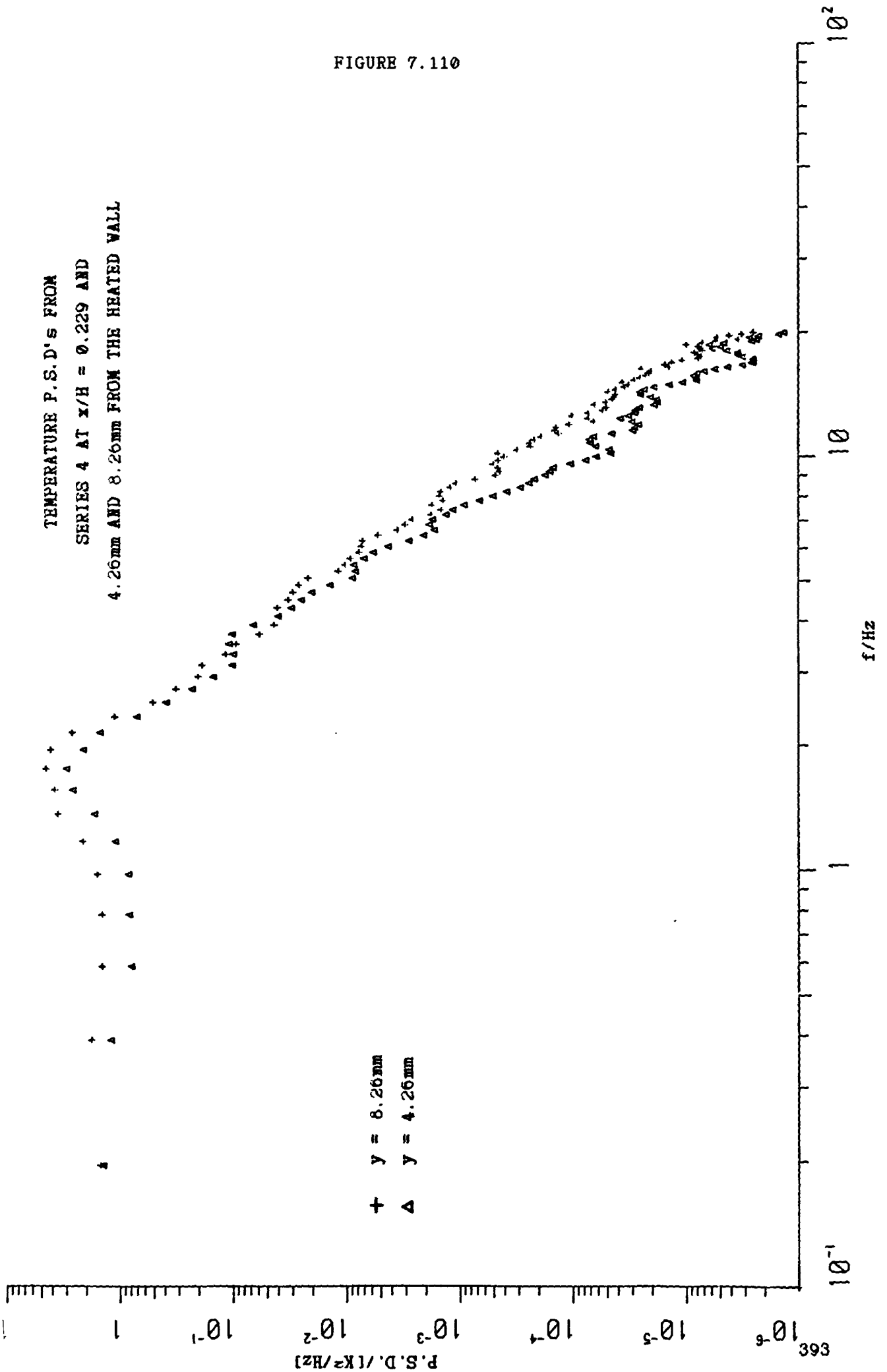
TEMPERATURE P.S.D's FROM
SERIES 4 AT x/H = 0.229 AND
4.26mm AND 8.26mm FROM THE HEATED WALL
+ y = 8.26mm
Δ y = 4.26mm
P.S.D./(K²/Hz)
f/Hz
10⁻⁶
10⁻⁵
10⁻⁴
10⁻³
10⁻²
10⁻¹
1
10⁻¹
1
10
10²

FIGURE 7.111

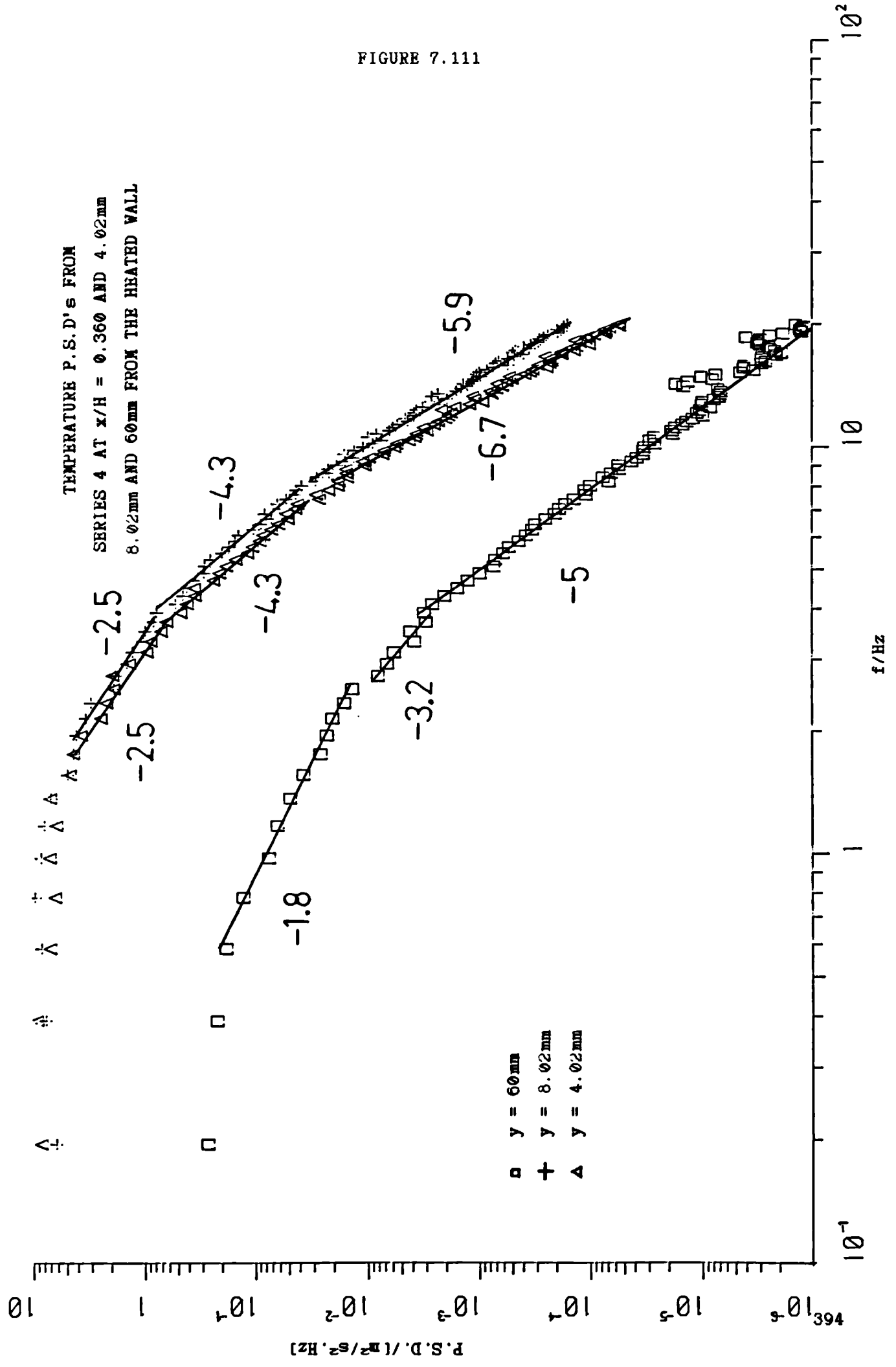
TEMPERATURE P.S.D'S FROM
SERIES 4 AT x/H = 0.360 AND 4.02mm
8.02mm AND 60mm FROM THE HEATED WALL
-2.5
-2.5
-4.3
-4.3
-5.9
-6.7
-5
-3.2
-1.8
y = 60mm
y = 8.02mm
y = 4.02mm
P.S.D./(m²/s².Hz)
f/Hz
10
1
10⁻¹
10²
10⁻⁴
10⁻³
10⁻²
10⁻¹
10⁻⁵
394

FIGURE 7.112

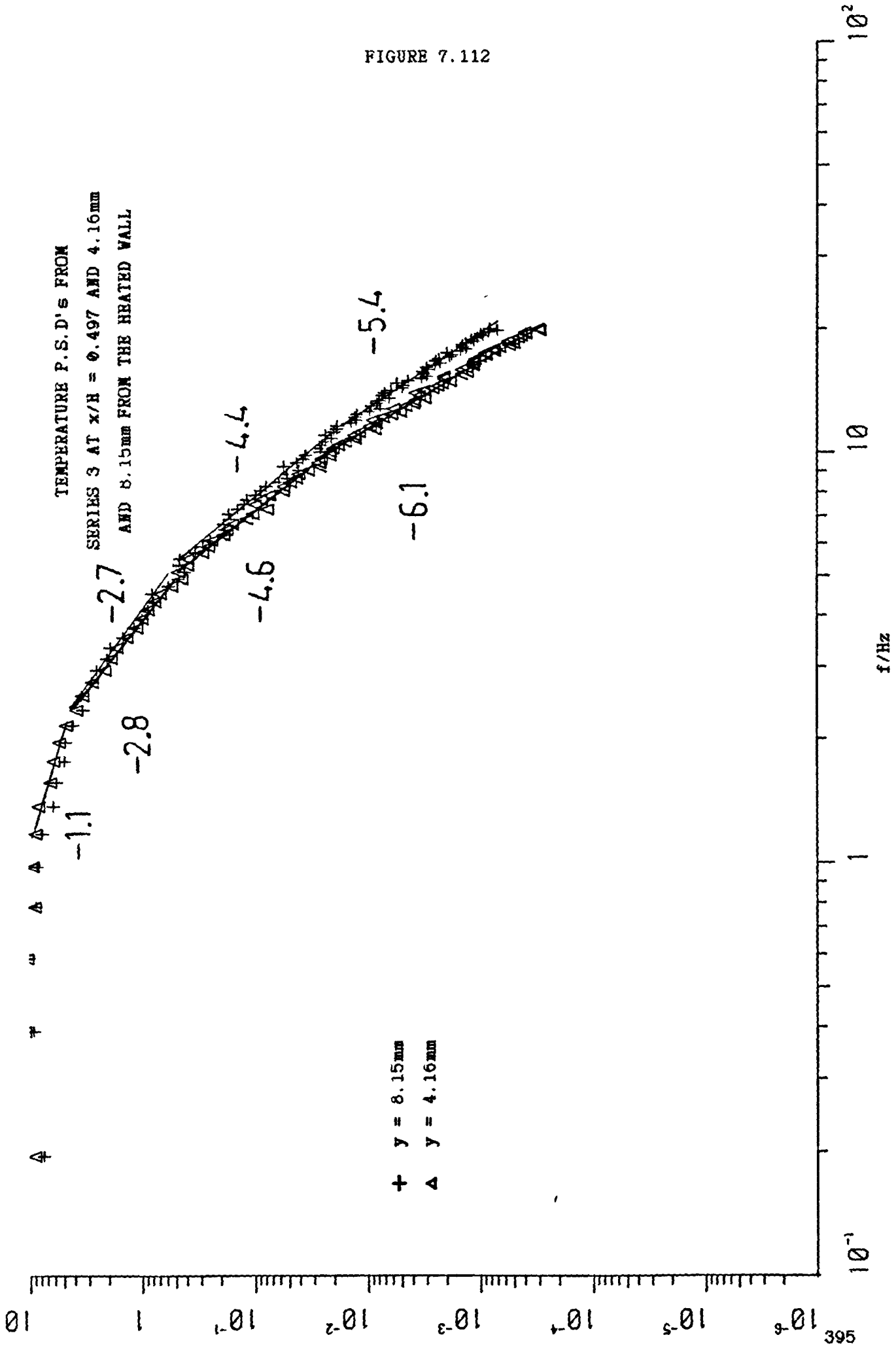
TEMPERATURE P.S.D's FROM
SERIES 3 AT x/H = 0.497 AND 4.16mm
AND 8.15mm FROM THE HEATED WALL
-1.1
-2.8
-2.7
-4.6
-4.4
-6.1
-5.4
+ y = 8.15mm
△ y = 4.16mm
P.S.D./(m²/s².Hz)
f/Hz
10⁻⁶
10⁻⁵
10⁻⁴
10⁻³
10⁻²
10⁻¹
1
10
10⁻¹
1
10
10²

FIGURE 7.113

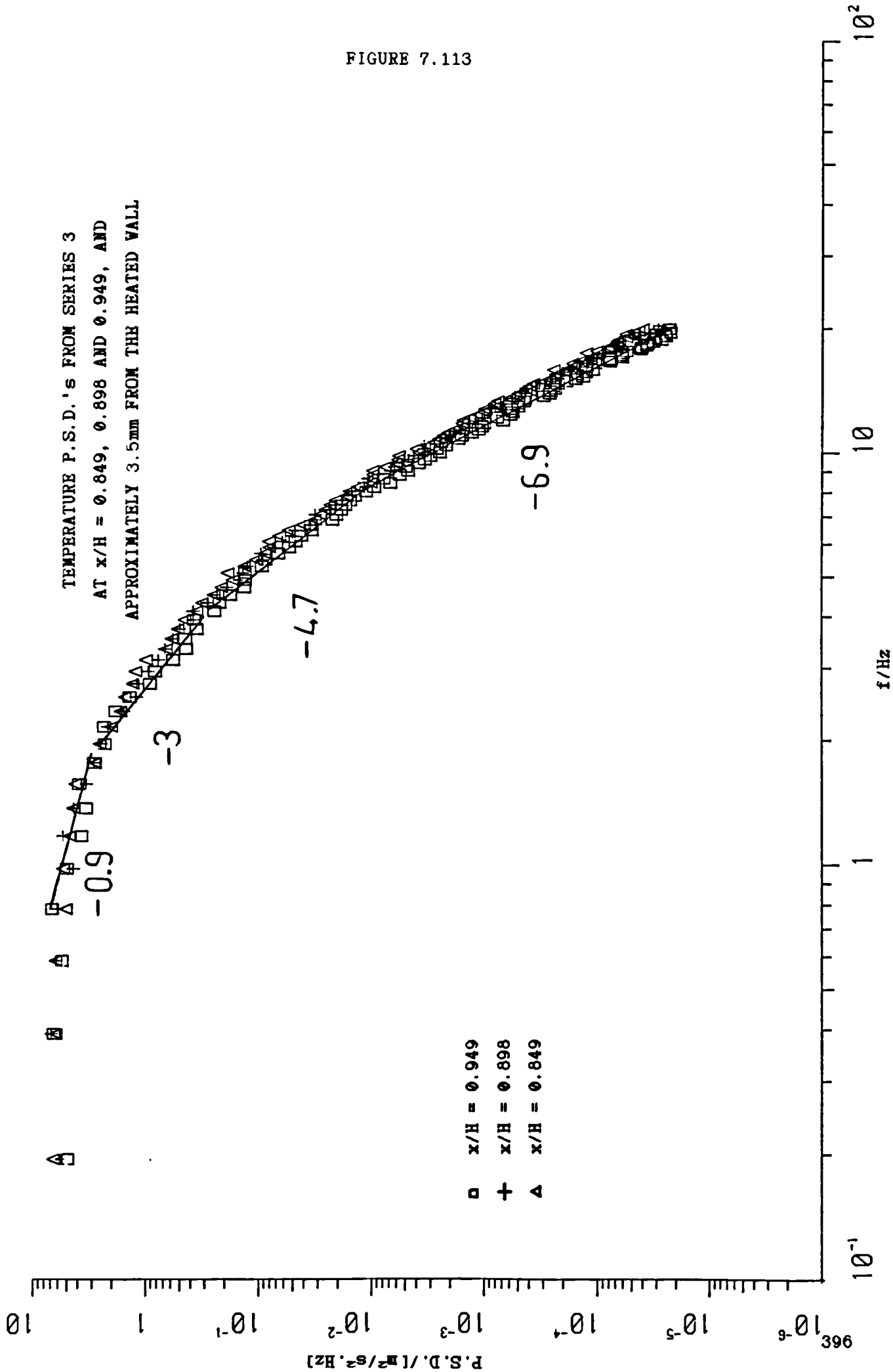
TEMPERATURE P.S.D.'s FROM SERIES 3
AT x/H = 0.849, 0.898 AND 0.949, AND
APPROXIMATELY 3.5mm FROM THE HEATED WALL
-0.9
-3
-4.7
-6.9
x/H = 0.949
x/H = 0.898
x/H = 0.849
P.S.D./[K²/S².Hz]
f/Hz
10
1
10⁻¹
10⁻²
10⁻³
10⁻⁴
10⁻⁵
10⁻⁶
10²

FIGURE 7.114

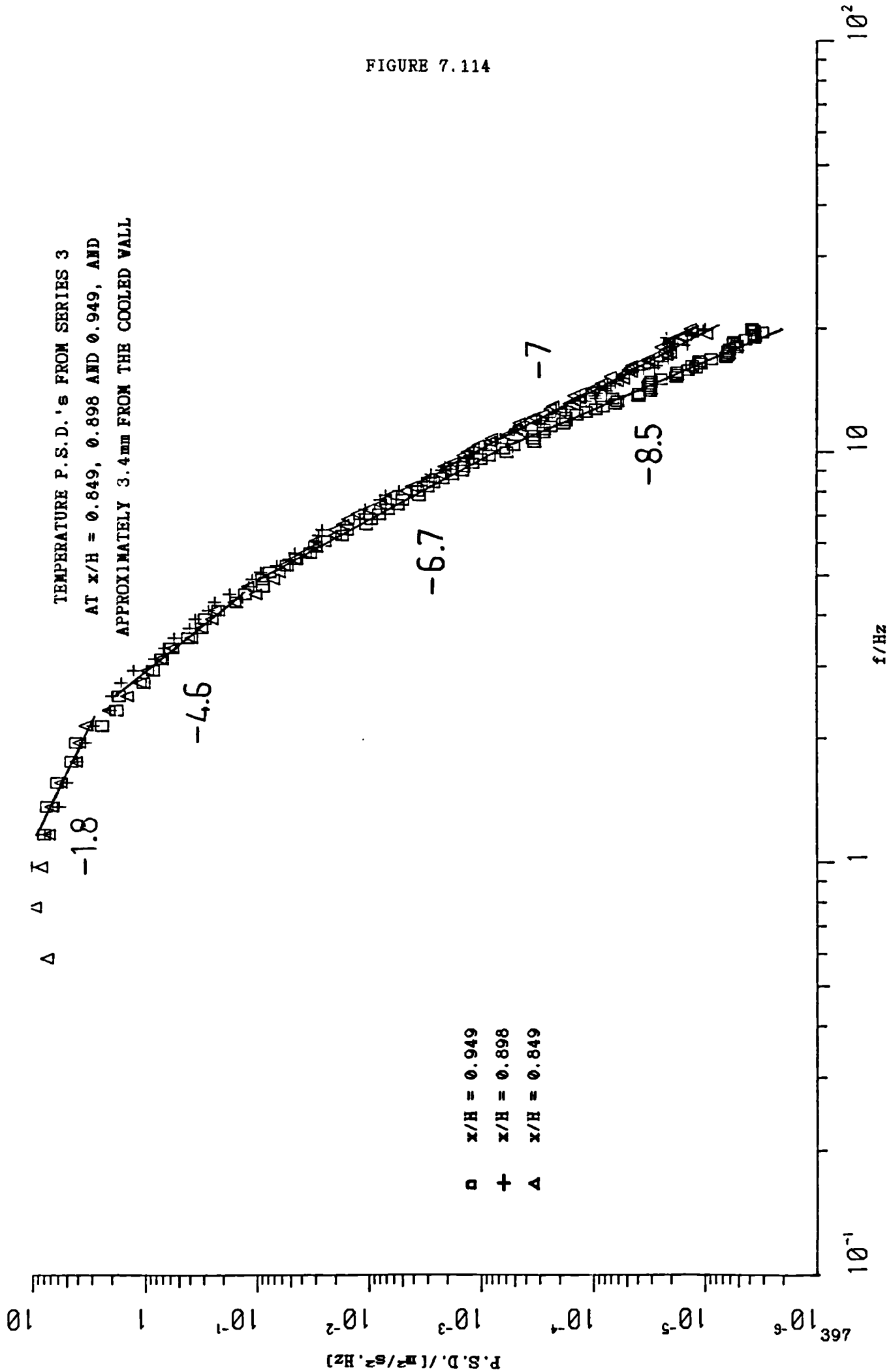
TEMPERATURE P.S.D.'s FROM SERIES 3
AT x/H = 0.849, 0.898 AND 0.949, AND
APPROXIMATELY 3.4mm FROM THE COOLED WALL
-1.8
-4.6
-6.7
-7
-8.5
x/H = 0.949
x/H = 0.898
x/H = 0.849
P.S.D./(m²/s².Hz)
f/Hz
10
1
10⁻¹
10⁻²
10⁻³
10⁻⁴
10⁻⁵
10⁻⁶
10²
397

FIGURE 7.115

TEMPERATURE BUOYANCY SUB-RANGE

INDEX AGAINST dT/dx, R_G AND R_F

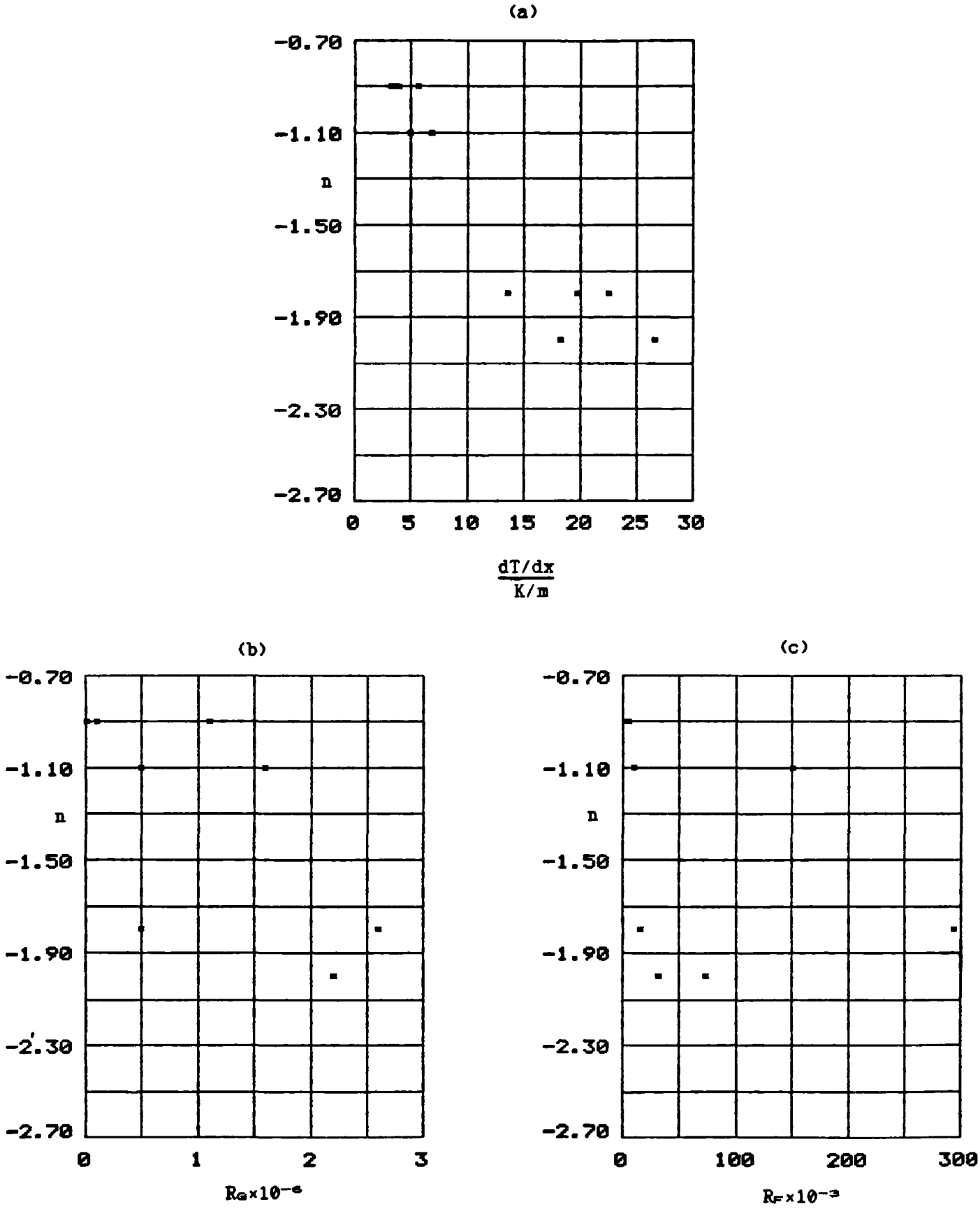

FIGURE 7.116

TEMPERATURE INERTIAL SUB-RANGE INDEX AGAINST dT/dx, R_α AND R_F

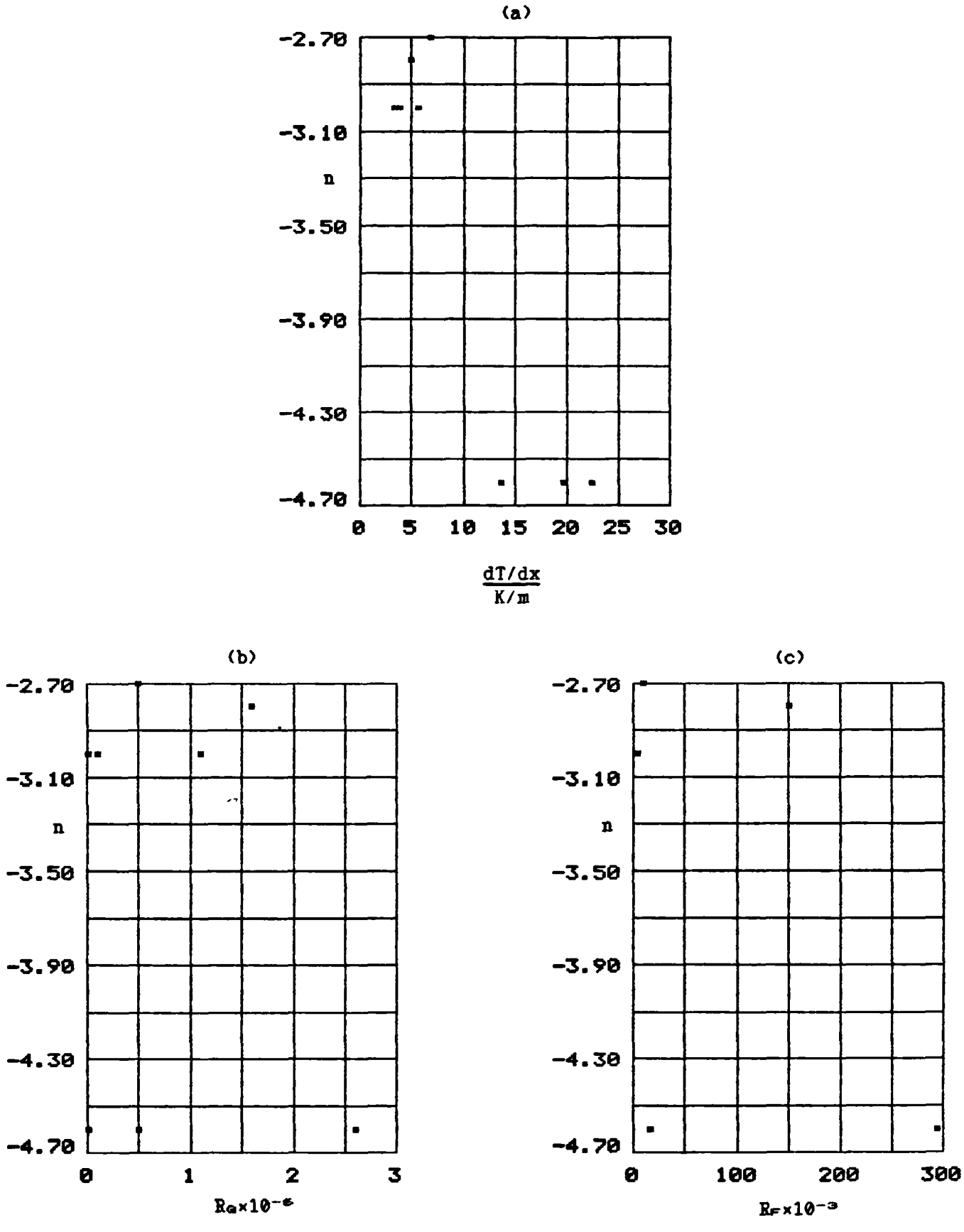

FIGURE 7.117

TEMPERATURE THIRD SUB-RANGE

INDEX AGAINST dT/dx, R_G AND R_F

(a)

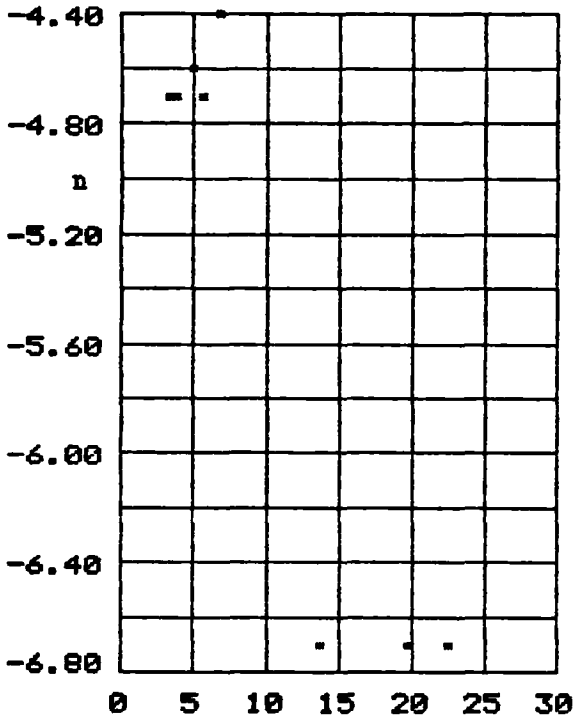

dT/dx
K/m

(b)

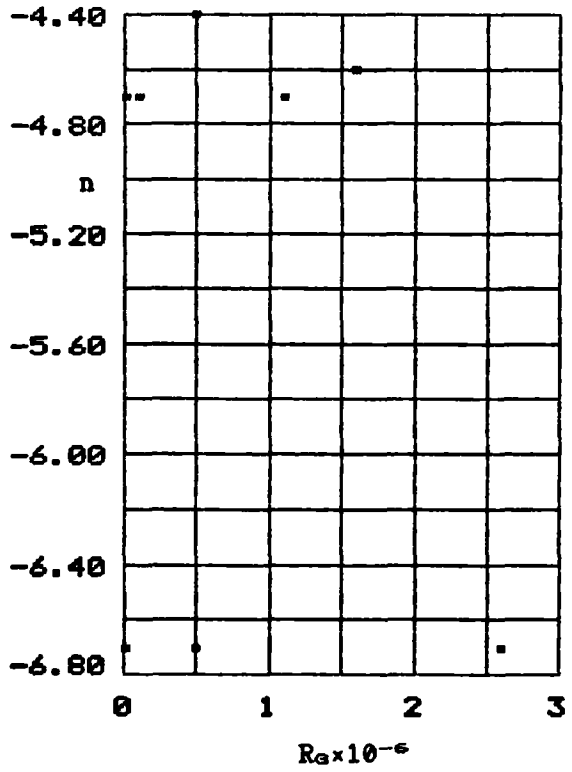

$R_G \times 10^{-6}$

(c)

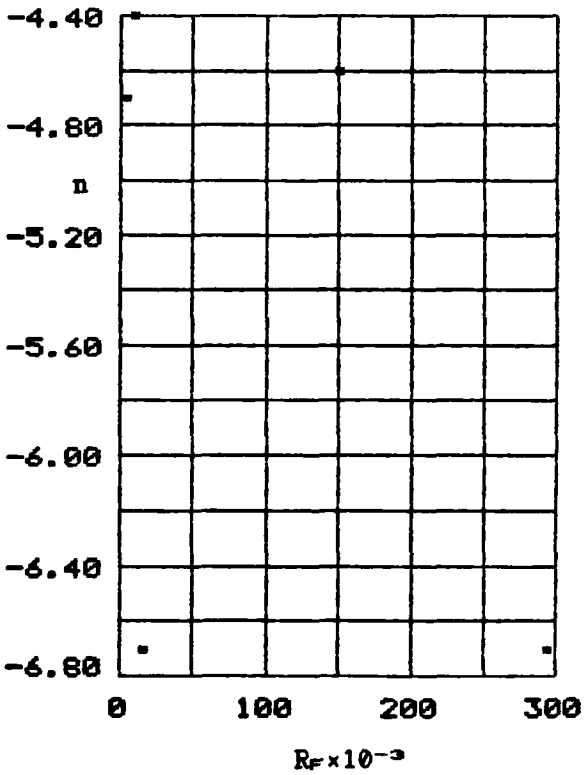

$R_F \times 10^{-3}$

FIGURE 7.118

TEMPERATURE DISSIPATION SUB-RANGE

INDEX AGAINST dT/dx, R_G AND R_F

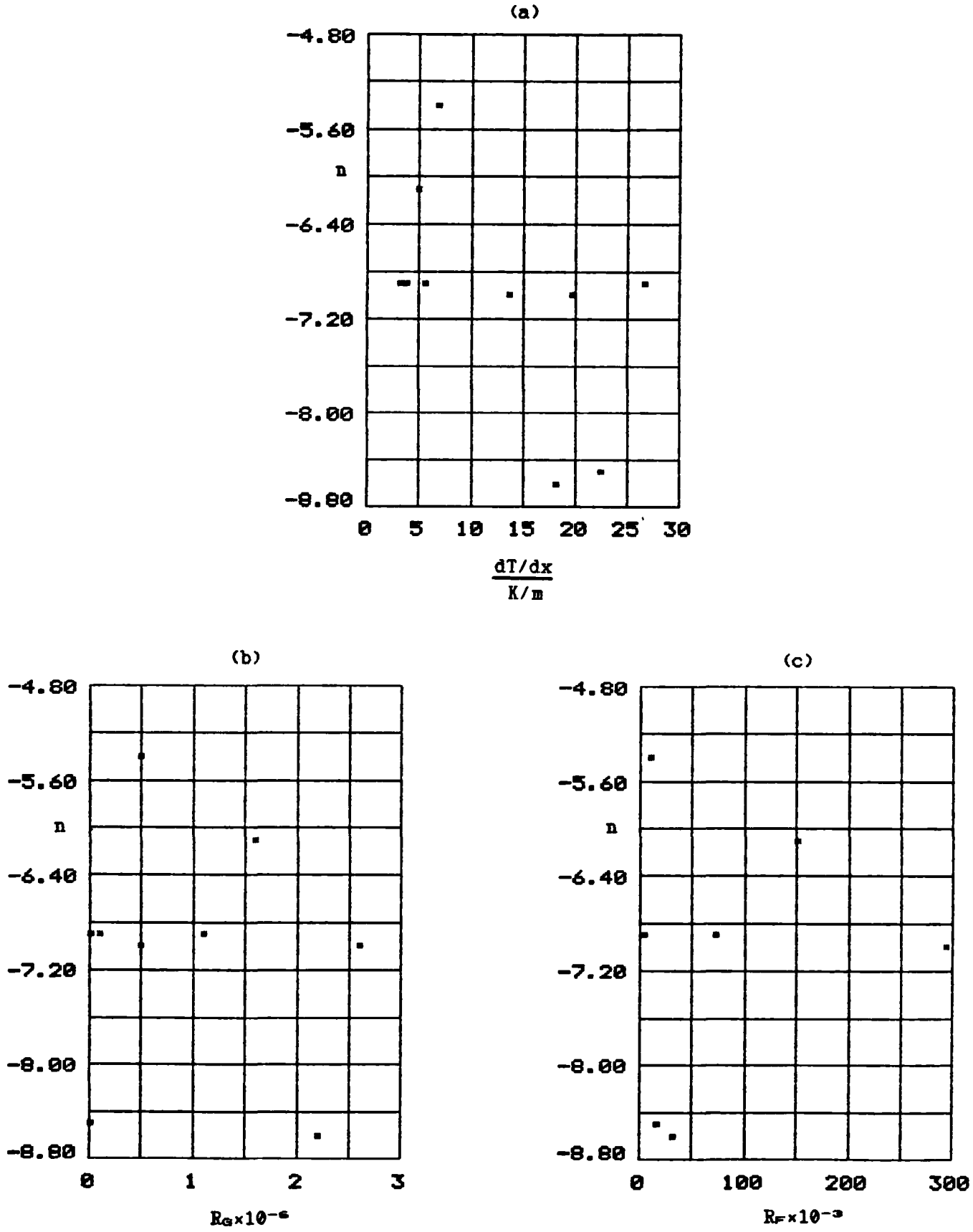

TABLE 7.1

HEAT TRANSFER COEFFICIENTS FOR SERIES 1 AND 2

	SERIES 1			SERIES 2	
$\frac{x}{H}$	$\frac{h_H}{kg/s^3K}$	$\frac{h_C}{kg/s^3K}$	$\frac{x}{H}$	$\frac{h_H}{kg/s^3K}$	$\frac{h_C}{kg/s^3K}$
0.950	4.059	5.974	0.950	4.346	5.393
0.900	4.240	4.818	0.900	4.461	4.686
0.850	4.232	4.131	0.850	4.183	3.984
0.766	4.030	4.432	0.766	4.188	4.157
0.633	4.099	4.216	0.633	4.215	4.137
0.500	4.147	4.004	0.500	4.347	4.239
0.366	4.213	4.278	0.366	4.391	4.139
0.233	3.714	4.408	0.233	3.384	4.546
0.150	3.375	4.301	0.150	3.185	4.704
0.100	3.721	4.369	0.100	3.628	4.278
0.050	4.444	3.622	0.050	4.207	4.300

TABLE 7.2

HEAT TRANSFER COEFFICIENTS FOR SERIES 3 AND 4

	SERIES 3			SERIES 4	
$\frac{x}{H}$	$\frac{h_H}{kg/s^3K}$	$\frac{h_C}{kg/s^3K}$	$\frac{x}{H}$	$\frac{h_H}{kg/s^3K}$	$\frac{h_C}{kg/s^3K}$
0.949	4.102	5.199	0.947	3.455	4.770
0.898	4.045	4.206	0.897	3.888	3.793
0.849	4.165	3.683	0.849	3.699	3.317
0.765	4.313	3.788	0.764	3.977	3.425
0.630	4.094	4.021	0.631	3.949	3.398
0.497	4.319	3.979	0.496	3.995	3.317
0.360	4.182	4.101	0.360	3.919	3.339
0.229	3.613	4.161	0.229	3.322	3.704
0.143	3.484	4.157	0.145	3.065	3.660
0.095	3.361	4.190	0.096	3.434	3.178
0.046	4.435	4.139	0.046	3.785	3.175

TABLE 7.3

HEAT TRANSFER COEFFICIENTS FOR SERIES 5

$\frac{x}{H}$	$\frac{h_H}{kg/s^3K}$	$\frac{h_C}{kg/s^3K}$
0.931	3.643	5.222
0.784	4.463	4.147
0.634	4.309	4.049
0.482	4.071	3.840
0.283	3.460	4.272
0.180	3.147	4.035
0.118	3.665	3.023
0.058	4.263	3.730

TABLE 7.4

HEAT TRANSFER COEFFICIENTS FOR SERIES 6 AND 7

SERIES 6			SERIES 7		
$\frac{x}{H}$	$\frac{h_H}{kg/s^3K}$	$\frac{h_C}{kg/s^3K}$	$\frac{x}{H}$	$\frac{h_H}{kg/s^3K}$	$\frac{h_C}{kg/s^3K}$
0.91	4.688	4.819	0.91	5.211	4.868
0.79	4.988	4.402	0.79	5.266	4.681
0.66	5.282	4.530	0.66	5.257	5.225
0.47	4.930	4.446	0.47	5.441	4.944
0.22	4.860	4.044	0.22	4.821	4.857
0.03	5.902	3.726	0.03	6.033	2.933

TABLE 7.5

LOCAL VALUES OF Nu_x, Gr_x AND Ra_x FROM SERIES 2

	HEATED WALL			COOLED WALL		
$\frac{x}{H}$	Nu_x	Gr_x	Ra_x	Nu_x	Gr_x	Ra_x
0.950	342.89	1.603×10^{10}	1.122×10^{10}	25.32	6.349×10^{6}	4.444×10^{6}
0.900	332.95	1.463×10^{10}	1.024×10^{10}	43.86	4.695×10^{7}	3.287×10^{7}
0.850	295.07	1.298×10^{10}	9.086×10^{9}	55.98	1.545×10^{8}	1.082×10^{8}
0.766	266.24	1.013×10^{10}	7.091×10^{9}	91.33	5.826×10^{8}	4.078×10^{8}
0.633	221.40	6.602×10^{9}	4.621×10^{9}	142.30	1.943×10^{9}	1.360×10^{9}
0.500	180.25	3.683×10^{9}	2.578×10^{9}	198.29	4.160×10^{9}	2.912×10^{9}
0.366	133.46	1.608×10^{9}	1.126×10^{9}	237.93	7.491×10^{9}	5.244×10^{9}
0.233	65.45	4.764×10^{8}	3.335×10^{8}	326.83	1.024×10^{10}	7.168×10^{9}
0.150	39.59	1.396×10^{8}	9.772×10^{7}	375.83	1.240×10^{10}	8.680×10^{9}
0.100	30.06	4.317×10^{7}	3.022×10^{7}	362.27	1.329×10^{10}	9.303×10^{9}
0.050	17.43	5.761×10^{6}	4.033×10^{6}	385.86	1.462×10^{10}	1.023×10^{10}

TABLE 7.6

LOCAL VALUES OF Nu_x, Gr_x AND Ra_x FROM SERIES 3

	HEATED WALL			COOLED WALL		
$\frac{x}{H}$	Nu_x	Gr_x	Ra_x	Nu_x	Gr_x	Ra_x
0.949	323.15	1.594×10^{10}	1.116×10^{10}	24.84	6.569×10^{6}	4.598×10^{6}
0.898	301.64	1.440×10^{10}	1.008×10^{10}	40.12	4.914×10^{7}	3.440×10^{7}
0.849	293.72	1.261×10^{10}	8.827×10^{9}	52.08	1.587×10^{8}	1.111×10^{8}
0.765	273.95	9.923×10^{9}	6.946×10^{9}	83.67	6.008×10^{8}	4.206×10^{8}
0.630	214.18	6.290×10^{9}	4.403×10^{9}	139.66	2.046×10^{9}	1.432×10^{9}
0.497	178.09	3.576×10^{9}	2.503×10^{9}	187.65	4.405×10^{9}	3.084×10^{9}
0.360	125.16	1.515×10^{9}	1.061×10^{9}	246.34	7.833×10^{9}	5.483×10^{9}
0.229	68.82	4.459×10^{8}	3.121×10^{8}	301.29	1.089×10^{10}	7.623×10^{9}
0.143	41.44	1.190×10^{8}	8.330×10^{7}	335.49	1.324×10^{10}	9.268×10^{9}
0.096	26.55	3.620×10^{7}	2.534×10^{7}	357.70	1.446×10^{10}	1.012×10^{10}
0.046	16.99	4.237×10^{6}	2.966×10^{6}	373.26	1.604×10^{10}	1.123×10^{10}

TABLE 7.7

LOCAL VALUES OF Nu_x, Gr_x AND Ra_x FROM SERIES 4

	HEATED WALL			COOLED WALL		
$\frac{x}{H}$	Nu_x	Gr_x	Ra_x	Nu_x	Gr_x	Ra_x
0.947	287.10	1.392×10^{10}	9.744×10^{9}	23.64	4.957×10^{6}	3.470×10^{6}
0.897	308.38	1.233×10^{10}	8.631×10^{9}	36.52	3.638×10^{7}	2.547×10^{7}
0.849	269.04	1.081×10^{10}	7.567×10^{9}	46.81	1.100×10^{8}	7.700×10^{7}
0.764	260.23	8.801×10^{9}	6.161×10^{9}	75.72	4.218×10^{8}	2.953×10^{8}
0.631	213.43	5.496×10^{9}	3.847×10^{9}	117.36	1.395×10^{9}	9.765×10^{8}
0.496	169.75	2.954×10^{9}	2.068×10^{9}	155.78	2.745×10^{9}	1.922×10^{9}
0.360	120.95	1.273×10^{9}	8.911×10^{8}	199.44	4.551×10^{9}	3.186×10^{9}
0.229	65.18	3.331×10^{8}	2.332×10^{8}	267.08	6.780×10^{9}	4.746×10^{9}
0.145	38.11	1.015×10^{8}	7.105×10^{7}	293.40	8.367×10^{9}	5.857×10^{9}
0.095	28.25	3.042×10^{7}	2.129×10^{7}	269.38	8.979×10^{9}	6.285×10^{9}
0.046	14.93	3.427×10^{6}	2.399×10^{6}	284.57	1.010×10^{10}	7.070×10^{9}

TABLE 7.8

LOCAL VALUES OF Nu_x, Gr_x AND Ra_x FROM SERIES 5

	HEATED WALL			COOLED WALL		
$\frac{x}{H}$	Nu_x	Gr_x	Ra_x	Nu_x	Gr_x	Ra_x
0.931	225.33	8.321×10^{9}	5.825×10^{9}	26.93	7.872×10^{6}	5.510×10^{6}
0.784	232.28	5.523×10^{9}	3.866×10^{9}	66.90	2.238×10^{8}	1.567×10^{8}
0.634	180.51	3.407×10^{9}	2.385×10^{9}	111.07	1.013×10^{9}	7.091×10^{8}
0.482	126.91	1.746×10^{9}	1.222×10^{9}	149.32	2.449×10^{9}	1.714×10^{9}
0.283	64.44	4.267×10^{8}	2.987×10^{8}	230.19	4.621×10^{9}	3.235×10^{9}
0.180	37.64	1.208×10^{8}	8.456×10^{7}	247.91	5.957×10^{9}	4.170×10^{9}
0.118	28.76	3.489×10^{7}	2.442×10^{7}	200.72	6.756×10^{9}	4.729×10^{9}
0.058	16.46	4.173×10^{6}	2.921×10^{6}	263.94	7.533×10^{9}	5.273×10^{9}

TABLE 7.9

LOCAL VALUES OF Nu_x, Gr_x AND Ra_x FROM SERIES 6

	HEATED WALL			COOLED WALL		
$\frac{x}{H}$	Nu_x	Gr_x	Ra_x	Nu_x	Gr_x	Ra_x
0.91	300.92	1.106×10^{10}	7.742×10^{9}	34.77	2.306×10^{7}	1.614×10^{7}
0.79	278.46	8.420×10^{9}	5.894×10^{9}	74.02	2.536×10^{8}	1.775×10^{8}
0.66	246.42	5.401×10^{9}	3.781×10^{9}	123.72	1.029×10^{9}	7.203×10^{8}
0.47	164.72	2.286×10^{9}	1.600×10^{9}	189.42	3.351×10^{9}	2.346×10^{9}
0.22	76.21	2.796×10^{8}	1.957×10^{8}	253.45	7.698×10^{9}	5.389×10^{9}
0.03	12.59	7.867×10^{5}	5.507×10^{5}	291.38	1.023×10^{10}	7.161×10^{9}

TABLE 7.10

LOCAL VALUES OF Nu_x, Gr_x AND Ra_x FROM SERIES 7

	HEATED WALL			COOLED WALL		
$\frac{x}{H}$	Nu_x	Gr_x	Ra_x	Nu_x	Gr_x	Ra_x
0.91	316.45	1.270×10^{10}	8.890×10^{9}	34.64	2.741×10^{7}	1.919×10^{7}
0.79	278.07	9.562×10^{9}	6.693×10^{9}	77.67	3.146×10^{8}	2.202×10^{8}
0.66	232.50	6.013×10^{9}	4.209×10^{9}	140.72	1.253×10^{9}	8.771×10^{8}
0.47	170.91	2.489×10^{9}	1.742×10^{9}	208.20	4.209×10^{9}	2.946×10^{9}
0.22	70.92	3.174×10^{8}	2.222×10^{8}	301.05	8.496×10^{9}	5.947×10^{9}
0.03	12.21	9.319×10^{5}	6.523×10^{5}	227.32	1.003×10^{10}	7.021×10^{9}

TABLE 7.11

OVERALL HEAT TRANSFER SERIES 1-7

SERIES	HEATED WALL	COOLED WALL	$\Delta Q'_{\omega}$	LOSS
1	266.2W/m	166.6W/m	99.6W/m	37.4%
2	263.0W/m	203.0W/m	60.0W/m	22.8%
3	269.5W/m	197.1W/m	72.4W/m	26.9%
4	178.3W/m	111.6W/m	66.7W/m	37.4%
5	210.7W/m	158.9W/m	51.8W/m	24.6%
6	269.7W/m	151.6W/m	118.1W/m	43.8%
7	412.6W/m	214.5W/m	198.1W/m	48.0%

TABLE 7.12

EXAMPLES OF THE AGREEMENT BETWEEN PREDICTED AND EXPERIMENTAL VELOCITIES

SERIES 3 x/H = 0.765			SERIES 4 x/H = 0.496			SERIES 6 x/H = 0.50		
$\frac{y}{mm}$	$\frac{u_P}{m/s}$	$\frac{u_E}{m/s}$	$\frac{y}{mm}$	$\frac{u_P}{m/s}$	$\frac{u_E}{m/s}$	$\frac{y}{mm}$	$\frac{u_P}{m/s}$	$\frac{u_E}{m/s}$
0.392	0.042	0.045	1.768	-0.119	-0.118	1.52	0.173	0.176
0.607	0.063	0.063	2.749	-0.160	-0.163	1.72	0.189	0.188
0.850	0.086	0.084	3.733	-0.187	-0.187	1.92	0.205	0.202
1.089	0.106	0.105				2.12	0.219	0.219
1.305	0.124	0.123				2.32	0.232	0.232
1.538	0.142	0.142				2.72	0.255	0.259
2.655	0.211	0.215						
3.363	0.243	0.241						

TABLE 7.13

WALL SHEAR STRESS DATA FOR SERIES 3

	HEATED WALL			COOLED WALL		
$\frac{x}{H}$	$\frac{\tau_w \times 10^3}{N/m^2}$	$\frac{\tau_w/\rho_w \times 10^3}{N.m/kg}$	$\frac{y_{COR}}{mm}$	$\frac{\tau_w \times 10^3}{N/m^2}$	$\frac{\tau_w/\rho_w \times 10^3}{N.m/kg}$	$\frac{y_{COR}}{mm}$
0.046	2.72	2.69	-0.34	1.08	0.92	-0.95
0.095	3.26	3.22	-0.23	1.13	0.98	-1.04
0.143	3.51	3.47	-0.38	1.32	1.13	-1.29
0.229	3.36	3.33	-0.10	1.57	1.35	-1.42
0.360	2.92	2.90	-0.49	2.02	1.75	-1.18
0.497	2.79	2.77	-0.53	2.32	2.00	-1.42
0.497PB	2.76	2.75	-0.55	2.34	2.02	-1.26
0.630	2.59	2.59	-0.67	2.50	2.17	-1.46
0.765	2.31	2.32	-0.26	2.67	2.33	-1.38
0.849	2.19	2.19	-0.77	2.73	2.39	-1.33
0.898	2.14	2.13	-0.93	2.51	2.18	-0.85
0.898R	2.14	2.12	-0.29	2.57	2.22	-0.96
0.949	1.89	1.87	-0.71	2.30	1.99	-0.42

PB - Run without probe block R - Repeat

TABLE 7.14

WALL SHEAR STRESS DATA FOR SERIES 4

	HEATED WALL			COOLED WALL		
$\frac{x}{H}$	$\frac{\tau_w \times 10^3}{N/m^2}$	$\frac{\tau_w/\rho_w \times 10^3}{N.m/kg}$	$\frac{y_{COR}}{mm}$	$\frac{\tau_w \times 10^3}{N/m^2}$	$\frac{\tau_w/\rho_w \times 10^3}{N.m/kg}$	$\frac{y_{COR}}{mm}$
0.046	2.20	2.12	-0.37	0.78	0.68	-1.09
0.096	2.53	2.43	-0.16	0.80	0.70	-1.12
0.145	2.69	2.61	-0.28	0.92	0.80	-1.60
0.229	2.75	2.65	-0.30	1.05	0.92	-1.37
0.360	2.38	2.31	-0.55	1.35	1.19	-1.09
0.496	2.22	2.14	-0.50	1.64	1.43	-1.29
0.631	2.06	1.99	-0.47	1.87	1.63	-1.26
0.764	1.88	1.80	-0.66	2.00	1.73	-1.11
0.849	1.72	1.66	-0.45	2.04	1.79	-1.07
0.897	1.66	1.58	-0.58	1.99	1.72	-1.17
0.947	1.64	1.57	-0.85	1.69	1.47	-0.45

TABLE 7.15

WALL SHEAR STRESS DATA FOR SERIES 5

	HEATED WALL			COOLED WALL		
$\frac{x}{H}$	$\frac{\tau_w \times 10^3}{N/m^2}$	$\frac{\tau_w/\rho_w \times 10^3}{N.m/kg}$	$\frac{y_{COR}}{mm}$	$\frac{\tau_w \times 10^3}{N/m^2}$	$\frac{\tau_w/\rho_w \times 10^3}{N.m/kg}$	$\frac{y_{COR}}{mm}$
0.058	2.71	2.68	-0.21	1.08	0.93	-1.61
0.118	3.21	3.21	-0.40	1.19	1.03	-1.51
0.180	3.53	3.50	-0.27	1.30	1.12	-1.15
0.283	3.45	3.44	-0.45	1.61	1.40	-1.29
0.482	2.74	2.71	-1.12	2.24	1.93	-0.47
0.634	2.41	2.38	-0.47	2.38	2.04	-1.78
0.784	2.10	2.07	-0.35	2.46	2.12	-0.82
0.931	1.74	1.72	-0.29	2.16	1.86	-0.56

TABLE 7.16

WALL SHEAR STRESS DATA FOR SERIES 6

	HEATED WALL			COOLED WALL		
$\frac{x}{H}$	$\frac{\tau_w \times 10^3}{N/m^2}$	$\frac{\tau_w/\rho_w \times 10^3}{N.m/kg}$	$\frac{y_{COR}}{mm}$	$\frac{\tau_w \times 10^3}{N/m^2}$	$\frac{\tau_w/\rho_w \times 10^3}{N.m/kg}$	$\frac{y_{COR}}{mm}$
0.12	3.03	2.78	-0.40	1.34	1.07	+0.35
0.25	3.11	2.84	-0.17	1.73	1.38	+0.37
0.50	2.80	2.57	-0.28	2.34	1.87	-0.11
0.65	2.74	2.53	-0.66	2.57	2.06	+0.13
0.80	2.34	2.17	+0.21	2.72	2.19	-0.21
0.95	2.03	1.88	+0.68	2.54	2.04	-0.12

TABLE 7.17

WALL SHEAR STRESS DATA FOR SERIES 7

	HEATED WALL			COOLED WALL		
$\frac{x}{H}$	$\frac{\tau_w \times 10^3}{N/m^2}$	$\frac{\tau_w/\rho_w \times 10^3}{N.m/kg}$	$\frac{y_{COR}}{mm}$	$\frac{\tau_w \times 10^3}{N/m^2}$	$\frac{\tau_w/\rho_w \times 10^3}{N.m/kg}$	$\frac{y_{COR}}{mm}$
0.12	3.97	3.89	+0.08	1.44	1.16	+0.18
0.25	4.03	3.98	-0.43	1.89	1.53	+0.27
0.50	3.59	3.55	-0.56	2.79	2.26	+0.43
0.65	3.30	3.24	+0.38	3.05	2.48	-0.13
0.80	2.95	2.95	+0.51	3.27	2.67	+0.43
0.95	2.63	2.60	+0.63	3.13	2.55	+0.04

TABLE 7.18

GROUPS FOR PROBABILITY DISTRIBUTION OF VELOCITY

GROUP	VELOCITY RANGE
1	-0.200m/s < u < -0.175m/s
2	-0.175m/s < u < -0.150m/s
3	-0.150m/s < u < -0.125m/s
4	-0.125m/s < u < -0.100m/s
5	-0.100m/s < u < -0.075m/s
6	-0.075m/s < u < -0.050m/s
7	-0.050m/s < u < -0.025m/s
8	-0.025m/s < u < 0.000m/s
9	0.000m/s < u < 0.025m/s
10	0.025m/s < u < 0.050m/s
11	0.050m/s < u < 0.075m/s
12	0.075m/s < u < 0.100m/s
13	0.100m/s < u < 0.125m/s
14	0.125m/s < u < 0.150m/s
15	0.150m/s < u < 0.175m/s
16	0.175m/s < u < 0.200m/s
17	0.200m/s < u < 0.225m/s
18	0.225m/s < u < 0.250m/s
19	0.250m/s < u < 0.275m/s
20	0.275m/s < u < 0.300m/s
21	0.300m/s < u < 0.325m/s
22	0.325m/s < u < 0.350m/s
23	0.350m/s < u < 0.375m/s
24	0.375m/s < u < 0.400m/s
25	0.400m/s < u < 0.425m/s
26	0.425m/s < u < 0.450m/s
27	0.450m/s < u < 0.475m/s
28	0.475m/s < u < 0.500m/s
29	0.500m/s < u < 0.525m/s
30	0.525m/s < u < 0.550m/s
31	0.550m/s < u < 0.575m/s
32	0.575m/s < u < 0.600m/s
33	0.600m/s < u < 0.625m/s
34	0.625m/s < u < 0.650m/s
35	0.650m/s < u < 0.675m/s
36	0.675m/s < u < 0.700m/s

TABLE 7.19

MASS FLOW FOR SERIES 1

$\frac{x}{H}$	$\dot{m}'_U \times 10^3$ kg/m.s	$\dot{m}'_D \times 10^3$ kg/m.s
0.950	17.4	15.2
0.900	17.7	14.5
0.850	17.3	13.9
0.766	19.0	12.6
0.633	20.7	15.5
0.500	18.3	15.3
0.366	14.8	13.3
0.233	9.3	8.7
0.150	6.2	5.3
0.100	4.5	4.7
0.050	3.5	4.6

TABLE 7.20

MASS FLOW FOR SERIES 3

$\frac{x}{H}$	$\dot{m}'_U \times 10^3$ kg/m.s	$\dot{m}'_D \times 10^3$ kg/m.s
0.949	14.82	12.90
0.898	12.90	9.38
0.849	12.09	8.67
0.765	13.51	8.47
0.630	15.62	11.79
0.497	14.92	13.01
0.360	9.68	9.57
0.229	5.04	4.84
0.143	3.43	3.53
0.096	2.72	2.12
0.046	2.42	2.21

TABLE 7.21

MASS FLOW FOR SERIES 4

$\frac{x}{H}$	$\dot{m}'_{U} \times 10^{3}$ kg/m.s	$\dot{m}'_{D} \times 10^{3}$ kg/m.s
0.947	13.806	12.129
0.897	11.291	9.677
0.849	11.355	8.516
0.764	12.904	7.484
0.631	13.806	10.452
0.496	12.710	10.838
0.360	7.807	7.549
0.229	4.323	4.194
0.145	2.516	2.645
0.096	2.194	2.000
0.046	1.935	2.458

TABLE 7.22

MEASURED v FOR SERIES 7, x/H = 0.50

$\frac{y}{mm}$	$\frac{v}{m/s}$	$\frac{v'_{r.m.s.}}{m/s}$
30	0.004	0.050
50	0.000	0.038
70	-0.002	0.035
90	0.004	0.030
110	0.004	0.034
130	0.003	0.039
150	0.006	0.041
170	0.007	0.033

TABLE 7.23

MEASURED v FOR SERIES 7, x/H = 0.65

y mm	v m/s	v'_{RMS} m/s
30	0.006	0.045
50	0.007	0.054
70	0.005	0.049
90	0.009	0.041
110	0.017	0.037
130	0.011	0.033
150	0.012	0.033
170	0.009	0.040

TABLE 7.24

MEASURED v FOR SERIES 7, x/H = 0.80

y mm	v m/s	v'_{RMS} m/s
30	0.010	0.057
45	0.011	0.054
60	0.014	0.056
80	0.012	0.054
100	0.014	0.043
120	0.010	0.033
140	0.014	0.034
155	0.013	0.031
170	0.014	0.036

TABLE 7.25

THE TURBULENCE QUANTITY $\overline{u'T'}$ AND G, THE PRODUCTION OF TURBULENCE KINETIC ENERGY BY BUOYANCY FOR x/H = 0.046

y mm	$\overline{u'T'} \times 10^3$ m.K/s	$-g\overline{u'\rho'} \times 10^3$ kg/[m.s^{-3}]
1.869	4.412	0.151
3.187	17.430	0.865
4.218	26.679	1.417
5.218	32.491	1.736
6.222	36.461	2.252
7.240	32.207	2.220
8.200	34.185	1.730
9.224	27.097	1.297
10.218	21.534	1.012
12.692	9.673	0.467
15.206	5.400	0.243
17.692	2.940	0.165
20.176	2.086	0.127
30.2	0.793	0.026
40.2	0.211	0.007
50.2	-0.356	-0.016
60.2	-0.350	-0.029
70.2	-0.247	-0.016
100.2	-0.313	-0.027
150.2	-0.164	-0.029
200.2	-0.152	-0.024
250.2	-0.096	-0.008
251.3	-0.180	0.000
301.3	-0.010	0.000
351.3	0.083	0.008
401.3	-0.111	-0.001
431.3	-1.414	-0.082
441.3	-1.651	-0.071
451.3	-1.132	-0.102
461.3	0.895	0.109
471.3	2.720	0.268
481.276	9.861	0.700
483.788	11.670	0.687
486.276	14.275	0.936
487.280	14.444	0.982
489.800	19.073	1.211
490.800	17.223	1.267
491.800	18.460	1.290
492.804	16.979	1.148
493.804	14.934	1.189
494.806	11.747	1.004
495.796	7.996	0.714
496.795	3.598	0.414

TABLE 7.26

THE TURBULENCE QUANTITY $\overline{u'T'}$ AND G, THE PRODUCTION OF TURBULENCE KINETIC ENERGY BY BUOYANCY FOR x/H = 0.096

y mm	$\overline{u'T'} \times 10^3$ m.K/s	$-g\overline{u'\rho'} \times 10^3$ kg/[m.s^3]
3.169	18.399	0.566
4.235	37.233	1.176
5.245	46.011	1.486
6.235	50.129	1.644
7.237	56.263	1.877
8.235	51.704	1.744
9.235	47.478	1.616
10.241	36.569	1.254
12.745	21.891	0.758
15.241	7.710	0.269
17.747	2.129	0.074
20.243	0.837	0.029
30.2	-0.233	-0.008
40.2	-0.120	-0.004
50.2	-0.077	-0.003
60.2	-0.075	-0.003
70.2	-0.073	-0.003
100.2	-0.056	-0.002
150.2	-0.037	-0.001
200.2	-0.033	-0.001
250.2	-0.058	-0.002
249.8	0.051	0.002
299.8	0.031	0.001
349.8	0.686	0.024
399.8	-0.482	-0.017
429.8	-4.453	-0.156
439.8	-7.131	-0.250
449.8	-5.798	-0.203
459.8	-3.005	-0.105
469.8	4.157	0.148
479.844	16.516	0.585
482.344	18.872	0.669
484.844	26.490	0.939
487.354	31.953	1.134
489.866	37.555	1.336
490.856	40.110	1.429
491.848	41.094	1.465
492.862	40.122	1.434
493.866	33.178	1.189
494.870	31.990	1.149
495.856	22.381	0.809
496.953	15.202	0.553

TABLE 7.27

THE TURBULENCE QUANTITY $\overline{u'T'}$ AND G, THE PRODUCTION OF TURBULENCE KINETIC ENERGY BY BUOYANCY FOR x/H = 0.143

y mm	$\overline{u'T'} \times 10^3$ m.K/s	$-g\overline{u'\rho'} \times 10^3$ kg/[m.s^3]
1.260	2.305	0.067
1.449	1.175	0.035
1.658	2.308	0.069
3.035	21.788	0.669
3.988	38.063	1.189
4.978	54.905	1.744
5.994	69.210	2.237
7.030	87.340	2.868
8.034	83.899	2.787
9.050	78.447	2.627
10.050	69.949	2.358
12.540	44.116	1.506
15.040	19.241	0.663
17.544	13.550	0.468
20.044	5.173	0.179
30.0	0.321	0.011
40.0	-0.064	-0.002
50.0	-0.062	-0.002
60.0	-0.060	-0.002
70.0	-0.032	-0.001
100.0	-0.028	-0.001
150.0	-0.018	-0.001
200.0	-0.031	-0.001
250.0	-0.023	-0.001
249.6	0.046	0.002
299.6	-0.005	0.000
349.6	1.237	0.043
399.6	-0.648	-0.022
429.6	-10.647	-0.369
439.6	-9.633	-0.334
449.6	-7.183	-0.248
459.6	-1.762	-0.060
469.6	4.859	0.171
479.589	20.974	0.734
482.095	28.334	0.993
484.591	30.382	1.065
487.089	42.021	1.475
489.569	49.274	1.734
490.569	47.400	1.670
491.573	47.501	1.676
492.577	47.649	1.685
493.575	45.258	1.603
494.583	42.298	1.504
495.585	29.894	1.068
496.601	21.950	0.788
497.945	9.452	0.345

TABLE 7.28

THE TURBULENCE QUANTITY $\overline{u'T'}$ AND G, THE PRODUCTION OF TURBULENCE KINETIC ENERGY BY BUOYANCY FOR x/H = 0.229

$\frac{y}{mm}$	$\frac{\overline{u'T'} \times 10^3}{m.K/s}$	$\frac{-g\overline{u'\rho'} \times 10^3}{kg/[m.s^3]}$
3.035	59.881	1.859
4.045	103.694	3.261
5.077	167.324	5.332
6.055	210.197	6.770
7.037	215.000	6.974
8.057	212.944	6.949
9.037	188.563	6.191
10.061	180.159	5.939
12.567	126.970	4.229
15.071	101.182	3.395
17.573	86.197	2.907
20.071	82.557	2.793
30.1	25.666	0.875
40.1	8.379	0.286
50.1	1.050	0.036
60.1	0.088	0.003
70.1	0.285	0.010
100.1	-0.026	-0.001
150.1	0.014	0.000
200.1	-0.009	0.000
250.1	0.210	0.007
249.6	-0.547	-0.019
299.6	0.485	0.017
349.6	5.334	0.183
399.6	-7.808	-0.266
429.6	-13.218	-0.450
439.6	-13.962	-0.475
449.6	-4.698	-0.159
459.6	3.227	0.111
469.6	15.431	0.529
479.579	37.135	1.277
482.093	43.461	1.495
484.597	52.034	1.792
487.111	60.120	2.074
489.611	70.981	2.457
490.617	65.121	2.258
491.623	61.770	2.145
492.621	58.356	2.031
493.615	61.040	2.131
494.619	44.894	1.574
495.617	34.812	1.227
496.324	28.370	1.004

TABLE 7.29

THE TURBULENCE QUANTITY $\overline{u'T'}$ AND G, THE PRODUCTION OF TURBULENCE KINETIC ENERGY BY BUOYANCY FOR x/H = 0.360

y mm	$\overline{u'T'} \times 10^3$ m.K/s	$-g\overline{u'\rho'} \times 10^3$ kg/[m.s^3]
1.599	14.468	0.431
3.037	71.295	2.186
4.039	116.098	3.605
5.037	153.850	4.826
6.039	166.272	5.250
7.039	177.438	5.637
8.037	183.266	5.846
9.053	186.534	5.975
10.059	178.471	5.735
12.571	158.953	5.140
15.055	136.132	4.425
17.573	118.154	3.854
20.093	111.633	3.651
30.1	74.970	2.474
40.1	41.086	1.363
50.1	21.559	0.718
60.1	9.904	0.330
70.1	4.277	0.143
100.1	0.571	0.019
150.1	0.362	0.012
200.1	0.391	0.013
250.1	1.280	0.043
249.6	-0.823	-0.028
299.6	3.514	0.118
349.6	0.982	0.033
399.6	-12.833	-0.428
429.6	-6.580	-0.219
439.6	-0.445	-0.014
449.6	13.680	0.458
459.6	25.045	0.839
469.6	39.838	1.337
479.6	62.029	2.092
482.104	73.804	2.494
484.604	82.969	2.809
487.116	84.692	2.874
489.624	95.353	3.246
490.630	97.719	3.337
491.634	93.413	3.197
492.644	89.625	3.076
493.634	78.360	2.698
494.648	70.235	2.428
495.636	52.100	1.808
496.666	33.292	1.167

TABLE 7.30

THE TURBULENCE QUANTITY $\overline{u'T'}$ AND G, THE PRODUCTION OF TURBULENCE KINETIC ENERGY BY BUOYANCY FOR x/H = 0.497

y mm	$\overline{u'T'}\times10^{3}$ m.K/s	$-g\overline{u'\rho'}\times10^{3}$ kg/[m.s^{3}]
1.230	5.785	0.169
1.411	9.405	0.276
1.593	11.172	0.330
3.141	53.668	1.634
4.157	93.762	2.883
5.167	115.657	3.587
6.147	135.832	4.236
7.155	151.401	4.744
8.147	147.229	4.635
9.143	156.363	4.944
10.151	154.773	4.902
12.661	142.188	4.527
15.167	131.565	4.205
17.687	114.570	3.675
20.187	100.237	3.223
30.2	76.021	2.466
40.2	53.678	1.748
50.2	32.436	1.060
60.2	19.556	0.640
70.2	9.520	0.312
100.2	-0.061	-0.002
150.2	0.802	0.026
200.2	0.644	0.021
250.2	1.021	0.036
249.8	-0.238	-0.008
299.8	-0.070	-0.002
349.8	0.697	0.023
399.8	-9.502	-0.311
429.8	-0.363	-0.011
439.8	8.915	0.293
449.8	20.592	0.678
459.8	34.774	1.146
469.8	52.513	1.737
479.792	73.061	2.428
482.302	84.766	2.823
484.796	92.975	3.105
487.302	102.030	3.418
489.808	109.653	3.691
490.804	102.889	3.471
491.808	111.727	3.777
492.808	98.199	3.330
493.814	96.901	3.298
494.808	78.535	2.685
495.798	54.057	1.860
496.708	32.404	1.125

TABLE 7.31

THE TURBULENCE QUANTITY $\overline{u'T'}$ AND G, THE PRODUCTION OF TURBULENCE KINETIC ENERGY BY BUOYANCY FOR x/H = 0.630

y mm	$\overline{u'T'} \times 10^3$ m.K/s	$-g\overline{u'\rho'} \times 10^3$ kg/[m.s^3]
1.236	4.252	0.123
1.433	6.464	0.189
2.823	31.152	0.939
3.819	53.751	1.640
4.831	94.792	2.914
5.851	109.636	3.386
6.831	131.346	4.080
7.831	139.475	4.347
8.871	143.187	4.477
9.815	150.365	4.711
12.321	136.522	4.300
14.805	122.031	3.861
17.307	119.288	3.783
19.811	104.248	3.316
29.8	71.871	2.302
39.8	47.021	1.512
49.8	35.940	1.159
59.8	20.957	0.677
69.8	11.264	0.364
99.9	-3.238	-0.105
149.8	-0.341	-0.011
199.8	1.784	0.058
249.8	1.615	0.052
249.4	-1.207	-0.039
299.4	-0.290	-0.009
349.4	-0.597	-0.019
399.4	-3.475	-0.112
429.4	-0.179	-0.005
439.4	6.512	0.211
449.4	19.407	0.629
459.4	33.418	1.085
469.4	51.385	1.673
479.425	86.740	2.844
481.945	96.831	3.182
484.455	101.107	3.331
486.947	119.438	3.946
489.447	137.470	4.565
490.477	141.418	4.711
491.469	139.096	4.645
492.453	134.870	4.522
493.487	122.827	4.136
494.471	109.512	3.705
495.469	85.488	2.911
496.822	36.141	1.250

TABLE 7.32

THE TURBULENCE QUANTITY $\overline{u'T'}$ AND G, THE PRODUCTION OF TURBULENCE KINETIC ENERGY BY BUOYANCY FOR x/H = 0.765

y mm	$\overline{u'T'} \times 10^3$ m.K/s	$-g\overline{u'\rho'} \times 10^3$ kg/[m.s^3]
0.652	1.961	0.056
0.867	3.190	0.092
1.110	4.839	0.140
1.349	5.555	0.162
1.565	11.544	0.337
1.798	15.223	0.447
2.925	40.166	1.202
3.623	59.399	1.791
5.007	102.380	3.120
6.027	115.712	3.543
7.027	120.065	3.693
8.027	117.588	3.628
9.027	124.288	3.846
10.027	119.439	3.699
12.527	129.292	4.030
15.033	116.402	3.637
17.527	112.699	3.531
20.049	101.991	3.201
30.0	63.318	2.000
40.0	48.481	1.538
50.0	31.462	1.000
60.0	16.110	0.513
70.0	8.855	0.282
100.0	-4.668	-0.150
150.0	-1.735	-0.556
200.0	1.567	0.050
250.0	1.653	0.053
249.2	-0.649	-0.021
299.2	-0.874	-0.028
349.2	-2.138	-0.068
399.2	-7.880	-0.249
429.2	-10.860	-0.343
439.2	-5.615	-0.177
449.2	3.692	0.118
459.2	26.562	0.848
469.2	53.622	1.716
479.176	98.317	3.164
481.674	104.745	3.381
484.164	133.794	4.332
486.684	140.186	4.557
489.170	167.506	5.474
490.206	182.278	5.980
491.206	194.745	6.408
492.206	184.179	6.088
493.206	174.567	5.789
494.210	183.132	6.113
495.202	147.066	4.951
496.180	97.572	3.319

TABLE 7.33

THE TURBULENCE QUANTITY $\overline{u'T'}$ AND G, THE PRODUCTION OF TURBULENCE KINETIC ENERGY BY BUOYANCY FOR x/H = 0.849

y mm	$\overline{u'T'} \times 10^3$ m.K/s	$-g\overline{u'\rho'} \times 10^3$ kg/[m.s^3]
1.141	3.193	0.092
1.336	4.036	0.117
2.603	20.074	0.597
3.440	38.667	1.161
4.440	55.872	1.688
5.460	80.852	2.457
6.502	94.811	2.893
7.524	104.088	3.186
8.564	109.555	3.361
9.602	108.241	3.327
12.118	99.025	3.059
14.652	103.976	3.220
17.170	95.024	2.950
19.690	86.515	2.691
29.7	56.459	1.767
39.7	45.754	1.435
49.7	26.170	0.823
59.7	16.835	0.531
69.7	7.031	0.221
99.7	-1.460	-0.047
149.7	-0.646	-0.021
199.7	1.128	0.036
249.7	2.767	0.088
250.4	-0.745	-0.023
300.4	-2.062	-0.065
350.4	-5.503	-0.173
400.4	-9.357	-0.293
430.4	-1.950	-0.060
440.4	6.167	0.195
450.4	12.353	0.391
460.4	21.283	0.672
470.4	46.517	1.472
480.372	99.733	3.170
482.872	105.058	3.346
485.372	118.760	3.794
487.872	144.183	4.623
490.372	173.483	5.608
491.380	167.512	5.429
492.386	177.063	5.773
493.398	148.392	4.867
494.388	121.385	4.018
495.388	90.242	3.016
496.390	59.411	2.014
497.370	22.200	0.766

TABLE 7.34

THE TURBULENCE QUANTITY $\overline{u'T'}$ AND G, THE PRODUCTION OF TURBULENCE KINETIC ENERGY BY BUOYANCY FOR x/H = 0.898

y mm	$\overline{u'T'} \times 10^3$ m.K/s	$-g\overline{u'\rho'} \times 10^3$ kg/[m.s^3]
1.683	5.722	0.167
2.781	18.649	0.554
3.502	32.561	0.976
4.530	66.306	2.000
5.580	83.300	2.526
6.570	91.144	2.773
7.580	102.911	3.141
8.558	103.511	3.168
9.596	101.922	3.124
12.108	106.414	3.274
14.610	106.758	3.293
17.116	94.083	2.907
19.620	-79.779	2.470
29.6	58.584	1.823
39.6	36.113	1.128
49.6	25.485	0.798
59.6	19.914	0.623
69.6	7.066	0.221
99.6	-0.864	-0.028
149.6	1.157	0.036
199.6	1.363	0.043
249.6	2.758	0.087
249.9	-0.573	-0.018
299.9	0.238	0.007
349.9	-1.464	-0.046
399.9	-0.878	-0.027
429.9	8.635	0.271
439.9	15.574	0.489
449.9	26.069	0.819
459.9	34.607	1.089
469.9	44.953	1.414
479.906	65.926	2.082
482.444	70.635	2.233
484.962	88.262	2.800
487.464	100.944	3.215
489.958	128.869	4.127
490.942	141.896	4.563
491.980	159.951	5.168
492.974	144.327	4.679
493.982	145.147	4.750
494.992	120.943	4.000
495.980	86.967	2.911
496.959	52.094	1.777

TABLE 7.35

THE TURBULENCE QUANTITY $\overline{u'T'}$ AND G, THE PRODUCTION OF TURBULENCE KINETIC ENERGY BY BUOYANCY FOR x/H = 0.949

y mm	$\overline{u'T'} \times 10^3$ m.K/s	$-g\overline{u'\rho'} \times 10^3$ kg/[m.s^3]
0.750	0.255	0.007
0.937	-0.485	-0.014
1.141	3.027	0.087
1.671	5.152	0.150
2.659	16.678	0.493
3.628	32.778	0.978
4.614	41.282	1.239
5.652	76.143	2.295
6.654	78.901	2.389
7.674	88.772	2.694
8.676	103.376	3.144
9.674	97.726	2.976
12.194	101.633	3.107
14.710	100.985	3.098
17.214	83.580	2.570
19.742	74.623	2.298
29.7	50.586	1.565
39.7	40.034	1.242
49.7	24.833	0.773
59.7	18.065	0.563
69.7	11.805	0.368
99.7	-1.446	-0.046
149.7	-0.789	-0.025
199.7	2.666	0.084
249.7	0.820	0.026
250.3	0.343	0.011
300.3	-2.667	-0.083
350.3	-3.902	-0.121
400.3	-2.419	-0.075
430.3	7.291	0.228
440.3	14.856	0.465
450.3	12.749	0.399
460.3	23.615	0.742
470.3	25.854	0.812
480.344	42.643	1.348
482.848	43.543	1.378
485.350	46.953	1.489
487.850	58.073	1.849
490.370	80.736	2.581
491.400	104.258	3.345
492.384	106.511	3.429
493.380	114.540	3.700
494.400	124.439	4.044
495.420	122.203	4.018
496.402	91.536	3.048

TABLE 7.36

THE TURBULENCE QUANTITY $\overline{v'T'}$

FOR x/H = 0.046

THE HEATED WALL

y mm	$\overline{v'T'} \times 10^3$ m.K/s
1	-1.16
2	3.27
3	3.96
4	-6.52
5	17.21
6	21.23
7	31.33
8	39.12
9	40.42
10	50.05
20	32.80
30	32.20
40	30.69
50	29.68
60	29.17
70	29.04
100	29.24
150	30.21
200	31.49
250	33.07

THE COOLED WALL

y mm	$\overline{v'T'} \times 10^3$ m.K/s
1	-0.07
2	4.35
3	6.90
4	11.90
5	13.94
6	15.33
7	19.33
8	22.00
9	22.89
10	23.55
20	22.40
30	18.50
40	16.25
50	15.37
60	15.27
70	14.82
100	15.61
150	18.48
200	20.36
250	21.62

TABLE 7.37

THE TURBULENCE QUANTITY $\overline{v'T'}$

FOR x/H = 0.096

THE HEATED WALL

y mm	$\overline{v'T'} \times 10^3$ m.K/s
1	-0.43
2	7.94
3	13.48
4	10.16
5	20.01
6	13.07
7	3.37
8	19.22
9	21.37
10	20.63
20	13.91
30	13.24
40	13.06
50	12.99
60	12.99
70	12.99
100	12.99
150	12.99
200	12.99
250	12.99

THE COOLED WALL

y mm	$\overline{v'T'} \times 10^3$ m.K/s
1	-0.14
2	3.01
3	7.92
4	10.31
5	16.01
6	17.27
7	18.48
8	20.77
9	22.00
10	22.12
20	17.13
30	11.70
40	7.15
50	4.34
60	3.41
70	3.83
100	8.51
150	16.66
200	20.60
250	23.32

TABLE 7.38

THE TURBULENCE QUANTITY $\overline{v'T'}$

FOR x/H = 0.143

THE HEATED WALL

y mm	$\overline{v'T'} \times 10^3$ m.K/s
1	-0.38
2	1.62
3	0.32
4	4.85
5	4.38
6	3.75
7	6.19
8	4.44
9	13.25
10	14.38
20	7.22
30	5.48
40	4.73
50	4.09
60	3.53
70	3.03
100	2.40
150	2.40
200	2.40
250	2.40

THE COOLED WALL

y mm	$\overline{v'T'} \times 10^3$ m.K/s
1	-0.19
2	0.64
3	4.41
4	10.88
5	15.63
6	20.27
7	23.49
8	23.69
9	23.46
10	22.95
20	17.20
30	9.00
40	1.69
50	-2.72
60	-5.07
70	-6.52
100	-8.15
150	-5.14
200	-3.22
250	-2.20

TABLE 7.39

THE TURBULENCE QUANTITY $\overline{v'T'}$

FOR x/H = 0.229

THE HEATED WALL

y mm	$\overline{v'T'} \times 10^3$ m.K/s
1	0.77
2	3.08
3	22.54
4	25.83
5	31.59
6	58.18
7	65.75
8	76.36
9	80.52
10	85.75
20	76.37
30	64.40
40	60.49
50	59.17
60	59.09
70	59.22
100	59.62
150	60.62
200	62.76
250	66.99

THE COOLED WALL

y mm	$\overline{v'T'} \times 10^3$ m.K/s
1	-0.13
2	5.65
3	8.67
4	17.23
5	21.78
6	23.27
7	25.78
8	29.34
9	29.92
10	30.01
20	24.65
30	15.28
40	6.38
50	-0.64
60	-5.24
70	-8.79
100	-14.34
150	-10.00
200	-3.71
250	-4.48

TABLE 7.40

THE TURBULENCE QUANTITY $\overline{v'T'}$

FOR x/H = 0.360

THE HEATED WALL

y mm	$\overline{v'T'} \times 10^3$ m.K/s
1	-0.48
2	5.34
3	36.09
4	45.15
5	52.99
6	62.30
7	70.32
8	76.86
9	76.45
10	77.03
20	51.50
30	19.77
40	-6.43
50	-24.48
60	-35.39
70	-40.91
100	-46.50
150	-46.08
200	-43.80
250	-40.14

THE COOLED WALL

y mm	$\overline{v'T'} \times 10^3$ m.K/s
1	-0.08
2	6.06
3	11.13
4	23.45
5	33.09
6	35.66
7	38.20
8	39.52
9	38.55
10	39.34
20	39.30
30	29.04
40	18.73
50	9.41
60	1.59
70	-4.46
100	-16.16
150	-18.47
200	-12.79
250	-9.34

TABLE 7.41

THE TURBULENCE QUANTITY $\overline{v'T'}$

FOR x/H = 0.497

THE HEATED WALL

y mm	$\overline{v'T'} \times 10^3$ m.K/s
1	0.08
2	5.02
3	36.90
4	53.94
5	60.46
6	65.77
7	70.63
8	75.46
9	78.89
10	80.49
20	62.81
30	46.48
40	30.47
50	17.83
60	8.52
70	0.48
100	-10.80
150	-11.54
200	-7.13
250	-0.89

THE COOLED WALL

y mm	$\overline{v'T'} \times 10^3$ m.K/s
1	-0.08
2	10.15
3	17.87
4	23.61
5	33.89
6	39.76
7	43.14
8	44.11
9	45.12
10	44.19
20	37.99
30	26.06
40	14.60
50	5.38
60	-1.93
70	-7.39
100	-15.87
150	-18.18
200	-17.38
250	-18.13

TABLE 7.42

THE TURBULENCE QUANTITY $\overline{v'T'}$

FOR x/H = 0.630

THE HEATED WALL

y mm	$\overline{v'T'} \times 10^3$ m.K/s
1	0.13
2	4.29
3	14.78
4	38.34
5	46.97
6	53.42
7	61.09
8	69.51
9	70.50
10	72.29
20	69.99
30	57.98
40	45.42
50	34.46
60	25.37
70	17.83
100	4.40
150	1.55
200	6.75
250	10.25

THE COOLED WALL

y mm	$\overline{v'T'} \times 10^3$ m.K/s
1	0.00
2	11.10
3	20.53
4	30.18
5	44.65
6	47.19
7	49.73
8	51.82
9	51.84
10	52.95
20	48.41
30	37.55
40	26.73
50	18.66
60	11.93
70	6.82
100	-1.21
150	-5.14
200	-6.68
250	-6.42

TABLE 7.43

THE TURBULENCE QUANTITY $\overline{v'T'}$

FOR x/H = 0.765

THE HEATED WALL

y mm	$\overline{v'T'} \times 10^3$ m.K/s
1	-0.16
2	10.43
3	26.72
4	40.51
5	45.90
6	55.03
7	62.02
8	65.62
9	66.47
10	67.24
20	63.29
30	50.15
40	36.35
50	23.63
60	12.27
70	3.68
100	-11.22
150	-15.37
200	-11.09
250	-7.93

THE COOLED WALL

y mm	$\overline{v'T'} \times 10^3$ m.K/s
1	-0.12
2	12.95
3	22.81
4	30.44
5	39.12
6	45.49
7	50.35
8	52.55
9	54.40
10	52.76
20	43.04
30	29.20
40	18.40
50	11.55
60	7.60
70	5.41
100	2.10
150	0.28
200	-0.46
250	-2.89

TABLE 7.44

THE TURBULENCE QUANTITY $\overline{v'T'}$

FOR x/H = 0.849

THE HEATED WALL

y mm	$\overline{v'T'} \times 10^3$ m.K/s
1	0.11
2	5.77
3	19.48
4	21.00
5	40.07
6	47.45
7	52.59
8	55.58
9	57.68
10	60.75
20	53.98
30	40.46
40	26.27
50	15.34
60	6.41
70	-0.68
100	-12.35
150	-11.10
200	-1.83
250	6.17

THE COOLED WALL

y mm	$\overline{v'T'} \times 10^3$ m.K/s
1	-0.45
2	-1.92
3	-4.53
4	16.13
5	19.42
6	25.22
7	28.34
8	30.08
9	32.94
10	34.64
20	23.38
30	12.24
40	5.30
50	0.22
60	-3.63
70	-6.77
100	-12.55
150	-14.55
200	-12.70
250	-12.15

TABLE 7.45

THE TURBULENCE QUANTITY $\overline{v'T'}$

FOR x/H = 0.898

THE HEATED WALL

y mm	$\overline{v'T'} \times 10^3$ m.K/s
1	-0.15
2	4.03
3	13.43
4	23.98
5	36.41
6	47.63
7	49.71
8	52.85
9	54.66
10	56.58
20	54.00
30	42.29
40	29.99
50	19.76
60	11.91
70	5.13
100	-7.09
150	-8.78
200	-2.46
250	0.68

THE COOLED WALL

y mm	$\overline{v'T'} \times 10^3$ m.K/s
1	-0.47
2	7.33
3	13.18
4	20.73
5	22.76
6	33.02
7	30.42
8	38.72
9	37.87
10	39.63
20	28.53
30	22.60
40	18.02
50	14.09
60	10.55
70	7.70
100	2.20
150	-0.58
200	0.64
250	1.75

TABLE 7.46

THE TURBULENCE QUANTITY $\overline{v'T'}$

FOR x/H = 0.949

THE HEATED WALL

y mm	$\overline{v'T'} \times 10^3$ m.K/s
1	0.11
2	4.69
3	13.39
4	28.08
5	36.05
6	42.30
7	44.83
8	50.45
9	53.57
10	55.08
20	55.77
30	46.08
40	37.98
50	30.55
60	24.79
70	19.17
100	6.85
150	1.48
200	6.40
250	12.93

THE COOLED WALL

y mm	$\overline{v'T'} \times 10^3$ m.K/s
1	-0.60
2	21.09
3	39.78
4	50.63
5	50.03
6	62.62
7	64.87
8	66.05
9	64.14
10	62.00
20	48.17
30	44.80
40	42.05
50	38.90
60	35.66
70	32.89
100	27.37
150	23.53
200	21.77
250	20.10

TABLE 7.47

THE TURBULENCE QUANTITY $\overline{u'v'}$ FOR x/H = 0.046

THE HEATED WALL

y mm	A×10³ m²/s²	B×10³ m²/s²	C×10³ m²/s²	D×10³ m²/s²	E×10³ m²/s²	$\overline{u'v'}$×10³ m²/s²
1	1.61	2.69	1.08	0.01	0.00	-0.01
2	0.74	2.69	1.99	0.05	0.00	-0.01
3	0.10	2.69	2.73	0.15	0.00	-0.01
4	-0.33	2.69	3.29	0.28	0.01	-0.02
5	-0.49	2.69	3.72	0.42	0.04	0.08
6	-0.47	2.69	4.03	0.54	0.10	0.23
7	-0.41	2.69	4.25	0.64	0.16	0.35
8	-0.37	2.69	4.39	0.70	0.23	0.40
9	-0.28	2.69	4.49	0.74	0.31	0.47
10	-0.18	2.69	4.55	0.76	0.36	0.56
20	-0.03	2.69	4.62	0.86	0.63	0.45
30	-0.01	2.69	4.59	0.86	0.63	0.44
40	-0.01	2.69	4.57	0.86	0.63	0.42
50	-0.01	2.69	4.56	0.86	0.63	0.41
60	-0.01	2.69	4.56	0.86	0.63	0.41
70	0.00	2.69	4.56	0.86	0.63	0.40
100	0.00	2.69	4.56	0.86	0.63	0.40
150	0.00	2.69	4.50	0.86	0.63	0.36
200	0.00	2.69	4.36	0.86	0.63	0.22
250	0.00	2.69	4.27	0.86	0.63	0.13

THE COOLED WALL

y mm	A×10³ m²/s²	B×10³ m²/s²	C×10³ m²/s²	D×10³ m²/s²	E×10³ m²/s²	$-\overline{u'v'}$×10³ m²/s²	$\overline{u'v'}$×10³ m²/s²
1	-0.65	-0.92	-0.28	0.00	0.00	-0.01	0.01
2	-0.40	-0.92	-0.51	0.02	0.00	-0.01	0.01
3	-0.21	-0.92	-0.69	0.04	-0.01	-0.01	0.01
4	-0.06	-0.92	-0.84	0.05	-0.01	-0.02	0.02
5	-0.02	-0.92	-0.97	0.06	-0.01	-0.12	0.12
6	0.11	-0.92	-1.06	0.08	-0.01	-0.10	0.10
7	0.03	-0.92	-1.14	0.10	-0.01	-0.28	0.28
8	0.00	-0.92	-1.20	0.12	-0.01	-0.39	0.39
9	0.05	-0.92	-1.25	0.14	-0.01	-0.41	0.41
10	0.06	-0.92	-1.30	0.15	0.00	-0.47	0.47
20	0.05	-0.92	-1.47	0.23	0.10	-0.83	0.83
30	0.04	-0.92	-1.45	0.34	0.20	-1.03	1.03
40	0.02	-0.92	-1.34	0.39	0.31	-1.10	1.10
50	0.02	-0.92	-1.18	0.41	0.39	-1.04	1.04
60	0.01	-0.92	-0.99	0.41	0.45	-0.92	0.92
70	0.01	-0.92	-0.81	0.41	0.49	-0.78	0.78
100	0.00	-0.92	-0.43	0.41	0.51	-0.43	0.43
150	0.00	-0.92	-0.14	0.41	0.52	-0.15	0.15
200	0.00	-0.92	-0.01	0.41	0.52	-0.02	0.02
250	0.00	-0.92	0.05	0.41	0.52	0.04	-0.04

TABLE 7.48

THE TURBULENCE QUANTITY $\overline{u'v'}$ FOR x/H = 0.095

THE HEATED WALL

y mm	A×10³ m²/s²	B×10³ m²/s²	C×10³ m²/s²	D×10³ m²/s²	E×10³ m²/s²	$\overline{u'v'}$×10³ m²/s²
1	2.14	3.22	1.08	0.00	0.00	0.00
2	1.18	3.22	2.03	0.02	-0.02	-0.01
3	0.40	3.22	2.83	0.08	-0.04	-0.03
4	-0.18	3.22	3.49	0.20	-0.04	-0.07
5	-0.42	3.22	4.03	0.38	-0.02	0.03
6	-0.59	3.22	4.45	0.56	0.04	0.04
7	-0.62	3.22	4.78	0.72	0.14	0.08
8	-0.60	3.22	5.02	0.84	0.25	0.11
9	-0.58	3.22	5.21	0.92	0.38	0.11
10	-0.62	3.22	5.34	0.98	0.53	-0.01
20	-0.03	3.22	5.61	1.16	1.38	-0.18
30	0.00	3.22	5.63	1.16	1.38	-0.13
40	0.00	3.22	5.65	1.16	1.38	-0.11
50	0.00	3.22	5.68	1.16	1.38	-0.08
60	0.00	3.22	5.71	1.16	1.38	-0.05
70	0.00	3.22	5.73	1.16	1.38	-0.03
100	0.00	3.22	5.78	1.16	1.38	0.02
150	0.00	3.22	5.82	1.16	1.38	0.06
200	0.00	3.22	5.78	1.16	1.38	0.02
250	0.00	3.22	5.74	1.16	1.38	-0.02

THE COOLED WALL

y mm	A×10³ m²/s²	B×10³ m²/s²	C×10³ m²/s²	D×10³ m²/s²	E×10³ m²/s²	$-\overline{u'v'}$×10³ m²/s²	$\overline{u'v'}$×10³ m²/s²
1	-0.68	-0.98	-0.30	0.00	0.00	0.00	0.00
2	-0.44	-0.98	-0.54	0.00	0.00	0.00	0.00
3	-0.23	-0.98	-0.74	0.01	0.00	0.00	0.00
4	-0.08	-0.98	-0.90	0.02	0.00	-0.02	0.02
5	0.00	-0.98	-1.03	0.03	0.00	-0.08	0.08
6	0.00	-0.98	-1.13	0.04	0.00	-0.19	0.19
7	0.00	-0.98	-1.21	0.06	0.00	-0.29	0.29
8	0.00	-0.98	-1.28	0.08	0.00	-0.38	0.38
9	0.07	-0.98	-1.33	0.09	0.00	-0.37	0.37
10	0.04	-0.98	-1.38	0.10	0.00	-0.46	0.46
20	0.05	-0.98	-1.51	0.22	0.06	-0.76	0.76
30	0.04	-0.98	-1.42	0.30	0.15	-0.85	0.85
40	0.03	-0.98	-1.22	0.34	0.26	-0.81	0.81
50	0.02	-0.98	-0.98	0.35	0.35	-0.70	0.70
60	0.01	-0.98	-0.78	0.36	0.42	-0.57	0.57
70	0.01	-0.98	-0.57	0.36	0.47	-0.41	0.41
100	0.01	-0.98	-0.16	0.36	0.56	-0.09	0.09
150	0.00	-0.98	0.01	0.36	0.56	0.07	-0.07
200	0.00	-0.98	-0.05	0.36	0.56	0.01	-0.01
250	0.00	-0.98	-0.07	0.36	0.56	-0.01	0.01

TABLE 7.49

THE TURBULENCE QUANTITY $\overline{u'v'}$ FOR x/H = 0.143

THE HEATED WALL

y mm	A×10³ m²/s²	B×10³ m²/s²	C×10³ m²/s²	D×10³ m²/s²	E×10³ m²/s²	$\overline{u'v'}$×10³ m²/s²
1	2.43	3.47	1.03	0.00	-0.01	0.00
2	1.50	3.47	1.93	0.02	-0.06	0.00
3	0.70	3.47	2.70	0.06	-0.12	-0.01
4	0.07	3.47	3.35	0.12	-0.15	-0.02
5	-0.17	3.47	3.92	0.23	-0.16	0.21
6	-0.51	3.47	4.37	0.37	-0.13	0.15
7	-0.62	3.47	4.74	0.49	-0.06	0.22
8	-0.67	3.47	5.02	0.62	0.03	0.23
9	-0.67	3.47	5.23	0.75	0.15	0.19
10	-0.62	3.47	5.40	0.86	0.28	0.17
20	-0.05	3.47	5.90	1.29	1.08	0.01
30	0.00	3.47	6.00	1.29	1.19	0.05
40	0.00	3.47	6.07	1.29	1.19	0.12
50	0.00	3.47	6.13	1.29	1.19	0.18
60	0.00	3.47	6.17	1.29	1.19	0.22
70	0.00	3.47	6.19	1.29	1.19	0.24
100	0.00	3.47	6.20	1.29	1.19	0.25
150	0.00	3.47	6.17	1.29	1.19	0.22
200	0.00	3.47	6.08	1.29	1.19	0.13
250	0.00	3.47	6.01	1.29	1.19	0.06

THE COOLED WALL

y mm	A×10³ m²/s²	B×10³ m²/s²	C×10³ m²/s²	D×10³ m²/s²	E×10³ m²/s²	$-\overline{u'v'}$×10³ m²/s²	$\overline{u'v'}$×10³ m²/s²
1	-0.82	-1.13	-0.31	0.00	0.00	0.00	0.00
2	-0.55	-1.13	-0.57	0.01	0.00	0.00	0.00
3	-0.34	-1.13	-0.78	0.02	0.00	-0.01	0.01
4	-0.16	-1.13	-0.94	0.04	0.00	-0.01	0.01
5	-0.10	-1.13	-1.09	0.06	0.00	-0.12	0.12
6	-0.07	-1.13	-1.19	0.08	0.00	-0.21	0.21
7	0.02	-1.13	-1.27	0.10	0.00	-0.22	0.22
8	0.08	-1.13	-1.33	0.13	0.00	-0.25	0.25
9	0.07	-1.13	-1.39	0.16	0.00	-0.35	0.35
10	0.03	-1.13	-1.43	0.20	0.00	-0.47	0.47
20	0.06	-1.13	-1.50	0.42	0.07	-0.80	0.80
30	0.05	-1.13	-1.29	0.57	0.20	-0.88	0.88
40	0.04	-1.13	-0.97	0.66	0.34	-0.80	0.80
50	0.03	-1.13	-0.62	0.70	0.47	-0.63	0.63
60	0.02	-1.13	-0.27	0.72	0.59	-0.43	0.43
70	0.02	-1.13	0.07	0.72	0.70	-0.20	0.20
100	0.00	-1.13	0.76	0.72	0.88	0.29	-0.29
150	0.00	-1.13	0.92	0.72	0.87	0.46	-0.46
200	0.00	-1.13	0.58	0.72	0.85	0.14	-0.14
250	0.00	-1.13	0.41	0.72	0.85	-0.03	0.03

TABLE 7.50

THE TURBULENCE QUANTITY $\overline{u'v'}$ FOR x/H = 0.229

THE HEATED WALL

y mm	A×10³ m²/s²	B×10³ m²/s²	C×10³ m²/s²	D×10³ m²/s²	E×10³ m²/s²	$\overline{u'v'}$×10³ m²/s²
1	2.39	3.33	0.96	0.00	0.02	0.00
2	1.60	3.33	1.79	0.00	0.06	0.00
3	0.93	3.33	2.51	0.01	0.10	0.00
4	0.37	3.33	3.13	0.02	0.12	0.03
5	-0.03	3.33	3.58	0.03	0.13	0.06
6	-0.29	3.33	4.00	0.04	0.12	0.22
7	-0.42	3.33	4.34	0.04	0.10	0.45
8	-0.42	3.33	4.63	0.06	0.07	0.75
9	-0.41	3.33	4.87	0.10	0.05	0.98
10	-0.43	3.33	5.07	0.14	0.03	1.14
20	-0.18	3.33	6.04	0.59	0.16	1.78
30	-0.04	3.33	6.28	0.78	0.43	1.70
40	-0.02	3.33	6.28	0.82	0.57	1.54
50	-0.01	3.33	6.23	0.83	0.64	1.42
60	0.00	3.33	6.16	0.83	0.67	1.33
70	0.00	3.33	6.08	0.83	0.67	1.25
100	0.00	3.33	5.86	0.83	0.67	1.03
150	0.00	3.33	5.47	0.83	0.67	0.64
200	0.00	3.33	5.08	0.83	0.67	0.25
250	0.00	3.33	4.91	0.83	0.67	0.08

THE COOLED WALL

y mm	A×10³ m²/s²	B×10³ m²/s²	C×10³ m²/s²	D×10³ m²/s²	E×10³ m²/s²	$-\overline{u'v'}$×10³ m²/s²	$\overline{u'v'}$×10³ m²/s²
1	-1.00	-1.35	-0.36	0.00	0.00	-0.01	0.01
2	-0.70	-1.35	-0.65	0.01	0.00	-0.01	0.01
3	-0.44	-1.35	-0.88	0.03	0.00	0.00	0.00
4	-0.26	-1.35	-1.07	0.05	-0.01	-0.02	0.02
5	-0.16	-1.35	-1.26	0.08	-0.01	-0.14	0.14
6	-0.08	-1.35	-1.39	0.12	-0.01	-0.23	0.23
7	0.00	-1.35	-1.49	0.15	-0.01	-0.28	0.28
8	0.03	-1.35	-1.56	0.19	-0.01	-0.36	0.36
9	0.03	-1.35	-1.63	0.22	-0.01	-0.46	0.46
10	0.02	-1.35	-1.68	0.25	-0.01	-0.55	0.55
20	0.06	-1.35	-1.74	0.54	0.06	-0.93	0.93
30	0.06	-1.35	-1.48	0.75	0.23	-1.05	1.05
40	0.05	-1.35	-1.08	0.89	0.43	-1.00	1.00
50	0.04	-1.35	-0.61	0.99	0.58	-0.79	0.79
60	0.03	-1.35	-0.12	1.04	0.73	-0.51	0.51
70	0.03	-1.35	0.36	1.06	0.91	-0.23	0.23
100	0.01	-1.35	1.46	1.07	1.27	0.48	-0.48
150	0.00	-1.35	2.01	1.07	1.38	0.91	-0.91
200	0.00	-1.35	1.47	1.09	1.28	0.45	-0.45
250	0.00	-1.35	1.07	1.09	1.27	0.06	-0.06

TABLE 7.51

THE TURBULENCE QUANTITY $\overline{u'v'}$ FOR x/H = 0.360

THE HEATED WALL

y mm	A×10³ m²/s²	B×10³ m²/s²	C×10³ m²/s²	D×10³ m²/s²	E×10³ m²/s²	$\overline{u'v'}$×10³ m²/s²
1	2.10	2.90	0.80	0.00	-0.01	0.01
2	1.40	2.90	1.47	0.00	-0.03	0.00
3	0.83	2.90	2.03	0.00	-0.05	0.01
4	0.39	2.90	2.49	0.00	-0.06	0.04
5	0.29	2.90	3.00	0.00	-0.06	0.45
6	0.02	2.90	3.36	0.00	-0.06	0.54
7	-0.06	2.90	3.68	0.00	-0.06	0.78
8	-0.11	2.90	3.95	0.00	-0.06	1.00
9	-0.11	2.90	4.20	0.01	-0.06	1.24
10	-0.13	2.90	4.42	0.04	-0.06	1.41
20	-0.12	2.90	5.91	0.57	-0.01	2.33
30	-0.10	2.90	6.73	1.27	0.17	2.29
40	-0.08	2.90	7.17	1.86	0.53	1.80
50	-0.07	2.90	7.41	2.18	1.05	1.21
60	-0.04	2.90	7.54	2.33	1.52	0.75
70	-0.03	2.90	7.61	2.40	1.82	0.46
100	0.00	2.90	7.73	2.42	2.28	0.13
150	0.00	2.90	7.78	2.42	2.30	0.16
200	0.00	2.90	7.65	2.42	2.30	0.03
250	0.00	2.90	7.53	2.42	2.30	-0.09

THE COOLED WALL

y mm	A×10³ m²/s²	B×10³ m²/s²	C×10³ m²/s²	D×10³ m²/s²	E×10³ m²/s²	$-\overline{u'v'}$×10³ m²/s²	$\overline{u'v'}$×10³ m²/s²
1	-1.30	-1.75	-0.45	0.00	0.00	0.00	0.00
2	-0.92	-1.75	-0.83	0.01	0.00	-0.01	0.01
3	-0.61	-1.75	-1.13	0.03	-0.01	-0.01	0.01
4	-0.37	-1.75	-1.38	0.06	-0.02	-0.04	0.04
5	-0.18	-1.75	-1.62	0.10	-0.03	-0.12	0.12
6	-0.11	-1.75	-1.79	0.13	-0.03	-0.25	0.25
7	0.00	-1.75	-1.94	0.16	-0.03	-0.32	0.32
8	0.00	-1.75	-2.06	0.19	-0.03	-0.47	0.47
9	0.17	-1.75	-2.17	0.23	-0.03	-0.45	0.45
10	0.04	-1.75	-2.25	0.26	-0.02	-0.70	0.70
20	0.08	-1.75	-2.61	0.50	0.02	-1.30	1.30
30	0.07	-1.75	-2.55	0.72	0.11	-1.56	1.56
40	0.06	-1.75	-2.30	0.91	0.22	-1.62	1.62
50	0.04	-1.75	-1.94	1.04	0.32	-1.51	1.51
60	0.04	-1.75	-1.51	1.15	0.41	-1.28	1.28
70	0.04	-1.75	-1.05	1.24	0.50	-1.00	1.00
100	0.02	-1.75	0.15	1.31	0.82	-0.21	0.21
150	0.00	-1.75	1.08	1.29	1.03	0.51	-0.51
200	0.00	-1.75	0.86	1.28	1.01	0.32	-0.32
250	0.00	-1.75	0.56	1.28	0.95	0.08	-0.08

TABLE 7.52

THE TURBULENCE QUANTITY $\overline{u'v'}$ FOR x/H = 0.497

THE HEATED WALL

y mm	A×10³ m²/s²	B×10³ m²/s²	C×10³ m²/s²	D×10³ m²/s²	E×10³ m²/s²	$\overline{u'v'}$×10³ m²/s²
1	2.05	2.77	0.72	0.00	0.00	0.00
2	1.45	2.77	1.32	0.00	0.00	0.00
3	0.96	2.77	1.83	0.00	0.00	0.02
4	0.58	2.77	2.25	0.00	0.00	0.06
5	0.25	2.77	2.72	0.00	0.00	0.20
6	0.12	2.77	3.05	0.00	0.00	0.40
7	0.00	2.77	3.34	0.01	0.00	0.56
8	-0.05	2.77	3.59	0.02	0.00	0.75
9	-0.09	2.77	3.81	0.03	0.00	0.92
10	-0.11	2.77	4.01	0.05	0.00	1.08
20	-0.10	2.77	5.34	0.33	0.01	2.13
30	-0.09	2.77	6.03	0.56	0.04	2.57
40	-0.08	2.77	6.39	0.70	0.09	2.75
50	-0.07	2.77	6.55	0.84	0.13	2.74
60	-0.06	2.77	6.58	1.00	0.24	2.51
70	-0.06	2.77	6.54	1.13	0.39	2.19
100	-0.03	2.77	6.28	1.30	0.79	1.39
150	0.00	2.77	5.80	1.31	0.98	0.74
200	0.00	2.77	5.34	1.31	0.98	0.28
250	0.00	2.77	5.11	1.31	0.98	0.05

THE COOLED WALL

y mm	A×10³ m²/s²	B×10³ m²/s²	C×10³ m²/s²	D×10³ m²/s²	E×10³ m²/s²	$-\overline{u'v'}$×10³ m²/s²	$\overline{u'v'}$×10³ m²/s²
1	-1.47	-2.00	-0.53	0.00	0.00	0.00	0.00
2	-1.01	-2.00	-0.98	0.01	0.00	0.00	0.00
3	-0.65	-2.00	-1.35	0.02	-0.01	-0.01	0.01
4	-0.36	-2.00	-1.66	0.04	-0.01	-0.05	0.05
5	-0.18	-2.00	-1.92	0.05	-0.01	-0.14	0.14
6	-0.08	-2.00	-2.14	0.06	-0.01	-0.27	0.27
7	0.00	-2.00	-2.32	0.08	-0.01	-0.39	0.39
8	0.02	-2.00	-2.48	0.08	-0.01	-0.53	0.53
9	0.08	-2.00	-2.62	0.08	-0.01	-0.61	0.61
10	0.05	-2.00	-2.74	0.08	-0.01	-0.76	0.76
20	0.08	-2.00	-3.39	0.09	-0.02	-1.38	1.38
30	0.08	-2.00	-3.57	0.06	-0.04	-1.51	1.51
40	0.07	-2.00	-3.52	-0.01	-0.07	-1.37	1.36
50	0.06	-2.00	-3.34	-0.04	-0.08	-1.16	1.16
60	0.06	-2.00	-3.10	-0.06	-0.08	-0.90	0.90
70	0.04	-2.00	-2.83	-0.09	-0.08	-0.62	0.62
100	0.02	-2.00	-2.08	-0.10	-0.07	0.11	-0.11
150	0.00	-2.00	-1.67	-0.10	-0.07	0.50	-0.50
200	0.00	-2.00	-2.01	-0.10	-0.07	0.16	-0.16
250	0.00	-2.00	-2.22	-0.10	-0.07	-0.05	0.05

TABLE 7.53

THE TURBULENCE QUANTITY $\overline{u'v'}$ FOR x/H = 0.630

THE HEATED WALL

y mm	A×10³ m²/s²	B×10³ m²/s²	C×10³ m²/s²	D×10³ m²/s²	E×10³ m²/s²	$\overline{u'v'}$×10³ m²/s²
1	1.94	2.59	0.65	0.00	0.00	0.00
2	1.38	2.59	1.21	-0.01	0.00	0.01
3	0.92	2.59	1.68	-0.02	0.00	0.03
4	0.55	2.59	2.07	-0.04	0.01	0.06
5	0.32	2.59	2.37	-0.06	0.02	0.14
6	0.16	2.59	2.65	-0.09	0.02	0.29
7	0.04	2.59	2.90	-0.11	0.02	0.44
8	0.00	2.59	3.11	-0.13	0.02	0.63
9	-0.02	2.59	3.29	-0.15	0.02	0.81
10	-0.03	2.59	3.46	-0.17	0.02	0.99
20	-0.10	2.59	4.49	-0.28	-0.03	2.11
30	-0.09	2.59	4.95	-0.34	-0.09	2.70
40	-0.07	2.59	5.11	-0.39	-0.14	2.98
50	-0.06	2.59	5.08	-0.41	-0.19	3.03
60	-0.06	2.59	4.93	-0.43	-0.19	2.90
70	-0.04	2.59	4.70	-0.44	-0.32	2.83
100	-0.03	2.59	3.85	-0.42	-0.46	2.11
150	0.00	2.59	2.57	-0.42	-0.51	0.91
200	0.00	2.59	1.86	-0.42	-0.51	0.20
250	0.00	2.59	1.67	-0.42	-0.51	0.01

THE COOLED WALL

y mm	A×10³ m²/s²	B×10³ m²/s²	C×10³ m²/s²	D×10³ m²/s²	E×10³ m²/s²	$-\overline{u'v'}$×10³ m²/s²	$\overline{u'v'}$×10³ m²/s²
1	-1.54	-2.17	-0.63	0.00	0.00	0.00	0.00
2	-1.02	-2.17	-1.15	0.00	0.00	0.00	0.00
3	-0.60	-2.17	-1.59	-0.01	0.00	-0.01	0.01
4	-0.29	-2.17	-1.95	-0.02	0.00	-0.05	0.05
5	-0.11	-2.17	-2.23	-0.03	0.00	-0.14	0.14
6	0.00	-2.17	-2.49	-0.04	0.00	-0.28	0.28
7	0.04	-2.17	-2.72	-0.06	0.00	-0.45	0.45
8	0.10	-2.17	-2.91	-0.09	0.00	-0.55	0.55
9	0.17	-2.17	-3.07	-0.11	0.00	-0.62	0.62
10	0.09	-2.17	-3.22	-0.13	0.00	-0.83	0.83
20	0.09	-2.17	-4.07	-0.35	0.01	-1.47	1.47
30	0.08	-2.17	-4.40	-0.56	0.02	-1.61	1.61
40	0.07	-2.17	-4.47	-0.71	0.02	-1.54	1.54
50	0.06	-2.17	-4.38	-0.84	0.00	-1.31	1.31
60	0.04	-2.17	-4.21	-0.94	-0.06	-1.00	1.00
70	0.03	-2.17	-4.02	-0.99	-0.13	-0.70	0.70
100	0.01	-2.17	-3.58	-1.05	-0.39	0.04	-0.04
150	0.00	-2.17	-3.38	-1.05	-0.41	0.25	-0.25
200	0.00	-2.17	-3.43	-1.05	-0.41	0.20	-0.20
250	0.00	-2.17	-3.46	-1.05	-0.41	0.17	-0.17

TABLE 7.54

THE TURBULENCE QUANTITY $\overline{u'v'}$ FOR x/H = 0.765

THE HEATED WALL

y mm	A×10³ m²/s²	B×10³ m²/s²	C×10³ m²/s²	D×10³ m²/s²	E×10³ m²/s²	$\overline{u'v'}$×10³ m²/s²
1	1.74	2.32	0.58	0.00	0.00	0.00
2	1.25	2.32	1.08	-0.01	0.01	0.01
3	0.84	2.32	1.49	-0.02	0.03	0.00
4	0.53	2.32	1.85	-0.03	0.04	0.05
5	0.32	2.32	2.11	-0.05	0.05	0.11
6	0.21	2.32	2.36	-0.08	0.05	0.28
7	0.10	2.32	2.57	-0.10	0.05	0.40
8	0.08	2.32	2.76	-0.12	0.05	0.59
9	0.04	2.32	2.93	-0.14	0.05	0.74
10	-0.01	2.32	3.09	-0.16	0.05	0.87
20	-0.09	2.32	4.02	-0.31	-0.03	1.95
30	-0.08	2.32	4.42	-0.41	-0.11	2.54
40	-0.07	2.32	4.54	-0.47	-0.19	2.81
50	-0.07	2.32	4.48	-0.51	-0.28	2.88
60	-0.06	2.32	4.32	-0.54	-0.36	2.84
70	-0.04	2.32	4.09	-0.57	-0.43	2.73
100	-0.03	2.32	3.25	-0.62	-0.69	2.21
150	0.00	2.32	1.92	-0.62	-0.93	1.15
200	0.00	2.32	1.14	-0.62	-0.95	0.39
250	0.00	2.32	0.91	-0.62	-0.95	0.16

THE COOLED WALL

y mm	A×10³ m²/s²	B×10³ m²/s²	C×10³ m²/s²	D×10³ m²/s²	E×10³ m²/s²	$-\overline{u'v'}$×10³ m²/s²	$\overline{u'v'}$×10³ m²/s²
1	-1.61	-2.33	-0.72	0.00	0.00	0.00	0.00
2	-1.00	-2.33	-1.33	0.00	0.00	0.00	0.00
3	-0.50	-2.33	-1.84	0.00	0.00	-0.01	0.01
4	-0.11	-2.33	-2.26	0.00	0.00	-0.04	0.04
5	-0.02	-2.33	-2.56	0.00	0.00	-0.25	0.25
6	0.08	-2.33	-2.84	-0.01	0.00	-0.42	0.42
7	0.05	-2.33	-3.08	-0.02	0.00	-0.68	0.68
8	0.08	-2.33	-3.28	-0.03	0.00	-0.84	0.84
9	0.22	-2.33	-3.46	-0.05	0.00	-0.86	0.86
10	0.16	-2.33	-3.61	-0.08	0.00	-1.04	1.04
20	0.11	-2.33	-4.42	-0.22	-0.04	-1.72	1.72
30	0.07	-2.33	-4.67	-0.38	-0.13	-1.75	1.76
40	0.06	-2.33	-4.67	-0.49	-0.26	-1.53	1.53
50	0.04	-2.33	-4.54	-0.53	-0.38	-1.26	1.26
60	0.03	-2.33	-4.36	-0.53	-0.48	-0.99	0.99
70	0.02	-2.33	-4.17	-0.52	-0.56	-0.74	0.74
100	0.01	-2.33	-3.73	-0.51	-0.61	-0.27	0.27
150	0.00	-2.33	-3.43	-0.51	-0.61	0.02	-0.02
200	0.00	-2.33	-3.44	-0.51	-0.61	0.01	-0.01
250	0.00	-2.33	-3.49	-0.51	-0.61	-0.04	0.04

TABLE 7.55

THE TURBULENCE QUANTITY $\overline{u'v'}$ FOR x/H = 0.849

THE HEATED WALL

y mm	A×10³ m²/s²	B×10³ m²/s²	C×10³ m²/s²	D×10³ m²/s²	E×10³ m²/s²	$\overline{u'v'}$×10³ m²/s²
1	1.66	2.19	0.53	0.00	0.00	0.00
2	1.20	2.19	0.99	0.00	0.01	-0.01
3	0.83	2.19	1.37	-0.01	0.02	0.00
4	0.53	2.19	1.69	-0.02	0.02	0.03
5	0.32	2.19	1.94	-0.02	0.02	0.07
6	0.23	2.19	2.18	-0.03	0.02	0.23
7	0.09	2.19	2.38	-0.04	0.02	0.30
8	0.00	2.19	2.56	-0.05	0.02	0.40
9	0.00	2.19	2.72	-0.08	0.02	0.59
10	-0.01	2.19	2.86	-0.10	0.02	0.74
20	-0.09	2.19	3.75	-0.29	-0.02	1.78
30	-0.09	2.19	4.17	-0.41	-0.06	2.36
40	-0.07	2.19	4.34	-0.50	-0.10	2.68
50	-0.06	2.19	4.36	-0.57	-0.16	2.84
60	-0.06	2.19	4.27	-0.61	-0.22	2.85
70	-0.06	2.19	4.10	-0.65	-0.29	2.79
100	-0.03	2.19	3.41	-0.68	-0.49	2.36
150	0.00	2.19	2.16	-0.68	-0.64	1.29
200	0.00	2.19	1.26	-0.68	-0.65	0.40
250	0.00	2.19	0.96	-0.68	-0.65	0.10

THE COOLED WALL

y mm	A×10³ m²/s²	B×10³ m²/s²	C×10³ m²/s²	D×10³ m²/s²	E×10³ m²/s²	$-\overline{u'v'}$×10³ m²/s²	$\overline{u'v'}$×10³ m²/s²
1	-1.65	-2.39	-0.73	0.01	0.00	0.00	0.00
2	-1.02	-2.39	-1.34	0.02	0.00	0.01	-0.01
3	-0.51	-2.39	-1.85	0.02	0.00	0.01	-0.01
4	-0.10	-2.39	-2.26	0.02	0.00	0.01	-0.01
5	0.00	-2.39	-2.58	0.01	0.00	-0.20	0.20
6	0.05	-2.39	-2.84	0.00	0.00	-0.40	0.40
7	0.13	-2.39	-3.06	-0.01	0.00	-0.53	0.53
8	0.37	-2.39	-3.22	-0.03	0.00	-0.43	0.43
9	0.67	-2.39	-3.35	-0.05	-0.01	-0.23	0.23
10	0.18	-2.39	-3.46	-0.08	-0.02	-0.79	0.79
20	0.11	-2.39	-3.87	-0.18	-0.08	-1.11	1.11
30	0.06	-2.39	-3.90	-0.18	-0.14	-1.13	1.13
40	0.03	-2.39	-3.78	-0.12	-0.16	-1.08	1.08
50	0.01	-2.39	-3.63	-0.08	-0.17	-0.98	0.98
60	0.02	-2.39	-3.48	-0.04	-0.14	-0.89	0.89
70	0.02	-2.39	-3.32	-0.01	-0.10	-0.80	0.80
100	0.01	-2.39	-2.87	0.03	0.00	-0.50	0.50
150	0.01	-2.39	-2.44	0.03	0.07	-0.14	0.14
200	0.00	-2.39	-2.37	0.03	0.07	-0.08	0.08
250	0.00	-2.39	-2.41	0.03	0.07	-0.12	0.12

TABLE 7.56

THE TURBULENCE QUANTITY $\overline{u'v'}$ FOR x/H = 0.898

THE HEATED WALL

y mm	A×10³ m²/s²	B×10³ m²/s²	C×10³ m²/s²	D×10³ m²/s²	E×10³ m²/s²	$\overline{u'v'}$×10³ m²/s²
1	1.62	2.13	0.51	0.00	0.00	0.00
2	1.17	2.13	0.94	-0.01	0.01	-0.02
3	0.81	2.13	1.31	-0.02	0.02	-0.01
4	0.51	2.13	1.61	-0.04	0.02	0.01
5	0.22	2.13	1.84	-0.06	0.02	-0.03
6	0.09	2.13	2.05	-0.10	0.02	0.09
7	0.03	2.13	2.24	-0.13	0.02	0.25
8	0.00	2.13	2.40	-0.17	0.02	0.42
9	0.00	2.13	2.54	-0.22	0.02	0.61
10	0.00	2.13	2.66	-0.25	0.02	0.76
20	-0.08	2.13	3.47	-0.55	-0.03	1.84
30	-0.08	2.13	3.88	-0.75	-0.12	2.54
40	-0.07	2.13	4.05	-0.81	-0.24	2.90
50	-0.07	2.13	4.06	-0.82	-0.36	3.04
60	-0.06	2.13	3.99	-0.84	-0.48	3.12
70	-0.04	2.13	3.85	-0.84	-0.58	3.10
100	-0.03	2.13	3.19	-0.78	-0.80	2.61
150	0.00	2.13	1.89	-0.75	-0.85	1.36
200	0.00	2.13	1.00	-0.81	-0.85	0.53
250	0.00	2.13	0.59	-0.82	-0.85	0.13

THE COOLED WALL

y mm	A×10³ m²/s²	B×10³ m²/s²	C×10³ m²/s²	D×10³ m²/s²	E×10³ m²/s²	$-\overline{u'v'}$×10³ m²/s²	$\overline{u'v'}$×10³ m²/s²
1	-1.47	-2.18	-0.73	-0.01	0.00	-0.01	0.01
2	-0.90	-2.18	-1.32	-0.04	0.00	0.00	0.00
3	-0.46	-2.18	-1.80	-0.08	0.00	0.00	0.00
4	-0.15	-2.18	-2.17	-0.13	0.00	-0.01	0.01
5	0.10	-2.18	-2.44	-0.21	0.00	0.05	-0.05
6	0.14	-2.18	-2.67	-0.27	-0.01	-0.07	0.07
7	0.14	-2.18	-2.83	-0.33	-0.02	-0.16	0.16
8	0.18	-2.18	-2.96	-0.40	-0.03	-0.17	0.17
9	0.22	-2.18	-3.05	-0.44	-0.05	-0.16	0.16
10	0.14	-2.18	-3.13	-0.48	-0.08	-0.25	0.25
20	0.07	-2.18	-3.35	-0.65	-0.19	-0.26	0.26
30	0.04	-2.18	-3.30	-0.56	-0.27	-0.25	0.25
40	0.04	-2.18	-3.17	-0.39	-0.29	-0.27	0.27
50	0.03	-2.18	-3.03	-0.27	-0.28	-0.27	0.27
60	0.02	-2.18	-2.89	-0.20	-0.27	-0.22	0.22
70	0.02	-2.18	-2.74	-0.17	-0.23	-0.14	0.14
100	0.02	-2.18	-2.35	-0.10	-0.11	0.06	-0.06
150	0.00	-2.18	-2.07	-0.09	0.00	0.20	-0.20
200	0.00	-2.18	-2.20	-0.09	0.01	0.06	-0.06
250	0.00	-2.18	-2.34	-0.09	0.01	-0.08	0.08

TABLE 7.57

THE TURBULENCE QUANTITY $\overline{u'v'}$ FOR x/H = 0.949

THE HEATED WALL

y mm	A×10³ m²/s²	B×10³ m²/s²	C×10³ m²/s²	D×10³ m²/s²	E×10³ m²/s²	$\overline{u'v'}$×10³ m²/s²
1	1.38	1.87	0.49	-0.01	0.00	0.01
2	0.95	1.87	0.91	-0.04	0.01	0.02
3	0.54	1.87	1.26	-0.11	0.02	0.02
4	0.18	1.87	1.56	-0.23	0.04	0.06
5	0.33	1.87	1.74	-0.39	0.08	0.51
6	0.19	1.87	1.95	-0.52	0.10	0.69
7	0.15	1.87	2.13	-0.62	0.12	0.91
8	0.11	1.87	2.28	-0.68	0.13	1.07
9	0.03	1.87	2.42	-0.73	0.14	1.17
10	0.00	1.87	2.54	-0.79	0.14	1.32
20	-0.08	1.87	3.26	-1.27	-0.11	2.69
30	-0.06	1.87	3.57	-1.79	-0.32	3.75
40	-0.06	1.87	3.64	-2.22	-0.54	4.47
50	-0.06	1.87	3.56	-2.45	-0.80	4.88
60	-0.04	1.87	3.37	-2.56	-1.03	5.05
70	-0.04	1.87	3.10	-2.59	-1.22	5.00
100	-0.02	1.87	2.09	-2.65	-1.55	4.40
150	0.00	1.87	0.23	-2.67	-1.73	2.76
200	0.00	1.87	-1.29	-2.71	-1.73	1.28
250	0.00	1.87	-1.91	-2.74	-1.73	0.69

THE COOLED WALL

y mm	A×10³ m²/s²	B×10³ m²/s²	C×10³ m²/s²	D×10³ m²/s²	E×10³ m²/s²	$-\overline{u'v'}$×10³ m²/s²	$\overline{u'v'}$×10³ m²/s²
1	-1.26	-1.99	-0.75	-0.02	0.00	0.00	0.00
2	-0.72	-1.99	-1.33	-0.08	0.01	0.01	-0.01
3	-0.35	-1.99	-1.76	-0.15	0.03	0.00	0.00
4	-0.18	-1.99	-2.08	-0.25	0.03	-0.05	0.05
5	0.08	-1.99	-2.32	-0.39	0.02	0.12	-0.12
6	0.08	-1.99	-2.50	-0.49	0.01	0.05	-0.05
7	0.08	-1.99	-2.63	-0.58	0.00	0.02	-0.02
8	0.08	-1.99	-2.73	-0.66	-0.02	0.02	-0.02
9	0.08	-1.99	-2.81	-0.72	-0.04	0.02	-0.02
10	0.08	-1.99	-2.87	-0.78	-0.07	0.05	-0.05
20	0.03	-1.99	-3.25	-1.13	-0.22	0.12	-0.12
30	0.02	-1.99	-3.45	-1.32	-0.31	0.19	-0.19
40	0.03	-1.99	-3.55	-1.38	-0.42	0.27	-0.27
50	0.03	-1.99	-3.59	-1.41	-0.53	0.37	-0.37
60	0.03	-1.99	-3.60	-1.45	-0.61	0.48	-0.48
70	0.02	-1.99	-3.61	-1.48	-0.69	0.57	-0.57
100	0.01	-1.99	-3.66	-1.53	-0.79	0.66	-0.66
150	0.00	-1.99	-3.99	-1.55	-0.79	0.34	-0.34
200	0.00	-1.99	-4.59	-1.55	-0.79	-0.26	0.26
250	0.00	-1.99	-4.96	-1.55	-0.79	-0.63	0.63

TABLE 7.58

VALUES OF $\overline{u'v'}$ AT THE CAVITY CENTRE LINE CALCULATED FROM EXPERIMENTAL DATA USING THE TURBULENCE ENERGY EQUATION

$\frac{x}{H}$	$\frac{\overline{u'v'} \times 10^3}{m^2/s^2}$
0.046	0.01
0.096	0.01
0.229	0.14
0.497	0.05
0.629	0.01
0.765	0.19
0.949	0.65-1.15

TABLE 7.59

VALUES OF $\overline{u'v'}$ AT THE CAVITY CENTRE LINE CALCULATED FROM EXPERIMENTAL DATA USING THE CORRELATION COEFFICIENT

$\frac{x}{H}$	$\frac{\overline{u'v'} \times 10^3}{m^2/s^2}$
0.046	0.10
0.096	0.02
0.229	0.12
0.497	0.06
0.629	0.12
0.765	0.23
0.949	1.20

TABLE 7.60

AFFECT OF CORRECTION TO CENTRE LINE

TEMPERATURE ON VALUES OF THE TURBULENCE QUANTITY $\overline{u'v'}$

THE HEATED WALL

y mm	$\overline{u'v'}\times10^{3}$ (original) m^2/s^2	$\overline{u'v'}\times10^{3}$ (corrected) m^2/s^2
1	0.00	0.00
2	0.01	0.01
3	0.00	0.00
4	0.05	0.05
5	0.15	0.11
6	0.32	0.28
7	0.45	0.40
8	0.65	0.59
9	0.81	0.74
10	0.94	0.87
20	2.08	1.95
30	2.75	2.54
40	3.09	2.81
50	3.23	2.88
60	3.26	2.84
70	3.23	2.73
100	2.94	2.21
150	2.26	1.15
200	1.88	0.39
250	1.84	0.16

THE COOLED WALL

y mm	$\overline{u'v'}\times10^{3}$ (original) m^2/s^2	$\overline{u'v'}\times10^{3}$ (corrected) m^2/s^2
1	0.00	0.00
2	0.00	0.00
3	0.01	0.01
4	0.04	0.04
5	0.27	0.22
6	0.45	0.39
7	0.71	0.65
8	0.88	0.81
9	0.90	0.83
10	1.09	1.01
20	1.83	1.69
30	1.94	1.73
40	1.78	1.50
50	1.58	1.23
60	1.38	0.96
70	1.20	0.71
100	0.93	0.24
150	0.98	-0.05
200	1.34	-0.04
250	1.56	0.01

TABLE 7.61

EXPERIMENTAL & CORRECTED CENTRE-LINE TEMPERATURES

	ORIGINAL		CORRECTED			
$\frac{x}{H}$	T_{HCLE} °C	T_{CCLE} °C	T_{HCLC} °C	T_{CCLC} °C	δT_H K	δT_C K
0.046	39.028	38.601	39.03	38.60	0.00	0.00
0.096	40.272	40.077	40.34	40.01	0.07	-0.07
0.143	41.373	41.349	41.46	41.52	0.09	0.17
0.229	43.874	43.814	44.24	44.13	0.37	0.32
0.360	47.860	47.555	48.11	47.82	0.25	0.27
0.497	51.156	50.911	51.47	51.05	0.31	0.14
0.629	54.000	54.096	54.22	53.94	0.22	-0.16
0.765	56.393	57.143	56.65	56.91	0.26	-0.23
0.848	56.883	58.499	58.12	58.59	1.24	0.09
0.898	58.278	59.141	59.00	59.37	0.72	0.23
0.949	59.867	59.912	60.36	60.40	0.49	0.49

TABLE 7.62

FLOW REVERSALS AND TEMPERATURE INVERSION

	HEATED WALL			COOLED WALL		
$\frac{x}{H}$	Δu m/s	ΔT K	$\Delta u/\Delta T$ m/s.K	Δu m/s	ΔT K	$\Delta u/\Delta T$ m/s.K
0.046	0.004	0.108	0.037	0.008	0.631	0.013
0.096	0.000	0.177	0.000	0.013	0.783	0.017
0.143	0.001	0.004	0.250	0.016	1.284	0.012
0.229	0.005	0.000	0.000	0.026	1.931	0.013
0.360	0.009	0.000	0.000	0.020	1.772	0.011
0.497	0.010	0.000	0.000	0.006	1.065	0.006
0.630	0.017	0.792	0.021	0.000	0.457	0.000
0.765	0.017	0.787	0.022	0.000	0.403	0.000
0.849	0.023	0.000	0.000	0.005	0.605	0.008
0.898	0.016	0.159	0.101	0.006	0.749	0.008
0.949	0.017	0.815	0.021	0.004	0.505	0.008

TABLE 7.63

DENSITY, REYNOLDS STRESS $\rho\overline{u'v'}$, TOTAL SHEAR STRESS, PRODUCTION OF TURBULENCE KINETIC ENERGY BY SHEAR AND MEAN LATERAL VELOCITY, v, FOR x/H = 0.046

THE HEATED WALL

y mm	ρ kg/m³	$\rho\overline{u'v'}\times10^3$ kg/m.s²	$\tau\times10^3$ N/m²	$-\rho\overline{u'v'}du/dy\times10^3$ kg/m.s³	v m/s
1	1.035	-0.01	1.68	0.84	0.0000
2	1.051	-0.01	0.79	0.40	-0.0001
3	1.072	-0.01	0.12	0.06	-0.0004
4	1.088	-0.02	-0.34	-0.40	-0.0009
5	1.101	0.09	-0.63	2.43	-0.0015
6	1.113	0.26	-0.78	6.87	-0.0022
7	1.122	0.39	-0.85	9.44	-0.0029
8	1.127	0.45	-0.87	9.88	-0.0035
9	1.132	0.53	-0.85	8.65	-0.0041
10	1.134	0.64	-0.84	6.66	-0.0044
20	1.140	0.51	-0.55	0.89	-0.0037
30	1.139	0.50	-0.51	0.36	-0.0025
40	1.139	0.48	-0.49	0.24	-0.0013
50	1.139	0.47	-0.48	0.24	-0.0013
60	1.139	0.47	-0.48	0.24	-0.0011
70	1.139	0.46	-0.46	0.00	-0.0011
100	1.139	0.46	-0.46	0.00	-0.0007
150	1.139	0.41	-0.41	0.00	-0.0013
200	1.139	0.25	-0.25	0.00	-0.0029
250	1.139	0.15	-0.15	0.00	-0.0063

THE COOLED WALL

y mm	ρ kg/m³	$\rho\overline{u'v'}\times10^3$ kg/m.s²	$\tau\times10^3$ N/m²	$-\rho\overline{u'v'}du/dy\times10^3$ kg/m.s³	v m/s
1	1.170	0.01	0.75	-0.48	-0.0001
2	1.165	0.01	0.45	-0.29	-0.0002
3	1.160	0.01	0.23	-0.15	-0.0005
4	1.157	0.02	0.05	-0.09	-0.0004
5	1.152	0.14	-0.12	-0.14	-0.0010
6	1.149	0.12	-0.24	0.70	-0.0012
7	1.148	0.32	-0.36	0.66	-0.0010
8	1.146	0.45	-0.45	0.00	-0.0011
9	1.145	0.47	-0.53	1.44	-0.0022
10	1.144	0.54	-0.61	1.82	-0.0030
20	1.141	0.95	-1.00	2.77	-0.0031
30	1.139	1.17	-1.22	2.65	-0.0052
40	1.139	1.25	-1.28	1.77	-0.0075
50	1.138	1.18	-1.21	1.16	-0.0060
60	1.138	1.05	-1.06	0.76	-0.0069
70	1.138	0.89	-0.90	0.47	-0.0067
100	1.139	0.49	-0.49	-0.02	-0.0050
150	1.139	0.17	-0.17	0.00	-0.0033
200	1.139	0.02	-0.02	0.00	-0.0046
250	1.139	-0.05	0.05	0.00	-0.0046

TABLE 7.64

DENSITY, REYNOLDS STRESS $\rho\overline{u'v'}$, TOTAL SHEAR STRESS, PRODUCTION OF TURBULENCE KINETIC ENERGY BY SHEAR AND MEAN LATERAL VELOCITY, v, FOR x/H = 0.095

THE HEATED WALL

y mm	ρ kg/m^3	$\rho\overline{u'v'}\times10^3$ kg/m.s^2	$\tau\times10^3$ N/m^2	$-\rho\overline{u'v'}du/dy\times10^3$ kg/m.s^3	v m/s
1	1.026	0.00	2.20	0.00	-0.0001
2	1.040	-0.01	1.24	0.63	-0.0003
3	1.056	-0.03	0.45	0.67	-0.0006
4	1.071	-0.07	-0.12	-0.73	-0.0012
5	1.083	0.03	-0.49	0.76	-0.0018
6	1.094	0.04	-0.69	1.45	-0.0023
7	1.103	0.09	-0.77	3.06	-0.0030
8	1.110	0.12	-0.79	4.23	-0.0036
9	1.116	0.12	-0.77	4.16	-0.0041
10	1.121	-0.01	-0.68	-0.40	-0.0045
20	1.132	-0.20	-0.41	-0.36	-0.0049
30	1.132	-0.15	-0.03	-0.03	-0.0047
40	1.132	-0.12	0.00	0.00	-0.0042
50	1.132	-0.09	0.00	0.00	-0.0040
60	1.132	-0.05	0.00	0.00	-0.0031
70	1.132	-0.03	0.00	0.00	-0.0031
100	1.132	0.02	0.00	0.00	-0.0033
150	1.132	0.06	0.00	0.00	-0.0042
200	1.132	0.02	0.00	0.00	-0.0042
250	1.132	-0.02	0.00	0.00	-0.0064

THE COOLED WALL

y mm	ρ kg/m^3	$\rho\overline{u'v'}\times10^3$ kg/m.s^2	$\tau\times10^3$ N/m^2	$-\rho\overline{u'v'}du/dy\times10^3$ kg/m.s^3	v m/s
1	1.160	0.00	0.79	0.00	0.0000
2	1.154	0.00	0.51	0.00	0.0000
3	1.150	0.00	0.26	0.00	-0.0001
4	1.145	0.02	0.07	-0.11	-0.0001
5	1.142	0.09	-0.09	0.00	-0.0004
6	1.139	0.22	-0.22	0.00	-0.0005
7	1.137	0.33	-0.33	0.00	-0.0005
8	1.135	0.43	-0.43	0.00	-0.0008
9	1.134	0.42	-0.50	1.71	-0.0009
10	1.134	0.52	-0.57	1.40	-0.0009
20	1.129	0.86	-0.91	2.76	-0.0031
30	1.127	0.96	-1.00	2.43	-0.0037
40	1.127	0.91	-0.95	1.97	-0.0056
50	1.127	0.79	-0.81	1.08	-0.0056
60	1.127	0.64	-0.65	0.56	-0.0072
70	1.127	0.46	-0.47	0.32	-0.0061
100	1.128	0.10	-0.11	0.00	-0.0055
150	1.128	-0.08	0.07	0.00	-0.0052
200	1.128	-0.01	0.01	0.00	-0.0033
250	1.128	0.01	-0.01	0.00	-0.0038

TABLE 7.65

DENSITY, REYNOLDS STRESS $\rho\overline{u'v'}$, TOTAL SHEAR STRESS, PRODUCTION OF TURBULENCE KINETIC ENERGY BY SHEAR AND LATERAL MEAN VELOCITY, v, FOR x/H = 0.143

THE HEATED WALL

y mm	ρ kg/m³	$\rho\overline{u'v'}\times10^3$ kg/m.s²	$\tau\times10^3$ N/m²	$-\rho\overline{u'v'}du/dy\times10^3$ kg/m.s³	v m/s
1	1.030	0.00	2.50	0.00	-0.0002
2	1.042	0.00	1.56	0.00	-0.0008
3	1.055	-0.01	0.75	0.39	-0.0014
4	1.066	-0.02	0.10	0.08	-0.0011
5	1.076	0.23	-0.41	2.10	-0.0013
6	1.087	0.16	-0.72	4.54	-0.0017
7	1.096	0.24	-0.92	8.25	-0.0021
8	1.104	0.25	-0.99	9.60	-0.0029
9	1.110	0.21	-0.95	7.97	-0.0032
10	1.115	0.19	-0.88	6.70	-0.0040
20	1.134	0.01	-0.07	0.04	-0.0062
30	1.131	0.05	-0.06	0.01	-0.0071
40	1.131	0.14	-0.14	0.00	-0.0077
50	1.131	0.20	-0.20	0.00	-0.0073
60	1.132	0.25	-0.25	0.00	-0.0073
70	1.132	0.27	-0.27	0.00	-0.0073
100	1.132	0.28	-0.28	0.00	-0.0072
150	1.132	0.25	-0.25	0.00	-0.0073
200	1.132	0.15	-0.15	0.00	-0.0073
250	1.132	0.07	-0.07	0.00	-0.0064

THE COOLED WALL

y mm	ρ kg/m³	$\rho\overline{u'v'}\times10^3$ kg/m.s²	$\tau\times10^3$ N/m²	$-\rho\overline{u'v'}du/dy\times10^3$ kg/m.s³	v m/s
1	1.166	0.00	0.96	0.00	0.0000
2	1.159	0.00	0.64	0.00	-0.0001
3	1.152	0.01	0.38	-0.24	-0.0001
4	1.147	0.01	0.17	-0.11	-0.0002
5	1.143	0.14	-0.02	-0.84	-0.0006
6	1.140	0.24	-0.16	-0.98	-0.0005
7	1.138	0.25	-0.27	0.26	-0.0006
8	1.137	0.28	-0.38	1.45	-0.0007
9	1.135	0.40	-0.48	1.62	-0.0007
10	1.134	0.53	-0.57	0.93	-0.0016
20	1.129	0.90	-0.97	3.15	-0.0033
30	1.127	0.99	-1.05	3.00	-0.0044
40	1.126	0.90	-0.94	2.22	-0.0064
50	1.126	0.71	-0.74	1.33	-0.0061
60	1.126	0.48	-0.51	0.68	-0.0084
70	1.126	0.23	-0.25	0.25	-0.0099
100	1.129	-0.33	0.33	0.00	-0.0099
150	1.130	-0.52	0.52	0.04	-0.0063
200	1.130	-0.16	0.16	0.00	-0.0071
250	1.130	0.03	-0.03	0.00	-0.0073

TABLE 7.66

DENSITY, REYNOLDS STRESS $\rho\overline{u'v'}$, TOTAL SHEAR STRESS, PRODUCTION OF TURBULENCE KINETIC ENERGY BY SHEAR AND LATERAL MEAN VELOCITY, v, FOR x/H = 0.229

THE HEATED WALL

y mm	ρ kg/m^3	$\rho\overline{u'v'}\times10^3$ kg/m.s^2	$\tau\times10^3$ N/m^2	$-\rho\overline{u'v'}du/dy\times10^3$ kg/m.s^3	v m/s
1	1.025	0.00	2.45	0.00	0.0004
2	1.038	0.00	1.66	0.00	0.0007
3	1.048	0.00	0.97	0.00	0.0008
4	1.057	0.03	0.36	-0.62	0.0006
5	1.068	0.06	-0.10	0.09	0.0008
6	1.076	0.24	-0.55	3.68	0.0008
7	1.083	0.49	-0.94	11.37	0.0009
8	1.089	0.82	-1.27	19.05	0.0010
9	1.093	1.07	-1.52	24.98	0.0009
10	1.097	1.25	-1.72	30.21	0.0005
20	1.112	1.98	-2.18	20.66	-0.0038
30	1.117	1.90	-1.94	5.05	-0.0069
40	1.118	1.72	-1.74	2.08	-0.0087
50	1.118	1.59	-1.60	0.78	-0.0093
60	1.118	1.49	-1.49	0.10	-0.0109
70	1.118	1.40	-1.40	0.00	-0.0101
100	1.118	1.15	-1.15	0.00	-0.0092
150	1.118	0.72	-0.72	0.00	-0.0087
200	1.118	0.28	-0.28	0.00	-0.0078
250	1.118	0.09	-0.09	0.00	-0.0079

THE COOLED WALL

y mm	ρ kg/m^3	$\rho\overline{u'v'}\times10^3$ kg/m.s^2	$\tau\times10^3$ N/m^2	$-\rho\overline{u'v'}du/dy\times10^3$ kg/m.s^3	v m/s
1	1.159	0.01	1.15	-0.72	0.0000
2	1.151	0.01	0.79	-0.49	-0.0001
3	1.145	0.00	0.50	0.00	-0.0002
4	1.138	0.02	0.27	-0.35	-0.0004
5	1.135	0.16	0.02	-1.46	-0.0005
6	1.132	0.26	-0.17	-1.33	-0.0007
7	1.128	0.32	-0.32	0.00	-0.0007
8	1.126	0.41	-0.44	0.83	-0.0009
9	1.125	0.52	-0.55	1.06	-0.0014
10	1.124	0.62	-0.64	0.66	-0.0013
20	1.117	1.04	-1.11	4.18	-0.0033
30	1.115	1.17	-1.24	4.13	-0.0056
40	1.114	1.11	-1.17	3.28	-0.0067
50	1.113	0.89	-0.92	2.28	-0.0037
60	1.113	0.57	-0.60	1.20	-0.0091
70	1.114	0.26	-0.29	0.43	-0.0096
100	1.116	-0.54	0.52	-0.39	-0.0110
150	1.119	-1.02	1.02	0.14	-0.0097
200	1.119	-0.50	0.50	0.03	-0.0080
250	1.119	-0.07	0.07	0.00	-0.0099

TABLE 7.67

DENSITY, REYNOLDS STRESS $\rho\overline{u'v'}$, TOTAL SHEAR STRESS, PRODUCTION OF TURBULENCE KINETIC ENERGY BY SHEAR AND LATERAL MEAN VELOCITY, v, FOR x/H = 0.360

THE HEATED WALL

y mm	ρ kg/m³	$\rho\overline{u'v'}\times10^3$ kg/m.s²	$\tau\times10^3$ N/m²	$-\rho\overline{u'v'}du/dy\times10^3$ kg/m.s³	v m/s
1	1.023	0.01	2.14	-1.07	-0.0002
2	1.037	0.00	1.45	0.00	-0.0002
3	1.046	0.01	0.86	-0.45	-0.0004
4	1.053	0.04	0.37	-0.86	-0.0003
5	1.060	0.48	-0.17	-7.33	-0.0002
6	1.065	0.58	-0.55	-0.61	0.0000
7	1.070	0.83	-0.90	2.65	-0.0001
8	1.073	1.07	-1.19	6.26	0.0001
9	1.076	1.33	-1.45	7.78	0.0000
10	1.078	1.52	-1.66	10.43	0.0000
20	1.090	2.54	-2.67	16.94	-0.0017
30	1.095	2.51	-2.62	14.09	-0.0048
40	1.098	1.98	-2.06	9.76	-0.0089
50	1.100	1.33	-1.41	5.47	-0.0143
60	1.101	0.83	-0.87	2.20	-0.0130
70	1.101	0.51	-0.54	0.83	-0.0155
100	1.101	0.14	-0.14	0.03	-0.0180
150	1.101	0.18	-0.18	0.00	-0.0188
200	1.101	0.03	-0.03	0.00	-0.0180
250	1.101	-0.09	0.10	0.00	-0.0168

THE COOLED WALL

y mm	ρ kg/m³	$\rho\overline{u'v'}\times10^3$ kg/m.s²	$\tau\times10^3$ N/m²	$-\rho\overline{u'v'}du/dy\times10^3$ kg/m.s³	v m/s
1	1.151	0.00	1.50	0.00	0.0000
2	1.142	0.01	1.04	-0.63	-0.0001
3	1.135	0.01	0.68	-0.41	-0.0003
4	1.128	0.04	0.37	-0.99	-0.0004
5	1.123	0.13	0.07	-1.37	-0.0004
6	1.119	0.28	-0.16	-1.71	-0.0006
7	1.117	0.36	-0.36	0.00	-0.0007
8	1.115	0.52	-0.52	0.00	-0.0009
9	1.112	0.50	-0.69	4.59	-0.0009
10	1.110	0.78	-0.82	1.59	-0.0014
20	1.102	1.43	-1.52	6.10	-0.0016
30	1.100	1.72	-1.79	6.45	-0.0027
40	1.098	1.78	-1.84	5.41	-0.0037
50	1.097	1.66	-1.70	4.42	-0.0028
60	1.096	1.40	-1.45	3.58	-0.0035
70	1.096	1.10	-1.14	2.54	-0.0038
100	1.098	0.23	-0.25	0.29	-0.0074
150	1.098	-0.56	0.56	-0.07	-0.0106
200	1.098	-0.35	0.35	0.04	-0.0115
250	1.098	-0.09	0.09	0.01	-0.0121

TABLE 7.68

DENSITY, REYNOLDS STRESS $\rho\overline{u'v'}$, TOTAL SHEAR STRESS, PRODUCTION OF TURBULENCE KINETIC ENERGY BY SHEAR AND MEAN LATERAL VELOCITY, v, FOR x/H = 0.497

THE HEATED WALL

y mm	ρ kg/m³	$\rho\overline{u'v'}\times10^3$ kg/m.s²	$\tau\times10^3$ N/m²	$-\rho\overline{u'v'}du/dy\times10^3$ kg/m.s³	v m/s
1	1.021	0.00	2.09	0.00	0.0001
2	1.032	0.00	1.50	0.00	0.0000
3	1.042	0.02	0.98	-0.99	0.0001
4	1.049	0.06	0.55	-1.81	0.0001
5	1.054	0.21	0.05	-2.68	0.0002
6	1.059	0.42	-0.30	-2.69	0.0000
7	1.062	0.59	-0.59	0.00	0.0001
8	1.066	0.80	-0.85	2.26	-0.0003
9	1.069	0.98	-1.08	4.69	-0.0001
10	1.071	1.16	-1.27	6.42	0.0000
20	1.081	2.30	-2.41	12.59	-0.0006
30	1.086	2.79	-2.89	12.78	-0.0009
40	1.089	2.99	-3.08	11.95	-0.0009
50	1.090	2.99	-3.06	10.93	-0.0017
60	1.091	2.74	-2.80	9.01	-0.0048
70	1.092	2.39	-2.46	7.20	-0.0043
100	1.092	1.52	-1.55	2.67	-0.0053
150	1.092	0.81	-0.81	0.00	-0.0084
200	1.092	0.31	-0.31	0.00	-0.0071
250	1.092	0.05	-0.05	0.00	-0.0069

THE COOLED WALL

y mm	ρ kg/m³	$\rho\overline{u'v'}\times10^3$ kg/m.s²	$\tau\times10^3$ N/m²	$-\rho\overline{u'v'}du/dy\times10^3$ kg/m.s³	v m/s
1	1.152	0.00	1.69	0.00	0.0000
2	1.141	0.00	1.15	0.00	-0.0001
3	1.131	0.01	0.72	-0.44	-0.0002
4	1.124	0.06	0.35	-1.19	-0.0002
5	1.120	0.16	0.04	-1.60	-0.0002
6	1.116	0.30	-0.21	-1.23	-0.0002
7	1.113	0.43	-0.43	0.00	-0.0002
8	1.110	0.59	-0.61	0.60	-0.0003
9	1.108	0.68	-0.76	2.76	-0.0004
10	1.106	0.84	-0.90	2.56	-0.0001
20	1.098	1.52	-1.60	6.44	0.0004
30	1.094	1.65	-1.74	6.39	0.0006
40	1.093	1.49	-1.56	4.94	0.0004
50	1.092	1.27	-1.33	3.95	0.0000
60	1.091	0.98	-1.05	2.66	0.0000
70	1.091	0.68	-0.72	1.65	-0.0002
100	1.092	-0.12	0.10	-0.16	0.0002
150	1.092	-0.55	0.55	-0.03	-0.0002
200	1.092	-0.17	0.17	0.00	-0.0016
250	1.092	0.05	-0.05	0.00	-0.0030

TABLE 7.69

DENSITY, REYNOLDS STRESS $\rho\overline{u'v'}$, TOTAL SHEAR STRESS, PRODUCTION OF TURBULENCE KINETIC ENERGY BY SHEAR AND LATERAL MEAN VELOCITY, v, FOR x/H = 0.630

THE HEATED WALL

y mm	ρ kg/m^3	$\rho\overline{u'v'}\times10^3$ kg/m.s^2	$\tau\times10^3$ N/m^2	$-\rho\overline{u'v'}du/dy\times10^3$ kg/m.s^3	v m/s
1	1.013	0.00	1.97	0.00	0.0001
2	1.023	0.01	1.40	-0.71	-0.0001
3	1.030	0.03	0.92	-1.44	0.0001
4	1.037	0.06	0.51	-1.75	0.0002
5	1.042	0.15	0.19	-2.39	0.0003
6	1.047	0.30	-0.14	-2.50	0.0005
7	1.051	0.46	-0.42	-0.98	0.0007
8	1.053	0.66	-0.66	0.00	0.0009
9	1.056	0.86	-0.88	0.99	0.0009
10	1.058	1.05	-1.08	1.60	0.0007
20	1.068	2.25	-2.36	12.03	0.0011
30	1.072	2.89	-2.99	13.98	0.0012
40	1.075	3.20	-3.28	11.88	0.0012
50	1.076	3.26	-3.32	10.60	0.0016
60	1.077	3.12	-3.19	8.90	0.0025
70	1.078	3.05	-3.09	8.11	0.0021
100	1.078	2.27	-2.31	4.50	0.0016
150	1.078	0.98	-0.98	0.09	0.0016
200	1.078	0.22	-0.22	0.02	0.0026
250	1.078	0.01	-0.01	0.00	0.0030

THE COOLED WALL

y mm	ρ kg/m^3	$\rho\overline{u'v'}\times10^3$ kg/m.s^2	$\tau\times10^3$ N/m^2	$-\rho\overline{u'v'}du/dy\times10^3$ kg/m.s^3	v m/s
1	1.148	0.00	1.77	0.00	0.0000
2	1.135	0.00	1.16	0.00	-0.0001
3	1.123	0.01	0.66	-0.40	-0.0001
4	1.117	0.06	0.27	-0.93	0.0000
5	1.110	0.16	-0.03	-0.95	0.0000
6	1.107	0.31	-0.31	0.00	0.0001
7	1.103	0.50	-0.54	1.01	0.0002
8	1.100	0.61	-0.72	3.09	0.0002
9	1.097	0.68	-0.87	6.24	0.0002
10	1.095	0.91	-1.01	4.04	0.0002
20	1.086	1.60	-1.69	7.26	-0.0005
30	1.082	1.74	-1.83	7.44	0.0000
40	1.080	1.66	-1.74	5.54	-0.0002
50	1.079	1.41	-1.48	3.97	0.0018
60	1.079	1.08	-1.12	2.28	0.0028
70	1.079	0.76	-0.79	1.45	0.0043
100	1.079	-0.04	0.03	-0.03	0.0042
150	1.079	-0.27	0.27	-0.01	0.0089
200	1.079	-0.22	0.22	0.00	0.0072
250	1.079	-0.18	0.18	0.00	0.0074

TABLE 7.70

DENSITY, REYNOLDS STRESS $\rho\overline{u'v'}$, TOTAL SHEAR STRESS, PRODUCTION OF TURBULENCE KINETIC ENERGY BY SHEAR AND LATERAL MEAN VELOCITY, v, FOR x/H = 0.765

THE HEATED WALL

y mm	ρ kg/m³	$\rho\overline{u'v'}\times10^3$ kg/m.s²	$\tau\times10^3$ N/m²	$-\rho\overline{u'v'}du/dy\times10^3$ kg/m.s³	v m/s
1	1.007	0.00	1.75	0.00	-0.0001
2	1.016	0.01	1.26	-0.63	0.0003
3	1.022	0.00	0.86	0.00	0.0003
4	1.029	0.05	0.48	-1.38	0.0002
5	1.033	0.11	0.22	-1.84	0.0004
6	1.037	0.29	-0.07	-2.98	0.0003
7	1.041	0.42	-0.31	-2.06	0.0005
8	1.042	0.61	-0.53	-2.24	0.0004
9	1.045	0.77	-0.73	-1.64	0.0004
10	1.046	0.91	-0.92	0.27	0.0006
20	1.055	2.06	-2.15	9.28	0.0016
30	1.059	2.69	-2.77	10.79	0.0017
40	1.062	2.98	-3.06	10.41	0.0022
50	1.063	3.06	-3.14	9.74	0.0026
60	1.064	3.02	-3.09	8.37	0.0026
70	1.064	2.90	-2.95	6.88	0.0033
100	1.065	2.35	-2.39	4.50	0.0040
150	1.064	1.22	-1.22	0.00	0.0064
200	1.064	0.41	-0.41	-0.03	0.0063
250	1.064	0.17	-0.17	-0.01	0.0078

THE COOLED WALL

y mm	ρ kg/m³	$\rho\overline{u'v'}\times10^3$ kg/m.s²	$\tau\times10^3$ N/m²	$-\rho\overline{u'v'}du/dy\times10^3$ kg/m.s³	v m/s
1	1.134	0.00	1.83	0.00	0.0000
2	1.120	0.00	1.12	0.00	0.0000
3	1.107	0.01	0.54	-0.32	0.0000
4	1.100	0.04	0.08	-0.28	0.0000
5	1.092	0.27	-0.25	-0.28	0.0000
6	1.086	0.46	-0.54	1.86	0.0000
7	1.081	0.74	-0.79	2.25	0.0000
8	1.078	0.91	-0.99	3.69	0.0002
9	1.075	0.92	-1.16	10.37	0.0002
10	1.073	1.12	-1.29	9.11	0.0004
20	1.061	1.82	-1.94	10.33	0.0010
30	1.058	1.86	-1.94	6.70	0.0033
40	1.056	1.62	-1.68	4.44	0.0043
50	1.055	1.33	-1.37	2.76	0.0052
60	1.055	1.04	-1.08	1.49	0.0064
70	1.055	0.78	-0.80	0.74	0.0058
100	1.056	0.29	-0.30	0.10	0.0011
150	1.056	-0.02	0.02	0.00	0.0011
200	1.056	-0.01	0.01	0.00	0.0027
250	1.056	0.04	-0.04	-0.01	0.0059

TABLE 7.71

DENSITY, REYNOLDS STRESS $\rho\overline{u'v'}$, TOTLA SHEAR STRESS, PRODUCTION OF TURBULENCE KINETIC ENERGY BY SHEAR AND LATERAL MEAN VELOCITY, v, FOR x/H = 0.849

THE HEATED WALL

y mm	ρ kg/m³	$\rho\overline{u'v'}\times10^3$ kg/m.s²	$\tau\times10^3$ N/m²	$-\rho\overline{u'v'}du/dy\times10^3$ kg/m.s³	v m/s
1	1.011	0.00	1.68	0.00	0.0001
2	1.020	-0.01	1.23	-0.61	0.0002
3	1.027	0.00	0.85	0.00	0.0001
4	1.030	0.03	0.52	-0.83	0.0001
5	1.034	0.07	0.26	-1.16	0.0001
6	1.037	0.24	0.00	-2.65	0.0002
7	1.040	0.31	-0.22	-1.33	0.0002
8	1.043	0.42	-0.42	0.00	0.0003
9	1.045	0.62	-0.62	0.00	0.0004
10	1.050	0.78	-0.79	0.32	0.0003
20	1.055	1.88	-1.97	8.49	0.0007
30	1.059	2.50	-2.59	11.17	0.0009
40	1.061	2.84	-2.92	10.23	0.0014
50	1.062	3.02	-3.08	9.53	0.0021
60	1.063	3.03	-3.09	8.77	0.0026
70	1.064	2.97	-3.03	7.83	0.0024
100	1.065	2.51	-2.55	4.64	0.0035
150	1.064	1.37	-1.37	0.00	-0.0002
200	1.064	0.43	-0.43	-0.06	-0.0005
250	1.064	0.11	-0.11	-0.01	-0.0011

THE COOLED WALL

y mm	ρ kg/m³	$\rho\overline{u'v'}\times10^3$ kg/m.s²	$\tau\times10^3$ N/m²	$-\rho\overline{u'v'}du/dy\times10^3$ kg/m.s³	v m/s
1	1.135	0.00	1.87	0.00	0.0000
2	1.124	-0.01	1.16	0.66	0.0000
3	1.110	-0.01	0.58	0.32	0.0000
4	1.100	-0.01	0.12	0.07	0.0001
5	1.091	0.22	-0.22	0.00	0.0004
6	1.085	0.43	-0.49	1.33	0.0002
7	1.080	0.57	-0.71	4.09	0.0003
8	1.075	0.46	-0.86	8.96	0.0003
9	1.071	0.25	-0.96	8.54	0.0003
10	1.068	0.84	-1.04	8.21	0.0002
20	1.061	1.18	-1.29	6.70	0.0014
30	1.059	1.20	-1.26	3.40	0.0008
40	1.058	1.14	-1.17	1.75	0.0011
50	1.058	1.04	-1.05	0.67	-0.0010
60	1.058	0.94	-0.96	1.20	-0.0024
70	1.058	0.85	-0.87	0.88	-0.0044
100	1.058	0.53	-0.54	0.37	-0.0036
150	1.059	0.15	-0.16	0.04	-0.0034
200	1.059	0.08	-0.10	0.00	-0.0025
250	1.059	0.13	-0.13	-0.01	-0.0015

TABLE 7.72

DENSITY, REYNOLDS STRESS $\rho\overline{u'v'}$, TOTAL SHEAR STRESS, PRODUCTION OF TURBULENCE KINETIC ENERGY BY SHEAR AND LATERAL MEAN VELOCITY, v, FOR x/H = 0.898

THE HEATED WALL

y mm	ρ kg/m³	$\rho\overline{u'v'}\times10^3$ kg/m.s²	$\tau\times10^3$ N/m²	$-\rho\overline{u'v'}du/dy\times10^3$ kg/m.s³	v m/s
1	1.014	0.00	1.64	0.00	0.0001
2	1.023	-0.02	1.22	1.19	0.0002
3	1.029	-0.01	0.84	0.42	0.0001
4	1.035	0.01	0.52	-0.27	0.0001
5	1.039	-0.03	0.26	0.34	0.0001
6	1.043	0.09	0.00	-0.43	0.0003
7	1.045	0.26	-0.23	-0.37	0.0005
8	1.047	0.44	-0.44	0.00	0.0006
9	1.049	0.64	-0.64	0.00	0.0008
10	1.051	0.80	-0.80	0.00	0.0008
20	1.057	1.94	-2.03	7.86	0.0024
30	1.060	2.69	-2.78	10.47	0.0032
40	1.062	3.08	-3.15	11.36	0.0030
50	1.064	3.23	-3.31	11.00	0.0035
60	1.064	3.32	-3.38	9.59	0.0042
70	1.065	3.30	-3.34	7.36	0.0039
100	1.066	2.78	-2.81	4.48	0.0025
150	1.066	1.45	-1.45	0.35	-0.0008
200	1.066	0.56	-0.56	-0.04	-0.0042
250	1.066	0.14	-0.14	-0.01	-0.0049

THE COOLED WALL

y mm	ρ kg/m³	$\rho\overline{u'v'}\times10^3$ kg/m.s²	$\tau\times10^3$ N/m²	$-\rho\overline{u'v'}du/dy\times10^3$ kg/m.s³	v m/s
1	1.144	0.01	1.67	-1.02	0.0000
2	1.126	0.00	1.01	0.00	0.0001
3	1.113	0.00	0.51	0.00	0.0002
4	1.102	0.01	0.15	-0.09	0.0003
5	1.094	-0.05	-0.05	-0.28	0.0008
6	1.087	0.08	-0.23	0.54	0.0014
7	1.081	0.17	-0.32	1.23	0.0014
8	1.078	0.18	-0.38	1.68	0.0019
9	1.075	0.17	-0.41	1.93	0.0020
10	1.073	0.27	-0.42	1.97	0.0020
20	1.066	0.28	-0.35	0.90	0.0025
30	1.064	0.27	-0.31	0.64	0.0024
40	1.064	0.29	-0.33	0.58	-0.0005
50	1.064	0.29	-0.32	0.46	-0.0002
60	1.064	0.23	-0.26	0.31	-0.0021
70	1.064	0.15	-0.17	0.17	-0.0031
100	1.064	-0.06	0.04	-0.06	-0.0033
150	1.065	-0.21	0.20	-0.05	-0.0046
200	1.065	-0.06	0.06	0.00	-0.0041
250	1.065	0.09	-0.09	0.00	-0.0041

TABLE 7.73

DENSITY, REYNOLDS STRESS $\rho\overline{u'v'}$, TOTAL SHEAR STRESS, PRODUCTION OF TURBULENCE KINETIC ENERGY BY SHEAR AND LATERAL MEAN VELOCITY, v, FOR x/H = 0.949

THE HEATED WALL

y mm	ρ kg/m³	$\rho\overline{u'v'}\times10^3$ kg/m.s²	$\tau\times10^3$ N/m²	$-\rho\overline{u'v'}du/dy\times10^3$ kg/m.s³	v m/s
1	1.019	0.01	1.40	-0.69	0.0001
2	1.027	0.02	0.96	-0.98	0.0002
3	1.033	0.02	0.54	-0.56	0.0001
4	1.037	0.06	0.12	-0.57	0.0012
5	1.041	0.53	-0.19	-8.82	0.0015
6	1.044	0.72	-0.52	-7.12	0.0019
7	1.047	0.95	-0.80	-7.07	0.0023
8	1.049	1.12	-1.01	-5.95	0.0027
9	1.050	1.23	-1.20	-1.73	0.0024
10	1.052	1.39	-1.39	0.00	0.0063
20	1.059	2.85	-2.93	11.25	0.0054
30	1.062	3.98	-4.05	12.66	0.0063
40	1.064	4.76	-4.82	13.75	0.0083
50	1.066	5.20	-5.27	13.84	0.0103
60	1.067	5.39	-5.43	13.20	0.0080
70	1.067	5.34	-5.38	11.74	0.0083
100	1.068	4.70	-4.72	6.67	0.0039
150	1.068	2.95	-2.95	0.59	-0.0003
200	1.068	1.37	-1.37	0.15	-0.0023
250	1.068	0.74	-0.74	0.08	-0.0017

THE COOLED WALL

y mm	ρ kg/m³	$\rho\overline{u'v'}\times10^3$ kg/m.s²	$\tau\times10^3$ N/m²	$-\rho\overline{u'v'}du/dy\times10^3$ kg/m.s³	v m/s
1	1.140	0.00	1.44	0.00	0.0001
2	1.123	-0.01	0.82	0.48	0.0004
3	1.105	0.00	0.39	0.00	0.0010
4	1.093	0.05	0.14	-0.55	0.0014
5	1.084	-0.13	0.04	-0.53	0.0020
6	1.077	-0.05	-0.03	-0.22	0.0030
7	1.073	-0.02	-0.06	-0.09	0.0040
8	1.070	-0.02	-0.06	-0.09	0.0043
9	1.069	-0.02	-0.06	-0.09	0.0042
10	1.068	-0.05	-0.03	-0.20	0.0052
20	1.066	-0.13	0.10	-0.18	0.0070
30	1.064	-0.20	0.18	-0.22	0.0072
40	1.063	-0.29	0.26	-0.53	0.0070
50	1.063	-0.39	0.36	-0.74	0.0040
60	1.063	-0.51	0.48	-0.88	0.0041
70	1.062	-0.61	0.58	-0.83	0.0056
100	1.063	-0.70	0.69	-0.58	-0.0006
150	1.063	-0.36	0.36	-0.01	-0.0010
200	1.063	0.28	-0.28	0.01	-0.0015
250	1.063	0.67	-0.67	0.02	-0.0019

CONCLUSIONS

The regime that existed in all Series was the transitional boundary layer regime. This was established for the Q.M.C. Series by visual inspection of the velocity profiles and confirmed by P.S.D. calculations. The Q.M.C. results allowed deductions to be made which inferred that the regime for the Poitiers Series was also transitional boundary layer.

The thermal boundary conditions on all closing boundaries were seen to affect both the temperature and velocity fields.

As the level of insulation on the vertical side walls increased, with all other parameters constant, the non-dimensional temperature at the vertical cavity centre-line increased. This lead to a decrease in the velocities at the heated wall, and an increase in the velocities at the cooled wall.

The increase in vertical side wall insulation also had another effect, this was to reduce the mass flow down the vertical side walls which originated from the flow across the ceiling.

The thermal boundary conditions at the floor were such that the turbulence in the floor boundary layer almost totally collapsed, whereas the thermal boundary conditions on the ceiling were such that the turbulence in the ceiling boundary layer only underwent partial collapse. This difference in the collapse of the turbulence in the floor and ceiling boundary layers resulted in velocity profiles which were not antisymmetric.

The collapse of the turbulence in the floor boundary layer meant that a fully discernible transition process occurred at the heated wall in all Series. The base frequencies of transition, detected by P.S.D. calculations using the Q.M.C. data, were in good agreement with those predicted using equation (2.5) from Gebhart and Mahajan [25]. The most important variable in their equation was the local temperature difference.

The data from the Q.M.C. Series also indicated that a very limited transition process took place in the near wall fluid at the cooled wall. The existence of transition processes at each wall was supported by the trends in $T'_{R.M.S.}$, $u'_{R.M.S.}$, τ_w, mass flow and the local heat transfer coefficient. The maximum in peak mean velocity was also seen to be associated with transition at the heated wall and did not occur at mid-height.

The non antisymmetric nature of the flow was emphasised by the comparison of temperature and velocity profiles from the heated and cooled walls. These were different thus showing that the flow characteristics in the fully developed regions of each boundary layer were different.

The non antisymmetric nature of the flow was again shown by the calculations for lateral velocity. These calculations showed the existence of a vortex in the central region of the upper third of the cavity. A complementary vortex was not found in the lower third of the cavity.

Horizontal temperature inversions were seen in regions of fully developed turbulence. These were associated with regions of velocity reversal. This observation was most striking in the Poitiers Series.

Excellent collapse of the mean temperature profiles from the Q.M.C. Series was found when using θ against Nu_Y where $\theta \equiv (T - T_{MIN})/(T_W - T_{MIN})$ and Nu_Y was evaluated at the wall temperature. The wall temperature was also found to be a suitable reference temperature for the calculations of local heat transfer and two component correlations.

Whilst this temperature representation again produced excellent collapse of the Poitiers data, the curve onto which they collapsed showed that the development of the temperature profiles in the two cavities were different. This was brought about by the reduction in cavity width, which also had other effects. In the fully developed turbulence regions of the Poitiers cavity the mean velocity profiles met at the cavity centre-line without there being any regions of reversed velocity as were seen in the Q.M.C. Series. The values of $u'_{R.M.S.}$ were also seen to be affected, as they were lower in the region of fully developed turbulence, and higher in the lower cavity region, for the Poitiers cavity, when both the Poitiers and Q.M.C. cavities were subject to a similar wall temperature difference with H being constant.

The non-dimensional centre-line temperature could be approximated to a straight line for the entire cavity height, but a better representation was of two straight lines, one applicable to the lower region where a flow with "laminar aspects" was present at the heated wall, and the other applicable to the rest of the cavity.

The equation for local heat transfer could also be divided into two regions, before and after transition, at each wall. For the regions of fully developed flow the power on Gr_x was always greater than the value of 1/3 which is considered applicable to vertical flat plate flow.

Of all the velocity scales proposed to-date, only the shear velocity was seen to be suitable for the present data when it was used in conjunction with Nu_Y in the near wall region, and y/δ for the entire boundary layer width.

For all Series the thermal sub-layer was found to be 1.6mm thick, whereas the viscous sub-layer was deduced as being 4mm thick.

The vertical turbulent transport of heat was seen to be in the positive x direction in both boundary layers, and the lateral turbulent transport of heat was found to be in the positive y direction at each wall.

The production of turbulence kinetic energy in the near wall region was found to be due to buoyancy, as no general region of negative $\overline{u'v'}$ was found to exist.

The distribution of total shear stress, τ, confirmed that there was no region of constant shear stress.

There was no consistency in either frequency or wavenumber for the limits of any sub-range found in the velocity or temperature P.S.D. distributions.

The exponent relating P.S.D. to frequency in any sub-range has been shown to vary. The variation of stratification with lateral position was only partially responsible for this.

Three sub-ranges were found within the velocity P.S.D. distributions, whilst four were found for the temperature data. The exponents for each corresponding buoyancy and inertial sub-range of the velocity and temperature data were generally similar, whereas those of the dissipative sub-range for the temperature data were generally lower than those for the velocity data.

REFERENCES

[1] Ziai, S., [1983].
Turbulent Natural Convection in a Large Rectangular Air Cavity.
Ph.D. Thesis, University of London, 1983.

[2] Batchelor, G.K., [1954].
Heat Transfer by Free Convection Across a Closed Cavity Between Vertical Boundaries at Different Temperatures.
Quarterly of Applied Mathematics, Vol. 12, No. 3, pp 209-233, 1954.

[3] Dixon, M. and Probert, S.D., [1975].
Heat-Transfer Regimes in Vertical, Plane-Walled, Air-Filled Cavities.
Int. J. Heat Mass Trans., Vol. 18, pp 709-710, 1975.

[4] Eckert, E.R.G., and Carlson, W.O., [1961].
Natural Convection in an Air Layer Enclosed Between Two Vertical Plates With Different Temperatures.
Int. J. Heat Mass Trans., Vol. 2, pp 106-120, 1961.

[5] Seki, N., Fukusako, S. and Inaba, H., [1978].
Heat Transfer of Natural Convection in a Rectangular Cavity With Vertical Walls of Different Temperatures.
Bull. J.S.M.E., Vol. 21, No. 152, pp 246-253, 1978.

[6] Bauman, F., Gadgil, A., Kammerud, R. and Greif, R., [1980].
Buoyancy Driven Convection in Rectangular Enclosures: Experimental Results and Numerical Calculations.
A.S.M.E. Paper 80-HT-66, 1980.

[7] Mull, W. and Reiher, H., [1930].
Beih., Gesundh.-Ing.
Reihe 1, Heft 28, 1930.

[8] MacGregor, R.K. and Emery, A.F., [1969].
Free Convection Through Vertical Plane Layers - Moderate and High Prandtl Number Fluids.
Trans. A.S.M.E. Series C, J. Heat Trans., Vol. 91, No. 3, pp 391-403, 1969.

[9] Elsherbiny, S.M., Raithby, G.D. and Hollands, K.G.T., [1982].
Heat Transfer by Natural Convection Across Vertical and Inclined Air Layers.
Trans. A.S.M.E. Series C, J. Heat Trans., Vol. 104, pp 96-102, 1982.

[10] Griffiths, E. and Davis, A.H., [1922].
The Transmission of Heat by Radiation and Convection.
Food Investigation Board, S.R.9, D.S.I.R., H.M. Stationary Office, London, 1922.

[11] Elder, J.W., [1965].
Turbulent Free Convection in a Vertical Slot.
J. Fluid Mech., Vol. 23, Part 1, pp 99-111, 1965.

[12] Cowan, G.H., Lovegrove, P.C. and Quarini, G.L., [1982].
Turbulent Natural Convection Heat Transfer in Vertical Single Water-Filled Cavities.
Proc. Int. Heat Trans. Conf., Munich, Vol. 2, Paper NC13, pp 195-203, 1982.

[13] MacGregor, R.K. and Emery, A.F., [1971].
Prandtl Number Effects on Natural Convection in an Enclosed Vertical Layer.
Trans. A.S.M.E. Series C, J. Heat Trans., Vol. 93, pp 253-254, 1971.

[14] Schmidt, F.W. and Wang, D.F., [1982].
Experimental Study of Turbulent Natural Convection in an Enclosure.
A.S.M.E. Paper, 82-WA/HT-72, 1982.

[15] Giel, P.W. and Schmidt, F.W., [1986].
An Experimental Study of High Rayleigh Number Natural Convection in an Enclosure.
Proc. Int. Heat Trans. Conf., San Francisco, Vol. 4, pp 1459-1464, 1986.

[16] Saunders, O.A., [1939].
Natural Convection in Liquids.
Proc. Roy. Soc. A, Vol. 172, p. 55, 1939.

[17] Raithby, G.D. and Hollands, K.G.T., [1975].
A General Method of Obtaining Approximate Solutions to Laminar and Turbulent Free Convection Problems.
Advances in Heat Transfer, Vol. 11, pp 266-317, 1975.

[18] Bohn, M.S., Kirkpatrick, A.T. and Olson, D.A., [1984].
Experimental Study of Three-Dimensional Natural Convection, High-Rayleigh Number.
Trans. A.S.M.E. Series C, J. Heat Trans., Vol. 106, pp 339-345, 1984.

[19] Godeaux, F. and Gebhart, B. [1974].
An Experimental Study of the Transition of Natural Convection Flow Adjacent to a Vertical Surface.
Int. J. Heat Mass Trans., Vol. 17, pp 93-107, 1974.

[20] Jaluria, Y. and Gebhart, B., [1974].
On Transition Mechanisms in Vertical Natural Convection Flow.
J. Fluid Mech., Vol. 66, Part 2, pp 309-337, 1974.

[21] Bergholz, R.F., [1978].
Instability of Steady Natural Convection in a Vertical Fluid Layer.
J. Fluid Mech., Vol. 84, Part 4, pp 743-768, 1978.

[22] Briggs, D.G. and Jones, D.N., [1985].
Two-Dimensional Periodic Natural Convection in a Rectangular Enclosure of Aspect Ratio One.
Trans. A.S.M.E. Series C, J. Heat Trans., Vol. 107, pp 850-854, 1985.

[23] Chenoweth, D.R. and Paolucci, S., [1986].
Natural Convection in an Enclosed Vertical Air Layer with Large Horizontal Temperature Differences.
J. Fluid Mech., Vol. 169, pp 173-210, 1986.

[24] Le Quere, P. and Alziary de Roquefort, T., [1986].
Transition to Unsteady Natural Convection of Air in Vertical Differentially Heated Cavities: Influence of Thermal Boundary Conditions on the Horizontal Walls.
Proc. Int. Heat Trans. Conf., San Francisco, Vol. 4, pp 1533-1538, 1986.

[25] Gebhart, B. and Mahajan, R., [1975].
Characteristic Disturbance Frequency in Vertical Natural Convection Flow.
Int. J. Heat Mass Trans., Vol. 18, pp 1143-1148, 1975.

[26] Dastbaz, A., [1983].
The Structure of Turbulence in a Natural Convection Boundary Layer on a Vertical Flat Plate.
Ph.D. Thesis, University of London, 1983.

[27] Smith, R.R., [1972].
Characteristics of Turbulence in Free Convection Flow Past a Vertical Plate.
Ph.D. Thesis, University of London, 1972.

[28] Cheesewright, R. and Doan, K.S., [1978].
Space-Time Correlation Measurements in a Turbulent Natural Convection Boundary Layer.
Int. J. Heat Mass Trans., Vol. 21, pp 911-921, 1978.

[29] Pera, L. and Gebhart, B., [1973].
On the Stability of Natural Convection Boundary Layer Flow Over Horizontal and Slightly Inclined Surfaces.
Int. J. Heat Mass Trans., Vol. 16, pp 1147-1163, 1973.

[30] Renault, C. and Doan-Kim-Son, [1983].
Turbulent Natural Convection in a Rectangular Enclosure.
Mechanics Reasearch Communications, Vol. 10, No. 4, pp 245-251, 1983.

[31] Ralph, S., Ince, N. and Betts, P.L., [1985].
The Measurement of Low Velocities in the Natural Convection of Air: Comparison of a Transient Recorder and a Counter System.
Int. Conf. on Laser Anemometry - Advances and Application, 16th-17th Dec., Manchester, U.K., Paper 7, pp 155-164, 1985.

[32] Renault, C., [1983].
Convection Naturelle Turbulente a Fort Nombre de Rayleigh dans une Cavite Paraellelepipedique de Grand Allongement.
These Pour Obtenir le Grade de Docteur Ingenieur, L'Universite de Poitiers, 1983.

[33] Ozoe, H., Mouri, A., Ohmuro, M., Churchill, S.W. and Lior, N., [1985].
Numerical Calculations of Laminar and Turbulent Natural Convection in Water in Rectangular Channels Heated and Cooled Isothermally on the Opposing Vertical Walls.
Int. J. Heat Mass Trans., Vol. 28, No. 1, pp 125-138, 1985.

[34] Markatos, N.C., and Pericleous, K.A., [1984].
Laminar and Turbulent Natural Convection in an Enclosed Cavity.
Int. J. Heat Mass Trans., Vol. 27, No. 5, pp 755-772, 1984.

[35] Kutateladze, S.S, Kirdyashkin, A.G. and Ivakin, V.P., [1972].
Turbulent Natural Convection on a Vertical Flat Plate and in a Vertical Layer.
Int. J. Heat Mass Trans., Vol. 15, pp 193-202, 1972.

[36] Bayley, F.J., [1955].
An Analysis of Turbulent Free-Convection Heat-Transfer.
Proc. Inst. Mech. Engs., Vol. 169, pp 361-368, 1955.

[37] Jaluria, Y. and Gebhart, B., [1974].
Stability and Transition of Buoyancy-Induced Flows in a Stratified Medium.
J. Fluid Mech., Vol. 66, Part 3, pp 593-612, 1974.

[38] Chen, C.C. and Eichhorn, R., [1976].
Natural Convection From a Vertical Surface to a Thermally Stratified Fluid.
Trans. A.S.M.E. Series C, J. Heat Trans., Vol. 98, pp 446-451, 1976.

[39] Gill, A.E., [1966].
The Boundary-Layer Regime for Convection in a Rectangular Cavity.
J. Fluid Mech., Vol. 26, Part 3, pp 515-536, 1966.

[40] deVahl Davis, G., [1968].
Laminar Natural Convection in an Enclosed Rectangular Cavity.
Int. J. Heat Mass Trans., Vol. 11, pp 1675-1693, 1968.

[41] Zhukauskas, A.A., [1984].
Enhancement of Convective Heat Transfer by Artificial Roughness.
Thermal Eng., Vol. 31, No. 3, pp 127-132, 1984.

[42] Ierokipiotis, E.G., [1983].
The Study of the Development of a Turbulent Natural Convection Boundary Layer Using Laser-Doppler Anemometry.
Ph.D. Thesis, University of London, 1983.

[43] Sparrow, E.M. and Azevedo, L.F.A., [1985].
Vertical-Channel Natural Convection Spanning Between the Fully-Developed Limit and the Single-Plate Boundary-Layer Limit.
Int. J. Heat Mass Trans., Vol. 28, No. 10, pp 1847-1857, 1985.

[44] Ostrach, S., [1972].
Natural Convection in Enclosures.
Advances in Heat Transfer, Vol. 8, pp 161-227, 1972.

[45] Miyamoto, M., Kajino, H., Kurima, J. and Takanami, I., [1982].
Development of Turbulence Characteristics in a Vertical Free Convection Boundary Layer.
Proc. Int. Heat Trans. Conf., Munich, Vol. 2, Paper NC34, pp 323-328, 1982.

[46] Kitamura, K., Koike, M., Fukuoka, I. and Saito, T., [1985].
Large Eddy Structure and Heat Transfer of Turbulent Natural Convection Along a Vertical Flat Plate.
Int. J. Heat Mass Trans., Vol. 28, No. 4, pp 837-850, 1985.

[47] To, W.M. and Humphrey, J.A.C., [1986].
Numerical Simulation of Buoyant, Turbulent Flow - 1. Free Convection Along a Heated, Vertical, Flat Plate.
Int. J. Heat Mass Trans., Vol. 29, No. 4, pp 573-592, 1986.

[48] Bill, R.G. and Gebhart, B., [1979].
The Development of Turbulent Transport in a Vertical Natural Convection Boundary Layer.
Int. J. Heat Mass Trans., Vol. 22, pp 267-276, 1979.

[49] Fraikin, M.P., Portier, J.J. and Fraikin, C.J., [1980].
Application of a k-ε Turbulence Model to an Enclosed Buoyancy Driven Recirculating Flow.
A.S.M.E. Paper 80-HT-68, 1980.

[50] Corrsin, S., [1951].
On the Spectrum of Isotropic Temperature Fluctuations in an Isotropic Turbulence.
J. Appl. Phys., Vol. 22, No. 4, pp 469-473, 1951.

[51] Bolgiano, R., [1959].
Turbulent Spectra in a Stably Stratified Atmosphere.
J. Geophys. Res., Vol. 64, No. 12, pp 2226-2229, 1959.

[52] Papailou, D.D. and Lykoudis, P.S., [1974].
Turbulent Free Convection Flow.
Int. J. Heat Mass Trans., Vol. 17, p. 161, 1974.

[53] Shur, G.N., [1962].
Eksperimental Nyye Issledovaniya Energeticheskogo Spectra Atmosfernoy Turbulentnost.
Trudy Vol. 43, p. 79, Trans. as AID Report T-63-55 Aerospace Info. Div. Lab. Cong., 1962.

[54] Lumley, J.L., [1964].
The Spectrum of Nearly Inertial Turbulence in a Stabily Stratified Fluid.
J. Atmos. Sci., Vol. 21, p. 99, 1964.

[55] Ostrach, S., [1982].
Natural Convection Heat Transfer in Cavities and Cells.
Proc. Int. Heat Trans. Conf., Munich, Vol 1, pp 365-379, 1982.

[56] George, W.K. and Capp, S.P., [1979].
A Theory for Natural Convection Turbulent Boundary Layers Next to Heated Vertical Surfaces.
Int. J. Heat Mass Trans., Vol. 22, pp 813-826, 1979.

[57] Cheesewright, R., [1985].
Turbulent Natural Convection.
Research Report EP5031, Dept. Mech. Eng., Queen Mary College, University of London, 1985.

[58] Zhong, Z.Y., Yang, K.T. and Lloyd, J.R., [1985].
Varaiable Property Effects in Laminar Natural Convection in a Square Enclosure.
Trans. A.S.M.E. Series C, J. Heat Trans., Vol. 107, pp 133-138, 1985.

[59] Cheesewright, R. and Ziai, S., [1986].
Distributions of Temperature and Local Heat-Transfer Rate in Turbulent Natural Convection in a Large Rectangular Cavity.
Proc. Int. Heat Trans. Conf., San Francisco, Vol. 4, pp 1465-1470, 1986.

[60] Siebers, D.L., Moffatt, R.F. and Schwind, R.G., [1985].
Experimental, Variable Properties Natural Convection From a Large, Vertical, Flat Surface.
Trans. A.S.M.E. Series C, J. Heat Trans., Vol. 107, pp 124-132, 1985.

[61] Cheesewright, R. and Ierokipiotis, E.G., [1982].
Velocity Measurements in a Turbulent Natural Convection Boundary Layer.
Proc. Int. Heat Trans. Conf., Munich, Vol. 2, Paper NC31, pp 305-309, 1982.

[62] Catton, I., Ayyaswamy, P.S. and Clever, R.M., [1974].
Natural Convection Flow in a Finite, Rectangular Slot Arbitrarily Oriented With Respect to the Gravity Vector.
Int. J. Heat Mass Trans., Vol. 17, pp 173-184, 1974.

[63] Elsherbiny, S.M., Hollands, K.G.T. and Raithby, G.D., [1982].
Effect of Thermal Boundary Conditions on Natural Convection in Vertical and Inclined Air Layers.
Trans. A.S.M.E. Series C, J. Heat Trans., Vol. 104, pp 515-520, 1982.

[64] Bilski, S.M., Lloyd, J.R. and Yang, K.T., [1986].
An Experimental Investigation of the Laminar Natural Convection Velocity Field in Square and Partitioned Enclosures.
Proc. Int. Heat Trans. Conf., San Francisco, Vol. 4, pp 1513-1518, 1986.

[65] Kim, D.M. and Viskanta, R., [1985].
Effect of Wall Heat Conduction on Natural Convection Heat Transfer in a Square Enclosure.
Trans. A.S.M.E. Series C, J. Heat Trans., Vol. 107, pp 139-146, 1985.

[66] Ozoe, H., Ohmuro, M., Mouri, A., Nishima, S., Sayama, H. and Churchill, S.W., [1983].
Laser-Doppler Measurements of the Velocity Along a Heated Vertical Wall of a Rectangular Enclosure.
Trans. A.S.M.E. Series C, J. Heat Trans., Vol. 105, pp 782-788, 1983.

[67] Mallinson, G.D., [1973].
Natural Convection in Enclosed Cavities.
Ph.D. Thesis, University of New South Wales, Australia, 1973.

[68] Webster, C.A.G., [1964].
An Experimental Study of Turbulence in a Density-Stratified Shear Flow.
J. Fluid Mech., Vol. 19, pp 221-245, 1964.

[69] Arya, S.P.S., [1975].
Buoyancy Effects in a Horizontal Flat-Plate Boundary Layer.
J. Fluid Mech., Vol. 68, pp 321-343, 1975.

[70] Gibson, M.M. and Launder, B.E., [1976].
On the Calculation of Horizontal, Turbulent, Free Shear Flows Under Gravitational Influence.
Trans. A.S.M.E. Series C, J. Heat Trans., Vol. 98, pp 81-87, 1976.

[71] Gibson, M.M. and Launder, B.E., [1978].
Ground Effects on Pressure Fluctuations in the Atmospheric Boundary Layer.
J. Fluid Mech., Vol. 86, pp 491-511, 1978.

[72] Launder, B.E., [1975].
On the Effects of a Gravitational Field on the Turbulent Transport of Heat and Momentum.
J. Fluid Mech., Vol. 67, pp 569-581, 1975.

[73] Morrison, G.L. and Tran, V.Q., [1978].
Laminar Flow Structure in Vertical Free Convective Cavities.
Int. J. Heat Mass Trans., Vol. 21, pp 203-213, 1978.

[74] Linthorst, S.J.M., Schinkel, W.M.M. and Hoogendoorn, C.J., [1981].
Flow Structure With Natural Convection in Inclined Air-Filled Enclosures.
Trans. A.S.M.E. Series C, J. Heat Trans., Vol. 103, pp 535-539, 1981.

[75] Churchill, S.W. and Chu, H.S., [1975].
Correlating Equations for Laminar and Turbulent Free Convection From a Vertical Plate.
Int. J. Heat Mass Trans., Vol. 18, pp 1323-1329, 1975.

[76] Viskanta, R., Kim, D.M. and Gau, C., [1986].
Three-Dimensional Natural Convection Heat Transfer of a Liquid Metal in a Cavity.
Int. J. Heat Mass Trans., Vol. 29, No. 3, pp 475-485, 1986.

[77] Fand, R.M. and Brucker, J., [1983].
A Correlation for Heat Transfer by Natural Convection From Horizontal Cylinders That Accounts for Viscous Dissipation.
Int. J. Heat Mass Trans., Vol. 26, No. 5, pp 709-726, 1983.

[78] Jakob, M., [1949].
Heat Transfer.
J. Wiley and Sons, 1949.

[79] Ziai, S. and Chessewright, R., [1980].
The Q.M.C. Large Air Cavity. An Apparatus for the Study of Turbulent Natural Convection in a Rectangular Enclosure.
HTFS/PFW197/P23/1980, AERE-G.1799, Nov. 1980.

[80] King, K.J., [1984].
A Summary of Laser Doppler Anemometry.
Q.M.C. Faculty of Engineering, Research Report EP 5032, Nov. 1984.

[81] King, K.J., [1984].
A Description of the DISA Laser Doppler Anemometer Used on the N.N.C. Cavity.
Q.M.C. Faculty of Engineering, Research Report EP 5033, Nov. 1984.

[82] King, K.J., [1985].
M.Phil. to Ph.D. Transition Report on Turbulent Natural Convection in Rectangular Cavities.
Dept. Mech. Eng., Q.M.C. Faculty of Engineering, Summer 1985.

[83] Gray, D.D. and Giorgini, A., [1976].
The Validity of the Boussinesq Approximation for Liquids and Gases.
Int. J. Heat Mass Trans., Vol 19, pp 545-551, 1976.

[84] Schlicting, H. [1948].
Boundary Layer Theory.
John Wiley and Sons, Inc., 1948.

[85] Cheesewright, R., King, K.J. and Ziai, S., [1986].
Experimental Data for the Validation of Computer Codes for the Prediction of Two-Dimensional Buoyant Cavity Flows.
ASME Winter Annual Meeting, Anaheim, U.S.A., December, 1986.

[86] Otnes, R.K. and Enochson, L., [1978].
Applied Time Series Analysis Volume 1 Basic Techniques.
John Wiley and Sons, Inc., 1978.

[87] Cheesewright, R. and King, K.J., [1985].
Laser-Doppler Measurements in Natural Convection Flows.
Int. Conf. on Laser Anemometry - Advances and Application, 16th-17th December, Manchester, U.K., 1985.

[88] Cheesewright, R. and King, K.J., [1986].
Velocity Survey of the Large Vertical Air Cavity at Q.M.C. Using Laser-Doppler Anemometry (5 to 1 Aspect Ratio Series 2, 3 and 4).
Q.M.C. Faculty of Engineering Report EP 5035, February 1986.

PUBLISHED MATERIAL

There have been two papers published to-date which have utilised data from the present study. These are Cheesewright et al [86] and Cheesewright and King [87]. In order to save space these have not been bound into this thesis.

[89] Bowles, A. and Cheesewright, R., [1989].
Direct Measurements of the Turbulence Heat Flux in a Large Rectangular Air Cavity.
Experimental Heat Transfer, Vol. 2, pp 59-69, 1989.

APPENDIX A

In order to save space, the entire set of raw data from all the experimental Series are not presented here. Instead a list of all the references containing the raw data are listed, together with contact addresses should the reader wish to contact the author to obtain a copy of the data.

The data from Series 1 have been published in King [82], and have been kept in the author's experimental results files.

The data from Series 2, 3 and 4 have been published in Cheesewright and King [88], and have been kept in the author's experimental results files.

The data from Series 5, 6 and 7 have been kept in the author's experimental results files.

Any communication with the author may be made through either of the two following addresses.

K. J. KING,
208, HIGH STREET,
CLAPHAM,
BEDFORD MK41 6BS
ENGLAND.

K. J. KING,
SOFTWARE SCIENCES LTD.,
MEUDON AVENUE,
FARNBOROUGH,
HAMPSHIRE,
ENGLAND.

Any communication with the author, or his supervisor, may also be made through the following address.

K. J. KING / R. CHEESEWRIGHT,
DEPT. MECH. ENG.,
QUEEN MARY COLLEGE,
UNIVERSITY OF LONDON,
MILE END ROAD,
LONDON E1 4NS
ENGLAND.

BIBL. LONDIN. UNIV